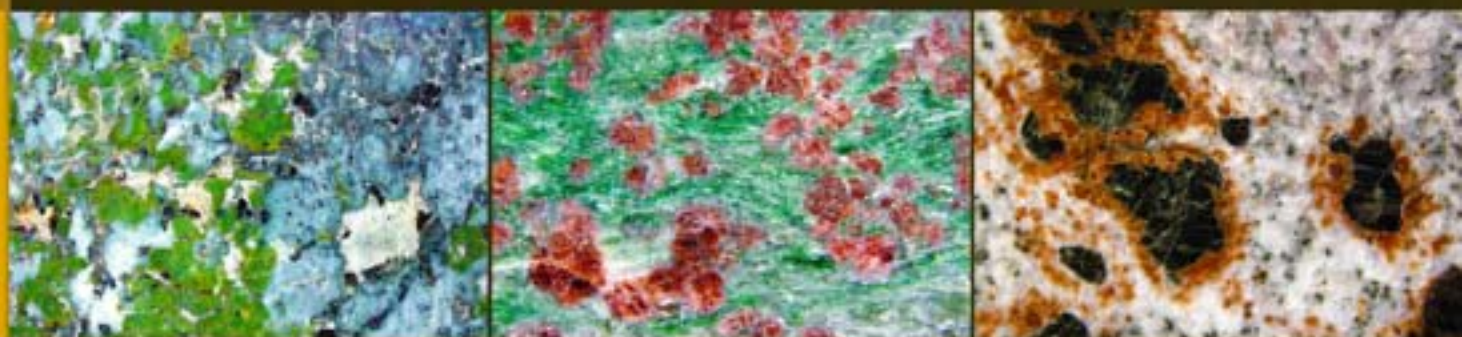



Kurt Bucher  
Rodney Grapes



# Petrogenesis of Metamorphic Rocks

*8th Edition*

 Springer

# Petrogenesis of Metamorphic Rocks



Kurt Bucher • Rodney Grapes

# Petrogenesis of Metamorphic Rocks

 Springer

Prof.Dr. Kurt Bucher  
University Freiburg  
Mineralogy Geochemistry  
Albertstr. 23 B  
79104 Freiburg  
Germany  
bucher@uni-freiburg.de

Prof. Rodney Grapes  
Department of Earth and Environmental  
Sciences  
Korea University  
Seoul  
Korea  
grapes@korea.ac.kr

ISBN 978-3-540-74168-8                      e-ISBN 978-3-540-74169-5  
DOI 10.1007/978-3-540-74169-5  
Springer Heidelberg Dordrecht London New York

Library of Congress Control Number: 2011930841

© Springer-Verlag Berlin Heidelberg 2011

This work is subject to copyright. All rights are reserved, whether the whole or part of the material is concerned, specifically the rights of translation, reprinting, reuse of illustrations, recitation, broadcasting, reproduction on microfilm or in any other way, and storage in data banks. Duplication of this publication or parts thereof is permitted only under the provisions of the German Copyright Law of September 9, 1965, in its current version, and permission for use must always be obtained from Springer. Violations are liable to prosecution under the German Copyright Law.

The use of general descriptive names, registered names, trademarks, etc. in this publication does not imply, even in the absence of a specific statement, that such names are exempt from the relevant protective laws and regulations and therefore free for general use.

*Cover design:* deblik

Printed on acid-free paper

Springer is part of Springer Science+Business Media ([www.springer.com](http://www.springer.com))

# Preface

This new edition of “Petrogenesis of Metamorphic Rocks” has several completely revised chapters and all chapters have updated references and redrawn figures. All chapters of Part II of the book have been rewritten. Also, the chapters “Introduction” and “Grade” have undergone several major changes. The references made to important web sites relating to metamorphic petrology tutorials, software, mail base, etc have been updated and extended. However, it should be noted that some of the links to these sites may fail to work in the future. A large number of new figures showing assemblage stability diagrams have been computed using the Theriak/Domino software by Ch. de Capitani of the University of Basel.

We encourage you to regularly read (or at least glance through) current issues of scientific journals in your library either online or paper copies. In the field of metamorphic petrology, the *Journal of Metamorphic Geology* is essential reading and some of the other particularly relevant journals include, *Journal of Petrology*, *Contributions to Mineralogy and Petrology*, *Geofluids*, *American Mineralogist*, *European Journal of Mineralogy*, *Lithos*, *Chemical Geology* and *Earth and Planetary Science Letters*.

Freiburg, Germany  
Seoul, South Korea  
November 2010

Kurt Bucher  
Rodney Grapes



# Contents

## Part I Introduction and General Aspects of Metamorphism

<b>1 Definition, Conditions and Types of Metamorphism</b> .....	3
1.1 Conditions of Metamorphism .....	4
1.1.1 Low-Temperature Limit of Metamorphism .....	4
1.1.2 High-Temperature Limit of Metamorphism .....	5
1.1.3 Low-Pressure Limit of Metamorphism .....	7
1.1.4 High-Pressure Limit of Metamorphism .....	7
1.2 Types of Metamorphism .....	8
1.2.1 Orogenic Metamorphism .....	8
1.2.2 Ocean-Floor Metamorphism .....	11
1.2.3 Other Types of Regional Metamorphism .....	11
1.2.4 Contact Metamorphism .....	13
1.2.5 Cataclastic Metamorphism .....	14
1.2.6 Hydrothermal Metamorphism .....	14
1.2.7 Other Types of Small-Scale Metamorphism .....	16
References and Further Reading .....	17
<b>2 Metamorphic Rocks</b> .....	21
2.1 Primary Material of Metamorphic Rocks .....	22
2.1.1 Chemical Composition of Protoliths of Metamorphic Rocks .....	23
2.1.2 Chemical Composition Classes of Metamorphic Rocks and Their Protoliths .....	25
2.2 The Structure of Metamorphic Rocks .....	26
2.3 Classification and Names of Metamorphic Rocks .....	29
2.3.1 Rock Names Referring to the Structure .....	31
2.3.2 Names for High-Strain Rocks .....	32
2.3.3 Special Terms .....	33
2.3.4 Modal Composition of Rocks .....	35
2.3.5 Names Related to the Origin of the Protolith .....	35
2.4 Mineral Assemblages and Mineral Parageneses .....	36



2.5 Graphical Representation of Metamorphic Mineral Assemblages .....	39
2.5.1 Mole Numbers, Mole Fractions and the Mole Fraction Line .....	39
2.5.2 The Mole Fraction Triangle .....	41
2.5.3 Projections .....	43
References and Further Reading .....	55
<b>3 Metamorphic Processes .....</b>	<b>57</b>
3.1 Principles of Metamorphic Reactions .....	58
3.2 Pressure and Temperature Changes in Crust and Mantle .....	65
3.2.1 General Aspects .....	65
3.2.2 Heat Flow and Geotherms .....	66
3.2.3 Temperature Changes and Metamorphic Reactions .....	71
3.2.4 Pressure Changes in Rocks .....	72
3.3 Gases and Fluids .....	74
3.4 Time Scale of Metamorphism .....	76
3.5 Pressure–Temperature–Time Paths and Reaction History .....	77
3.6 Chemical Reactions in Metamorphic Rocks .....	81
3.6.1 Reactions Among Solid-Phase Components .....	82
3.6.2 Reactions Involving Volatiles as Reacting Species .....	83
3.7 Reaction Progress .....	99
3.8 Phase Diagrams .....	102
3.8.1 Phase Diagrams, General Comments and Software .....	102
3.8.2 The Phase Rule .....	103
3.8.3 Construction of Phase Diagrams for Multicomponent Systems After the Method of Schreinemakers .....	105
3.8.4 Use of Phase Diagrams, an Example .....	109
References and Further Reading .....	113
<b>4 Metamorphic Grade .....</b>	<b>119</b>
4.1 General Considerations .....	119
4.2 Index Minerals and Mineral Zones .....	120
4.3 Metamorphic Facies .....	122
4.3.1 Origin of the Facies Concept .....	122
4.3.2 Metamorphic Facies Scheme .....	124
4.3.3 Pressure–Temperature Conditions of Metamorphic Facies ...	131
4.4 Isograds .....	131
4.4.1 The Isograd Concept .....	131
4.4.2 Zone Boundaries, Isograds and Reaction-Isograds .....	133
4.4.3 Assessing Isograds, Isobars and Isotherms .....	135
4.5 Bathozones and Bathograds .....	139
4.6 Petrogenetic Grid .....	141
4.6.1 Polymorphic Transitions .....	142

4.7	Geothermobarometry .....	146
4.7.1	Concept and General Principle .....	147
4.7.2	Assumptions and Precautions .....	149
4.7.3	Exchange Reactions .....	153
4.7.4	Net-Transfer .....	158
4.7.5	Miscibility Gaps and Solvus Thermometry .....	162
4.7.6	Uncertainties in Thermobarometry .....	166
4.7.7	Thermobarometry Using Multi-equilibrium Calculations (MET) .....	167
4.8	Gibbs Method .....	168
4.9	Assemblage Stability Diagrams .....	170
4.10	More $P$ - $T$ Tools .....	171
4.10.1	Reactions Involving Fluid Species .....	171
4.10.2	$P$ - $T$ Tools for Very Low Grade Rocks .....	173
	References and Further Reading .....	174

## Part II Metamorphism of Specific Rock Types

<b>5</b>	<b>Metamorphism of Ultramafic Rocks .....</b>	<b>191</b>
5.1	Introduction .....	191
5.2	Ultramafic Rocks .....	191
5.2.1	Rock Types .....	193
5.2.2	Chemical Composition .....	194
5.3	Metamorphism in the MSH System .....	196
5.3.1	Chemographic Relations in the MSH System .....	196
5.3.2	Progressive Metamorphism of Maximum Hydrated Harzburgite .....	198
5.4	Metamorphism in the CMASH System .....	202
5.4.1	Progressive Metamorphism of Hydrated Al-Bearing Lherzolite .....	202
5.4.2	Effects of Rapid Decompression and Uplift Prior to Cooling .....	204
5.5	Isograds in Ultramafic Rocks .....	204
5.6	Mineral Assemblages in the Uppermost Mantle .....	206
5.7	Serpentinization of Peridotite .....	208
5.8	Ultramafic Rocks at High Temperature .....	210
5.9	Thermometry and Geobarometry in Ultramafic Rocks .....	211
5.10	Carbonate-Bearing Ultramafic Rocks .....	212
5.10.1	Metamorphism of Ophicarbonates .....	212
5.10.2	Soapstone and Sagvandite .....	215
5.11	Open System Reactions in Ultramafic Rocks .....	219
5.12	Potassium-Bearing Peridotites .....	221
	References and Further Reading .....	221

<b>6</b>	<b>Metamorphism of Dolomites and Limestones</b>	225
6.1	Introduction	225
6.1.1	Rocks	225
6.1.2	Minerals and Rock Composition	227
6.1.3	Chemographic Relationships	228
6.2	Orogenic Metamorphism of Siliceous Dolomite	230
6.2.1	Modal Evolution Model	232
6.3	Orogenic Metamorphism of Limestone	233
6.4	Contact Metamorphism of Dolomites	235
6.4.1	Modal Evolution Model	238
6.5	Contact Metamorphism of Limestones	239
6.6	Isograds and Zone Boundaries in Marbles	243
6.7	Metamorphic Reactions Along Isothermal Decompression Paths	244
6.8	Marbles Beyond the CMS-HC System	246
6.8.1	Fluorine	247
6.8.2	Aluminium	248
6.8.3	Potassium	248
6.8.4	Sodium	251
6.9	Thermobarometry of Marbles	251
6.9.1	Calcite–Dolomite Miscibility Gap	252
6.10	High-Pressure and Ultrahigh-Pressure Metamorphism of Carbonate Rocks	252
	References and Further Reading	253
<b>7</b>	<b>Metamorphism of Pelitic Rocks (Metapelites)</b>	257
7.1	Metapelitic Rocks	257
7.2	Pelitic Sediments	257
7.2.1	General	257
7.2.2	Chemical Composition	258
7.2.3	Mineralogy	258
7.3	Pre-metamorphic Changes in Pelitic Sediments	258
7.4	Intermediate-Pressure Metamorphism of Pelitic Rocks	259
7.4.1	Chemical Composition and Chemography	259
7.4.2	Mineral Assemblages at the Beginning of Metamorphism	260
7.4.3	The ASH System	262
7.4.4	Metamorphism in the FASH System	264
7.4.5	Mica-Involving Reactions	267
7.4.6	Metamorphism in the KFMASH System (AFM System)	269
7.5	Low-Pressure Metamorphism of Pelites	278
7.5.1	FASH System	278
7.5.2	KFMASH System	280
7.6	High-Temperature Metamorphism of Pelites: Metapelitic Granulites	284

7.6.1	Cordierite–Garnet–Opx–Spinel–Olivine Equilibria	285
7.6.2	The Excess Quartz Condition	286
7.6.3	Partial Melting and Migmatite	288
7.6.4	More About Granulites	292
7.7	Metamorphism of Mg-rich “Pelites”	296
7.8	High Pressure: Low Temperature Metamorphism of Pelites	298
7.9	Additional Components in Metapelites	302
	References and Further Reading	306
<b>8</b>	<b>Metamorphism of Marls</b>	<b>315</b>
8.1	General	315
8.2	Orogenic Metamorphism of Al-Poor Marls	316
8.2.1	Phase Relationships in the KCMAS-HC System	317
8.2.2	Prograde Metamorphism in the KCMAS-HC System at Low $X_{\text{CO}_2}$	319
8.3	Orogenic Metamorphism of Al-Rich Marls	321
8.3.1	Phase Relationships in the CAS-HC System	323
8.3.2	Phase Relationships in the KNCAS-HC System	325
8.4	Increasing Complexity of Metamarls	332
8.5	Low Pressure Metamorphism of Marls	333
	References and Further Reading	336
<b>9</b>	<b>Metamorphism of Mafic Rocks</b>	<b>339</b>
9.1	Mafic Rocks	339
9.1.1	Hydration of Mafic Rocks	340
9.1.2	Chemical and Mineralogical Composition of Mafic Rocks	342
9.1.3	Chemographic Relationships and ACF Projection	343
9.2	Overview of Metamorphism of Mafic Rocks	348
9.2.1	Plagioclase in Mafic Rocks, Equilibria in the Labradorite System (NCASH System)	352
9.3	Subgreenschist Facies Metamorphism	353
9.3.1	General Aspects	353
9.3.2	Metamorphism in the CMASH and NCMASH Systems	356
9.3.3	Transition to Greenschist Facies	362
9.4	Greenschist Facies Metamorphism	363
9.4.1	Introduction	363
9.4.2	Mineralogical Changes Within the Greenschist Facies	363
9.4.3	Greenschist–Amphibolite Facies Transition	365
9.5	Amphibolite Facies Metamorphism	367
9.5.1	Introduction	367
9.5.2	Mineralogical Changes Within the Amphibolite Facies	367
9.5.3	Low-Pressure Series Amphibolites	368
9.5.4	Amphibolite–Granulite Facies Transition	370
9.6	Granulite Facies and Mafic Granulites	371

9.7 Blueschist Facies Metamorphism .....	374
9.7.1 Introduction .....	374
9.7.2 Reactions and Assemblages .....	374
9.8 Eclogite Facies Metamorphism .....	378
9.8.1 Eclogites .....	378
9.8.2 Reactions and Assemblages .....	380
9.8.3 Eclogite Facies in Gabbroic Rocks .....	383
References and Further Reading .....	387
<b>10 Metamorphism of Quartzofeldspathic Rocks .....</b>	<b>395</b>
10.1 Quartzofeldspathic Rocks .....	395
10.2 Metagraywackes .....	395
10.2.1 Introduction .....	395
10.2.2 Metamorphism of Metagraywacke (Metasparmitic) Compositions .....	397
10.2.3 Orogenic Metamorphism of Metagraywackes .....	398
10.2.4 Contact Metamorphism of Metagraywackes and Metasparmites .....	400
10.3 Granitoids .....	406
10.3.1 Prehnite and Pumpellyite .....	406
10.3.2 Stilpnomelane .....	406
10.3.3 The Microcline–Sanidine Isograd .....	407
10.3.4 Eclogite and Blueschist Facies Granitoids .....	408
10.3.5 Migmatitic Granitoids and Charnockite .....	409
References and Further Reading .....	411
<b>Appendix: Symbols for rock forming minerals .....</b>	<b>415</b>
<b>Index .....</b>	<b>419</b>



# Part I Introduction and General Aspects of Metamorphism

Kyanite-eelolite from Verpeneset, Nordfjord, Norway. Omphacite (*green*), garnet (*red brown, zoned*) are the main minerals, additional minerals include kyanite, zoisite and phengite. The rock formed by Caledonian high-pressure metamorphism



# Chapter 1

## Definition, Conditions and Types of Metamorphism

Rock metamorphism is a geological process that changes the mineralogical and chemical composition, as well as the structure of rocks. Metamorphism is typically associated with elevated temperature and pressure, thus it affects rocks within the earth's crust and mantle. The process is driven by changing physical and/or chemical conditions in response to large-scale geological dynamics. Consequently, it is inherent in the term, that metamorphism always is related to a precursor state where the rocks had other mineralogical and structural attributes. Metamorphism, metamorphic processes and mineral transformations in rocks at elevated temperatures and pressures are fundamentally associated with chemical reactions in rocks. Metamorphism does not include, by definition, similar processes that occur near the earth's surface such as weathering, cementation and diagenesis. The transition to igneous processes is gradual, and metamorphism may include partial melting. The term metasomatism is used if modification of the rocks bulk composition is the dominant metamorphic process. Metamorphic rocks are rocks that have developed their mineralogical and structural characteristics by metamorphic processes.

The most typical metamorphism transforms sedimentary rocks to metamorphic rocks by addition of heat during mountain building or by a large volume of magma in the crust. For example, Upper Ordovician shales and nodular limestone (Fig. 1.1) in the Permian Oslo rift were heated to about 420°C by syenite plutons. The gray fissile shales composed predominantly of diagenetic clay minerals and quartz were transformed to dark splintery rocks called hornfels, which contain metamorphic minerals such as biotite, cordierite, K-feldspar and sillimanite. The limestone nodules consist of pure CaCO<sub>3</sub> in the unmetamorphic sedimentary rock (Fig. 1.1a). At the temperature of metamorphism calcite reacted with the minerals of the shale. The reaction produced concentrically zoned nodules consisting of the Ca-silicates anorthite, wollastonite and diopside, so-called calcsilicate rocks (Fig. 1.1b). All calcite has been used up in the reaction and all CO<sub>2</sub> once present has left the rock together with H<sub>2</sub>O produced by the dehydration of the clay minerals. The example shows all characteristic features of metamorphism: The nodular limestone and shale were the precursor rocks (so-called protolith) of the newly formed metamorphic hornfels. A set of new minerals formed on the expense of previous minerals by chemical reactions in the rocks. The reactions were driven by heat added to the rock. The structure of the original rock was modified as



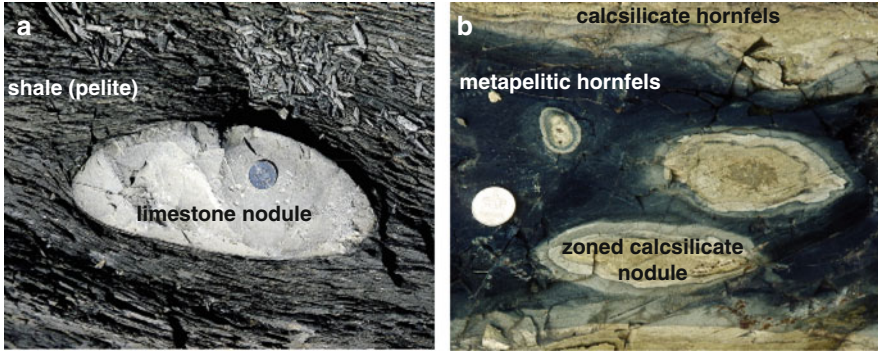


**Fig. 1.1** Metamorphic transformation of sedimentary rocks (a) to metamorphic hornfels (b) in a contact aureole of Permian plutons in the Oslo rift, Norway: (a) Upper Ordovician shale with fossiliferous limestone nodules. (b) Same rock as (a) but heated to about 430°C by a nearby pluton. Shale transformed to hornfels and limestone nodules reacted to zoned calcisilicate rock with anorthite and diopside as main minerals

expressed by new ultrafine grainsize in the hornfels and by the concentric arrangement of chemically distinct reaction zones in the calcisilicate nodules as a result of small scale redistribution of chemical constituents in the rock. Obviously also the chemical composition of the rocks were changed on a local scale because the volume once occupied by carbonate (limestone nodule) was replaced by silicates during the metamorphic process and the rock is devoid of  $\text{CO}_2$  and  $\text{H}_2\text{O}$ .

## 1.1 Conditions of Metamorphism

Large scale geologic events such as global lithospheric plate movements, subduction of oceanic lithosphere, continent–continent collision and ocean floor spreading all have the consequence of moving rocks and transporting heat. Consequently, changes in pressure (depth) and temperature are the most important variables in rock metamorphism. As an example, consider a layer of sediment on the ocean floor that is covered with more sediment layers through geologic time and finally subducted at a destructive plate margin. The mineral, chemical and structural transformations experienced by the sediment can be related to a gradually increasing temperature with time. The question may be asked: at what temperature does metamorphism begin?

### 1.1.1 Low-Temperature Limit of Metamorphism

Temperatures at which metamorphism sets in are strongly dependent on the material under investigation. Transformation of evaporites, of vitreous material and of

organic material, for example, begins to take place at considerably lower temperatures than chemical reactions in most silicate and carbonate rocks. This book is not concerned with the metamorphism of organic material, i.e. coalification (maturation). For a review on this subject the reader is referred to Teichmüller (1987) (see also Ruppert et al. 2010). Correlation between the rank of coalification and mineralogical changes in slightly metamorphosed sediments and volcanic rocks are reviewed by Kisch (1987).

In many rocks mineral transformations begin shortly after sedimentation and proceed continuously with increasing burial. Whether such reactions are called “diagenetic” or “metamorphic” is largely arbitrary. Further examples of processes that are intimately related to metamorphism include low temperature alteration of volcanic rocks, precipitation of mineral coatings in fractures and low-temperature rock–water reactions that produce mineral-filled veins and fissures. Hence, metamorphic processes occur in a temperature continuum from surface temperature upward. However, the low-temperature limit of metamorphism has been arbitrarily set to  $150^{\circ}\text{C} \pm 50^{\circ}\text{C}$  in this book and most of our phase-diagrams show phase equilibria above  $200^{\circ}\text{C}$  or  $300^{\circ}\text{C}$ .

Some minerals are considered distinctly metamorphic, that is they form at elevated temperature and are not found in diagenetically transformed sediments. In a regime of increasing temperature, the first occurrence of such minerals in sediments thus marks the onset of metamorphism. Indicators of beginning of metamorphism include: carpholite, pyrophyllite, Na-amphibole, lawsonite, paragonite, prehnite, pumpellyite, or stilpnomelane. Note, however, that these minerals may also be found as detrital grains in unmetamorphosed sediments. In this case, textural evidence from thin-sections will distinguish between a neof ormation or a detrital origin. For a more detailed discussion of problems dealing with the low-temperature limit of metamorphism and its delimitation from diagenesis the reader is referred to Frey and Kisch (1987) and Robinson and Merriman (1999).

### ***1.1.2 High-Temperature Limit of Metamorphism***

Ultimately, at high temperature, rocks will start to melt and dealing with silicate melts is the subject of igneous petrology. However, partial melting has always, both, a metamorphic and an igneous aspect. Crustal rocks that are characteristically produced by partial melting, so called migmatites, are made up of a residual metamorphic rock and an igneous rock component. Nevertheless, melting temperatures of rocks define the high-temperature limit of metamorphism. Melting temperatures are strongly dependent on pressure, rock composition and the amount of water present. For example, at 500 MPa and in the presence of an aqueous fluid, granitic rocks begin to melt at a temperature of about  $660^{\circ}\text{C}$  while basaltic rocks need a much higher temperature of about  $800^{\circ}\text{C}$  (Fig. 1.2). If  $\text{H}_2\text{O}$  is absent, melting temperatures are much higher. Granitic gneisses will not melt below about  $1,000^{\circ}\text{C}$ , mafic rocks such as basalt require  $> 1,120^{\circ}\text{C}$  to melt. The highest temperatures

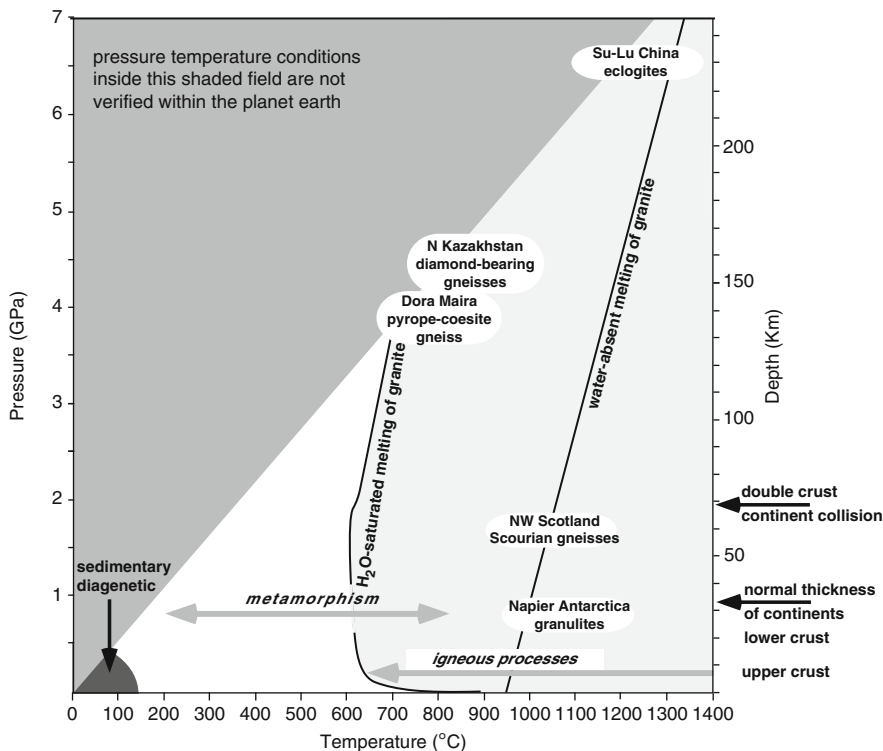


**Fig. 1.2** The pressure temperature range of metamorphic processes. The  $P$ - $T$  gradients of four typical geodynamic settings are shown. The boundary between diagenesis and metamorphism is gradational, but a  $T$ -value of  $\sim 150^{\circ}\text{C}$  is shown for convenience. Note that the metamorphic field has no upper  $P$ - $T$  limit on this diagram, and that there is a large overlap for metamorphic and magmatic conditions. Extreme  $P$ - $T$  conditions are shown for the following areas: (1) Sapphirine quartzite from the Napier Complex, Antarctica (Harley and Motoyoshi 2000); (2) Scourian granulites from NW Scotland (Lamb et al. 1986, Fig. 3); (3) Pyrope-coesite rocks from Dora Maira, western Alps (Schertl et al. 1991); (4) diamond-bearing metamorphic rocks from the Kokchetav massif, northern Kazakhstan (Shatsky et al. 1995); (5) Garnet peridotite from the Su-Lu unit, east central China (Yang et al. 1993). The *wet granite melting curve* is after Stern and Wyllie (1981), and the *dry granite melting curve* is after Newton (1987, Fig. 1)

reported from crustal metamorphic rocks are  $1,000$ – $1,150^{\circ}\text{C}$  (e.g. Lamb et al. 1986; Ellis 1980; Harley and Motoyoshi 2000; Hokada 2001; Sajeew and Osanai 2004), determined by indirect methods of thermobarometry as explained in Sect. 4.7. Such rocks are termed ultra high temperature (UHT) metamorphic rocks and are typically magnesian- and aluminous-rich gneisses, e.g. Napier Complex (Antarctica), Scourian gneiss (Scotland), the Highland Complex (Sri Lanka). Temperatures in the lower continental crust of geologically active areas are inferred to be about  $750$ – $850^{\circ}\text{C}$  and the rocks produced under these conditions are termed granulites. This is also the typical upper temperature limit of crustal metamorphism. However,

metamorphism is not restricted to the Earth's crust. A given volume of rock in the convecting mantle continuously undergoes metamorphic processes such as recrystallization and various phase transformations in the solid state at temperatures in excess of 1,500°C.

### ***1.1.3 Low-Pressure Limit of Metamorphism***

Ascending hot silicate magmas are a typical and globally important occurrence in geologically active areas. The heat released by the cooling magma causes metamorphism in the surrounding country rocks to produce so-called contact aureoles at shallow depth and pressures of a few megapascal.

### ***1.1.4 High-Pressure Limit of Metamorphism***

For a long time it was believed that maximum pressures in metamorphic crustal rocks did not exceed 1.0 GPa, which corresponds to the lithostatic pressure at the base of a normal continental crust with a thickness of 30–40 km (pressure units used in this book: Pa – pascal,  $1 \text{ Pa} = 1 \text{ N/m}^2 = 1 \text{ kg/(m s}^2\text{)}$ ;  $10^5 \text{ Pa} = 1 \text{ bar}$ ;  $1 \text{ GPa} = 10^9 \text{ Pa}$ ;  $1 \text{ MPa} = 10^6 \text{ Pa}$ ;  $100 \text{ MPa} = 1 \text{ kbar}$ ). As better data on mineral stability relations became available, it was found that mineral assemblages in some metamorphic mafic rocks often recorded pressures of 1.5–2.0 GPa. It was recognized early that these rocks, called eclogites, represented high density and consequently high pressure equivalents of basalts (Eskola 1921). Spectacular high-pressure rocks of clearly crustal origin were discovered in the Dora-Maira massif of the Alps (Chopin 1984). Gneisses with pure pyrope garnet containing coesite inclusions indicate pressures of at least 3.0 GPa. Similar super-high-pressure rock have been discovered in many other places in the world (e.g. Reinecke 1991; Wain et al. 2000) since. Today, eclogites with coesite inclusions in garnet and even diamond-bearing eclogites have been reported (Smith and Lappin 1989; Okay 1993; Zhang and Liou 1994; Coleman et al. 1995; Schreyer 1995; Ernst 1999; Lü et al. 2009). Some of these rocks require at least 6.0 GPa to form. Rock transformations at such high pressures are called ultra-high-pressure (UHP) metamorphism. It is clear that such super-high pressures must be related to transport of crustal rocks to very great depth of >100 km.

Yet, metamorphism as stated above, is not confined to the Earth's crust or to subducted crustal rocks. Mantle rocks such as garnet peridotites (or garnet–olivine–pyroxene–granofelses) from ophiolite complexes or from xenoliths in kimberlite record pressures of >3–4 GPa (e.g. Yang et al. 1993; Song et al. 2009). Consequently, it is possible to find and study rocks that formed 100–200 km below the earth surface corresponding to pressures >3–6 GPa.

Temperature	Pressure
<i>Low T-limit</i> 0°C for processes in near surface environments, rock–water reactions Conventionally, the term metamorphism implies $T > 150\text{--}200^\circ\text{C}$	<i>Low P-limit</i> 0.1 MPa at contact to lava flows at the surface
<i>Upper T-limit</i> In crustal rocks: $750\text{--}850^\circ\text{C}$ (max. recorded $T \sim 1,150^\circ\text{C}$ ) In many regional scale metamorphic areas $T$ does not exceed $\sim 650\text{--}700^\circ\text{C}$	<i>High P-limit</i> Presently, some rocks collected at the earth surface are known to have once formed at 100–200 km depth, = 3–6 GPa

## 1.2 Types of Metamorphism

On the basis of geological setting, we distinguish between metamorphism of local and regional extent:

Regional extent	Local extent
Orogenic metamorphism (regional metamorphism)	Contact (igneous) metamorphism
Subduction metamorphism	Cataclastic metamorphism
Collision metamorphism	Hydrothermal metamorphism
Ocean-floor metamorphism	<i>Exotic local metamorphism</i>
Burial metamorphism	Impact metamorphism
	Lightning metamorphism
	Combustion metamorphism

Such a subdivision is certainly useful, but it should be kept in mind that there commonly exist transitional forms between regional and contact (igneous) categories of metamorphism.

### 1.2.1 Orogenic Metamorphism

Orogenic metamorphism (Miyashiro 1973, p. 24) is caused by mountain building or orogenic process. It acts upon large volumes of rocks and the metamorphic effects of a specific mountain building episode are found over large, regional scale dimensions. The term regional metamorphism can be used as a word with the same meaning. This is the most significant type of metamorphism affecting the rocks of the continental crust on a large scale. Consequently this book deals almost exclusively with orogenic metamorphism supplemented with some aspects of low-P contact metamorphism (Sect. 1.2.4).

Metamorphism associated with a specific mountain building episode may show characteristic features. As an example; Alpine metamorphism in the Alps is collectively used for all metamorphic processes associated with the formation of the Alps

in late Cretaceous and Tertiary times. It affected rocks that experienced metamorphic transformations for the first time, i.e. Mesozoic sediments and volcanics. It also once more transformed rocks that already have been metamorphosed during earlier orogenic periods, such as Variscian gneisses, Caledonian metasediments and even rocks with Precambrian mineral assemblages. Rocks subjected to orogenic metamorphism usually extend over large belts, hundreds or thousands of kilometers long and tens or hundreds of kilometers wide.

In many higher temperature parts of orogenic metamorphic belts, syn- or late-tectonic granites are abundant. Orogenic metamorphism and granitic plutons are often intimately associated. In the middle and upper crust, rising granitic magma carries heat and thereby contributes to the increase of temperature on a regional scale leading to typical high-temperature low-pressure terranes. In the lower to middle crust, the granitic magmas were generated by partial melting as a consequence of high-grade metamorphism.

Orogenic metamorphism is commonly characterized by two fundamentally different kinds of regional scale metamorphic transformations that follow each other in time. An early high-pressure low-temperature type metamorphism is related to a subduction zone process, a later younger regional metamorphism following a moderate  $P$ - $T$  gradient is related to continental collision. This dualism of orogenic metamorphism is related to major intervals of a Wilson cycle of mountain building (Wilson 1966; Murphy and Nance 1992; Duncan and Turcotte 1994).

Typically, metamorphic recrystallization in orogenic belts is accompanied by deformation. Such metamorphic rocks exhibit a penetrative fabric with preferred orientation of mineral grains. Examples are phyllites, schists and gneisses. Orogenic metamorphism is a long-lasting process of millions or tens of millions of years duration. It includes a number of distinct episodes of crystallization and deformation. Individual deformation phases appear to have definite characteristics, like attitude and direction of schistosity, folds, and lineations. Therefore, several phases of deformation can perhaps be recognized in the field and they often can be put into a time sequence. Texture observations in thin sections under the microscope can unravel the relationships between structural features and mineral growth, and establish the time relations of deformation and metamorphism (e.g. Vernon 1976, p. 224).

Deformation is intimately associated with most forms of metamorphic recrystallization. Almost all metamorphic rocks show distinct features of ductile (Fig. 1.3) or brittle (Fig. 1.4) deformation. Metamorphic rocks are commonly intensely folded like the banded marbles shown in Fig. 1.3a from Engabreen, Nordland, Norway. The marbles represent former calcareous sediments, including limestone, marl and dolomite. The dolomite marble contains tremolite, diopside and phlogopite as characteristic metamorphic minerals. Granites and other unfoliated plutonic rocks can be progressively sheared resulting the transformation to gneiss. The Matorello granite is shown as an example on Fig. 1.3b from the Lagetti locality (Valle Maggia, Ticino, Swiss Alps). It shows the gradual transition of undeformed granite (upper left) to strongly foliated and sheared gneiss (lower right). Deformation is monitored by a regular increasing flattening of spherical mafic inclusions (strain

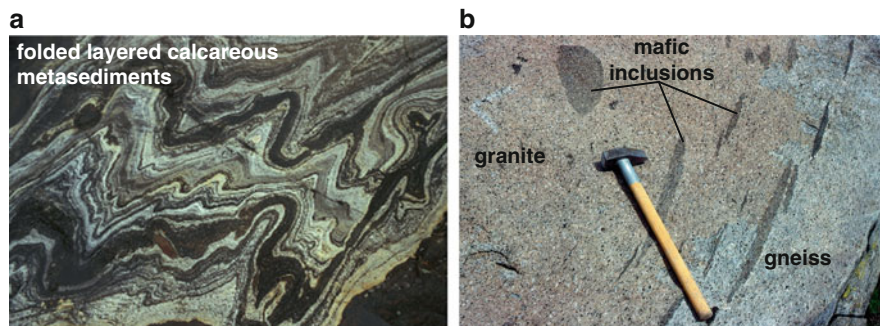


**Fig. 1.3** Ductile deformation associated with metamorphic transformation: **(a)** Intensely folded banded marbles representing former calcareous sediments, including limestone, marl and dolomite. The dolomite marble contains tremolite, diopside and phlogopite as characteristic metamorphic minerals (Engabreen, Nordland, Norway). **(b)** Gradual transition of undeformed granite (*upper left*) to strongly foliated and sheared gneiss (*lower right*). Deformation is monitored by increasing flattening of spherical mafic inclusions (*strain markers*) in the undeformed granite (Matorello granite, Lagetti, Valle Maggia, Ticino, Swiss Alps)

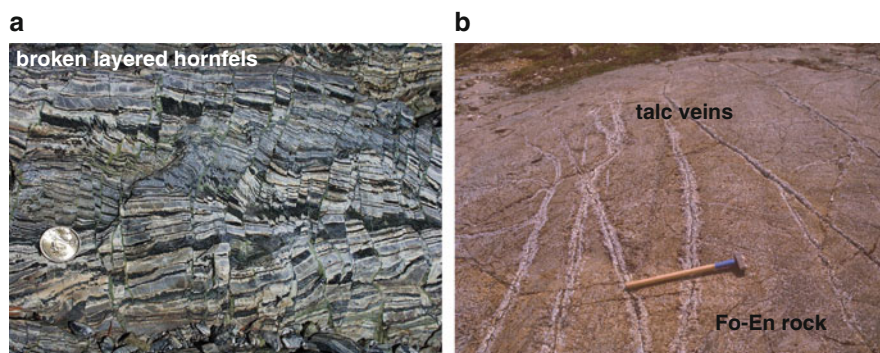


**Fig. 1.4** Brittle deformation associated with metamorphic transformation: **(a)** Intensely broken fine banded hornfels formed from volcanoclastic rocks in the contact aureole of a pluton (Saddlebag Lake, near Tioga Pass, Sierra Nevada, California, USA). Note that the porosity of the brittle fractures is sealed by hydrothermal mineral deposits (epidote, pumpellyite and chlorite). **(b)** Fractured metamorphic olivine–enstatite rock (metaharzburgite) with talc-rich replacement zones indication the reaction of hot water with the ultramafic rock (Flisarvatnet, Oppland, Norway)

markers) in the undeformed granite (Ramsay and Allison 1979). Also brittle deformation can be associated with metamorphic transformation. Figure 1.4a shows intensely broken fine banded hornfels that formed from volcanoclastic rocks in the contact aureole of a pluton (Saddlebag Lake, near Tioga Pass, Sierra Nevada, California, USA). Note that the porosity of the brittle fractures is sealed by greenish hydrothermal mineral deposits (epidote, pumpellyite and chlorite). Figure 1.4b shows fractured metamorphic olivine–enstatite rock (metaharzburgite) from the Scandinavian Caledonides (Flisarvatnet, Oppland, Norway). The fractures

served as conduits for hot fluid that contained dissolved silica. The reaction of this fluid with the ultramafic rock produced talc-rich replacement zones along the fractures. Both examples show that metamorphic minerals formed by reaction of fluid with rocks and that the hydrothermal metamorphism (see below) is associated with brittle deformation.

Some features of orogenic metamorphism are summarized in Table 1.1. Rocks produced by regional orogenic and local contact metamorphism differ significantly in their fabric, being schistose as opposed to non-schistose, respectively. Furthermore, orogenic metamorphism takes place at higher pressures, while the temperature regime is often the similar in both types.

### ***1.2.2 Ocean-Floor Metamorphism***

This type of regional metamorphism was introduced by Miyashiro (1971) for transformations in the oceanic crust in the vicinity of mid-ocean ridges. The metamorphic rocks thus produced are moved laterally by ocean-floor spreading, covering large areas of the oceanic floor. The ocean-floor metamorphic rocks are mostly of basic and ultrabasic composition (basalt, peridotite). As most of these rocks are non schistose, ocean-floor metamorphism resembles continental burial metamorphism (see below), although the thermal gradient is much higher, up to several 100°C/km. A further characteristic of ocean-floor metamorphic rocks is their extensive veining and metasomatism, produced by the convective circulation of large amounts of heated sea water. This process leads to chemical interaction between rocks and sea water; in this respect, ocean-floor metamorphism resembles hydrothermal metamorphism (see below).

Some features of ocean-floor metamorphism are briefly stated in Table 1.1.

### ***1.2.3 Other Types of Regional Metamorphism***

Burial metamorphism was introduced by Coombs (1961) for low temperature regional metamorphism affecting sediments and interlayered volcanic rocks in a geosyncline without any influence of orogenesis or magmatic intrusion. Lack of schistosity is an essential characteristic of resultant rocks. This means that original rock fabrics are largely preserved. Mineralogical changes commonly are incomplete, so that the newly-formed mineral assemblage is intimately associated with relict mineral grains inherited from the original rock. Burial metamorphism in fact merges into and cannot be sharply distinguished from deep-seated diagenesis. Metamorphic changes are often not distinguishable in hand specimen; only in thin sections can they be clearly recognized.

Well-known examples of burial metamorphism include those described from southern New Zealand (e.g. Kawachi 1975; Boles and Coombs 1975), eastern



Table 1.1 Typical features of important types of metamorphism

Type of metamorphism	Orogenic (subduction type)	Orogenic (collision type)	Ocean-floor	Contact
Geologic setting	In orogenic belts, extending for several 1,000 km <sup>2</sup> Early phase of orogenic metamorphism	In orogenic belts, extending for several 1,000 km <sup>2</sup> Late phase of orogenic metamorphism	In oceanic crust and upper mantle, extending for several 1,000 km <sup>2</sup>	Proximity to contacts to shallow level igneous intrusions; contact aureole of a few m up to a some kilometer width
Static/dynamic regime	Dynamic; generally associated with thrusting, slicing	Dynamic, generally associated with polyphase deformation, foliation and folding	± Static, extensive fracturing and veining, no foliation associated with extension and sea floor spreading	Static, no foliation
Temperature	150–700°C (>700°C in deep subduction)	150–850°C (max. T ~ 1,050°C)	150–500°C (>500°C close to magmas)	150–600°C (>600°C at gabbro contacts)
Lithostatic pressure	200–3,000 MPa for crustal rocks	200–1,000 MPa (in some collision belts up to 14 kbars, "double crust")	<300 MPa	From a few tens MPa to 3,000 MPa
Temperature gradients	5–12°C/km (vertical) gradient depends on subduction velocity	12–60°C/km (vertical) gradients depends on associated igneous activity	50–500°C/km (vertical or horizontal)	100°C/km or higher (horizontal)
Processes	Associated with subduction of oceanic lithosphere (ophiolites) and partly also continental rocks	Continent–continent collision, lithospheric thickening, compression and heating	Heat supply by ascending asthenosphere and intruding mafic magmas at mid-ocean ridges, combined with circulation of sea-water through fractured hot rocks in an extensional regime	Heat supply by igneous intrusions, commonly also associated with extensive metasomatism caused by convective hydrothermal circulation,
Typical metamorphic rocks	Blueschist, eclogite, serpentinite,	Slate, phyllite, schist, gneiss, migmatite, marble, quartzite, greenschist, amphibolite, granulite	Metabasalt, greenstone, metagabbro, serpentine; primary structure often well preserved	Hornfels, marble, calc-silicate granulites, skarn

Australia (e.g. Smith 1969), Japan (e.g. Seki 1973), and Chile (e.g. Levi et al. 1982). Well-known examples of burial metamorphism in metapelitic and metabasic rocks are also described by Merriman and Frey (1999) and Robinson and Bevins (1999), respectively.

**Diastathermal metamorphism** is a term proposed by Robinson (1987) for burial metamorphism in extensional tectonic settings showing enhanced heat flow. An example of this type of regional metamorphism was described from the Welsh Basin (Bevins and Robinson 1988; see also Merriman and Frey 1999; Robinson and Bevins 1999).

### ***1.2.4 Contact Metamorphism***

**Contact metamorphism** usually takes place in rocks in the vicinity of plutonic or extrusive igneous bodies. Metamorphic changes are caused by the heat given off by the cooling igneous body and also by gases and fluids released by the crystallizing magma. The zone of contact metamorphism is termed a contact aureole, the rocks affected are the country rocks of the magma body. The width of contact metamorphic aureoles typically varies in the range of several meters to a few kilometers. Local deformation associated with emplacement of the igneous mass can be observed in some aureoles.

Specifically, the width of aureoles depends on the volume, composition, intrusion depth of a magmatic body and also the properties of the country rocks, especially their fluid content and permeability. A larger volume of magma carries more heat with it than a smaller one, and the temperature increase in the bordering country rock will last long enough to cause mineral reactions. Rocks adjacent to small dikes, sills or lava flows are barely metamorphosed, whereas larger igneous bodies give rise to a well-defined contact aureole of metamorphic rocks.

The temperature of the various types of magma differs widely. Typical solidus temperatures of gabbroic (mafic, basaltic) magmas are well over 1,000°C. In contrast, many granitic plutons are formed from water-rich melts at temperatures close to 650–700°C. Large granitoid plutons formed from water-deficient magmas, (e.g. charnockite, mangerite) have solidus temperatures close to 900–950°C. However, because water-rich granites are the most common plutonic bodies in the continental crust, contact aureoles around granites are the most common examples of contact metamorphism.

The intrusion depth of a magmatic body determines the thermal gradient and heat flow across the magma-country rock contact. Exceptionally high thermal gradients are generally confined to the upper 10 km of the Earth's crust because, at deeper levels, the country rocks are already rather hot and, hence, obvious thermal aureoles are seldom produced.

The effects of contact metamorphism are most obvious where non-metamorphic sedimentary rocks, especially shales and limestones, are in contact with large magmatic bodies as detailed in later chapters. On the other hand, country rocks

that experienced medium- or high-temperature regional metamorphism prior to the intrusion show limited effects of contact metamorphic overprinting because the older mineral assemblages persist at contact metamorphic conditions.

Contact metamorphic rocks are generally fine-grained and lack schistosity. The most typical example is called hornfels (see Chap. 2 for nomenclature); but foliated rocks such as spotted slates and schists are occasionally present. Some features of contact metamorphism are stated briefly in Table 1.1 (for more details see Kerrick 1991).

**Pyrometamorphism** is a special kind of contact metamorphism. It shows the effects of particularly high temperatures at the contact of a rock with magma under volcanic or quasi-volcanic conditions, e.g. in xenoliths. Partial melting is common, producing glass-bearing rocks called buchites, and in this respect pyrometamorphism may be regarded as being intermediate between metamorphism and igneous processes. A detailed discussion of pyrometamorphism illustrated by numerous examples of rocks of different compositions is given by Grapes (2006) and is not discussed further here.

### *1.2.5 Cataclastic Metamorphism*

Cataclastic metamorphism is confined to the vicinity of faults and overthrusts, and involves purely mechanical forces causing crushing and granulation of the rock fabric. Experiments show that cataclastic metamorphism is favored by high strain rates under high shear stress at relatively low temperatures. The resulting cataclastic rocks are non-foliated and are known as fault breccia, fault gouge, or pseudotachylite. A pseudotachylite consists of an aphanitic groundmass that looks like black basaltic glass (tachylite). Note that mylonites are not regarded as cataclastic rocks, because some grain growth by syntectonic recrystallization and neoblastesis is involved (see e.g. Wise et al. 1984).

Dislocation or dynamic metamorphism are sometimes used as synonyms for cataclastic metamorphism; but these terms were initially coined to represent what is now called regional metamorphism. In order to avoid misunderstanding, the name “cataclastic metamorphism” is preferred.

### *1.2.6 Hydrothermal Metamorphism*

**Hydrothermal metamorphism** was originally introduced as a term by Coombs (1961). In hydrothermal metamorphism, hot aqueous solutions or gases flow through fractured rocks causing mineralogical and chemical changes in the rock matrix. The study of hydrothermal processes experienced a dramatic expansion during the last decades. It has been generalized and today the research on water–rock interaction

is a focus of modern petrology and geochemistry (e.g. Giggenbach 1981, 1984; Gillis 1995; Buick and Cartwright 1996, Droop and Al-Filali 1996; Alt 1999; Gianelli and Grassi 2001). Water–rock interaction and hydrothermal processes are particularly relevant for the making of ore deposits (Burnham 1979), rock leaching and alteration, formation of vein systems and fissure deposits. Understanding hydrothermal processes is also important in the context of geothermal energy production, use of thermal water in spas, design of radioactive waste repositories and many other areas.

Hydrothermal metamorphism in active geothermal areas are known from many areas including well studied examples in California, Mexico, Iceland, Italy, Japan, the Philippines (Fig. 1.5) and New Zealand. However, water–rock interaction takes place whenever circulating water in pores and fractures has a composition that is not in equilibrium with the rock matrix. Consequently, water–rock reactions occur at all temperatures from the surface to very hot conditions. At present, a few research boreholes in continental crust have reached several kilometer depth and temperatures in excess of 200°C. The fracture pore space was found to be fluid-filled in all boreholes and progressing fluid-rock reactions are evident from the

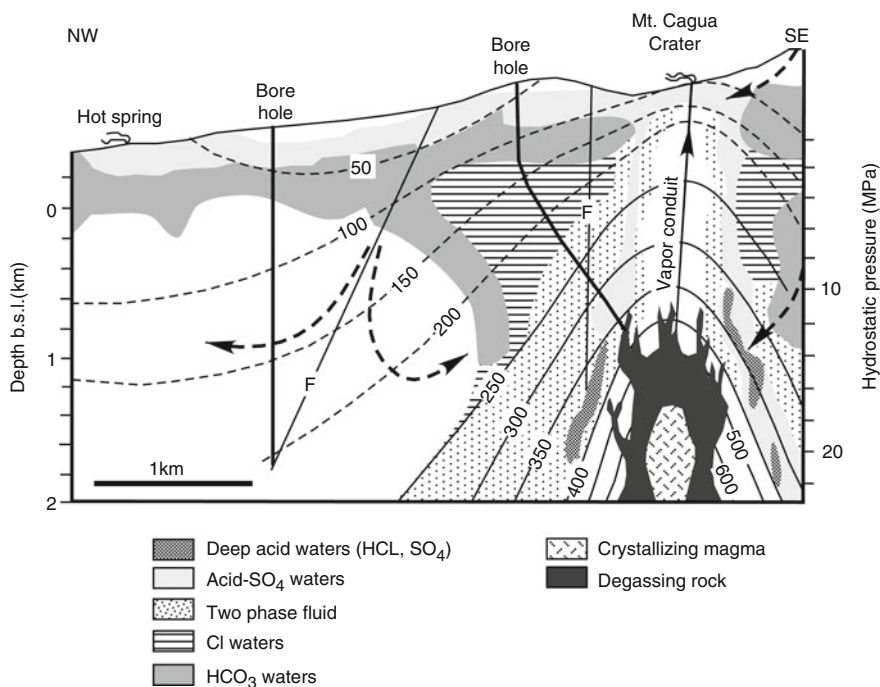


**Fig. 1.5** The magmatic-hydrothermal metamorphic system of Mt. Cagua, Philippines, showing thermal structure and chemical characteristics of hydrothermal fluids. *Dashed arrowed lines* indicate inferred meteoric water flow direction (Redrawn from Reyes et al. (2003, Fig. 16)

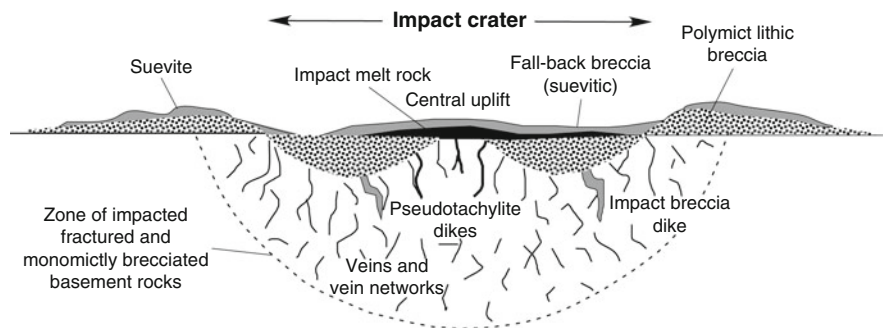


**Fig. 1.6** Diagram showing the geology of a meteorite impact crater and associated impact metamorphic effects and products

surface to bottom hole (Kozlovsky 1984; Emmermann and Lauterjung 1997; Möller and Cast 1997; Stober and Bucher 2007; Bucher and Stober 2010).

To study present-day metamorphism in active hydrothermal areas or in research wells is very attractive because temperature, pressure, and fluid compositions can be determined directly in boreholes. Normally, metamorphic rocks at surface outcrops represent cold and fluid-free final products of rock transformation. The conditions under which these rocks once formed, such as temperature, pressure and fluid composition, must be derived indirectly through the study of mineral assemblages (these techniques are detailed in later chapters).

### 1.2.7 Other Types of Small-Scale Metamorphism

All other forms of small scale metamorphism are rather “exotic” and are briefly mentioned here for the sake of completeness.

**Impact metamorphism** is a type of shock metamorphism (Dietz 1961) in which the shock waves and the observed changes in rocks and minerals result from the hypervelocity impact of a meteorite. The duration is very short, i.e. a few microseconds resulting in melting and vaporization of the impacted rocks. Typical maximum pressures and temperatures at the point of impact are in the order of several 100 GPa or greater and several tens of thousands of degrees. Mineralogical characteristics involve the presence of shocked quartz and the neof ormation of very high pressure coesite and stishovite as well as minute diamonds. Brecciated and partly melted rock produced by the impact is known as suevite (Fig. 1.6). Reviews of impact metamorphism and impactites are provided by Grieve (1987) and Stöffler and Grieve (2007) respectively, and this type of metamorphism is not considered further.

**Lightning metamorphism** can be regarded as a type of highly localised impact metamorphism caused by lightning strikes at very high temperatures that can exceed 2,000°C, resulting, as with meteorite impact metamorphism, in melting,

vaporization, and extreme chemical reduction, e.g. Essene and Fisher (1986). In soils and sands, the products of lightning metamorphism are typically glassy tubes called fulgurites. Examples of lightning metamorphism are summarized in Grapes (2006).

**Combustion metamorphism** is a type of pyrometamorphism caused by spontaneous combustion of organic matter, coal, oil and gas at or near the earth's surface. Temperatures can be extreme, i.e., 1,000–1,500°C, and with increasing temperature burnt rocks, clinkers, and slag or paralava are produced. Although contact aureoles caused by combustion metamorphism are generally only a few meters thick, and more rarely may be up to several tens of meters, burnt rocks may crop out over a large area, especially where combusted organic-bearing strata are gently dipping, e.g. >518,000 km<sup>2</sup> in the case of the great western coal-bearing Cretaceous–Tertiary basins of the United States extending from Texas in the south to Canada in the north. The interested reader is referred to numerous examples of combustion metamorphism described in Grapes (2006).

## References and Further Reading

- Alt JC (1999) Very low-grade hydrothermal metamorphism of basic igneous rocks. In: Frey M, Robinson D (eds) *Low-grade metamorphism*. Blackwell Science, Oxford, pp 169–201
- Bevins RE, Robinson D (1988) Low grade metamorphism of the Welsh Basin Lower Paleozoic succession: an example of diastothermal metamorphism? *J Geol Soc Lond* 145:363–366
- Boles JR, Coombs DS (1975) Mineral reactions in zeolitic Triassic tuff, Hokonui Hills, New Zealand. *Geol Soc Am Bull* 86:163–173
- Bucher K, Stober I (2010) Fluids in the upper continental crust. *Geofluids* 10:241–253
- Buick IS, Cartwright I (1996) Fluid–rock interaction during low-pressure polymetamorphism of the reynolds range group, Central Australia. *J Petrol* 37:1097–1124
- Burnham CW (1979) Magmas and hydrothermal fluids. In: Barnes HL (ed) *Geochemistry of hydrothermal ore deposits*. Wiley, New York, pp 71–136
- Chopin C (1984) Coesite and pure pyrope in high-grade blueschists of the western Alps: a first record and some consequences. *Contrib Miner Petrol* 86:107–118
- Coleman RG, Wang X (eds) (1995) *Ultrahigh pressure metamorphism*. Cambridge University Press, Cambridge, 528 pp
- Coombs DS (1961) Some recent work on the lower grades of metamorphism. *Aust J Sci* 24:203–215
- Dietz RS (1961) Astroblemes. *Sci Am* 205:50–58
- Droop GTR, Al-Filali IY (1996) Interaction of aqueous fluids with calcareous metasediments during high-T, low-P regional metamorphism in the Qadda area, southern Arabian Shield. *J Metamorph Geol* 14:613–634
- Duncan CC, Turcotte DL (1994) On the breakup and coalescence of continents. *Geology* 22:103–106
- Ellis DJ (1980) Osumilite-sapphirine-quartz-granulites from Enderby Land, Antarctica: P-T conditions of metamorphism, implications for garnet-cordierite equilibria and the evolution of the deep crust. *Contrib Miner Petrol* 74:201–210
- Emmermann R, Lauterjung J (1997) The German Continental Deep Drilling Program KTB. *J Geophys Res* 102:18179–18201
- Ernst WG (1999) Metamorphism, partial preservation, and exhumation of ultrahigh-pressure belts. *I Arc* 8:125–153
- Eskola P (1921) On the eclogites of Norway. *Skr Vidensk Selsk Christiania, Mat-nat Kl I* 8:1–118

- Essene EJ, Fisher DC (1986) Lightning strike fusion: extreme reduction and metal-silicate liquid immiscibility. *Science* 234:189–193
- Frey M, Kisch HJ (1987) Scope of subject. In: Frey M (ed) *Low temperature metamorphism*. Blackie, Glasgow, pp 1–8
- Gianelli G, Grassi S (2001) Water-rock interaction in the active geothermal system of Pantelleria, Italy. *Chem Geol* 181:113–130
- Giggenbach WF (1981) Geothermal mineral equilibria. *Geochim Cosmochim Acta* 45:393–410
- Giggenbach WF (1984) Mass transfer in hydrothermal alteration systems – a conceptual approach. *Geochim Cosmochim Acta* 48:2693–2711
- Gillis KM (1995) Controls on hydrothermal alteration in a section of fast-spreading oceanic crust. *Earth Planet Sci Lett* 134:473–489
- Grapes R (2006) *Pyrometamorphism*. Springer, Berlin, Heidelberg, 275 pp
- Grieve RAF (1987) Terrestrial impact structures. *Ann Rev Earth Planet Sci* 15:245–270
- Harley SL, Motoyoshi Y (2000) Al zoning in orthopyroxene in a sapphirine quartzite: evidence for >1120°C UHT metamorphism in the Napier Complex, Antarctica, and implications for the entropy of sapphirine. *Contrib Miner Petrol* 138:293–307
- Hokada T (2001) Feldspar thermometry in ultrahigh-temperature metamorphic rocks: Evidence of crustal metamorphism attaining  $\approx 1100^\circ\text{C}$  in the Archean Napier Complex, East Antarctica. *Am Mineralog* 86:932–938
- Kawachi DE (1975) Pumpellyite-actinolite and contiguous facies metamorphism in the Upper Wakatipu district, southern New Zealand. *NZ J Geol Geophys* 17:169–208
- Kerrick DM (1991) Contact metamorphism., vol 26, *Reviews in mineralogy*. Mineralogical Society of America, Washington DC, 847 pp
- Kisch HJ (1987) Correlation between indicators of very-low-grade metamorphism. In: Frey M (ed) *Low temperature metamorphism*. Blackie, Glasgow, pp 227–300
- Kozlovsky YeA (1984) The world's deepest well. *Sci Am* 251:106–112
- Lamb RC, Smalley PC, Field D (1986) P-T conditions for the Arendal granulites, southern Norway: implications for the roles of P, T and  $\text{CO}_2$  in deep crustal LILE-depletion. *J Metamorph Geol* 4:143–160
- Levi B, Aguirre L, Nystroem JO (1982) Metamorphic gradients in burial metamorphosed vesicular lavas; comparison of basalt and spilite in Cretaceous basic flows from central Chile. *Contrib Mineralog Petrol* 80:49–58
- Lü Z, Zhang L, Du J, Bucher K (2009) Petrology of coesite-bearing eclogite from Habutengsu Valley, western Tianshan, NW China and its tectonometamorphic implication. *J Metamorph Geol* 27:773–787
- Merriman RJ, Frey M (1999) Patterns of very low-grade metamorphism in metapelitic rocks. In: Frey M, Robinson D (eds) *Low-grade metamorphism*. Blackwell Science, Oxford, pp 61–107
- Miyashiro A (1971) Pressure and temperature conditions and tectonic significance of regional and ocean floor metamorphism. *Tectonophysics* 13:141–159
- Miyashiro A (1973) *Metamorphism and metamorphic belts*. Allen & Unwin, London, 492 pp
- Möller P et al (1997) Paleo- and recent fluids in the upper continental crust – results from the German Continental deep drilling Program (KTB). *J Geophys Res* 102:18245–18256
- Murphy JB, Nance RD (1992) Mountain belts and the supercontinent cycle. *Sci Am* 266:84–91
- Newton RC (1987) Petrologic aspects of Precambrian granulite facies terrains bearing on their origins. In: Kröner A (ed) *Proterozoic lithospheric evolution*, vol 17, *Geodynamics series*. American Geophysical Union, Washington, DC, pp 11–26
- Okay AI (1993) Petrology of a diamond and coesite-bearing metamorphic terrain: Dabie Shan, China. *Eur J Miner* 5:659–675
- Ramsay JG, Allison I (1979) Structural analysis of shear zones in an alpinised Hercynian granite (Maggia Nappen, Pennine zone, central Alps). *Schweiz Miner Petrogr Mitt* 59:251–279
- Reinecke T (1991) Very-high-pressure metamorphism and uplift of coesite-bearing metasediments from the Zermatt-Saas zone, Western Alps. *Eur J Miner* 3:7–17

- Reyes AG, Grapes R, Clemente VC (2003) Fluid-rock interaction at the magmatic-hydrothermal interface of the Mount Cagua geothermal field, Philippines. *Soc Econ Geol Spec Publ* 10:197–222
- Robinson D (1987) Transition from diagenesis to metamorphism in extensional and collision settings. *Geology* 15:866–869
- Robinson D, Bevins RE (1999) Patterns of regional low-grade metamorphism in metabasites. In: Robinson D, Frey M (eds) *Low-grade metamorphism*. Blackwell Science, Oxford, pp 143–168
- Robinson D, Merriman RJ (1999) Low-temperature metamorphism: an overview. In: Frey M, Robinson D (eds) *Low-grade metamorphism*. Blackwell Science, Oxford, pp 1–9
- Ruppert LF, Hower JC, Ryder RT, Trippi MH, Grady WC, Levine JR (2010) Geologic controls on observed thermal maturation patterns in Pennsylvanian coal-bearing rocks in the Appalachian basin. *Int J Coal Geol* 81:169–181
- Sajeev K, Osanai Y (2004) Ultrahigh-temperature metamorphism (1150°C, 12 kbar) and multi-stage evolution of Mg-, Al-rich granulites from the Central Highland Complex, Sri Lanka. *J Petrol* 45:1821–1844
- Schertl HP, Schreyer W, Chopin C (1991) The pyrope-coesite rocks and their country rocks at Parigi, Dora Maira Massif, Western Alps: detailed petrography, mineral chemistry and PT-path. *Contrib Miner Petrol* 108:1–21
- Schreyer W (1995) Ultradeep metamorphic rocks: the retrospective viewpoint. *J Geophys Res* 100:8353–8366
- Seki Y (1973) Temperature and pressure scale of low-grade metamorphism. *J Geol Soc Jpn* 79:735–743
- Shatsky VS, Sobolev NV, Vavilov MA (1995) Diamond-bearing metamorphic rocks of the Kokchetav massif (Northern Kazakhstan). In: Coleman RG, Wang X (eds) *Ultrahigh pressure metamorphism*. Cambridge University Press, Cambridge, pp 427–455
- Smith RE (1969) Zones of progressive regional burial metamorphism in part of the Tasman geosyncline, eastern Australia. *J Petrol* 10:144–163
- Smith DC, Lappin MA (1989) Coesite in the Straumen kyanite-eclogite pod, Norway. *Terra Nova* 1:47–56
- Song SG, Niu YL, Zhang LF, Bucher K (2009) The Luliangshan garnet peridotite massif of the North Qaidam UHPM belt, NW China – a review of its origin and metamorphic evolution. *J Metamorph Geol* 27:621–638
- Stem CR, Wyllie PJ (1981) Phase relationships of I-type granite with H<sub>2</sub>O to 35 kilobars: the Dinkey Lakes biotite-granite from the Sierra Nevada batholith. *J Geophys Res* 86(B11):10412–10422
- Stober I, Bucher K (2007) Hydraulic properties of the crystalline basement. *Hydrogeol J* 15:213–224
- Stöckler D, Greive RAF (2007) Impactites. In: Fettes D, Desmonds J (eds) *Metamorphic rocks – a classification and glossary of terms; recommendations of the International Union of Geological Sciences Subcommittee on the systematics of metamorphic rocks*. Cambridge University Press, New York, pp 82–92
- Teichmüller M (1987) Organic material and very low-grade metamorphism. In: Frey M (ed) *Low temperature metamorphism*. Blackie, Glasgow, pp 114–161
- Vernon RH (1976) *Metamorphic processes*. Allen & Unwin, London, 247 pp
- Wain A, Waters D, Jephcoat A, Olijnyk H (2000) The high-pressure to ultrahigh-pressure eclogite transition in the Western Gneiss Region, Norway. *Eur J Miner* 12:667–688
- Wilson JT (1966) Did the Atlantic close and then re-open? *Nature* 211:676–681
- Wise DU, Dunn DE, Engelder JT, Geiser PA, Hatcher RD, Kish SA, Odon AL, Schamel S (1984) Fault-related rocks: suggestions for terminology. *Geology* 12:391–394
- Yang J, Godard G, Kienast JR, Lu Y, Sun J (1993) Ultrahigh-pressure (60 kbar) magnesite-bearing garnet peridotites from northeastern Jiangsu, China. *J Geol* 101:541–554
- Zhang R-Y, Liou JG (1994) Coesite-bearing eclogite in Henan Province, central China: detailed petrography, glaucophane stability and PT-path. *Eur J Miner* 6:217–233





## Chapter 2

# Metamorphic Rocks

This chapter deals with the descriptive characterization of metamorphic rocks. Metamorphic rocks are derived from other rocks of igneous, sedimentary or metamorphic origin. The chemical composition of this primary material (=protolith) determines the chemical and mineralogical composition of metamorphic rocks to a large degree. The compositional variation found in the primary material of metamorphic rocks is reviewed in Sect. 2.1.

The structure of metamorphic rocks is often inherited from the precursor material. In low-grade metasedimentary rocks, for example, the sedimentary bedding and typical structures of sedimentary rocks such as cross-bedding and graded bedding may be preserved. Ophitic structure, characteristic of basaltic lava, may be preserved in mafic metamorphic rocks. Very coarse-grained structures of igneous origin can occasionally be found even in high-grade metamorphic rocks. Most metamorphic rocks, however, exhibit structures that are of distinct metamorphic origin. The structures typically result from a combination of deformation and recrystallization. Deformation normally accompanies large-scale tectonic processes causing metamorphism. Some descriptive terms of metamorphic structures are defined in Sect. 2.2. Classification principles and nomenclature of metamorphic rocks are explained in Sect. 2.3.

Large scale tectono-thermal processes move rocks along unique paths in pressure–temperature–time (P–T–t) space. Rocks may undergo continuous recrystallization and new minerals may replace old ones in a complex succession. Earlier-formed minerals and groups of minerals often experience metastable survival because of unfavorable reaction kinetics. This happens particularly if an aqueous fluid phase is absent. Metamorphism may proceed episodically. The study of metamorphic rocks aims at the correct identification of the group of minerals that may have coexisted in chemical equilibrium at one stage during the evolutionary history of the metamorphic rock. This group of minerals is the **mineral assemblage**. The total succession of mineral assemblages preserved in a metastable state in the structure of a metamorphic rock is designated **mineral paragenesis**. Some aspects regarding the mineral assemblage and the mineral paragenesis are discussed in Sect. 2.4.

Discussion and analysis of phase relationships in metamorphic rocks is greatly facilitated by the use of composition phase diagrams. Their construction is explained

in the last section of this chapter (Sect. 2.5) on graphical representation of mineral assemblages. However, the quantitative computation of equilibrium composition phase diagrams is not discussed in this book.

## 2.1 Primary Material of Metamorphic Rocks

All metamorphic rock-forming processes make rocks from other rocks. The precursor rock or **protolith** determines many attributes of the new metamorphic rock.

Metamorphism results from the addition (or removal) of heat and material to discrete volumes of the crust or mantle by tectonic or igneous processes. Metamorphism, therefore, may affect all possible types of rock present in the Earth's crust or mantle. Protoliths of metamorphic rocks comprises rocks of all possible chemical compositions and include the entire range of sedimentary, igneous and metamorphic rocks.

Metamorphic processes tend to change the original composition of the protolith. Addition of heat to rocks typically results in the release of volatiles ( $H_2O$ ,  $CO_2$ , etc.) that are stored in hydrous minerals (e.g. clay, micas, amphiboles), carbonates and other minerals containing volatile components. Therefore, many metamorphic rocks are typically depleted in volatiles relative to their protoliths. Metamorphism that releases only volatiles from the protolith is, somewhat illogically, termed isochemical. On a volatile-free basis, the chemical composition of protolith and product rock is identical in isochemical metamorphism. In truly isochemical metamorphism, protolith and product rocks are of identical composition including the volatile content. Recrystallization of sedimentary calcite to coarse grained calcite marble is an example of isochemical metamorphism in a strict sense. It affects the structure of the rock, no new minerals are formed.

Many, if not most, metamorphic processes also change the cation composition of the protolith. This type of metamorphism is termed allochemical metamorphism or metasomatism. The aqueous fluid released by dehydration reactions during metamorphism generally contains dissolved solutes. These are then carried away with the fluid and lost by the rock system. It has been found, for example, that many granulite facies gneisses are systematically depleted in alkalis (Na and K) relative to their amphibolite facies precursor rocks. This can be explained by alkali loss during dehydration. Silica saturation is a general feature of nearly all metamorphic fluids. Pervasive or channelled regional scale flow of silica-saturated dehydration fluids may strongly alter silica-deficient rocks (ultramafic rocks, dolomite marbles) that come in contact with these fluids. Unique metamorphic rock compositions may result from metasomatism on a local or regional scale. Efficient diffusion and infiltration metasomatism requires the presence of a fluid phase. Metasomatism is a process of fluid-rock interaction combined with transfer of material between the systems at elevated temperature and pressure. Fluid-rock interaction processes are dominant in chemical weathering, in sedimentary, diagenetic, groundwater, hydrothermal and other near surface environments, but they play an important role also in

the metamorphic domain. In fact, isochemical metamorphism of rocks may be viewed as interaction of rocks with an internally derived fluid that makes dissolution of unstable and precipitation of more stable mineral assemblages possible.

Interaction of rocks with externally derived fluids is referred to as allochemical metamorphism. The volatile composition of the fluid may not be in equilibrium with the mineral assemblage of the rock and, consequently, the rock may be altered. Some examples: flushing of rocks with pure H<sub>2</sub>O at high-P–T conditions may initiate partial melting, it may form mica and amphibole in pyroxene-bearing rocks, it may induce wollastonite or periclase formation in marbles. CO<sub>2</sub> metasomatism is particularly common in very high-grade rocks. Metasomatism can create rocks of extreme composition which, in turn, may serve as a protolith in subsequent metamorphic cycles. Metasomatic rocks of unusual composition are widespread in regional metamorphic terrains and contact aureoles. However, the total volume of such types of rocks is negligible. Although interesting petrologically, these exotic rocks will not be discussed in Part II where we present a systematic treatment of prograde metamorphism of the most important types of bulk rock compositions.

### 2.1.1 Chemical Composition of Protoliths of Metamorphic Rocks

The average composition of crust and mantle is listed in Table 2.1. The mantle constitutes the largest volume of rocks on planet Earth. From geophysical and petrophysical evidence and from mantle fragments exposed at the surface, we know that the mantle consists predominantly of ultramafic rocks of the peridotite family. The bulk of the mantle is in a solid state and experiences continuous recrystallization as a result of large-scale convective flow in the sub-lithospheric mantle and tectonic processes in the lithospheric mantle. Therefore, nearly all mantle rocks represent metamorphic rocks. The composition of the mantle (Table 2.1) is representative for the most prominent type of metamorphic rock of this planet. However, mantle rocks can only be transported through the lid of crust to the surface of the Earth by active tectonic or igneous processes. Although outcrops of ultramafic

**Table 2.1** Composition of the Earth's crust and mantle (After Carmichael 1989)

	Peridotite mantle	Continental crust	Oceanic crust	Basalt	Tonalite
SiO <sub>2</sub>	45.3	60.2	48.6	47.1	61.52
TiO <sub>2</sub>	0.2	0.7	1.4	2.3	0.73
Al <sub>2</sub> O <sub>3</sub>	3.6	15.2	16.5	14.2	16.48
FeO	7.3	6.3	8.5	11.0	5.6
MgO	41.3	3.1	6.8	12.7	2.8
CaO	1.9	5.5	12.3	9.9	5.42
Na <sub>2</sub> O	0.2	3.0	2.6	2.2	3.63
K <sub>2</sub> O	0.1	2.8	0.4	0.4	2.1
H <sub>2</sub> O	<0.1	1.4	1.1	<1.0	1.2
CO <sub>2</sub>	<0.1	1.4	1.4	<1.0	0.1

rocks are common and widespread, particularly in orogenic belts, the total volume of ultramafic rocks exposed on continents is small.

Crustal rocks may be divided into rocks from oceanic and continental environments. Characteristic compositions of continental (tonalite) and oceanic crust (basalt) are listed in Table 2.1. It is evident that the average composition of oceanic crust is well represented by an average basalt composition, and the average composition of continental crust can be described by an average tonalite composition. The composition of the continental crust is more heterogeneous than the oceanic crust which is ~99% basaltic. Table 2.2 lists abundances of types of rocks that make up typical crust and are the predominant protoliths of metamorphic rocks. Igneous rocks of mafic composition (basalts, gabbros of Mid Ocean Ridge Basalt [MORB] affinity) form the oceanic crust which covers much larger areas than continental crust, and constitute an important chemical group of metamorphic rocks (greenschist, amphibolite, granulite, eclogite).

Granite and related rocks such as granodiorite and quartz–diorite (typical granite and tonalite compositions given in Table 2.3) dominate the continental crust. They make up the family of metamorphic rocks termed meta-granitoids (= quartzofeldspathic rocks) and represent 33% of all igneous rocks of the Earth's crust (Table 2.2).

**Table 2.2** Abundance of rocks (vol%) in the crust (After Carmichael 1989)

Igneous rocks	64.7		
Sedimentary rocks	7.9		
Metamorphic rocks	27.4		
<i>Igneous rocks (64.7)</i>		<i>Sedimentary rocks (7.9)</i>	
Granites	16	Shales	82
Granodiorites/diorites	17	Sandstones, arkoses	12
Syenites	0.6	Limestones	6
Basalts/gabbros	66		
Peridotites/dunites	0.3		

**Table 2.3** Chemical composition of sedimentary and igneous rocks (After Carmichael 1989)

	Sandstones, graywackes	Shales (platforms)	Pelites, pelagic clays	Carbonates (platforms)	Tonalite	Granite	Basalt MORB
SiO <sub>2</sub>	70.0	50.7	54.9	8.2	61.52	70.11	49.2
TiO <sub>2</sub>	0.58	0.78	0.78	–	0.73	0.42	2.03
Al <sub>2</sub> O <sub>3</sub>	8.2	15.1	16.6	2.2	16.48	14.11	16.09
Fe <sub>2</sub> O <sub>3</sub>	0.5	4.4	7.7	1.0	–	1.14	2.72
FeO	1.5	2.1	2.0	0.68	5.6	2.62	7.77
MgO	0.9	3.3	3.4	7.7	2.8	0.24	6.44
CaO	4.3	7.2	0.72	40.5	5.42	1.66	10.46
Na <sub>2</sub> O	0.58	0.8	1.3	–	3.63	3.03	3.01
K <sub>2</sub> O	2.1	3.5	2.7	–	2.1	6.02	0.14
H <sub>2</sub> O	3.0	5.0	9.2	–	1.2	0.23	0.70
CO <sub>2</sub>	3.9	6.1	–	35.5	0.1		
C	0.26	0.67	–	0.23			

On a global basis, sedimentary rocks are dominated by shales and clays of pelagic and platform (shelf) environments (82% of all sediments, Table 2.2). Compositions of typical shales from continental and oceanic settings are listed in Table 2.3. Pelagic clays represent the typical sediments of the deep oceans and these extremely fine-grained clay-rich sediments are designated as pelites. They form the most important type of metamorphic rock of sedimentary origin (metapelites).

Shales deposited on continental shelves typically contain carbonate minerals as reflected in the chemical composition of the average analysis given in Table 2.3. Such carbonate-rich shales are usually referred to as marls and their metamorphic equivalents, e.g. calcareous mica-schists are important types of metasediments in orogenic belts.

With reference to Table 2.2, sandstones (e.g. graywacke, arkose) and carbonate rocks (limestone) are the remaining important groups of rocks. The former dominate the sedimentary rocks in continental basins and subduction related trenches, whereas carbonate sequences (including marls) are characteristic of continental shelf (platform) depositional environments. Characteristic compositions of graywacke sandstone and platform carbonate are listed in Table 2.3.

If metamorphic rocks become a protolith in a new cycle of metamorphism, their composition will comprise those of the most common sedimentary and igneous rocks as given in Table 2.3. Thus, all metamorphic rocks can be grouped into seven classes of characteristic bulk rock composition.

### ***2.1.2 Chemical Composition Classes of Metamorphic Rocks and Their Protoliths***

The seven classes are arranged according to increasing chemical complexity.

1. *Ultramafic rocks*. Usually mantle-derived, very Mg-rich family of rocks (typical peridotite composition in Table 2.1). Metamorphism of ultramafic rocks produces hydrous and non-hydrous Mg-silicate minerals and is discussed in Chap. 5.
2. *Carbonate rocks*. These are chemical sedimentary rocks modally dominated by carbonate minerals (calcite, dolomite) (Table 2.3). Their metamorphosed equivalents, marble, calc-silicate rocks or metacarbonate, are dominated by Ca–Mg and Ca-silicate minerals in addition to calcite and are described in Chap. 6.
3. *Pelites (shales)*. Pelitic rocks such as shale are the most common type of sedimentary rock. Pelagic clays (true pelites) are poor in calcium compared with shales from continental platforms (Table 2.3). Pelites constitute a separate composition group and their metamorphic equivalents are termed metapelites (metapelitic slate, phyllite, schist and gneiss) characterized by the formation of K–Al and Al-rich silicate minerals as detailed in Chap. 7.

4. *Marls*. Marls are shales containing a significant proportion of carbonate minerals (usually calcite) (Table 2.3), and metamorphic equivalents are dominated by Ca–Al silicate minerals as discussed in Chap. 8.
5. *Mafic rocks*. Metamorphic mafic rocks (e.g. greenstone, mafic schist and gneiss, greenschist, amphibolite) are derived from mafic igneous rocks, mainly basalt (but also andesite) and, of lesser importance, gabbro (Tables 2.1 and 2.3). Based on total volume, basalts are the most important group of volcanic rocks, and metabasalts or metabasites are common in many metamorphic terrains. Metamorphic assemblages in mafic rocks are dominated by Ca–Mg–Fe–Al silicate minerals that define the intensity of metamorphism in the metamorphic facies concept (Chap. 4). Prograde metamorphism of mafic rocks is described in Chap. 9.
6. *Quartzo-feldspathic rocks*. Metamorphic rocks of sedimentary (arkose, sandstone, siltstone, greywacke) or igneous origin (granite, granodiorite, tonalite, monzonite, syenite, etc.) which are modally dominated by quartz and feldspar (Table 2.3) are described in Chap. 10. Gneisses derived from igneous rocks of the granite family may be designated as metagranitoids.
7. *Other bulk compositions*. All remaining compositions of protoliths of metamorphic rocks are of minor and subordinate importance. They include manganese sediments and chert, volcanogenic sediments, ironstones, laterites, evaporites and alkaline igneous rocks, to name only a few.

## 2.2 The Structure of Metamorphic Rocks

Most metamorphic rocks originate from large-scale tectonic processes (deformation) and associated changes in pressure and temperature. Metamorphism involves chemical reactions in rocks that replace minerals and mineral assemblages in the original material by new minerals or groups of minerals. The orientation and geometric arrangement of new inequant metamorphic minerals is largely controlled by the anisotropic pressure field associated with the tectonic processes.

Therefore, metamorphic rocks display not only a characteristic metamorphic mineral content they are also characterized by distinctive **metamorphic structures**. The structure of metamorphic rocks is used for the classification of the rocks. The structures of metamorphic rocks inherit essential information about the type of tectonic setting in which they formed and about the nature of metamorphism. Structural and chemical (petrological) aspects of metamorphic rocks are of equal importance in the study of metamorphism and the characterization of metamorphic rocks requires a description of their structure. Some important and typical structures of metamorphic rocks are defined by descriptive terms. The definition of terms given in this chapter partly follows recommendations of the “International Union Commission of Geological Sciences Subcommission on the Systematics of Metamorphic Rocks” (Fettes and Desmonds 2007).

*Structure.* The arrangement of parts of a rock mass irrespective of scale, including geometric interrelationships between the parts, their shapes and internal features. The terms micro-, meso- and mega- can be used as a prefix to describe the scale of the feature. Micro- is used for a thin-section scale, meso- for hand-specimen and outcrop scale, mega- for larger scales.

*Fabric.* The kind and degree of preferred orientation of parts of a rock mass. The term is used to describe the crystallographic and/or shape orientation of mineral grains or groups of grains, but can also be used to describe meso- and mega-scale features.

*Layer.* One of a sequence of near parallel tabular-shaped rock bodies. The sequence is referred to as being layered (equivalent expressions: bands, banded, laminated).

*Foliation.* Any repetitively occurring or penetrative planar structural feature in a rock body. Some examples:

- Regular layering on a cm or smaller scale
- Preferred planar orientation of inequant mineral grains
- Preferred planar orientation of lenticular (elongate) grain aggregates

More than one kind of foliation with more than one orientation may be present in a rock. Foliations may become curved (folded) or distorted. The surfaces to which they are parallel are designated **s-surfaces** (Fig. 2.1).

*Schistosity.* A type of foliation produced by deformation and/or recrystallization resulting in a preferred orientation of inequant mineral grains. It is common practice in phyllosilicate-rich rocks to use the term slaty cleavage instead of schistosity when individual grains are too small to be seen by the unaided eye (Fig. 2.1).

*Cleavage.* A type of foliation consisting of a regular set of parallel or sub-parallel closely spaced surfaces produced by deformation along which a rock body will usually preferentially split. More than one cleavage may be present in a rock.

*Slaty cleavage.* Perfectly developed foliation independent of bedding resulting from the parallel arrangement of very fine-grained phyllosilicates (Fig. 2.1).

*Fracture cleavage.* A type of cleavage defined by a regular set of closely spaced fractures.

*Crenulation cleavage.* A type of cleavage related to microfolding (crenulation) of a pre-existing foliation. It is commonly associated with varying degrees of metamorphic segregation.

*Gneissose structure.* A type of foliation on hand-specimen scale, produced by deformation and recrystallization, defined by:

- Irregular or poorly defined layering
- Augen and/or lenticular aggregates of mineral grains (augen structure, flaser structure)
- Inequant mineral grains which are present, however, only in small amounts or which display only a weak preferred orientation, thus defining only a poorly developed schistosity

*Lineation.* Any repetitively occurring or penetrative visible linear feature in a rock body (Fig. 2.1). This may be defined by, for example:



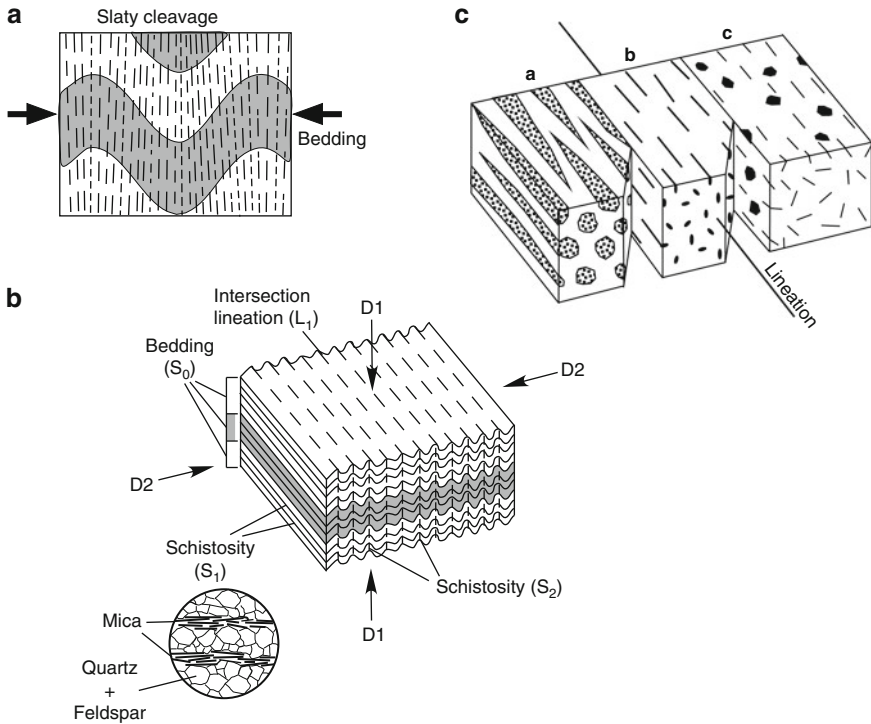


**Fig. 2.1** Diagrams to illustrate some structure features in metamorphic rocks. (a) Folded sedimentary rocks and slaty cleavage; (b) Schist with alternating mica and quartz–feldspar foliation displaying two schistosity planes ( $S_1$  and  $S_2$ ) related to deformation events  $D_1$  and  $D_2$ , respectively; The first schistosity,  $S_1$ , is parallel to sedimentary bedding planes ( $S_0$ ); intersection of  $S_1$  and  $S_2$  planes produce an intersection lineation ( $L_1$ ); (c) Examples of metamorphic lineation, a = alignment of mineral aggregates; b = alignment of elongate mineral grains (e.g. hornblende); c = alignment of tabular mineral grains (e.g. mica)

- Alignment of the long axes of elongate mineral grains (= mineral lineation)
- Alignment of elongate mineral aggregates
- Alignment of elongate objects, bodies (e.g. strongly deformed pebbles in a meta-conglomerate)
- Common axis of intersection of tabular mineral grains (or bodies)
- Intersection of two foliations (intersection lineation)
- Parallelism of hinge lines of small scale folds
- Slickenside striations
- Striations due to flexural slip

More than one kind of lineation, with more than one orientation, may be present in a rock. Lineations may become curved or distorted. The lines to which they are parallel are called **L-lines**. Reference to a lineation is incomplete without indication of the type concerned.

*Joint.* A single fracture in a rock with or without a small amount (<1 cm) of either dilatational or shear displacement (joints may be sealed by mineral deposits during or after their formation).

*Cataclasis.* Rock deformation accomplished by some combination of fracturing, rotation, and frictional sliding producing mineral grain and/or rock fragments of various sizes and often of angular shape.

*Metamorphic differentiation.* Redistribution of mineral grains and/or chemical components in a rock as a result of metamorphic processes. Metamorphic process by which mineral grains or chemical components are redistributed in such a way to increase the modal or chemical anisotropy of a rock (or portion of a rock) without changing the overall chemical composition.

*Textural zones.* Regional geological mapping of metamorphic terranes is typically based on criteria such as lithologic associations, metamorphic zones and structural zones. Field and petrographic subdivision of metamorphic rocks has also been made on the basis of textural zones that subdivide rocks in terms of the degree of recrystallization, e.g. foliation, mineral segregation, increasing grain size, with increasing metamorphism. For example, four textural zones have been established for quartzofeldspathic rocks (metagreywacke) that comprise the Otago Schist, New Zealand (Fig. 2.2) in which the boundaries of the 10–50 km wide zones are gradational and are termed **isotects** (Bishop 1972; Turnbull et al. 2001). The macroscopic/microscopic criteria used to distinguish textural zones are essentially a mapping tool and cannot be used as a mineralogical or isochemical  $P$ – $T$  indicator.

## 2.3 Classification and Names of Metamorphic Rocks

The names of metamorphic rocks are usually straightforward and self-explanatory. The number of special terms and cryptic expressions is relatively small. Nevertheless in order to be able to communicate with other geologists working with metamorphic rocks it is necessary to define commonly used names and expressions and to briefly review currently used classification principles for metamorphic rocks.

There is not one sole classification principle used for the description of metamorphic rocks, which consequently means that all metamorphic rocks may have a series of perfectly correct and accepted names. However, **modal mineral composition and mesoscopic structure are the main criteria for naming metamorphic rocks**. In addition, the **composition and the nature of the protolith** (original material) is an important classification criterion. Finally, some well-established **special names** are used also in metamorphic geology.

The names of metamorphic rocks consist of a **root** name and a series of **prefixes**. The root of the name may be a special name (e.g. amphibolite) or a name describing

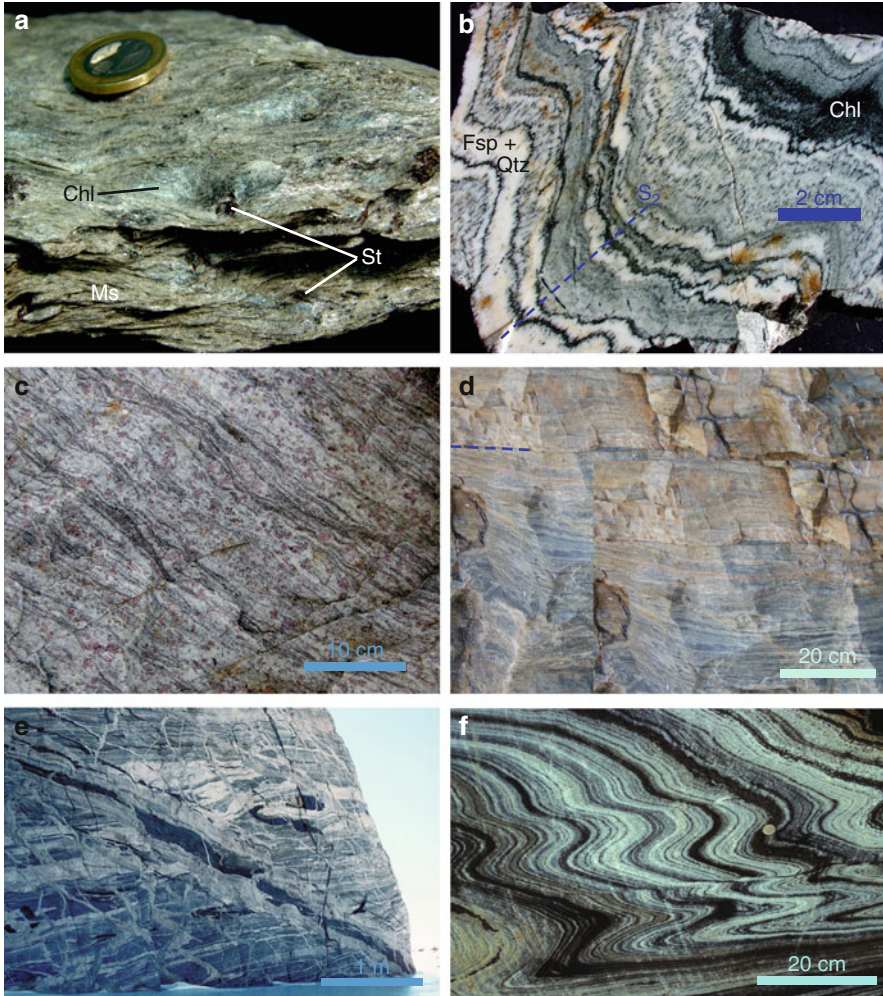


**Fig. 2.2** Photos illustrating metamorphic rock fabrics. (a) St–Chl micaschist and schistosity (Saltdalen, Norway); (b) Banded and folded lower greenschist facies granite–gneiss; deformation and low grade metamorphism produced a banded orthogneiss from a Variscan granite, metamorphic segregation associated with deformation resulted in alternating white bands of Fsp + Qtz and green Chl bands, note Chl sheets oriented parallel to axial plains of folds (Arolla Gneiss, Matterhorn, Alps); (c) Gneiss and gneissosity, high-grade Spl–Sil–Bt–Grt gneiss (Jøkelfjorden, Norway); (d) Mylonite at the basal thrust of the Helvetic nappe complex (Glarus thrust, Piz Sardona, Swiss Alps); (e) Amphibolite facies banded orthogneiss with granite veins, *dark band in the upper part of picture* is a amphibolitized mafic dyke (Thor Range, Antarctica); (f) Upper amphibolite facies banded and folded marble, note extreme boudinage of bands of silicate rock (Engabreen, Svartisen, Norway)

the structure of the rock (e.g. gneiss). The root name always embraces some modally dominant metamorphic minerals (amphibolite is mainly composed of amphibole + plagioclase; gneiss is mainly composed of feldspar ± quartz).

The rock may be further characterized by adding prefixes to the root name. The prefixes may specify some typical structural features of the rock or may give some additional mineral information (e.g. banded epidote-bearing garnet–amphibolite, folded leucocratic garnet–hornblende gneiss). The prefixes are optional and the name may consist of the root only.

### 2.3.1 Rock Names Referring to the Structure

The structure of a rock concerns the characteristic distribution of its constituents (minerals, aggregates, layers etc.). It results from the geometrical arrangement of minerals, mineral aggregates with non-equant crystal shapes and other structural features, as discussed above. This structure is largely controlled by mechanical deformation and chemical segregation processes which are almost always associated with metamorphism. Expressions that mainly characterize the structure of metamorphic rocks are often used as root names. Metamorphic rocks are named primarily by using **descriptive structural terms**. The most important of these terms are:

*Gneiss*. A metamorphic rock displaying a gneissose structure (Fig. 2.2). The term gneiss may also be applied to rocks displaying a dominant linear fabric rather than a gneissose structure, in which case the term lineated gneiss may be used. This term gneiss is almost exclusively used for rocks containing abundant feldspar ( $\pm$ quartz), but may also be used in exceptional cases for other compositions (e.g. feldspar-free cordierite–anthophyllite gneiss). Examples: garnet–biotite gneiss, granitic gneiss, ortho-gneiss, migmatitic gneiss, banded gneiss, garnet–hornblende gneiss, mafic gneiss.

*Schist*. A metamorphic rock displaying on the hand-specimen scale a pervasive, well-developed schistosity defined by the preferred orientation of abundant inequant mineral grains (Fig. 2.2). For phyllosilicate-rich rocks the term schist is usually reserved for medium- to coarse-grained varieties, whilst finer-grained rocks are termed slates or phyllites. The term schist may also be used for rocks displaying a strong linear fabric rather than a schistose structure. Examples: epidote-bearing actinolite–chlorite schist (=greenschist), garnet–biotite schist, micaschist, calcareous micaschist, antigorite schist (=serpentinite), talc–kyanite schist (=whiteschist).

*Phyllite*. A fine-grained rock of low metamorphic grade displaying a perfect penetrative schistosity resulting from parallel arrangement of phyllosilicates. Foliation surfaces commonly show a lustrous sheen.

*Slate*. A very fine-grained rock of low metamorphic grade displaying slaty cleavage (Fig. 2.1).

*Granofels*. A metamorphic rock lacking schistosity, gneissose structure, and mineral lineations.

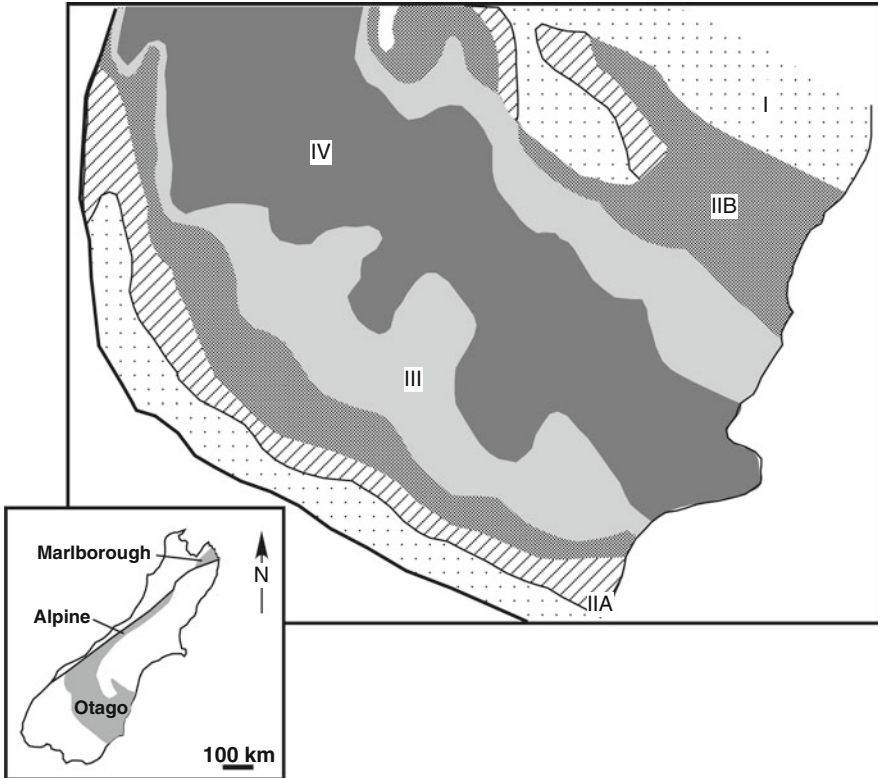


**Fig. 2.3** Map showing distribution of textural zones (TZ's) delineating transition from non-schistose to schistose metagreywacke rocks, Otago, South Island of New Zealand (inset map shows distribution of Otago, Alpine and Marlborough schist) (Redrawn from Turnbull et al. 2001, Fig. 1D). TZI. Non foliated or spaced fracture cleavage. TZIIA. Weak-moderate, anastomosing, penetrative foliation that is stronger in fine-grained rocks. Sedimentary bedding dominant over cleavage. Rocks break into wedge-shaped blocks. Lowest grade semischist (sandstone = phyllite; mudstone = slate). TZIIB. Strong, penetrative foliation. Cleavage dominant over bedding which is transposed. No foliation parallel segregation of quartz and mica. Rocks break into parallel-sided slabs. Highest grade semischist (sandstone = phyllite; mudstone = slate). TZIII. Strong, penetrative foliation undulating on millimeter-scale. Distributed foliation-parallel quartz segregation lenses <1 mm thick. Psammitic-pelitic contacts sharp on millimeter scale. Lowest grade schist. TZIV. Strong, penetrative foliation undulating on millimeter- to centimeter-scale. Segregation banding (<1 mm thick) of quartz and mica. Psammitic-pelitic contacts blurred on millimeter-scale but distinguishable on centimeter-scale. Higher grade schist

### 2.3.2 Names for High-Strain Rocks

Metamorphism may locally be associated with an extremely high degree of rock deformation. Localized high strain in metamorphic terrains produces rocks with distinctive structures. Some widely used special names for high-strain rocks are defined below:

*Mylonite*. A rock produced by mechanical reduction of grain size as a result of ductile, non-cataclastic deformation in localized zones (shear zones, fault zones), resulting in the development of a penetrative fine-scale foliation, and often with an associated mineral and stretching lineation (Fig. 2.2).

*Ultramylonite*. A mylonite in which most of the megacrysts or lithic fragments have been eliminated (>90% fine-grained matrix).

*Augen mylonite (blastomylonite)*. A mylonite containing distinctive large crystals or lithic fragments around which the fine-grained banding is wrapped.

*Cataclasite*. A rock which underwent cataclasis.

*Fault breccia*. Cataclasite with breccia-like structure formed in a fault zone.

*Pseudotachylite*. Ultra-fine-grained vitreous-looking material, flinty in appearance, occurring as thin veins, injection veins, or as a matrix to pseudo-conglomerates or -breccias, which seals dilatancy in host rocks displaying various degrees of fracturing.

### 2.3.3 Special Terms

Some commonly used and approved special terms (names, suffixes, prefixes) include:

*Mafic minerals*. Collective expression for ferro-magnesian minerals.

*Felsic minerals*. Collective term for quartz, feldspar, feldspathoids and scapolite.

*Mafic rock*. Rock mainly consisting of mafic minerals (mainly  $\equiv$  modally >50%).

*Felsic rock*. rock mainly consisting of felsic minerals.

*Meta-*. If a sedimentary or igneous origin of a metamorphic rock can be identified, the original igneous or sedimentary rock term preceded by “meta” may be used (e.g. metagabbro, metapelite, metasediment, metasupracrustal). Also used to generally indicate that the rock in question is metamorphic (e.g. metabasite).

*Ortho- and para-*. A prefix indicating, when placed in front of a metamorphic rock name, that the rock is derived from an igneous (ortho) or sedimentary (para) rock respectively (e.g. orthogneiss, paragneiss).

*Acid, intermediate, basic, ultrabasic*. Terms defining the SiO<sub>2</sub> content of igneous and metamorphic rocks (respectively, >63, 63–52, 52–45, <45 wt% SiO<sub>2</sub>).

*Greenschist and greenstone*. Schistose (greenschist) or non-schistose (greenstone) metamorphic rock whose green color is due to the presence of minerals such as chlorite, actinolite, and epidote (greenschist e.g. epidote-bearing actinolite-chlorite schist; greenstone, e.g. chlorite-epidote granofels).

*Blueschist*. Schistose rock whose bluish color is due to the presence of sodic amphibole (e.g. glaucophane schist). However, the “blue” color of a blueschist will not easily be recognized by a non-geologist (i.e. it is not really blue, although very rare outcrops of really blue glaucophanites do exist). Blueschists are schistose rocks containing amphibole with significant amounts of the M(4) cation position in the amphibole structure occupied by Na (glaucophane, crossite).

- Amphibolite*. Mafic rock predominantly composed of hornblende (>40%) and plagioclase.
- Granulite*. Metamorphic rock in or from a granulite facies terrain exhibiting characteristic granulite facies mineral assemblages. Anhydrous mafic minerals are modally more abundant than hydrous mafic minerals. Muscovite is absent in such rocks. Characteristic is the occurrence of metamorphic orthopyroxene in both mafic and felsic rocks. The term is not used for marbles and ultramafic rocks in granulite facies terranes.
- Charnockite, mangerite, jotunite, enderbyite*. Terms applied to orthopyroxene-bearing rocks with igneous texture and granitic (charnockite), monzonitic (mangerite, jotunite), and tonalitic (enderbyite) composition, irrespective of whether the rock is igneous or metamorphic.
- Eclogite*. A plagioclase-free mafic rock mainly composed of omphacite and garnet, both of which are modally abundant.
- Eclogitic rock*. Rocks of any composition containing diagnostic mineral assemblages of the eclogite facies (e.g. jadeite–kyanite–talc granulites).
- Marble*. A metamorphic rock mainly composed of calcite and/or dolomite (e.g. dolomitic marble).
- Calc-silicate rock*. Metamorphic rock which, besides 0–50% carbonates, is mainly composed of Ca-silicates such as epidote, zoisite, vesuvianite, diopside–hedenbergite, Ca-garnet (grossular–andradite), wollastonite, anorthite, scapolite, Ca-amphibole.
- Skarn*. A metasomatic Ca–Fe–Mg–(Mn)-silicate rock often with sequences of compositional zones and bands, formed by the interaction of a carbonate and a silicate system in mutual contact. Typical skarn minerals include, wollastonite, diopside, grossular, zoisite, anorthite, scapolite, margarite (Ca skarns); hedenbergite, andradite, ilvaite (Ca–Fe skarns); forsterite, humites, spinel, phlogopite, clintonite, fassaite (Mg skarns); rhodonite, tephroite, piemontite (Mn skarns).
- Blackwall*. A chlorite- or biotite-rich rock developed by metasomatic reaction between serpentinised ultramafic rocks and mafic rocks or quartzo-feldspathic rocks, respectively.
- Rodingite*. Calc-silicate rock, poor in alkalis and generally poor in carbonates, generated by metasomatic alteration of mafic igneous rocks enclosed in serpentinised ultramafic rocks. The process of rodingitization is associated with oceanic metamorphism (serpentinization of peridotite, rodingitization of enclosed basic igneous rocks such as gabbroic/basaltic dykes). Metarodingite is a prograde metamorphic equivalent of rodingite produced by oceanic metamorphism.
- Quartzite or metachert*. A metamorphic rock containing more than about 80% quartz.
- Serpentinite*. An ultramafic rock composed mainly of minerals of the serpentine group (antigorite, chrysotile, lizardite), e.g. diopside–forsterite–antigorite schist.
- Hornfels*. Is a non-schistose very fine-grained rock mainly composed of silicate  $\pm$  oxide minerals that shows substantial recrystallization due to contact metamorphism. Hornfels often retain some features inherited from the original rock such as graded bedding and cross-bedding in hornfelses of sedimentary origin.

*Migmatite*. Composite silicate rock, pervasively heterogeneous on a meso- to megascopic scale, found in medium- to high-grade metamorphic terrains (characteristic rocks for the middle and lower continental crust). Migmatites are composed of dark (mafic) parts (**melanosome**) and light (felsic) parts (**leucosome**) in complex structural association. The felsic parts formed by crystallization of locally derived partial melts or by metamorphic segregation, the mafic parts represent residues of the inferred partial melting process or are formed by metamorphic segregation. Parts of the felsic phases may represent intruded granitic magma from a more distant source.

*Restite*. Remnant of a rock, chemically depleted in some elements relative to its protolith. The depletion is the result of partial melting of that rock, e.g. emery rock.

### 2.3.4 Modal Composition of Rocks

The mineral constituents of metamorphic rocks are classified as follows: (1) *Major constituent*: present in amounts >5 vol%. To account for a major constituent not included in the definition of a rock name, the mineral name is put in front of the rock name (e.g. muscovite-gneiss, epidote–amphibolite). It follows from this that epidote–amphibolite is a rock which is mainly composed of epidote, hornblende and plagioclase. A garnet–staurolite gneiss is a metamorphic rock which is mainly composed of feldspar and quartz (included in the root name “gneiss”). In addition, it contains modally more staurolite than garnet as major constituents. (2) *Minor constituent*: present in amounts <5 vol%. If one wishes to include a minor constituent mineral in the rock name it is connected with “-bearing”, e.g. rutile–ilmenite-bearing garnet–staurolite gneiss (contains less rutile than ilmenite). (3) *Critical mineral (or mineral assemblage)*: indicating distinctive conditions for the formation of a rock (or distinct chemical composition of the rock) based on the presence or absence of a critical mineral or mineral assemblage. The critical mineral(s) may be present as a major or/and minor constituent(s).

It is up to the geologist to decide how many and which of the minerals that are not included in the definition of the rock name need to be prefixed. It is also possible to use abbreviations of mineral names in naming rocks, e.g. Bt–Ms gneiss for biotite–muscovite gneiss. Recommended standard abbreviations for mineral names are listed in the *Appendix* and are used throughout this book.

### 2.3.5 Names Related to the Origin of the Protolith

Metamorphic rocks can be grouped into seven chemical composition classes according to the most common rock types in the crust and mantle.



Examples of such rock names include: metapelite, metabasite, metabasalt, metapsamite, metamarl (e.g. calcareous micaschist), metagranite, metagabbro, semi-pelitic gneiss, metaeclogite.

## 2.4 Mineral Assemblages and Mineral Parageneses

The petrogenesis of metamorphic rocks is often a long-lasting complicated process in time and space which perhaps may endure for 30 Ma or so (see Chap. 3). The geologists collect the end product of such a long-drawn-out process at the Earth's surface (0.1 MPa and 25°C). The geologist is, of course, interested in finding out something about the evolution, the petrogenesis of the collected rock at this sample locality, to compare it with rocks from other localities and finally draw some logical conclusions on the large-scale processes that caused the metamorphism of the observed rock.

One of the important and successful methods to decipher the petrogenesis and evolution of metamorphic rocks is the application of chemical thermodynamics to the heterogeneous chemical systems exemplified by rocks. Rocks are usually composed of a number of different minerals that represent chemical subspaces of the rock, so-called phases. Most metamorphic rocks are also composed of a number of different chemical constituents that are designated system components. The chemical constituents that make up the bulk composition of rocks are distributed among a group of mineral species or phases, each with a distinct composition (heterogeneous system). The number, composition and identity of the minerals is uniquely defined by the laws of thermodynamics and depends exclusively on the prevailing intensive variables such as pressure and temperature. The group of minerals that make up a rock at equilibrium is designated as the **equilibrium mineral assemblage** or equilibrium phase assemblage. The succession of mineral assemblages that follow and replace one another during the metamorphic evolution of a given terrain are designated **mineral parageneses**.

In practical work with metamorphic rocks it is impossible to demonstrate that a given mineral assemblage once coexisted in chemical equilibrium. Therefore, one uses a less rigorous definition: a **mineral assemblage** is an association of mineral species in mutual grain contact. The assemblage occurs in a chemically homogeneous portion of a rock. With thin section examination, it is convenient to use a matrix table for marking all observed two-phase grain contacts. An example: in a thin section of a metamorphic rock showing a coarse-grained mosaic structure, the following mafic minerals are identified: staurolite, garnet, biotite and kyanite. All observed grain contacts between two of these minerals are marked with an "X" in Table 2.4. The thin-section observations summarized in Table 2.4 imply that the four minerals indeed represent a mineral assemblage.

In rocks displaying clear disequilibrium features (compositional zoning of minerals, reaction rims, symplectitic structures, replacement structures, exsolution

**Table 2.4** Practical determination of a mineral assemblage

Mineral	Staurolite	Garnet	Biotite	Kyanite
Staurolite	X	X	X	X
Garnet		X	X	X
Biotite			X	X
Kyanite				X

A cross in the Grt–St cell means; garnet and staurolite have mutual grain contacts in thin section

structures), it is often difficult to determine mineral assemblages that represent a particular stage in the evolutionary history of the rock.

One has to keep in mind that mineral assemblages are usually identified in thin sections which represent a two-dimensional section through a volume of rock. In such sections, only two and a maximum of three minerals may be in mutual grain contact. In the three-dimensional rock a maximum of four minerals can be in contact at a point in space, three minerals form contacts along a line, and two minerals contact along surfaces (that show as lines in thin sections). It is therefore strongly recommended to study **more than one thin section** from the most significant and interesting samples. As an example, in a series of 20 thin-sections of a single hand specimen of a coarse-grained sapphirine–granulite from the Western Alps, unique assemblages and unique structures were found in nearly all of the sections. The problem is especially acute in coarse-grained samples, where the scale of chemical homogeneity may considerably exceed the size of a thin section.

In extremely fine-grained samples the mineral assemblage must be determined by X-ray techniques. In this case it is not possible to maintain the requirement of mutual grain contact in the definition of an assemblage. However, this shortcoming may be overcome by using the high magnification backscatter image mode of an electron probe microanalyser (EPMA).

Rocks should always be examined by X-ray techniques in order to identify minerals which are difficult to distinguish under the microscope (e.g. muscovite, paragonite, talc, pyrophyllite, also quartz and untwinned albite).

Staining techniques help in distinguishing some important rock-forming minerals with similar optical properties such as calcite from dolomite.

Minerals occurring as inclusions in refractory minerals such as garnet but not in the matrix of the rock do not belong to the main matrix assemblage. In the example of the staurolite–garnet–biotite–kyanite assemblage cited above, garnet may show small composite two-phase inclusions of chlorite and chloritoid. In this case, chlorite–chloritoid–garnet constitutes another, earlier assemblage of the rock.

During metamorphism some earlier-formed minerals may become unstable and react chemically to form a new, more stable assemblage. However, metastable relics of the early assemblage may partly survive. Great care must be taken in the study of metamorphic micro-structures in order to avoid mixing up mineral assemblages. The correct identification of a successive series of mineral assemblages, i.e. the paragenesis of a metamorphic rock, represents the “great art” of metamorphic petrology. It can be learned only by experience.

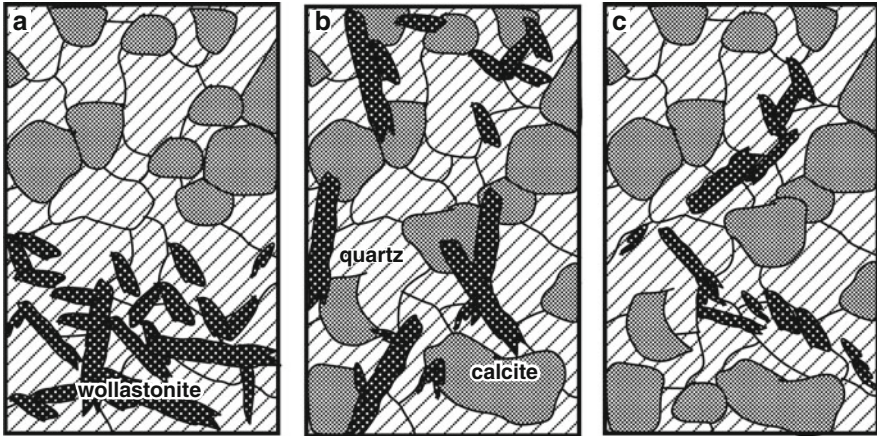


**Fig. 2.4** (a–c) Mineral assemblages in three different rocks all containing wollastonite, calcite and quartz

Figure 2.4 shows some of the aspects related to the recognition of mineral assemblages. Three fictive rocks all contain the minerals, quartz, calcite and wollastonite on the scale of a thin section. The general micro-structure of the three sections (Fig. 2.4) shows the distribution of the three minerals in their respective rocks. Rock A is clearly heterogeneous on the scale of a thin section, the upper part contains the assemblage Qtz + Cal, the lower half of the section is free of carbonate and contains the assemblage Qtz + Wo. The rock does not contain the assemblage Qtz + Cal + Wo. The two parts of the section are different in overall composition. Note, however, on a volatile-free basis, the two domains of the rock may have very similar or identical compositions (same Ca/Si ratio). In rock B, obviously all three minerals can be found in mutual grain contact, and Qtz + Cal + Wo constitutes the mineral assemblage. In rock C, which appears to be compositionally homogeneous on thin-section scale, Qtz + Cal and Qtz + Wo form common grain boundaries. However, no Wo + Cal grain boundaries can be observed. Thus, although the three phases Qtz + Cal + Wo do not strictly represent a mineral assemblage, many petrologists would probably approve it being labeled as an equilibrium assemblage. [Comment: after the publication of the first edition of this book Fig. 2.4 (originally Fig. 2.1), inspired a lively discussion among petrologists on the geo-metamorphism mailbase. A number of comments were made and it was suggested that the figure be modified. We prefer to keep it essentially in its original form and some aspects of the debate will be discussed in Sect. 3.7. We strongly recommend that the reader and anyone interested in rock metamorphism subscribe to the mailbase geo-metamorphism where one sometimes captures a stimulating dispute on questions related to geo-metamorphism. The present address is: [geo-metamorphism@jiscmail.ac.uk](mailto:geo-metamorphism@jiscmail.ac.uk): you need to send an e-mail with only the following in the body of the message: *subscribe geo-metamorphism*].

## 2.5 Graphical Representation of Metamorphic Mineral Assemblages

Once the mineral assemblage of a rock has been identified, it is convenient or even necessary to represent graphically the chemical composition of the minerals that constitute the assemblage. Such a figure is called a **chemograph** and represents a **composition phase diagram**. The geometric arrangement of the phase relationships on such a phase diagram is called the **topology**. Composition phase diagrams can be used only to document the assemblages found in rocks of a given metamorphic terrain or outcrop. However, such diagrams are an indispensable tool for the analysis of metamorphic characteristics and evolution of a terrain. They can be used to deduce sequences of metamorphic mineral reactions. Finally, composition phase diagrams can also be calculated theoretically from thermodynamic data of minerals which permits the quantitative calibration of field-derived chemographs.

Composition phase diagrams display the chemical composition of minerals and the topologic relationships of mineral assemblages. Variables on the diagrams are concentrations or amounts of chemical entities. All other variables that control the nature of the stable mineral assemblage such as pressure and temperature must be constant. Thus, composition phase diagrams are isothermal and isobaric. Also, not more than two composition variables can conveniently be displayed on a two-dimensional xy-diagram (sheet of paper, computer screen).

### 2.5.1 Mole Numbers, Mole Fractions and the Mole Fraction Line

It is useful to change the scale for the compositional variables from wt% to mol%, mole fractions or mole numbers. Most chemographs use mol% or mole fraction as units for the composition variables. The mineral forsterite (Fo), for example, is composed of 42.7 wt% SiO<sub>2</sub> and 57.3 wt% MgO. Mole numbers and mole fractions for this mineral are calculated as follows:

SiO<sub>2</sub>:  $42.7/60.1$  (molecular weight SiO<sub>2</sub>) = **0.71** (number of moles of SiO<sub>2</sub> per 100 g Fo)

MgO:  $57.3/40.3$  (molecular weight MgO) = **1.42** (number of moles of MgO per 100 g Fo)

Forsterite has a MgO/SiO<sub>2</sub> ratio of  $1.42/0.71 = 2$  and thus has 2 mol MgO per 1 mol SiO<sub>2</sub>. The composition is reported as Mg<sub>2</sub>SiO<sub>4</sub> or (2MgO SiO<sub>2</sub>) or 66.66% MgO + 33.33% SiO<sub>2</sub> or 2/3MgO + 1/3SiO<sub>2</sub>. This is all equivalent. However, the last version has many advantages ⇒ mole fraction basis.

The mole fraction is defined as follows:

$$X_{\text{MgO}} = \frac{\text{(Number of moles of MgO)}}{\text{(Number of moles of MgO)} + \text{(Number of moles of SiO}_2\text{)}}$$

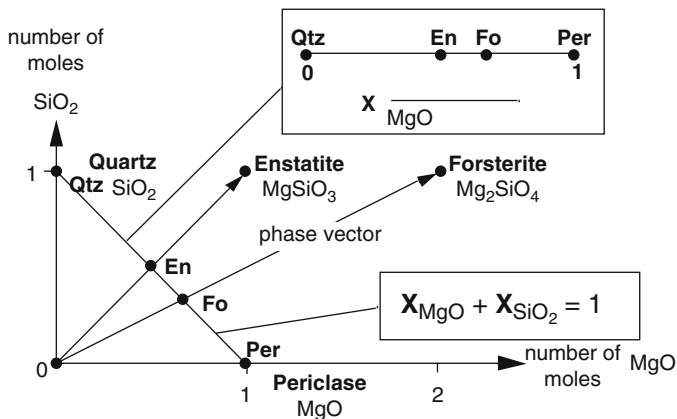


Fig. 2.5 Composition space and the two-component MgO–SiO<sub>2</sub> system

For the example above:  $X_{MgO} = 2/(2 + 1) = 1.42/(1.42 + 0.71) = 0.66$  (dimensionless quantity).

Figure 2.5 shows a graphical representation of the two component system MgO and SiO<sub>2</sub> in a rectangular coordinate system. The two components MgO and SiO<sub>2</sub> define the two-dimensional **composition space**. The graphical representation of the compositions of forsterite, enstatite, quartz and periclase is a point in the Cartesian coordinate system with the axes: numbers of moles MgO and numbers of moles SiO<sub>2</sub>. It is apparent in Fig. 2.5 that the composition of forsterite, for example, can also be viewed as a vector in the composition space with the elements (2,1). Mineral compositions are unequivocally characterized by a vector, the **phase vector**, in the composition space.

Mineral compositions can also be represented in terms of mole fractions rather than mole numbers. The mole fractions of the two **system components** MgO and SiO<sub>2</sub> sum to unity in all four minerals represented in Fig. 2.5. This can be expressed by the general relationship:

$$X_{MgO} + X_{SiO_2} = 1$$

This equation represents a straight line in Fig. 2.5 connecting  $X_{MgO} = 1$  with  $X_{SiO_2} = 1$ . The phase vectors of forsterite and enstatite intersect the mole fraction line at unique positions (En and Fo, respectively; Fig. 2.5). It is, therefore, not necessary to represent phase composition in a two-component system on a two-dimensional diagram. The topologic information is contained on the mole fraction line. The dimension of the graph can be reduced from two to one. If the concentration of one component is known in a phase that is composed of two components, the second concentration is known as well. In an n-component system there are  $n - 1$  independent compositional variables, the remaining

concentration is given by the equation (or:  $n$  composition variables and one equation relating them):

$$\sum_{i=1}^n X_i = 1$$

Note also, for example, that enstatite compositions expressed as  $\text{MgSiO}_3$ ,  $\text{Mg}_2\text{Si}_2\text{O}_6$ ,  $\text{Mg}_4\text{Si}_4\text{O}_{12}$  all have the same intersection point with the mole fraction line (multiplying the phase vector for enstatite with a scalar preserves its position on the mole fraction line). Phase compositions in a two-component system can be represented on a mole fraction line as shown in Fig. 2.5.

### 2.5.2 The Mole Fraction Triangle

The mineral talc (Tlc) is composed of three simple oxide components and its composition can be written as:  $\text{H}_2\text{Mg}_3\text{Si}_4\text{O}_{12}$ . Based on a total of 12 oxygens per formula unit, talc consists of 1 mol  $\text{H}_2\text{O}$ , 3 mol  $\text{MgO}$  and 4 mol  $\text{SiO}_2$ . A graphical representation of the talc composition in the three-component system is shown in Fig. 2.6. The three components,  $\text{MgO}$ ,  $\text{SiO}_2$  and  $\text{H}_2\text{O}$ , define a Cartesian coordinate system with numbers of moles of the components displayed along the coordinate axes. The unit vectors of the system components span the composition space. The talc composition is represented by a phase vector with the elements;  $\times 3$  the unit vector of  $\text{MgO}$ ,  $\times 4$  the unit vector of  $\text{SiO}_2$  and  $\times 1$  the unit vector of  $\text{H}_2\text{O}$ .

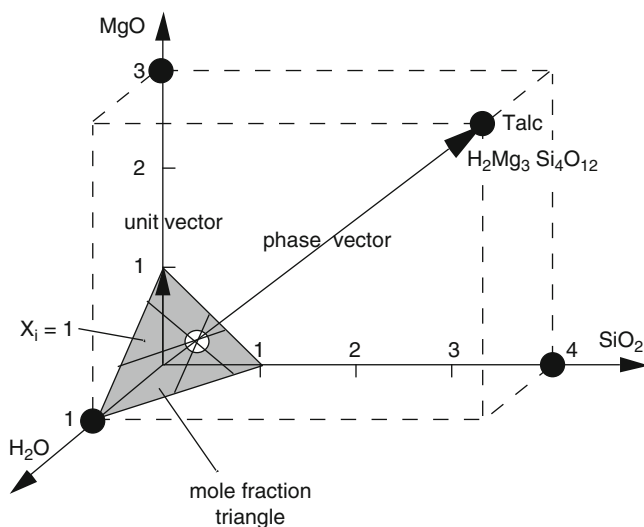


Fig. 2.6 Composition space and the three-component  $\text{MgO-H}_2\text{O-SiO}_2$  system

The total number of moles of system components is 8 and the composition of talc can be normalized to a total number of 8 mol of system components. In this case the talc composition will be expressed by  $\Rightarrow$  mole fractions:  $X_{\text{H}_2\text{O}} = 1/8$ ,  $X_{\text{MgO}} = 3/8$ ,  $X_{\text{SiO}_2} = 4/8$ , or:  $X_{\text{H}_2\text{O}} = 0.125$ ,  $X_{\text{MgO}} = 0.375$ ,  $X_{\text{SiO}_2} = 0.50$ ; in mol%:  $\text{H}_2\text{O} = 12.5\%$ ,  $\text{MgO} = 37.5\%$ ,  $\text{SiO}_2 = 50\%$ . Graphic representation of the talc composition on a mole fraction basis is given by the intersection of the talc phase vector in Fig. 2.6 and the plane  $\sum X_i = 1$ . The mole fraction plane is a regular triangle with the corners  $X_i = 1$ . This triangle is called the **mole fraction triangle**.

A representation of the mole fraction triangle is shown in Fig. 2.7. The lines of constant  $X_i$  are parallel with the base lines of the triangle. This follows from Fig. 2.6, where it can be seen that the planes  $X_i = \text{constant}$  and  $X_{j \neq i} = 0$  intersect the mole fraction plane along lines parallel to the base line  $X_i = 0$ . Three rulers with  $X_i = 0.1$  increments are also shown in Fig. 2.7 for the three components. Triangular coordinate paper is available on the market.

A further example of a mineral composition in a three-component system  $\text{MgO-SiO}_2\text{-H}_2\text{O}$  is the chemical formula of chrysotile (one of many serpentine minerals) that can be written as,  $\text{H}_4\text{Mg}_3\text{Si}_2\text{O}_9$ . The sum of moles of system components is 7;  $\Rightarrow$  mole fractions:  $X_{\text{H}_2\text{O}} = 2/7$ ,  $X_{\text{MgO}} = 3/7$ ,  $X_{\text{SiO}_2} = 2/7$ , or equivalent:  $X_{\text{H}_2\text{O}} = 0.29$ ,  $X_{\text{MgO}} = 0.42$ ,  $X_{\text{SiO}_2} = 0.29$ ; expressed in mol%:  $\text{H}_2\text{O} = 29\%$ ,  $\text{MgO} = 42\%$ ,  $\text{SiO}_2 = 29\%$ .

Because triangular coordinate drawing paper is not always at hand for plotting composition data, the formulae for recalculation into Cartesian coordinates are given in Fig. 2.8 together with the position of the serpentine composition. The value of the scaling factor “f” depends on the desired size of the figure. The scaling factor must be multiplied by 100 when using mole fractions rather than mol%.

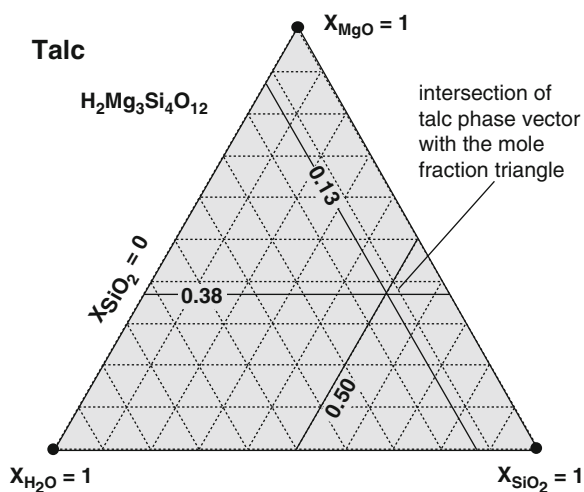


**Fig. 2.7** Mole fraction triangle  $\text{MgO-H}_2\text{O-SiO}_2$  and intersection coordinates of the talc phase vector with the mole fraction triangle

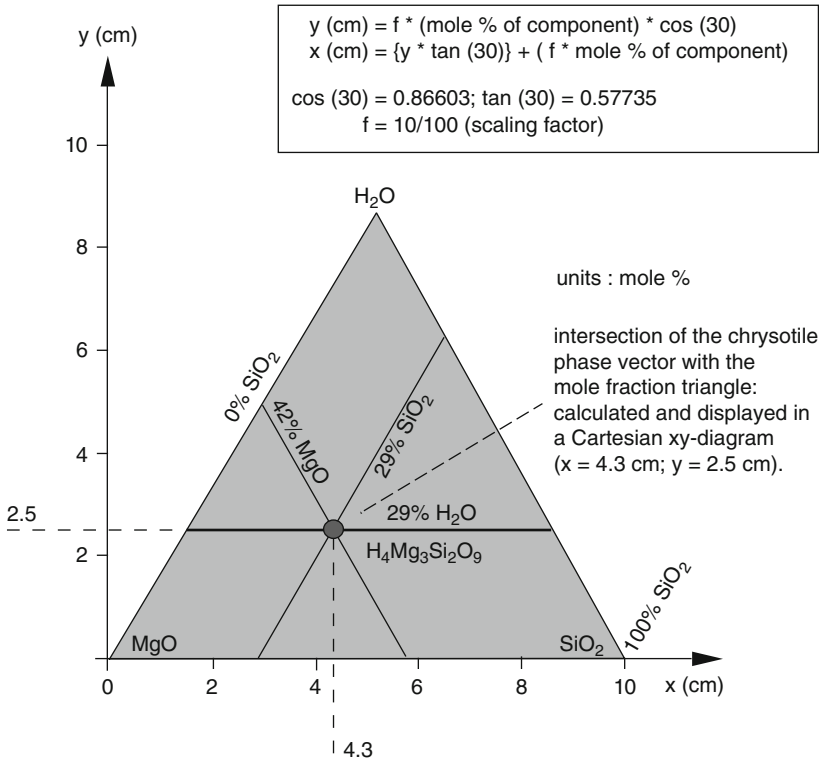


**Fig. 2.8** Mole fraction triangle MgO–H<sub>2</sub>O–SiO<sub>2</sub> in the Cartesian coordinate system

### 2.5.3 Projections

#### 2.5.3.1 Simple Projections

On a mole fraction triangle two compositional variables of a three-component system can be depicted. Most rocks, however, require more than three components to describe and to understand the phase relationships. Graphical representation of an eight component system requires a seven-dimensional figure. Projection phase diagrams are graphical representations of complex n-component systems that show two composition variables at a time while keeping the other n – 3 composition variables constant. The remaining variable is given by the mole fraction equation as outlined above.

In a suite of samples of similar bulk composition (e.g. 20 samples of metapelite), one often finds certain mineral species that are present in many of them. This circumstance permits projection of the phase compositions from the composition of one such mineral which is present in excess. For instance, in many metapelitic rocks quartz is modally abundant whereas calcite is the main mineral in most marbles.



Composition phase diagrams for metapelites can therefore be constructed by projecting through  $\text{SiO}_2$  onto an appropriate mole fraction triangle, and for marbles by projection the phase compositions from  $\text{CaCO}_3$ .

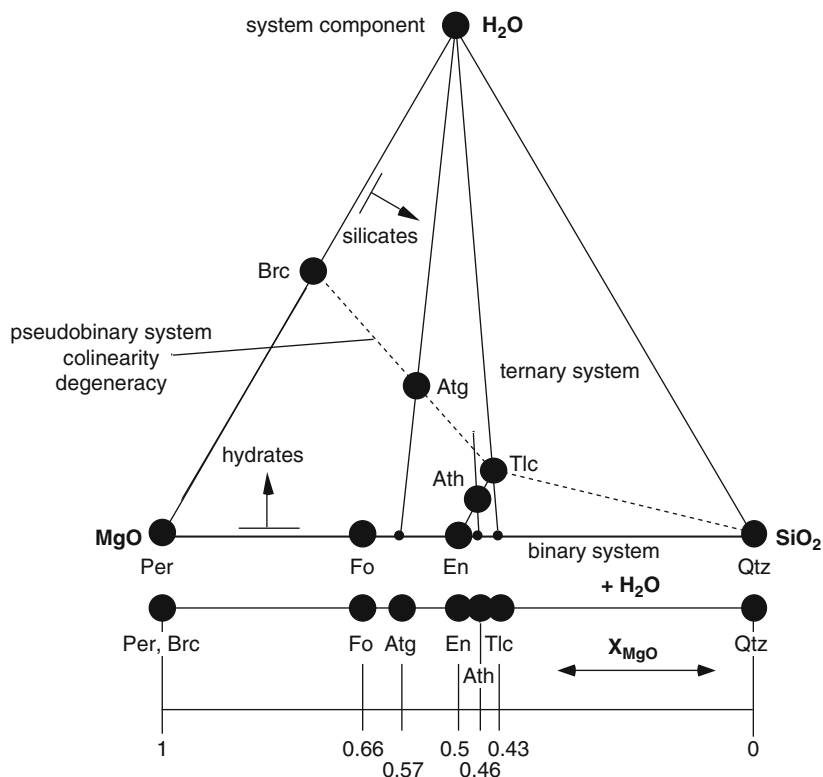
The system  $\text{MgO-SiO}_2\text{-H}_2\text{O}$  (MSH system) can be used to explain the basic principle of making projections. Some phase compositions in the MSH system are given in Table 2.5. This table represents a **composition matrix** with oxide components defining unit vectors of the composition space and the mineral compositions used as column vectors.

Figure 2.9 shows the chemographic relationships in the ternary system  $\text{H}_2\text{O-MgO-SiO}_2$ . The corners of the triangle represent  $X_i = 1$  or 100 mol% of the system components. The lines connecting them are the binary subsystems of the three-component system. The compositions of the black circles occur as stable phases in nature (phase components). The ternary system has three binary subsystems ( $\text{MgO-SiO}_2$ ,  $\text{MgO-H}_2\text{O}$ , and  $\text{SiO}_2\text{-H}_2\text{O}$ ). Some phase compositions in the ternary system fall on straight lines such as  $\text{Tlc-Ath-En}$  and  $\text{Brc-Atg-Tlc}$ . This means that the phase compositions along a straight line, e.g.  $\text{Tlc-Ath-En}$ , are linearly dependent; one of these compositions can be expressed by the other two ( $4\text{En} + \text{Tlc} = \text{Ath}$ ). Therefore, there are only two components required to describe the compositions of the other phases on the straight line  $\Rightarrow$  **pseudobinary join**. The colinearity is also said to be a **compositional degeneracy** in the system.

Now, one might wish to analyze and discuss phase relationships among the minerals shown in Fig. 2.9 for geologic situations in which an aqueous fluid phase ( $\text{H}_2\text{O}$ ) is present in all rocks and in equilibrium with the solid phase assemblage. The presence of excess water in all the considered rocks permits projection of the other phase compositions through water onto the  $\text{MgO-SiO}_2$ -binary (in principle on any pseudobinary as well). Imagine that you are standing in the  $\text{H}_2\text{O}$  corner of Fig. 2.9. What you will see from there is shown at the bottom of Fig. 2.9. The

**Table 2.5** Phase compositions in the MSH-system

(a) Composition matrix (moles); columns are phase vectors, composition space defined by the system components $\text{SiO}_2$ , $\text{MgO}$ , $\text{H}_2\text{O}$									
	Fo	Brc	Tlc	En	Ath	Qtz	Per	Atg	Fl
$\text{SiO}_2$	1	0	4	2	8	1	0	2	0
$\text{MgO}$	2	1	3	2	7	0	1	3	0
$\text{H}_2\text{O}$	0	1	1	0	1	0	0	2	1
Sum	3	2	8	4	16	1	1	7	1
(b) Composition matrix (mole fractions); columns are normalized phase vectors, values are coordinates on the molefraction triangle									
$\text{SiO}_2$	0.33	0.00	0.50	0.50	0.50	1.00	0.00	0.29	0.00
$\text{MgO}$	0.67	0.50	0.38	0.50	0.44	0.00	1.00	0.43	0.00
$\text{H}_2\text{O}$	0.00	0.50	0.13	0.00	0.06	0.00	0.00	0.29	1.00
Sum	1	1	1	1	1	1	1	1	1
(c) Composition matrix (mole fractions); projected through $\text{H}_2\text{O}$ , columns are normalized phase vectors, values are coordinates on the $\text{SiO}_2\text{-MgO}$ -binary (mole fraction line)									
$\text{SiO}_2$	0.33	0.00	0.56	0.50	0.53	1.00	0.00	0.40	0.00
$\text{MgO}$	0.67	1.00	0.43	0.50	0.47	0.00	1.00	0.60	0.00



**Fig. 2.9** Projection of phase compositions in the MgO–H<sub>2</sub>O–SiO<sub>2</sub> system through H<sub>2</sub>O onto the MgO–SiO<sub>2</sub> binary

chemography on the MgO–SiO<sub>2</sub> binary is a projected chemography and the positions of the mineral compositions on this binary are expressed in terms of mole fractions  $X_{\text{Mg}}$ . They can be calculated from the composition matrix (Table 2.5b) by first; deleting the row containing the component one wishes to project from (in this case H<sub>2</sub>O) and second; renormalizing the column vectors to unity (Table 2.5c). It follows that projections from quartz, periclase and H<sub>2</sub>O can be prepared using the composition matrix of Table 2.5b. It must be stressed again, however, that the projections are meaningful only if the projection component is present as a phase of fixed composition in all rocks of interest. The projected chemography in Fig. 2.9 cannot be used in H<sub>2</sub>O-absent situations. Likewise, an analogous projection through MgO onto the SiO<sub>2</sub>–H<sub>2</sub>O–binary requires that periclase is present in all assemblages, and projection through SiO<sub>2</sub> onto the MgO–H<sub>2</sub>O–binary requires that quartz is present in all assemblages. It is therefore necessary to write the projection compositions on any projected composition phase diagram. In simple projections, the projecting phase component is identical with one of the simple oxide system components.

### 2.5.3.2 Projection of Solid-Solution Phases

In nature, the magnesian minerals shown in Fig. 2.9 have variable substitution of Mg by Fe. If the restriction of water saturation is maintained, phase compositions in the FeO–MgO–SiO<sub>2</sub>–H<sub>2</sub>O system can be projected from H<sub>2</sub>O onto the mole fraction triangle FeO–MgO–SiO<sub>2</sub>, as shown in Fig. 2.10. In certain applications one does not wish to consider the complexity arising from the Fe–Mg substitution. In such cases, one projects the compositions onto the MgO–SiO<sub>2</sub>–binary parallel to the direction of the substitution vector MgFe<sub>-1</sub>. The resulting projection is identical to the binary chemography shown in Fig. 2.9. All solid-solution phases must be projected along exchange vectors. More examples will be given below.

### 2.5.3.3 Complex Projections

The technique of projecting phase compositions in the m-dimensional space from one system component onto a subspace with m – 1 dimensions is one of the two key steps in producing geologic composition phase diagrams. In the MSH system, used as an example here, the projection was made from the H<sub>2</sub>O component in the three-component space onto the MgO–SiO<sub>2</sub> binary. However, often one wishes to project from a composition other than the original system components. Most commonly, it is necessary to find a projection from a composition of a phase that is present in excess. In order to make this possible, the composition matrix has to be

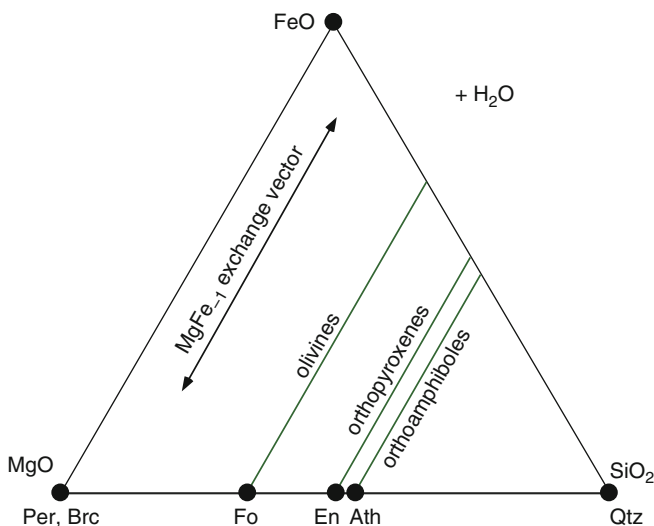


**Fig. 2.10** Projection of phase compositions in the FeO–MgO–H<sub>2</sub>O–SiO<sub>2</sub> system through H<sub>2</sub>O and along the MgFe<sub>-1</sub> exchange vector onto the MgO–SiO<sub>2</sub> binary

rewritten in terms of a set of new system components. One of these new components must be the desired new projection composition.

For example, we would like to prepare a figure representing the phase compositions in the MSH system on a mole fraction triangle with the corners  $\text{Mg}_2\text{SiO}_4$  (Fo),  $\text{Mg}(\text{OH})_2$  (Brc), and  $\text{Mg}_3\text{Si}_4\text{O}_{10}(\text{OH})_2$  (Tlc). Secondly, we would like to study phase relationships in rocks which contain excess forsterite and need a projection from  $\text{Mg}_2\text{SiO}_4$  (Fo) onto the Brc–Tlc-binary.

The solution to the problem is shown in Table 2.6. In Table 2.6a the phase compositions are expressed in terms of the new system components  $\text{Mg}_2\text{SiO}_4$  (Fo),  $\text{Mg}(\text{OH})_2$  (Brc), and  $\text{Mg}_3\text{Si}_4\text{O}_{10}(\text{OH})_2$  (Tlc). As an example, the composition of enstatite can be expressed by  $2\text{Fo} - 1\text{Brc} + 1\text{Tlc}$ , which is equivalent to  $6\text{MgO} + 6\text{SiO}_2$ . Table 2.6b gives the coordinates of the mineral compositions in the mole fraction triangle Fo–Brc–Tlc. The algebraic operation which transforms the composition space expressed in terms of simple oxide components (Table 2.5a) to the composition space expressed in terms of  $\text{Mg}_2\text{SiO}_4$  (Fo),  $\text{Mg}(\text{OH})_2$  (Brc), and  $\text{Mg}_3\text{Si}_4\text{O}_{10}(\text{OH})_2$  (Tlc) components (Table 2.6a) is also given in Table 2.6. It can be seen that the operation is a pre-multiplication of Table 2.5a by the inverse of the leading  $3 \times 3$  square matrix in Table 2.5a. The result of the operation is the composition matrix (Table 2.7a) with the mineral compositions expressed by the new set of system components. Today, any standard commercial spreadsheet

**Table 2.6** Phase compositions in the Fo–Brc–Tlc-system

(a) Composition matrix in terms of moles; columns are phase vectors, composition space defined by the system components

	Fo	Brc	Tlc	En	Ath	Qtz	Per	Atg	Fl
Fo	1.00	0.00	0.00	2.00	4.00	-1.00	4.00	0.00	-4.00
Brc	0.00	1.00	0.00	-1.00	-2.00	-1.00	1.00	3.00	5.00
Tlc	0.00	0.00	1.00	1.00	5.00	1.00	-1.00	1.00	1.00

(b) Composition matrix in terms of mole fractions; columns are normalized phase vectors, values are coordinates on the mole fraction triangle

	Fo	Brc	Tlc	En	Ath	Qtz	Per	Atg	Fl
Fo	1.00	0.00	0.00	1.00	0.57	1.00	1.00	0.00	-2.00
Brc	0.00	1.00	0.00	-0.50	-0.29	1.00	0.25	0.75	2.50
Tlc	0.00	0.00	1.00	0.50	0.71	-1.00	-0.25	0.25	0.50

Initial composition matrix (old system components):  $[A][B_{OC}]$  (Table 2.5a)

New matrix (new system components)  $[I][B_{NC}]$  (Table 2.6a)

Matrix operation:  $[A^{-1}][A][B_{OC}] \Rightarrow [I][B_{NC}]$

Old basis [A]	Inverse of old basis $[A^{-1}]$						Identity matrix [I]		
1	0	4	-0.33	0.67	-0.67	1	0	0	
2	1	3	-0.33	0.17	0.83	0	1	0	
0	1	1	0.33	-0.17	0.17	0	0	1	

(c) Composition matrix in terms of mole fractions; projection through  $\text{Mg}_2\text{SiO}_4$  (Fo), columns are normalized phase vectors, values are coordinates on the mole fraction line

	Fo	Brc	Tlc	En	Ath	Qtz	Per	Atg	Fl
Brc	0.00	1.00	0.00	-1.00	-0.69	1.00	0.00	0.75	0.83
Tlc	0.00	0.00	1.00	1.00	1.69	-1.00	0.00	0.25	0.17

**Table 2.7** Composition matrix for minerals in the KFMASH-system

(a) Composition matrix in terms of oxide components																		
	Ky	Qtz	Ms	Fl	FeO	MgO	Alm	Prp	Ann	Phl	FEs	Es	St	Cld	Crd	OPX	Spl	Chl
SiO <sub>2</sub>	1	1	6	0	0	0	3	3	6	6	5	5	8	2	5	1.8	0	3
Al <sub>2</sub> O <sub>3</sub>	1	0	3	0	0	0	1	1	1	1	2	2	9	2	2	0.2	1	1
FeO	0	0	0	0	1	0	3	0	6	0	5	0	4	2	0	0.5	0	0
MgO	0	0	0	0	0	1	0	3	0	6	0	5	0	0	2	1.3	1	5
K <sub>2</sub> O	0	0	1	0	0	0	0	0	1	1	1	1	0	0	0	0.0	0	0
H <sub>2</sub> O	0	0	2	1	0	0	0	0	2	2	2	2	2	2	0	0.0	0	4

(b) Inverse of leading 6 × 6 square matrix (A-matrix ⇒ A <sup>-1</sup> )																		
	0.00	1.00	0.00	0.00	-3.00	0.00												
	1.00	-1.00	0.00	0.00	-3.00	0.00												
	0.00	0.00	0.00	0.00	1.00	0.00												
	0.00	0.00	0.00	0.00	-2.00	1.00												
	0.00	0.00	1.00	0.00	0.00	0.00												
	0.00	0.00	0.00	1.00	0.00	0.00												

(c) Composition matrix in terms of Ky, Qtz, Ms, H <sub>2</sub> O, FeO and MgO																		
	Ky	Qtz	Ms	Fl	FeO	MgO	Alm	Prp	Ann	Phl	Fe-Es	Es	St	Cld	Crd	OPX	Spl	Chl
Ky	1.00	0.00	0.00	0.00	0.00	0.00	1.00	1.00	-2.00	-2.00	-1.00	-1.00	9.00	2.00	2.00	0.20	1.00	1.00
Qtz	0.00	1.00	0.00	0.00	0.00	0.00	2.00	2.00	2.00	2.00	0.00	0.00	-1.00	0.00	3.00	1.60	-1.00	2.00
Ms	0.00	0.00	1.00	0.00	0.00	0.00	0.00	0.00	1.00	1.00	1.00	1.00	0.00	0.00	0.00	0.00	0.00	0.00
Fl	0.00	0.00	0.00	1.00	0.00	0.00	0.00	0.00	0.00	0.00	0.00	0.00	2.00	2.00	0.00	0.00	0.00	4.00
FeO	0.00	0.00	0.00	0.00	1.00	0.00	3.00	3.00	6.00	6.00	0.00	5.00	4.00	2.00	0.00	0.50	0.00	0.00
MgO	0.00	0.00	0.00	0.00	0.00	1.00	0.00	3.00	0.00	6.00	0.00	5.00	0.00	0.00	2.00	1.30	1.00	5.00

(d) Renormalized composition matrix, column vectors are coordinates of mineral compositions in the mole fraction triangle Ky (A), FeO (F) and MgO (M) (⇒ AFM-diagram), projection through Qtz, Ms and H <sub>2</sub> O																		
	Ky	Qtz	Ms	Fl	FeO	MgO	Alm	Prp	Ann	Phl	Fe-Es	Es	St	Cld	Crd	OPX	Spl	Chl
Ky	1.00	0.00	0.00	0.00	0.00	0.00	0.25	0.25	-0.50	-0.50	-0.25	-0.25	0.69	0.50	0.50	0.10	0.50	0.17
FeO	0.00	0.00	0.00	0.00	1.00	0.00	0.75	0.00	1.50	0.00	1.25	0.00	0.31	0.50	0.00	0.25	0.00	0.00
MgO	0.00	0.00	0.00	0.00	0.00	1.00	0.00	0.75	0.00	1.50	0.00	1.25	0.00	0.00	0.50	0.65	0.50	0.83

program running on a PC or MAC will do these algebraic operations for you (e.g. Excel). We are now ready for the construction of the desired forsterite projection. Just as in simple projections, delete the Fo-row in Table 2.6b and renormalize to constant sum. Table 2.6c shows the coordinates of the phase compositions along the Brc–Tlc binary. Some of the compositions project to the negative side of talc, and periclase cannot be projected onto the Brc–Tlc binary at all. This is apparent also from Fig. 2.9, where it can be recognized that, seen from forsterite, periclase projects away from the Brc–Tlc binary. It is also clear from the procedure outlined above, that the compositions which one chooses to project from or which one wants to see at the apexes of the mole fraction triangle must be written as column vectors in the original A-matrix.

With the two basic operations, projection and redefinition of system components, one can construct any thermodynamically valid composition phase diagram for any geologic problem.

#### 2.5.3.4 AFM Projections

A classical example of a composite projection is the AFM projection for metapelitic rocks (see also Chap. 7). Many of the phase relationships in metapelitic rocks can be described in the six-component system  $K_2O$ – $FeO$ – $MgO$ – $Al_2O_3$ – $SiO_2$ – $H_2O$  (KFMASH system). A graphical representation of the system requires projection from at least three fixed compositions. Many of the metapelitic rocks contain excess quartz and some aspects of metamorphism can be discussed for water-present conditions. Therefore, a projection from  $SiO_2$  and  $H_2O$  can be easily prepared. However, none of the remaining four components is present as a phase in such rocks. On the other hand, in low- and medium-grade metapelites muscovite is normally present as an excess phase, and in high-grade rocks muscovite is replaced by K-feldspar. Therefore, a useful diagram could be prepared by projecting through muscovite or K-feldspar onto the plane  $Al_2O_3$ – $FeO$ – $MgO$ . Furthermore, under the condition of excess quartz an  $Al_2SiO_5$  polymorph is always more stable than corundum. This, in turn, requires that the composition matrix for minerals in metapelitic rocks is rewritten in terms of the new system components  $KAl_3Si_3O_{10}(OH)_2$ – $Al_2SiO_5$ – $FeO$ – $MgO$ – $SiO_2$ – $H_2O$  as shown in Table 2.7. The coordinates of the phase compositions in the AFM mole fraction triangle can then be represented in an AFM diagram (Fig. 2.11). All Mg–Fe-free Al-silicates project to the A apex, pure enstatite, talc and anthophyllite are located at the M apex, ferrosilite and Fe-anthophyllite project to the F apex. Biotites have negative A-coordinates. The iron-magnesium substitution ( $FeMg_{-1}$  exchange) in the ferromagnesian minerals is parallel to the AM binary, the Mg-tschermak substitution ( $2AlSi_{-1}Mg_{-1}$  exchange) is parallel to the AM binary. Minerals such as staurolite, chloritoid, garnet, cordierite and spinel do not show any tschermak variation, their compositional variation is exclusively parallel to the  $FeMg_{-1}$  exchange vector. Other minerals such as chlorites, biotites, orthopyroxenes and orthoamphiboles show both  $FeMg_{-1}$  exchange and  $2AlSi_{-1}Mg_{-1}$  exchange. The compositions of

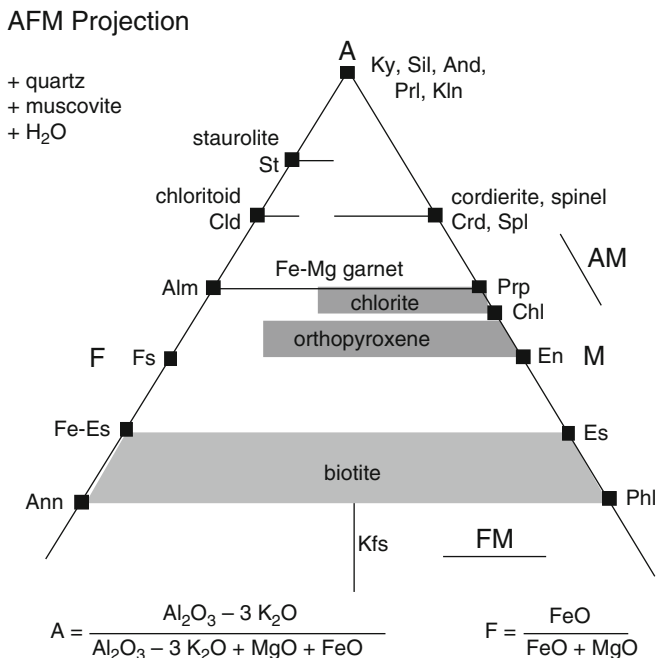


**Fig. 2.11** Coordinates of phase compositions in the  $K_2O$ - $FeO$ - $MgO$ - $Al_2O_3$ - $SiO_2$ - $H_2O$  system projected through muscovite, quartz and  $H_2O$  onto the plane  $Al_2O_3$ ,  $FeO$  and  $MgO$  (AFM projection)

these minerals are represented by fields in an AFM diagram. The AFM projection (Fig. 2.11) can be used exclusively for rocks with excess quartz and muscovite and for water-present conditions. Similar projections can readily be prepared from the composition matrix in Table 2.7c if one wants to analyze phase relationships for rocks containing excess muscovite, quartz and Al-silicate but treating  $H_2O$  as a compositional variable on the diagram. Such a WFM diagram can be constructed by deleting the rows Ky, Qtz and Ms and renormalizing the remaining three rows. A QFM diagram (Qtz- $FeO$ - $MgO$ ) projecting through Ms, Ky and  $H_2O$  can be constructed from Table 2.7c for discussing rocks with excess Al-silicate and muscovite but not excess quartz. To project from K-feldspar rather than muscovite, the Ms column in Table 2.7a has to be replaced by the column vector of K-feldspar. The subsequent procedure is the same as that described above. If, for example in low-grade rocks, muscovite contains a significant tschermak component (phengite), one may replace the Ms column vector (endmember muscovite) in Table 2.7a by the analyzed mica composition.

Figure 2.11 shows the general projection coordinates of AFM phases. However, composition phase diagrams are used to represent phase relationships at a given pressure and temperature. A specific example of an AFM diagram at a distinct P and T is shown in Fig. 2.12. Present in excess is quartz, muscovite and  $H_2O$ . The AFM surface is divided into a number of sub-regions. Three types can be distinguished:

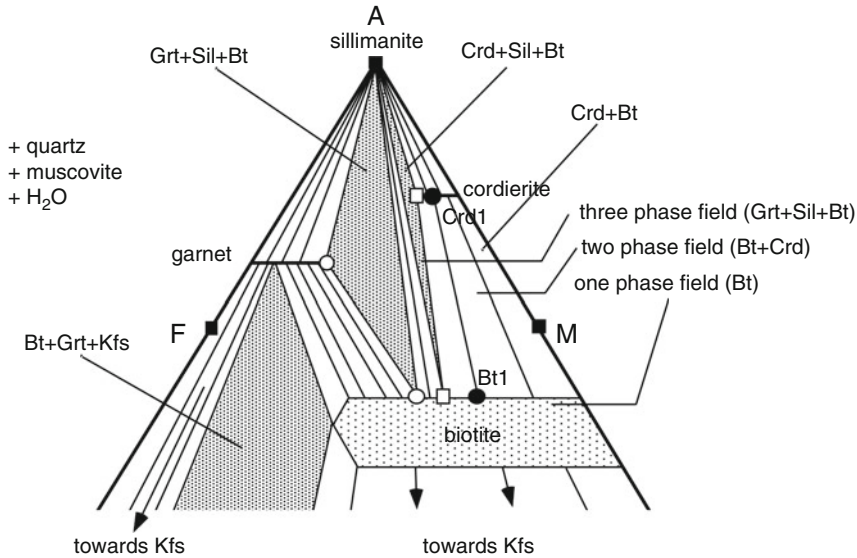


**Fig. 2.12** AFM-diagram at a specified pressure and temperature showing phase relationships among some typical AFM phases

1. *One-phase fields.* If the total rock composition projects inside, for example, the one phase field for biotite, it will be composed of quartz, muscovite and biotite. The composition of biotite is given by the composition of the rock. One-phase fields are divariant fields because the composition of the mineral freely changes with the two composition variables of the bulk rock.
2. *Two-phase fields.* If the total rock composition projects inside the two-phase field biotite + cordierite it will contain the assemblage  $M_s + Qtz + Crd + Bt$ . The composition of coexisting biotite and cordierite can be connected with a tie line (isopotential line) passing through the projection point of the bulk rock composition (e.g. Bt1–Crd1 in Fig. 2.12). A tie line can be drawn through any bulk composition inside the two-phase field which connects the two coexisting minerals (tie line bundle). It follows that all bulk rock compositions on a specific Crd–Bt tie line (at a given P and T) contain minerals of identical composition. If the rock composition projects close to cordierite it will contain abundant cordierite and little biotite (and vice versa). The mineral compositions are controlled by the Fe–Mg exchange equilibrium between cordierite and biotite (see Chap. 3). Also the tschermak exchange in biotite is controlled by the assemblage. Consider, for example, a rock composition which projects in the garnet + biotite field. For a given biotite composition, the composition of the coexisting garnet is fixed by the tie line passing through the given biotite composition and the projection point of the bulk rock.
3. *Three phase fields.* If the rock composition projects inside the three-phase field biotite + cordierite + sillimanite it will contain the assemblage  $M_s + Qtz + Crd + Bt + Sil$ . Here the compositions of all minerals are entirely controlled by the



assemblage (open squares in Fig. 2.12). All bulk rock compositions which project in the three-phase field Crd + Bt + Sil will be composed of these three minerals of identical composition in modal proportions depending on the composition of the rock. Three-phase fields are invariant fields at constant  $P$  and  $T$ , because the mineral compositions do not vary with rock composition. The cordierite coexisting with biotite and sillimanite has the most Fe-rich composition of all cordierite at the  $P$ - $T$  conditions of the AFM diagram. Note that, in general, all three-phase fields on an AFM diagram must be separated from each other by two-phase fields. In the three-phase field Grt + Sil + Bt, the mineral compositions are controlled by the assemblage as well (open circles in Fig. 2.12). It follows that biotite in this assemblage must be more Fe-rich than biotite in the assemblage Crd + Sil + Bt. The garnet coexisting with Bt + Sil has the most Mg-rich composition of all garnets at the given pressure and temperature.

AFM-type diagrams will be extensively used for discussing metamorphism in metapelitic rocks in Chap. 7.

### 2.5.3.5 ACF Projections

Composition phase diagrams for assemblages in marbles, calc-silicate rocks, calcareous metapelites and other rocks with calcic phases such as mafic rocks, can be prepared, for example, for a simple CFMAS system. Calcic phases may include amphiboles, plagioclase, epidote, diopside and carbonate minerals. A graphic representation of the phase relationships can, for instance, be made by projecting from quartz (if present in excess) and from a  $\text{CO}_2$ - $\text{H}_2\text{O}$  fluid phase of constant composition onto the mole fraction triangle  $\text{Al}_2\text{O}_3$ - $\text{CaO}$ - $\text{FeO}$  (ACF diagram, Fig. 2.13). The ACF diagram is also a projection parallel to the  $\text{FeMg}_{-1}$  exchange vector. All minerals of the AFM system can also be represented on ACF diagrams provided that one also projects through muscovite or K-feldspar. The coordinates of mineral compositions can be calculated as explained above for the MSH and KFMASH systems, respectively. Figure 2.14 is a typical ACF diagram, showing phase relationships at a certain pressure and temperature. The tschermak variation is parallel to the AF binary and affects mainly chlorite and amphibole (and pyroxene which is not present at the  $P$ - $T$  conditions of the figure). The three-phase fields Pl + Am + Grt and Ky + Grt + Pl are separated by a two-phase field Grt + Pl because of  $\text{CaMg}_{-1}$ -substitution in garnet (grossular component). Both garnet and plagioclase show no compositional variation along the TS exchange vector. Any mineral which can be described by the components  $\text{K}_2\text{O}$ - $\text{CaO}$ - $\text{FeO}$ - $\text{MgO}$ - $\text{Al}_2\text{O}_3$ - $\text{SiO}_2$ - $\text{H}_2\text{O}$ - $\text{CO}_2$  can be represented on an ACF diagram such as Fig. 2.13. However, the consequences of  $\text{FeMg}_{-1}$  substitution in minerals cannot be discussed by means of ACF diagrams. Therefore, any discontinuous reaction relationship deduced from an ACF diagram is in reality continuous and dependent on the Fe-Mg variation (if it involves Fe-Mg minerals). For example, replacement of the Pl-Grt tie line by a more stable tie line between kyanite and amphibole can be related to the

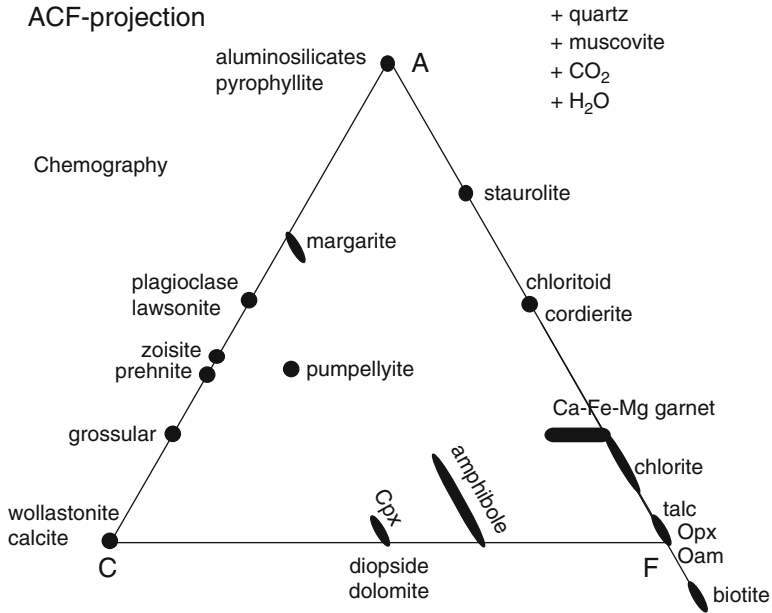


**Fig. 2.13** Coordinates of phase compositions in the  $(K_2O)-CaO-FeO-MgO-Al_2O_3-SiO_2-H_2O-CO_2$  system projected through (muscovite), quartz,  $CO_2$  and  $H_2O$  and parallel to the  $MgFe_{-1}$  exchange vector onto the plane  $Al_2O_3, FeO$  and  $MgO$  (ACF projection). *Upper* coordinates of some ACF phase compositions; *lower* phase relationships among some typical ACF phases at a specified pressure and temperature

reaction:  $Pl + Grt \Rightarrow Am + Ky \pm Qtz \pm H_2O$ . Equilibrium of the reaction, however, depends not only on pressure and temperature but also on the Fe–Mg variation in garnet and amphibole. The projection coordinates of a selection of mineral compositions is shown in the chemograph above Fig. 2.13.

In Fig. 2.14, the same mineral chemography is shown together with two protolith compositions listed in Table 2.3. As the  $P-T$  conditions shown on Fig. 2.14 are those of the amphibolite facies (Barrovian kyanite zone) conditions, it can be seen that metamorphosed MOR basalt, would consist of  $Pl + Am + Grt$  and would be rich in amphibole. The platform carbonate plots in the  $Cal + Am + Zo$  triangle.

**2.5.3.6 Other Projections**

Any other graphic representation of phase relationships on composition phase diagrams can be prepared by the procedure outlined above. The type of graphic representation of assemblages is entirely dictated by the material one is working with and by the problem one wants to solve. The following steps are a guide to the production of adequate phase composition diagrams.

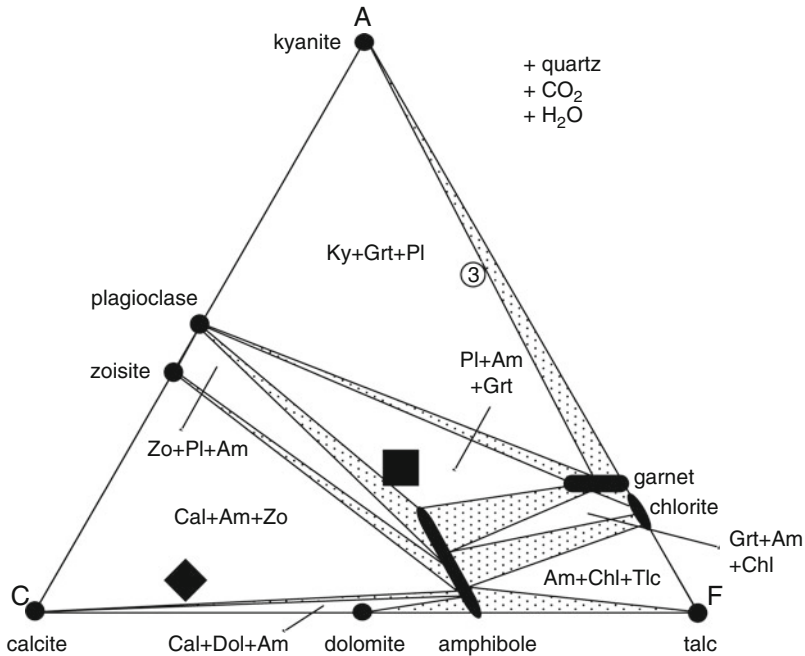


**Fig. 2.14** ACF projection of phase relationships of typical ACF phases at a specified pressure and temperature (same as lower diagram in Fig. 2.13). MORB composition projected at *black square*, platform carbonate at *black diamond* (rock compositions listed in Table 2.3)

1. Group the collected rocks in populations with similar bulk compositions, e.g. “normal” metapelites, metabasalts, etc.
2. Identify minerals which are present in the majority of a given group of rocks (e.g. muscovite and quartz in metapelites). Special assemblages require a special treatment, e.g. in quartz-absent corundum-bearing metapelites one may project through corundum onto an QFM plane.
3. If the excess minerals are not composed of simple oxide components, rewrite the composition matrix in terms of the compositions of the excess phases and the desired compositions at the corners of the mole fraction triangle selected as the new projection plane.
4. Delete rows in the composition matrix containing the excess phases and renormalize the column vectors. Draw the diagram and keep in mind the proper distribution of one- two- and three-phase fields. Do not forget to write the compositions of the projection phases on the diagram (without this information your figure is meaningless).

**In Part II** we will make extensive use of various kinds of composition phase diagrams.

## References and Further Reading

### *Cited References*

- Bishop DG (1972) Progressive metamorphism from prehnite-pumpellyite to greenschist facies in the Danseys Pass area, Otago, New Zealand. *Geo Soc Am Bull* 83:3177–3198
- Carmichael RS (1989) Practical handbook of physical properties of rocks and minerals. CRC Press, Boca Raton, 834 pp
- Fettes D, Desmons J (eds) (2007) Metamorphic rocks – a classification and glossary of terms; recommendations of the International Union of Geological Sciences Subcommittee on the systematics of metamorphic rocks. Cambridge University Press, New York, pp 244
- Turnbull IM, Mortimer N, Craw D (2001) Textural zones in the Haast Schist—a reappraisal. *NZ J Geol Geophys* 44:171–183

### *Further Reading*

- Ashworth JR (1985) Migmatites. Blackie, Glasgow, 301 pp
- Bell TH, Johnson SE (1992) Shear sense: a new approach that resolves conflicts between criteria in metamorphic rocks. *J Metamorph Geol* 10:99–124
- Brodie KH, Rutter EH (1985) On the relationship between deformation and metamorphism with special reference to the behaviour of basic rocks. In: Thompson AB, Rubie DC (eds) *Advances in physical geochemistry*. Springer, Berlin, Heidelberg, New York, pp 138–179
- Cooke RA, O'Brien PJ, Carswell DA (2000) Garnet zoning and the identification of equilibrium mineral compositions in high-pressure-temperature granulites from the Moldanubian Zone, Austria. *J Metamorph Geol* 18:551–569
- Greenwood HJ (1975) Thermodynamically valid projections of extensive phase relationships. *Am Mineralog* 60:1–8
- Kisch HJ (1992) Development of slaty cleavage and degree of very low-grade metamorphism: a review. *J Metamorph Geol* 9:735–750
- Orville PM (1969) A model for metamorphic differentiation origin of thin-layered amphibolites. *Am J Sci* 267:64–68
- Rudnick RL, Gao S (2003) Nature and composition of the continental crust. In: *Treatise on geochemistry*, vol 3. Elsevier, Amsterdam, pp 1–64
- Selverstone J (1993) Micro- to macroscale interactions between deformational and metamorphic processes, Tauern Window, Eastern Alps. *Schweiz Miner Petrogr Mitt* 73:229–239
- Spear FS (1988) Thermodynamic projection and extrapolation of high-variance assemblages. *Contrib Mineralog Petrol* 98:346–351
- Spear FS (1999) Real-time AFM diagrams on your Macintosh. *Geol Mater Res* 1:1–18
- Spear FS, Rumble D III, Ferry JM (1982) Linear algebraic manipulation of n-dimensional composition space. In: Ferry JM (ed) *Characterization of metamorphism through mineral equilibria*, vol 10, *Reviews in mineralogy*. Mineralogical Society of America, Washington, DC, pp 53–104
- Spry A (1969) *Metamorphic textures*. Pergamon Press, Oxford
- Thompson JB (1957) The graphical analysis of mineral assemblages in pelitic schists. *Am Mineralog* 42:842–858
- Thompson JB (1982) Composition space; an algebraic and geometric approach. In: Ferry JM (ed) *Characterization of metamorphism through mineral equilibria*, vol 10, *Reviews in mineralogy*. Mineralogical Society of America, Washington, DC, pp 1–31

- Tracy RJ, Robinson P (1983) Acadian migmatite types in pelitic rocks of Central Massachusetts. In: Atherton MP, Gribble CD (eds) *Migmatites, melting and metamorphism*. Shiva, Nantwich, pp 163–173
- Williams ML (1994) Sigmoidal inclusion trails, punctuated fabric development and interactions between metamorphism and deformation. *J Metamorph Geol* 12:1–21
- Zeck HP (1974) Cataclastites, hemiclastites, holoclastites, blasto-ditto and myloblastites – cataclastic rocks. *Am J Sci* 274:1064–1073

## Chapter 3

# Metamorphic Processes

Rock metamorphism is always associated with processes and changes. Metamorphism reworks rocks in the Earth's crust and mantle. Typical effects of rock metamorphism include:

- Minerals and mineral assemblages originally not present in a rock may form, the new mineral assemblages grow at the expense of old ones. Consequently older minerals may disappear (e.g. metapelitic gneiss may originally contain Sil + Grt + Bt. A metamorphic event transforms this rock into one that contains Crd + Grt + Bt in addition to the Qtz and Fsp that also have been previously present in the rock; the old rock contained Sil, the new one Crd).
- The relative abundance of minerals in a rock may systematically change and the new rock may have a different modal composition (metamorphism may increase the amount of Crd present in the rock and decrease the volume proportion of Grt + Bt).
- Metamorphic minerals may systematically change their composition (e.g. the  $X_{\text{Fe}}$  of Grt and Crd may simultaneously increase during metamorphism).
- The structure of rocks in crust and mantle may be modified (e.g. randomly oriented biotite flakes may be parallel aligned after the process).
- The composition of the bulk rock may be altered during metamorphism by adding or removing components to, or from the rock from a source/sink outside the volume of the rock considered (e.g. removing  $\text{K}_2\text{O}$ ,  $\text{MgO}$  and  $\text{FeO}$  dissolved in a coexisting aqueous solution from a Grt + Crd + Bt rock may result in the formation of sillimanite).

Typical changes in the modal composition of rocks and in the chemical composition of minerals that constitute the rocks are caused by heterogeneous chemical reactions progressing in the rocks. The principles of metamorphism are, therefore, strongly related to the principles of chemical reactions. Mineral- and rock-forming metamorphic processes are mainly controlled by the same parameters that control chemical reactions. Metamorphic petrology studies reaction and transport processes in rocks. Metamorphic processes are caused by transient chemical, thermal and mechanical disequilibrium in confined volumes of the Earth's crust and mantle. These disequilibrium states ultimately result from large-scale geological processes and the dynamics of the Earth's planetary system as a whole. Metamorphic processes

always result from disequilibrium and gradients in parameters that control reaction and transport in rocks; they cease when the rocks reach an equilibrium state. Chemical reaction is always inherent in the term metamorphism. The term metamorphosis actually means transformation, modification, alteration, conversion and thus is clearly a process-related expression.

Metamorphism is a very complex occurrence that involves a large number of chemical and physical processes at various scales. Metamorphic processes can be viewed as a combination of (1) chemical reactions between minerals and between minerals and gasses, liquids and fluids (mainly H<sub>2</sub>O) and (2) transport and exchange of substances and heat between domains where such reactions take place. The presence of an aqueous fluid phase in rocks undergoing metamorphism is critical to the rates of both chemical reactions and chemical transport. Consequently, an advanced understanding of metamorphism requires a great deal of insight into the quantitative description of chemical reactions and chemical transport processes, especially reversible and irreversible chemical thermodynamics.

The term metamorphism as it is related to processes, changes and reactions clearly also includes the aspect of time. Metamorphism occurs episodically and is particularly related to mountain-building or orogenic episodes at convergent plate margins (collision zones) and during subsequent uplift and extension of continental crust, but also during sea-floor spreading and continental rifting.

### 3.1 Principles of Metamorphic Reactions

In the following we briefly explain some basic aspects of metamorphic reactions and introduce some elementary principles that are essential for a basic understanding of metamorphism. The treatment is not sufficient for a thorough understanding of metamorphic processes and chemical reactions in rocks. It is therefore recommended for the reader who needs to know more, to study textbooks on chemical thermodynamics (e.g. Guggenheim 1986; Lewis and Randall 1961; Moore 1972; Prigogine 1955; Denbigh 1971) or textbooks that deal particularly with the application of thermodynamics to mineralogy and petrology (Ferry 1982; Fraser 1977; Greenwood 1977; Lasaga and Kirkpatrick 1981; Powell 1978; Saxena and Ganguly 1987; Wood and Fraser 1976). We recommend Chatterjee (1991), Fletcher (1993), Nordstrom and Munoz (1994), Anderson and Crerar (1993), and Ganguly (2008).

First, let us consider, for example, a rock that contains the minerals albite and quartz. The Ab–Qtz rock is located at a certain depth in the crust (e.g. at point T<sub>h</sub> = 1.25 GPa, 550°C in Fig. 3.1). At that given pressure and temperature the two minerals (phases) are associated with unique values of molar Gibbs free energy. The Gibbs free energy, usually abbreviated with the symbol **G**, is a thermodynamic potential with the dimension joules/mole (energy/mole) and it is a function of pressure and temperature. The free energy of minerals and their mixtures are negative quantities (because they refer to the free energy of formation from the elements or oxides rather than absolute energies, e.g. *G* of albite at 900 K and

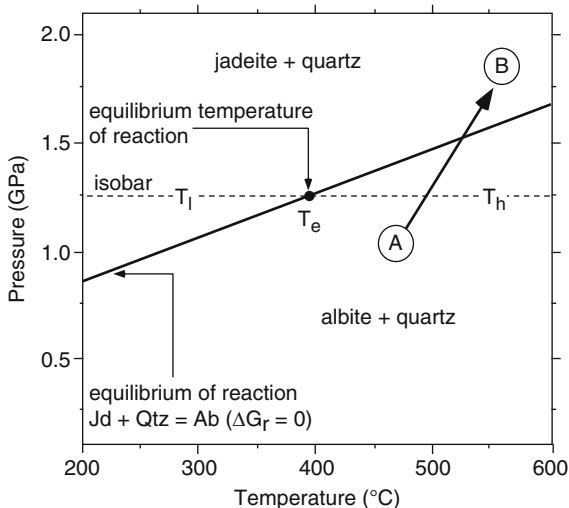


**Fig. 3.1** Pressure–temperature diagram showing equilibrium conditions of the reaction jadeite + quartz = albite

0.1 MPa is  $-3,257.489$  kJ/mol). The considered Ab + Qtz rock can be formed by mechanically mixing, for example, 1 mol albite and 1 mol quartz. All rocks represent, thermodynamically speaking, mechanical mixtures of phases and are therefore heterogeneous thermodynamic systems.<sup>1</sup> The phases, in turn, can be viewed as chemically homogeneous sub-spaces of the considered system, e.g., a volume of rock. Minerals, aqueous fluids, gasses and melts are the thermodynamic phases in rocks. These phases are usually chemical mixtures of a number of phase components (most minerals are solid chemical solutions and show a wide range in composition). In our example, albite and quartz shall be pure  $\text{NaAlSi}_3\text{O}_8$  and  $\text{SiO}_2$  respectively. The total free energy of the rock is the sum of the free energies of its parts, that is in our case,  $n_{\text{Ab}}G_{\text{Ab}} + n_{\text{Qtz}}G_{\text{Qtz}}$  (where  $n_i$  = number of moles of substance  $i$ ). The rock is characterized by a unique value of  $G$  and, by taking 1 mole of each substance, its total composition is  $\text{NaAlSi}_4\text{O}_{10}$ . However, the composition of such a mechanical mixture ( $\equiv$  rock) can also be obtained by mixing (powders of) jadeite ( $\text{NaAlSi}_2\text{O}_6$ ) and quartz in the appropriate proportions. It is clear also that this rock has a unique Gibbs free energy at the given pressure and temperature and that it corresponds to the sum of  $G_{\text{Jd}} + 2G_{\text{Qtz}}$ . The free energy of the Ab–Qtz rock may be designated  $G_{\text{AQ}}$  and that of the Jd–Qtz rock  $G_{\text{JQ}}$ . The Gibbs free energies of the two rocks at  $P$  and  $T$  can be calculated from (3.1) and (3.2) provided that the free energy values of the three minerals can be calculated for that  $P$  and  $T$ :

<sup>1</sup>The thermodynamic description of heterogeneous systems has been developed and formulated mainly by W. Gibbs (1878, 1906). Gibbs scientific contributions were fundamental for the development of modern quantitative petrology.



$$G_{AQ} = G_{Ab} + G_{Qtz} \quad (3.1)$$

$$G_{JQ} = G_{Jd} + 2G_{Qtz} \quad (3.2)$$

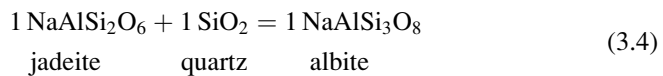
The Gibbs free energies of the three minerals at P and T can be calculated from thermodynamic data and equations of state given by the laws of chemical thermodynamics. The question one may ask now is, which one of the two possible rocks, the albite + quartz rock or the jadeite + quartz rock, will be present at the conditions  $T_h$  (Fig. 3.1). According to the thermodynamic laws it is always the mixture with the lowest total free energy at the prevailing conditions that is the **stable** mixture (assemblage) while the other mixture is **metastable**. These laws can be summarized and expressed by the following statement:

The chemical components (constituents) making up the bulk composition of a rock are distributed into a group of homogeneous phases, (minerals and fluid(s)), that constitute the assemblage with the lowest Gibbs free energy for the system at that given pressure and temperature. This assemblage is called the equilibrium phase assemblage.

At  $T_h$ ,  $G_{AQ}$  is more negative than  $G_{JQ}$  and thus the albite + quartz rock is stable, while the jadeite + quartz assemblage is metastable or less stable than Ab + Qtz. The free energy difference of the two rocks can be calculated by subtracting (3.2) from (3.1):

$$\Delta G = G_{AQ} - G_{JQ} = G_{Ab} - G_{Jd} - G_{Qtz} \quad (3.3)$$

$\Delta G$  is the free energy difference of the two rocks with identical composition but different mineral content. The minerals of the two rocks are connected by a reaction that can be expressed by the stoichiometric equation:



The stoichiometric coefficients in this particular reaction equation are all equal to 1. The equation suggests that albite in the Ab + Qtz rock that is stable at  $T_h$  may decompose to jadeite + quartz at some other conditions than  $T_h$ . Similarly, the reaction (3.4) describes the formation of 1 mol Na-feldspar from 1 mol jadeite + 1 mol quartz. The free energy change of the reaction  $\Delta G_r$  is calculated from:

$$\Delta G_r = G_{Ab} - G_{Jd} - G_{Qtz} \quad (3.5)$$

By convention, the stoichiometric coefficients on the right hand side of a reaction equation are always taken as positive, while those on the left hand side are taken as negative. In the example given here the energy difference of the two rocks (3.3) is identified as the free energy change of the albite-forming reaction.

$\Delta G_r$  is, like  $G$  of the individual phases, a function of  $P$  and  $T$ . Three basic cases may be distinguished:

$$\Delta G_r < 0 \quad (3.6)$$

At all pressure and temperature conditions that satisfy (3.6) the products of the reaction are stable and the reactants are metastable. At  $T_h$ ,  $\Delta G_r$  is negative and  $Ab + Qtz$  constitute the stable assemblage. A rock with  $Jd + Qtz$  is metastable at  $T_h$ .

$$\Delta G_r > 0 \quad (3.7)$$

At all conditions that satisfy (3.7) the reactants of the reaction are stable and the products are metastable. At  $T_l$ ,  $\Delta G_r$  is positive and  $Jd + Qtz$  constitute the stable assemblage (Fig. 3.1). A rock with  $Ab + Qtz$  is metastable at  $T_l$ .

$$\Delta G_r = 0 \quad (3.8)$$

At all conditions that satisfy (3.8) the reactants and products of the reaction are simultaneously stable. These conditions are referred to as the **equilibrium conditions of the reaction**. In Fig. 3.1, the equilibrium condition of the reaction expressed by (3.8) is represented by a straight line. Along that line all three minerals are simultaneously stable. At a pressure of 1.25 GPa, the equilibrium temperature of the reaction is 400°C and corresponds to the point  $T_e$  along the isobar of Fig. 3.1. At this unique temperature the rock may contain all three minerals in stable equilibrium. At any temperature other than  $T_e$  the reaction is not at equilibrium and it will proceed in such a way as to produce the assemblage with the most negative free energy for the given temperature. In Fig. 3.1, the equilibrium line of the reaction divides the  $P$ - $T$  space into two half spaces with two distinct stable assemblages. In this way, the  $P$ - $T$  diagram represents a Gibbs free energy map of the considered system. Like a topographic map where the surface of the Earth is projected along a vertical axis, a  $P$ - $T$  phase diagram represents a map where the lowest Gibbs free energy surface of the system is projected along the  $G$ -axis onto the  $P$ - $T$  plane.

At equilibrium, the mineralogical composition of a rock is entirely dictated by its composition, the pressure and the temperature. If temperature and pressure change, new assemblages may have a lower Gibbs free energy, and chemical reaction will replace the old assemblage by a new, more stable assemblage. A rock always tries to reach a state of equilibrium by minimizing its Gibbs free energy content. This is accomplished by readjusting the mineralogy or the composition of minerals if necessary.

Stable assemblages cannot be distinguished from metastable ones by any petrographic technique, and metastable equilibria cannot be separated from stable equilibria. This becomes obvious if we look at a rock sample collected on a rainy day that contains the three Al-silicate minerals, kyanite, andalusite, sillimanite in addition to quartz. All three Al-silicates are metastable in the presence of quartz and water under

surface conditions relative to the *hydrous* Al-silicate, kaolinite. In general, at some arbitrary metamorphic  $P$ - $T$  condition only one Al-silicate + quartz can be stable, the other two possible two-phase assemblages must be metastable. Metastable persistence of metamorphic minerals and assemblages is common in metamorphic rocks. This is, of course, an extremely fortunate circumstance for metamorphic petrologists. Rocks that formed in the deep crust or mantle with characteristic high-pressure and high-temperature mineral assemblages may be collected at the Earth's surface. If metastable assemblages were not common in metamorphic rocks we would find only low- $P$ - $T$  rocks at the surface. Metastable assemblages may even survive over geological time scales (hundreds of millions of years). It is obvious from Fig. 3.1 that a rock containing Jd + Qtz is metastable under conditions at the surface of the Earth. However, rocks containing Jd + Qtz are found at surface outcrops and provide evidence that they were formed originally at very high pressures.

Some criteria and methods to detect **disequilibrium** in rocks do exist, however. One may distinguish two main kinds of disequilibrium; structural or textural disequilibrium and chemical disequilibrium. Structural disequilibrium is indicated by distinct shapes and forms of crystals and spatial distribution and arrangement of groups of minerals in heterogeneous systems. Structural disequilibrium may be found in rocks that underwent chemical reactions or successive series of reactions that all ceased before equilibrium structures developed and overall chemical equilibrium was reached. For example, zoned minerals with relic, often resorbed cores, representing an earlier metamorphism overgrown and partly replaced by compositionally different rims that formed during later metamorphism. Many different kinds of compositional features of metamorphic rocks and minerals may indicate chemical disequilibrium. As an illustration we can use our Jd + Qtz example again, except that in this case the rock that contains omphacite (Omp) + quartz (sodium-rich clinopyroxene where jadeite is present as a phase component). Independent information suggests that this example rock formed at about 600°C. The rock may also contain pure albite in domains, local patches or veins and its composition clearly indicates chemical disequilibrium. The minerals Omp + Ab + Qtz never coexisted in stable or metastable equilibrium because the pyroxene contains a calcic component (diopside) and the feldspar does not (the phase component anorthite is not present in Pl). However, at the inferred temperature of 600°C, plagioclase in an omphacite-bearing rock should, in an equilibrium situation (stable or metastable), contain some anorthite component. The presence of albite in such a rock must be related to some metamorphic process that progressed under conditions other than the equilibration of the Omp + Qtz assemblage. It is, on the other hand, important to note that the assemblage Omp + Qtz + Ab represents an overall disequilibrium but the assemblages Omp + Qtz and Ab + Qtz may well be equilibrium assemblages that equilibrated at different times at different  $P$ - $T$  conditions. The question of equilibrium is always related to the scale of equilibrium domains. Disequilibrium may exist between large rock bodies in the crust, layers of rocks of different composition in an outcrop, between local domains of a thin section or between two minerals in mutual grain contact. Any chemically zoned mineral also represents disequilibrium. At some scale there is always disequilibrium at any time.

Chemical properties of coexisting minerals in a rock are often used to help resolve the question of equilibrium. As an example, a series of garnet–biotite pairs have been analyzed from a homogeneous Grt–Bt schist and the data are schematically shown in Fig. 3.2. The data pairs can be arranged into two groups. *Group a* represents matrix biotite in contact with the rim of garnet; *group b* represents analyses of biotite grains included in the core of the garnet. Overall chemical equilibrium (stable or metastable) between garnet and biotite requires that both minerals have a uniform composition in the rock. Crossing tie lines are inconsistent with overall equilibrium. However, it is evident that the Grt–Bt pairs from each group are not in conflict with the requirements of chemical equilibrium. They are likely to constitute two different **local equilibrium** systems. However, the Grt–Bt pair connected with a dashed line in Fig. 3.2 shows crossing tie-line relationships within *group a* pairs and clearly represents a disequilibrium pair. Note that the absence of crossing tie-line relationships does not necessarily prove that the rock was in a state of overall equilibrium. The lack of obvious disequilibrium phenomena can be taken as evidence for, but not proof of, equilibrium.

Metastable persistence of minerals and mineral assemblages and also the obvious disequilibrium features in many rocks reflects the controlling factors and circumstances of reaction kinetics. The rate of a mineral reaction may be slower than the rate of, e.g., cooling of a volume of rock. Lacking activation energy for reaction in cooling rocks and nucleation problems of more stable minerals typically affects reaction kinetics. The kinetics of reactions in rocks is extremely sensitive to the presence or absence of H<sub>2</sub>O. Aqueous fluids serve as both a solvent and a reaction medium for mineral reactions. For example, if kyanite-bearing rocks are brought to pressure and temperature conditions where andalusite is more stable than kyanite, kyanite may be replaced by andalusite in rocks containing a free aqueous fluid in the pore space or along grain boundaries, whilst andalusite may fail to form in fluid-absent or dry rocks.

It is commonly reasonable to assume that during **prograde** metamorphism rocks pass through successive sequences of equilibrium mineral assemblages. These sequences can be viewed as a series of stages, each of them characterized by an equilibrium assemblage and the different stages are connected by mineral reactions.

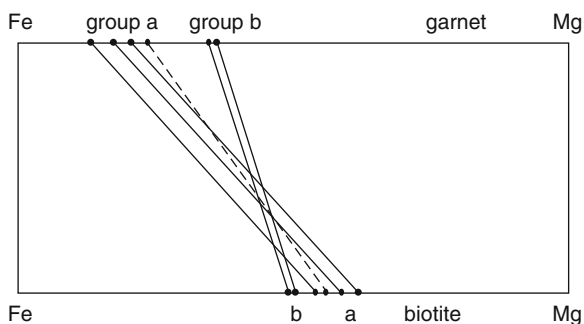


**Fig. 3.2** Schematic diagram showing the Fe–Mg distribution between coexisting garnet and biotite pairs in a single rock

This assumption is founded on convincing evidence that prograde metamorphism takes place under episodic or continuous water-present conditions. One would therefore expect to find disequilibrium and metastable assemblages particularly in rocks that were metamorphosed under fluid-absent or fluid-deficient conditions. Aqueous fluids are typically not present in cooling rocks after they have reached maximum metamorphic pressure and temperature conditions. Textural and chemical disequilibrium is also widespread in very high-grade rocks of the granulite facies that have lost their hydrous minerals and aqueous fluids during earlier stages of prograde metamorphism. Microstructures such as reaction rims, symplectites, partial replacement, corrosion and dissolution of earlier minerals are characteristic features of granulite facies rocks. They indicate that, despite relatively high temperatures (700–900°C), equilibrium domains were small and chemical communication and transport were hampered as a result of dry or H<sub>2</sub>O-poor conditions.

To further illustrate some aspects of disequilibrium, we may consider large bodies of incompatible rock types in the crust. In many orogenic fold belts (e.g. Alps, Caledonides, Tianshan) mantle-derived ultramafic rock fragments were emplaced in the continental crust during the collision phase and stacking of nappes. Mantle fragments (harzburgites, lherzolites, serpentinites) of various dimensions can be found as lenses in granitic crust (Fig. 3.3). Forsterite (in the mantle fragment) + quartz (in the crustal rocks) is metastable relative to enstatite at any geologically accessible pressure and temperature conditions. The presence of Fo-bearing mantle rocks in Qtz-rich crustal rocks represents a large-scale disequilibrium feature. Chemical mass transfer across the contact of the incompatible rock types results in the formation of shells of reaction zones that encapsulate the mantle fragment. The nature of the minerals found in the reaction zones depends on the *P–T* conditions at the reaction site. In our example, the reaction shells may consist of

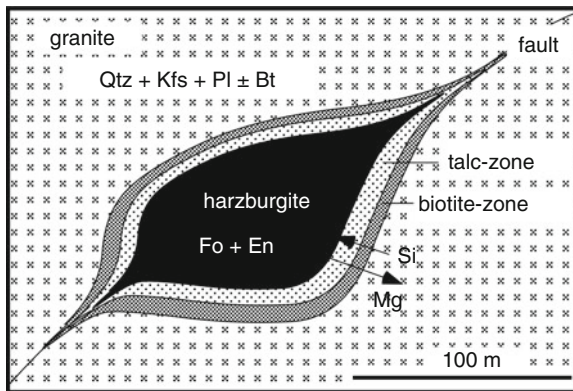


**Fig. 3.3** Large-scale disequilibrium between a tectonic lens of harzburgite (ultramafic rock fragment from the upper mantle) in granitic (gneissic) crust. The harzburgite lens is enveloped by protective shells of talc and biotite. These shells were produced by chemical reaction between incompatible rocks (rocks of radically different compositions) and their formation required transfer of, e.g. Si from granite to harzburgite and Mg from harzburgite to granite

tal- and biotite-rich zones that are typically nearly monomineralic (Fig. 3.3). Biotite-, chlorite- or amphibole-rich zones that form as a result of disequilibrium on a macroscopic scale and subsequent chemical transport and reaction are also known as blackwall. The process is one of contact metasomatism, Chemical communication, transport and reaction are most efficient if aqueous fluids are present in excess and wet the grain boundaries in the incompatible rock bodies. Metasomatism proceeds until the incompatible mineralogy has been used up by the process or the rocks lose their aqueous fluid phase. In rocks with dry grain boundaries, diffusional mass transfer is extremely slow and inefficient even over geological time spans.

Returning again to the Jd–Qtz–Ab example. At the conditions of point A in Fig. 3.1, a rock containing Ab + Qtz is more stable than a rock composed of Jd + Qtz. Consider an Ab + Qtz rock that has reached a state of chemical and structural (textural) equilibrium at conditions of point A. The assemblage of this rock may be replaced by Jd + Qtz by reaction (3.4) if the rock is brought to the conditions at point B (increasing temperature and pressure during prograde metamorphism). It is obvious that a transfer from A to B would shift the Ab + Qtz rock into the field where Jd + Qtz represents the stable assemblage. The causes of such changes in P and T are explained in the following section.

## 3.2 Pressure and Temperature Changes in Crust and Mantle

### 3.2.1 General Aspects

Changes in pressure and temperature are the prime causes of metamorphism. This raises the question: what kind of geologic processes lead to changes in pressure and temperature in the crust or the mantle?

In a general way, such changes are caused by some force that acts on rocks (driving force: driving the process or change). Any kind of force applied to a rock will cause some flow or transfer of a property in such a way as to reduce the size of the applied force.

Temperature differences between volumes of rocks result in the transfer of heat (heat flow) from hot rock to cold rock until both rocks reach the same temperature. A simple linear equation describes this process:

$$J_Q = -L_Q \nabla T \quad (3.9)$$

Equation (3.9) states that a non-uniform temperature distribution in a system will transfer heat (Q) in the direction normal to the isotherms of the temperature field and from high temperature to low temperature in order to decrease the temperature difference. The linear equation (known as Fourier's law) describes heat flow in systems with small temperature differences (such as most geologic systems).  $L_Q$  is

a material-dependent constant related to the thermal conductivity of the material  $\kappa$ .  $J_Q$  is the rate of heat transfer per unit area (heat flow vector) parallel to the highest gradient in the temperature field ( $J_Q = \partial Q / \partial t$ ).  $\nabla T$  represents the gradients in temperature in the three-dimensional space. If there are only linear temperature gradients in one direction, the  $\nabla T$  in (3.9) reduces to  $(T_{x1} - T_{x2})$ , the temperature difference between two points. The general expression presented above shows that gradients in intensive variables in a system ultimately cause “processes” and “changes”, geological or other. As metamorphism is mainly related to chemical reactions in rocks that are largely controlled by changes in temperature, pressure and rock composition, it is useful to discuss geological aspects of heat transfer, pressure changes and chemical mass transfer in the crust and mantle in some detail.

### 3.2.2 Heat Flow and Geotherms

Fourier’s law states that heat will be transported from a place at high temperature to an area at low temperature. In the case of the Earth, and looking at it on a large scale, there is a hot interior and a cold surface. This necessarily results in transport of heat from the center to the surface. The surface of the earth is at a nearly constant temperature (about 10°C) and the core mantle boundary is probably also at a constant temperature as a result of the liquid state of the outer core that permits very rapid convection and heat transport. The general situation is depicted in Fig. 3.4. A consequence of the temperature difference between the two surfaces is a steady and continuous heat flow from the interior to the surface.

Heat flow is measured in watt per square meter ( $W/m^2$ ); however, in the literature heat flow data are often given in “HFU” (heat flow units). A HFU is defined as  $\mu\text{cal cm}^{-2} \text{s}^{-1}$ , that is equivalent to  $4.2 \mu\text{J s}^{-1} \text{cm}^{-2}$  or  $0.042 \text{J s}^{-1} \text{m}^{-2}$ .

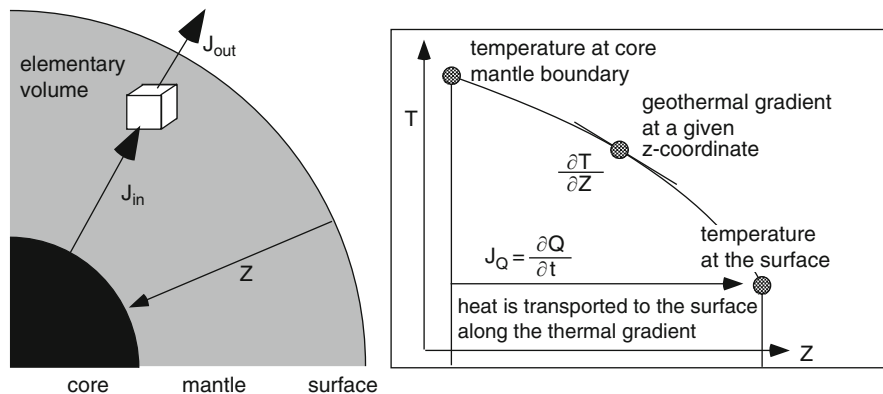


Fig. 3.4 Conductive heat transfer between hot interior and cold surface of the Earth

Because  $J/s^2$  is equivalent to W (watt), it follows that 1 HFU is equal to  $0.042 W/m^2$ . (or more convenient  $42 mW/m^2$ ).

The heat flow from the interior of the Earth is on the order of  $30 mW/m^2$ . However, heat flow measurements at the surface of the Earth vary between about  $30$  and  $120 mW/m^2$ . The total heat flow at the surface is composed of a number of contributions: (1) heat flow from the interior resulting from conductive heat transport as described by Fourier's law, (2) transport of heat by convective mass flow in the mantle (Fig. 3.5), (3) transport of heat generated by decay of radioactive elements.

The continental crust consists mostly of granitic rocks that produce about  $30 mJ$  heat per kilogram and year. Oceanic crust, that is generally composed of basaltic rocks, produces about  $5 mJ$  heat per kilogram and year, whereas mantle rocks produce only a small amount of radioactive heat (ca.  $0.1 mJ$  heat per kilogram and year). The extra heat produced in the crust by decay of radioactive elements thus contributes significantly to the observed heat flow at the surface.

Heat flow through a specified volume of the crust may occur under the following conditions:

- (a) Heat flow into the crustal volume is equal to the heat flow out from that volume. In this case the temperature in the volume remains constant. The temperature profile along thermal gradient  $z$  in Fig. 3.4 is independent of time (**steady-state geotherm**).

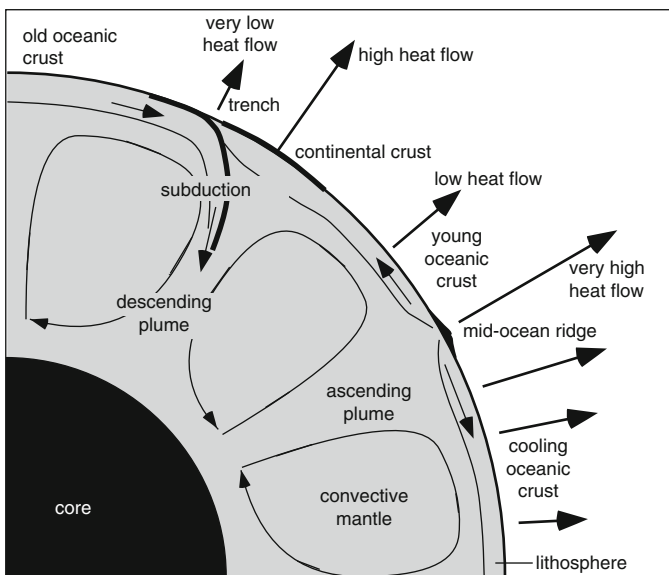


**Fig. 3.5** Modification of steady-state heat flow resulting from conductive heat transfer by active tectonic processes. Heat flow at the surface varies by a factor of 4



- (b) Heat flow into the crustal volume is greater than the heat flow out from that volume. The excess heat put into the crustal volume will be used in two different ways: (1) to increase the temperature of the rock volume, (2) to drive endothermic chemical reactions in rocks.
- (c) Heat flow into the crustal volume is lower than the heat flow out of the volume. In this case the heat loss of the volume of rock results in a temperature decrease (the rock cools). In this situation exothermic chemical reactions may produce extra heat to some extent. These reactions have the effect of preventing the rocks from cooling.

Different heat flow at the surface also has the consequence that rocks at the same depth in the crust and upper mantle may be at different temperatures leading to lateral heat transport parallel to the earth surface (parallel to  $xy$ -surfaces). This is shown in Fig. 3.6. Along a profile from Denmark to southern Norway the observed surface heat flows have been used by Balling (1985) to model the temperature field in the crust and mantle shown in Fig. 3.6. Because flow vectors are always normal to the force field from which the flow results, the heat flow trajectories will roughly look like the flow vectors shown in Fig. 3.6. It is obvious from this two dimensional section that at a given point in the crust the heat flow has a vertical **and** a horizontal component. Also note that the MOHO under the mid-Paleozoic continental crust of central Europe (Denmark) is at about 700°C whereas the MOHO under the Precambrian crust of the Baltic Shield in the north is only at about 350°C. It follows that the base of continental crust may be at largely different temperatures

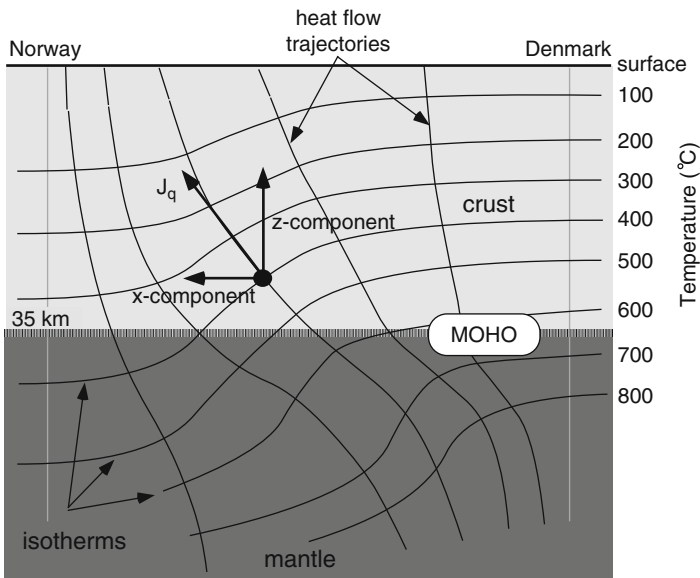


**Fig. 3.6** Modelled temperature field along a cross section from Denmark to Norway (After Balling 1985)

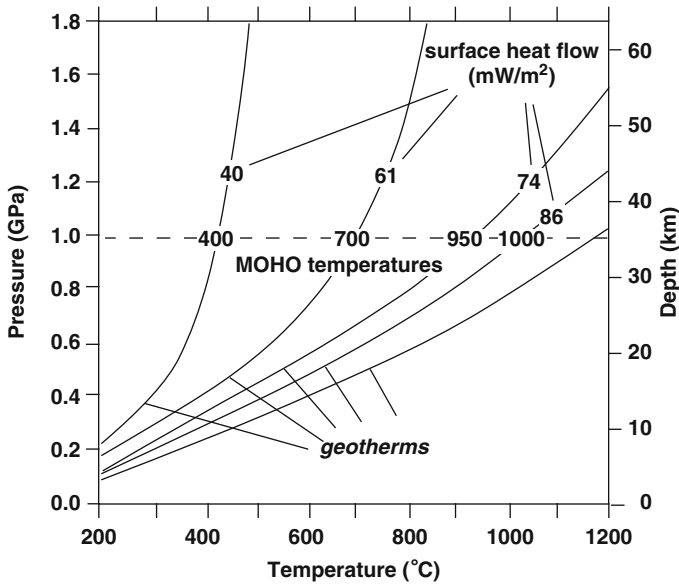


Fig. 3.7 Model geotherms with associated surface heat flow values and MOHO temperatures

depending on the state and evolutionary history of a lithosphere segment and on the thermal regime deeper in the mantle. Observed surface heat flows can be translated into geotherms that may be time-dependent geotherms or steady-state geotherms. Such model geotherms are shown in Fig. 3.7 together with typical associated surface heat flows and temperatures at an average MOHO depth beneath continents of about 35 km (1.0 GPa). The geotherms represent curves that relate temperature with depth. The geothermal gradient (expressed as  $dT/dz$ ) is the slope of the geotherm at a given depth in the crust or mantle and characterizes the temperature increase per or depth increment. In this book, you will see many  $P$ - $T$ -diagrams with  $T$  on the x-axis and  $P$  on the y-axis. Pressure increases proportional with depth (for details see Sect. 3.2.4). Thus steep geotherms (or paths of metamorphism) on these figures correspond to low geothermal gradients, flat geotherms represent high geothermal gradients. Geotherms have high gradients near the surface and the gradients become progressively lower with increasing depth.

### 3.2.2.1 Transient Geotherms

Temperature changes in the crust and mantle are caused by adding or removing extra heat to or from the rocks. Heat flow changes may have a number of geological causes. Deep-seated causes include changes in the relative positions of lithosphere plates and their continental rafts relative to mantle convection systems (Fig. 3.5). Collision of lithosphere plates may lead to subduction of oceanic crust and cause

abnormal thermal regimes. Collision of continental rafts leads to extreme crustal thickening (from 35 km of normal continental thickness to 70 km in active collision zones, active example: Himalayas). Smaller volumes of crust can be moved relative to each other, for instance during a continent–continent collision. The formation of nappes and the stacking of slices of crust are typical examples of redistribution of rocks in crust and mantle. A very efficient way to transfer large amounts of heat to the crust is the transport by melts (magmatic heat transfer). Large volumes of mantle-derived basaltic melt may underplate continental areas and release enormous amounts of latent heat of fusion during solidification. Heat transported to the crust by upward migrating magma chambers locally disturbs the thermal regime and the temperature field in the crust.

Also, all tectonic transport disturbs the pre-tectonic steady-state geotherm. At any one instant during active tectonics, the crust is characterized by a specific geotherm that relates temperature to depth. The geotherm is now changing with depth. These **transient geotherms** describe the temperature–depth relationship at a given time and for a given geographic location (xy-coordinates). Some aspects of tectonic transport and its effect on the instantaneous geotherm are depicted in Fig. 3.8. The figure shows schematically the temperature field along a cross section through an Andean-type convergent margin. The down-going slab of oceanic lithosphere is relatively cold. Thermal relaxation is a slow process compared to plate movement. The continental lithosphere above the subducted oceanic plate is characterized by a complex, thermally anomalous region that results from magmatic heat transfer and from smaller scale deformation in the crust (nappes). The geotherm at location **a** at a given instant (instantaneous geotherm) in the active history of the subduction event may look like the geotherm shown at the left side of Fig. 3.8. Tectonic transport may even be fast enough to create temperature inversion in a transient geotherm. Such temperature inversions will, however, be a very short-lived phenomena and they will be eliminated rapidly if subduction ceases.

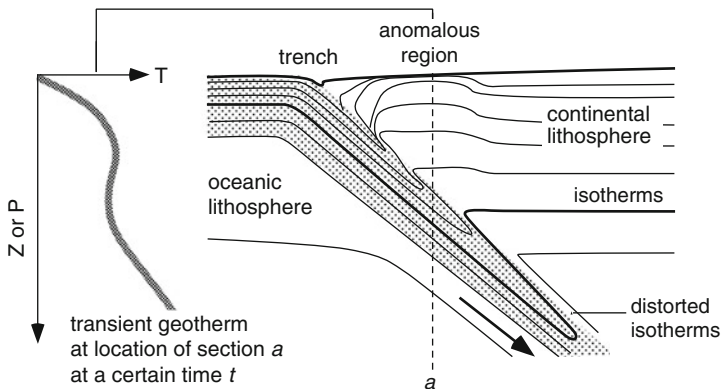


**Fig. 3.8** Isotherm configuration within a cross section through an Andean-type subduction zone and a transient geotherm at location **a** (Peacock 1990)

### 3.2.3 Temperature Changes and Metamorphic Reactions

If a crustal volume receives more heat than required to maintain a steady-state geotherm, the volume of rock will experience an increase in temperature and it will undergo **prograde metamorphism**. The heat capacity of the rock determines how much the temperature rises in relation to the heat added. Typical heat capacities for silicate rocks are on the order of 1 kJ per kg rock and °C. Suppose a quartzite layer in the crust receives 100 kJ/kg rock extra heat, this heat will increase the temperature of the quartzite by 100°C. When heated, some rocks must adjust their mineralogy by chemical reactions in order to maintain a state of minimized total Gibbs free energy (as explained above). These endothermic reactions will consume part of the heat added to the rock. Dehydration reactions are typical during prograde metamorphism. The reactions replace hydrous minerals (such as zeolites, micas, chlorite, amphibole) by less hydrous or anhydrous minerals and release H<sub>2</sub>O to a fluid phase. This fluid may or may not escape from the site of production. Such reactions are strongly endothermic and consume a large amount of heat (about 90 kJ/mol H<sub>2</sub>O released from hydrous minerals). Consider a layer of mica schist in the crust containing about 1 mol H<sub>2</sub>O/kg rock. A temperature increase of 100°C (as in the quartzite layer) may result in complete destruction of the hydrous minerals in this rock, and a total of 190 kJ/kg of schist is required to obtain the same temperature increase (100 kJ for the temperature increase and 90 kJ for the reaction).

The heat effect of mineral reactions in rocks also influences the temperature–time relationship in a volume of reactive rock. The case is illustrated in Fig. 3.9 using the  $Qtz + Jd \Rightarrow Ab$  reaction as an example. Supply of excess heat (in addition to the steady state heat flow) will cause an increase in temperature until the equilibrium conditions ( $T_e$ ) of the chemical reaction are reached. The heat input will then be used for the reaction<sup>2</sup> over a certain period of time and the temperature

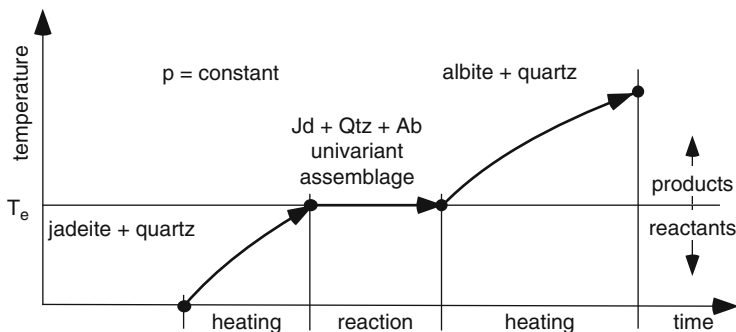


**Fig. 3.9** Diagram showing phase relationships between jadeite, quartz and albite as a function of time during a period of increased heat flow

<sup>2</sup>Note: the heat required for this type of H<sub>2</sub>O-absent reaction is much less than the heat consumption for a dehydration reaction discussed above.

remains constant until one of the two reactant minerals (in this case Jd) is used up. After completion of the reaction, the temperature of the rock will continue to increase. The effect is analogous to heating water to its boiling point. The temperature of the water increases to the boiling temperature as heat is added to the water. During boiling the water temperature remains constant and the heat is used to drive the reaction (phase transition) liquid water  $\Rightarrow$  steam. After all the water is boiled off, further addition of heat will increase the temperature of the steam.

If a crustal volume receives less heat than it requires to maintain a steady state geotherm, it will cool and the rocks will be potentially affected by **retrograde metamorphism**. During cooling, it may become necessary for the rock to change its mineralogical composition in order to maintain a state of minimum Gibbs free energy. In our example, for a rock consisting of Ab + Qtz, the reaction  $\text{Ab} \Rightarrow \text{Qtz} + \text{Jd}$  converts all albite into jadeite and quartz as the rock cools to  $T_c$  (Fig. 3.9) under equilibrium conditions. The heat released by the reaction buffers the temperature to a constant value ( $T_c$ ) until all Ab has been used up and further cooling can take place. The situation is analogous to removing heat from water. The temperature will decrease until water begins to freeze. As long as both reactant (liquid water) and product (ice) are present in the system, the temperature is confined to the freezing temperature. After conversion of all water into ice the temperature will continue to fall if further heat is removed from the ice.

### 3.2.4 Pressure Changes in Rocks

Normally, pressure in the crust and mantle is characterized by isobaric surfaces that are approximately parallel to the Earth's surface. As outlined above, the Gibbs free energy of minerals and associations of minerals (rocks) is also a function of pressure. Pressure changes in rocks are related to the change of position along the vertical space coordinate ( $z$ -axis in Fig. 3.4). The prevailing pressure at a given depth in a crustal profile with a steady-state geotherm is given by the density of the material above the volume of interest. It can be calculated from ( $dP/dz = -g\rho$ ):

$$P_{(z)} = -g \int_0^z \rho_{(z)} dz + P_{(z=0)} \quad (3.10)$$

where  $g$  is the acceleration due to gravity ( $9.81 \text{ m/s}^2$ ),  $\rho$  is the density of the rock at any  $z$  (e.g.  $2.7 \text{ g/cm}^3 = 2,700 \text{ kg m}^{-3}$ ) and  $P_{(z=0)}$  is the pressure at the surface (e.g.  $10^5 \text{ Pa} = 1 \text{ bar} = 10^5 \text{ N/m}^2 = 10^5 \text{ kg m}^{-1} \text{ s}^{-2}$ ). The  $z$ -axis direction is always taken as negative. With a constant, depth independent density, (3.10) reduces to the simple relationship  $P = g \rho z$ . The pressure, for example at 10 km (10,000 m) depth, is then calculated for an average rock density of  $2,700 \text{ kg/m}^3$  as 265 MPa or 2.65 kbar. The pressure at the base of continental crust of normal thickness (35–40 km)

is about 1.0 GPa. The pressure at  $z$  results from the weight of the rock column above the volume of interest and is designated as the **lithostatic pressure**. This pressure is usually nearly isotropic. Non-isotropic pressure (stress) may occur as a result of a number of geologically feasible processes and situations as discussed below.

A pressure difference of about 10 MPa at a depth of, e.g. 10 km ( $P \sim 270$  MPa) will occur if a column of nearby rocks has a different average density (e.g. 2,800 instead of 2,700 kg/m<sup>3</sup>). If the density contrast of two columns of rock is 300 kg/m<sup>3</sup> a  $\Delta P$  of  $\sim 9$  MPa at a depth of 30 km is possible. This is nearly a 100 MPa at a total pressure of  $\sim 0.8$  GPa. However, because crustal material has similar densities, possible pressure differences between columns of rock at the same depth are limited to relatively small fractions of the lithostatic pressure (typically  $< 10\%$ ). However, such pressure gradients may cause flow of fluids stored in the interconnected pore space of rocks according to Darcy's law. The transport of fluids may cause chemical reactions in rocks through which the fluids pass if they are not in equilibrium with the solid assemblage of the rock.

Non-isotropic pressure (stress) also results from tectonic forces and from volume changes associated with temperature changes and composition changes of rocks and minerals. Stress is one of the major controlling factors of the structure of metamorphic rocks. It is also a very important force for small-scale migration and redistribution of chemical components in metamorphic rocks. The processes of pressure solution, formation of fabric (such as foliation) and formation of metamorphic banding from homogeneous protolith rocks are caused by non-isotropic pressure distribution in rocks and associated transport phenomena (Fig. 2.2b). The redistribution of material in stressed rocks attempts to reduce the non-isotropic pressure and to return to isotropic lithostatic pressure conditions.

There are two basic regimes how rocks respond by deformation to applied stresses. At high temperatures and lithostatic pressures rocks react by ductile deformation to stress, whereas brittle deformation is dominant at low- $T$  and shallow depth. The two deformation regimes grade into one another at the brittle–ductile transition zone, which is located at about 12 km depth corresponding to about 318 MPa (3.2 kbar) pressure in typical anorogenic continental crust. The temperature at this depth is about 300°C. The  $P$ – $T$  conditions at the brittle–ductile transition zone correspond to those of the lower greenschist facies (see Chap. 4). The precise depth of the brittle–ductile transition depends on the amount of applied stress, the mechanical properties of the rocks (dependent on the type of rocks present) and the presence or absence of an aqueous fluid. In the brittle deformation regime rocks break and fracture in response to applied stress. The created fractures fill normally with an aqueous fluid (liquid water) because the  $P$ – $T$  conditions are in the field of liquid water (below the critical point of water, see Sect. 3.3). The fractures in crustal rocks above the brittle–ductile transition are typically well connected and form a permeable fracture network. The water in the fracture system is under hydrostatic pressure rather than lithostatic pressure conditions as described above. Thus hydrostatic pressure operating on water in an extension fracture at 10 km depth is about 100 MPa rather than the lithostatic 270 MPa as on the rock matrix on both sides of

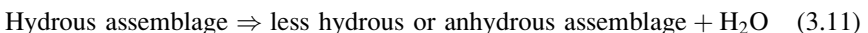
the fracture. Hydrothermal metamorphism, precipitation of fissure minerals, low-T rock alteration and similar processes occur typically under hydrostatic pressure conditions. Within the ductile deformation regime fluids tend to be close to lithostatic pressure or if present in isolated pores even at lithostatic pressure.

In general, the lithostatic pressure acting on a volume of rock changes as a result of a change of depth of that rock volume (change of the position along the  $z$ -direction). In almost all geological occurrences, depth changes are caused by tectonic processes (that ultimately are also the result of thermal processes, e.g. mantle convection, density changes resulting from temperature changes). A lithosphere plate can be subducted in a collision zone and be transported to great depth in the mantle before it is resorbed by the mantle. Some of the subducted material may return to the surface before a normal steady-state geotherm is established. Metamorphic rocks of sedimentary or volcanic origin with mineral assemblages that formed at pressures in excess of 3.0 GPa have been reported from various orogenic belts; 3.0 GPa pressure is equivalent to about 100 km subduction depth ( $z = -P/(g\rho)$ ). In continental collision zones the continental crust often is thickened to double its normal pre-collision thickness. At the base of the thickened crust the pressure increases from 0.9 to 1.8 GPa. The changes in mineralogical composition of the rocks undergoing such dramatic pressure changes depend on the nature and composition of these rocks and will be discussed in Part II.

Variations in depth and associated pressure changes also can be related to subsiding sedimentary basins where a given layer **a** of sediment is successively overlain and buried by new layers **b**, **c** . . . of sediments. Layer **a** experiences a progressive increase in pressure and temperature. If sedimentation and subsidence is slow, layer **a** may follow a steady state geotherm. Metamorphism experienced by layer **a** is commonly described under the collective term **burial metamorphism** as defined in Sect. 1.2.3. Crustal extension or lithosphere thinning is often the cause for the required subsidence creating deep sedimentary basins. Burial metamorphism is therefore also caused by tectonic processes.

### 3.3 Gases and Fluids

Sedimentary rocks such as shales often contain large modal proportions of hydrous minerals. In fact, sediments deposited in marine environments can be expected to contain, under equilibrium conditions, a mineral association that corresponds to a **maximum hydrated state**. Adding heat to the hydrous minerals (clays) of a sediment during a metamorphic event will drive reactions of the general form:



The general reaction (3.11) describes the dehydration process taking place during prograde metamorphism. The important feature of dehydration reactions is the release of  $\text{H}_2\text{O}$ . Steam is, in contrast to solid minerals, a very compressible

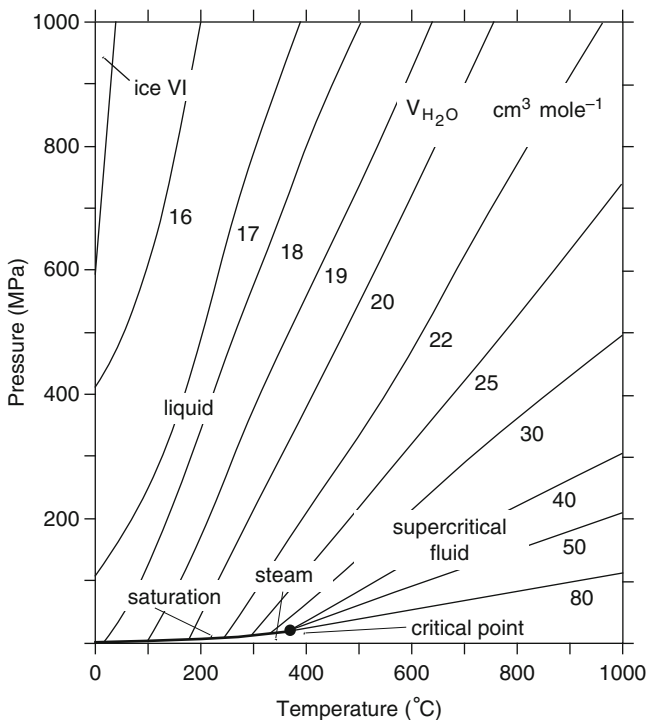


**Fig. 3.10** Isochores of  $\text{H}_2\text{O}$  as a function of pressure and temperature (Helgeson and Kirkham 1974)

phase and its volume is strongly dependent on pressure and temperature. In Fig. 3.10, the molar volume of  $\text{H}_2\text{O}$  is shown as a function of pressure and temperature. At low temperatures,  $\text{H}_2\text{O}$  occurs either as a high density liquid phase or as a low density steam phase depending on the prevailing pressure. The phase boundary between liquid and steam  $\text{H}_2\text{O}$  is the boiling curve. With increasing temperature the density contrast between steam and liquid  $\text{H}_2\text{O}$  continuously decreases along the boiling curve. At the critical point, steam and liquid have the same density and the distinction between steam and liquid becomes redundant. At temperatures above the critical point the  $\text{H}_2\text{O}$  phase is therefore a supercritical fluid phase or simply a fluid. Water in metamorphic systems at temperatures above  $374^\circ\text{C}$  is referred to as an (aqueous) **fluid phase** or a **fluid**. The critical point of  $\text{H}_2\text{O}$  is at  $374^\circ\text{C}$  and 21.77 MPa.

Metamorphic fluids usually predominantly consist of  $\text{H}_2\text{O}$ . The  $\text{H}_2\text{O}$  of aqueous fluids in metamorphic rocks has its origin from various sources: (1) relic formation waters of sedimentary rocks, (2) dehydration water from  $\text{H}_2\text{O}$  originally stored in hydrous minerals, (3) meteoric water, and (4) magmatic water released from solidifying magmas. In the lower crust and in crustal segments with abundant carbonate rocks,  $\text{CO}_2$  may become an additional important component in the fluid



phase. Aqueous fluids also may contain significant amounts of dissolved salts (NaCl) and other solutes (e.g. aqueous silica complexes). At temperatures below 265°C (at 200 MPa), H<sub>2</sub>O and CO<sub>2</sub> mixtures form two separate phases. At higher temperatures, H<sub>2</sub>O and CO<sub>2</sub> form continuous solutions ranging from pure H<sub>2</sub>O to pure CO<sub>2</sub>. However, extremely NaCl-rich brines may unmix into a dense aqueous brine and a low density CO<sub>2</sub>-rich vapor phase even under fairly high metamorphic P–T conditions. The composition of the most common binary metamorphic CO<sub>2</sub>–H<sub>2</sub>O fluids is normally reported in terms of mole fraction X<sub>H<sub>2</sub>O</sub> (or X<sub>CO<sub>2</sub></sub>). The mole fraction is defined as:

$$X_{\text{H}_2\text{O}} = \frac{n_{\text{H}_2\text{O}}}{n_{\text{H}_2\text{O}} + n_{\text{CO}_2}} \quad (3.12)$$

The dimensionless quantity X<sub>H<sub>2</sub>O</sub> is the ratio of the number of moles of H<sub>2</sub>O and the total number of moles of H<sub>2</sub>O and CO<sub>2</sub> in the fluid phase. An X<sub>H<sub>2</sub>O</sub> of 0.5 indicates, for example, a fluid with equal amounts of H<sub>2</sub>O and CO<sub>2</sub> on a mole basis. Other molecular gas species found in metamorphic fluids include: CH<sub>4</sub>, N<sub>2</sub>, HCl, HF, and many others.

The low density fluid produced during prograde dehydration is transported away from the site of production through interconnected pore space and lost to the system. If the rate of H<sub>2</sub>O production exceeds the rate of transport, then the local pore pressure increases. However, the fluid pressure that may build up this way does not greatly exceed the lithostatic pressure imposed on the solid rock, but if the mechanical strength of the rocks is exceeded, then failure occurs. This mechanism of **hydraulic fracturing** produces the necessary transport system for dehydration water. The fluid released is quickly transported and channelled away from the area undergoing dehydration. Suppose a rock undergoes dehydration at 0.5 GPa and 600°C. The produced fluid (Fig. 3.10) has a molar volume of about 22 cm<sup>3</sup> that corresponds to a density of about 0.82 g/cm<sup>3</sup>. This is a remarkably high density for H<sub>2</sub>O at 600°C but it is still much lower than the typical density of rock-forming minerals of about 3 ± 0.5 /cm<sup>3</sup>. The large density contrast between fluid and solids results in strong buoyancy forces and a rapid escape of the fluid from the rocks. Most metamorphic rocks are probably free of fluid during periods without reaction with the exception of fluids trapped in isolated pore spaces, as thin films along grain boundaries, and as inclusions in minerals (**fluid inclusions**).

In most cases, the bulk composition of a metamorphic rock determines the mineral assemblage present at any point on a prograde P–T path. In turn, the mineral assemblage will control (buffer) the composition path followed by the fluid. Thus, in most metamorphic rocks the fluid composition is internally controlled.

### 3.4 Time Scale of Metamorphism

Some simple considerations allow for an estimate of the time scale of typical orogenic metamorphism (see also Walther and Orville 1982). The range of reasonable heat flow differences in the crust that can drive metamorphic processes is

constrained by maximum heat flow differences observed at the surface. The highest heat flows are measured along mid-ocean ridges ( $120 \text{ mW/m}^2$ ), whilst the lowest are in old continental cratons ( $30 \text{ mW/m}^2$ ). Consider a crustal layer with a heat flow difference between bottom ( $75 \text{ mW/m}^2$ ) and top ( $35 \text{ mW/m}^2$ ) of  $40 \text{ mW m}^{-2}$ . This means that every second the rock column receives  $0.04 \text{ J heat (per m}^2\text{)}$ . If the layer consists of shales (heat capacity =  $1 \text{ kJ kg}^{-1} \text{ }^\circ\text{C}^{-1}$ ) with a volatile content ( $\text{H}_2\text{O}$  and  $\text{CO}_2$ ) of about  $2 \text{ mol/kg}$ , the heat received will be used to increase the temperature of the rock and to drive endothermic devolatilization reactions. About  $90 \text{ kJ}$  heat are required to release  $1 \text{ mol H}_2\text{O}$  or  $\text{CO}_2$ . If complete devolatilization occurs in the temperature interval  $400\text{--}600^\circ\text{C}$ , a total of  $380 \text{ kJ}$  will be consumed by the shale ( $180 \text{ kJ}$  for the reactions and  $200 \text{ kJ}$  for the temperature increase from  $400$  to  $600^\circ\text{C}$ ). It takes  $9.5 \times 10^6 \text{ s}$  ( $0.3 \text{ years}$ ) to supply  $1 \text{ kg}$  of rock with the necessary energy. Using a density of  $2.63 \text{ g/cm}^3$ ,  $1 \text{ kg}$  of rock occupies a volume of  $380 \text{ cm}^3$  and it represents a column of  $0.38 \text{ mm}$  height and  $1 \text{ m}^2$  ground surface. From this it follows that metamorphism requires about  $8 \text{ years}$  to advance by  $1 \text{ cm}$ . Eight million years (Ma) are required to metamorphose a  $10 \text{ km}$  thick layer of shale. Similarly, if the heat flow difference is only  $20 \text{ mW/m}^2$ , and the shale layer is  $20 \text{ km}$  thick layer with an initial temperature  $200^\circ\text{C}$ , it will require about  $48 \text{ Ma}$  of metamorphism to convert the hydrous  $200^\circ\text{C}$  shale to an anhydrous  $600^\circ\text{C}$  meta-pelitic gneiss.

This crude calculation shows that typical time spans for regional scale metamorphic processes are on the order of  $10\text{--}50$  million years. Similar time scales have been derived from radiometric age determinations.

### 3.5 Pressure–Temperature–Time Paths and Reaction History

During tectonic transport, any given volume of rock follows its individual and unique path in space and time. Each volume of rock may experience loss or gain of heat, and changes of its position along the  $z$ -coordinate result in changes in lithostatic pressure loaded on the rock. Figure 3.11 shows again a simple model of a destructive plate margin. The situation here depicts a continent–continent collision with the formation of continental crust twice its normal thickness. In A at  $t_1$  ( $0 \text{ Ma}$ ) there is a volume of rock (a rock unit indicated by an open square) at depth  $c$ , the position of which changes depth with time ( $t_1$  through to  $t_6$  at  $30 \text{ Ma}$ ). In B through E, the position of the rock unit (filled squares) during tectonic transport is shown in terms of  $P$ – $T$  space. The time slices are arbitrary and have been chosen in accordance with time scales of the formation of Alpine-type orogenic belts. At  $t_1$  the rock unit lies on a stable steady-state geotherm. At  $t_2$  ( $10 \text{ Ma}$ ) tectonic transport moves the crust together with the rock unit beneath another continental crust of normal  $35 \text{ km}$  thickness. Increasing depth of the rock unit is accompanied by increasing pressure (3.10). At the same time, the rock unit begins to receive more heat than at its former position at  $t_1$ . However, because heat transport is a slow process compared with tectonic transport,  $dP/dT$  tends to be much steeper

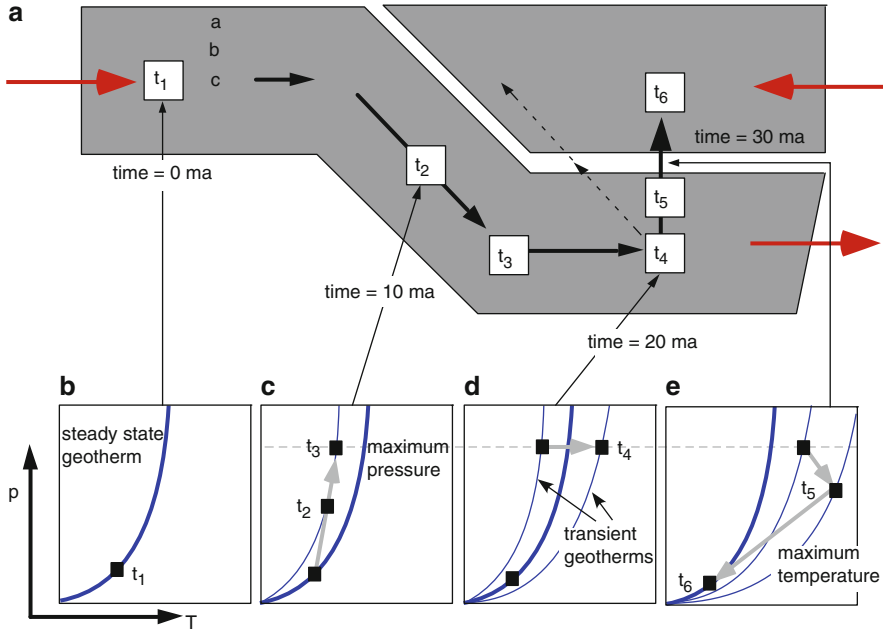


**Fig. 3.11** (a–e) Schematic diagram showing the position of a rock unit in the crust as a function of time during continent–continent collision and the corresponding paths followed by the rock unit in  $P$ – $T$  space

(Fig. 3.11c) than the corresponding  $dP/dT$  slope of the initial steady-state geotherm (Fig. 3.11b). Between  $t_1$  and  $t_2$ , the rock unit has traveled in  $P$ – $T$  space along a path that is on the high-pressure side of the initial steady-state geotherm. The rock unit is now on a transient geotherm that changes its shape as time progresses. At  $t_3$  the crust is twice its normal thickness (about 70 km), which is about the maximum thickness in continent–continent collision zones. The rocks have reached their maximum depth and consequently their maximum pressure of about 2 GPa (Fig. 3.11c). Continued plate motion does not increase the thickness of the crust and pressure remains constant as long as underthrusting is going on. On the other hand, heat transfer to the rock unit in question increases the temperature as shown in Fig. 3.11d ( $t_4$ ). From this time, a number of feasible mechanisms may control the path of the rock unit. Continued tectonic transport may return slices and fragments of rock to shallower levels in a material counter current (dashed arrow in Fig. 3.11a), or simply, after some period of time, plate convergence stops, e.g. because frictional forces balance the force moving the plate. The thickened crust starts to uplift, and erosion restores the crust to its original thickness. By this mechanism the rock unit may return to its original depth position and, given enough time, the stable steady-state geotherm will be re-established. The path between  $t_4$  and  $t_5$  is characterized by decompression (transport along the  $z$ -axis). If initial uplift rates are slow compared with heat transport rates, the rocks will experience

a continued temperature increase during uplift as shown in Fig. 3.11e). However, at some stage along the path the rocks must start to lose more heat to the surface than they receive from below, and consequently cooling begins. The point  $t_5$  in Fig. 3.11e represents the maximum temperature position of the path traveled by the rock unit. At  $t_6$  the rock has returned to its former position on the steady state geotherm (Fig. 3.11a).

The consequences for pressure and temperature of the geologic process illustrated in Fig. 3.11 are summarized in Fig. 3.12. A rock at depth  $c$  ( $P$ – $T$ – $t$ -path 3) follows a clockwise pressure–temperature loop. Such clockwise  $P$ – $T$ – $t$  paths are a characteristic feature of orogenic metamorphism and have been documented from such diverse mountain belts as the Scandinavian Caledonides, western Alps, Appalachians, and Himalayas. In detail, clockwise  $P$ – $T$ – $t$  loops may show a number of additional complications and local features. Counter-clockwise  $P$ – $T$ – $t$  paths have been reported from granulite facies terrains where an event of heating from igneous intrusions precedes crustal thickening. They may also occur in terrains that have experienced an initial phase of crustal extension. Very often “normal” orogenesis, is characterized by the following sequence of  $P$ – $T$ – $t$  path sections: isothermal thickening, isobaric heating, isothermal decompression and isobaric cooling. Returning to Fig. 3.12a, it is evident that the maximum temperature point along the  $P$ – $T$ – $t$  path followed by a metamorphic rock does not necessarily coincide with the maximum pressure point of the path. This means that maximum pressure and maximum temperature will be generally diachronous.

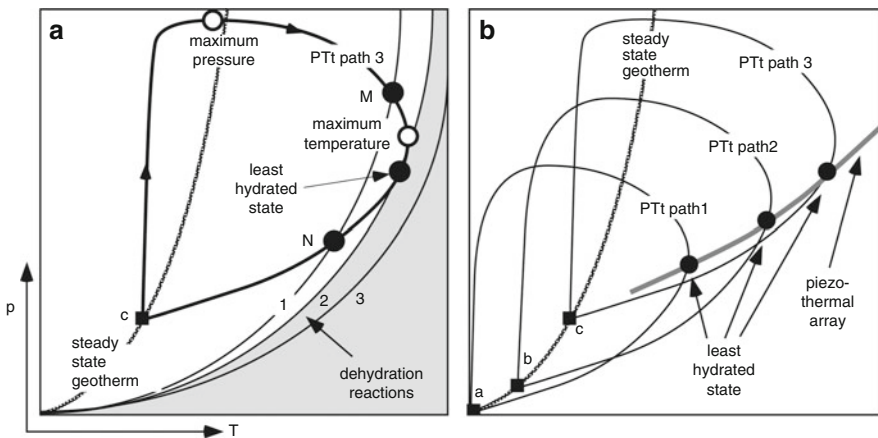


**Fig. 3.12** (a, b) (a)  $P$ – $T$ – $t$  path of a rock unit at depth  $c$  in 0. The mineral assemblage stable at the tangent point of the path with dehydration reaction 2 will, in general, be preserved in metamorphic rocks. The tangent point corresponds to the least hydrated state of the rock. (b) Clockwise  $P$ – $T$ – $t$  loops for crustal rock units from different depth levels (0). The mineral assemblage of the individual rock units corresponds to the least hydrated state. The  $P$ – $T$  points of the least hydrated state from all rocks of a metamorphic terrain define a curve that is known as a *piezo-thermal array* (~metamorphic field gradient)

What do we see of the path traveled by a rock in  $P$ - $T$ - $t$  space when we study a metamorphic rock? If the rock has always maintained an equilibrium state and metamorphism is strictly isochemical, we will not find any relics of its metamorphic history. However, rocks that formed at, for example, 800°C and 1.0 GPa can be collected at the surface and they *do* show characteristic high- $P$ - $T$  mineral assemblages! This immediately tells us that at some stage during the reaction history a certain high-grade mineral assemblage has not been converted to low-grade assemblages on the way back to the surface. The question is: which point (or points) on the  $P$ - $T$  path is preserved and recorded by the mineral assemblage(s) of the rock? The answer may be difficult to find in a specific geologic situation and for specific samples. However, low-grade rocks e.g., shale, often contain modally large amounts of hydrates and are, therefore, affected by a series of discontinuous and continuous dehydration reactions during prograde metamorphism. In the pressure-temperature range typical of crustal metamorphism, dehydration reactions have equilibrium conditions as shown in Fig. 3.12a (reactions 3.1–3.3). Path 3 will be shaped by dehydration reactions and when crossing dehydration reaction (3.1) at point **M** a rock will partially lose water and continue as a rock containing a smaller amount of hydrous minerals (mica, chlorite, amphibole). Dehydration of the rock will continue until the tangent point of the  $P$ - $T$  path where the last active dehydration reaction is reached. This point corresponds to the **least hydrated state** in the metamorphic history of the rock. It does not necessarily correspond to the maximum temperature point reached by the rock. If the  $P$ - $T$ - $t$  path shows a pronounced period of rapid uplift and decompression, the  $P$ - $T$  coordinates of the least hydrated state may be dramatically different from maximum  $P$  and  $T$ . At this point the rock contains a prograde assemblage in equilibrium with an aqueous fluid phase saturating the mineral grain boundaries and filling the pore space. However, the total amount of free fluid is extremely small in most metamorphic rocks. Typical porosities of metamorphic rocks at  $P$  and  $T$  are on the order of 0.2 vol% (e.g. 2 cm<sup>3</sup> H<sub>2</sub>O per 1,000 cm<sup>3</sup> rock). After having passed the point of the least hydrated state, the rock crosses the dehydration reactions in the reversed direction. The reactions consume water and form hydrates from anhydrous (or less hydrous) minerals and the minute amount of free fluid will be readily used up by the first rehydration reaction. For example, 2% free H<sub>2</sub>O in a rock of an appropriate composition and mineral assemblage at 0.9 GPa and 700°C (corresponding to 0.1 mol H<sub>2</sub>O per 1,000 cm<sup>3</sup> of rock) can be used to form 15 cm<sup>3</sup> biotite per 1,000 cm<sup>3</sup> rock (1.5 vol% biotite). The rock will then be devoid of a free fluid phase which effectively prevents its minerals adjusting to changing  $P$ - $T$  conditions. This is because water is not only essential in dehydration reactions but plays a central role as a transport medium and catalyst for chemical reactions in rocks. Its final loss marks the closure the reaction history of a rock. Even reconstructive phase transitions, e.g. kyanite = sillimanite, require the presence of water in order to proceed at finite rates even over geological time scales. Consequently, by studying the phase relationships of metamorphic rocks, one will in general only be able to determine the  $P$ - $T$  conditions corresponding to the least hydrated state. This is close to the conditions when a free aqueous fluid was last present in the rock.

On its way to the surface the rock crosses reaction (3.1) at point N (Fig. 3.12a). However, the reaction will affect the rock only if water is available for the back reaction. Rehydration (retrograde metamorphism) is widespread and very common in metamorphic rocks. However, rehydration reactions very often do not run to completion, and assemblages from the least hydrated state more often than not survive as relics. The necessary water for retrograde metamorphism is usually introduced to the rocks by late deformation events. Deformation may occur along discrete shear zones that also act as fluid conduits. The shear zone rocks may contain low-grade mineral assemblages whereas the rocks unaffected by late deformation still show the high-grade assemblage. With some luck, it is possible to identify in a single rock sample a series of mineral assemblages that formed at consecutive stages of the reaction history. The reaction history of rocks can often be well documented for all stages that modified the assemblage of the least hydrated state.

Relics from earlier portions of the  $P$ - $T$  path (before it reached its least hydrated state) are seldom preserved in metasedimentary rocks. Occasionally, early minerals survive as isolated inclusions in refractory minerals such as garnet. Garnet in such cases effectively shields and protects the early mineral from reacting with minerals in the matrix of the rock with which it is not stable at some later stage of the rock's history. Rocks with water-deficient protoliths such as basalts, gabbros and other igneous rocks may better preserve early stages of the reaction history. In some reported case studies, meta-igneous rocks record the entire  $P$ - $T$ - $t$  path from the igneous stage to subduction metamorphism and subsequent modifications at shallower crustal levels (see Sect. 9.8.2.1).

Rocks collected in a metamorphic terrain may originate from different depth levels in the crust (Fig. 3.11, depths a-c). All rocks follow their individual  $P$ - $T$  path as indicated in Fig. 3.12b. Analysis of phase relationships and geologic thermobarometry may therefore yield a series of different  $P$ - $T$  coordinates corresponding to the least hydrated states of the individual samples. The collection of all  $P$ - $T$ -points from a given metamorphic terrain define a so-called **piezo-thermic array**. Its slope and shape characterize the specific terrain. The details of a piezo-thermic array of a given terrain depend on the geologic history and dynamic evolution of the area. The term "**metamorphic field gradient**" is preferred by some petrologists over the expression piezo-thermic array, but both expressions mean essentially the same thing. It is an arrangement of  $P$ - $T$ -points of least-hydrated state conditions reached during a now **fossil** metamorphism by rocks that are exposed **today** on the erosion surface. It is important to note that this two-dimensional array of  $P$ - $T$ -points should *not* be confused with a geotherm.

### 3.6 Chemical Reactions in Metamorphic Rocks

Chemical reactions in rocks may be classified according to a number of different criteria. Below follows a brief presentation of various kinds of reactions that modify the mineral assemblage or the mineral composition of metamorphic rocks.

### 3.6.1 Reactions Among Solid-Phase Components

These are often termed “solid–solid” reactions because only phase components of solid phases occur in the reaction equation. Typical “solid–solid” reactions are, for example:

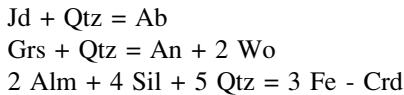
#### 3.6.1.1 Phase Transitions, Polymorphic Reactions

$\text{Al}_2\text{SiO}_5$	Ky = And; Ky = Sil; Sil = And
$\text{CaCO}_3$	Calcite = aragonite
C	Graphite = diamond
$\text{SiO}_2$	$\alpha$ -Qtz = $\beta$ -Qtz; $\alpha$ -Qtz = coesite, .....
$\text{KAlSi}_3\text{O}_8$	Microcline = sanidine

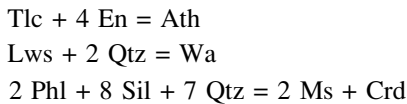
#### 3.6.1.2 Net-Transfer Reactions

Such reactions transfer the components of reactant minerals to minerals of the product assemblage.

Reactions involving anhydrous phase components only



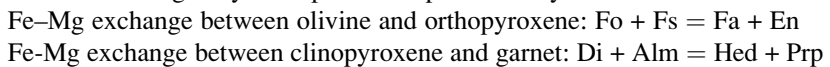
Volatile-conserving “solid–solid” reactions



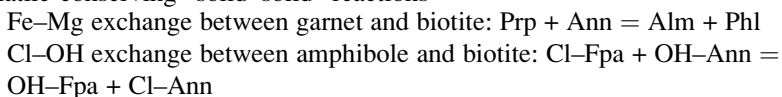
#### 3.6.1.3 Exchange Reactions

These reactions exchange components between a set of minerals.

Reactions involving anhydrous phase components only



Volatile-conserving “solid–solid” reactions



### 3.6.1.4 Exsolution Reactions/Solvus Reactions

High-T alkali feldspar = K-feldspar + Na-feldspar

Ternary high-T feldspar = meso-perthite + plagioclase

Mg-rich calcite = calcite + dolomite

High-T Cpx = diopside + enstatite

Al-rich Opx = enstatite + garnet

The common feature of all “solid–solid” reactions is that equilibrium conditions of the reaction are independent of the fluid phase composition, or more generally speaking, of the chemical potentials of volatile phase components during metamorphism. It is for this reason that all “solid–solid” reactions are potentially useful geologic thermometers and barometers. The absence of volatile components in the reaction equation of “solid–solid” reactions should not be confused with general fluid-absent conditions during reaction progress. Metamorphic reactions generally require the presence of an aqueous fluid phase in order to achieve significant reaction progress even in geological time spans, attainment of chemical equilibrium in larger scale domains and chemical communication over several grain-size dimensions. Although  $P$ – $T$  coordinates of the simple reconstructive phase transition kyanite = sillimanite are independent of  $\mu_{\text{H}_2\text{O}}$ , the detailed reaction mechanism may involve dissolution of kyanite in a saline aqueous fluid and precipitation of sillimanite from the fluid at nucleation sites that can be structurally unrelated to the former kyanite (e.g. Carmichael 1968). It is clear that the chlorine-hydroxyl exchange between amphibole and mica represents a process that requires the presence of an saline aqueous fluid. However, the equilibrium of the exchange reaction is independent on the composition of that fluid.

Phase transitions, “solid–solid” net transfer and exchange reactions often show straight line equilibrium relationships in  $P$ – $T$  space. The slope of the equilibrium line of such reactions can be readily calculated (estimated) from the Clausius–Clapeyron equation (Fig. 3.13).

## 3.6.2 Reactions Involving Volatiles as Reacting Species

### 3.6.2.1 Dehydration Reactions

Reactions involving  $\text{H}_2\text{O}$  are the most important metamorphic reactions. Low-grade metasediments contain modally abundant hydrous minerals. Pelitic and mafic rocks from the subgreenschist facies consist mainly of clay minerals (and zeolites). Serpentine minerals make up lower-grade ultramafic rocks. These sheet silicates contain up to about 12 wt%  $\text{H}_2\text{O}$ . The hydrous minerals are successively removed from the rocks by continuous and discontinuous dehydration reactions as heat is added to them as shown in Fig. 3.14 for a shale and basaltic rock. Release of  $\text{H}_2\text{O}$  during prograde metamorphism of  $\text{H}_2\text{O}$ -rich protoliths ensures that a free  $\text{H}_2\text{O}$  fluid is present in the rocks either permanently or periodically during the progress of dehydration reactions. This in turn often permits discussion of metamorphism for conditions



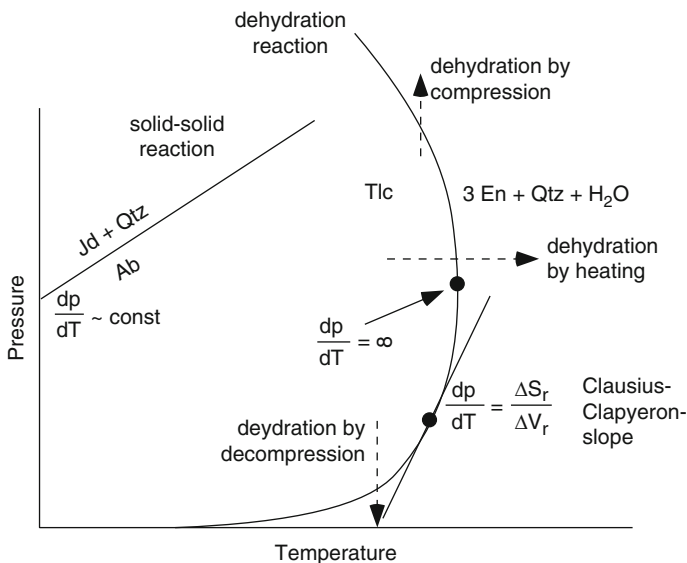
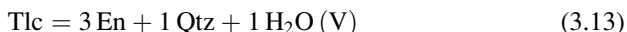


**Fig. 3.13** Schematic equilibrium conditions of solid–solid and dehydration reactions in  $P$ – $T$  space and the Clausius–Clapeyron equation ( $\Delta S_r$  = entropy change and  $\Delta V_r$  = volume change of the reaction)

where the lithostatic pressure acting on the solids also applies to a free fluid phase. If the fluid is pure  $H_2O$  (and choosing an appropriate standard state), the condition is equivalent to  $a_{H_2O} = 1$ . The general shape of dehydration equilibria is shown schematically in Fig. 3.13. Using the talc breakdown reaction as an example, the general curve shape of dehydration reactions on  $P$ – $T$  diagrams can be deduced as follows:



The  $dP/dT$ -slope of a tangent to the equilibrium curve is given at any point along the curve by the Clapeyron equation. All dehydration reactions have a positive  $\Delta S_r$  (entropy change of reaction) and the curvature is largely controlled by the volume change of the reaction. The volume term can be separated into a contribution from the solids and the volume of  $H_2O$ , respectively:

$$\Delta V_r = \Delta V_{\text{solids}} + \Delta V_{H_2O} \quad (3.14)$$

The volume change of the solids can be calculated from:

$$\Delta V_{\text{solids}} = 3 V_{\text{En}} + 1 V_{\text{Qtz}} - 1 V_{\text{tlc}} \quad (3.15)$$

$\Delta V_{\text{solids}}$  is a small and negative quantity and varies very little with  $P$  and  $T$ . Consequently, the curve shape of dehydration reactions largely reflects the volume function of  $H_2O$ , that is shown in Fig. 3.10. At low pressures,  $V_{H_2O}$  is large and the

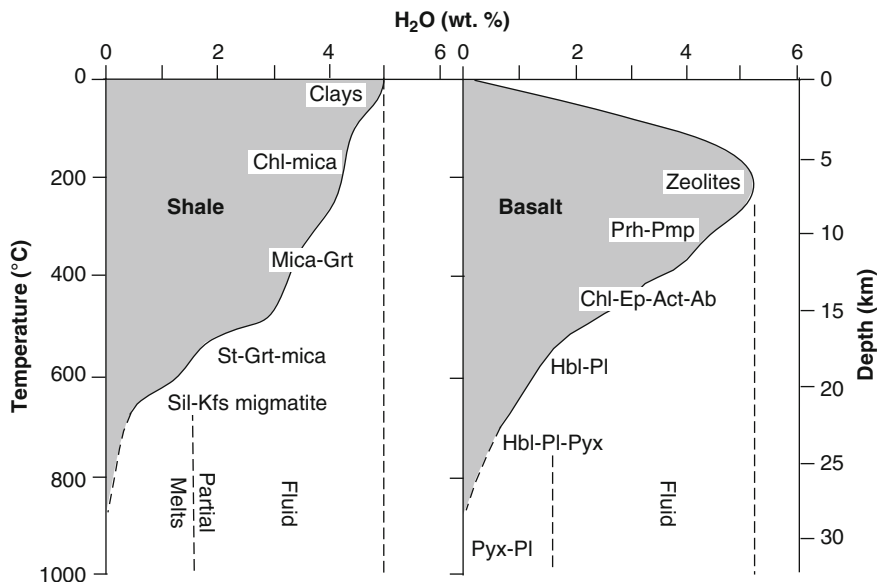


**Fig. 3.14** Diagrams showing water-release curves of hydrous mineral assemblages during prograde dehydration reactions in shale and basalt along a  $30^{\circ}\text{C}/\text{km}$  geotherm (Redrawn from Fyfe et al. 1978). Changes in the slopes of the water-release curves relate to the beginning and completion of dehydration of the main hydrous silicates. In the pelagic shale, partial melting to form migmatite can occur at  $\sim 620^{\circ}\text{C}$  depending on composition and remaining water content. Note that in the case of the basalt, which is essentially dry, hydration initially takes place to produce a zeolite facies assemblage with  $\sim 5$  wt%  $\text{H}_2\text{O}$ . Partial melting of the basalt to form a mafic migmatite could occur at  $\sim 800^{\circ}\text{C}$

$dP/dT$ -slope small. In the pressure range of about 200–300 MPa, the molar volume of  $\text{H}_2\text{O}$  rapidly decreases and dehydration reactions tend to be strongly curved. At pressures greater than about 300 MPa and up to 1.0–1.5 GPa, the volume of  $\text{H}_2\text{O}$  is usually comparable to the volume change of the solids and  $\Delta V_r$  tends to be very small. Perceptively,  $dP/dT$  slopes are very large in this pressure range. At even higher pressures, the volume of  $\text{H}_2\text{O}$  cannot compensate the negative  $\Delta V_{\text{solids}}$  and  $\Delta V_r$  and the  $dP/dT$ -slope also become negative. From the general shape of dehydration equilibria in  $P$ - $T$  space shown in Fig. 3.13, it is evident that talc, for instance, can be dehydrated either by heating, by decompression or by compression.

The dehydration of zeolite minerals is often accompanied by large negative  $\Delta V_{\text{solids}}$  and the dehydration equilibria have negative slopes already at moderate or low pressures. For example, the reaction  $\text{analcime} + \text{quartz} \Rightarrow \text{albite} + \text{H}_2\text{O}$  has a  $\Delta V_{\text{solids}}$  of  $-20.1 \text{ cm}^3/\text{mol}$  and the equilibrium has a negative slope above pressures of about 200 MPa.

In contrast to dehydration reactions,  $dP/dT$ -slopes of “solid–solid” reactions (and phase transitions) are nearly constant (Fig. 3.13).

The equilibrium constant of the talc breakdown reaction (3.13) can be expressed by the mass action equation:

$$K = \frac{a_{\text{En}}^3 a_{\text{Qtz}} a_{\text{H}_2\text{O}}}{a_{\text{Tlc}}} \quad (3.16)$$

where  $a_i$  denotes the activity of the subscripted phase component. The activity of a phase component is a function of the composition of the phase. Its numerical value also depends on the choice of a standard state, explicitly the conditions where the activity shall be equal to one. The equilibrium constant  $K$  of a chemical reaction has a fixed value at a given  $P$  and  $T$  (a constant as the name suggests). It can be calculated from the fundamental equation that is also extremely useful for geological applications:

$$-RT \ln K = \Delta G_r^0 \quad (3.17)$$

The standard state Gibbs free energy change of the reaction on the right hand side of equation (3.17) can be calculated for  $P$  and  $T$  of interest provided the thermodynamic data for all phase components in the reaction are known ( $R$  = universal gas constant;  $T$  = temperature in K). For the talc reaction (3.13) the logarithmic form of (3.16) and (3.17) is:

$$\ln K = \{ \ln a_{\text{H}_2\text{O}} + [\ln a_{\text{En}}^3 + \ln a_{\text{Qtz}} - \ln a_{\text{Tlc}}] \} = -\Delta G_r^0 / (R T) \quad (3.18)$$

With the appropriate standard state and by considering pure end member solids  $i$  ( $a_i=1$ ), the expression in square brackets becomes zero and the equilibrium is dependent on the activity of  $\text{H}_2\text{O}$ . The equilibrium is shown in Fig. 3.13 for the case  $P_{\text{H}_2\text{O}} = P_{\text{lithostatic}}$  (pure  $\text{H}_2\text{O}$  fluid present,  $a_{\text{H}_2\text{O}} = 1$ ). Equation (3.18) is graphically represented in Fig. 3.15 for three values of  $a_{\text{H}_2\text{O}}$ . It can be seen from Fig. 3.15, that the equilibrium conditions for dehydration reactions are displaced to lower temperatures (at  $P$  = constant) by decreasing  $a_{\text{H}_2\text{O}}$ . Solutions of (3.18) for different  $a_{\text{H}_2\text{O}}$  are shown in Fig. 3.16. It follows from Fig. 3.15 that the maximum temperature for the talc-breakdown reaction is given by the condition  $a_{\text{H}_2\text{O}} = 1$  that is equivalent to  $P_{\text{H}_2\text{O}} = P_{\text{hydrostatic}}$  and the presence of a pure  $\text{H}_2\text{O}$  fluid.

It also follows from Fig. 3.15, that talc dehydrates to enstatite and quartz at lower temperatures if  $a_{\text{H}_2\text{O}} < 1.0$  at any pressure. The  $P$ - $T$  space can, therefore, be contoured with a series of dehydration curves of constant  $a_{\text{H}_2\text{O}}$ . Geologically, the condition of  $a_{\text{H}_2\text{O}} < 1.0$  can be realized basically in two different situations: (1) the fluid is not a pure  $\text{H}_2\text{O}$  fluid but is rather a mixture of  $\text{H}_2\text{O}$  and some other components not taking part in the reaction (e.g.  $\text{CH}_4$ ,  $\text{N}_2$ ,  $\text{CO}_2$ ), (2) there is no free fluid phase present at all.

The equilibrium curve for the condition  $P_{\text{H}_2\text{O}} = P_{\text{hydrostatic}}$  has a shape similar to the  $P_{\text{H}_2\text{O}} = P_{\text{lithostatic}}$  curve. The two curves converge at very low pressures. Note, however, that here  $a_{\text{H}_2\text{O}} = 1$  along the curve (standard state: pure  $\text{H}_2\text{O}$  at  $T$  and

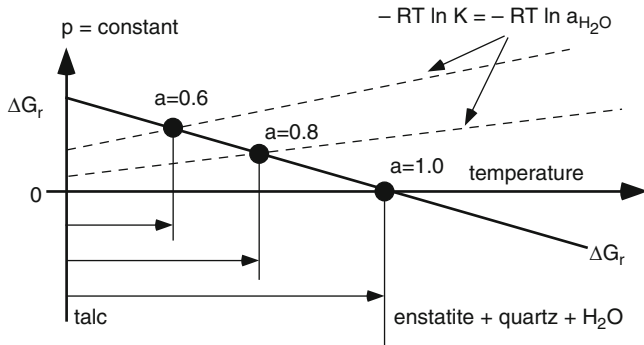


Fig. 3.15 Solutions of the equation  $\Delta G_r^0 = -RT \ln K$  for dehydration reactions and three different values of  $a_{H_2O}$

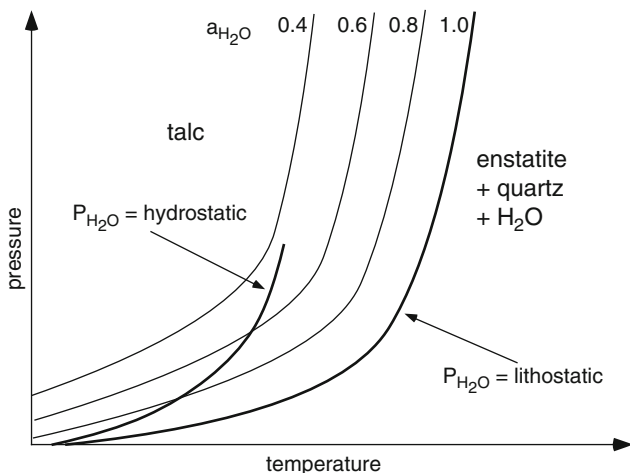


Fig. 3.16 Schematic equilibrium conditions of dehydration reactions for various  $a_{H_2O}$  conditions

$P_{hydrostatic}$ ), and that it does not vary with increasing pressure. Also note that under the condition  $P_{H_2O} = P_{hydrostatic}$ , the pressure is different for the solids and the fluid. This means that such a system is not in mechanical equilibrium. Hydrostatic pressure conditions may occur in very porous or strongly fractured rocks at shallow crustal levels. Typical geologic settings where such conditions may occur include hydrothermal vein formation, oceanic metamorphism, shallow level contact aureoles, deep groundwater in basement rocks. Hydrostatic pressures usually cannot be maintained at typical metamorphic pressures of several hundred megapascal. Pressure solution and local chemical redistribution of material rapidly isolates the fluid phase and the system returns to mechanical equilibrium. Geologically then, the situation  $P_{H_2O} = P_{lithostatic}$  is the most important one and the curves  $a_{H_2O} < 1$  may be relevant in rocks with an impure aqueous fluid or in “dry” environments.

### 3.6.2.2 Decarbonation Reactions

This type of reaction describes the decomposition of carbonate minerals such as calcite and dolomite. For example, adding heat to a rock containing calcite and quartz will eventually cause the following reaction:  $\text{Cal} + \text{Qtz} = \text{Wo} + \text{CO}_2$  (Fig. 3.17). The form of the equilibrium conditions in  $P$ - $T$  space is analogous to the dehydration reactions depicted in Fig. 3.16 as are the effects of variations in  $a_{\text{CO}_2}$  ( $P_{\text{CO}_2}$ ). The highest temperature of the reaction at any pressure occurs where  $a_{\text{CO}_2} = 1$ . In metamorphosed carbonate rocks, the fluid phase rarely consists of pure  $\text{CO}_2$ , and is usually a mixture of  $\text{CO}_2$  and  $\text{H}_2\text{O}$  (and other volatile species).

### 3.6.2.3 Mixed Volatile Reactions

In rocks containing both, hydrous minerals (sheet silicates and amphiboles) and carbonates, reactions may produce or consume both  $\text{CO}_2$  and  $\text{H}_2\text{O}$  simultaneously. In such rock types the fluid phase contains at least the two volatile species,  $\text{CO}_2$  and  $\text{H}_2\text{O}$ . Under certain conditions, for instance where graphite is present, other species such as  $\text{H}_2$  and  $\text{CH}_4$  may be occur in the fluid phase in significant amounts. However, the fluid composition in most carbonate-bearing rocks can be assumed to be a binary mixture of  $\text{CO}_2$  and  $\text{H}_2\text{O}$ . One compositional variable is therefore sufficient to describe the fluid composition. Usually this variable is defined as the mole fraction of  $\text{CO}_2$  in the fluid ( $X_{\text{CO}_2}$ ).  $X_{\text{CO}_2}$  is zero in pure  $\text{H}_2\text{O}$  fluids and equal to one in pure  $\text{CO}_2$  fluids. Consider the following characteristic mixed volatile reaction:

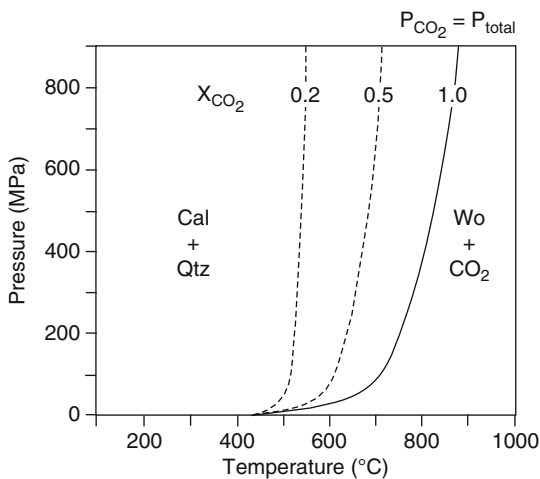
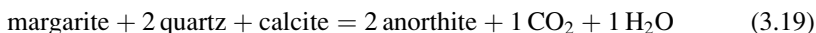


**Fig. 3.17** Univariant decarbonation curves for the breakdown reaction  $\text{Cc} + \text{Qtz} = \text{Wo} + \text{CO}_2$  as a function of  $T$ ,  $P$  ( $P_{\text{fluid}} = P_{\text{CO}_2}$ ) and fluid composition ( $X_{\text{CO}_2}$ )

For pure solid phases, the equilibrium constant is,  $K_{P,T} = a_{\text{CO}_2} a_{\text{H}_2\text{O}}$ . Equilibrium conditions depend on the activities of  $\text{CO}_2$  and  $\text{H}_2\text{O}$  in addition to pressure and temperature. However, if we assume that the fluid is a binary  $\text{CO}_2$ - $\text{H}_2\text{O}$  mixture (and using an ideal solution model for the fluid;  $a = X$ ), the equilibrium constant reduces to,  $K_{P,T} = X_{\text{CO}_2}(1 - X_{\text{CO}_2})$  or  $K_{P,T} = X_{\text{CO}_2}(X_{\text{CO}_2})^2$ . Depending on the actual value of the equilibrium constant at  $P$  and  $T$ , this quadratic equation may have no, one or two solutions. The equilibrium conditions of the margarite breakdown reaction (3.19) is visualized as a complex surface in  $P$ - $T$ - $X_{\text{CO}_2}$  space. Because it is inconvenient to work graphically in a three-dimensional space, mixed volatile reactions are most often represented on isobaric  $T$ - $X$  diagrams or isothermal  $P$ - $X$  diagrams, depending on the geological problem one wants to solve. It is also possible to select a certain metamorphic  $P$ - $T$  field gradient that best describes the regional metamorphic area under consideration and construct  $(P$ - $T$ )- $X_{\text{CO}_2}$  sections (examples are given in Chap. 6). For instance, take the case where  $P$  is kept constant. The quadratic equation above can be solved for a series of temperatures and the results shown on an isobaric  $T$ - $X$  section (Fig. 3.18). At  $T_1$  the four-mineral assemblage, margarite + quartz + calcite + anorthite, may coexist with either very  $\text{H}_2\text{O}$ -rich or very  $\text{CO}_2$ -rich fluids. At one unique temperature,  $T_2$ , the equation has only one solution. Temperature  $T_2$  represents the maximum temperature for the reactant assemblage, as above it, no margarite, calcite and quartz can coexist. At  $T_3$  no (real) solution for the equation exists and the product assemblage may coexist with binary  $\text{CO}_2$ - $\text{H}_2\text{O}$  fluids of any composition. The heavy solid curve in Fig. 3.18 connects all solutions of the equilibrium constant equation and represents the

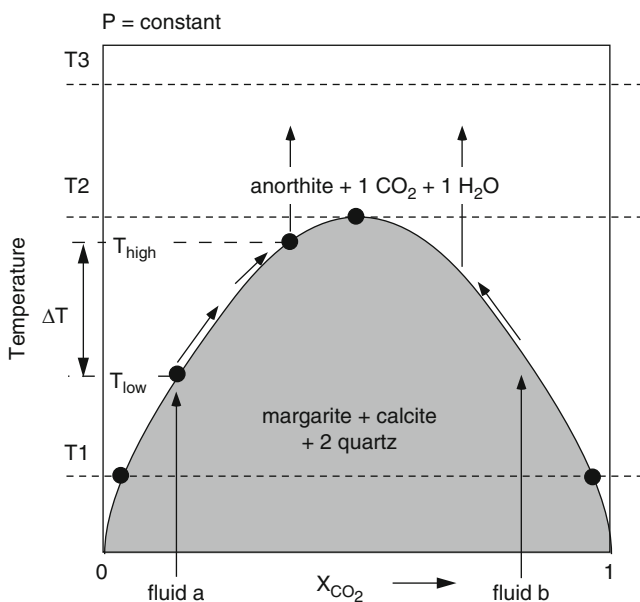
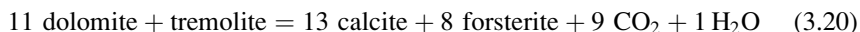


Fig. 3.18 Schematic equilibrium conditions of a mixed volatile reaction (isobaric  $T$ - $X$  diagram)

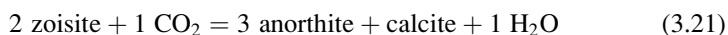
reaction equilibrium of the margarite breakdown reaction in quartz- and calcite-bearing rocks. The curve separates a  $T$ - $X$  field where the reactants are stable (shaded) from an area where the products are stable. At any temperature  $<T_2$ , the products are stable in  $H_2O$ -rich or  $CO_2$ -rich fluids, respectively. The reactants may coexist with fluids of intermediate compositions.

Consider now a margarite-bearing rock containing excess quartz and calcite and a pore fluid of composition " $a$ ". Adding heat to this rock raises its temperature until the reaction boundary is reached at  $T_{low}$ . Further temperature increase causes the production of anorthite and a fluid with equal proportions of  $CO_2$  and  $H_2O$  (3.19). Because the produced fluid is more  $CO_2$ -rich than the original pore fluid of the rock (fluid  $a$ ), the total fluid composition is driven to more  $CO_2$ -rich compositions. The original fluid becomes progressively more diluted with the fluid produced by the reaction; ultimately the fluid is entirely dominated by the reaction fluid and has the composition  $X_{CO_2} = 0.5$  (1 mol  $CO_2$  and 1 mol  $H_2O$ ). This will be the case at  $T_2$ , the maximum temperature of the reactant assemblage. However, the reactant assemblage may become exhausted with respect to one or more reactant minerals before reaching  $T_2$ . For example, if the original rock contains 1 mol margarite, 3 mol calcite and 5 mol quartz per 1,000  $cm^3$ , the reaction will consume all margarite during the reaction progress at some temperature along the isobaric univariant curve ( $T_{high}$ ). The rock consists then of anorthite, calcite and quartz, and a fluid of the composition at  $T_{high}$ . Further addition of heat will increase the temperature of the rock, but the fluid composition will remain unchanged. Therefore, the univariant assemblage margarite + anorthite + calcite + quartz is stable over a temperature interval  $\Delta T$  and coexists with fluids with increasing  $CO_2$  content. The temperature interval  $\Delta T$  is also associated with gradual changes in modal composition in the rock. At  $T_{low}$  the first infinitesimally small amount of anorthite appears and it continuously increases in modal abundance as the reaction progresses towards  $T_{high}$  where the last small amount of margarite disappears. The fluid composition at the maximum temperature  $T_2$  depends exclusively on the reaction stoichiometry. Consider the reaction that makes olivin marbles from tremolite marbles:



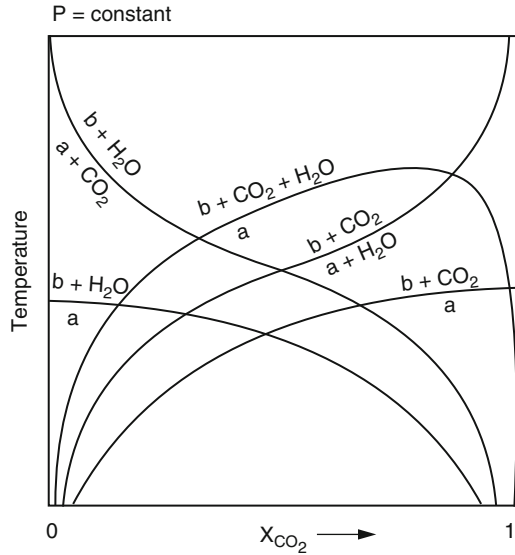
In this reaction, the produced fluid has the composition  $X_{CO_2} = 0.9$  (9 mol  $CO_2$  and 1 mol  $H_2O$ ) and the temperature maximum of the equilibrium is at the same fluid composition. The general shape of reaction equilibria for reactions of the type:  $a = b + mH_2O + nCO_2$  (both fluid species are products of the reaction) is shown in Fig. 3.19 together with mixed volatile reactions with other reaction stoichiometries.

The equilibrium constant of the reaction:

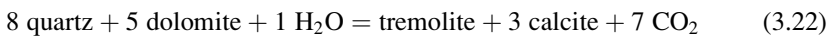


can be written as,  $K = (1 / X_{CO_2}) - 1$ . It varies between zero and  $+\infty$  ( $\ln K - \infty$ ,  $+\infty$ ). Consequently, the univariant assemblage coexists with  $CO_2$ -rich fluids at low

**Fig. 3.19** Schematic equilibrium conditions of mixed volatile reactions with different reaction stoichiometries (isobaric  $T$ - $X$  diagram)



temperatures and with  $\text{H}_2\text{O}$ -rich fluids at high temperatures. The general shape of reactions  $a + \text{CO}_2 = b + \text{H}_2\text{O}$  can be seen in Fig. 3.19. The reaction that produces tremolite marbles from siliceous dolomitic limestone:



represents a reaction of the type:  $a + \text{H}_2\text{O} = b + \text{CO}_2$  and has, compared to reaction (3.21), an inverse shape in  $T$ - $X$ -diagrams (Fig. 3.19). It follows from the earlier discussion on pure dehydration and decarbonation reactions (see Figs. 3.15–3.17) that they must have general curve shapes as shown in Fig. 3.19. The figures presented so far also permit a deduction of the general shape of mixed volatile reaction equilibria in isothermal  $P$ - $X$  sections (you may try to draw a  $P$ - $X$  figure at constant temperature similar to Fig. 3.19).

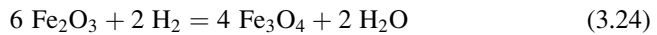
### 3.6.2.4 Oxidation/Reduction Reactions

A number of cations making up minerals occur in different oxidation states. Examples are,  $\text{Fe}^{2+}/\text{Fe}^{3+}$ ,  $\text{Cu}^+/\text{Cu}^{2+}$ ,  $\text{Mn}^{2+}/\text{Mn}^{3+}$ . The most important REDOX couple in common rock-forming silicates and oxides is  $\text{Fe}^{2+}/\text{Fe}^{3+}$ . The two iron oxides hematite and magnetite are related by the reaction:





The equilibrium conditions of this reaction are given (for pure hematite and magnetite) by  $K = a_{O_2}$ . Again, the equilibrium depends on three variables; P, T and  $a_{O_2}$ . As the pressure dependence is very small for this REDOX reaction, the equilibrium is commonly depicted on isobaric T versus  $\log a_{O_2}$  diagrams (Fig. 3.20). In the literature, the activity is often replaced by  $f_{O_2}$  (fugacity of  $O_2$ ).  $\ln f_{O_2}$  is numerically identical to  $\log a_{O_2}$  if an appropriate standard state is chosen. The fugacity is close to the partial pressure of  $O_2$  under low pressure conditions. However, fugacity can be related to the partial pressure of  $O_2$  at any pressure. The partial pressure of  $O_2$  in crustal metamorphic rocks is extremely small (on the order of  $10^{-20}$ – $10^{-40}$  bar). However, coexistence of hematite and magnetite may also be formulated in the presence of water as,



and the equilibrium can be shown on T versus  $\log a_{H_2}$  diagrams.

The assemblage biotite + K-feldspar + magnetite is common in high-grade metamorphic and in igneous rocks. The REDOX reaction:

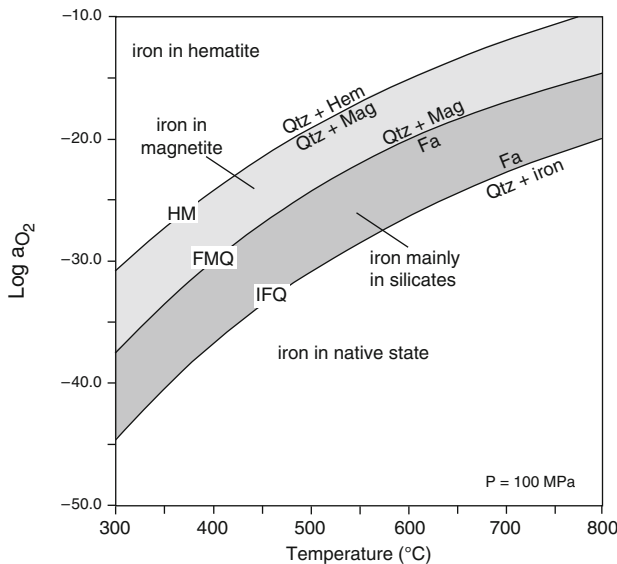
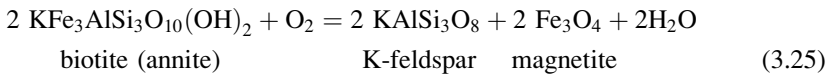


**Fig. 3.20** Log oxygen activity–T diagram showing various oxidation states of iron in the system Fe–Si–O at 100 MPa. Oxygen buffered along curves by HM = hematite–magnetite; FMQ = fayalite–magnetite–quartz; IFQ = iron–fayalite–quartz. Standard state for  $O_2$ : pure gas at T and  $10^5$  Pa

depends on  $O_2$  (and  $H_2O$ ). If  $O_2$  is increased then biotite is oxidized to Kfs + Mag, if  $O_2$  is lowered then Kfs + Mag is reduced to biotite (Fig. 3.21). Expressed in another way, the three mineral assemblage, Bt + Kfs + Mt, defines the activity of  $O_2$  in the presence of water.

The model reaction (3.25) helps to understand the REDOX behaviour of  $Fe^{2+}$ -bearing silicate minerals such as micas, amphiboles and pyroxenes in general. The reaction transfers the Fe-biotite component annite to feldspar and Fe-oxide thus leaving behind the Mg-biotite component phlogopite in the mica. Hence, the Mg/Fe ratio of silicates, the ferrous/ferric ratio of coexisting oxides, and oxygen activity are interrelated. At high  $a_{O_2}$ , Fe–Mg silicates tend to be Mg-rich and coexist with hematite and at lower  $a_{O_2}$  silicates contain less of the Mg phase component and tend to occur with magnetite  $\pm$  ilmenite under at the same temperature. In layered rocks with contrasting silicate + oxide assemblages, this implies that the rocks have retained the oxidation state of their protolith and that oxygen activity is controlled by the mineral assemblage in the rocks. Where extensive reaction with a fluid phase during metamorphism has occurred such primary oxidation variation may be eliminated and the oxygen activity is imposed externally.

REDOX reactions do not necessarily involve molecular gas species. Redox reactions may also be formulated in ionic form (e.g. the Mag–Hem reaction):

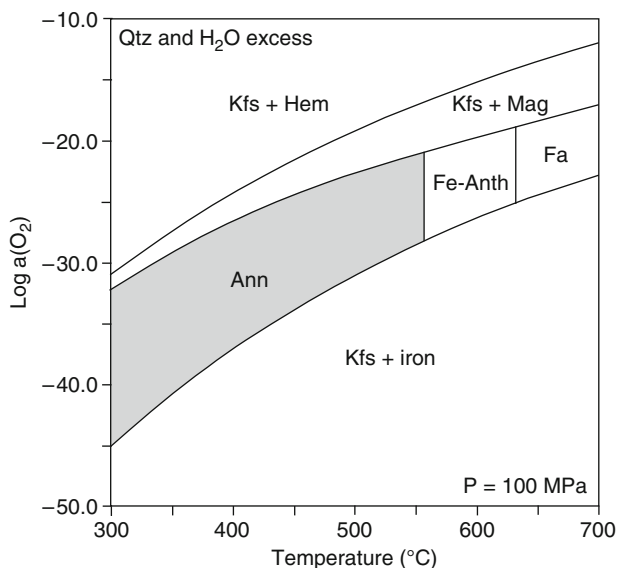
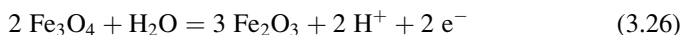


**Fig. 3.21** Log oxygen activity– $T$  diagram at 200 MPa showing stability fields for Fe-biotite (annite) (*shaded field*), Fe-anthophyllite, fayalite, and K-feldspar (microcline/sanidine) coexisting with iron, magnetite, hematite, in the presence of excess quartz and water. Standard state for  $O_2$ : pure gas at  $T$  and  $10^5$  Pa

Oxidation of magnetite to hematite in the presence of water produces two  $H^+$  and two electrons. This formulation shows that oxydation produces electrons, reduction consums electrons ( $Fe^{2+} = Fe^{3+} + e^-$ ). The magnetite–hematite reaction (3.26) depends on the REDOX potential ( $p_e = -\log a_{e^-}$ ) and on the activity of the hydrogen ion ( $p_H = -\log a_{H^+}$ ). Graphical representation of equilibria of the type (3.26) is often done by means of  $p_e$  (oxidation potential) versus  $p_H$  diagrams (see Garrels and Christ 1965).

### 3.6.2.5 Reactions Involving Sulfur

Sulfides are widespread accessory minerals in metamorphic rocks. Most common are pyrrhotite ( $FeS$ ) and pyrite ( $FeS_2$ ). If both Fe-sulfides occur in a metamorphic rock, their stable coexistence requires equilibrium of the reaction:



The dominant sulfur species in metamorphic fluids is either  $H_2S$  or  $SO_2$ . If one wishes to discuss sulfide-involving reactions in terms of the most abundant species, (3.27) can be rewritten in the presence of water ( $2H_2O = 2H_2 + O_2$ ;  $2H_2S = 2H_2 + S_2$ ) as:



Graphical representation of sulfide-involving reactions depends on the actual problem but partial pressure (activity, fugacity) of a sulfur species in the fluid versus temperature diagrams are popular. If sulfide reactions are combined with REDOX reactions, oxygen (hydrogen) versus sulfur diagrams are useful. As an example, Fig. 3.22 shows the phase relationships among some iron oxides and sulfides in terms of  $a_{H_2}$  and  $a_{H_2S}$ . The diagram shows that the presence of one Fe-sulfide and one Fe-oxide in a metamorphic rock (e.g. magnetite and pyrrhotite) fixes the activities of  $H_2$  and  $H_2S$  to distinct values along a univariant line at a given P and T in the presence of water. Rocks may be zoned with respect to oxides and sulfides depending on gradients in  $a_{H_2S}$ , e.g. under reducing conditions, rocks may contain magnetite, pyrrhotite or pyrite with increasing  $a_{H_2S}$ .

### 3.6.2.6 Reactions Involving Halogens

Fluorine and chlorine may replace OH groups in all common rock-forming hydrous minerals, notably mica, talc and amphibole (less so in serpentine minerals and chlorite). The halogen content of common rock-forming minerals may be related to exchange reactions of the type (e.g. fluorine-hydroxyl exchange between biotite [phlogopite] and fluid):

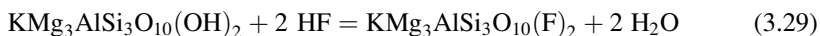
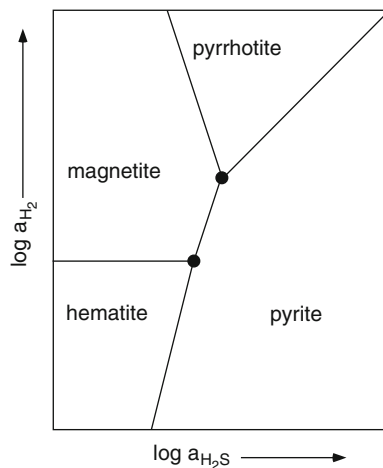


**Fig. 3.22** Qualitative phase relationships among hematite, magnetite, pyrrhotite and pyrite in a  $\log a_{\text{H}_2}$  versus  $\log a_{\text{H}_2\text{S}}$  activity–activity diagram

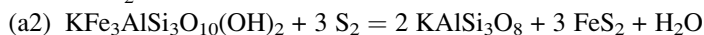
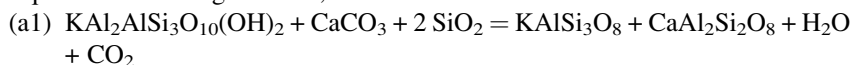


Also in this case, equilibria of the type (3.29) are commonly shown and discussed in terms of partial pressure (fugacity, activity) of a gaseous halogen species ( $\text{HCl}$ ,  $\text{HF}$ ) versus temperature diagrams or in terms of  $\mu$ – $\mu$ -diagrams (or activity–activity diagrams).

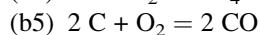
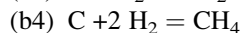
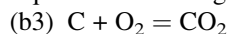
### 3.6.2.7 Complex Mixed Volatile Reactions and Fluids

It is a common situation in metamorphic rocks, that they contain simultaneously halogen-bearing hydrous silicates, carbonates, sulfides, and oxides. Dealing with such rocks consequently means that all types of metamorphic reactions must be considered together. For example, consider a typical calcareous mica schist containing the minerals: calcite, quartz, K-feldspar, plagioclase, muscovite, biotite, graphite and pyrite. Among the minerals and nine potentially important fluid species the following linearly independent equilibria can be written:

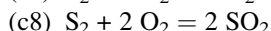
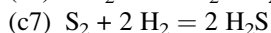
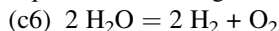
(a) Equilibria involving silicates, sulfides and carbonates



(b) Equilibria involving graphite



(c) Equilibria involving fluid species only



A mass action equation can be formulated for all eight equilibria [see, for example (3.16)]. Mass action equations express the equilibrium constant in terms of activities at constant pressure and temperature. In addition, in the presence of a free fluid phase in the rock, the following mass balance equation (total pressure equation) can be written:

$$(d9) \quad p_{\text{total}} = p_{\text{fluid}} = p_{\text{H}_2\text{O}} + p_{\text{CO}_2} + p_{\text{O}_2} + p_{\text{H}_2} + p_{\text{CH}_4} + p_{\text{CO}} + p_{\text{S}_2} + p_{\text{H}_2\text{S}} + p_{\text{SO}_2}$$

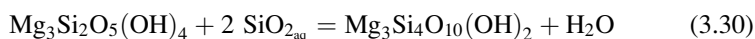
Equation (d9) states that the sum of the partial pressures of the fluid species is equal to the total lithostatic rock pressure. Together with activity (fugacity) – partial pressure functions for the species in the fluid, the set of nine equations can be solved iteratively for the nine unknown partial pressures and hence the fluid composition. This means that the mineral assemblage of the calcareous mica schist defines and completely controls the composition of the coexisting fluid phase at any given pressure and temperature. In other words, the minerals of the rock **buffer** the fluid composition. In most metamorphic fluids the partial pressures of  $\text{O}_2$  and  $\text{CO}$  are extremely low compared with the total pressure.  $\text{H}_2$  is usually also low in most metamorphic fluids. The dominant sulfur species in the fluid is  $\text{H}_2\text{S}$  at low temperatures and  $\text{SO}_2$  at high temperatures.  $\text{CH}_4$  may be high in some fluids at lower temperature.  $\text{CO}_2$  is dominant at higher temperatures.

### 3.6.2.8 Reactions Involving Minerals and Dissolved Components in Aqueous Solutions

The fluids that are associated with rock metamorphism in crust and mantle inevitably migrate from the source area. They come in contact with other rocks with which they may not be in equilibrium. Chemical reactions that attempt to establish equilibrium between the solid rock assemblage and the fluid are termed “**fluid–rock interactions**”. Fluid–rock interaction is important in, for example, the formation of hydrothermal ore deposits, contact metasomatism, large-scale infiltration and reaction during orogenesis, in shear zone metasomatism, fissure mineral deposition and in geothermal fields. As an example, take a crustal volume containing rocks with the assemblage margarite + calcite + quartz (Fig. 3.18). An externally-derived fluid with the composition  $X_{\text{CO}_2} = 0.01$  infiltrates this rock at  $T_{\text{high}}$ . The fluid is in equilibrium with the product assemblage of reaction (3.19) rather than with the reactant assemblage that is actually present. A consequence of fluid infiltration is that the fluid will drive the reaction until it reaches equilibrium with the solid phase assemblage. In this case the rock cannot buffer the fluid composition and is controlled by the external fluid.

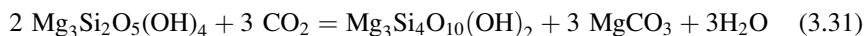
Commonly, metamorphic fluids are saline brines containing high concentrations of metal ions and complexes. Therefore, infiltrating fluids may also have a cation composition that is not in equilibrium with the solid phase assemblage it comes in contact with. An essential aspect of fluid-rock interaction is the reaction of phase components of the solid mineral assemblage of the rock and dissolved species in the external fluid. Some examples:

1. Formation of talc schist by interaction of serpentinite with silica-rich fluids:

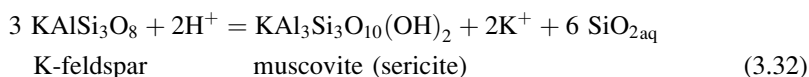


where  $\text{SiO}_{2\text{aq}}$  refers to an uncharged hydrous silica complex in the aqueous fluid. In many cases, the  $\text{SiO}_2$ -rich fluid infiltrating the serpentinite is saturated with respect to quartz, which results from interaction of the fluid with granitic gneiss or quartzo-feldspathic schist that encloses the serpentinite body.

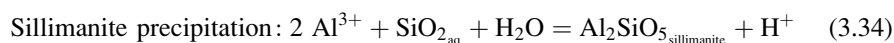
2. Formation of soapstone (Tlc + Mgs rock) by interaction of serpentinite with  $\text{CO}_2$ -bearing fluids:



3. Sericitization of K-feldspar is a widespread process during retrograde metamorphism:



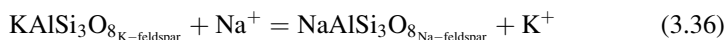
Reactions of the type (3.32) are important in geology and are referred to as **hydrolysis reactions**. Any other kind of metamorphic mineral reaction can be viewed as a linear combination of a series of hydrolysis reactions. For example, the phase transition kyanite = sillimanite can be viewed as a result of two hydrolysis reactions (Carmichael 1968):



In extremely acid aqueous fluids,  $\text{Al}^{3+}$  is the dominant Al species, but similar reactions can be written with other Al species such as  $\text{Al}(\text{OH})^{2+}$ ,  $\text{Al}(\text{OH})_2^+$ ,  $\text{Al}(\text{OH})_3^0$ ,  $\text{Al}(\text{OH})_4^-$ , depending on the pH of the fluid.

The above example of the  $Ky = Sil$  reaction illustrates the most efficient mechanism by which old unstable minerals or mineral assemblages are replaced by more stable ones. The unstable reactant minerals dissolve in the aqueous solution because they have a higher solubility than the stable product minerals. The more stable minerals and mineral assemblages precipitate from the aqueous solution after a certain threshold degree of supersaturation is reached and nucleation and growth of the reaction products begin. This general process mechanism of dissolution and precipitation that involves an aqueous fluid is fundamental to water–rock interaction in hydrothermal and geothermal systems (and weathering, diagenesis and other near surface processes as well). However, it is also expected to be the most efficient processes mechanism in metamorphism at high  $P$ – $T$  conditions. Strong evidence for this claim is, that in high-grade metamorphism structural disequilibrium and persistence of metastable assemblages increases with grade. This is unexpected at a first glimpse because reaction kinetics and diffusive transport is favored by increasing temperature. However, at high  $P$  and  $T$  metamorphic rocks tend to lose the aqueous fluid and thus the efficient dissolution–precipitation mechanism vanishes with the fluid.

A further important fluid–rock interaction process is the albitization of K-feldspar. It is an **ion exchange reaction** that occurs during low-grade alteration of granite and granite-gneiss:



Ionic reactions in the formation of hydrothermal ore deposits are also important and can be illustrated by the dependence of the solubility of covellite ( $CuS$ ) on  $p_H$ .



Suppose there is an acid metamorphic fluid with some  $Cu^{2+}$ . Covellite will precipitate from that fluid as a result of increasing  $p_H$  caused by feldspar alteration (3.32). Alteration processes such as reaction (3.32) (micas from feldspars, chlorite from amphiboles) increase the  $p_H$  and lead to precipitation of metal oxides and sulfides.

Graphically, ionic (complex) reactions can be represented by means of  $p_H$  versus gas pressure (activity, fugacity) diagrams, activity–activity diagrams (or  $\mu$ – $\mu$  diagrams), activity–temperature diagrams, etc., depending on the actual geological problem. A computed quantitative activity–activity diagram for the system  $Na$ – $K$ – $Al$ – $Si$ – $O$ – $H$  (Fig. 3.23) shows the fields for alkali-feldspars (K-feldspar and albite), micas (muscovite, paragonite), and an Al-silicate with respect to the activity of alkali oxides. The diagram shows that at low  $a_{K_2O}$  and  $a_{Na_2O}$ , Al-silicate is stable, whereas the opposite stabilizes feldspars. Micas are present at intermediate activities of alkali oxides. The activities of the alkali metal oxides can be converted to conventional ionic species in an aqueous fluid by the equations:  $Na_2O + 2H^+ = 2Na^+ + H_2O$  and  $K_2O + 2H^+ = 2K^+ + H_2O$  corresponding to  $\log a_{Na_2O} = 2 \log(a_{Na^+}/a_{H^+})$  and  $\log a_{K_2O} = 2 \log(a_{K^+}/a_{H^+})$ . The phase boundaries are markedly curved near the transitions of Kfs to Ab and Ms to Pg as a result of  $Na$   $K_{-1}$  exchange in Fsp and white mica.

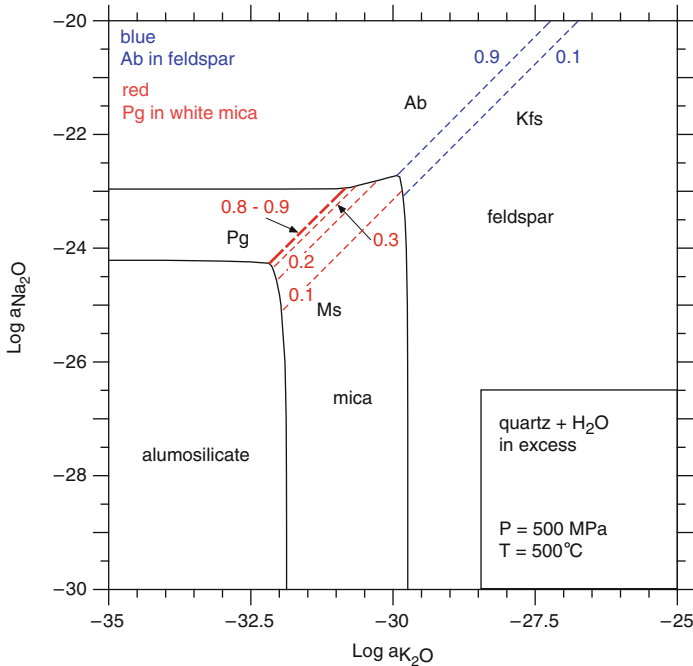
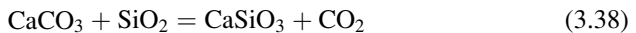


Fig. 3.23 Computed, quantitative activity-activity diagram for the system Na-K-Al-Si-O-H

### 3.7 Reaction Progress

Chemical reactions in rocks proceed in response to gradients in intensive variables (e.g. increase in temperature). The progress of a chemical reaction can be illustrated by using the wollastonite-producing reaction (Fig. 3.17) as an example:



Calcite and quartz may react and produce wollastonite and release CO<sub>2</sub> gas. The equilibrium conditions of the reaction are shown in Fig. 3.24 as a function of temperature and the composition of a binary CO<sub>2</sub>-H<sub>2</sub>O fluid at a total pressure of 200 MPa. A calcite- and quartz-bearing rock with an initial pore space of 1% may contain a fluid of the composition X<sub>CO<sub>2</sub></sub> = 0.01. Adding heat to this rock brings it to the reaction boundary of the wollastonite-producing reaction at a temperature of about 450°C. Further addition of heat will produce wollastonite and the fluid becomes enriched in CO<sub>2</sub> as a result of CO<sub>2</sub> released by the reaction. Suppose the rock finally reaches a temperature of 600°C and contains the isobaric univariant assemblage calcite + quartz + wollastonite. It is a simple matter to calculate the modal amount of wollastonite produced by the reaction:



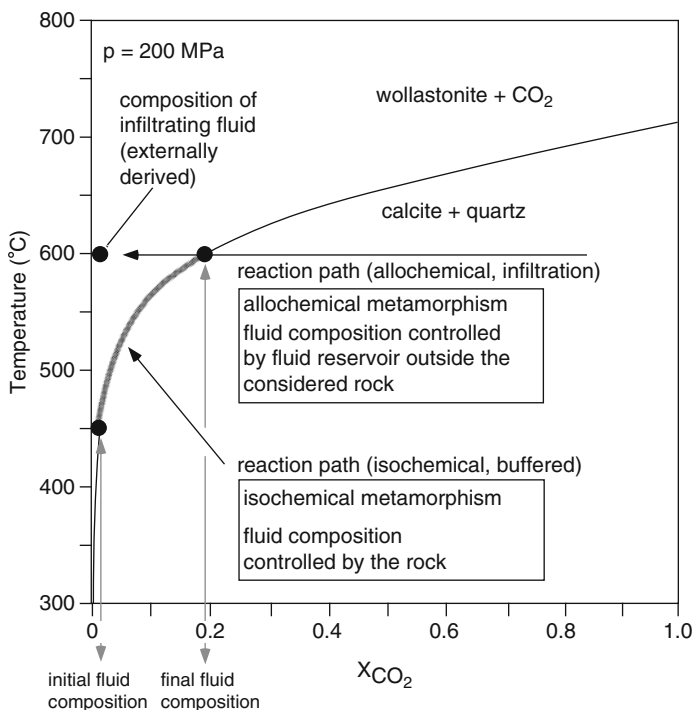


**Fig. 3.24** Quantitative temperature versus fluid composition phase diagram showing the equilibrium conditions of the wollastonite reaction at 200 MPa

Reference volume: 1,000 cm<sup>3</sup> rock

1% pore space = 10 cm<sup>3</sup> fluid per 1,000 cm<sup>3</sup>

Cal + Qtz reaches equilibrium with Wo at 450°C (200 MPa) and  $X_{\text{CO}_2} = 0.01$  (Fig. 3.24)

Cal + Qtz + Wo assemblage at 600°C (200 MPa) and  $X_{\text{CO}_2} = 0.19$  (Fig. 3.24)

Molar volume of H<sub>2</sub>O at 450°C, 200 MPa = 24 cm<sup>3</sup>/mol (Fig. 3.10)

Initial fluid 99 mol% H<sub>2</sub>O + 1 mol% CO<sub>2</sub> (assume for simplicity pure H<sub>2</sub>O)

Number of moles of H<sub>2</sub>O in the initial fluid:  $n_{\text{H}_2\text{O}}^0 = 10/24 = 0.42$  mol H<sub>2</sub>O

Initial  $X_{\text{CO}_2}^0 = n_{\text{CO}_2}^0 / (n_{\text{CO}_2}^0 + 0.42)$

Final  $X_{\text{CO}_2}^f = n_{\text{CO}_2}^f / (n_{\text{CO}_2}^f + 0.42)$

Solving for:

Number of moles of CO<sub>2</sub> in the initial fluid:  $n_{\text{CO}_2}^0 = 4.21$  mmol

Number of moles of CO<sub>2</sub> in the final fluid:  $n_{\text{CO}_2}^f = 4.21$  mmol

CO<sub>2</sub> produced by the reaction:  $\Delta n_{\text{CO}_2} = n_{\text{CO}_2}^f - n_{\text{CO}_2}^0 = 96.5 - 4.21 = 92.34$  mmol

With reference to (3.38): 92.34 mmol CO<sub>2</sub> is equivalent to 92.34 mmol of wollastonite produced by the reaction per 1,000 cm<sup>3</sup> rock.

The molar volume of wollastonite is:  $V^0 = 40$  cm<sup>3</sup>/mol

Wollastonite produced by buffered reaction: 3.7 cm<sup>3</sup> (0.367 vol%)

The amount of wollastonite is very small and would hardly be detected under the petrographic microscope.

Let us now consider a calcite- and quartz-bearing rock with 20 vol% wollastonite that equilibrated at 600°C and 200 MPa. From the calculations above it is evident that isochemical metamorphism can produce only a very small modal amount of wollastonite (at 600°C and 200 MPa). Consequently, a very wollastonite-rich rock that formed at these conditions must be the result of interaction of the rock with an externally-derived H<sub>2</sub>O-rich fluid that pushed conditions across the reaction equilibrium into the wollastonite field shown in Fig. 3.24. The question is how much H<sub>2</sub>O must be added to the rock in order to produce the observed modal proportion of wollastonite? This can be readily calculated:

20 vol% wollastonite ( $V^0 = 40 \text{ cm}^3/\text{mole}$ ) = 0.5 mol/100 cm<sup>3</sup>  
 The rock contains 5 mol wollastonite per 1,000 cm<sup>3</sup> rock. It follows from the reaction stoichiometry of reaction (3.38) that the reaction also produced 5 mol of CO<sub>2</sub>.  
 However the final  $X^f_{\text{CO}_2} = n^f_{\text{CO}_2} / (n^f_{\text{CO}_2} + n^f_{\text{H}_2\text{O}})$  is equal to 0.19 (Fig. 3.24).  
 Solving for:  $n_{\text{H}_2\text{O}} = n^f_{\text{CO}_2} (1 - X^f_{\text{CO}_2}) / X^f_{\text{CO}_2}$   
 gives:  $n_{\text{H}_2\text{O}} = 5 \times 0.81 \times (1/0.19) = 21.315 \text{ mol H}_2\text{O}$   
 The molar volume of H<sub>2</sub>O is:  $V^0 (600^\circ\text{C}, 200 \text{ MPa}) = 31 \text{ cm}^3$  (Fig. 3.10)  
 The total volume of H<sub>2</sub>O that reacted with the rock is:  $V_{\text{H}_2\text{O}} = 660 \text{ cm}^3 / 1,000 \text{ cm}^3 \text{ rock}$

In conclusion, a rock with 20 vol% wollastonite that formed from calcite + quartz at 600°C and 200 MPa requires interaction with 660 cm<sup>3</sup> H<sub>2</sub>O per 1,000 cm<sup>3</sup> rock. This represents a minimum value. If the composition of the interacting fluid is more CO<sub>2</sub>-rich, more fluid is required to produce the observed amount wollastonite in the rock. The deduced amount of interacting external fluid may be expressed in terms of a time-integrated fluid to rock ratio: fluid–rock ratio = 660 cm<sup>3</sup>/1,000 cm<sup>3</sup> = 0.66

A brief comment may be added here with reference to Fig. 2.4. This fictive wollastonite–calcite–quartz rock was used to illustrate how the mineral assemblage is related to the structure of the rock, i.e., how the three minerals are distributed in the rock. We now relate the three rocks to reaction (3.38) and Fig. 3.24.

The rock texture shown in Fig. 2.4a is chemically layered with a marble layer at the top and a calc-silicate layer below. The two rock “layers” may have similar Ca/Si ratios. However, it follows from Fig. 3.24 that, at a given temperature (e.g. 600°C) the marble layer is consistent with a fluid with  $X_{\text{CO}_2}$  greater than the  $X_{\text{CO}_2}$  corresponding to equilibrium of reaction (3.38). The Wo + Qtz rock of the lower calc-silicate layer is consistent with  $X_{\text{CO}_2}$  smaller than the  $X_{\text{CO}_2}$  corresponding to the equilibrium of reaction (3.38). Consequently, if a fluid is present in the rock it is of different composition in the two chemically distinct parts of the rock. The two layers are isolated with respect to the fluid and the two minerals in the top layer do not form an assemblage with the two minerals of the bottom layer. At the

interface between the two layers two different fluids may be present over a very small interval. Such “fluid-discontinuities” are commonly observed in hydrothermal veins, finely-banded impermeable metasediments, and other rocks showing large compositional heterogeneity.

The rock in Fig. 2.4b contains the true assemblage Cal–Qtz–Wo that is stable at any temperature along the equilibrium curve of reaction (3.38) shown in Fig. 3.24. It is also clear that at a given temperature (e.g. 600°C) the three minerals buffer the fluid composition, they fix the composition of the fluid to a specific  $X_{\text{CO}_2}$  value at P and T.

The rock in Fig. 2.4c is difficult to interpret on the basis of Fig. 3.24. A plausible explanation might be that very small-scale fluid heterogeneity existed in this rock with water-rich fluid probably channeled along small-scale pathways. Actually, two very small-scale veinlets can be discerned from the structure shown in Fig. 2.4c. Along them, wollastonite was produced from reaction of Cal + Qtz with H<sub>2</sub>O-rich fluid. But remember, this is a computer-generated diagram of a fictive rock texture.

## 3.8 Phase Diagrams

### 3.8.1 Phase Diagrams, General Comments and Software

Phase diagrams display equilibrium relationships among phases and phase assemblages in terms of intensive, extensive or mixed variables. A widely used type of phase diagram in metamorphic petrology is the  $P$ – $T$  diagram. It shows the equilibrium relationships among minerals (and fluids) as a function of the intensive variables pressure and temperature. The chosen ranges of the parameter values define a  $P$ – $T$  window that is appropriate for the problem of interest. Mineral and fluid compositions may be constant or variable on such a diagram. Composition phase diagrams show the phase relationships in terms of extensive variables at specified values of pressure and temperature. AFM and ACF diagrams described in Chap. 2 are examples of such composition phase diagrams.

Phase diagram software is routinely used to compute and display petrologic phase diagrams from published sets of thermodynamic data of phase components and models of the thermodynamic properties of fluid and solid solutions. All phase diagrams in this book were computed by using the program package THERIAK/DOMINO, a multipurpose software system that permits the construction of remarkably complex phase diagrams (de Capitani and Petrakakis 2010) together with updated versions of the data base of Berman (1988).

Other petrologic programs include (see Chap. 4 for more information about some of these programs): PERPLEX by Connolly (1990), Connolly and Kerrick (1987); THERMOCALC by Powell and Holland (1985, 1988); TWQ or TWEEQU by Berman (1991); SUPCRT92 by Johnson et al. (1992); PTPATH by Spear et al. (1991)

and THERMO by Perkins et al. (1987). Compilations of thermodynamic data for substances of geologic interest are found in Clark (1966), Burnham et al. (1969), Stull and Prophet (1971), Robie et al. (1978), Helgeson et al. (1978), Holland and Powell (1985, 1990, 1998), Powell and Holland (1985, 1988), Berman (1988), Johnson et al. (1992). The thermodynamic data sets of Berman (1988) [RB88] and Holland and Powell (1990, 1998) [HP90; HP98] are classified as so-called internally consistent data sets because of the specific data retrieval technique used in deriving the data. These two sets are particularly well suited for use in conjunction with the two mentioned programs and are widely used by metamorphic petrologists. Thermodynamic data can be derived from calorimetric measurements and, especially, from experimental phase equilibrium data. Nearly all phase diagrams shown in this book have been generated by THERIAK/DOMINO using the RB88 data base (or updated versions of it).

Phase diagrams are indispensable tools for the description, analysis and interpretation of metamorphic rocks and metamorphism. The ability to read and understand phase diagrams is central and essential in metamorphic petrology. The capability to calculate and construct phase diagrams is important for all those who are in need of phase diagrams for phase assemblages and phase compositions that are unique for the geologic problem in question. It may also be necessary to modify published phase diagrams and adapt them to the actual problem, e.g. change the  $P$ - $T$  frame or other parameter values or modify solid solution models or add data for new phase components to the data base.

It is also clear, that phase diagrams depict the equilibrium state of a system and thus represent the target configuration for a system adjusting to disequilibrium. They give the framework for the ultimate order when processes and reactions cease and come to an end. However, it is a terribly trivial insight that metamorphism is more than phase diagrams. Metamorphic processes and reactions are caused by disequilibrium in the system as discussed in various parts of the text so far. Reaction kinetics and local mass transfer coupled with deformation determine the structure of metamorphic rocks and control how close the mineral assemblages approach the equilibrium case depicted on phase diagrams.

### **3.8.2 *The Phase Rule***

Although it is not the intention of this book to give a comprehensive treatment of the computation and construction of phase diagrams, it is useful to briefly introduce two important aspects of phase diagrams: the phase rule and Schreinemakers rules.

The state of a heterogeneous system, such as a rock, depends on a number of state variables such as pressure, temperature and chemical potentials. The requirements of heterogeneous equilibrium impose some restrictions on these variables (equilibrium constraints). The phase rule relates the number of variables in a system and the

number of equations that can be written among them at equilibrium. In a system with a total number of  $c$  components and composed of  $p$  phases the number of variables is:

- For each phase: T, P, and  $c-1$  compositional variables =  $c + 1$
- For the system of  $p$  phases:  $p(c + 1)$

Equilibrium constraints:

- The temperature of all phases must be the same (thermal equilibrium)  $\Rightarrow$
- $p - 1$  equations of the type: T of phase  $\alpha =$  T of phase  $\beta$
- The pressure on all phases must be the same (mechanical equilibrium)  $\Rightarrow$
- $p - 1$  equations of the type P on phase  $\alpha =$  P on phase  $\beta$
- The chemical potential of component  $i$  must be the same in all phases (chemical equilibrium)  $\Rightarrow$
- $c(p - 1)$  equations of the type  $\mu_{i\alpha} = \mu_{i\beta}$ ;  $p - 1$  equations for each component from 1 to  $c$

Hence, the number of variables  $n_v$  is:  $p(c + 1)$ , and the number of equations  $n_e$ :  $2(p - 1) + c(p - 1)$ .

Now let us define a variable  $f$  as the difference between  $n_v$  and  $n_e$ .  $f$  simply expresses how many variables can be changed independently in a system at equilibrium

$$f = n_v - n_e = [p(c + 1) - 2(p - 1) - c(p - 1)]; \text{ or simply}$$

$$\mathbf{f = c + 2 - p} \quad (3.39)$$

This equation is known as the **phase rule**.  $f$  is often referred to as **variance** or **degrees of freedom** of the system. A consequence of the phase rule is that the number of phases cannot exceed the number of components by more than 2.

In a one-component system (e.g.  $\text{Al}_2\text{SiO}_5$ ) consisting of one phase (e.g. kyanite), there are two variables which can be varied independently, i.e. P and T. If there are two phases present (sillimanite and kyanite), only one variable can be specified independently. If there are three phases present (andalusite, sillimanite and kyanite), the number of variables equals the number of equations ( $f = 0$ ) and the system of equations has one unique solution. In other words, coexistence of all three aluminosilicates completely defines the state of the system and this is only possible at a unique value of P and T (the triple point, invariant point). Another well-known one-component system is the system  $\text{H}_2\text{O}$ . Ice has  $f = 2$ , melting ice has  $f = 1$  and ice, water and steam ( $f = 0$ ) may be in equilibrium at the unique P and T values of the triple point.

### 3.8.2.1 Phase Rule in Reactive Systems

Consider a system with  $N$  phase components (chemical species), some inert, some at reaction equilibrium.  $R$  is the number of independent reactions and  $p$  the number of phases.

Number of variables:  $p(N + 1)$

Number of equations:  $(N + 2)(p - 1) + R$

$R$  = number of conditions of reaction equilibrium  $\sum \nu \mu = 0$

$$f = n_v - n_e = N - R + 2 - p \quad (3.40)$$

An example; the mineral assemblage Grt + Crd + Sil + Qtz consists of four phases and we may consider seven phase components (garnet: Grs, Prp, Alm ; cordierite: Fe–Crd, Mg–Crd; sillimanite: Sil; quartz: Qtz). The seven phase components are related by two independent reactions (net transfer:  $2\text{Alm} + 5\text{Qtz} + 4\text{Sil} = 3\text{Fe–Crd}$ ; exchange:  $\text{FeMg}_{-1}(\text{Grt}) = \text{FeMg}_{-1}(\text{Crd})$ ). The variance of the assemblage calculated from (3.40) is 3. This means that the system of equations has a unique solution if three variables can be specified independently. If, for example, the Alm and Prp content of the garnet and the Fe–Crd content of the cordierite were measured in a rock containing the four minerals in equilibrium, then the system is uniquely defined and the equilibrium pressure and temperature can be calculated. By defining  $c = N - R$ , the two forms of the phase rule become formally identical. The number of components in the sense of the phase rule is therefore taken as the total number of phase components (chemical species) minus the number of independent reactions between them. In the example used above, the number of system components is five (seven phase components – two independent reactions). Simple oxide components are often selected as system components and the five components CaO–MgO–FeO–Al<sub>2</sub>O<sub>3</sub>–SiO<sub>2</sub> (CMFAS) define the composition space of the Grt + Crd + Sil + Qtz rock. For a comprehensive treatment of the composition space and reaction space see Thompson (1982a, b). The phase rule derivation has been adapted from Denbigh (1971).

### 3.8.3 Construction of Phase Diagrams for Multicomponent Systems After the Method of Schreinemakers

A binary system of four phases is, according to the phase rule, invariant. The four minerals may occur at a unique pair of temperature and pressure (or any other two intensive variables). Graphically the four-phase assemblage occurs at a point (invariant point) on a  $P$ – $T$  diagram. From this point four univariant assemblages represented by univariant lines (curves) radiate into the  $P$ – $T$  plane (surface). The univariant lines are characterized by the absence of one of the phases occurring at the invariant point and divide the  $P$ – $T$  plane in four divariant sectors. Each of these sectors is characterized by one unique two-phase assemblage that occurs in only one sector. The geometric distribution of univariant and divariant assemblages follows strict rules that may be derived from chemical thermodynamics. These rules were formulated by F.A.H. Schreinemakers, in a series of articles between 1915 and 1925 and are known today as Schreinemakers rules. Figure 3.25a shows the geometry of the general binary four-phase system and Fig. 3.25b represents a

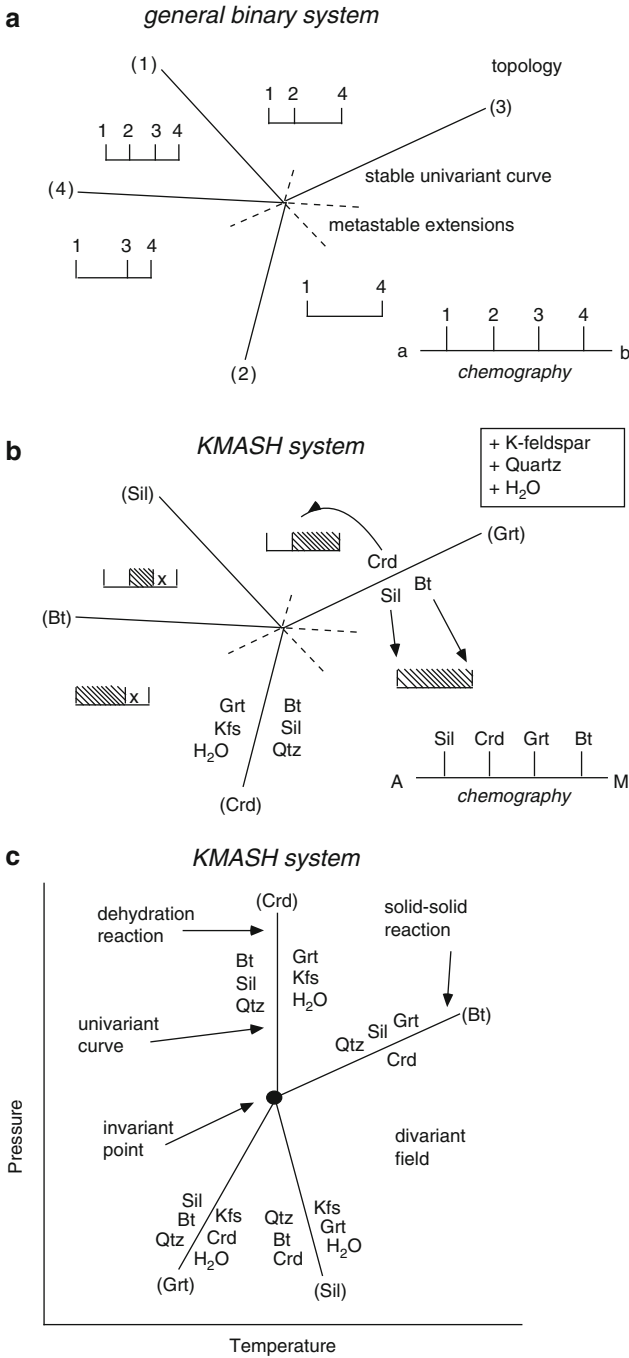


**Fig. 3.25** Schreinemaker diagram for general binary four phase assemblages (a), an example assemblage, Sil, Fe-Crd, Fe-Grt, and Fe-Bt projected from K-feldspar, quartz and H<sub>2</sub>O (b), and the translation of the relationships shown in (b)3.25 into P-T space (c)

specific geologic example. For three-component five-phase systems and complications arising from compositional degeneracies, the reader is referred to Zen (1966).

The general geometry of the binary system (Fig. 3.25a) shows an invariant assemblage of four phases with the compositions 1–4 in the two-component system a–b. The space around the invariant point is divided into four sectors by four univariant curves. Each of these curves is characterized by the absence of one phase of the invariant four-phase assemblage. The name of the absent phase is enclosed by brackets. The sectors contain either two, one or no metastable extension of the four univariant curves. The sector between the curves (2) and (3) contains two metastable extensions and is characterized by the presence of the divariant assemblage 1 + 4 which occurs only in this sector. The assemblage contains the most a-rich and the most b-rich phase, respectively. If the sector boundary (3) is crossed, 1 + 4 form phase 2, which is a new phase of intermediate composition (3 does not participate in the reaction, (3) is absent). If the sector boundary (1) is crossed, 3 forms from 2 + 4 (1 is absent). In the sector between (1) and (4), three two-phase assemblages may be present depending on the relative proportions of the components *a* and *b* in the rock. However, only one of the three assemblages is unique for the sector, namely 2 + 3. Crossing the sector boundary (4), phase 2 decomposes to 1 + 3 (4 does not participate in the reaction). Finally, crossing univariant curve (2) removes 3 by the reaction  $3 = 1 + 4$ .

Figure 3.25b shows a specific geologic example. In rocks containing excess quartz and K-feldspar and for H<sub>2</sub>O-saturated conditions, the four minerals garnet, cordierite, biotite and sillimanite can be represented in a binary chemographic diagram. The diagram is a projection through quartz, K-feldspar and H<sub>2</sub>O (and parallel to the MgFe<sub>-1</sub> exchange vector). The geometry shown for the general binary case in Fig. 3.25a may be readily translated into Fig. 3.25b. The unique divariant assemblage for each sector is shaded in Fig. 3.25b. Note, however, that some assemblages, e.g. garnet + biotite, occur in more than one sector. Any assemblage occurring in two sectors (in the binary case) contains the phase which is absent at the sector boundary (biotite in our case). This is because biotite + garnet is not affected by the biotite-absent reaction  $\text{Crd} = \text{Sil} + \text{Grt}$ . Also note for instance, that in the cordierite-absent reaction  $\text{Bt} + \text{Sil} = \text{Grt}$ , the assemblage containing biotite must be in the sector that is not bounded by the biotite-absent reaction, and garnet must be in the sector that is not bounded by the garnet-absent reaction. This is a general rule and must be obeyed by all univariant assemblages along any of the curves.

Once the correct sequence and geometry of univariant assemblages is established around an invariant point the sequence may be translated into pressure-temperature space (Fig. 3.25c).

Three of the four reactions in our example are dehydration reactions. It is fairly safe to assume that H<sub>2</sub>O is released from biotite as temperature increases. The reactions (Crd), (Grt) and (Sil) should therefore be arranged in such a way that H<sub>2</sub>O appears on the high-temperature side of the univariant curve. In addition, dehydration reactions commonly have steep slopes on *P*–*T*-diagrams. Two solutions are possible; (1) the (Crd) reaction extends to high pressures from the invariant point



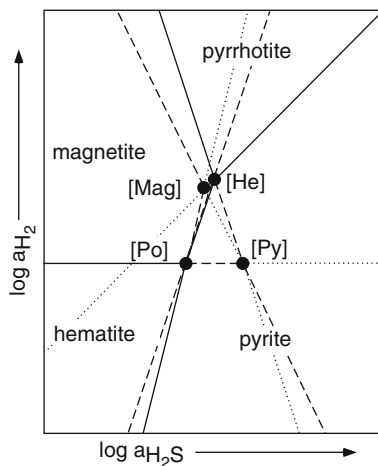
(the reactions (Grt) and (Sil) extend to the low-pressure side), or (2) (Crd) extends to low pressures. Both solutions are geometrically correct. Solution (1) is shown in Fig. 3.25c because cordierite is a mineral that typically occurs in low- to medium-pressure metapelites. In solution (2), cordierite is restricted to high pressures, which is not consistent with geological observations. The slope of the solid–solid reaction (Bt) cannot be constrained in a way similar to that for the dehydration reactions. However, it must extend from the invariant point into the sector between (Sil) and the metastable extension of (Grt). This follows from Fig. 3.25b. Therefore, it may have a positive or a negative slope. The equilibrium of the reaction is in reality rather independent of temperature and it represents an example of a geologic barometer.

The geometric arrangement of univariant curves around invariant points on any kind of phase diagram must be strictly consistent with Schreinemakers rules. Part II, on progressive metamorphism of various rock types, provides many examples of Schreinemakers bundles in two- and three-component systems on various types of phase diagrams.

Once the correct arrangement of univariant curves around an invariant point is known the connection of this invariant point to other (if any) invariant points in the system can be examined. If, for example, spinel needs to be considered in the example used, five invariant assemblages exist in the system. The one already considered was Grt + Crd + Bt + Sil that is characterized by the absence of spinel and the invariant point of Fig. 3.25 is consequently the [Spl] absent invariant point. According to the phase rule, the system has a variance of  $-1$ . Systems with negative  $f$ -values are called multisystems where more than one invariant assemblage exists. Some of the invariant assemblages may be stable, others are metastable. In general, the minerals of a multisystem cannot all simultaneously coexist at equilibrium. On phase diagrams multisystems are characterized by the presence of more than one, and usually several invariant points.

A simple example can be made by reconsidering the phase relationships shown in Fig. 3.22 where the minerals pyrite, pyrrhotite, hematite, magnetite and an  $H_2O$ -fluid in the four component system Fe–O–H–S are depicted. It follows from the phase rule that  $f = 1$ . Under isobaric isothermal conditions ( $P$  and  $T$  fixed),  $f = -1$  and five invariant assemblages exist. In the presence of an  $H_2O$ -fluid, there are four invariant assemblages involving three minerals each and lacking one mineral. Consequently, the invariant assemblages are [Po],[Py],[He] and [Mag]. As shown in Fig. 3.26, the pair [Po][He] is stable and [Mag][Py] is metastable at the selected  $P$ – $T$  conditions. Note that the univariant curves change their stability level at invariant points as indicated by different dashes of the metastable extensions of the stable curves. The Schreinemakers rules are also observed by the metastable invariant points, e.g. [Py]. Also note that the metastable invariant point [Mag] is inside the field of stable magnetite and that the metastable invariant point [Py] is inside the field of stable pyrite. Furthermore, there is one forbidden assemblage, namely pyrrhotite + hematite. The Po + He equilibrium has no stable sector in Fig. 3.26, as it connects as a metastable curve the two metastable invariant points [Mag] and [Py].

**Fig. 3.26** Qualitative phase relationships among hematite, magnetite, pyrrhotite and pyrite in a  $\log a_{\text{H}_2}$  versus  $\log a_{\text{H}_2\text{S}}$  activity-activity diagram (see also Fig. 3.22). Stable equilibria = *full lines*; metastable level 1 equilibria = *dashed lines*; metastable level 2 equilibria = *dotted lines*. Invariant points [Po][He] are stable; [Mag][Py] are metastable



Metastable phase relations are not normally shown on geologic phase diagrams. However, these are sometimes useful to consider and most phase diagram software permit the construction of diagrams showing the metastable phase patterns.

### 3.8.4 Use of Phase Diagrams, an Example

A phase diagram relevant for discussing metamorphism of carbonate rocks is used as an example to explain general properties and the use of phase diagrams. Metamorphism of marbles and carbonate-rich rocks will be presented in more detail in Chap. 6.

An isobaric  $T$ - $X_{\text{CO}_2}$  diagram (Fig. 3.27a) shows stable mineral assemblages in siliceous dolomite. Calcite and dolomite are present in excess (however, dolomite is replaced by brucite or periclase in the upper left area of the diagram) and each field on the diagram is characterized by one diagnostic mineral. The diagram can be understood as a map showing at each point the mineral with the lowest Gibbs free energy that coexists with calcite and dolomite and a fluid of the composition given along the x-axis at the temperature given along the y-axis and at a pressure of 200 MPa. The field boundaries shown in Fig. 3.27 represent reaction equilibria of mixed volatile reactions (see Sect. 3.6.2.3). The shapes of the curves correspond to those shown in Fig. 3.19 and they are given by the stoichiometry of the reactions. The equilibrium curves terminate at intersections with other equilibria (invariant points, see also Sect. 3.8.2) or they end at the boundaries of the selected parameter window. Only stable sections of reaction equilibria are shown; metastable equilibria have been omitted.

How can this figure be used for practical purposes? Before using this figure one must be convinced that the pressure of 200 MPa is significant to the actual

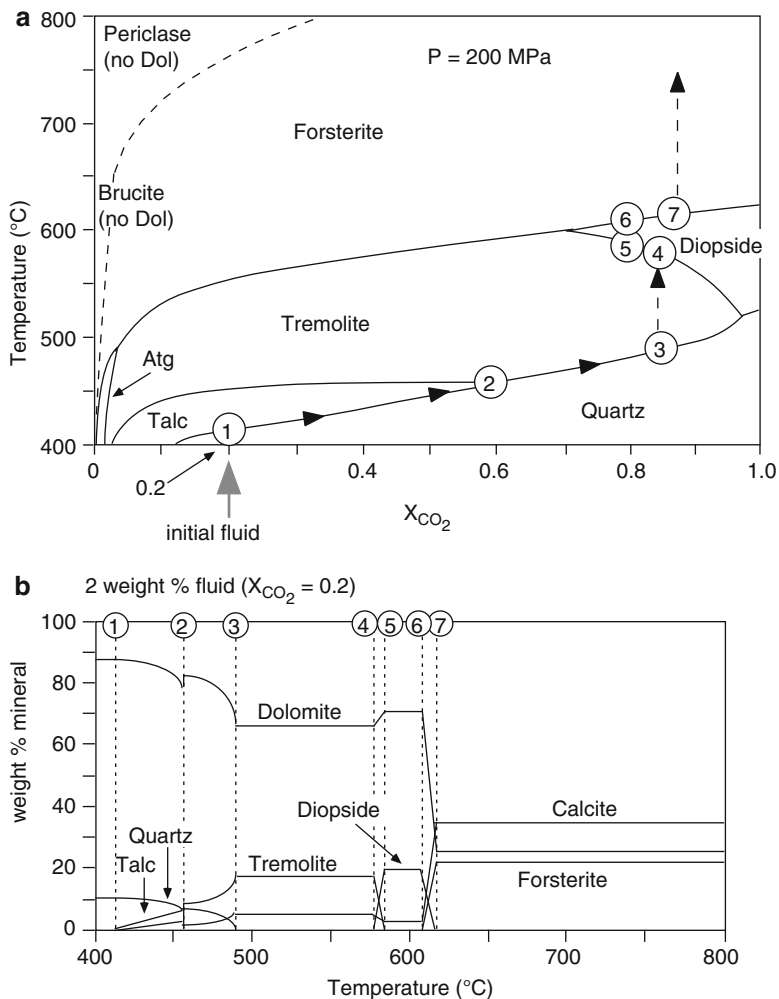


**Fig. 3.27** A quantitative model for isobaric metamorphism of siliceous dolomites in terms of a quantitative isobaric  $T-X$  diagram (a) and a modal composition versus  $T$  diagram (b). The diagram has originally been calculated using the computer code EQUILAS written by Brown and Skinner (1974)

geological situation of interest and that a binary  $CO_2-H_2O$  fluid was present during petrogenesis. If this is accepted, then two types of simple applications are obvious:

1. Given a marble with calcite + dolomite + diopside, at what possible  $T-X$  pairs was this rock stable? The answer would be: temperature was above  $520^\circ C$  and below  $630^\circ C$  and  $X_{CO_2}$  was greater than 0.7. An independent estimate of the

temperature at which the marble equilibrated can be made from Cal–Dol thermometry (see Chap. 4). If the temperature estimate for the rock is 550°C, then it follows that the diopside marble indicates the presence of an extremely CO<sub>2</sub>-rich fluid (>93 mol% CO<sub>2</sub>). If the diopside marble is the product of prograde metamorphism, what were the possible precursor assemblages? The answer: either Tr + Cal + Dol or Qtz + Cal + Dol.

- Given that a temperature of about 500°C has been reached during contact metamorphism at a certain distance from the contact of a granite pluton. The temperature may be determined, for example, from theoretical thermal modeling, from assemblages in other associated rocks of different composition, from fluid inclusion data, from Cal–Dol thermometry or from stable isotope data. What kind of marbles can be expected? The answer: tremolite marble is the obvious candidate. Quartz may still be present in rocks with an unusually CO<sub>2</sub>-rich fluid. Forsterite marble is possible but it would require an extremely H<sub>2</sub>O-rich fluid to form. If forsterite marble is present at this locality, one would suspect that it formed as a result of infiltration of an external fluid (see Fig. 3.24). This is even more likely for the assemblage Fo + Brc + Cal close to the X<sub>CO<sub>2</sub></sub> = 0 axis.

The phase diagram (Fig. 3.27a) can also be used to deduce complete paths of prograde metamorphism taken by a particular marble sample, e.g. a marble containing initially 88 wt% dolomite, 10 wt% quartz and 2 wt% fluid (with the composition 20 mol% CO<sub>2</sub> and 80 mol% H<sub>2</sub>O). The question is, what will happen to this rock if it is progressively heated to 800°C? The following discussion assumes that the volatile components released by the reactions are taken up by the fluid and remain in the rock. When heated, the model marble starts its reaction history at point (1) where talc becomes stable. The rock will be buffered along the talc field boundary by the talc-producing reaction exactly analogous to that explained in Sects. 3.6.2.3 and 3.7. How far the metamorphic path follows the talc field boundary can be calculated from the initial composition of the marble and the reaction stoichiometry (see Sect. 3.7). In the present example, the path reaches the invariant point Tlc + Tr + Qtz (point (2) in Fig. 3.27a). At this point, all previously formed talc is converted to tremolite. The path then continues along the tremolite field boundary until all quartz is used up by the tremolite-producing reaction at point (3). With continued heating, the Tr + Dol + Cal marble crosses the divariant field until diopside production sets in at point (4). All tremolite is then converted to diopside along the diopside field boundary. At point (5), the marble runs out of tremolite and at point (6), it reaches equilibrium conditions with forsterite. Forsterite replaces diopside between points (6) and (7) and at point (7) diopside has disappeared from the marble. With further heating, the Fo–Dol–Cal marble is simply heated through the divariant forsterite field to its final temperature of 800°C.

The modal composition of the marble at any point along the reaction path in Fig. 3.27a can be calculated in the same way as in Sect. 3.7 for the wollastonite reaction. Figure 3.27b shows changes in the modal composition of the marble with

increasing temperature. The specific metamorphic mileposts along the path are labeled from (1) through (7). The markers correspond to those in Fig. 3.27a: (1) onset of continuous talc production; (2) talc disappears and significant modal amounts of tremolite are produced by the reaction at the invariant point; (3) last quartz disappears; (4) onset of continuous diopside production; (5) the rock runs out of tremolite; (6) onset of continuous forsterite production; (7) rock runs out of diopside. The end product of metamorphism is a high-grade forsterite marble with 25% Fo, 38% Cal, 32% Dol and fluid.

The two types of diagrams are helpful tools for the study of metamorphic rocks. The equilibrium phase diagram (Fig. 3.27a) relates the assemblages to the conditions under which they have formed, the composition phase diagram illustrates modal changes resulting from reactions in a rock of specific composition (Fig. 3.27b). Note however, that Fig. 3.27b is a special variant of a composition phase diagram because it combines composition with the intensive variable temperature, and is in fact a mixed variable diagram. On the other hand, a  $T-X_{\text{CO}_2}$  diagram is not a mixed variable diagram because the  $\text{CO}_2$  and  $\text{H}_2\text{O}$  represented along the x-axis are actually related to the chemical potential of the two volatile species. Chemical potentials are intensive variables like temperature and pressure.

The model metamorphism outlined above is truly prograde. This means that with progressive metamorphism the rock (in this case, marble) advances from low to high temperature (= prograde), in which case, the rock increases in metamorphic grade and metamorphism becomes more intense (see Chap. 4). Along the reaction path, the rock maintains equilibrium at all times and one stage follows the next in a continuous series. The highest grade end-product of metamorphism is a forsterite marble that went through all lower grades in a succession of continuous prograde transformations. An inverse equilibrium path from high to low temperature would be progressively retrograde. However, retrograde metamorphism very rarely follows a strict equilibrium path in contrast to prograde metamorphism which produces its own fluid phase.

As a final remark, the metamorphism of a model marble illustrated in Fig. 3.27 can be understood in both a temporal or spatial sense. The former describes the metamorphic reactions experienced over time by a volume of rock at a given position in space. In the latter case the metamorphic reactions explain the mineral distribution and content of the maximum grade reached by all marble in an area. An example of the spatial viewpoint would be: from Fig. 3.27 it follows that a contact metamorphic aureole (200 MPa) in dolomitic country rock of a granite will show a regular systematic zonation with minor talc in the outermost (coldest) parts, followed by a zone of tremolite marble, a narrow zone with diopside marble and, closest to the contact with the granite (the heat source), a zone of forsterite marble. In contrast, the time aspect is exemplified in the following: a specific small outcrop of forsterite marble formed from diopside marble, which earlier was a tremolite marble that formed initially from talc marble which originated from the sedimentary siliceous dolomitic limestone protolith.

## References and Further Reading

### *Cited References*

- Anderson GM, Crerar DA (1993) *Thermodynamics in geochemistry: the equilibrium model*. Oxford University Press, New York
- Balling NP (1985) Thermal structure of the lithosphere beneath the Norwegian-Danish basin and the southern baltic shield: a major transition zone. *Terra Cognita* 5:377–378
- Berman RG (1988) Internally-consistent thermodynamic data for minerals in the system: Na<sub>2</sub>O–K<sub>2</sub>O–CaO–MgO–FeO–Fe<sub>2</sub>O<sub>3</sub>–Al<sub>2</sub>O<sub>3</sub>–SiO<sub>2</sub>–TiO<sub>2</sub>–H<sub>2</sub>O–CO<sub>2</sub>. *J Petrol* 29:445–522
- Berman RG (1991) Thermobarometry using multi-equilibrium calculations: a new technique, with petrological applications. *Can Mineralog* 29:833–856
- Brown TH, Skinner BJ (1974) Theoretical prediction of equilibrium phase assemblages in multicomponent systems. *Am J Sci* 274:961–986
- Burnham CW, Holloway JR, Davis NF (1969) Thermodynamic properties of water to 1000°C and 10,000 bars. *Geol Soc Am Spec Pap* 132:96
- Carmichael DM (1968) On the mechanism of prograde metamorphic reactions in quartz-bearing pelitic rocks. *Contrib Mineralog Petrol* 20:244–267
- Chatterjee ND (1991) *Applied mineralogical thermodynamics*. Springer, Berlin, Heidelberg, New York, 321 pp
- Clark SP (1966) *Handbook of physical constants*. Geological Society of America Memoir, Washington, DC, 587 pp
- Connolly JAD (1990) Multivariable phase diagrams: an algorithm based on generalized thermodynamics. *Am J Sci* 290:666–718
- Connolly JAD, Kerrick DM (1987) An algorithm and computer program for calculating computer phase diagrams. *Calphad* 11:1–55
- De Capitani C, Petrakakis K (2010) The computation of equilibrium assemblage diagrams with Theriak/Domino software. *Am Mineralog* 95:1006–1016
- Denbigh K (1971) *The principles of chemical equilibrium*. Cambridge University Press, London, 494 pp
- Ferry JM (1982) Characterization of metamorphism through mineral equilibria, vol 10, *Reviews in mineralogy*. Mineralogical Society of America, Washington, DC, 397 pp
- Fletcher P (1993) *Chemical thermodynamics for earth scientists*. Longman Scientific & Technical, Essex, 464 pp
- Fraser DG (ed) (1977) *Thermodynamics in geology*. NATO Advanced Study Institutes Series 30. D. Reidel, Dordrecht, 410 pp
- Fyfe WS, Price NJ, Thompson AB (1978) *Fluids in the earth's crust*. Elsevier, New York, 383 pp
- Ganguly J (2008) *Thermodynamics in earth and planetary sciences*. Springer, Heidelberg, 501 p. ISBN 978-3-540-77305-4
- Garrels RM, Christ CL (1965) *Solutions, minerals and equilibria*. Freeman & Cooper, San Francisco, 450 pp
- Gibbs JW (1878) On the equilibrium of heterogeneous substances. *Am J Sci (Trans Conn Acad)* 16:343–524
- Gibbs JW (1906) *The scientific papers of J. Willard Gibbs, thermodynamics*. Longmans & Greed, London
- Greenwood HJ (ed) (1977) *Application of thermodynamics to petrology and ore deposits*. Short Course 2. Mineralogical Society of Canada, Vancouver, 230 pp
- Guggenheim EA (1986) *Thermodynamics*. North-Holland Physics, Amsterdam, 390 pp
- Helgeson HC, Delany JM, Nesbitt HW, Bird DK (1978) Summary and critique of the thermodynamic properties of rock-forming minerals. *Am J Sci* 278A:229 pp

- Helgeson HC, Kirkham DH (1974) Theoretical prediction of the thermodynamic behaviour of aqueous electrolytes at high pressures and temperatures. I. Summary of the thermodynamic/electrostatic properties of the solvent. *Am J Sci* 274:1089–1098
- Holland TJB, Powell R (1985) An internally consistent dataset with uncertainties and correlations: 2. Data and results. *J Metamorph Geol* 3:343–370
- Holland TJB, Powell R (1990) An enlarged and updated internally consistent thermodynamic dataset with uncertainties and correlations: the system K<sub>2</sub>O- Na<sub>2</sub>O- CaO- MgO- MnO- FeO- Fe<sub>2</sub>O<sub>3</sub>- Al<sub>2</sub>O<sub>3</sub>- TiO<sub>2</sub>- SiO<sub>2</sub>- C- H<sub>2</sub>-O<sub>2</sub>. *J Metamorph Geol* 8:89–124
- Holland TJB, Powell R (1998) An internally-consistent thermodynamic dataset for phases of petrological interest. *J Metamorph Geol* 16:309–343
- Johnson JW, Oelkers EH, Helgeson HC (1992) SUPCRT92: a software package for calculating the standard molal thermodynamic properties of minerals, gases, aqueous species, and reactions from 1 to 5000 bars and 0 to 1000°C. *Comput Geosci* 18:899–947
- Lasaga AC, Kirkpatrick RJ (eds) (1981) Kinetics of geochemical processes, *Reviews in mineralogy*. Mineralogical Society of America, Washington, DC, 398 pp
- Lewis GN, Randall M (1961) *Thermodynamics*. Revised by Pitzer KS, Brewer L. McGraw-Hill, New York, 723 pp
- Moore WL (1972) *Physical chemistry*. Longman, London, 977 pp
- Nordstrom DK, Munoz JL (1994) *Geochemical thermodynamics*, 2nd edn. Blackwell Scientific Publications, Boston, p 493
- Peacock SM (1990) Numerical simulation of metamorphic pressure-temperature-time paths and fluid production in subducting slabs. *Tectonics* 9:1197–1211
- Perkins D, Essene EJ, Wall VJ (1987) THERMO: a computer program for calculation of mixed-volatile equilibria. *Am Mineralog* 72:446–447
- Powell R (1978) *Equilibrium thermodynamics in petrology, an introduction*. Harper & Row, New York, 284 pp
- Powell R, Holland TJB (1985) An internally consistent dataset with uncertainties and correlations: 1. Methods and a worked example. *J Metamorph Geol* 3:327–342
- Powell R, Holland TJB (1988) An internally consistent dataset with uncertainties and correlations: 3. Applications to geobarometry, worked examples and a computer program. *J Metamorph Geol* 6:173–204
- Prigogine I (1955) *Thermodynamics of irreversible processes*. Wiley, New York, 147 pp
- Robie RA, Hemingway BS, Fisher JR (1978) Thermodynamic properties of minerals and related substances at 298.15 K and 1 bar (10<sup>5</sup> Pascals) pressure and at higher temperatures. *US Geol Surv Bull* 1452:456 pp
- Saxena S, Ganguly J (1987) *Mixtures and mineral reactions*. Minerals and rocks. Springer, Berlin, Heidelberg, New York, 260 pp
- Spear FS, Peacock SM, Kohn MJ, Florence FP, Menard T (1991) Computer programs for petrologic P-T-t path calculations. *Am Mineralog* 76:2009–2012
- Stull DR, Prophet H (eds) (1971) *JANAF thermochemical tables*. Mat. Standards Ref Data Ser National Bureau of Standards, Washington, DC, 1141 pp
- Thompson JB (1982a) Composition space; an algebraic and geometric approach. In: Ferry JM (ed) *Characterization of metamorphism through mineral equilibria*, *Reviews in mineralogy*. Mineralogical Society of America, Washington, DC, pp 1–31
- Thompson JB (1982b) Reaction space; an algebraic and geometric approach. In: Ferry JM (ed) *Characterization of metamorphism through mineral equilibria*, *Reviews in mineralogy*. Mineralogical Society of America, Washington, DC, pp 33–52
- Walther JV, Orville PM (1982) Rates of metamorphism and volatile production and transport in regional metamorphism. *Contrib Mineralog Petrol* 79:252–257
- Wood BJ, Fraser DG (1976) *Elementary thermodynamics for geologists*. Oxford University Press, Oxford, 303 pp
- Zen E-An (1966) Construction of pressure-temperature diagrams for multi-component systems after the method of Schreinemakers – a geometrical approach. *US Geol Surv Bull* 1225:56 pp

### ***Further Reading and Additional Literature***

- Armstrong TR, Tracy RJ, Hames WE (1992) Contrasting styles of Taconian, Eastern Acadian and Western Acadian metamorphism, central and western New England. *J Metamorph Geol* 10:415–426
- Baxter EF, DePaolo DJ (2002) Field measurement of high temperature bulk reaction rates I: theory and technique. *Am J Sci* 302:442–464
- Bell TH, Cuff C (1989) Dissolution, solution transfer, diffusion versus fluid flow and volume loss during deformation/metamorphism. *J Metamorph Geol* 7:425–448
- Bell TH, Hayward N (1991) Episodic metamorphic reactions during orogenesis: the control of deformation partitioning on reaction sites and reaction duration. *J Metamorph Geol* 9:619–640
- Bell TH, Mares VM (1999) Correlating deformation and metamorphism around orogenic arcs. *Am Mineralog* 84:1727–1740
- Berman RG, Brown TH, Perkins EH (1987) GEØ-CALC: software for calculation and display of pressure–temperature–composition phase diagrams. *Am Mineralog* 72:861
- Bickle MJ, McKenzie D (1987) The transport of heat and matter by fluids during metamorphism. *Contrib Mineralog Petrol* 95:384–392
- Brady JB (1988) The role of volatiles in the thermal history of metamorphic terranes. *J Petrol* 29:1187–1213
- Brodie KH, Rutter EH (1985) On the relationship between deformation and metamorphism with special reference to the behaviour of basic rocks. In: Thompson AB, Rubie DC (eds) *Advances in Physical Geochemistry*. Springer, Berlin, Heidelberg, New York, pp 138–179
- Brown GC, Mussett AE (1981) *The inaccessible Earth*. Allen & Unwin, London, 235 pp (p 152, Fig.8.15)
- Cermak V, Rybach L (1987) Terrestrial heat flow and the lithosphere structure. *Terra Cognita* 7:685–687
- Chapman DS (1986) Thermal gradients in the continental crust. The nature of the lower continental crust. In: Dawson JB, Carswell DA, Hall J, Wedepohl KH (eds) *The nature of the lower continental crust*. Geological Society of London Special Publication, Blackwell, London, pp 63–70
- Clarke GL, Fitzherbert JA, Milan LA, Daczko NR, Degeling HS (2010) Anti-clockwise P-T paths in the lower crust: an example from a kyanite-bearing regional aureole, George Sound, New Zealand. *J Metamorph Geol* 28:77–96
- Coelho J (2006) GEOISO-A Windows™ program to calculate and plot mass balances and volume changes occurring in a wide variety of geologic processes. *Comput Geosci* 32:1523–1528
- Davy P, Gillet P (1986) The stacking of thrust slices in collision zones and its thermal consequences. *Tectonics* 5:913–929
- Day HW (1972) Geometrical analysis of phase equilibria in ternary system of six phases. *Am J Sci* 272:711–734
- Day HW, Chamberlain CP (1989) Implications of thermal and baric structure for controls on metamorphism, northern New England, USA. In: Daly S, Cliff A, Yardley BWD (eds) *Evolution of metamorphic belts*. Geological Society of London Special Publication, Blackwell, London, pp 215–222
- Durney DW (1972) Solution transfer, an important geological deformation mechanism. *Nature* 235:315–317
- England PC, Richardson SW (1977) The influence of erosion upon the mineral facies of rocks from different metamorphic environments. *J Geol Soc Lond* 134:201–213
- England PC, Thompson AB (1984) Pressure-temperature-time paths of regional metamorphism I. Heat transfer during the evolution of regions of thickened continental crust. *J Petrol* 25:894–928
- England PC, Thompson AB (1986) Some thermal and tectonic models for crustal melting in continental collision zones. In: Coward MP, Ries AC (eds) *Collision tectonics*. Geological Society of London Special Publication, Blackwell, London, pp 83–94



- Ernst WG (1976) Petrologic phase equilibria. Freeman, San Francisco, 333 pp
- Eugster HP (1959) Oxidation and reduction in metamorphism. In: Abelson PH (ed) *Researches in geochemistry*. Wiley, New York, pp 397–426
- Eugster HP (1977) Compositions and thermodynamics of metamorphic solutions. In: Fraser DG (ed) *Thermodynamics in geology*. Reidel, Dordrecht, pp 183–202
- Eugster HP (1986) Minerals in hot water. *Am Mineralog* 71:655–673
- Eugster HP, Gunter WD (1981) The compositions of supercritical metamorphic solutions. *Bull Minér* 104:817–826
- Eugster HP, Wones DR (1962) Stability relations of ferruginous biotite, annite. *J Petrol* 3:82–125
- Ferry JM (1980) A case study of the amount and distribution of heat and fluid during metamorphism. *Contrib Mineralog Petrol* 71:373–385
- Ferry JM (1983) Application of the reaction progress variable in metamorphic petrology. *J Petrol* 24:343–376
- Ferry JM (2000) Patterns of mineral occurrence in metamorphic rocks. *Am Mineralog* 85:1573–1588
- Froese E (1977) Oxidation and sulphidation reactions. In: Greenwood HJ (ed) *Application of thermodynamics to petrology and ore deposits*. Short course 2. Mineralogical Society of Canada, Vancouver, pp 84–98
- Frost BR (1988) A review of graphite-sulfide-oxide-silicate equilibria in metamorphic rocks. *Rend Soc Ital Miner Petrol* 43:25–40
- Frost BR (1991) Introduction to oxygen fugacity and its petrologic importance. In: Lindsley DH (ed) *Oxide minerals: petrologic and magnetic significance*, vol 25, *Reviews in mineralogy*. Mineralogical Society of America, Washington, DC, pp 1–9
- Frost BR, Tracy RJ (1991) P-T paths from zoned garnets: some minimum criteria. *Am J Sci* 291:917–939
- Fyfe WS, Turner FJ, Verhoogen J (1958) Metamorphic reactions and metamorphic facies. *Geol Soc Am Mem.* 73:260pp
- Greenwood HJ (1975) Buffering of pore fluids by metamorphic reactions. *Am J Sci* 275:573–594
- Harker A (1932) *Metamorphism. A study of the transformation of rock masses*. Methuen, London
- Harte B, Dempster TJ (1987) Regional metamorphic zones: tectonic controls. *Philos Trans R Soc Lond A* 321:105–127
- Jamieson RA, Beaumont C, Hamilton J, Fullsack P (1996) Tectonic assembly of inverted metamorphic sequences. *Geology* 24:839–842
- Jones KA, Brown M (1990) High-temperature ‘clockwise’ P-T paths and melting in the development of regional migmatites: an example from southern Brittany, France. *J Metamorph Geol* 8:551–578
- Karabinos P, Ketcham R (1988) Thermal structure of active thrust belts. *J Metamorph Geol* 6:559–570
- Kretz R (1991) A note on transfer reactions. *Can Mineralog* 29:823–832
- Krogh EJ, Oh CW, Liou JG (1994) Polyphase and anticlockwise P-T evolution for Franciscan eclogites and blueschists from Jenner, California, USA. *J Metamorph Geol* 12:121–134
- Kukkonen IT, Cermák V, Hurtig E (1993) Vertical variation of heat flow density in the continental crust. *Terra* 5:389–398
- Lasaga AC, Jianxin J (1995) Thermal history of rocks: P-T-t paths from geospeedometry, petrologic data, and inverse theory techniques. *Am J Sci* 295:697–741
- Lasaga AC, Lüttge A, Rye DM, Bolton EW (2000) Dynamic treatment of invariant and univariant reactions in metamorphic systems. *Am J Sci* 300:173–221
- Lasaga AC, Rye DM (1993) Fluid flow and chemical reaction kinetics in metamorphic systems. *Am J Sci* 293:361–404
- Lenardic A, Kaula WM (1995) Mantle dynamics and the heat flow into the Earth’s continents. *Nature* 378:709–711
- Lux DR, DeYoreo JJ, Guidotti CV, Deker ER (1986) Role of plutonism in low-pressure metamorphic belt formation. *Nature* 323:794–797

- MacFarlane AM (1995) An evaluation of the inverted metamorphic gradient at Langtang National Park, Central Nepal Himalaya. *J Metamorph Geol* 13:595–612
- Manning CE, Ingebritsen SE (1999) Permeability of the continental crust: Implications of geothermal data and metamorphic systems. *Rev Geophys* 37:127–150
- Martignole J, Martelat JE (2003) Regional-scale Grenvillian-age UHT metamorphism in the Mollendo-Camana block (basement of the Peruvian Andes). *J Metamorph Geol* 21:99–120
- Miyashiro A (1961) Evolution of metamorphic belts. *J Petrol* 2:277–311
- Miyashiro A (1964) Oxidation and reduction in the earth's crust, with special reference to the role of graphite. *Geochim Cosmochim Acta* 28:717–729
- Munoz JL, Ludington SD (1974) Fluoride-hydroxyl exchange in biotite. *Am J Sci* 274:396–413
- Nisbet EG, Fowler CMR (1988) Heat, metamorphism and tectonics. Short course 14. St. John's Newfoundland, Mineralogical Society of Canada, Vancouver, 319 pp
- Norris RJ, Henley RW (1976) Dewatering of a metamorphic pile. *Geology* 4:333–306
- Norton D, Knight J (1977) Transport phenomena in hydrothermal systems: cooling plutons. *Am J Sci* 277:937–981
- Ohmoto H (2003) Nonredox transformations of magnetite-hematite in hydrothermal systems. *Econ Geol* 98:157–161
- Oxburgh ER (1974) The plain man's guide to plate tectonics. *Proc Geol Assoc* 85:299–358
- Oxburgh ER, England PC (1980) Heat flow and the metamorphic evolution of the Eastern Alps. *Eclogae Geol Helv* 73:379–398
- Oxburgh ER, Turcotte DL (1971) Origin of paired metamorphic belts and crustal dilation in island arc regions. *J Geophys Res* 76:1315–1327
- Oxburgh ER, Turcotte DL (1974) Thermal gradients and regional metamorphism in overthrust terrains with special reference to the Eastern Alps. *Schweiz Miner Petrogr Mitt* 54:642–662
- Petrini K, Podladchikov Yu (2000) Lithospheric pressure-depth relationship in compressive regions of thickened crust. *J Metamorph Geol* 18:67–77
- Ramberg H (1952) The origin of metamorphic and metasomatic rocks. University of Chicago Press, Chicago, 317 pp
- Roselle GT, Engi M (2002) Ultra high pressure (UHP) terrains: lessons from thermal modeling. *Am J Sci* 302:410–441
- Roselle GT, Thüring M, Engi M (2002) MELONPIT: a finite element code for simulating tectonic mass movement and heat flow within subduction zones. *Am J Sci* 302:381–409
- Rubenach MJ (1992) Proterozoic low-pressure/high-temperature metamorphism and an anti-clockwise P-T-t path for the Hazeldene area, Mount Isa Inlier, Queensland, Australia. *J Metamorph Geol* 10:333–346
- Scambelluri M, Philippot P (2001) Deep fluids in subduction zones. *Lithos* 55:213–227
- Sclater JG, Jaupart C, Galson D (1980) The heat flow through oceanic and continental crust and the heat loss of the Earth. *Rev Geophys Space Phys* 18:269–311
- Seyfried WE (1987) Experimental and theoretical constraints on hydrothermal alteration processes at mid-ocean ridges. *Ann Rev Earth Planet Sci Lett* 15:317–335
- Skippen GB, Carmichael DM (1977) Mixed-volatile equilibria. In: Greenwood HJ (ed) Application of thermodynamics to petrology and ore deposits. Short course. Mineralogical Society of Canada, Vancouver, pp 109–125
- Skippen GB, Marshall DD (1991) The metamorphism of granulites and devolatilization of the lithosphere. *Can Mineralog* 29:693–706
- Sleep NH (1979) A thermal constraint on the duration of folding with reference to Acadian geology, New England, USA. *J Geol* 87:583–589
- Spear FS (1993) Metamorphic phase equilibria and pressure-temperature-time paths, vol 824, Monograph. Mineralogical Society of America, Washington, DC, 824 pp
- Spear FS, Peacock SM (1989) Metamorphic pressure-temperature-time paths. Short course in geology, vol 7. American Geophysical Union, Washington, DC, 102 pp
- Spear FS, Rumble D III, Ferry JM (1982) Linear algebraic manipulation of n-dimensional composition space. In: Ferry JM (ed) Characterization of metamorphism through mineral

- equilibria, Mineralogical Society of America. Reviews in mineralogy, Washington, DC, pp 53–104
- Spear FS, Selverstone J, Hickmont D, Crowley P, Hodges KV (1984) P-T paths from garnet zoning: a new technique for deciphering tectonic processes in crystalline terranes. *Geology* 12:87–90
- Spies R, Bell TH (1996) Microstructural controls on sites of metamorphic reaction: a case study of the inter-relationship between deformation and metamorphism. *Eur J Mineralog* 1:165–186
- Spooner ETC, Fyfe WS (1973) Sub-sea-floor metamorphism, heat and mass transfer. *Contrib Mineralog Petrol* 42:287–304
- Stephenson BJ, Waters DJ, Searle MP (2000) Inverted metamorphism and the Main Central Thrust: field relations and thermobarometric constraints from the Kishtwar Window, NW Indian Himalaya. *J Metamorph Geol* 18:571–590
- Stern T, Smith EGC, Davey FJ, Muirhead KJ (1987) Crustal and upper mantle structure of the northwestern North Island, New Zealand, from seismic refraction data. *Geophys J R Astron Soc* 91:913–936
- Thompson AB (1981) The pressure-temperature (P, T) plane viewed by geophysicists and petrologists. *Terra Cognita* 1:11–20
- Thompson AB, England PC (1984) Pressure-temperature-time paths of regional metamorphism II. Their inference and interpretation using mineral assemblages in metamorphic rocks. *J Petrol* 25:929–955
- Thompson AB, Ridley JR (1987) Pressure-temperature-time (P-T-t) histories of orogenic belts. *PhilosTrans R Soc Lond A321*:27–45
- Thompson AB, Tracy RJ, Lyttle PT, Thompson JB (1977) Prograde reaction histories deduced from compositional zonation and mineral inclusions in garnet from the Gassetts schist, Vermont. *Am J Sci* 277:1152–1167
- Touret JLR (2001) Fluids in metamorphic rocks. *Lithos* 55:1–25
- Vernon RH (1996) Problems with inferring P-T-t paths in low-P granulite facies rocks. *J Metamorph Geol* 14:143–153
- Vigneresse JL (1988) Heat flow, heat production and crustal structure in peri-Atlantic regions. *Earth Planet Sci Lett* 87:303–312
- Vigneresse JL, Cuney M (1991) What can we learn about crustal structure from thermal data? *Terra Nova* 3:28–34
- Whitney DL, Lang HM, Ghent ED (1995) Quantitative determination of metamorphic reaction history: mass balance relations between groundmass and mineral inclusion assemblages in metamorphic rocks. *Contrib Mineralog Petrol* 120:404–411
- Wickham S, Oxburgh ER (1985) Continental rifts as a setting for regional metamorphism. *Nature* 318:330–333
- Winslow DM, Bodnar RJ, Tracy RJ (1994) Fluid inclusion evidence for an anticlockwise metamorphic P-T path in central Massachusetts. *J Metamorph Geol* 12:361–371
- Wintsch RP (1975) Solid-fluid equilibria in the system  $KAlSi_3O_8$ - $NaAlSi_3O_8$ - $Al_2SiO_5$ - $SiO_2$ - $H_2O$ - $HCl$ . *J Petrol* 16:57–79
- Wood BJ, Walther JV (1984) Rates of hydrothermal reactions. *Science* 222:413–415
- Zhang L, Ellis DJ, Arculus RJ, Jiang W, Wei C (2003) ‘Forbidden zone’ subduction of sediments to 150 km depth – the reaction of dolomite to magnesite + aragonite in the UHPM metapelites from western Tianshan, China. *J Metamorph Geol* 21:523–529
- Zwart HJ (1962) On the determination of polymetamorphic mineral associations, and its application to the Bosot area (central Pyrénées). *Geol Rundsch* 52:38–65

# Chapter 4

## Metamorphic Grade

### 4.1 General Considerations

The intensity of metamorphism and the vigor of metamorphic transformation is expressed by the term metamorphic grade. If for instance a granitic pluton intrudes sedimentary rocks, the resulting contact metamorphic aureole will contain rocks of higher grade close to the contact of the granite (heat source) and rocks of low grade at greater distance from the granite where the sediments were only moderately heated. Similarly, in an mountain chain a metamorphic terrain may have developed and is presently at the erosion surface where rock samples can be collected. The rocks contain mineral assemblages that represent the least hydrated state attained during a metamorphic cycle. The assemblages define a metamorphic field gradient (see Chap. 3) and rocks on this  $P$ - $T$ -array are said to be of low grade at low  $P$ - $T$  and of successively higher grade with higher  $P$ - $T$  conditions. The term metamorphic grade is a qualitative indicator of the physical conditions that have been operating on the rocks. Increasing  $P$ - $T$  conditions produce rocks of increasingly higher metamorphic grade. It is a useful term for comparison of rocks within a single prograde metamorphic area but when applied to rocks in different regions, its meaning is not always clear, and the exact nature of the term should be clearly defined.

According to Turner (1981, p. 85), the term metamorphic grade or grade of metamorphism was originally introduced by Tilley (1924) “to signify the degree or state of metamorphism” (p. 168) and, more specifically, “the particular pressure-temperature conditions under which the rocks have arisen” (p. 167). Since reliable  $P$ - $T$  values were not known for metamorphic rocks at that time, and since temperature was generally accepted as the most important factor of metamorphism (cf. Chap. 3), it became current usage to equate grade rather loosely with temperature. As a further example, Winkler (1979, p. 7) suggested a broad fourfold division of the  $P$ - $T$  regime of metamorphism primarily based on temperature, which he named very low-, low-, medium-, and high-grade metamorphism. Even though Winkler noted that information on pressure should be stated as well, a subdivision of metamorphic grade with respect to pressure seemed to be less important. This is well understandable because most of Winkler’s  $P$ - $T$  diagrams were limited to

$P < 1.2$  GPa (12 kbar), whilst the present-day  $P$ – $T$  space of metamorphism has been extended to much higher pressures (Fig. 1.1).

Today, as explained in previous chapters of this book, metamorphism is understood in a geodynamic context. This means that the grade of metamorphic rocks is only a meaningful term for rocks that reached a metamorphic field gradient (or piezo-thermic array) during a single geodynamic process, e.g. a collision event. When, for example, studying a particular shale unit in the Western Alps, it is useful to describe a sillimanite–garnet–biotite schist as a high-grade rock and a chlorite–pyrophyllite schist as a low grade rock. However, comparing the metamorphic grade of an eclogite (2.5 GPa, 600°C) with that of an amphibolite (0.6 GPa, 750°C) is meaningless in most cases because the two rocks were produced in different geodynamic settings.

In the following, various concepts to determine metamorphic grade will be discussed.

## 4.2 Index Minerals and Mineral Zones

Mineral zones were mapped for the first time by Barrow (1893, 1912) in pelitic rocks of the Scottish Highlands. He recognized the systematic entrance of new minerals proceeding up-grade; these minerals were designated as index minerals. The following succession of index minerals with increasing metamorphic grade has been distinguished:

- Chlorite  $\Rightarrow$  Biotite  $\Rightarrow$  Almandine–Garnet  $\Rightarrow$  Staurolite  $\Rightarrow$  Kyanite  $\Rightarrow$  Sillimanite

The individual minerals are systematically distributed in distinct regional zones in the field (Figs. 4.1 and 4.2), and corresponding mineral zones are defined as follows. The low grade limit is determined by a line on a map joining points of the first appearance of a certain index mineral, after which the zone is named. The high grade limit of a particular zone is indicated by a similar line for the following (higher grade) index mineral. A line separating two adjacent mineral zones will be termed a mineral zone boundary (and not an isograd, see below). The biotite zone, for instance, is the zone occurring between the biotite and almandine–garnet mineral zone boundaries. Note that an index mineral generally persists to higher grades than the zone which it characterises, but is sometimes restricted to a single mineral zone (e.g. kyanite in Figs. 4.1 and 4.2).

The zonal sequence elaborated by Barrow are called Barrovian zones. These mineral zones have since been found in many other areas and are characteristic for medium-pressure metapelites. Sequences of mineral zones other than those found by Barrow have been identified in other areas. In the Buchan region of NE Scotland (Fig. 4.1), the Buchan zones are defined by the index minerals staurolite, cordierite, andalusite, and sillimanite. The Buchan zones represent a different metamorphic field gradient involving relatively lower pressures than those represented by the Barrovian zones.

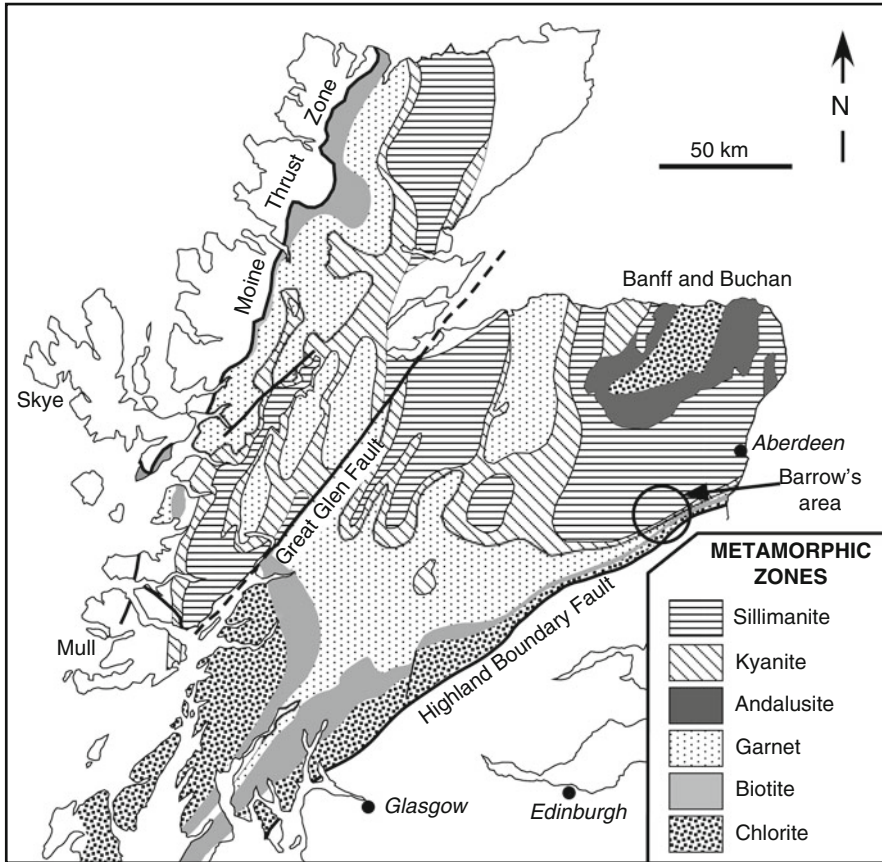


**Fig. 4.1** Map showing the distribution of regional metamorphic rocks in northern Scotland showing index mineral zones of progressive metamorphism (see Fig. 4.2 for mineral zonation of Barrovian intermediate  $P-T$  type metamorphism first delineated by Barrow 1893, 1912). Note the sequence chlorite  $\Rightarrow$  andalusite  $\Rightarrow$  sillimanite in the Buchan area from which low  $P-T$  Buchan-type metamorphism is named (Redrawn from Gillen 1982)

The two zonal schemes (Barrovian and Buchan) have been mapped in pelites from many orogenic metamorphic terrains. It should be made clear, however, that mineral zones can be mapped, in principle, in many types of rock belonging to any type of metamorphism.

The mapping of mineral zones in determining metamorphic grade has the great advantage that it is a simple and rapid method, because the distribution of index minerals becomes obvious from inspection of hand specimens and thin sections. When working in an area for the first time, mineral zoning provides a first insight into the pattern of metamorphism. On the other hand, several shortcomings should be mentioned as well. First, by mapping mineral zones, a single mineral in each rock is considered instead of a mineral assemblage which contains potentially more

Mineral zoning	Chlorite zone	Biotite zone	Almandine zone	Staurolite zone	Kyanite zone	Sillimanite zone
Chlorite			--			
Muscovite						
Biotite						
Almandine						
Staurolite						
Kyanite						
Sillimanite						
Sodic plagioclase						
Quartz						

**Fig. 4.2** Distribution of some metamorphic minerals in pelitic rocks from the Barrovian zones of the Scottish Highlands (see Fig. 4.1)

petrogenetic information. Second, variations in rock composition are not adequately taken into account, and some index minerals will appear at a higher or lower grade in layers of different composition. Care must be taken to refer the mapped zonal pattern to a specific rock type, i.e. a specific rock composition. In order to circumvent these drawbacks, metamorphic zones are currently distinguished by associations of two, three or even more minerals rather than by single index minerals.

### 4.3 Metamorphic Facies

#### 4.3.1 Origin of the Facies Concept

The concept of metamorphic facies was introduced by Eskola (1915). He emphasized that mineral assemblages rather than individual minerals are the genetically important characteristics of metamorphic rocks, and a regular relationship between mineral assemblages and rock composition at a given metamorphic grade was proposed. From this it was concluded that mineral assemblages of metamorphic rocks that had reached chemical equilibrium under the same  $P$ - $T$ -conditions depended only on the bulk rock chemical composition.

Eskola (1915, p. 115) defined a metamorphic facies as follows: "A metamorphic facies includes rocks which . . . may be supposed to have been metamorphosed under identical conditions. As belonging to a certain facies we regard rocks which, if having an identical chemical composition, are composed of the same minerals." This definition has been a problem ever since Eskola first introduced the idea as discussed below:

1. A metamorphic facies includes mineral assemblages of a set of associated rocks covering a wide range of composition, all formed under the same broad metamorphic conditions ( $P$  and  $T$  according to Eskola). Therefore, a metamorphic facies in its original meaning does not refer to a single rock-type, even though many facies are named after some characteristic metabasic rocks, e.g. greenschist, amphibolite, eclogite. Furthermore, some mineral assemblages have a large stability range and may occur in several metamorphic facies, whilst other assemblages have a more restricted stability range and may be diagnostic of only one facies. In addition, some rock-types do not show diagnostic assemblages at a particular metamorphic grade, e.g. many metapelites metamorphosed under subgreenschist facies conditions or metacarbonates metamorphosed under eclogite facies conditions. From these considerations it is obvious that we should look for diagnostic mineral assemblages, and it may be sufficient to recognize a metamorphic facies with the aid of only one such assemblage. On the other hand, in areas devoid of rock compositions suitable for forming these diagnostic assemblages, assignment to a facies cannot be made.
2. It should be remembered that Eskola proposed the idea of metamorphic facies before there were any significant experimental or thermodynamic data on the stability of metamorphic minerals. Under these circumstances it is understandable that the only factors, which this early scheme considered to be variable during metamorphism were temperature and lithostatic pressure. Additional variables, e.g. the composition of fluids present, if any, were not yet recognized, and it was assumed that  $P_{\text{H}_2\text{O}} = P_{\text{tot}}$ . Since that time, experimental and theoretical studies have shown that minerals and mineral assemblages including, e.g. antigorite, lawsonite, prehnite or zeolites, are stable only in the presence of a very water-rich fluid, and are absent if the fluid contains appreciable concentrations of  $\text{CO}_2$ . Fluid composition controls the  $P$ - $T$  stability of mineral assemblages (Chap. 3). For example, the transition from amphibolite facies to granulite facies rocks depends critically upon the partial pressure of  $\text{H}_2\text{O}$ . This means that a more complete representation of metamorphic facies should involve relationships in  $P$ - $T$ - $X$  space, but detailed information on fluid composition is often missing.
3. Eskola's definition allows for an unlimited number of metamorphic facies. During his lifetime, Eskola increased the number of facies he recognized from five to eight. As more information on mineral assemblages became available, more metamorphic facies have been added by other petrologists and many have been divided into "subfacies" or zones. At some point, facies classification became impracticable. Some metamorphic petrologists proposed to retain broad divisions, but others have advocated for the abolition of metamorphic facies.

Notwithstanding the inherent weaknesses of the concept, the metamorphic facies scheme continues to be used and is as popular as ever. It is convenient as a broad genetic classification of metamorphic rocks, in terms of two major variables: lithostatic pressure and temperature. It is especially useful for regional or reconnaissance



studies in metamorphic regions, e.g. the large-scale metamorphic maps of Europe (Zwart 1973), but is too broad for detailed metamorphic studies.

### 4.3.2 Metamorphic Facies Scheme

The metamorphic facies scheme proposed in this book is shown in Fig. 4.3, and some diagnostic mineral assemblages are listed in Table 4.1. The simple facies scheme of Fig. 4.3 closely follows Eskola's classic treatment and the facies names are linked to characteristic rocks of mafic composition. The system is fairly straight-forward. First, we select a standard mafic reference rock composition; Mid Ocean Ridge Basalt (MORB) is the obvious choice. This rock type is then placed in  $P$ - $T$  space (Fig. 4.3) for all possible pairs of pressure-temperature conditions. A pure  $H_2O$ -fluid is deemed to be present so that  $P_{H_2O} = P_{tot}$ . The equilibrium phase assemblage in the metabasalt at each  $P$ - $T$  point is characteristic for the facies fields of Fig 4.3 and defines the facies. The characteristics of each, essentially regional, metamorphic facies are summarized below.

Contrary to other schemes, no facies for low-pressure contact metamorphism are distinguished here, because such facies are only of local extent and metamorphic zones are sufficient to characterize the grade pattern around an igneous intrusion.

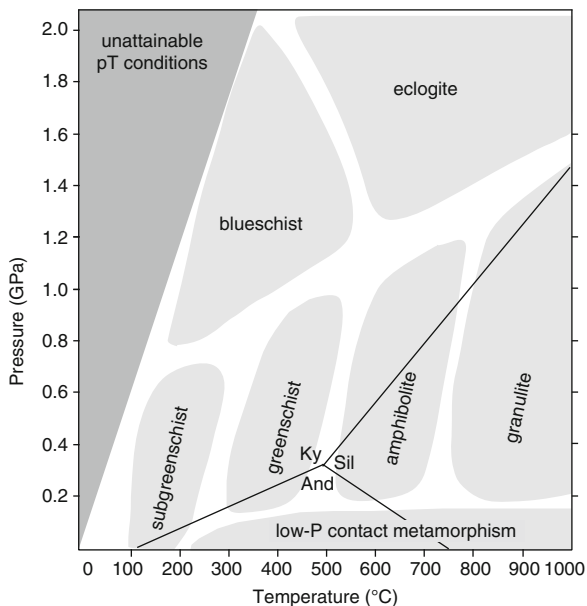


**Fig. 4.3** Pressure-temperature fields of metamorphic facies

**Table 4.1** Metamorphic facies and diagnostic assemblages

	Ultramafic rocks	Marbles	Metapelites	Metamafels	Metabasalts	Metagranitoids	Fluids
Protolith	Ol + Opx ± Cpx ± Spl ± Grt	Cal + Dol + Qtz + Kfs ± Chl, ± Ab, ± "clay"	"Clay", + Qtz ± Ab ± Kfs	Cal + "clay"	Pl + Cpx ± Opx ± Qtz Pl + Cpx ± Opx ± Ol ± Opx	Pl + Kfs + Qtz ± Hbl ± Bt ± Ol ± Cpx ± Opx	H <sub>2</sub> O-CH <sub>4</sub>
Subgreenschist	Chrysotil + Brc + Act ± Chl	Cal + Dol + Qtz + Kfs	Kln(Pr) + Chl + Illite + Qtz	Cal + Kln(Pr) + Chl + Illite + Qtz	Zeolites Pmp + Pth + Chl + Ab ± Ep	"Clay", illite, zeolites Prh, Stlp, Chl + Kfs	H <sub>2</sub> O
Greenschist	Atg + Brc + Di + Chl + Tlc + Di + Chl + Fo + Di + Chl	Cal + Dol + Qtz + Chl + Kfs + Ab	Pr(Als) + Chl + Ms ± Pg ± Cld, ± Bt, ± Grt	Cal + Qtz + Mrg + Chl + Ms ± Ep	Ab + Chl + Ep + Act ± Phe, ± Bt, ± Stp	Ab + Kfs + Chl + Qtz ± Bt ± Act ± Ep	H <sub>2</sub> O
Amphibolite	Atg + Fo + Tr + Chl + Fo + Tr + Chl + Ath + Fo + Tr + Chl + En + Fo + Tr + Chl + En + Fo + Hbl + Spl	Cal + Dol + Qtz + Tlc + Dol + Tr + Phl + Dol + Di + Phl + Qtz + Tr + Di + Phl	St + Chl + Grt + Ms St + Bt + Als + Ms St + Bt + Grt + Ms Crd + Bt + Grt + Ms Bt + Als + Kfs + Grt	Cal + Qtz + Pl ± Hbl ± Grt ± Bt	Pl + Hbl + Ep Pl + Hbl + Grt Pl + Hbl + Cpx ± Bt	Pl + Kfs + Qtz ± Bt ± Ms ± Hbl	H <sub>2</sub> O-CO <sub>2</sub>
Granulite	En + Fo + Di + Spl	Cal + Dol + Di + Spl + Dol + Fo + Spl + Qtz + Di + Spl	Opx + Qtz Opx + Crd + Bt + Qtz Opx + Als + Qtz ± Spr ± Spl	Cal + Qtz + Pl + Cpx ± Grt	Pl + Cpx + Grt Pl + Cpx + Opx ± Hbl ± Bt	Opx + Qtz + Fsp ± Ol ± Cpx Mesoperthite	No fluid or CO <sub>2</sub>
Blueschist	Atg + Fo + Di + Chl	CaCO <sub>3</sub> + Dol + Qtz + Phe	Campholite Phe + Tlc + Grt Phe + carpholite	Cal + Gin + Ep + Phe + Pg	Gln + Lws + Chl ± Pg Gln + Ep ± Grt ± Pg ± Cld ± Tlc ± Chl	Gln + Lws + Chl ± Pg Jd + Qtz ± Phe ± Ky	H <sub>2</sub> O-(CO <sub>2</sub> )
Eclogite	Atg + Fo + Di + Chl + En + Fo + Di + Grt	Tlc + Ky Jd + Qtz(Coe) + Tlc + Ky			Omp + Grt ± Ky Omp + Grt ± Zo ± Phe Omp + Grt ± Zo ± Tlc ± Cld	Jd + Qtz ± Phe ± Ky	H <sub>2</sub> O-N <sub>2</sub>

"Clay" includes: kaolinite, smectite, montmorillonite, vermiculite, saponite and many others; Metagranitoids include metagranitoidspathic (metapsammite) rocks

### 4.3.2.1 Sub-Blueschist-Greenschist Facies

We continue to use this broad facies name after having introduced it in the first edition of this book. Eskola remained unconvinced that certain feebly recrystallized zeolite-bearing rocks contained equilibrium assemblages; hence he chose not to establish a separate metamorphic facies. However, work by Coombs et al. (1959) in New Zealand revealed the ubiquitous, systematic occurrence of such assemblages, and accordingly he proposed two very low-grade metamorphic facies, the *zeolite facies* and the *prehnite–pumpellyite facies*. Subsequently, another subfacies, the *pumpellyite–actinolite facies*, was introduced to define higher grade rocks transitional to those of the greenschist facies proper. These three facies can be recognized in metabasalts and in other rocks such as meta-andesite, metapsammite and meta-granitoid. Zeolites occur in hydrothermally altered basalts at very low-grade. The distribution of the various zeolite species is systematic and characteristic of  $P$ – $T$  conditions (see Chap. 9). Prehnite and pumpellyite are widespread in metabasalts that have been metamorphosed under conditions between those of the zeolite and pumpellyite–actinolite facies that lack prehnite. Metamorphism has obviously been insufficient to produce the characteristic assemblages of the greenschist and blueschist facies. In regional orogenic metamorphism, the first greenschist facies assemblages (without pumpellyite and prehnite) develop in metabasalts at about 300°C.

Sub-blueschist-greenschist facies therefore represents metamorphism at all  $P$ – $T$  conditions too weak to produce greenschist or blueschist from basalt. The lower limit of metamorphism has arbitrarily been set to 200°C (Chap. 1) and diagenetic processes in sediments are normally excluded from the term metamorphism. However, hydrothermal alteration of igneous rocks such as zeolitization of basalt, low-grade alteration of basement gneisses or fissure mineral formation in granite are typical processes at low-grade conditions, often as low as 100°C. Obviously, metamorphic petrologists are interested in such processes and not sedimentologists. The temperature range of 100–300°C includes a wealth of metamorphic transformation processes and most of them are, in a broad sense, related to the interaction of meteoric water with rocks. Water-rock interaction (WRI) research is a flourishing inter- and multi-disciplinary field in geosciences and almost all WRI research concentrates on processes and products in sub-blueschist-greenschist facies rocks.

Because the term sub-blueschist-greenschist facies is rather awkward we suggest to use the simplified version: sub-greenschist facies (subgreenschist facies).

### 4.3.2.2 Greenschist Facies

At  $P$ – $T$  conditions of the greenschist facies (Fig. 4.3), meta-MORB is transformed to greenschist with the mineral assemblage, actinolite + chlorite + epidote + albite ± quartz. The first three minerals give the rock type its characteristic green color. The four mineral assemblage is mandatory for a greenschist and hence for the greenschist facies. Other rock compositions such as shales (pelites) and sandstone (psammites) develop slightly different assemblages if metamorphosed under the

same conditions. The chlorite, biotite and garnet Barrovian zones in metapelites belong to this facies, and more Al-rich metapelites may contain chloritoid. The metamorphic facies concept implies that a metapelitic schist containing muscovite + chlorite + chloritoid + albite, or a metapsammitic schist containing muscovite + actinolite + chlorite + albite, are said to be of greenschist grade, i.e. metamorphosed under the greenschist facies conditions, although they are not actually greenschists. If the metapelitic schist above (Ms + Act + Chl + Ab) occurs at an outcrop with metabasalt, that metabasalt would be a greenschist with the assemblage actinolite + chlorite + epidote + albite  $\pm$  quartz.

The greenschist facies roughly covers the temperature range from 300°C to 500°C at low to intermediate pressures. The transition to amphibolite facies is rather gradual. Above about 450°C, metabasic rocks gradually develop hornblende in place of actinolite as a result of reaction of epidote and chlorite, and plagioclase more calcic than albite appears reflecting the presence of miscibility gaps in the low-T Na-plagioclase series (peristerite gap) and the actinolite–hornblende series (Fig. 4.4a). A transitional *epidote–amphibolite facies* (for metabasic rocks), or simply *transition facies* (for metabasic and metaquartzofeldspathic rocks) is often referred to in the literature and this important transition can be included in both the greenschist and amphibolite facies. The upper temperature of the transition facies where only Hbl and Pl occur (true amphibolite facies conditions) depends on pressure as illustrated by closure of the plagioclase peristerite solvus in Fig. 4.4b.

#### 4.3.2.3 Amphibolite Facies

Under the  $P$ – $T$  conditions of the amphibolite facies metabasalt converts to amphibolite containing plagioclase (oligoclase – andesine) + hornblende  $\pm$  quartz. In amphibolite hornblende is modally abundant (typically >50%). At lower temperature in the amphibolite facies, epidote may still be present and garnet also typically occurs in many amphibolites. In the upper amphibolite facies, clinopyroxene may appear, however, together with garnet only at relatively high pressure. In any case, the diagnostic assemblage in basic rocks is Hbl + Pl. Other rocks such as metapelites contain a large variety of assemblages depending on the rock composition and the precise  $P$ – $T$  conditions. The staurolite, kyanite and sillimanite Barrovian zones belong to this facies. Tremolite-bearing marbles are also characteristic. The key point here is that a metapelite, a calcsilicate rock or a metalherzolite is said to be of amphibolite facies grade or has been metamorphosed under amphibolite facies conditions if a metabasalt (if present or not at the same locality) would have developed Hbl + Pl  $\pm$  Qtz.

#### 4.3.2.4 Granulite Facies

The granulite facies comprises the high-grade rocks formed at the highest temperatures of orogenic metamorphism. Under granulite facies conditions, the MOR-basalt

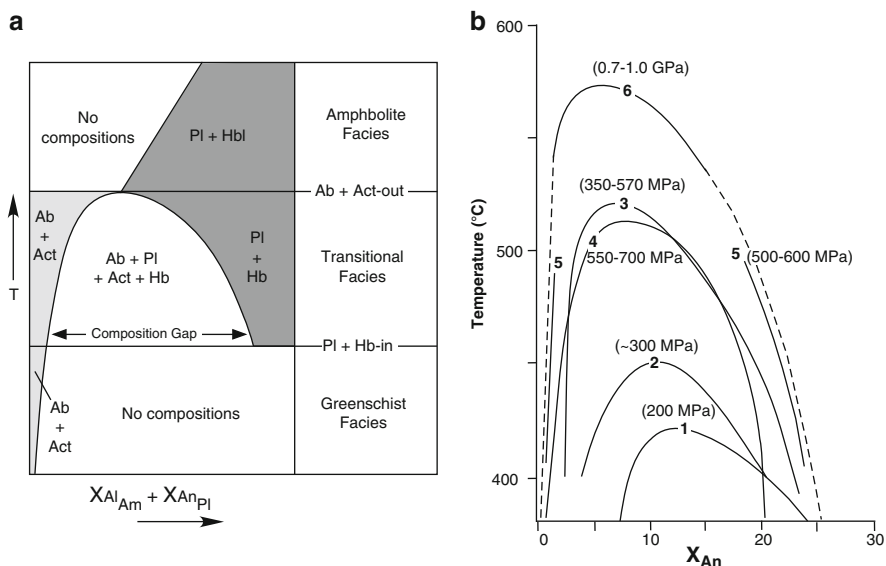


**Fig. 4.4** The greenschist–amphibolite transition. **(a)** Schematic diagram illustrating the greenschist–amphibolite transition in terms of  $X_{Al}$  (amphibole) and  $X_{An}$  (plagioclase) versus temperature at a specified pressure, showing position of a composition gap (= miscibility gap) that defines the temperature interval of a transition facies in metabasic (with Am + Pl) and meta-quartzofeldspathic (with Pl) rocks. Pl = oligoclase–andesine compositions. In the greenschist facies albite + actinolite (together with chlorite and epidote) are stable; in the transition facies, the coexisting pairs, albite and oligoclase–andesine, actinolite and hornblende occur; in the amphibolite facies hornblende + oligoclase–andesine are stable. **(b)** Plots of  $X_{An}$  versus  $T$  that define the shape of the plagioclase peristerite solvus or miscibility gap for various metamorphic terranes. Pressures given in *brackets*. 1 Metabasalt, contact aureole of Kasugamura granite, Japan (Maruyama et al. 1981); 2 Metabasalt, Yap Island, Western Pacific (Maruyama et al. 1983); 3 Carbonate-bearing metapelites, Vermont, USA (Crawford 1966; Nord et al. 1978; Spear 1980); 4 Quartzofeldspathic (metagreywacke) schist, Southern Alps, New Zealand (Grapes and Otsuki 1983); 5 Metabasite and quartzofeldspathic (metagreywacke) schist (Haast schist), New Zealand (Crawford 1966; Cooper 1972); 6 Mafic and pelitic schist, Sanbagawa belt, Japan (Enami 1981) (Diagram modified after Maruyama et al. (1983, Fig. 7)

facies reference rock contains clinopyroxene + plagioclase  $\pm$  Qtz  $\pm$  Opx. Note that Cpx + Pl was also the original igneous assemblage of the basalt, but here we are dealing with a new metamorphic (neometamorphic) Cpx + Pl pair where Cpx has replaced hornblende of the amphibolite facies (Fig. 9.12a, b).

There are several problems with definition of the granulite facies and, in fact, the term granulite and granulite facies is used in different ways by metamorphic petrologists. The problem has many different causes. The most obvious is that the pair Cpx + Pl also occurs in rocks that contain Hbl + Pl, i.e. amphibolites. One could circumvent the problem by requiring that hornblende or any other hydrous mineral such as mica should not present in the granulite facies. However, hornblende (and biotite) can persist to very high temperature ( $>950^{\circ}\text{C}$ ) in metabasaltic

compositions. Most petrologists would consider this temperature to be well within the granulite facies. In some mafic rocks and under certain conditions within the granulite facies, orthopyroxene forms in addition to Cpx + Pl and a metabasalt that contains Opx + Cpx + Pl is termed a two-pyroxene granulite. There is general agreement that this assemblage is diagnostic for granulite facies conditions even if hornblende (and biotite) is present in the two-pyroxene-granulite. Unfortunately, the diagnostic Opx + Cpx + Pl assemblage in metabasalt is restricted to the low-pressure part of the granulite facies. At high-pressures in the granulite facies (Fig. 4.3), Opx is replaced by garnet ( $\text{Opx} + \text{Pl} = \text{Cpx} + \text{Grt}$ ). However, rocks with the assemblage Grt + Cpx + Pl that also contain Hbl may occur under  $P$ - $T$  conditions of *both* the amphibolite and the granulite facies. Also note that, in the light of the comments above, the upper limit of the amphibolite facies is difficult to define, since the pair Hbl + Pl occurs well within the granulite facies.

Granulite facies rocks are strongly dehydrated and their formation should be promoted by low water pressure. Conditions of  $P_{\text{H}_2\text{O}} < P_{\text{total}}$  have been indeed reported from many granulite facies terrains although, water saturation is implicit in Fig. 4.3. High  $\text{CO}_2$  concentrations in fluid inclusions and an abundance of such inclusions have been reported from granulites world wide (see references).

At high water pressure, rocks melt either partially or completely under  $P$ - $T$  conditions of the granulite facies. Also partial melting of metabasalt occurs if  $P_{\text{H}_2\text{O}}$  is high and mafic migmatite rocks are the result of this process. Many rock-forming processes in the granulite facies involve partial melting in the presence of a  $\text{H}_2\text{O}$ -poor fluid phase or in the absence of a free fluid phase.

Few subjects in petrology are equally interesting and involved as the amphibolite-granulite facies transition. Perhaps, granulite facies conditions should not be tied to metabasaltic compositions because of the lack of truly unique assemblages in such rocks that are unequivocally diagnostic for the granulite facies. In fact, in Chap. 2 we have defined the term granulite to include, both, mafic and felsic rock compositions. Mineral assemblages of felsic granulites are better suited for defining the granulite facies. The mineral pair Opx + Qtz is the most diagnostic and widespread pair indicative of granulite facies conditions in rocks of all compositions at pressures up to 0.8–1.0 GPa. In an outcrop, where Opx + Qtz occurs in felsic granulite, associated mafic granulites would contain either  $\text{Opx} + \text{Cpx} + \text{Pl} \pm \text{Qtz} \pm \text{Hbl}$  or  $\text{Grt} + \text{Cpx} + \text{Pl} \pm \text{Qtz} \pm \text{Hbl}$ .

#### 4.3.2.5 Blueschist Facies

The name blueschist facies is derived from the presence of blue glaucophane and other sodic amphiboles. They are typically found in mineral assemblages together with lawsonite, zoisite, epidote, garnet, chlorite, phengite, paragonite, chloritoid, talc, kyanite, jadeitic pyroxene, ankerite and aragonite. In the blueschist facies feldspar is absent and also biotite is not found in such rocks. Blueschist facies assemblages are formed at low temperatures and relatively high pressures, i.e. along low geothermal gradients typically related to subduction dynamics. This facies was

originally named as glaucophane–schist facies by Eskola. The lawsonite–albite or lawsonite–albite–chlorite facies of some authors are included in this book in the sub-blueschist–greenschist facies.

Metabasaltic rocks of blueschist facies grade are typically found in subducted and later exhumed ophiolite complexes. The most characteristic mineral assemblage is glaucophane + epidote + phengite + paragonite + chlorite  $\pm$  Mg–chloritoid  $\pm$  quartz  $\pm$  garnet. Bulk rock compositions other than that of basic rocks do not develop especially diagnostic assemblages and blueschist facies conditions are difficult to recognize if no mafic rocks occur in a metamorphic complex.

#### 4.3.2.6 Eclogite Facies

In the eclogite facies, metabasaltic rocks contain the characteristic assemblage omphacite + garnet. Plagioclase is not present in eclogite facies rocks. Eclogites are high pressure rocks that formed over a wide range of temperatures and occur in very different geodynamic settings. Low-T eclogites may result from subduction of oceanic lithosphere. In the Western Alps, for instance, pillow basalt of ophiolite complexes that have been subducted and later exhumed contain a number of characteristic, often hydrous minerals such as chloritoid, zoisite and talc in addition to Grt + Omp. Intermediate-T eclogites may result from thickening caused by nappe-stacking of continental crust. Such eclogites may still contain hydrous minerals, mainly zoisite + phengite. At high-T, hydrous phases are absent from eclogite and kyanite is often a characteristic additional mineral associated with Grt + Omp.

Eclogites occur as tectonically-transported blocks enclosed in rocks of some other facies or in chaotic mélangé zones that commonly occur in accretionary subduction zone wedges and blueschist terranes. Other eclogites show a regular zonal mineral distribution suggestive of progressive metamorphism, and isofacial metapelites and metagranitoids with distinct mineral assemblages are known from a number of occurrences. Other rock compositions also develop distinct high-pressure assemblages. Eclogite facies lherzolites may contain the pair olivine + garnet. Metagranites contain jadeite + quartz instead of Na-rich plagioclase and talc + kyanite in Mg-rich metapelites are examples of eclogitic facies rocks. Even mafic rocks may not be converted to eclogite under the very high-P conditions of the eclogite facies. For example, Mg-rich gabbros in the Western Alps contain Jd + Ky + Zo + Omp + Tlc + Phe + Cld  $\pm$  Qtz but lack garnet. Pillow metabasalts associated with the eclogitic gabbros are ordinary eclogites with abundant Omp + Grt.

Xenoliths of eclogite, sometimes associated with garnet lherzolite are found in basalt, derived from an upper mantle source region of around 100 km depth.

There is no defined high-pressure limit of the eclogite facies. The highest pressure reported from rocks exposed at the today's surface is about 6.5 GPa. Crustal rocks containing diamond and coesite (typically as inclusions in garnet and zircon) indicating pressures of  $>4$ –5 GPa have been reported from a number of localities, e.g. Dabie–Sulu metamorphic belts, China; Kokchetav Massif, Kazakhstan; Dora Maira Massif, Western Alps (Fig. 1.1). These rocks also belong to the eclogite facies. The term ultra-high pressure metamorphism (UHPM) is used

for eclogite facies rocks containing coesite or have been metamorphosed under conditions where coesite would be stable.

### 4.3.3 Pressure–Temperature Conditions of Metamorphic Facies

The  $P$ – $T$  limits of the various metamorphic facies in Fig. 4.3 should not be taken too literally, and boundaries between facies are gradational because (1) most characterizing mineral assemblages form by continuous reactions over  $P$ – $T$  intervals as a consequence of mineral solid solution; (2) the assumption of  $P_{\text{H}_2\text{O}} = P_{\text{total}}$  may be incorrect since many metamorphic fluids are compositionally complex solutions. In addition, some data on  $P$ – $T$  stabilities of mineral assemblages are still ambiguous. Some specific problems related to facies boundaries have been discussed above.

In different orogenic belts, Miyashiro (1961) emphasized that certain metamorphic facies are commonly associated to the exclusion of others. The sequence of facies characteristic of an individual area or terrane was named a metamorphic facies series. Miyashiro recognized three principal types of facies series: (1) a low- $P$ , high- $T$  type, in which andalusite and sillimanite are formed (LP type); (2) an intermediate- $P$  and intermediate- $T$  type characterized by kyanite and sillimanite (IP type); and (3) a high- $P$ , low- $T$  type, indicated by the occurrence of jadeitic pyroxene and glaucophane (HP type). Facies series (1) and (2) can now be extended to higher temperatures to include UHT metamorphic terranes (e.g. Fig. 1.1), and facies series (3) can be extended to include UHP metamorphic terranes. In a  $P$ – $T$  diagram, each facies series can be represented by a different  $P$ – $T$  gradient (Fig. 4.5). Miyashiro also noted the existence of a metamorphic facies series intermediate to the three types mentioned above. All intergradations are possible, and result from the fact that each metamorphic belt has been subjected to its own unique set of physical conditions as illustrated by the prograde metamorphic arrays from various metamorphic terranes in Fig. 4.5. The metamorphic facies series concept is useful because it links regional orogenic metamorphism to its geodynamic causes. In the broadest sense, LP type facies metamorphism is typically related to extension tectonics and heat transfer by igneous intrusions. IP type metamorphism is the typical collision belt, crustal thickening metamorphism (Barrovian metamorphism). HP-type metamorphism normally results from subduction dynamics.

## 4.4 Isograds

### 4.4.1 The Isograd Concept

In principle, an isograd is a line on a map connecting points of equal metamorphic grade. The isograd method has been applied by many geologists for several decades, but semantic confusion has arisen because its significance is more complex than was originally assumed. When coining the word “isograd”, Tilley (1924,



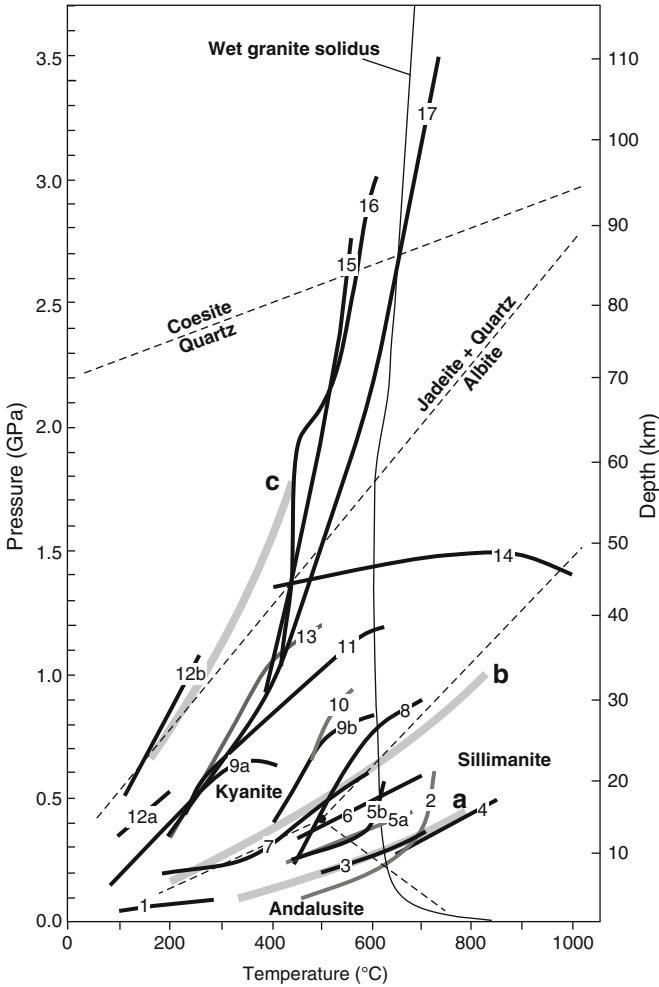


**Fig. 4.5** Metamorphic facies series (*thick gray lines* labelled A, B, C) and prograde  $P$ - $T$  paths of various metamorphic terranes (numbered) in relation to the  $\text{Al}_2\text{SiO}_5$  polymorphs, the  $\text{Ab} = \text{Jd} + \text{Qtz}$  equilibrium, and  $\text{Qtz} = \text{Cs}$  transition. A = Low- $P$ , B = Medium- $P$ , C = High- $P$  facies series of Miyashiro (1961). 1 Zeolite-prehnite-pumpellyite facies metamorphism, Puerto Rico (Turner 1981, Fig. 11.5); 2 Acadian metamorphism, Massachusetts and SW New Hampshire, USA (Schumacher et al. 1989); 3 Southern Hidaka metamorphic belt, Hokkaido, Japan (Shiba 1988); 4 Namaqualand granulites, South Africa (Waters 1989); 5a East Buchan metamorphic series, NE Scotland (Hudson 1980); 5b West Buchan metamorphic series, NE Scotland (Hudson 1980); 6 Barrovian metamorphic series (Stonehaveian), NE Scotland (Hudson 1980); 7 Archean Slave Province, NW Canadian Shield (Thompson 1989); 8 Idaho, USA (Perchuk 1989); 9a NW Otago schist, New Zealand (Yardley 1982); 9b Alpine schist, central Southern Alps, New Zealand (Grapes and Watanabe 1992); 10 Sulitjelma fold-nappe, central Scandinavian Caledonides (Burton et al. 1989); 11 Sanbagawa Metamorphic belt, Shikoku, Japan (Banno and Sakai 1989); 12a Franciscan metamorphic belt (metagreywacke with *detrital* jadeite origin), California (Brothers and Grapes 1989); 12b Franciscan metamorphic belt (metagreywacke/metabasite),

p. 169) referred to the boundaries of Barrow's mineral zones as a "... line joining the points of entry of ... (an index mineral) in rocks of the same composition ...". He defined the term isograd "as a line joining points of similar  $P$ - $T$  values, under which the rocks as now constituted, originated". This definition is inappropriate because in practice it can never be more than an inference; in addition, there are several arguments which indicate that the stipulation of "similar  $P$ - $T$  values" may be incorrect (see below).

Later, it was proposed to relate an isograd to a specific metamorphic reaction across the "isograd line". Since a metamorphic reaction depends on temperature, pressure, and fluid composition, an isograd will in general, represent sets of  $P$ - $T$ - $X$  conditions satisfying the reaction equilibrium and not points of equal  $P$ - $T$ - $X$  conditions. Therefore, whenever the reaction is known, the term isograd should be replaced by the term reaction-isograd. A reaction-isograd is a line joining points that are characterized by the equilibrium assemblage of a specific reaction. This line is not necessarily a line of equal or similar grade and therefore it is not an isograd in its proper meaning.

#### 4.4.2 Zone Boundaries, Isograds and Reaction-Isograds

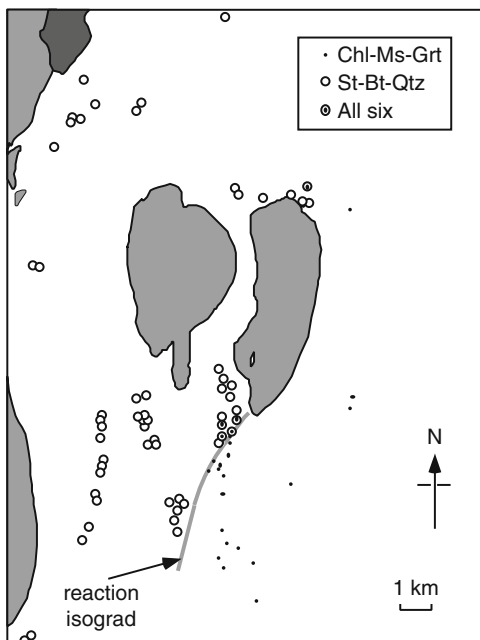
Tilley's definition of an isograd is identical to what we have called a mineral zone boundary earlier in this chapter, with the additional assumption of similar  $P$ - $T$  values existing along this boundary. In order to avoid this assumption, the terms mineral zone boundary or reaction-isograd will be used in this book together with the term isograd. The distinction between a mineral zone boundary and a reaction-isograd should be again clarified. Mapping a mineral zone boundary is based on the first appearance of an index mineral, whilst locating a reaction-isograd involves mapping reactants and products of a chemical reaction in rocks (Fig. 4.6). Such reactions may be simple phase transitions such as  $Ky = Sil$  or  $Qtz = Coesite$ . The field geologist will then find an area with kyanite and another area with sillimanite. The line drawn on a map separating the two areas is the reaction-isograd of the  $Ky$ - $Sil$  phase transition. Unfortunately, one will commonly find kyanite in sillimanite grade rocks as well. This complication arises from the fact that metastable persistence of reactants or products of a reaction on the "wrong" side of the line is a common occurrence.

The problem is less severe if reaction-isograds involving hydrous minerals are mapped. At very low grade, kaolinite decomposes to pyrophyllite in the presence of



**Fig. 4.5** (Continued) California (Radvanec et al. 1998; Banno et al. 2000); 13 New Caledonia (Bell and Brothers 1985); 14 Scourian granulite complex, NW Scotland (Cartwright and Barnicoat 1989); 15 Zermatt-Saas ophiolite, Western Alps (Bucher et al. 2005); 16 Lago di Cignana, Western Alps (Reinecke 1991); 17 Dora-Maira massif, Western Alps (Compagnoni and Rolfo 2003)

**Fig. 4.6** Reaction-isograd in metapelitic rocks based on the reaction  $\text{Chl} + \text{Ms} + \text{Grt} = \text{St} + \text{Bt} + \text{Qtz} + \text{H}_2\text{O}$  from the Whetstone Lake area, Ontario, Canada (After Carmichael 1970, Fig. 3). *Shaded areas:* granitic rocks



quartz. The corresponding reaction is  $\text{Kln} + 2 \text{Qtz} = \text{Prl} + \text{H}_2\text{O}$ . This reaction has been mapped as a reaction-isograd in the Central Alps and it was found that kaolinite does not persist into the pyrophyllite + quartz zone (Frey 1987). Ultramafic rocks are very well suited for reaction-isograd mapping because they contain relatively simple mineral compositions. For example, in the contact aureole of the Bergell pluton, Trommsdorff and Evans (1972) mapped several reaction-isograds in serpentinite, such as the breakdown of antigorite  $\Rightarrow$  talc + forsterite +  $\text{H}_2\text{O}$ . Trommsdorff and Evans (1977) later mapped a series of reaction-isograds in complex ophicarbonate rocks within the same aureole (see Chap. 5). In fact, the later study even involved the mapping of isobaric invariant-reaction-isograds. These isograds thus came very close to representing true isograds, i.e. lines on a map connecting rocks of the same metamorphic grade.

Reactions that involve minerals of variable composition may be complex and the mass balance coefficients of such reactions are obtained by applying least-squares regression techniques, e.g.  $3.0 \text{Chl} + 1.5 \text{Grt} + 3.3 \text{Ms} + 0.5 \text{Ilm} = 1.0 \text{St} + 3.1 \text{Bt} + 1.5 \text{Pl} + 3.3 \text{Qtz} + 10.3 \text{H}_2\text{O}$  (Lang and Rice 1985a). The reaction-isograd related to this reaction separates an area on the map with Chl – Grt micaschist from an area with St – Bt schist. Many other excellent field studies have mapped reaction-isograds. The mapping of reaction-isograds in the field is more time-consuming and more ambitious than the mapping of mineral zone boundaries. On the other hand, a reaction-isograd provides more petrogenetic information for two reasons:

1. The position of a reaction-isograd is bracketed by reactants and products, but a mineral zone boundary is limited only towards higher grade and may possibly be displaced towards lower grade as more field data become available. As an example, the chloritoid mineral zone boundary of the Central Alps has been replaced by the reaction-isograd  $\text{Prl} + \text{Chl} \Rightarrow \text{Cld} + \text{Qtz} + \text{H}_2\text{O}$ , located some 10 km down grade (Frey and Wieland 1975).
2. A reaction-isograd may yield information about conditions of metamorphism provided  $P$ - $T$ - $X$  conditions of the corresponding metamorphic reaction are known from experimental or thermodynamic data. This information is dependent on the type of mineral reaction (Chap. 3), its location in  $P$ - $T$ - $X$  space, and the distribution of isotherms and isobars in a rock body as detailed below.

### 4.4.3 Assessing Isograds, Isobars and Isotherms

Isograds have been used by field geologists to present information about the intensity of metamorphism on a geological map. In principle, an isograd (a line connecting equal metamorphic grade on a map) is conceptually simple. However, in practice, many geologic features make it almost impossible to define such lines in the field. The first problem is that rocks collected from surface exposures are unrelated to the metamorphic structure that was established many million of years ago. The second point is that the intersection of an isobaric and an isothermal surface in 3D-space is the true line connecting equal  $P$ - $T$  conditions at a given instant in time. When transected by an erosion surface, this line appears as a point on a map rather than a line! Most metamorphic rocks conserve the least hydrated state attained during their metamorphic evolution and this state is characterized by a unique  $P$ - $T$  pair for each rock. Rocks with equal  $P$ - $T$  conditions at the least hydrated state lie on a line in 3D space and are represented as a single point on an erosion surface. Therefore, except for some special cases related to contact aureoles, true isograds are not mappable features.

Because one would like to relate isograds to mappable relationships the concept must work in the field. Consider a  $P$ - $T$  diagram where isotherms are perpendicular to isobars. If a metamorphic reaction was dependent upon temperature only, the reaction-isograd would parallel an isothermal surface and it could be mapped in the field as a line connecting rocks that experienced the same temperature. Nothing could be said about the pressure during metamorphism. Similarly, a reaction dependent upon pressure only would produce a reaction-isograd parallel to an isobaric surface. However, metamorphic reactions are, in general, dependent upon both  $P$  and  $T$  and their equilibria have general slopes on a  $P$ - $T$  diagram. Yet, many dehydration reactions are nearly isothermal over some pressure range, and this is also true for some polybaric traces of isobaric invariant assemblages in mixed-volatile systems e.g. see the tremolite-in curve in Fig. 6.14. We can conclude that, although most mapped reaction-isograds are lines with variable  $P$  and  $T$ , this variation may be relatively small for many dehydration reaction-based isograds.

Further insight into the significance of reaction-isograds with respect to the  $P$ - $T$  distribution during orogenic metamorphism is obtained by considering the relative position of isotherms and isobars in a cross-section, termed a  $P$ - $T$  profile by Thompson (1976). Let us assume that isobars are parallel to the Earth's surface during metamorphism. In a stable craton or during burial metamorphism isotherms are also be parallel to the Earth's surface, and in this limiting case  $P$  and  $T$  are not independent parameters; at a given pressure, the temperature is fixed, and reaction-isograds corresponding to mineral equilibria are isothermal and isobaric (Chinner 1966). During orogenic metamorphism, however, isotherms are rarely expected to be parallel to isobars (Fig. 4.7). Furthermore, the temperature gradient – the increase in temperature perpendicular to isotherms; not to be confused with the geothermal gradient, the increase of temperature with depth, both expressed in  $^{\circ}\text{C}/\text{km}$ , is not likely to be constant. Thompson (1976) and Bhattacharyya (1981) have analyzed the geometrical relations among reaction-isograds, the angle ( $\alpha$ ) between isotherms and isobars, and the temperature gradient (Fig. 4.7). It was shown that temperature gradient and angle  $\alpha$  are important in determining  $P$ - $T$  distributions from reaction-isograd patterns besides, of course, the slope of the corresponding mineral reaction on a  $P$ - $T$  diagram. As an example, for a given metamorphic reaction with a low  $dT/dP$  slope of  $8^{\circ}\text{C}/\text{kbar}$ , if temperature

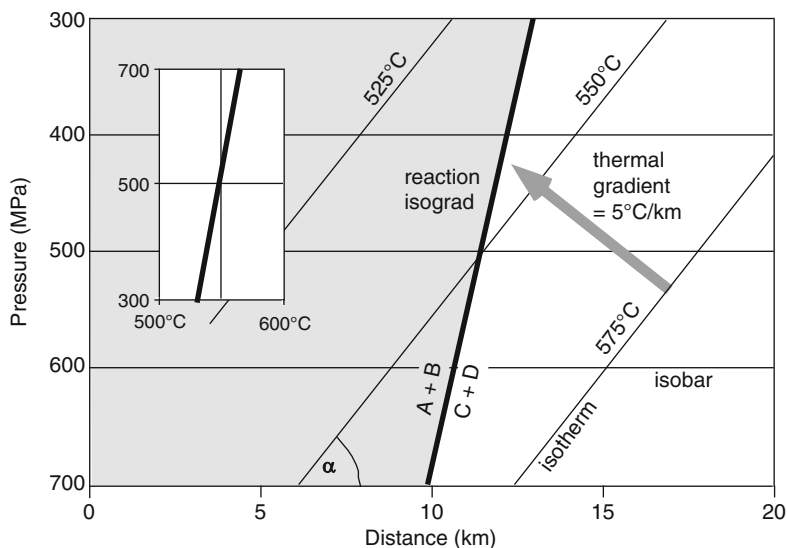


**Fig. 4.7** Geometrical relations between a hypothetical mineral reaction  $A + B = C + D$ , isotherms, and isobars in a  $P$ - $T$  profile. The mineral reaction has an assumed  $dP/dT$  slope of  $8^{\circ}\text{C}/0.1 \text{ GPa}$  as shown in the *inset*  $P$ - $T$  diagram. Isobars are horizontal with a pressure gradient of  $28.6 \text{ MPa}/\text{km}$  (corresponding to a mean rock density of  $2.8 \text{ g}/\text{cm}^3$ ). Isotherms are inclined with respect to isobars at an angle of  $60^{\circ}$  with a thermal gradient of  $5^{\circ}\text{C}/\text{km}$ . Note the relatively large angle between the mineral reaction and isotherms in the  $P$ - $T$  profile

gradients are low the angle between such reaction-isograds and isotherms can be large (Fig. 4.7).

From the preceding discussion it is clear that along a reaction-isograd, both  $P$  and  $T$  will generally vary, and that “similar  $P$ – $T$  values” as suggested by Tilley either require the special precondition of isotherms being parallel to isobars, or may be true for nearby localities only. Reaction-isograds intersecting at high angles as described by Carmichael (1970) provide further convincing evidence for changing  $P$ – $T$ – $X$  conditions along such metamorphic boundaries.

Reaction-isograds mentioned so far refer to univariant or discontinuous mineral reactions. In the field, such reaction-isograds can be defined as relatively sharp lines that can be mapped to within  $\pm 10$  to 100 m (e.g. Fig. 4.6). However, many metamorphic reactions are continuous in nature due to extensive solid-solution in minerals, e.g. Mg–Fe phases such as cordierite, biotite, chlorite and garnet in metapelites. Corresponding reaction-isograds are not mappable as distinct lines and rocks containing the reactant or the product assemblage of the reaction will occur together over an interval of several 100 m or even km because of the range of  $P$ – $T$  conditions over which a continuous reaction occurs between minerals with different Mg/Fe ratios in the rocks.

A reaction-isograd line recorded on a map is only a two-dimensional representation of a reaction-isograd, which is a surface in three dimensions as already noted by Tilley (1924). The form of reaction-isograd surfaces in orogenic belts is of great interest from a geodynamic point of view; but unfortunately in many areas such information is difficult to obtain because of insufficient relief (in addition to poor exposure or scarcity of rock horizons of suitable composition). A few examples are known, however, from Alpine areas where the attitude of reaction-isograd surfaces have been determined with some confidence (e.g. Bearth 1958; Fox 1975; Thompson 1976; Grapes and Watanabe 1992). But even for areas with a long erosion history and where the relief is low, Thompson (1976) has described a method to reconstruct the distribution of isotherms in a portion of the Earth’s crust at the time of metamorphism from the mapped pattern of reaction-isograds.

Metamorphic zone boundaries can often be mapped by hand specimen examination whereas reaction-isograd mapping normally requires microscope observation of rock thin sections. If, in a regional-scale study, mineral composition data are available from a large number of rocks of similar composition, then  $P$ – $T$  data can be derived for each sample using thermobarometric methods (as will be discussed below). One of the few studies that systematically analyzed  $P$ – $T$  data derived from thermobarometry of metapelitic rocks on a regional scale is that of Engi et al. (1995) and Todd and Engi (1997) in relation to the Tertiary orogenic collision- type metamorphic structure of the Ticino area in the Central Alps (Fig. 4.8). Engi et al. were able to map the metamorphic structure as intersections of 25 Ma isobaric and isothermal surfaces with the present day erosion surface (iso- $T$  and iso- $P$  contours). It can be seen from Fig. 4.8 that the location of the highest temperature does not coincide with the location that experienced the highest pressure. As an instructive exercise you can plot the  $P$ – $T$  data along a

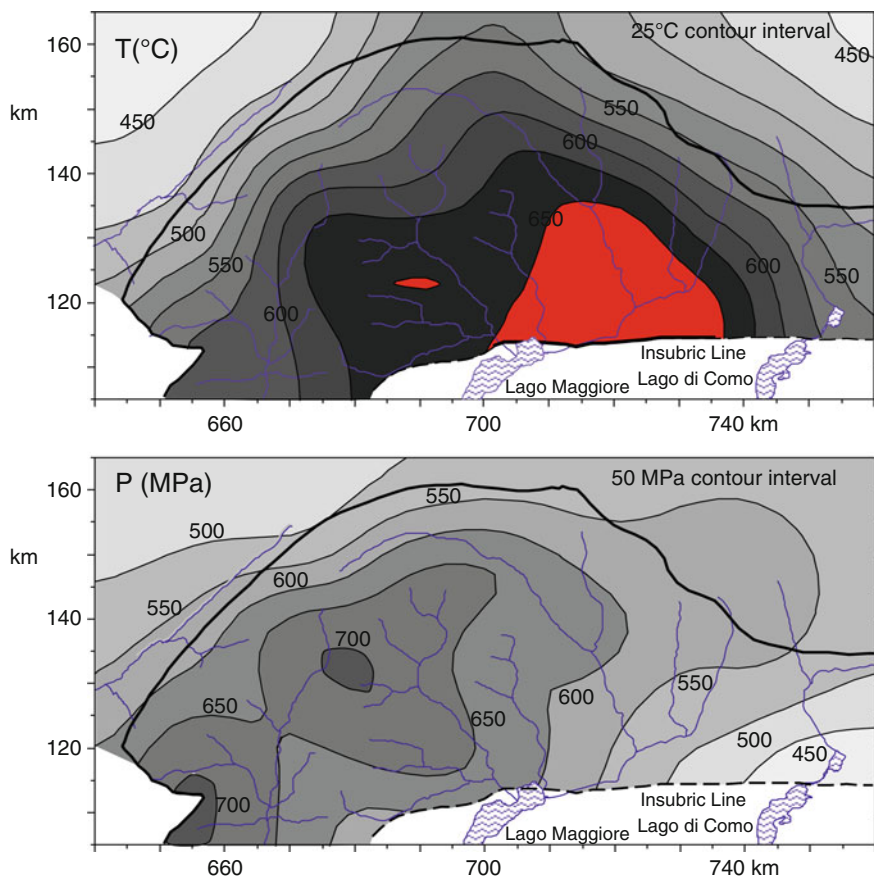


**Fig. 4.8** Isotherm and isobar map of the Tertiary metamorphism of the Ticino area, Central Alps (Todd and Engi 1997). Numbers on axes refer to the Swiss coordinate network in kilometre. The metamorphic pattern is typical of Barrovian regional orogenic metamorphism. It is the result of late stage continent-collision during formation of the Alps and has been modified by even younger processes particularly along the Insubric Line (the major suture zone of the Alps). It is important to understand that the isotherms and the isobars are diachronous. The temperature at location  $xy$  is about maximum  $T$  during the last thermal event and the pressure at the same location is assumed to be  $P$  at  $T_{\max}$ . The  $P$ - $T$  data were derived from a statistical analysis of MET solutions (see Sect. 4.7.7) from a large number of samples

number of sections on a  $P$ - $T$  diagram and evaluate your own ideas about metamorphic field gradients. By combining the  $T$  and  $P$  maps (Fig. 4.8) it can be seen that the e.g. the 600°C isotherm and e.g. the 600 MPa isobar intersect at one single point. That point represents the “isograd” condition of equal metamorphic grade, and all 600°C–600 MPa pairs lie on a line in 3D that intersects the erosion surface at that point on the map.

## 4.5 Bathozones and Bathograds

This concept, proposed by Carmichael (1978), relies on the following considerations. On a  $P$ - $T$  diagram, any invariant point in any model system separates a lower- $P$  mineral assemblage from a higher- $P$  assemblage. An invariant model reaction relates these two critical assemblages, which have no phase in common, i.e. these assemblages are, at least in part, different from divariant assemblages derived from a Schreinemakers analysis. A bathograd is then defined “as a mappable line that separates occurrences of the higher- $P$  assemblage from occurrences of the lower- $P$  assemblage” (Carmichael 1978, p. 771). The field or area between two neighboring bathograds is termed a bathozone.

Carmichael considered five invariant points in a model pelitic system: four are based on intersections of the  $\text{Al}_2\text{SiO}_5$  phase boundaries with three curves referring to the upper thermal stabilities of  $\text{St} + \text{Ms} + \text{Qtz}$  and  $\text{Ms} + \text{Qtz} \pm \text{Na-feldspar}$ , one invariant point corresponds to the  $\text{Al}_2\text{SiO}_5$  triple point (Fig. 4.9). The invariant reactions are as follows (with  $P$  increasing from left to right and in sequential order, and numbers referring to bathozones defined below):

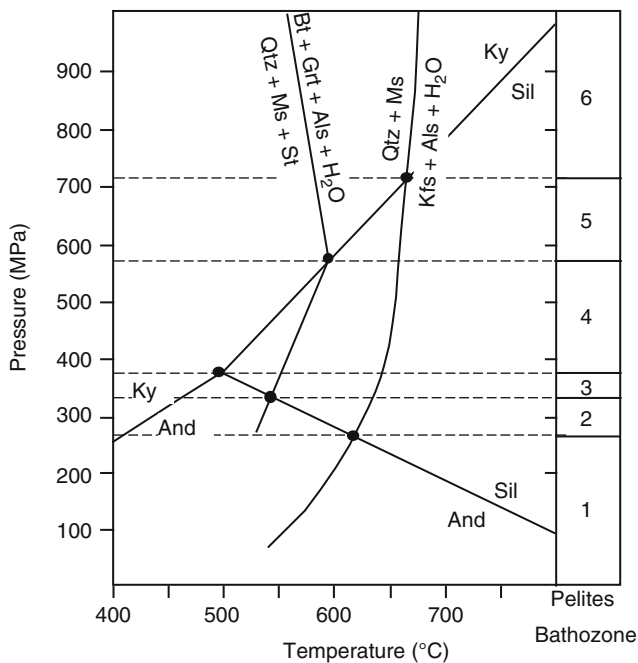


**Fig. 4.9**  $P$ - $T$  phase diagram for pelitic rocks divided into bathozones (After Carmichael 1978, Fig. 2; Archibald et al. 1984, Fig. 2)



Bathograd	Invariant model reaction
1/2	$\text{Kfs} + \text{And} + \text{H}_2\text{O} = \text{Qtz} + \text{Ms} + \text{Sil}$
2/3	$\text{Bt} + \text{Grt} + \text{And} + \text{H}_2\text{O} = \text{Qtz} + \text{Ms} + \text{St} + \text{Sil}$
3/4	$\text{And} = \text{Ky} + \text{Sil}$
4/5	$\text{Qtz} + \text{Ms} + \text{St} + \text{Sil} = \text{Bt} + \text{Grt} + \text{Ky} + \text{H}_2\text{O}$
5/6	$\text{Qtz} + \text{Ab} + \text{Ms} + \text{Sil} = \text{Kfs} + \text{Ky} + \text{granitic liquid}$

Reactants and products of these reactions define diagnostic mineral assemblages of six bathozones. With the exception of bathozones 1 and 6, which are “open-ended” and therefore characterized by a single diagnostic assemblage, each bathozone is defined by two diagnostic assemblages, one to constrain the lower-*P* boundary and the other to constrain the higher-*P* boundary:

Bathozone	Diagnostic assemblage		Pressure range
	Lower limit	Upper limit	
1		Kfs + And	$P < 220 \text{ MPa}$
2	Qtz + Ms + Sil	Bt + Grt + And	$P = 220\text{--}350 \text{ MPa}$
3	Qtz + Ms + St + Sil	And	$P = 350\text{--}380 \text{ MPa}$
4	Ky + Sil	Qtz + Ms + St + Sil	$P = 380\text{--}550 \text{ MPa}$
5	Bt + Grt + Ky	Qtz + Ab + Ms + Sil	$P = 550\text{--}710 \text{ MPa}$
6	Kfs + Ky (+neosomes)		$P > 710 \text{ MPa}$

These bathozones are shown in Fig. 4.9. Note that the apparently precise pressure calibration is somewhat misleading; no errors in the equilibrium curves have been taken into account, and several of the reactions are continuous in rocks and also depend on the activity of water. In fact, the equilibrium  $\text{Qtz} + \text{Ms} + \text{St} = \text{Bt} + \text{Grt} + \text{Als} + \text{H}_2\text{O}$  was located by Carmichael (1978, p. 793) to be “consistent with a huge body of field data” and later slightly adjusted by Archibald et al. (1984, Fig. 2), but is inconsistent with available experimental and thermodynamic data (see Chap. 7).

Nevertheless, Carmichael’s scheme provides an elegant and simple reconnaissance geobarometry of amphibolite facies metapelites, requiring only thin-section observation. Figure 4.10 illustrates an example of a bathozone and bathograd map from the Bergell granite pluton of the Central Alps. The erosion surface intersects the eastern part of the pluton at high crustal levels (bathozones 1 and 2). A well developed contact metamorphic aureole is exposed in the east and pressures range from 200 to 300 MPa. Towards the west, pressure rapidly increases and deeper parts of the pluton are exposed. Bathozones increase progressively from 1 in the east to 5 in the west. Bathozone 5 defines a minimum pressure of about 600 MPa along the western contact of the pluton. Consequently, the narrow eastern contact metamorphic aureole widens towards the west and grades into the regional orogenic metamorphic terrain of the Central Alps.

Powell et al. (1993) defined a bathograd and two bathozones for low-grade metabasic rocks. The assemblages Prh + Chl and Act + Pmp + Ep + Qtz provide low-pressure and high-pressure constraints, respectively, of a bathograd that corresponds to a pseudo-invariant point at which  $\text{Chl} + \text{Ep} + \text{Prh} + \text{Pmp} + \text{Act} + \text{Qtz} + \text{H}_2\text{O}$  coexist. *P*–*T* coordinates of the invariant point determined for metabasites of

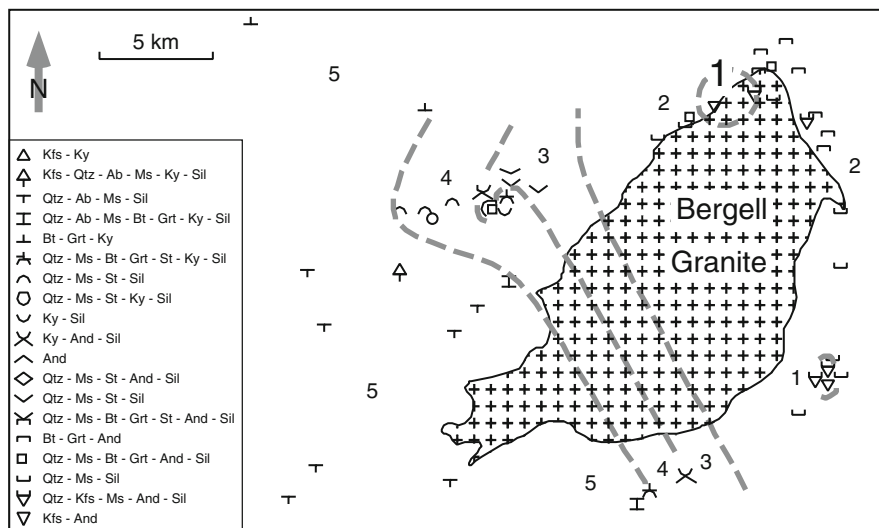


**Fig. 4.10** Bathozones in metapelites from the Bergell Alps of Switzerland and Italy (After Carmichael 1978, Fig. 6)

the Abitibi greenstone belt, Canada, suggest that this sub-greenschist bathograd corresponds approximately to the Sil–Ms–Qtz bathograd, separating bathozones 1 and 2 of Carmichael (1978), for amphibolite facies metapelites. Accordingly, the lower-*P* bathozone, as defined in the low-grade metabasites, is referred to as bathozone 1 and the higher-*P* bathozone as bathozone 2.

## 4.6 Petrogenetic Grid

*P–T* curves of different mineral equilibria generally have different slopes and will therefore intersect. Such intersecting curves will thus divide a *P–T* diagram into a grid which Bowen (1940, p. 274) called a “petrogenetic grid”. His idea was to construct a *P–T* grid with univariant reaction curves bounding all conceivable divariant mineral assemblages for a given bulk chemical composition. Each mineral assemblage would thus fall within a unique *P–T* field and indicate the conditions of metamorphism. When proposing the concept, Bowen regarded it more as a vision than a tool, realizing that “the determinations necessary for the production of such a grid constitute a task of colossal magnitude . . .” (p. 274). In general, a petrogenetic grid is a diagram whose coordinates are intensive parameters characterizing the rock-forming conditions, e.g. *P* and *T*, on which may be plotted equilibrium curves delimiting the stability fields of specific minerals and mineral assemblages.

Early petrogenetic grids consisted of a few experimentally determined mineral equilibria belonging to different chemical systems, and thus the geometrical rules of Schreinemakers could not be applied. This resulted in rather vague conclusions

with regard to the conditions of formation of associated rocks. Univariant curves delineating stability limits of many end-member minerals and mineral assemblages have since been determined by experimental studies. Furthermore, internally consistent sets of thermodynamic data derived from the experimental data are available for many rock-forming minerals, making it possible to calculate petrogenetic grids with all stable reaction curves related to some model systems.

However, even after five decades of extensive experimental and theoretical work, the goal of a wholly comprehensive petrogenetic grid has not been achieved. The main difficulty arises from the lack of data for the comprehensive thermodynamic description of solid-solution properties of common rock-forming minerals like feldspar, chlorite, mica, garnet, pyroxene, and amphibole. Further research will, hopefully, provide the experimental basis for deriving activity-composition functions for solid-solution phases. It is astonishing that, after decades of research, there is still no solution model for the most common crustal mineral, plagioclase, and its various low- $T$  miscibility gaps. Nevertheless, available petrogenetic grids for simple end-member systems provide important constraints on the  $P$ - $T$  conditions of metamorphism in chemically complex systems.

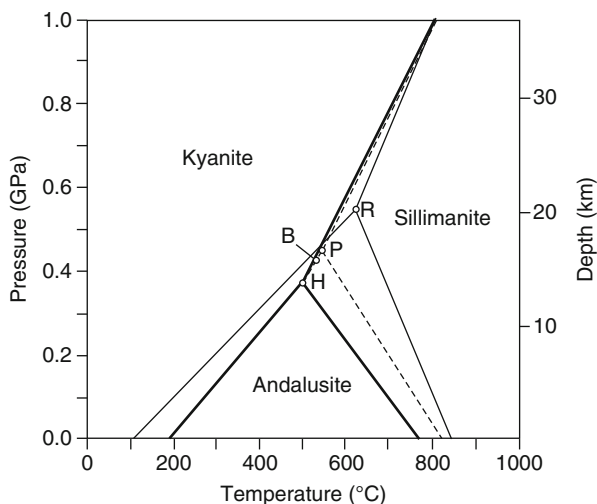
### 4.6.1 Polymorphic Transitions

Examples of polymorphic transitions in metamorphic rocks include andalusite–kyanite–sillimanite, calcite–aragonite, quartz–coesite, and diamond–graphite. Theoretically these simple conversions correspond to univariant reactions which are relatively well known in  $P$ - $T$  space (Fig. 4.11). Due to the small energy changes involved in these reactions, however, such equilibria may become divariant through preferential incorporation of minor elements and by order-disorder states. Reaction kinetics and the influence of strain effects may further complicate the phase transition. Neglecting these complications for the moment, polymorphic transitions are easy to apply to rocks because the presence of an appropriate phase (or pseudomorphs of) is sufficient to yield some  $P$ - $T$  information. A disadvantage is that only  $P$ - $T$  limits are usually provided, and absolute  $P$ - $T$  values can be determined only in rare cases where univariant assemblages are preserved. In principle, using polymorphic transitions as  $P$ - $T$  indicators is related to petrogenetic grids rather than to thermobarometry proper.

#### 4.6.1.1 Andalusite–Kyanite–Sillimanite

Because of their common occurrence in peraluminous rocks, the three  $\text{Al}_2\text{SiO}_5$  polymorphs have been widely used as index minerals, for the definition of facies series (Sect. 4.3), and for estimating  $P$ - $T$  in metamorphic rocks (e.g. Sect. 4.5). The system  $\text{Al}_2\text{SiO}_5$  has an eventful history of experimentation (see e.g. Kerrick 1990, for a review). In the 1970s and 1980s, most petrologists referred to the  $\text{Al}_2\text{SiO}_5$

**Fig. 4.11** Aluminium silicate stability diagram showing experimental results of Richardson et al. (1969) (R); Holdaway (1971) (H) and Bohlen et al. (1991) (B), together with a combined field, experimental and thermodynamic determination (Pattison 1992) (P)



triple point of Richardson et al. (1969) at 550 MPa and 620°C, or that of Holdaway (1971) at 380 MPa and 500°C. Both determinations were obtained using a hydrostatic pressure apparatus. The main difference between the two results concerns the And = Sil equilibrium. Richardson et al. used fibrolitic sillimanite whilst Holdaway used coarse grained sillimanite as the starting material, and Salje (1986) suggests that different thermodynamic properties of these materials could account for the experimental discrepancies.

Bohlen et al. (1991) performed phase equilibrium experiments for the system  $\text{Al}_2\text{SiO}_5$ . Combining the  $dP/dT$  slopes of the equilibria  $\text{Ky} = \text{Sil}$  and  $\text{Ky} = \text{And}$ , these authors obtained a revised triple point at  $420 \pm 30$  MPa and  $530^\circ\text{C} \pm 20^\circ\text{C}$ . Considering the low angle of intersection of the two equilibria mentioned above, the small uncertainty appears rather optimistic. Pattison (1992) combined field data from a contact aureole (Ballachulish aureole, Scotland; see Chap. 7) with available experimental and thermodynamic data in order to constrain the triple point. Firstly, the  $P$ - $T$  position of the And = Sil equilibrium in the aureole was estimated. Secondly, this equilibrium was extrapolated, using entropy and volume data, to intersect the  $\text{Ky} = \text{And}$  and  $\text{Ky} = \text{Sil}$  equilibria, giving an estimated triple point of  $450 \pm 50$  MPa and  $550^\circ\text{C} \pm 35^\circ\text{C}$ . Differences in the location of the Al-silicate triple point mainly affect the position of the andalusite-sillimanite transition curve as shown in Fig. 4.11.

Both experimental and field evidence indicate that  $\text{Fe}^{3+}$  and  $\text{Mn}^{3+}$  have an effect on the stability relations of the  $\text{Al}_2\text{SiO}_5$  polymorphs (see Kerrick 1990, for details). Grambling and Williams (1985) have shown that these transition metals stabilize the And-Ky-Sil assemblage, in apparent chemical equilibrium, across a  $P$ - $T$  interval of 500–540°C, 380–460 MPa.

In summary, it is clear that a single  $\text{Al}_2\text{SiO}_5$  triple point exists on petrogenetic grids only, but depending on the degree of “fibrolitization” of sillimanite and the

transition metal content of the aluminosilicate, some variation in the location of the triple point is to be expected in nature. Nevertheless, the 450 MPa and 550°C triple point is consistent with field data world-wide and the  $P$ - $T$  coordinates are generally accepted by the petrologic community.

#### 4.6.1.2 Calcite–Aragonite

At ambient  $P$ - $T$  the stable polymorph is calcite, at high pressure, however, aragonite is the stable Ca-carbonate (Fig. 4.12). Consequently, the presence of aragonite may be a valuable pressure indicator in rocks of the blueschist facies. Interestingly, aragonite is widespread at the surface of the Earth in marine animal shells and spring sinters, etc. This aragonite is metastable relative to calcite, and forms, e.g. as a result of biological activity.

A large number of experimental attempts to define the stable polymorphic transition Cal = Arg are reviewed by Newton and Fyfe (1976); see also Carlson (1983). Only small discrepancies exist between results obtained in the pure  $\text{CaCO}_3$

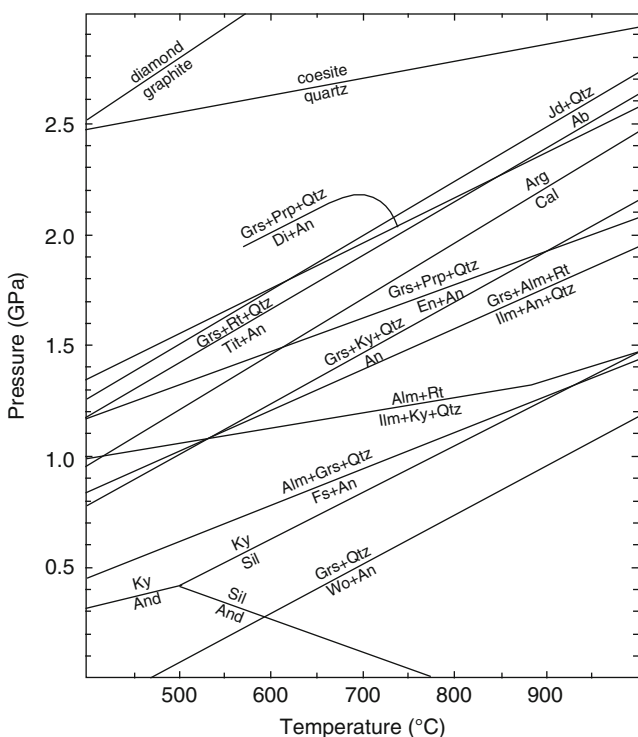


**Fig. 4.12** Some solid-solid reaction equilibria calculated from HP98

system by different workers in the late 1960s and early 1970s. The effects of solid solution have been evaluated for Mg and Sr. Common Mg and Sr contents in metamorphic carbonates result in small displacements of the equilibrium boundary, not exceeding a few tens of MPa's.

Application of the simple equilibrium reaction  $\text{Cal} = \text{Arg}$  to metamorphic rocks is, however, complicated by several factors. Firstly, aragonite is a widely distributed phase in some high-pressure metagreywacke rocks of the Franciscan Formation in California, but is uncommon in other blueschist terranes. These field observations have been explained by high reaction rates, meaning that aragonite-bearing rocks enroute to the surface must enter the calcite stability field between 125°C and 175°C (Carlson and Rosenfeld 1981), and this aragonite will be transformed into calcite if it crosses the equilibrium curve at higher temperatures. Secondly, metastable growth of aragonite in modern and ancient oceans and its subsequent conversion to calcite is a well-known phenomena, and one wonders whether metamorphic aragonite might form outside its stability field as well. It has been shown that aragonite can form instead of calcite at much lower pressures if it is precipitated from fluids with other dissolved ions, rather than from solution in pure water. The frequent occurrence of aragonite in the Franciscan metagreywacke as coarse crystals in late-stage veins suggests that it may have formed by a dissolution-precipitation process. The question remains open as to whether such metastable aragonite grows at lower pressures outside its equilibrium stability field. Thirdly, severely deformed calcite will accumulate strain energy, and Newton et al. (1969) were able to grow aragonite at the expense of calcite strained by prolonged mortar grinding at pressures several hundred MPa's below the aragonite stability limit. This suggests that deformational energy can be a significant factor in Cal-Arg stability considerations.

In summary, more experimental and field work will be needed to establish the circumstances under which aragonite forms in nature. Where associated with other high-pressure minerals such as jadeite or glaucophane, it is likely that aragonite occurring in metamorphic rocks is an indicator of high pressure (see Chap. 6).

### 4.6.1.3 Quartz-Coesite

Coesite, a high-pressure polymorph of  $\text{SiO}_2$ , has been found at many locations worldwide. Its presence in eclogites and subducted supracrustal rocks have generated great interest in the quartz-coesite transition. The Qtz-Cs equilibrium has been well located experimentally as a function of P and T (Bohlen and Lindsley 1987, Fig. 1) and it has been observed in experiments that conversion of one polymorph to the other is rapid. It is thus astonishing that coesite has survived the long return path from great depth to the Earth's surface. Under static conditions, the experimental results imply unusually high metamorphic pressures of 2.2–3.0 GPa (Figs. 4.5 and 4.12) for stable coesite to form. Depending on temperature, this pressure range corresponds to depths in excess of 75 km. However, an important question is whether coesite formed under static conditions or not, because it has been shown

experimentally that coesite can grow from highly strained quartz as much as 1.0 GPa below the transition determined under static conditions. From descriptions of several coesite localities, it appears that strain energy is considered to be an irrelevant factor, and that the presence of coesite actually indicates very high pressures of formation.

## 4.7 Geothermobarometry

Pressures and temperatures at which rocks formed can be accessed by various methods. Finding the field for a characteristic mineral assemblage on a petrogenetic grid is one commonly used method (see Sect. 4.6). An even more powerful technique to obtain  $P$ – $T$  data for metamorphic rocks is geologic thermometry and barometry or, geothermobarometry (GTB). The  $P$ – $T$  conditions of the least hydrated state of a rock along a metamorphic evolution path holds much geologic information and is of great geodynamic significance. Such conditions can be inferred from mineral equilibria (stable or metastable) together with the chemical composition of minerals in a specific sample, especially from the distribution of elements between coexisting minerals in that sample.

Reliable analysis of  $P$ – $T$  conditions prevailing during metamorphism that created a sampled metamorphic rock is based on data from laboratory experiments, thermodynamic probe micro and calculations, and mineral analyses obtained by the electron microprobe analyzer (EPMA). Geothermobarometry made considerable progress in the 1980s and evolved into a standard technique in metamorphic petrology. General reviews on this topic are provided by Essene (1982, 1989), Bohlen and Lindsley (1987), and Yardley and Schumacher (1991). More specific reviews refer to the geobarometry of granulites (Bohlen et al. 1983a; Newton 1983; Pattison et al. 2003) and the geothermobarometry of eclogites (Newton 1986; Carswell and Harley 1989, Ravna and Paquin 2003).

Today, several software packages greatly facilitate the use of geothermobarometry and allow the technique to be widely used. A useful program is for instance “Thermobarometry” by Spear and Kohn (1999). The program can be downloaded from the site <http://ees2.geo.rpi.edu/MetaPetaRen> and a comprehensive manual and tutorial is provided by the authors. The version for download is GTB 2003, and it seems that the program has not been updated recently. A number of EXCEL spreadsheets have been created by different authors and can be googled and downloaded from the scientists web sites. Two particularly useful GTB collections are those of Chun-Ming WU (four GTB EXCEL sheets) based on four publications by Wu and co-authors (see references, the EXCEL sheets are deposited as supplementary materials and can be downloaded from the cited journal papers) and Erling Ravna Krogh’s “ $P$ – $T$  CALC eclogite” (a useful GTB system for eclogites based on Ravna and Terry 2004).

### 4.7.1 Concept and General Principle

The basic idea of geothermobarometry is simple: (1) find a suitable equilibrium phase assemblage in a rock that allows you to formulate two reactions among the phase components, and (2) solve for the equilibrium pressure and temperature conditions of the two reactions. The equilibrium conditions of the two reactions are two lines on a  $P$ - $T$  diagram, the  $P$ - $T$  intersection indicates the conditions of simultaneous equilibrium of the two reactions in one rock and, hence, the values of  $P$ - $T$  at which the assemblage equilibrated.

The two reactions must be independent of the composition of a now vanished fluid phase. Consequently, no dehydration reactions or other reactions that involve volatile species can be used in geothermobarometry (GTB). There are NO exceptions from this rule. This does not mean that only anhydrous minerals are suitable for thermobarometry. It means that if hydrous minerals participate in the reactions, their OH-groups must be conserved among the solid phases.

The most commonly used GTB applications utilize one exchange reaction and one net transfer reaction to determine the  $P$ - $T$  intersection and therefore the condition of “rock formation”. In Chap. 3, the reaction  $\text{Gr} + \text{Qtz} = \text{An} + 2\text{Wo}$  was used as an example of a net-transfer reaction.

This reaction has some relevance for calcisilicate rocks and is used in the following to illustrate the concept of GTB. The equilibrium conditions of the reaction can be calculated from thermodynamic data and are shown on Fig. 4.13. At low temperature  $\text{Grs} + \text{Qtz}$  is stable, at high- $T$  the products of the reaction,

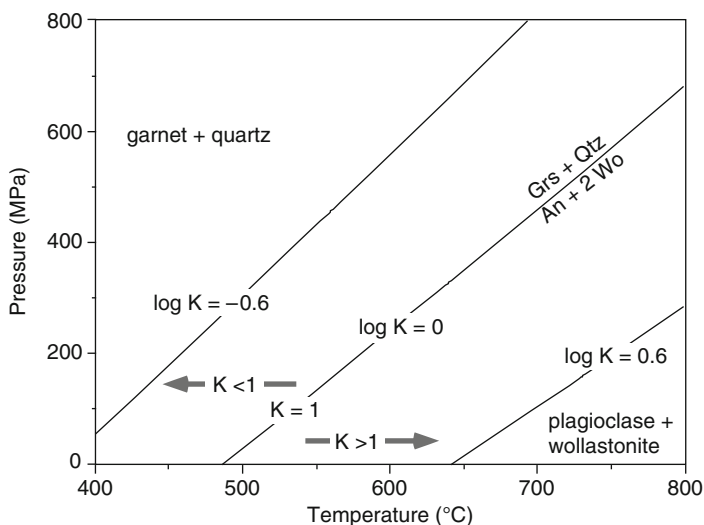


**Fig. 4.13** Equilibrium conditions of the  $\text{Grs} + \text{Qtz} = \text{An} + 2 \text{Wo}$  (GWAQ) reaction for three different values of  $\log K$ . The  $\log K = -0.6$  contour corresponds to  $\text{An}_{20}$  and  $\text{Grs}_{80}$  composition of Pl and Grt, respectively, using the solution model  $a = X$  (thermodynamic data of phase components from Berman 1988)



An + Wo are stable. In contact aureoles, calcisilicate rocks may contain all four minerals, Grs-rich garnet + plagioclase + wollastonite + quartz. Assuming equilibrium among the phase components of the reaction above, we may write an expression for the equilibrium constant:

$$\log K_{PT} = \log a_{An} - \log a_{Gr} \quad (4.1)$$

Microprobe analysis of coexisting plagioclase and garnet in a particular sample are recalculated to, e.g.  $X_{An} = 0.2$  and  $X_{Grs} = 0.8$ . If we have a function  $a = f(X)$ , called a solution model, the required activities of the phase components and the equilibrium constant can be calculated. The simplest function is  $a = X$ . This will serve the purpose of illustrating the GTB principle here with the result that  $\log K = -0.6$ . The solution model also implies  $a_{Wo} = a_{Qtz} = 1$  and the corresponding  $\log a_i$  of Wo and Qtz are equal to zero.

The second GTB step is to determine P and T. For this purpose, we use the equation from Chap. 3:

$$\log K_{PT} = -0.6 = -\Delta G_r^\circ / RT \quad (4.2)$$

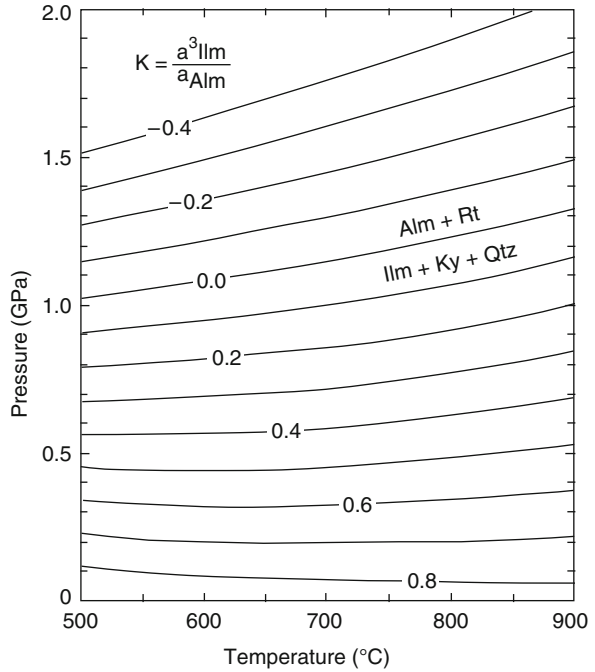
The problem is to find all P and T pairs where  $\Delta G_r^\circ$  has values that satisfy this equation representing the equilibrium condition of the reaction. In other words, we need an equation that permits us to calculate the right-hand-side of the Eq. 4.2 at any P and T. The most popular form of such an equation is:

$$\log K_{PT} = -(A/T) + B + (C/T)P \quad (4.3)$$

In this equation based on thermodynamics, the coefficients A, B, and C are constants, specific to a thermometer or barometer, that have been determined experimentally or have been calculated from thermodynamic data. The equation describes a straight line in a  $P$ - $T$  diagram with the slope (B/C) and the intercept  $-(A/C)$  for a given value of  $\log K$  (Fig. 4.13). The equation represents a family of lines for specific values of  $\log K$ , one of which is  $\log K = 0$ , the equilibrium among end-member phase components An and Grs. Another line represents  $\log K = -0.6$ , the equilibrium between  $An_{20}$  and  $Grs_{80}$  in the presence of Qtz + Wo. There is, of course, an infinite number of lines for all possible values of  $\log K$ . For practical purposes, one can contour a  $P$ - $T$  frame by a series of lines with constant  $\log K$ . Such a figure permits direct graphic application of a thermobarometer, e.g. Fig. 4.14.

From the above, it follows that an equilibrium with a steep slope in  $P$ - $T$  space depends mostly on T and one with a flat slope mainly on P. The first type of reaction is a preferred thermometer, the second type an excellent barometer. The slope (B/C) is, in fact, the so called Clausius-Clapeyron slope given by  $\Delta S_r / \Delta V_r$  (see also Fig. 3.13). An good thermometer has a large entropy change and a small volume change of reaction, a good barometer is one with a large volume change. From Chap. 3 we may recall that exchange reactions are typically associated with small  $\Delta V_r$  and make good thermometers. Net transfer reactions are the prime candidates for barometers.

**Fig. 4.14** In K contours for equilibrium conditions of the GRAIL reaction (Grt–Rt–Als (Ky)–Ilm–Qtz assemblage)



After having solved the above thermobarometer for all possible  $P$ – $T$  solutions, we know that the equilibrium conditions of the GWAK reaction in our rock can be anywhere along a line in  $P$ – $T$  space. In order to find a  $P$ – $T$  point that we then can associate with the least hydrated state or generally speaking with the “peak conditions” of metamorphism, we need a second geothermobarometric equilibrium in our rock sample. The equilibrium conditions of this second reaction represent a second line in  $P$ – $T$  space.

In general, two (straight) lines intersect somewhere on a  $P$ – $T$  diagram and great care and geological common sense must be used in the interpretation of such  $P$ – $T$  data. Never think the numbers are “true” because they are derived from a “clever” computer program. Obvious cases are intersections at negative pressure or negative temperature that indicate calculation errors or severe disequilibrium. More difficult to detect are erroneous  $P$ – $T$  solutions in plausible  $P$ – $T$  portions of  $P$ – $T$  space. Some of the pitfalls of GTB are briefly discussed below.

### 4.7.2 Assumptions and Precautions

Successful geothermobarometry relies on several assumptions and many pitfalls have to be avoided. Studies dealing with errors and difficulties in geothermobarometry include Carson and Powell (1997) and Holdaway (2001).

### 4.7.2.1 Question of Equilibrium

The basic assumption of thermobarometry is that the considered mineral assemblage formed at equilibrium, but it is impossible to prove that minerals in an individual rock ever achieved equilibrium (Chaps. 2 and 3). On the other hand, it is highly desirable to find different generations of sub-assemblages in the same rock, each hopefully preserved in a state of small-scale domain equilibrium. It might then be possible to infer the pressures and temperatures at various stages in the history of a rock, and to reconstruct its pressure-temperature-time path. As an example, St-Onge (1987) describes zoned poikiloblastic garnets with inclusions of biotite, plagioclase, quartz, and less commonly  $\text{Al}_2\text{SiO}_5$ . This enabled simultaneous determination of successive metamorphic  $P$  and  $T$  conditions from core to rim of a single garnet grain, using the garnet-biotite (Fe–Mg) exchange reaction and the garnet –  $\text{Al}_2\text{SiO}_5$  – plagioclase – quartz solid-solid reaction. Over the years, many studies have appeared in the literature that have successfully deduced  $P$ – $T$  paths taken by a single sample using thermobarometry data (see references).

### 4.7.2.2 Retrograde Effects

If an equilibrium assemblage has remained unchanged after its formation, determined  $P$ – $T$  values presumably refer to peak temperature conditions (= least hydrated state; see Chap. 3). Such situations may be nearly valid for some quickly cooled or low temperature rocks, but are not realized in slowly cooled rocks formed at high temperatures such as those of higher amphibolite facies and granulite facies conditions. In some cases retrogression is obvious from thin-section examination, e.g. chloritisation of biotite and garnet, pinitisation of cordierite, or exsolution in feldspars, carbonates, oxides, and sulphides. In other cases, however, retrograde diffusion may be revealed only by careful microchemical analysis. The following two examples serve to demonstrate how such problems may be overcome. Bohlen and Essene (1977) used feldspar and iron–titanium–oxide equilibria to determine metamorphic temperatures in a granulite facies terrain. Exsolution of albite in alkali feldspar and of ilmenite in magnetite was observed, and geologically reasonable temperatures were obtained only after reintegration of the exsolved components. Edwards and Essene (1988) applied two-feldspar and garnet–biotite thermometry to an amphibolite–granulite facies transition zone. Biotite–garnet pairs gave erratic temperatures compared to two-feldspar temperatures. In detail, it was found that some garnets were homogeneous in composition, and some were zoned with rapidly changing composition near the rim but with sillimanite included. Biotites had different compositions depending on whether they were included in garnet, contacting grains not included in garnet, or in contact with garnet. In addition, included and contacting biotites from the same sample had highly variable Fe/Mg ratios, whereas biotites not in contact with garnet tended to have the same composition. These observations were explained by the retrograde exchange of Fe and Mg

between biotite and garnet and by the retrograde hydration reaction  $\text{Grt} + \text{Kfs} + \text{H}_2\text{O} = \text{Bt} + \text{Sil} + \text{Qtz}$ . It is clear by using compositions of biotite not actually in contact with garnet and those of garnet cores should have indicated peak metamorphic temperatures, but this was not the case with the calibrations applied.

#### 4.7.2.3 Quality of Calibration

The applied reaction or equilibrium must be well calibrated, either from direct experimental or from thermodynamic data. Experiments used to calibrate a given system should be well reversed and not rely on synthesis runs only. Furthermore, starting materials and run products need to be carefully characterized.

#### 4.7.2.4 Large Extrapolations of $P$ – $T$

Some geothermobarometers have been calibrated at much higher  $P$ – $T$  conditions than those of typical crustal metamorphism, generating significant errors if large extrapolations are required. As an example, the reaction  $\text{Grs} + 2 \text{Ky} + \text{Qtz} = 3 \text{An}$  has been determined experimentally over the temperature range of 900–1,600°C, but may also be applicable at temperatures as low as 500°C. This extrapolation problem may be minimized if an “accurate” reaction slope calculation is feasible, although calculated uncertainty limits may turn out to be disappointingly large (see e.g. Hodges and McKenna 1987, Fig. 4).

#### 4.7.2.5 Sensitivity of Thermobarometers

Some systems are sensitive over a restricted  $P$ – $T$  range only. For example, many solvus thermometers are useful at relatively high temperatures, but less so at relatively low temperatures where mineral compositions are located on the steep limbs of the solvus. In such cases even small errors involved in the location of the solvus as well as the mineral analyses will produce large errors in inferred temperatures. In contrast to solvus thermometry, fractionation of oxygen isotopes between coexisting minerals are most sensitive at low temperatures, because fractionation decreases to almost zero at high temperatures (800–1,000°C).

#### 4.7.2.6 Variable Structural State

Many minerals have variably ordered cation distributions, and the extent and temperature dependence of the ordering process are presently not well known for most phases. In an ideal case, the synthetic products should have the same structural state that the metamorphic minerals had at the time of metamorphism, although, the structural state of disordered metamorphic minerals may reset upon cooling.

In using feldspar thermometry, for instance, one must decide whether the metamorphic feldspars were ordered, partially disordered or completely disordered.

#### 4.7.2.7 Effect of Other Components

Most geothermobarometers are based on mineral equilibria that are calibrated using simple mineral compositions, although most minerals in rocks contain additional components and form complex solid solutions. Thermodynamic solution models can account for these compositional complexities. This requires the accurate knowledge of activity-composition relations. The activities of all phase components of a reaction equilibrium must be calculated from mineral composition data that are analyzed with an electron probe microanalyser. The activities are inserted into an equilibrium constant expression that can be solved for  $P$  and  $T$ . The activity-composition function,  $a = fX$ , is commonly known as the solution model. Unfortunately, the connection between activity and composition is often complex and only poorly known for most minerals. As a consequence, there is often disagreement among petrologists about the most suitable solution model for a given mineral species. This has led to the widespread practice of reporting multiple  $P$ - $T$  estimates reflecting the effects of different solution models. As an example, for the garnet-biotite thermometer (see below) at least seven calibrations based on the experimental study of Ferry and Spear (1978) are currently available. "In some cases,  $P$ - $T$  estimates calculated using different solution models can vary widely, implying that uncertainties in solution behavior constitute a major source of error in thermobarometry. In general, this error cannot be quantified because the assumptions inherent in different models are often mutually exclusive" (Hodges and McKenna 1987, p. 672).

If the composition of a metamorphic mineral, e.g. garnet, deviates strongly from that used in the calibration experiment for the geothermobarometer, then the effect of "other" components will lead to large errors of extrapolation. For instance, the garnet- $\text{Al}_2\text{SiO}_5$ -quartz-plagioclase thermobarometer is commonly applied to metapelites containing garnets with only 5–10% grossular component and plagioclase with only 10–30% anorthite component. The experimental calibration is only available for the end-member equilibrium  $\text{Grs} + 2 \text{Als} + \text{Qtz} = 3 \text{An}$ .

#### 4.7.2.8 Estimation of $\text{Fe}^{2+}/\text{Fe}^{3+}$ in Mineral Analysis

The electron probe microanalyzer provides information on total iron content expressed either as  $\text{FeO}$  or  $\text{Fe}_2\text{O}_3$ , and the ferric and ferrous iron contents of a mineral analysis must be calculated assuming charge balance and some site occupancy model. For relatively simple minerals with low ferric iron (e.g. pelitic garnets, some pyroxenes) such calculations can be done in principle. For other, more complex minerals with partially vacant cation sites and variable  $\text{H}_2\text{O}$  content (e.g. amphiboles and micas) such calculations are often questionable or even

meaningless. Calculation of ferric iron in garnet and pyroxene (and spinel, etc.) requires microprobe data of excellent quality. Routine data are not good enough! In a given sample, calculated  $\text{Fe}^{3+}/\text{Fe}^{2+}$  ratios in Grt and Pyx, for example, should not vary by more than ~5%. The REDOX conditions do not normally vary from grain to grain or within a grain of a given sample. A larger variation of  $\text{Fe}^{3+}/\text{Fe}^{2+}$  ratio is not permitted because of the assumption that the rock has recrystallised under equilibrium conditions and therefore mineral compositions represent an equilibrium state. This is a simple, but very restrictive quality test. If the variation is large, then one usually relies on  $\text{Fe}_{\text{total}} = \text{Fe}^{2+}$ . Spinel is notoriously difficult because of the common presence of vacancies and of  $\text{Fe}^{3+}$ , and few spinels are simple hercynite–spinel solutions. Assuming  $\text{Fe}_{\text{total}} = \text{Fe}^{2+}$  is recommended for amphiboles, micas and other complex minerals. However, if excellent garnet and pyroxene data from a sample indicate the presence of some ferric iron, one might consider a fixed  $\text{Fe}^{3+}/\text{Fe}^{2+}$  in coexisting amphibole and mica. In any case,  $\text{Fe}^{3+}/\text{Fe}^{2+}$  calculations from microprobe data need to be done on good quality analyses and the data used thoughtfully (see also Droop 1987; Schumacher 1991).

### 4.7.3 Exchange Reactions

Exchange equilibria involve interchange of two similar atoms between different sites in one mineral (*intracrystalline exchange*) or between two minerals (*intercrystalline exchange*). The atoms may be elements of equal charge and similar ionic radius or isotopes of the same element. Because the volume changes involved are very small and the entropy changes are relatively large, exchange reactions are largely independent of pressure and have good potential as thermometers. Unfortunately, retrograde exchange by diffusion below peak metamorphic conditions occurs very easily in many cases and generally leaves no textural evidence. This is especially true for intracrystalline cation distributions because diffusion paths are but a fraction of a unit cell. Consequently, intracrystalline exchange reactions are unsuitable for peak metamorphic thermometry and will not be considered further.

The most widely applied exchange thermometers in metamorphic rocks involve  $\text{Fe}^{2+}$  and Mg, and involve the minerals, olivine, garnet, clinopyroxene, orthopyroxene, spinel, ilmenite, cordierite, biotite, phengite, chlorite and hornblende. For many mineral pairs of this list there are calibrations for some end-member mineral compositions, either from experimental work or from thermodynamic calculation. In a few cases, experimental calibrations are also available for complex “natural” systems. Based on these calibrations, many reformulations exist, using different solution models to account for the effects of “impurities”. Furthermore, some exchange thermometers are empirically calibrated against natural assemblages. Currently, data for about 20 systems are available and some of these are given in Table 4.2. Most of the experiments on the anhydrous pairs listed were obtained at  $T > 800^\circ\text{C}$  and many were not compositionally reversed. If not reset by retrograde exchange, their best application is for high-temperature rocks from the granulite

**Table 4.2** Some Fe–Mg exchange reactions used for geothermometry

No.	Mineral pair	Exchange reaction	Range of application <sup>b</sup>	References <sup>c</sup>
1	Ol–Spl	Fo + Hc = Fa + Spl	GRE, AMP, GRA	
2	Ol–Opx	Fo + Fs = Fa + En	GA, ECL	Docka et al. (1986) Carswell and Harley (1989)
3	Ilm–Opx	Gei + Fs = Ilm + En	GRA	Docka et al. (1986)
4	Ilm–Cpx	Gei + Hd = Ilm + Di	GRA, AMP	Docka et al. (1986)
5	Ilm–Ol	Gei + Fa = Ilm + Fo	GRA	Docka et al. (1986)
6	Opx–Cpx	En + Hd = Fs + Di	GRA	Stephenson (1984) Docka et al. (1986)
7	Opx–Bt	En + Ann = Fs + Phl	GRA	Fonarev and Konilov (1986) Sengupta et al. (1990)
8	Crd–Spl	Mg–Crd + Hc = Fe–Crd + Spl	GRA	Vielzeuf (1983)
9	Grt–Ol	Prp + Fa = Alm + Fo	GRA, ECL	Carswell and Harley (1989)
10	Grt–Opx	Prp + Fs = Alm + En	GRA, ECL	Carswell and Harley (1989) Bhattacharya et al. (1991)
11	Grt–Cpx	Prp + Hd = Alm + Di	GRA, ECL, ± AMP	Pattison and Newton (1989) Carswell and Harley (1989)
12	Grt–Crd	Prp + Fe–Crd = Alm + Mg–Crd	GRA	Bhattacharya et al. (1988)
13	Grt–Bt	Prp + Ann = Alm + Phl	AMP, GRE, ± GRA	Thoenen (1989)
14	Grt–Phe	Prp + Fe–Cel = Alm + Mg–Cel	ECL, BLU	Carswell and Harley (1989)
15	Grt–Hbl <sup>a</sup>	Prp + Fprg = Alm + Prg	AMP, ± GRA	Graham and Powell (1984)
16	Grt–Chl	Prp + Fe–Chl = Alm + Mg–Chl	GRE, BLU, ± AMP	Laird (1988) Grambling (1990)

<sup>a</sup>Empirical calibrations; all other calibrations were determined by experiment or by calculation

<sup>b</sup>Abbreviations of metamorphic facies: *AMP* Amphibolite, *BLU* Blueschist, *ECL* Eclogite, *GRA* Granulite, *GRE* Greenschist

<sup>c</sup>One or two references for each reaction are given only

facies and the mantle, and extrapolation of these data to relatively low temperatures is often unjustified. The potential problem with Mg–Fe<sup>2+</sup> thermometry in using microprobe analyses is discussed in Sect. 4.7.2.8.

In the following, the two most commonly used Fe–Mg exchange thermometers are briefly reviewed.

#### 4.7.3.1 Garnet–Clinopyroxene

The Grt–Cpx thermometer has been considered by many petrologists because of its potential importance for garnet-granulites, garnet-amphibolites, garnet-peridotites and eclogites. There exist at least ten calibrations of this thermometer derived from a large body of experimental work. Experiments were conducted in the temperature range of 600–1,500°C, but predominantly at  $T > 900^\circ\text{C}$ . Only three calibrations

will be mentioned here, whilst references to other studies can be found in Pattison and Newton (1989).

The most often used calibration of the Grt–Cpx thermometer is that derived by Ellis and Green (1979). These authors first experimentally evaluated the effect of grossular substitution ( $X_{Ca}^{Grt}$ ) on the exchange reaction 11 (Table 4.2) and derived the following equation:

$$T(^{\circ}\text{C}) = (3030 + 10.86 P \text{ (kbar)} + 3104 X_{Ca}^{Grt}) / (\ln K_D + 1.9034) - 273 \quad (4.4)$$

where  $K_D$  is the distribution ratio  $(\text{Fe}^{2+}/\text{Mg})^{\text{Grt}}/(\text{Fe}^{2+}/\text{Mg})^{\text{Cpx}}$ . More recent experimental studies have shown that the Ellis and Green geothermometer overestimates temperatures when applied to granulites formed at about 1.0 GPa. According to Green and Adam (1991, p. 347) “this overestimate could be of the order of 50–150°C”. However, no new thermometric equation was presented.

Using earlier experimental data, Krogh (1988) derived an expression for the Grt–Cpx thermometer with a curvilinear relationship between  $\ln K_D$  and  $X_{Ca}^{Grt}$ .

$$T(^{\circ}\text{C}) = \{1879 + 10 P \text{ (kbar)} - 6173 (X_{Ca}^{Grt})^2 + 6731 X_{Ca}^{Grt}\} / (\ln K_D + 1.393) - 273 \quad (4.5)$$

A large set of new experimental data presented by Pattison and Newton (1989) indicated that the Grt–Cpx Fe/Mg distribution curves are asymmetric, implying non-ideal solid solution behavior, in contrast to those of previous experimental studies. The Grt–Cpx thermometer as formulated by Pattison and Newton (1989) appears to work for upper amphibolite facies, granulite facies and high-T eclogite facies rocks. Application to low- and medium-T crustal eclogites is uncertain because they contain clinopyroxene that is ordered omphacite with a high jadeite content, very different from those of the simpler system investigated by Pattison and Newton. In most recent studies, the Ellis and Green (1979) calibration has been applied to eclogites. In many cases a large temperature extrapolation is involved, and in this respect the lowest T estimates obtained are critical, i.e. in the range of 400–500°C. As an example, Schliestedt (1986) determined Grt–Cpx temperatures of  $471^{\circ}\text{C} \pm 31^{\circ}\text{C}$  (range = 392–512°C, 16 samples) for eclogites and blueschists from Sifnos, based on a preliminary version of the Krogh (1988) calibration. Schliestedt concluded that these temperatures were in accordance with those estimated by other methods (calcite-dolomite solvus and oxygen isotope fractionation). Note that the Ellis and Green (1979) thermometer gave equilibrium temperatures ca. 50°C too high for these rocks (Krogh 1988). These limited data seem to indicate that reasonable results can be obtained with the Krogh formulation, even in low-T eclogites.

The Grt–Cpx thermometer calibrations mentioned above do not include the possible effects of chemical variations in Cpx. Such effects were noted for variations in the jadeite content, with  $K_D$  tending to decrease with increasing of  $X_{Jd}^{\text{Cpx}}$  of sodic omphacite, and especially at  $X_{Jd}^{\text{Cpx}} > 0.6$  (e.g. Koons 1984; Heinrich 1986;



Benciolini et al. 1988). However,  $X_{Jd}^{Cpx}$  will in most cases be lower than 0.6 and will exert only a minor effect on  $K_D$ . On the other hand, no definite compositional dependence of  $K_D$ 's on the  $Fe^{3+}$  content in clinopyroxene (aegirine component) was observed by Benciolini et al. (1988), but it should be remembered that the problem of the determination of ferrous/ferric iron in the clinopyroxene from microprobe data is not solved. Additional chemical effects on the Fe–Mg partition coefficient  $K_D$  are discussed by Krogh (1988).

In conclusion, the present status of Grt–Cpx Fe–Mg exchange geothermometry is certainly far from being perfect, but nevertheless it is a valuable thermometer for granulites and eclogites. The calibration of Krogh (1988) (by using Erling Ravna Krogh's spreadsheet) is recommended for low-T//medium-T eclogites and that of Pattison and Newton (1989) for high-T eclogites/granulites, respectively.

#### 4.7.3.2 Garnet–Biotite

The garnet–biotite exchange thermometer is the most popular of all geothermometers because of its wide application to a large variety of rocks covering a broad range of metamorphic grade. At least eighteen versions of this thermometer are available: three have been calibrated by field observations, two by laboratory experimentation, and thirteen were derived from the experimental calibrations using different non-ideal mixing models for garnet and biotite.

Ferry and Spear (1978) published experimental data on the Fe–Mg exchange between synthetic annite–phlogopite and almandine–pyrope in systems with  $Fe/(Fe + Mg)$  held at 0.9. The following equation was derived:

$$T(^{\circ}C) = \{[2089 + 9.56 P \text{ (kbar)}]/(0.782 - \ln K_D)\} - 273 \quad (4.6)$$

with  $K_D = (Fe/Mg)^{Bt}/(Fe/Mg)^{Grt}$ . As it is likely that solid solution of additional components affects this thermometer, Ferry and Spear (1978) suggested that it should be restricted for garnet low in Ca and Mn, with  $(Ca + Mn)/(Ca + Mn + Fe + Mg) \leq 0.2$ , and with biotite low in  $Al^{VI}$  and Ti, with  $(Al^{VI} + Ti)/(Al^{VI} + Ti + Fe + Mg) \leq 0.15$ .

Perchuk and Lavrent'eva (1983) performed a second experimental study on the Fe–Mg exchange between garnet and biotite. For most experiments natural minerals served as starting materials in systems that covered a range of 0.3–0.7  $Fe/(Fe + Mg)$ . As pointed out by Thoenen (1989), the thermometric equation given by Perchuk and Lavrent'eva is unlikely because it gives negative Clausius–Clapeyron slopes. A corrected version of the equation is:

$$T(^{\circ}C) = \{[3890 + 9.56 P \text{ (kbar)}]/(2.868 - \ln K_D)\} - 273 \quad (4.7)$$

Temperatures obtained from this calibration are  $\sim 30^{\circ}C$  higher in the  $500^{\circ}C$  temperature range, but  $\sim 60^{\circ}C$  lower in the  $700^{\circ}C$  temperature range compared to the Ferry and Spear calibration.

Several modifications of the Ferry and Spear calibration have been made, based upon the effects of Ca and Mn in garnet and of Al and Ti in biotite. Despite considerable research, the magnitude of the effects of these elements on the Fe–Mg exchange between garnet and biotite is still not sufficiently well known (for a discussion, see Bhattacharya et al. 1992). This makes it difficult to choose between the many versions of this geothermometer. Some authors have tried to evaluate the quality of different calibrations by comparing the calculated temperatures with T estimates based on other mineral equilibria or by comparing the scatter of data within a given metamorphic zone. Another approach was taken by Chipera and Perkins (1988) who applied a trend surface analysis to determine how well the temperatures fitted a regional temperature surface across their study area. Eight calibrations of the garnet-biotite thermometer were compared and it was found that the Perchuk and Lavrent'eva (1983) thermometer yielded the most precise results.

In general, the Grt–Bt thermometer seems to work fairly well for rocks metamorphosed under high-T greenschist facies and the amphibolite facies conditions. For several areas, Grt–Bt temperatures indicate a regular increase in temperature with increasing metamorphic grade over a range of some 100–150°C (e.g. Ferry 1980; Lang and Rice 1985b; Holdaway et al. 1988). In the upper amphibolite facies and granulite facies, however, retrograde Fe–Mg exchange generally occurs, resulting in anomalously low Grt–Bt temperatures if garnet-rims and adjacent biotites are analyzed. Nevertheless, reasonable prograde temperatures can still be obtained from garnets that have undergone retrograde reactions. As suggested by Tracy et al. (1976), in biotite-rich rocks retrograde reactions will cause negligible changes in matrix biotite composition while there is a significant change garnet-rim compositions. In biotite-rich rocks, therefore, reasonable estimates of maximum prograde temperatures can be made using garnet-core and matrix biotite compositions (provided these two mineral compositions were once in chemical equilibrium).

The GTB program of Spear and Kohn (1999) offers a choice of 11 different Bt–Grt thermometers, including calibrations by Patiño Douce et al. (1993), Holdaway et al. (1997), Gessmann et al. (1997), Kleemann and Reinhardt (1994). We tested the thermometers with various Bt and Grt data from amphibolite facies metapelites and found that the Ferry and Spear (1978), Hodges and Spear (1982), Perchuk and Lavrent'eva (1983) and Patiño Douce et al. (1993) formulations gave consistent and plausible temperatures.

### 4.7.3.3 Isotopic Exchange Thermometry

Most exchange thermometers involve cations. Isotopic thermometers are an important exception that are based on the temperature dependence of the equilibrium partition of light stable isotopes (typically of the elements C, O, S) between two coexisting phases. Stable isotopes are used because their ratios do not vary with time because of radioactive decay. Heavy isotopes are not useful for thermometry because they do not fractionate as much as light isotopes. Fractionation between light isotopes is dependent on temperature, mineral chemical composition and crystal structure.

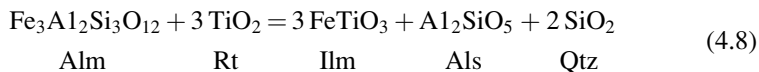
Fractionation between two coexisting minerals is largest at low temperatures and decreases to almost zero at high temperatures (800–1,000°C). Fractionation tends to be greatest between phases of widely different compositions and structures, so that mineral pairs such as magnetite–quartz, ilmenite–quartz, rutile–quartz, and calcite–quartz are most useful. Isotopic exchange has virtually no volume change, which means that this thermometer is effectively independent of pressure.

Isotopic thermometry is potentially very useful because it appears to be the ideal thermometer for metamorphic rocks, but there are several problems. Different experimentally determined calibration curves are in use which, in general, are not internally consistent. Retrograde isotopic exchange will occur during slow cooling from high temperatures, yielding discordant temperature values for different mineral pairs from the same rock. A set of paleotemperatures obtained for a rock will generally give neither mineral closure temperatures nor formation or crystallization temperatures. On the other hand, the cooling rate of the rock may be derived from the data (Giletti 1986). Lack of equilibrium may be a problem, especially during contact metamorphism and at low temperatures. For further information the reader is referred to Valley (1986), Hoefs (1987) and Savin and Lee (1988).

#### 4.7.4 Net-Transfer

The prime equilibria in geobarometry are net-transfer reactions in which one or more of the involved minerals shows variable composition. Due to their generally small positive slope in  $P$ – $T$  space, solid-solid transfer reactions are primarily used as pressure indicators and the temperature can be retrieved from exchange or other thermometers. Net-transfer reactions are continuous or sliding equilibria that are multivariant in  $P$ – $T$ – $X$  space and, as a result, the entire thermobarometric assemblage can coexist over a wide range of  $P$  and  $T$ . Application of these reactions requires that (1) the appropriate univariant end-member equilibrium has been well calibrated, (2) the chemical compositions of the phases are known, and (3) activity-composition relations are available for those minerals with appreciable solid-solution. The net-transfer reaction  $\text{Grt} + \text{Qtz} = 2 \text{Wo} + \text{An}$  has been used in Sect. 4.7.1 to illustrate the general principles of thermobarometry.

As a further example, consider the assemblage  $\text{Grt} + \text{Rt} + \text{Als} + \text{Ilm} + \text{Qtz}$  (GRAIL) typical of some metapelitic rocks. The following end-member reaction can be formulated:



Equilibrium of the reaction is shown in Fig. 4.14. The effect of solid solution in garnet and ilmenite leads to isopleths of  $\log K_{PT} = 3 \log a_{\text{Ilm}} - \log a_{\text{Alm}}$  contoured on a  $P$ – $T$  diagram. If chemical analyses of coexisting Ilm and Grt can be converted to activities of the respective Fe end-member phase components by using an

appropriate solution model, then  $\log K$  for the specific assemblage in the rock can be calculated. This specific  $\log K$  value corresponds to one  $P$ - $T$  line or a nearby line on Fig. 4.14.

As mentioned above, thermodynamic models of activity-composition relations are a prerequisite for application of thermobarometers involving solid solutions. Unfortunately, solution models for the minerals most commonly employed in thermobarometry are poorly constrained (see e.g. Essene 1989, p. 2), and this represents one of the main obstacles to obtaining accurate geothermobarometry. For this reason, the use of any thermodynamic model at large dilutions, i.e. where the actual mineral compositions deviate significantly from those of the calibrated end-member reaction, should be avoided or at least regarded with skepticism, except where experimental  $a$ - $X$  data are available.

Some of the more commonly used net transfer reactions together with some potentially useful solid-solid end-member reactions in thermobarometry are listed in Table 4.3, together with their range of applicability in terms of metamorphic facies. Note that these reactions are listed with increasing number of phases involved, ranging from two to five. Before some specific reactions are considered, a few general comments concerning Table 4.3 are given.

1. No equilibria involving cordierite or sapphirine have been considered because the effects of various fluid species (contained in cordierite), order/disorder, and non-ideal  $a$ - $X$  relations are not sufficiently well known.
2. There are two calibrated reactions available for six of the mineral assemblages listed, one each for the Fe and Mg end-members respectively.
3. Most of the thermobarometers have a rather restricted range of applicability, often limited to one or two metamorphic facies.
4. There are at least 19 thermobarometers based on solid-solid reactions available for the granulite facies and a further 9 for the amphibolite facies, but their application to other facies is not appropriate.

#### 4.7.4.1 Garnet–Aluminosilicate–Quartz–Plagioclase (GASP)

The equilibrium  $\text{Grs} + 2 \text{Als} + \text{Qtz} = 3 \text{An}$  (Table 4.3) has become the most widely used barometer for amphibolite and granulite facies rocks. The advantage of this tool is the widespread occurrence of the GASP assemblage in metapelites due to extensive solid solution in garnet and plagioclase. An expression of the popularity of this geobarometer is the existence of at least eight different calibrations. However, the large uncertainties involved (see below) is cause for concern for the successful application of this barometer.

The end-member reaction has been calibrated in several studies (see e.g. Koziol and Newton 1988, for references) in the temperature range 900–1,400°C. Application to rocks that equilibrated between 500°C and 800°C requires a rather considerable extrapolation and this contributes to the large uncertainty in  $P$  estimates from this barometer. Based on 27 brackets from 5 different experimental studies, McKenna and

**Table 4.3** Some net-transfer reactions used in geothermobarometry

No.	Mineral assemblage	Net-transfer reaction	Range of application <sup>c</sup>	Reference <sup>d</sup>
1	Gr <sub>t</sub> -Opx	1 Prp = 1 En + 1 MgTs	ECL	Carswell and Harley (1989)
2	Opx-Ol-Qtz	1 Fs = 1 Fa + 1 Qtz	GRA	Bohlen and Boettcher (1981) Newton (1983)
3	Cpx-Pl-Qtz	1 CaTs + 1 Qtz = 1 An	GRA	Newton (1983) Gasparik (1984)
4	Cpx-Pl-Qtz	1 Jd + 1 Qtz = 1 Ab	BLU, ECL, ± GRA	Liou et al. (1987) Carswell and Harley (1989)
5	Gr <sub>t</sub> -Pl-Ol	1 Grs + 2 Prp = 3 An + 3 Fo	GRA	Johnson and Essene (1982)
6	Gr <sub>t</sub> -Pl-Ol (GAF) <sup>a</sup>	1 Grs + 2 Alm = 3 An + 3 Fa	GRA	Bohlen et al. (1983a)
7	Sp-Po-Py	-	GRE, AMP, GRA ± BLU	Jamieson and Craw (1987) Bryndzia et al. (1988, 1990)
8	Wo-Pl-Gr <sub>t</sub> -Qtz (WAGS) <sup>a</sup>	1 Grs + 1 Qtz = 1 An + 2 Wo	AMP, GRA	Huckenholz et al. (1981)
9	Gr <sub>t</sub> -Spl-Sil-Qtz	1 Alm + 2 Sil = 3 Hc + 5 Qtz	GRA	Bohlen et al. (1983b)
10	Gr <sub>t</sub> -Spl-Sil-Crn	1 Alm + 5 Crn = 3 Hc + 3 Sil	GRA	Shulters and Bohlen (1989)
11	Gr <sub>t</sub> -Pl-Opx-Qtz (GAES) <sup>a</sup>	1 Grs + 2 Prp + 3 Qtz = 3 An + 3 En	GRA	Eckert et al. (1991)
12	Gr <sub>t</sub> -Pl-Opx-Qtz (GAFS) <sup>a</sup>	1 Grs + 2 Alm + 3 Qtz = 3 An + 3 Fs	GRA	Faulhaber and Raith (1991)
13	Gr <sub>t</sub> -Pl-Cpx-Qtz (GADS) <sup>a</sup>	2 Grs + 1 Prp + 3 Qtz = 3 An + 3 Di	GRA	Eckert et al. (1991)
14	Gr <sub>t</sub> -Pl-Cpx-Qtz (GAHS) <sup>a</sup>	2 Grs + 1 Alm + 3 Qtz = 3 An + 3 Hd	GRA	Moecher et al. (1988)
15	Gr <sub>t</sub> -Als-Qtz-Pl (GRIPS) <sup>a</sup>	1 Grs + 2 Als + 1 Qtz = 3 An	AMP, GRA	Koziol and Newton (1988) McKenna and Hodges (1988)
16	Gr <sub>t</sub> -Hbl-Pl-Qtz <sup>b</sup>	2 Grs + 1 Prp + 3 Prg + 18 Qtz = 6 An + 3 Ab + 3 Tr	AMP, GRA	Kohn and Spear (1989)
17	Gr <sub>t</sub> -Hbl-Pl-Qtz <sup>b</sup>	2 Grs + 1 Alm + 3 Fprg + 18 Qtz = 6 An + 3 Ab + 3 Fac	AMP, GRA	Kohn and Spear (1989)
18	Gr <sub>t</sub> -Ms-Pl-Bt <sup>b</sup>	1 Grs + 1 Prp + 1 Ms = 3 An + 1 Phl	AMP	Powell and Holland (1988)
19	Gr <sub>t</sub> -Ms-Pl-Bt <sup>b</sup>	1 Grs + 1 Alm + 1 Ms = 3 An + 1 Ann	AMP	Powell and Holland (1988)
20	Ttn-Ky-Pl-Rt	1 Ttn + 1 Ky = 1 An + 1 Rt	ECL	Manning and Bohlen (1991)
21	Gr <sub>t</sub> -Opx-Cpx-Pl-Qtz	1 Prp + 1 Di + 1 Qtz = 2 En + 1 An	GRA	Paria et al. (1988)
22	Gr <sub>t</sub> -Opx-Cpx-Pl-Qtz	1 Alm + 1 Hd + 1 Qtz = 2 Fs + 1 An	GRA	Paria et al. (1988)
23	Gr <sub>t</sub> -Rt-Als-Ilm-Qtz (GRAIL) <sup>a</sup>	1 Alm + 3 Rt = 3 Ilm + 1 Als + 2 Qtz	AMP, GRA	Bohlen et al. (1983b)
24	Gr <sub>t</sub> -Rt-Pl-Ilm-Qtz (GRIPS) <sup>a</sup>	1 Grs + 2 Alm + 6 Rt = 3 An + 6 Ilm + 3 Qtz	AMP, GRA	Bohlen and Liotta (1986) Anovitz and Essene (1987)

<sup>a</sup>Abbreviations according to Essene (1989)

<sup>b</sup>Empirical calibrations; all other calibrations were determined by experiment or by calculation

<sup>c</sup>Abbreviations of metamorphic facies: AMP Amphibolite, BLU Blueschist, ECL Eclogite, GRA Granulite, GRE Greenschist

<sup>d</sup>One or two references for each reaction are given only

Hodges (1988) give the following equation for use in thermobarometry with kyanite as the aluminosilicate polymorph:

$$P \text{ (MPa)} = (2.20 \pm 0.15) T \text{ (}^\circ\text{K)} - (620 \pm 300) \quad (4.9)$$

where the uncertainties are at the 95% confidence level. According to McKenna and Hodges (1988) these inaccuracies propagate into paleopressure uncertainties of  $\pm 0.25$  MPa.

An additional problem with this barometer is the generally small content of grossular component in metapelitic garnets. This leads to relatively large errors in analyzing small concentrations of Ca in garnet. Moreover, this entails greater extrapolations in composition as well because the experimental data refer to a pure Grs-component. Furthermore, the activity of Grs in garnet at such extreme dilution is unknown which results in large additional uncertainties in applying solution models. Our recommendation is to use this thermobarometer with caution for high-pressure amphibolite and granulite facies rocks (see also Todd 1998; Holdaway 2001). It works best for high-P mafic rocks containing An-rich plagioclase and fairly Grs-rich garnet ( $P = 0.6\text{--}1.0$  GPa).

#### 4.7.4.2 Garnet–Rutile–Aluminosilicate–Ilmenite–Quartz (GRAIL)

1. The GRAIL reaction (Fig. 4.14 and Table 4.3) has been tightly experimentally-reversed by Bohlen et al. (1983b) in the temperature range 750–1,100°C. The reaction has many advantages as a barometer for amphibolite and granulite facies metapelites
2. It was calibrated within or in the vicinity of the  $P$ – $T$  range for which it will be used and, therefore, long extrapolations are unnecessary
3. Its location is insensitive to temperature (Fig. 4.14)
4. Only two minerals in the requisite assemblage, garnet and ilmenite, have appreciable solid solution in ordinary metamorphic rocks
5. Analyses of garnet and ilmenite are for their major components, and long compositional extrapolations are not required

Furthermore, in the absence of rutile, the GRAIL barometer may be used to estimate an upper pressure limit. Application of this barometer in numerous metamorphic terrains yields geologically reasonable pressures that are in good agreement with other barometers.

#### 4.7.4.3 Clinopyroxene–Plagioclase–Quartz

The reaction  $Jd + Qtz = Ab$  (Table 4.3) provides the basis for a widely used thermobarometer. Because of its petrological significance, this reaction has been evaluated in several experimental studies (for references see, e.g. Essene 1982, p. 176; Berman 1988, Fig. 38). These experiments have been performed at  $T > 500^\circ\text{C}$  using high albite as the starting material. Many petrologists have used the calibration of Holland (1980) for  $P$ – $T$  estimates, and this procedure is also recommended by Carswell and Harley (1989, p. 93) for eclogite facies rocks. However, Liou et al. (1987, p. 91) found that Holland's data are not consistent with some observed mineral assemblages and mineral composition data from the blueschist facies.

For this reason, at low temperatures, Liou et al. recommended to use the Jd–Ab–Qtz stability relations determined by Popp and Gilbert (1972).

Application of the jadeitic pyroxene equilibrium to natural assemblages is complicated by the difficulty to accurately measure sodium in clinopyroxene, by order-disorder transitions in albite and clinopyroxene, and by limited  $a = f(X)$  data for Ca–Na pyroxenes. For a recent discussion of some of these questions the reader is referred to Carswell and Harley (1989) and Meyre et al. (1997). Also note that eclogite facies assemblages are, by definition, devoid of plagioclase and many eclogites also do not contain quartz. Therefore, the jadeite content of clinopyroxene in such rocks will yield only a minimum pressure of formation.

#### 4.7.4.4 Sphalerite–Pyrrhotite–Pyrite

The iron content of sphalerite in equilibrium with hexagonal pyrrhotite and pyrite continuously decreases as a function of pressure, and provides a barometer in the temperature range 300–750°C (e.g. Bryndzia et al. 1988, 1990). Applications of this barometer to metamorphic rocks has yielded both excellent and poor results. At  $T < 300^\circ\text{C}$ , extensive resetting of sulphide compositions and transformation of hexagonal to monoclinic pyrrhotite occurs, resulting in decreased FeS contents in sphalerite and high apparent pressures. It is important to use unexsolved, coexisting three-phase assemblages following the textural criteria proposed by Hutchison and Scott (1980), and we caution against the indiscriminant use of this sphalerite geobarometer. Sulfide barometers for mantle samples can be found in Egglar and Lorand (1993).

#### 4.7.5 *Miscibility Gaps and Solvus Thermometry*

Some mineral pairs with similar structure but different composition show a mutual solubility that increases with temperature. The immiscible region is called a miscibility gap. Well known examples include the pairs K-feldspar – albite, calcite – dolomite, peristerite albite – oligoclase and actinolite – hornblende mentioned in Sect. 4.3.2.2. At some temperature, e.g. 400°C, Kfs can dissolve a certain amount of Ab and vice versa. With increasing temperature the composition of Kfs becomes more sodic and the coexisting Nafs contains an increasing amount of K. At some critical temperature the two feldspars have an identical composition and the miscibility gap has closed. At higher T, Na–K feldspar forms a continuous solid solution. In the temperature region where a miscibility gap exists, the composition of the two coexisting minerals can be used for thermometry. Most gaps are little pressure dependent, however, some are and therefore the pressure dependence should not be ignored. A miscibility gap between isostructural phases is called a solvus. The term solvus is quite often also used for all miscibility gaps and also for

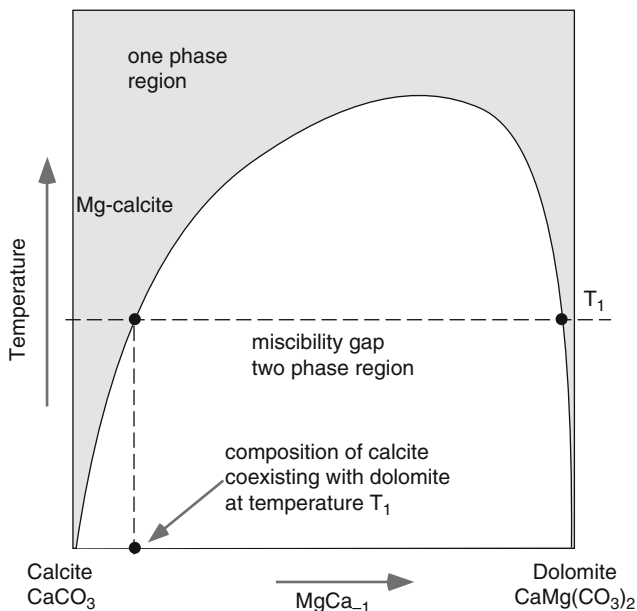


**Fig. 4.15** Schematic  $T$ - $X$  diagram showing the asymmetric miscibility gap between calcite and dolomite (compositional variable is  $\text{MgCa}_{-1}$ ; this is 0 in  $\text{CaCO}_3$  and 1 in  $\text{CaMg}(\text{CO}_3)_2$ ). A given Mg-content in calcite coexisting with dolomite corresponds to an equilibrium temperature of the Ca-Mg exchange equilibrium between Cal and Dol. A given analytical error translates to a large  $T$  error at low  $T$  and a smaller  $T$  error at high  $T$

the curve that separates the two-phase from the one-phase region as well (Fig. 4.15). Although this is not completely accurate we will follow this practice here.

Because of the general shape of miscibility gaps (Fig. 4.15), small variations in mineral composition correspond to a large temperature difference on the steep limbs at low  $T$ , and moderate temperature difference at higher  $T$ . Thus, mineral solvus geothermometers become more sensitive temperature indicators as temperature increases. If disorder occurs in one or both minerals, then there will be a continuum of solvi with gradually increasing partial disorder.

The following mineral pairs are often used for solvus geothermometry; orthopyroxene–clinopyroxene, plagioclase–alkali feldspar, calcite–dolomite, and muscovite–paragonite, and are briefly discussed below.

#### 4.7.5.1 Orthopyroxene–Clinopyroxene

There exists a large body of experimental and theoretical data on the enstatite–diopside solvus, and it has been shown that at high temperatures, above about  $800^\circ\text{C}$ , the diopside limb of the asymmetrical solvus is strongly temperature-dependent. Because natural pyroxenes rarely belong to the binary join  $\text{Mg}_2\text{Si}_2\text{O}_6$ – $\text{CaMgSi}_2\text{O}_6$ , the major problem with this thermometer lies in correction for



additional components. This has led to the formulation of several multicomponent two-pyroxene thermometers. If applied to ultramafic rocks, where pyroxenes closely approach the enstatite–diopside binary join, satisfactory results have been obtained, e.g. Carswell and Gibb (1987), but much less so for iron-rich pyroxenes from granulites.

A different, and more successful approach to Opx–Cpx thermometry was proposed by Lindsley (1983). In this case, phase equilibria for pure Ca–Mg–Fe pyroxenes over the temperature range of 800–1,200°C and for pressures up to 1.5 GPa were determined. Solvus isotherms for coexisting Opx–Cpx are displayed graphically in the quadrilateral pyroxene system Di–Hd–En–Fs. The effect of pressure was found to be  $\leq 8^\circ\text{C}/100\text{ MPa}$ , and graphs are presented for solvus relations at 1 atm and at 0.5, 1.0, and 1.5 GPa, along with approximate formulas for interpolating between these pressures. Pyroxenes with appreciable contents of nonquadrilateral components require special projections onto the Di–Hd–En–Fs pyroxene quadrilateral, and a corresponding method is presented by Lindsley and Andersen (1983) and Lindsley (1983). This correction scheme is largely empirical and Lindsley (op. cit.) suggests that application be limited to pyroxenes with relatively low (<10%) amounts of nonquadrilateral components. An updated version of Cpx–Opx thermometry is implemented in the code QUILF (Andersen et al. 1993). QUILF is briefly described in Sect. 4.10.1.2 on ilmenite–magnetite oxygen-barometry.

Slowly cooled pyroxenes often show exsolution lamellae, and reintegration of exsolved material in form of microprobe analyses is necessary to obtain meaningful thermometric results (e.g. Sandiford and Powell 1986). Also, incorrect calculation of ferric iron will affect this geothermometer.

#### 4.7.5.2 Plagioclase-Alkali Feldspar

Most feldspars consist of the three components Ab, Or, An, with extensive solid solution between Ab and An (the plagioclase series) and between Ab and Or (the alkali feldspar series). The composition of coexisting feldspars contain important thermometric information. The majority of formulations of the two-feldspar thermometer concentrate on two feldspar binaries, Ab–An and Ab–Or, and obtain temperatures from the partitioning of the Ab- component between coexisting plagioclase and alkali feldspar (e.g. Stormer 1975; Haselton et al. 1983). This approach may be valid at lower temperatures where feldspars have only trivial amounts of the third component. At higher temperatures, however, the effects of ternary solution become increasingly important. Thus, most feldspar thermometers are based on ternary solution models that account for the effects of K in plagioclase and Ca in alkali feldspar (e.g. Fuhrman and Lindsley 1988; Elkins and Grove 1990). A great advantage of the ternary approach is that it allows three temperatures to be calculated, one for each component, providing a valuable test of equilibrium. The more sophisticated thermometers cannot be published as a simple thermometric equations, but in many cases a computer program can be downloaded from the web

sites of the authors. A very good program for ternary feldspar thermometry is SOLV CALC (Wen and Nekvasil 1994). SOLV CALC is a windows-based interactive graphics program package for calculating the ternary feldspar solvus and for two-feldspar geothermometry. It is available via the Software List provided by the Department of Geosciences, North Dakota State University.

Two-feldspar thermometry has been applied with some success to high-grade gneisses from granulite facies terranes (e.g. Bohlen et al. 1985; see also Fuhrman and Lindsley 1988). In such rocks, exsolutions of Ab-rich plagioclase from alkali feldspar and of K-rich feldspar from plagioclase upon cooling are common phenomena, and it is essential that exsolved grains are reintegrated to obtain compositions of the original feldspars (see Bohlen et al. 1985, for analytical details). Applications of feldspar geothermometry to rocks from the amphibolite and greenschist facies have been less successful, often yielding unreasonable low temperatures. Evidently, alkali exchange with a fluid phase below peak metamorphic conditions has occurred.

#### 4.7.5.3 Calcite–Dolomite

In the system  $\text{CaCO}_3\text{--CaMg}(\text{CO}_3)_2$  a miscibility gap exists and the two phases on either side of the gap are calcite and dolomite, respectively (Fig. 4.15). The amount of  $\text{MgCO}_3$  in calcite in equilibrium with dolomite can be used for estimating metamorphic temperatures. This strongly asymmetric solvus appears to be well determined and the effect of pressure on temperature estimates is small. Most natural carbonates, however, contain additional components such as  $\text{FeCO}_3$  or  $\text{MnCO}_3$ , and the effect of  $\text{FeCO}_3$  on calcite–dolomite thermometry has been evaluated, e.g. by Powell et al. (1984) and Anovitz and Essene (1987).

Application of the two-carbonate thermometer to metamorphic rocks is complicated by retrograde resetting. Magnesian calcite may exsolve dolomite which must be reintegrated in microprobe analyses. Occasionally, the original high Mg-content of calcite is obliterated through diffusion, yielding temperatures, e.g. of 300–400°C for high-grade marbles (e.g. Essene 1983). Therefore, this thermometer is more useful in low-grade orogenic metamorphic rocks and in contact metamorphic rocks where cooling rates are high.

Ferry (2001) demonstrated that a high Mg-content of calcite can be preserved by calcite inclusions in forsterite of high-grade marble. Small calcite crystals were trapped by growing forsterite in dolomite marble and did not exsolve Dol or loose Mg during cooling. Computed Cal–Dol solvus temperatures (600–700°C) are high and evidently reflect the temperature at the time of forsterite growth.

#### 4.7.5.4 Muscovite–Paragonite

The binary solvus between coexisting muscovite and paragonite has been repeatedly investigated experimentally (see Essene 1989, p. 8, for references), a detailed study being that of Flux and Chatterjee (1986). However, the solvus is not well

constrained because it is only bracketed by three experimental runs, of which one bracket was determined using 1 M mica run products instead of the stable 2M<sub>1</sub> mica polytype. The solvus calculated by Chatterjee and Flux (1986) shows a considerable pressure-dependence.

Application of the muscovite-paragonite solvus geothermometer has not been successful in the past (see, e.g. Guidotti 1984, p. 409). Nevertheless, the muscovite limb of the solvus determined by Chatterjee and Flux (1986, Fig. 6) may be provisionally used to obtain geothermometric data for coexisting muscovite-paragonite pairs, provided (1) the equilibrium pressure is independently known and (2) the chemical composition of the micas is close to the ideal muscovite-paragonite join. This last requirement is, however, rarely the case for phengitic muscovites formed at high pressures and/or low temperatures, and use of the solvus should be restricted to muscovite with Si < 3.05 atoms per formula unit.

#### 4.7.6 *Uncertainties in Thermobarometry*

The development of geothermobarometry has been one of the most exciting advances in metamorphic petrology because it allowed petrologists to quantify pressure and temperature conditions of metamorphism. But how accurate are such data? Ideally, application of geothermobarometry should be accompanied by a statement regarding the uncertainties of T and P. In practice, however, uncertainties are rarely reported because it is difficult to quantify several sources of error.

Kohn and Spear (1991) performed an evaluation of pressure uncertainty when a barometer is applied to a mineral assemblage in a rock. Four barometers were considered, including GASP and GRAIL discussed above. Sources of error considered included (with estimated 1 $\sigma$  uncertainties in P given in brackets); accuracy of the experimentally determined, barometric end-member reaction ( $\pm 30$  to  $\pm 40$  MPa); volume measurement errors ( $\pm 0.25$  to  $\pm 1$  Mpa); analytical imprecision of mineral analyses using an electron microprobe ( $\pm 0.5$  to  $\pm 1.8$  MPa); thermometer calibration errors ( $\pm 25$  to  $\pm 100$  MPa); variation in garnet and plagioclase activity models ( $\pm 0.6$  to  $\pm 150$  MPa); and compositional heterogeneity of natural minerals ( $\pm 1.5$  to  $\pm 5$  MPa). Collectively, the accuracy of a barometer may typically range from  $\pm 6$  to  $\pm 325$  MPa (1 $\sigma$ ), with the most significant sources of error being uncertainty in thermometer calibration and poorly constrained activity models. However, continued experimental and empirical work should substantially reduce these uncertainties.

The situation is much better, however, if we are interested in comparative thermobarometry, which involves applying a single pair of thermobarometers to different samples in order to calculate differences in *P-T* conditions. In this case, the systematic errors associated with experimental calibrations and solution modeling are eliminated, leaving only the effects of analytical uncertainties. It is then possible to confidently resolve *P-T* differences of as little as a few MPa's and a few tens of degrees.

### 4.7.7 Thermobarometry Using Multi-equilibrium Calculations (MET)

Above, we used two intersecting equilibria to determine possible  $P$ – $T$  conditions of rock formation (the  $P$ – $T$  conditions of the least hydrated state). Many rocks, however, contain mineral assemblages that allow for the formulation of more than two reactions among phase components of the assemblage. Often a large number of reactions can be written for the assemblage of a metamorphic rock. If the rock achieved a state of equilibrium at one point in  $P$ – $T$  space all reactions must be simultaneously in equilibrium at this point. A set of equations, one for each reaction, can be solved for these conditions using (1) a consistent set of thermodynamic data for all phase components involved in the reactions, (2) appropriate equations of state to describe thermodynamic properties of all phase components at  $P$  and  $T$ , (3) appropriate solution models to describe the thermodynamics of solid and fluid solutions for all minerals and fluids involved, and (4) an efficient computer code that performs the desired computation of the equilibrium conditions. The equilibrium conditions of all reactions will appear as lines on a  $P$ – $T$  diagram that intersect at one point, the “frozen-in” equilibrium conditions of  $P$  and  $T$  for that metamorphic rock (Fig. 4.16).

All four prerequisites for successful MET applications are available today and the appropriate tools can be downloaded from web sites. The technique is widely used, albeit sometimes a little carelessly. Thermodynamic data sets particularly useful for metamorphic rocks have been published by Berman (1988) and Holland and Powell (1990). The data bases are regularly maintained and expanded as new experimental

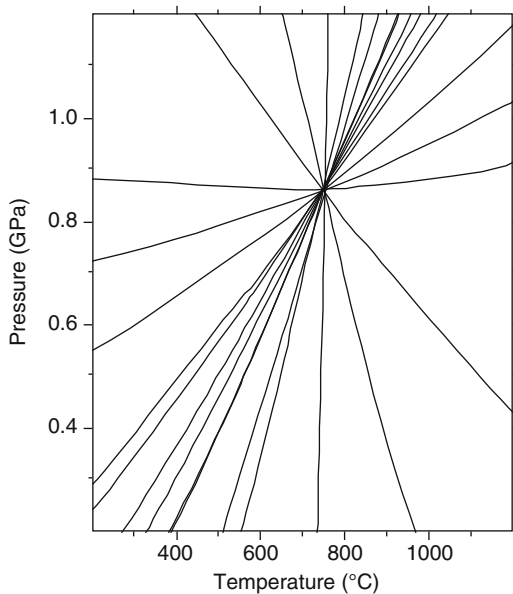


**Fig. 4.16**  $P$ – $T$  diagram showing the results of a TWEEQU calculation for an amphibolite with the mineral assemblage Grt–Cpx–Hbl–Pl–Qtz–Ilm–Rt. Fourteen equilibria among (Grs–Alm–Prp)–(Di–Hd)–An–Qtz–Ilm–Rt, excluding hornblende, were considered. Note that only 3 of the 14 equilibria are linearly independent (From Lieberman and Petrakakis 1991, Fig. 8b)

data become available or the science makes progress in some other way. The latest version is HP98 (Holland and Powell 1998) and this is currently the most widely used geologic data set.

The computer program of choice for MET calculations is TWQ or TWEEQU (Thermobarometry With Estimation of Equilibration State). It is an interactive program for calculation of mineral–fluid equilibria. It has been developed and maintained by Rob Berman of the Geological Survey of Canada (Berman 1991). Although it can calculate many types of phase diagrams, its primary application is geothermobarometry using internally consistent thermodynamic data for endmembers and solid solutions that have been derived simultaneously from relevant experimental constraints. The program can be downloaded from the site (last update in 2008): [http://gsc.nrcan.gc.ca/sw/twq\\_e.php](http://gsc.nrcan.gc.ca/sw/twq_e.php).

Other, highly recommended programs that can also be used for MET-type calculations are DOMINO/THERIAK (De Capitani and Petrakakis 2010), PERPLEX (Connolly and Kerrick 1987; Connolly 1990) and THERMOCALC (Powell and Holland 1988; Powell et al. 1998). All three program packages are regularly maintained and updated and can be downloaded from the authors web sites free of charge (the authors of this book would like to express our sincere thanks to the authors of these outstanding and powerful software packages that revolutionized metamorphic petrology research. The generous position of the authors of metamorphic petrology software is by no means obvious as the software used in the geochemistry community shows). We recommend viewing the web to find the many sites that provide and maintain geologic software links. A good start is the Software List provided by the Department of Geosciences, North Dakota State University, where you will find links to the web addresses of a large variety of geologic and petrologic software.

If you process rocks through the computer mill, please don't stop thinking, be judicious and observant. The perfectly well-behaved sample does not exist in practice. Multi-equilibria rarely intersect in one  $P$ – $T$  point (except for linear dependent equilibria that always intersect at one point and are therefore no proof of MET success). Significant deviations from this ideal single point case often occur. When results for several rocks are compared to each other and with petrographic observations, it may be possible to conclude whether inaccurate thermodynamic data, compositional data, or disequilibrium may be the cause of discrepant results. In some samples subsets of the assemblage may intersect at one  $P$ – $T$  point and another subset may define a second intersection. Some examples of MET calculations can be found in Vidal et al. (2001) and an example using granulite facies metapelitic rocks from the Thor Range, Antarctica, are shown in Fig. 4.17.

## 4.8 Gibbs Method

In a classic benchmark paper, Spear et al. (1982) introduced “the Gibbs method” to applications in petrology. The method is based on differential thermodynamics and permits the computation of successive pressure–temperature differences ( $P$ – $T$

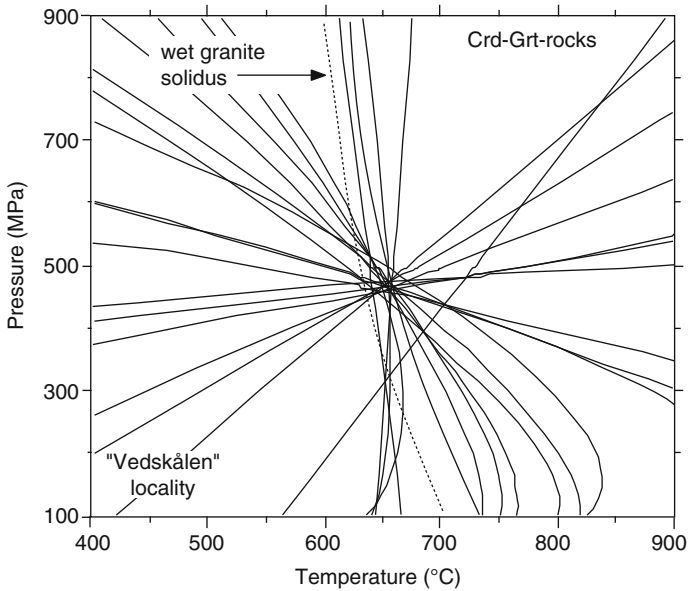


**Fig. 4.17** MET solution for a cordierite gneiss from the Thor Range, Antarctica (mineral data from Bucher and Otha 1993). Assemblage: Qtz + Pl + Grt + Crd + Sil + Bt + Kfs. Software: PTAX now TWQ (Berman et al. 1987)

paths) recorded by chemically zoned minerals in rocks. The method essentially solves a set of partial differential equations that express the thermodynamic consequences of chemically zoned minerals. It has been mostly used to model  $P$ - $T$  paths from compositional zoning of pelitic garnets. It has been very successful in resolving remarkably detailed paths taken by garnet-bearing metapelitic schists in  $P$ - $T$  space. The differential calculations are tied to a starting point in  $P$ - $T$  space where an assemblage and the associated mineral compositions are well known. From there the movements of the garnet-bearing sample can be reconstructed with high resolution of a few  $^{\circ}\text{C}$  and MPa's (e.g. Selverstone et al. 1984).

The software for GIBBS method calculations can be downloaded from the web site of the metamorphic petrology group at Rensselaer Polytechnic Institute. The entire package includes the programs, GIBBS, GTB, plus tutorial notes (pdf format) for running the software. The texts were originally prepared for a Short Course given at the Northeast Section Meeting of the Geological Society of America at the University of Vermont, Burlington, Vermont, in 2001. An excellent account of differential thermobarometry using zoned minerals can be found in Spear (1993); Chap. 17: "The origin and interpretation of zoned metamorphic minerals".

## 4.9 Assemblage Stability Diagrams

Assemblage stability diagrams, or *pseudosections*, are diagrams that display the stable mineral assemblages for a specific bulk rock composition over a range of  $P$ - $T$  conditions. Pseudosections are relatives of the petrogenetic grid. The great advantage of pseudosections is that they predict the stable mineral assemblage and the composition of minerals at  $P$ - $T$ - $X$  conditions for the specific rock of interest.

Pseudosections can be computed by very different techniques and, consequently, different computer programs. One popular method of computation is utilized by the code THERMOCALC. It employs the methods of integrated thermodynamics in the same way as the construction of  $P$ - $T$  curves, grids and contour diagrams. Using divariant contour routines (PERPLEX also provides this option), one can draw 0.0 mol. contours for a phase. The contours must be truncated at the absolute stability limit of the assemblage defined by univariant reactions. THERMOCALC and tutorials can be downloaded from Roger Powell's web site: <http://www.earthsci.unimelb.edu.au/tpg/thermocalc/>.

THERMOCALC is a very versatile program that can be used for conventional phase diagram calculations, creation of petrogenetic grids and, as mentioned, for the construction of pseudosections. The program is a highly sophisticated problem solver in metamorphic petrology and its versatility and complexity necessarily takes an advanced level of understanding to be able to use so that the code is well suited for petrologists with a higher skill level than imparted by reading this book.

Finally, the most elegant and mature concept in the field of assemblage stability diagram computation is perhaps the program package THERIAK/DOMINO by Prof. de Capitani, at the University of Basel, that is extensively used in Part II of this book. It is based on a Gibbs free energy minimization algorithm and solves directly for the assemblage with the lowest Gibbs free energy at a specified  $P$ - $T$  for a given bulk rock composition in the multi-dimensional composition space and utilizing a general thermodynamic description of multi-component solid-solutions (de Capitani and Brown 1987; de Capitani and Petrakakis 2010). The general and unique approach is an offspring of an ingenious early program EQUILAS by Brown and Skinner (1974). An example of a modified EQUILAS computation is shown on Fig. 3.27b. The DOMINO part of the software package calculates and draws  $x$ - $y$  equilibrium phase diagrams ( $x, y = P, T, a_i, \ln a_i, \log a_i$  or a pseudo-binary or -ternary system). The diagram shows either areas of equal assemblages, isopleths or the amount of a phase (or many other user selectable variables). All assemblage stability diagrams shown in the second part of this book have been computed with the THERIAK/DOMINO software and using updated data collections based on the original Berman (1988) data set. The chosen bulk composition for the diagram is given on the diagram in atoms of the variable system components. Components of excess phases need to be added to the indicated composition as well as the appropriate amount of oxygen atoms. The software package can be downloaded together with examples and a tutorial from: <http://titan.minpet.unibas.ch/minpet/theriak/theruser.html>.

An alternative program package based on Gibbs free energy minimization is PERPLEX written and maintained by Prof. J. Connolly from ETH Zurich (Connolly and Kerrick 1987; Connolly 1990, 2005, 2009; Connolly and Petrini 2002). The following site provides program, documentation and tutorial downloads: <http://www.perplex.ethz.ch/>.

THERIAK/DOMINO, THERMOCALC and PERPLEX packages are ideal for the experienced specialist with a sound knowledge of thermodynamics, particularly thermodynamics of solid solutions. The user must be able to critically evaluate the thermodynamic data and the solution models used in the calculations. If necessary these data and models must be modified or adjusted for obtaining meaningful results. Many of the comments made in Sect. 4.7.2 also apply to the computation of assemblage stability diagrams. Nevertheless, we encourage the not-so-specialised reader to update themselves with the most recent advances of our science.

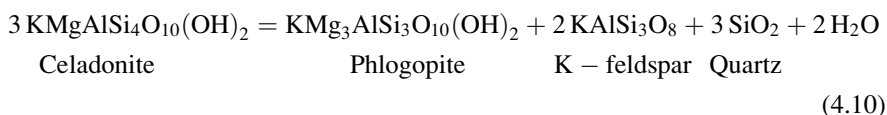
## 4.10 More $P$ - $T$ Tools

### 4.10.1 Reactions Involving Fluid Species

Univariant equilibria involving volatile components cannot be directly applied to thermobarometry because their position in  $P$ - $T$  space depends on properties of a now vanished fluid phase (Chap. 3). Dehydration reactions are often used in constructing petrogenetic grids assuming  $P_{\text{H}_2\text{O}} = P_{\text{S}}$  or  $a_{\text{H}_2\text{O}} = 1$ , but it is now well known that  $\text{CH}_4$  is a significant fluid species in many low- $T$  rocks whilst  $\text{CO}_2$  is abundant in many high- $T$  rocks. For this reason  $P$ - $T$  estimates based on dehydration reactions are, with one exception, not considered further.

#### 4.10.1.1 Phengite-Biotite-K-Feldspar-Quartz

The white mica phengite is an intermediate member of the muscovite-celadonite solid-solution series. The two end-members are related by the exchange of Tschermak component,  $[(\text{Mg}, \text{Fe}^{2+})\text{Si}(\text{AlAl})_{-1}]$  and the silica content of phengite is the preferred measure of this substitution. Field observations and data have shown that the Si-content of phengitic mica increases from nearly 3.0 per formula unit to almost 4.0 with increasing pressure. In the KMASH assemblage phengite + biotite + K-feldspar + quartz, the composition of phengite is invariant at fixed  $P$ ,  $T$  and  $a_{\text{H}_2\text{O}}$ . The reaction:



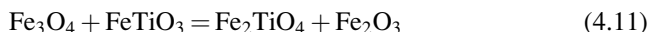


has been investigated experimentally by Massonne and Schreyer (1987) for varying Si content in phengite. Si-isopleths have a small positive  $P$ - $T$  slope and the Si-content of phengite increases strongly and linearly with pressure. In practice, in rocks with the assemblage Phe–Bt–Kfs–Qtz, only phengite is chemically analyzed and its Si-content used for a pressure estimate.

This is a powerful geobarometer, especially in low to medium grade rocks, where calibrated barometers are scarce. However, there are several drawbacks: (1) The isopleths determined by Massonne and Schreyer (1987) are based on synthesis experiments that produced mainly 1 M and Md K-white mica polytypes; (2) Since the above reaction involves dehydration, estimates of  $a_{\text{H}_2\text{O}}$  are crucial for correct application; water activities below unity shift the Si-isopleths of phengite towards higher pressure; (3) Experiments were conducted in an iron-free system whilst natural micas may contain considerable amounts of  $\text{Fe}^{2+}$  and  $\text{Fe}^{3+}$ . Since the ratio  $\text{Fe}^{2+}/\text{Mg}$  is generally higher in biotite than coexisting muscovite, the introduction of Fe will stabilize biotite + K-feldspar and thus reduce the celadonite content of the K-white mica, displacing the Si-isopleths to higher pressure (Evans and Patrick 1987). Application of the Massonne and Schreyer phengite geobarometer yielded reasonable results for eclogite facies metagranites (Massonne and Chopin 1989), but gave pressures up to 400 MPa too high for greenschist and amphibolite facies metamorphic rocks (Patrick and Ghent 1988). The phengite geobarometer may be most useful for obtaining relative pressure estimates across a metamorphic terrane.

#### 4.10.1.2 Magnetite–Ilmenite Equilibria and the “QUILF” System

Two Fe–Ti oxides, magnetite and ilmenite, coexist in some metamorphic rocks. Magnetite shows solid-solution with ulvöspinel ( $\text{Fe}_2\text{TiO}_4$ ) whilst ilmenite shows solid-solution with hematite. Chemical equilibrium between titanian magnetite and ferrian ilmenite can be described by a temperature-dependent Fe–Ti exchange reaction:



and a redox reaction:



Buddington and Lindsley (1964) present a graphical form of this thermometer and oxybarometer. They contoured isopleths of ilmenite ( $X_{\text{FeTiO}_3}$ ) and ulvöspinel ( $X_{\text{Fe}_2\text{TiO}_4}$ ) on a  $\log f_{\text{O}_2}$  –  $T$  diagram and showed that intersection of these isopleths yields  $f_{\text{O}_2}$  (equals  $a_{\text{O}_2}$  using an appropriate standard state) and  $T$ . Since Buddington and Lindsley’s work, there have been a number of other thermodynamic treatments.

Application of the Mag–Ilm thermometer is limited because these oxides are easily reset during retrogression. Upon cooling, Ti-bearing magnetite will typically be oxidized with the formation of ilmenite lamellae within the magnetite;

conversely,  $\text{Fe}_2\text{O}_3$ -rich ilmenite will be reduced, yielding lamellae of Ti-magnetite within ilmenite. In order to obtain peak metamorphic temperatures, these “exsolution” lamellae must be reintegrated (Bohlen and Essene 1977).

However, spinel-ilmenite equilibria can be combined with equilibria involving silicate minerals in high-grade rocks. In this way, Lindsley and Frost (1992) and Frost and Lindsley (1992) have developed an excellent system of thermobarometers. The system and the code *QUILF* (Andersen et al. 1993) can be used for  $P$ - $T$ - $a_{\text{O}_2}$  estimates among Cpx-Opx-pigeonite-Ol-SiO<sub>2</sub>-Ilm-Spl. The program can be downloaded from the address Prof D. Lindsley’s web site (2010): <http://www.geosciences.stonybrook.edu/people/faculty/lindsley/lindsley.html>.

The program is particularly useful for igneous rocks but can also be applied to granulite facies mafic rocks and felsic rocks such as charnockite and other Opx-bearing meta-granitoids.

## 4.10.2 $P$ - $T$ Tools for Very Low Grade Rocks

None of the many geothermobarometers mentioned above is applicable to sub-blueschist-greenschist facies conditions. Fortunately, a few other methods are available to estimate  $T$ , and sometimes also  $P$ , at very low metamorphic grade.

### 4.10.2.1 Fluid Inclusions

Fluid inclusions in metamorphic rocks generally yield information about their retrograde  $P$ - $T$  path, but at very low metamorphic grade it is possible to obtain thermobarometric data about peak (or near-peak) conditions of metamorphism (e.g. Mullis 1987). This author developed a method to determine approximate  $P$  and  $T$  values of fluid-trapping based on fluid inclusion studies from vein quartz. The micro-thermometric method takes advantage of immiscibility in  $\text{H}_2\text{O}$ - $\text{CH}_4$  fluids. As a result, the homogenization temperature of water-rich inclusions saturated with  $\text{CH}_4$  can be interpreted in terms of temperature of formation. Methane-rich inclusions, on the other hand, allow measurement of the density of  $\text{CH}_4$ . With these data the pressure of inclusion formation can be determined from known experimental  $P$ - $V$ - $T$ - $X$  properties. Application of this method has recorded temperatures of up to 270°C and pressures of up to about 300 MPa.

### 4.10.2.2 Vitrinite Reflectance

Vitrinite is a predominant constituent in many coals and in finely dispersed organic matter in sedimentary rocks. As organic material is converted from complex hydrocarbons to graphite, the optical reflectance of vitrinite increases and indicates the degree of transformation. There are various models relating vitrinite reflectance

and physical variables. While temperature is regarded uniformly as the main controlling variable, the role played by the time factor is controversial and ranges from “important” to “negligible”. Possibly the best model available is that of Sweeney and Burnham (1990), called EASY%R<sub>0</sub>, based on a chemical kinetic model of vitrinite maturation proposed by Burnham and Sweeney (1989). In this Arrhenius reaction model, equations were integrated over temperature and time to account for the elimination of water, carbon dioxide, methane, and higher hydrocarbons from vitrinite. The model can be implemented on a spreadsheet or in a small computer program on a PC, but the results are also shown graphically in nomograms of vitrinite reflectance versus exposure time and maximum temperature (Fig. 5 of Sweeney and Burnham 1990). EASY%R<sub>0</sub> can be used for vitrinite reflectance values of 0.3–4.5%, and for heating rates ranging from those related to igneous intrusions (1°C/day), and geothermal systems (10°C/100 year) to burial diagenesis (1°C/10 Ma) (see also Carr 1999; Wangen et al. 2007).

#### 4.10.2.3 Conodont Color Alteration Index (CAI)

Conodonts are apatitic marine microfossils that contain trace amounts of organic material that colors them. They range in age from Cambrian to the Triassic and are mainly found in carbonate rocks. In the temperature range of diagenesis and incipient metamorphism, five stages of CAI are distinguished according to changes in color from pale yellow to brown to black (Voldman et al. 2010). Epstein et al. (1977) and Rejebian et al. (1987) reproduced these color changes by heating in the laboratory and found a time and temperature dependence. Experimental data obtained between 300°C and 950°C and time up to 10<sup>3</sup> h that was extrapolated to geologic time. A graph of reciprocal absolute temperature versus a logarithmic time scale forms then the basis of this geothermometer, which has a resolution of ca. 50°C. An advantage of the conodont method is that it can be used in carbonate rocks in which vitrinite is rarely present.

## References and Further Reading

### *Cited References*

- Andersen DJ, Lindsley DH, Davidson PM (1993) QUILF: A PASCAL program to assess equilibria among Fe-Mg-Mn-Ti oxides, pyroxenes, olivine, and quartz. *Comput Geosci* 19:1333–1350
- Anovitz IM, Essene EJ (1987) Phase equilibria in the system CaCO<sub>3</sub>-MgCO<sub>3</sub>-FeCO<sub>3</sub>. *J Petrol* 28:389–414
- Archibald DA, Krogh TE, Armstrong RL, Farrar E (1984) Geochronology and tectonic implications of magmatism and metamorphism, southern Kootenay Arc and neighbouring regions, southeastern British Columbia. Part II: Mid-Cretaceous to Eocene. *Can J Earth Sci* 21:567–583

- Banno S, Sakai C (1989) Geology and metamorphic evolution of the Sanbagawa metamorphic belt, Japan. In: Daly JS, Cliff RA, Yardley BWS (eds) Evolution of metamorphic belts. Geological Society Special Publication 43 (Blackwell), Oxford, pp 519–532
- Banno S, Shibakusa H, Enami M, Wang C-L, Ernst WG (2000) Chemical fine structure of Franciscan jadeitic pyroxene from Ward Creek, Cazadero area, California. *Am Mineralog* 85:1795–1798
- Barrow G (1893) On an intrusion of muscovite biotite gneiss in the S.E. Highlands of Scotland and its accompanying metamorphism. *Q J Geol Soc London* 49:330–358
- Barrow G (1912) On the geology of lower Deeside and the southern Highland border. *Proc Geol Assoc* 23:268–284
- Bearth P (1958) Ueber einen Wechsel der Mineralfazies in der Wurzelzone des Penninikums. *Schweiz Mineralog Petrogr Mitt* 38:363–373
- Benciolini L, Lombardo B, Martin S (1988) Mineral chemistry and Fe/Mg exchange geothermometry of ferrogabbro-derived eclogites from the Northwestern Alps. *N Jahrb Mineral Abh* 159: 199–222
- Berman RG (1988) Internally-consistent thermodynamic data for minerals in the system  $K_2O$ - $Na_2O$ - $CaO$ - $MgO$ - $FeO$ - $Fe_2O_3$ - $Al_2O_3$ - $SiO_2$ - $TiO_2$ - $H_2O$ - $CO_2$ . *J Petrol* 29:445–522
- Berman RG (1991) Thermobarometry using multi-equilibrium calculations: a new technique, with petrological applications. *Can Mineralog* 29:833–856
- Berman RG, Brown TH, Perkins EH (1987) GEØ-CALC: software for calculation and display of P-T-X phase diagrams. *Am Mineralog* 72:861–862
- Bhattacharya A, Mohanty L, Maji A, Sen SK, Raith M (1992) Non-ideal mixing in the phlogopite-annite binary: constraints from experimental data on Mg-Fe partitioning and a reformulation of the biotite-garnet geothermometer. *Contrib Mineralog Petrol* 111:87–93
- Bhattacharyya DS (1981) Geometry of isograds in metamorphic terrains. *Tectonophys* 73: 385–395
- Bohlen SR, Essene EJ (1977) Feldspar and oxide thermometry of granulites in the Adirondack Highlands. *Contrib Mineralog Petrol* 62:153–169
- Bohlen SR, Lindsley DH (1987) Thermometry and barometry of igneous and metamorphic rocks. *Ann Rev Earth Planet Sci* 15:397–420
- Bohlen SR, Montana A, Kerrick DM (1991) Precise determinations of the equilibria kyanite = sillimanite and kyanite = andalusite and a revised triple point for  $Al_2SiO_5$  polymorphs. *Am Mineralog* 76:677–680
- Bohlen SR, Valley JW, Essene EJ (1985) Metamorphism in the Adirondacks. 1. Pressure and temperature. *J Petrol* 26:971–992
- Bohlen SR, Wall VJ, Boettcher AL (1983a) Experimental investigation and application of garnet granulite equilibria. *Contrib Mineralog Petrol* 83:52–61
- Bohlen SR, Wall VJ, Boettcher AL (1983b) Experimental investigations and geologic applications of equilibria in the system  $FeO$ - $TiO_2$ - $Al_2O_3$ - $SiO_2$ - $H_2O$ . *Am Mineralog* 68:1049–1058
- Brothers RN, Grapes RH (1989) Clastic lawsonite, glaucophane, and jadeitic pyroxene in Franciscan metagreywackes from the Diablo Range, California. *Geol Soc Am Bull* 101:24–26
- Brown TH, Skinner BJ (1974) Theoretical prediction of equilibrium phase assemblages in multicomponent systems. *Am J Sci* 274:961–986
- Bryndzia LT, Scott SD, Spry PG (1988) Sphalerite and hexagonal pyrrhotite geobarometer: experimental calibration and application to the metamorphosed sulfide ores of Broken Hill, Australia. *Econ Geol* 83:1193–1204
- Bryndzia LT, Scott SD, Spry PG (1990) Sphalerite and hexagonal pyrrhotite geobarometer: correction in calibration and application. *Econ Geol* 85:408–411
- Bucher K, Fazio Y, de Capitani C, Grapes R (2005) Blueschists, eclogites, and decompression assemblages of the Zermatt-Saas ophiolite: high-pressure metamorphism of subducted Tethys lithosphere. *Am Mineralog* 90:821–835
- Buddington AF, Lindsley DH (1964) Iron-titanium oxide minerals and their synthetic equivalents. *J Petrol* 5:310–357

- Burnham AK, Sweeney JJ (1989) A chemical kinetic model of vitrinite reflectance maturation. *Geochim Cosmochim Acta* 53:2649–2657
- Burton KW, Boyle AP, Kirk WL, Mason R (1989) Pressure, temperature and structural evolution of the Sulitjelma fold-nappe, central Scandanavian Caledonides. In: Daly JS, Cliff RA, Yardley BWS (eds) *Evolution of metamorphic belts*. Geological Society Special Publication 43: Blackwell, Oxford, pp 392–411
- Carlson WD (1983) The polymorphs of  $\text{CaCO}_3$  and the aragonite-calcite transformation. In: Reeder RJ (ed) *Carbonates: mineralogy and chemistry*. Reviews in mineralogy, vol 11. Mineralogical Society of America, Washington, DC, pp 191–225
- Carlson WD, Rosenfeld JL (1981) Optical determination of topotactic aragonite-calcite growth kinetics: metamorphic implications. *J Geol* 89:615–638
- Carmichael DM (1970) Intersecting isograds in the Whetstone Lake area, Ontario. *J Petrol* 11: 147–181
- Carmichael DM (1978) Metamorphic bathozones and bathograds: a measure of the depth of post-metamorphic uplift and erosion on the regional scale. *Am J Sci* 278:769–797
- Carr AD (1999) A vitrinite reflectance kinetic model incorporating overpressure retardation. *Mar Petrol Geol* 16:355–377
- Carson CJ, Powell R (1997) Garnet-orthopyroxene geothermometry and geobarometry; error propagation and equilibration effects. *J Metamorph Geol* 15:679–686
- Carswell DA, Gibb FGF (1987) Evaluation of mineral thermometers and barometers applicable to garnet lherzolite assemblages. *Contrib Mineralog Petrol* 95:499–511
- Carswell DA, Harley SL (1989) Mineral barometry and thermometry. In: Carswell DA (ed) *Eclogites and related rocks*. Blackie, Glasgow, pp 83–110
- Cartwright I, Barnicoat AC (1989) Evolution of the Scourian complex. In: Daly JS, Cliff RA, Yardley BWS (eds) *Evolution of metamorphic belts*. Geological Society Special Publication 43: Blackwell, Oxford, pp 297–301
- Chatterjee ND, Flux S (1986) Thermodynamic mixing properties of muscovite-paragonite crystal-line solutions at high temperatures and pressures, and their geological applications. *J Petrol* 27: 677–693
- Chinner GA (1966) The distribution of pressure and temperature during Dalradian metamorphism. *Q J Geol Soc Lond* 122:159–186
- Chipera SJ, Perkins D (1988) Evaluation of biotite-garnet geothermometers: application to the English River subprovince, Ontario. *Contrib Mineralog Petrol* 98:40–48
- Compagnoni R, Rolfo F (2003) UHPM units in the Western Alps. In: Carswell DA, Compagnoni R (eds) *High pressure metamorphism*, European Mineralogical Union notes in mineralogy, vol 5. Eötvös University Press, Budapest, pp 13–49
- Connolly JAD (1990) Multivariable phase-diagrams – an algorithm based on generalized thermodynamics. *Am J Sci* 290:666–718
- Connolly JAD (2005) Computation of phase equilibria by linear programming: a tool for geodynamic modeling and its application to subduction zone decarbonation. *Earth Planet Sci Lett* 236:524–541
- Connolly JAD (2009) The geodynamic equation of state: what and how. *Geochem Geophys Geosyst* 10:Q10014 DOI:[10.1029/2009GC002540](https://doi.org/10.1029/2009GC002540)
- Connolly JAD, Kerrick DM (1987) An algorithm and computer program for calculating computer phase diagrams. *Calphad* 11:1–55
- Connolly JAD, Petrini K (2002) An automated strategy for calculation of phase diagram sections and retrieval of rock properties as a function of physical conditions. *J Metamorph Petrol* 20: 697–708
- Coombs DS, Ellis AJ, Fyfe WS, Taylor AM (1959) The zeolite facies, with comments on the interpretation of hydrothermal syntheses. *Geochim Cosmochim Acta* 17:53–107
- Cooper AF (1972) Progressive metamorphism of metabasic rocks from the Haast schist group of Southern New Zealand. *J Petrol* 13:457–492

- Crawford MJ (1966) Composition of plagioclase and associated minerals in some schists from Vermont, USA, and South Westland, New Zealand, with inferences about peristerite solvus. *Contrib Mineralog Petrol* 13:269–294
- de Capitani C, Brown TH (1987) The computation of chemical equilibrium in complex systems containing non-ideal solutions. *Geochim Cosmochim Acta* 51:2639–2652
- de Capitani C, Petrakakis K (2010) The computation of equilibrium assemblage diagrams with Theriak/Domino software. *Am Mineralog* 95:1006–1016
- Droop GTR (1987) A general equation for estimating  $\text{Fe}^{3+}$  concentrations in ferromagnesian silicates and oxides from microprobe analyses, using stoichiometric criteria. *Mineralog Mag* 51:431–435
- Edwards RL, Essene EJ (1988) Pressure, temperature and C-O-H fluid fugacities across the amphibolite-granulite facies transition, NW Adirondack Mtns., NY. *J Petrol* 29:39–72
- Eggler DH, Lorand JP (1993) Mantle sulfide geobarometry. *Geochim Cosmochim Acta* 57: 2213–2222
- Elkins LT, Grove TL (1990) Ternary feldspar experiments and thermodynamic models. *Am Mineralog* 75:544–559
- Ellis DJ, Green DH (1979) An experimental study of the effect of Ca upon garnet-clinopyroxene Fe-Mg exchange equilibria. *Contrib Mineralog Petrol* 7:13–22
- Enami M (1981) On sodic plagioclase in some rocks of the Sanbagawa Metamorphic Belt in the Bessi district, Shikoku, Japan. *Proc Jpn Acad* 57:188–193
- Engi M, Todd CS, Schmatz DR (1995) Tertiary metamorphic conditions in the eastern Lepontine Alps. *Schweiz Mineralog Petrogr Mitt* 75:347–369
- Epstein AG, Epstein JB, Harris LD (1977) Conodont color alteration – an index to organic metamorphism. *US Geol Surv Prof Pap* 955:1–27
- Eskola P (1915) On the relations between the chemical and mineralogical composition in the metamorphic rocks of the Orijarvi region. *Bull Comm Geol Fin* 44:109–143
- Essene EJ (1982) Geologic thermometry and barometry. In: Ferry JM (ed) *Characterization of metamorphism through mineral equilibria, reviews in mineralogy, vol 10*. Mineralogical Society of America, Washington, DC, pp 153–205
- Essene EJ (1983) Solid solutions and solvi among metamorphic carbonates with applications to geologic thermometry. In: Reeder RJ (ed) *Carbonates: mineralogy and chemistry, reviews in mineralogy, vol 11*. Mineralogical Society of America, Washington, DC, pp 77–96
- Essene EJ (1989) The current status of thermobarometry in metamorphic rocks. In: Daly JS, Cliff RA, Yardley BWD (eds) *Evolution of metamorphic belts*. Geological Society Special Publication, Blackwell, Oxford, pp 1–44
- Evans BW, Patrick BE (1987) Phengite-3 T in high-pressure metamorphosed granitic orthogneisses, Seward Peninsula, Alaska. *Can Mineralog* 25:141–158
- Faulhaber S, Raith M (1991) Geothermometry and geobarometry of high-grade rocks: a case study on garnet-pyroxene granulites in southern Sri Lanka. *Mineralogical Magazine*, 55:33–56
- Ferry JM (1980) A comparative study of geothermometers and geobarometers in pelitic schists from southern-central Maine. *Am Mineralog* 65:720–732
- Ferry JM (2001) Calcite inclusions in forsterite. *Am Mineralog* 86:773–779
- Ferry JM, Spear FS (1978) Experimental calibration of the partitioning of Fe and Mg between biotite and garnet. *Contrib Mineralog Petrol* 66:113–117
- Flux S, Chatterjee ND (1986) Experimental reversal of the Na-K exchange reaction between muscovite-paragonite crystalline solutions and a 2 molal aqueous (Na, K)Cl fluid. *J Petrol* 27:665–676
- Fox JS (1975) Three-dimensional isograds from the Lukmanier Pass, Switzerland, and their tectonic significance. *Geol Mag* 112:547–564
- Frey M (1987) The reaction-isograd kaolinite + quartz = pyrophyllite +  $\text{H}_2\text{O}$ , Helvetic Alps, Switzerland. *Schweiz Mineralog Petrogr Mitt* 67:1–11
- Frey M, Wieland B (1975) Chloritoid in autochthon-parautochthonen Sedimenten des Aarmassivs. *Schweiz Mineralog Petrogr Mitt* 55:407–418
- Frost BR, Lindsley DH (1992) Equilibria among Fe-Ti oxides, pyroxenes, olivine, and quartz: Part II. Application. *Am Mineralog* 77:1004–1020

- Fuhrman ML, Lindsley DH (1988) Ternary feldspar modeling and thermometry. *Am Mineralog* 73:201–215
- Gasparik T (1984) Experimental study of subsolidus phase relations and mixing properties of pyroxene in the system CaO-Al<sub>2</sub>O<sub>3</sub>-SiO<sub>2</sub>. *Geochimica Cosmochimica Acta*, 48:2537–2546
- Gessmann CK, Spiering B, Raith M (1997) Experimental study of the Fe-Mg exchange between garnet and biotite: constrains on the mixing behaviour and analysis of the cation exchange mechanisms. *Am Mineralog* 82:1225–1240
- Giletti BJ (1986) Diffusion effects on oxygen isotope temperatures of slowly cooled igneous and metamorphic rocks. *Earth Planet Sci Lett* 77:218–228
- Gillen C (1982) *Metamorphic geology*. George Allen and Urwin, London
- Grambling JA, Williams ML (1985) The effects of Fe<sup>3+</sup> and Mn<sup>3+</sup> on aluminum silicate phase relations in north-central New Mexico, U.S.A. *J Petrol* 26:324–354
- Grapes RH, Otsuki M (1983) Pserisite compositions in quartzofeldspathic schists, Franz Josef-Fox Glacier area, New Zealand. *J Metamorph Geol* 1:47–62
- Grapes RH, Watanabe T (1992) Metamorphism and uplift of the Alpine Schist in the Franz Josef-Fox Glacier area of the Southern Alps, New Zealand. *J Metamorph Geol* 10:171–180
- Guidotti CV (1984) Micas in metamorphic rocks. In: Bailey SW (ed) *Micas, reviews in mineralogy*, vol 13. Mineralogical Society of America, Washington, DC, pp 357–467
- Haselton HT, Hovis GL, Hemingway BS, Robie RA (1983) Calorimetric investigation of the excess entropy of mixing in analbite-sanidine solid solutions: lack of evidence for Na, K short range order and implications for two-feldspar thermometry. *Am Mineralog* 68:398–413
- Heinrich CA (1986) Eclogite facies regional metamorphism of hydrous mafic rocks in the Central Alpine Adula Nappe. *J Petrol* 27:123–154
- Hodges KV, McKenna LW (1987) Realistic propagation of uncertainties in geologic thermobarometry. *Am Mineralog* 72:671–680
- Hoefs J (1987) *Stable isotope geochemistry*, 3rd edn. Springer, Berlin, Heidelberg, New York, 241 pp
- Holdaway MJ (1971) Stability of andalusite and the aluminum silicate phase diagram. *Am J Sci* 271:97–131
- Holdaway MJ (2001) Recalibration of the GASP geobarometer in light of recent garnet and plagioclase activity models and versions of the garnet-biotite geothermometer. *Am Mineralog* 86:1117–1129
- Holdaway MJ, Dutrow BL, Hinton RW (1988) Devonian and Carboniferous metamorphism in west-central Maine: the muscovite-almandine geobarometer and the staurolite problem revisited. *Am Mineralog* 73:20–47
- Holdaway MJ, Mukhopadhyay B, Dyar MD, Guidotti CV, Dutrow BL (1997) Garnet-biotite geothermometry revised; new Margules parameters and a natural specimen data set from Maine. *Am Mineralog* 82:582–595
- Holland TJB (1980) The reaction albite = jadeite + quartz determined experimentally in the range 600–1200°C. *Am Mineralog* 65:129–134
- Holland TJB, Powell R (1990) An enlarged and updated internally consistent thermodynamic dataset with uncertainties and correlations: the system K<sub>2</sub>O-Na<sub>2</sub>O-CaO-MgO-MnO-FeO-Fe<sub>2</sub>O<sub>3</sub>-Al<sub>2</sub>O<sub>3</sub>-TiO<sub>2</sub>-SiO<sub>2</sub>-C-H<sub>2</sub>-O<sub>2</sub>. *J Metamorph Geol* 8:89–124
- Holland TJB, Powell R (1998) An internally-consistent thermodynamic dataset for phases of petrological interest. *J Metamorph Geol* 16:309–343
- Hudson NFC (1980) Regional metamorphism of some Dalradian pelites in the Buchan area, N.E. Scotland. *Contrib Mineralog Petrol* 73:39–51
- Hutchison MN, Scott SD (1980) Sphalerite geobarometry applied to metamorphosed sulfide ores of the Swedish Caledonides and U.S. Appalachians. *Nor Geol Unders* 360:59–71
- Johnson CA, Essene EJ (1982) The formation of garnet in olivine-bearing metagabbros from the Adirondacks. *Contributions Mineralogy Petrology*, 81:240–251
- Kerrick DM (ed) (1990) *The Al<sub>2</sub>SiO<sub>5</sub> polymorphs*. *Reviews in mineralogy*, vol 22. Mineralogical Society of America, Washington DC, p 406

- Kleemann U, Reinhardt J (1994) Garnet-biotite thermometry revisited I effect AlVI Ti biotite. *Eur J Mineralog* 6:925–941
- Kohn MJ, Spear FS (1991) Error propagation for barometers: 2. Application rocks. *Am Mineralog* 76:138–147
- Koons PO (1984) Implications to garnet-clinopyroxene geothermometry of non-ideal solid solution in jadeitic pyroxenes. *Contrib Mineralog Petrol* 88:340–347
- Koziol AM, Newton RC (1988) Redetermination of the garnet breakdown reaction and improvement of the plagioclase-garnet- $Al_2SiO_5$ -quartz geobarometer. *Am Mineralog* 73:216–223
- Krogh EJ (1988) The garnet-clinopyroxene Fe-Mg geothermometer – a reinterpretation of existing experimental data. *Contrib Mineralog Petrol* 99:44–48
- Laird J (1988) Chlorites: Metamorphic petrology. In: Bailey SW (ed) *Hydrous phyllosilicates, Reviews in Mineralogy* 19, Mineralogical Soc of America, 404–454
- Lang HM, Rice JM (1985a) Regression modeling of metamorphic reactions in metapelites, Snow Peak, northern Idaho. *J Petrol* 26:857–887
- Lang HM, Rice JM (1985b) Geothermometry, geobarometry and T-X (Fe-Mg) relations in metapelites, Snow Peak, northern Idaho. *J Petrol* 26:889–924
- Lieberman J, Petrakakis K (1991) TWEEQU thermobarometry: analysis of uncertainties and applications to granulites from western Alaska and Austria. *Can Mineralog* 29:857–887
- Lindsley DH (1983) Pyroxene thermometry. *Am Mineralog* 68:477–493
- Lindsley DH, Andersen DJ (1983) A two-pyroxene thermometer: proceedings of the 13th lunar and planetary science conference, part 2. *J Geophys Res* 88(Suppl):A887–A906
- Lindsley DH, Frost BR (1992) Equilibria among Fe-Ti oxides, pyroxenes, olivine, and quartz. I Theory. *Am Mineralog* 77:987–1003
- Liou JG, Maruyama S, Cho M (1987) Very low-grade metamorphism of volcanic and volcanoclastic rocks – mineral assemblages and mineral facies. In: Frey M (ed) *Low temperature metamorphism*. Blackie, Glasgow, pp 59–114
- Maruyama H, Liou JG, Suzuki K (1981) The peristerite gap in low-grade metamorphic rocks. *Contrib Mineralog Petrol* 81:268–276
- Maruyama H, Suzuki K, Liou JG (1983) Greenschist-amphibolite transition equilibria at low pressures. *J Petrol* 24:583–604
- Massonne HJ, Chopin C (1989) P-T history of the Gran Paradiso (western Alps) metagranites based on phengite geobarometry. In: Daly JS, Cliff RA, Yardley BWD (eds) *Evolution of metamorphic belts*. Geological Society Special Publication 43: Blackwell, Oxford, pp 545–549
- Massonne HJ, Schreyer W (1987) Phengite geobarometry based on the limiting assemblage with K-feldspar, phlogopite, and quartz. *Contrib Mineralog Petrol* 96:212–224
- McKenna LW, Hodges KV (1988) Accuracy versus precision in locating reaction boundaries: implications for the garnet-plagioclase-aluminum silicate-quartz geobarometer. *Am Mineralog* 73:1205–1208
- Meyre C, de Capitani C, Partsch JH (1997) A ternary solid solution model for omphacite and its application to geothermobarometry of eclogites from the Middle Adula nappe (Central Alps, Switzerland). *J Metamorph Geol* 15:687–700
- Miyashiro A (1961) Evolution of metamorphic belts. *J Petrol* 2:277–318
- Mullis J (1987) Fluid inclusion studies during very low-grade metamorphism. In: Frey M (ed) *Low temperature metamorphism*. Blackie, Glasgow, pp 162–199
- Newton RC (1983) Geobarometry of high-grade metamorphic rocks. *Am J Sci* 283A:1–28
- Newton RC (1986) Metamorphic temperatures and pressures of Group B and C, eclogites. *Geol Soc Am Sp Pap* 164:17–30
- Newton RC, Fyfe WS (1976) High pressure metamorphism. In: Bailey DK, MacDonald R (eds) *The evolution of the crystalline rocks*. Academic, London, pp 100–186
- Newton RC, Goldsmith JR, Smith JV (1969) Aragonite crystallization from strained calcite at reduced pressures and its bearing on aragonite in low-grade metamorphism. *Contrib Mineralog Petrol* 22:335–348



- Nord GL, Hammarstrom J, E-an Z (1978) Zoned plagioclase and peristerite formation in phyllites from southwestern Massachusetts. *Am Mineralog* 63:947–955
- Patrick BE, Ghent ED (1988) Empirical calibration of the K-white mica + feldspar + biotite geobarometer. *Miner Soc Can program abstracts* 13:A95
- Pattison DRM (1992) Stability of andalusite and sillimanite and the  $Al_2SiO_5$  triple point: constraints from the Ballachulish aureole, Scotland. *J Geol* 100:423–446
- Pattison DRM, Chako T, Farquhar J, McFarlane CRM (2003) Temperatures of granulite-facies metamorphism: constraints from experimental phase equilibria and thermobarometry corrected from retrograde exchange. *J Petrol* 44:867–900
- Pattison DRM, Newton RC (1989) Reversed experimental calibration of the garnet-clinopyroxene Fe-Mg exchange thermometer. *Contrib Mineralog Petrol* 101:87–103
- Perchuk LL (1989) P-T-fluid regimes of metamorphism and related magmatism with special reference to the granulite-facies Sharyzhalgay complex of Lake Baikal. In: *Evolution of metamorphic belts*. Geological Society Special Publication 43: Blackwell, Oxford, pp 275–291
- Perchuk LL, Lavrent'eva IV (1983) Experimental investigation of exchange equilibria in the system cordierite-garnet-biotite. In: Saxena SK (ed) *Kinetics and equilibrium in mineral reactions, advances in physical geochemistry*, vol 3, Springer. Berlin, Heidelberg, New York, pp 199–239
- Popp RK, Gilbert MC (1972) Stability of acmite-jadeite pyroxenes at low pressure. *Am Mineralog* 57:1210–1231
- Powell R, Holland TJB (1988) An internally consistent dataset with uncertainties and correlations: 3. Applications to geobarometry, worked examples and a computer program. *J Metamorph Geol* 6:173–204
- Powell R, Holland T, Worley B (1998) Calculating phase diagrams involving solid solutions via non-linear equations, with examples using THERMOCALC. *J Metamorph Geol* 16:577–588
- Powell WG, Carmichael DM, Hodgson CJ (1993) Thermobarometry in a sub-greenschist to greenschist transition in metabasites of the Abitibi greenstone belt, Superior Province, Canada. *J Metamorph Geol* 11:165–178
- Ravna EJ, Paquin J (2003) Thermobarometric methodologies applicable to eclogites and garnet ultrabasites. In: Carswell DA, Compagnoni R (eds) *High pressure metamorphism*, European Mineralogical Union Notes in mineralogy, vol 5. Eötvös University Press, Budapest, pp 229–259
- Ravna EJK, Terry MP (2004) Geothermobarometry of UHP and HP eclogites and schists – an evaluation of equilibria among garnet-clinopyroxene-kyanite-phengite-coesite/quartz. *J Metamorph Geol* 22:593–604
- Radvanec M, Banno S, Ernst WG (1998) Chemical microstructure of Franciscan jadeite from Pacheco Pass, California. *Am Mineralog* 83:273–279
- Reinecke T (1991) Very-high-pressure metamorphism and uplift of coesite-bearing metasediments from the Zermatt-Saas zone, Western Alps. *Eur J Mineralog* 3:7–17
- Rejebian VA, Harris AG, Huebner JS (1987) Conodont color and textural alteration: an index to regional metamorphism, contact metamorphism, and hydrothermal alteration. *Geol Soc Am Bull* 99:471–479
- Richardson SW, Gilbert MC, Bell PM (1969) Experimental determination of kyanite-andalusite and andalusite-sillimanite equilibrium; the aluminium silicate triple point. *Am J Sci* 267: 259–272
- Salje E (1986) Heat capacities and entropies of andalusite and sillimanite: the influence of fibrolization on the phase diagram of the  $Al_2SiO_5$  polymorphs. *Am Mineralog* 71:1366–1371
- Sandiford M, Powell R (1986) Pyroxene exsolution in granulites from Fyfe Hills, Enderby Land, Antarctica: evidence for 1000°C metamorphic temperatures in Archean continental crust. *Am Mineralog* 71:946–954
- Savin SM, Lee M (1988) Isotopic studies of phyllosilicates. In: Bailey SW (ed.) *Hydrous phyllosilicates, Reviews in Mineralogy* 19, Mineralogical Soc America, 189–223
- Schliestedt M (1986) Eclogite-blueschist relationships as evidenced by mineral equilibria in the high-pressure metabasic rocks of Sifnos (Cycladic Islands), Greece. *J Petrol* 27:1437–1459

- Schumacher JC (1991) Empirical ferric iron corrections: necessity, assumptions and effects on selected geothermobarometers. *Mineralog Mag* 55:3–18
- Schumacher JC, Schumacher R, Robinson P (1989) Acadian metamorphism in central Massachusetts and south-western New Hampshire: evidence for contrasting *P-T* trajectories. In: Daly JS, Cliff RA, Yardley BWS (eds) *Evolution of metamorphic belts*. Geological Society Special Publication 43: Blackwell, Oxford, pp 453–460
- Selverstone J, Spear FS, Franz G, Morteani G (1984) High-pressure metamorphism in the SW Tauern Window, Austria: *P-T* paths from Hornblende-Kyanite-Stauroilite Schists. *J Petrol* 25:501–531
- Shiba M (1988) Metamorphic evolution of the southern part of Hidaka belt, Hokkaido, Japan. *J Metamorph Geol* 6:273–296
- Spear FS (1980)  $\text{NaSi} \rightleftharpoons \text{CaAl}$  exchange equilibrium between plagioclase and amphibole. *Contrib Mineralog Petrol* 72:33–41
- Spear FS (1993) *Metamorphic phase equilibria and pressure-temperature-time path* (monograph). Mineralogical Society of America, Washington, DC, 824 pp
- Spear F, Kohn M (1999) *GTB program manual: Program Thermobarometry Version 2.1* May, 1999, Department of Geology, Rensselaer Polytechnic Institute, Troy, New York 12180 (<http://ees2.geo.rpi.edu/MetaPetaRen>)
- Spear FS, Ferry JM, Rumble D III (1982a) Analytical formulation of phase equilibria: the Gibbs' method. In: Ferry JM (ed) *Characterization of metamorphism through mineral equilibria, reviews in mineralogy*, reviews in mineralogy, vol 10. Mineralogical Society of America, Washington, DC, pp 105–152
- St-Onge MR (1987) Zoned poikiloblastic garnets: *P-T* paths and syn-metamorphic uplift through 30 km of structural depth, Wopmay Orogen, Canada. *J Petrol* 28:1–21
- Stormer JC (1975) A practical two-feldspar geothermometer. *Am Mineralog* 60:667–674
- Sweeney JJ, Burnham AK (1990) Evaluation of a simple model of vitrinite reflectance based on chemical kinetics. *Am Assoc Petrol Geol Bull* 74:1559–1570
- Thoenen T (1989) *A comparative study of garnet-biotite geothermometers*. Unpublished Doctoral Dissertation, University of Basel, 118 pp
- Thompson PH (1976) Isograd patterns and pressure-temperature distributions during regional metamorphism. *Contrib Mineralog Petrol* 57:277–295
- Thompson PH (1989) An empirical model for metamorphic evolution of the Archaean Slave Province and adjacent Thelon Tectonic Zone, north-western Canadian Shield. In: Daly JS, Cliff RA, Yardley BWS (eds) *Evolution of metamorphic belts*. Geological Society Special Publication 43: Blackwell, Oxford, pp 245–263
- Tilley CE (1924) The facies classification of metamorphic rocks. *Geol Mag* 61:167–171
- Todd CS (1998) Limits on the precision of geobarometry at low grossular and anorthite content. *Am Mineralog* 83:1161–1167
- Todd CS, Engi M (1997) Metamorphic field gradients in the Central Alps. *J Metamorph Geol* 15:513–530
- Tracy RJ, Robinson P, Thompson AB (1976) Garnet composition and zoning in the determination of temperature and pressure of metamorphism, Central Massachusetts. *Am Mineralog* 61:762–775
- Trommsdorff V, Evans BW (1972) Progressive metamorphism of antigorite schist in the Bergell tonalite aureole (Italy). *Am J Sci* 272:487–509
- Trommsdorff V, Evans BW (1977) Antigorite – ophicarbonates: contact metamorphism in Valmalenco, Italy. *Contrib Mineralog Petrol* 62:301–312
- Turner FJ (1981) *Metamorphic petrology – mineralogical, field and tectonic aspects*, 2nd edn. McGraw-Hill, New York
- Valley JW (1986) Stable isotope geochemistry of metamorphic rocks. In: Valley JW, Taylor HP, O-Neil JR (eds) *Stable isotopes in high temperature geological processes, reviews in mineralogy*, vol 16. Mineralogical Society of America, Washington DC, pp 445–489

- Vidal O, Parra T, Trotet F (2001) A thermodynamic model for Fe-Mg aluminous chlorite using data from phase equilibrium experiments and natural pelitic assemblages in the 100° to 600°C, 1 to 15 kb range. *Am J Sci* 301:557–592
- Voldman GG, Bustos-Marun RA, Albanesi GL (2010) Calculation of the conodont Color Alteration Index (CAI) for complex thermal histories. *Int J Coal Geol* 82:45–50
- Wangen M, Throndsen T, Halvorsen G (2007) The Paleo heat flow contents in vitrinite reflectance observations. *Math Geol* 39:491–511
- Wen S, Nekvasil H (1994) SOLVCALC: An interactive graphics program package for calculating the ternary feldspar solvus and for two-feldspar geothermometry. *Comput Geosci* 20:1025–1040
- Winkler HGF (1979) *Petrogenesis of metamorphic rocks*. Springer, Heidelberg, 348 pp
- Wu CM, Zhang J, Ren LD (2004) Empirical garnet – biotite – plagioclase – quartz (GBPQ) geobarometry in medium- to high-grade metapelites. *J Petrol* 45:1907–1921
- Wu CM, Zhao GC (2006) Recalibration of the garnet – muscovite (GM) geothermometer and the garnet – muscovite – plagioclase – quartz (GMPQ) geobarometer for metapelitic assemblages. *J Petrol* 47:2357–2368
- Wu CM, Zhao GC (2007a) A recalibration of the garnet-olivine geothermometer and a new geobarometer for garnet-olivine-plagioclase-bearing granulites. *J Metamorph Geol* 25:497–505
- Wu CM, Zhao GC (2007b) The metapelitic garnet – biotite – muscovite – aluminosilicate – quartz (GBMAQ) geobarometer. *Lithos* 97:365–372
- Yardley BWD (1982) The early metamorphic history of the Haast schists and related rocks of New Zealand. *Contrib Mineralog Petrol* 81:317–327
- Yardley BWD, Schumacher JC (1991) Geothermometry and geobarometry. *Mineral Mag (special volume on GTB)* 55:378
- Zwart HJ (1973) *Metamorphic map of Europe*. Leiden/UNESCO, Paris

### ***Further References and Recommended Reading***

- Aranovich LY, Podlesskii KK (1989) Geothermobarometry of high-grade metapelites: simultaneously operating reactions. In: Daly JS, Cliff RA, Yardley BWD (eds) *Evolution of metamorphic belts geological society special publication*. Blackwell, Oxford, pp 45–62
- Auzanneau E, Schmidt MW, Vielzeuf D, Connolly JAD (2010) Titanium in phengite: a geobarometer for high temperature eclogites. *Contrib Mineralog Petrol* 159:1–24
- Barton MD, Staude JM, Snow EA, Johnson DA (1991) Aureole systematics. In: Kerrick DM (ed) *Contact metamorphism, reviews in mineralogy*, vol 26. Mineralogical Society of America, Washington, DC, pp 723–847
- Bégin NJ (1992) Contrasting mineral isograd sequences in metabasites of the Cape Smith Belt, northern Québec, Canada: three new bathograds for mafic rocks. *J Metamorph Geol* 10:685–704
- Bell TM, Brothers RN (1985) Development of *P-T* prograde and *P*-retrograde, *T*-prograde isogradic surfaces during blueschist to eclogite regional deformation/metamorphism in New Caledonia, as indicated by progressively developed porphyroblast microstructures. *J Metamorph Geol* 3:59–79
- Benisek A, Kroll H, Cemic L (2004) New developments in two-feldspar thermometry. *Am Mineralog* 89:1496–1504
- Bertrand P, Mercier J-CC (1985) The mutual solubility of coexisting ortho- and clinopyroxene: toward an absolute geothermometer for the natural system? *Earth Planet Sci Lett* 76:109–122
- Beysac O, Goffé B, Chopin C, Rouzaud JN (2002) Raman spectra of carbonaceous material in metasediments: a new geothermometer. *J Metamorph Geol* 20:859–871
- Bhattacharya A, Krishnakumar KR, Raith M, Sen SK (1991) An improved set of *a-X* parameters for Fe-Mg-Ca garnets and refinements of the orthopyroxene-garnet thermometer and the orthopyroxene-garnet-plagioclase-quartz barometer. *J Petrol* 32:629–656

- Bhattacharya A, Mazumdar AC, Sen SK (1988) Fe-Mg mixing in cordierite: constraints from natural data and implications for cordierite-garnet geothermometry in granulites. *Am Mineralog* 73:338–344
- Bohlen SR, Boettcher AL (1981) Experimental investigations and geological applications of orthopyroxene geobarometry. *Am Mineralog* 66:951–964
- Bohlen SR, Dollase WA, Wall VJ (1986) Calibration and application of spinel equilibria in the system FeO-Al<sub>2</sub>O<sub>3</sub>-SiO<sub>2</sub>. *J Petrol* 27:1143–1156
- Bohlen SR, Liotta JJ (1986) A barometer for garnet amphibolites and garnet granulites. *J Petrol* 27:1025–1056
- Bowen NL (1940) Progressive metamorphism of siliceous limestone and dolomites. *J Geol* 48:225–274
- Brey GP, Koehler T (1990) Geothermobarometry in four-phase lherzolites II. New thermobarometers, and practical assessment of existing thermobarometers. *J Petrol* 31:1353–1378
- Brown TH, Berman RG, Perkins EH (1989) PTA-SYSTEM; a GeO-Calc software package for the calculation and display of activity-temperature-pressure phase diagrams. *Am Mineralog* 74:485–487
- Bucher K, Ohta Y (1993) Granulites and garnet-cordierite gneisses from Dronning Maud Land, Antarctica. *J Metamorph Geol* 11:691–703
- Carmichael DM (1991) Univariant mixed-volatile reactions: pressure-temperature phase diagrams and reaction isograds. *Can Mineralog* 29:741–754
- Carrington DP, Harley SL (1995) The stability of osumilite in metapelitic granulites. *J Metamorph Geol* 13:613–625
- Connolly JAD, Trommsdorff V (1991) Petrogenetic grids for metacarbonate rocks: pressure-temperature phase-diagram projection for mixed-volatile systems. *Contrib Mineralog Petrol* 108:93–105
- Cooke RA, O'Brien PJ, Carswell DA (2000) Garnet zoning and the identification of equilibrium mineral compositions in high-pressure-temperature granulites from the Moldanubian Zone, Austria. *J Metamorph Geol* 18:551–569
- Currie KL, Van Staal CR (1999) The assemblage stilpnomelane-chlorite-phengitic mica: a geothermobarometer for blueschist and associated greenschist terranes. *J Metamorph Geol* 17:613–620
- Dachs E (1994) Uncertainties in the activities of garnets and their propagation into geothermobarometry. *Eur J Mineralog* 6:291–295
- Das K, Fujino K, Tomioka N, Miura H (2006) Experimental data on Fe and Mg partitioning between coexisting sapphirine and spinel: an empirical geothermometer and its application. *Eur J Mineralog* 18:49–58
- Dobrzhinetskaya L, Bozhilov KN, Green HW (1999) The solubility of TiO<sub>2</sub> in olivine: implications for the mantle wedge environment. *Chem Geol* 160:357–370
- Docka JA, Berg JH, Klewin K (1986) Geothermometry in the Kiglapait aureole. II. Evaluation of exchange thermometry in a well-constrained setting. *J Petrol* 27:605–626
- Eckert JO, Newton RC, Kleppa OJ (1991) The  $\Delta H$  of reaction and recalibration of garnet-pyroxene-plagioclase-quartz geobarometers in the CMAS system by solution calorimetry. *Am Mineralog* 76:148–160
- El-Shazly AK, Liou JG (1991) Glaucofan chloritoid-bearing assemblages from NE Oman: petrologic significance and a petrogenetic grid for high P metapelites. *Contrib Mineralog Petrol* 107:180–201
- Ernst WG (1976) Petrologic phase equilibria. Freeman, San Francisco, 333 pp
- Evans BW (1990) Phase relations of epidote-blueschists. *Lithos* 25:3–23
- Evans BW, Guidotti CV (1966) The sillimanite-potash feldspar isograd in western Maine, USA. *Contrib Mineralog Petrol* 12:25–62
- Ferry JM (2000) Patterns of mineral occurrence in metamorphic rocks. *Am Mineralog* 85:1573–1588
- Fonarev VI, Konilov AN (1986) Experimental study of Fe-Mg distribution between biotite and orthopyroxene at P = 490 MPa. *Contrib Mineralog Petrol* 93:227–235

- Frey M, De Capitani C, Liou JG (1991) A new petrogenetic grid for low-grade metabasites. *J Metamorph Geol* 9:497–509
- Frost BR, Chacko T (1989) The granulite uncertainty principle: Limitations on thermobarometry in granulites. *J Geol* 97:435–450
- Fyfe WS, Turner FJ, Verhoogen J (1958) Metamorphic reactions and metamorphic facies. *Geol Soc Am Bull* 73:259
- Ghent ED, Gordon TM (2000) Application of INVEQ to the geothermobarometry of metamorphic rocks near a kyanite-sillimanite isograd, Mica Creek, British Columbia. *Am Mineralog* 85:9–13
- Graham CM, Powell R (1984) A garnet-hornblende geothermometer and application to the Pelona Schist, southern California. *J Metamorph Geol* 2:13–32
- Grambling JA (1990) Internally-consistent geothermometry and H<sub>2</sub>O barometry in metamorphic rocks: the example garnet-chlorite-quartz. *Contrib Mineralog Petrol* 105:617–628
- Green TH, Adam J (1991) Assessment of the garnet-clinopyroxene Fe-Mg exchange thermometer using new experimental data. *J Metamorph Geol* 9:341–347
- Guidotti CV, Dyar MB (1991) Ferric iron in metamorphic biotite and its petrologic and crystal-chemical implications. *Am Mineralog* 76:161–175
- Guidotti CV, Sassi FP, Blencoe JG, Selverstone J (1994) The paragonite-muscovite solvus: I. P-T-X limits derived from the Na-K compositions of natural, quasibinary paragonite-muscovite pairs. *Geochim Cosmochim Acta* 58:2269–2275
- Guiraud M, Holland T, Powell R (1990) Calculated mineral equilibria in the greenschist-blueschist-eclogite facies in Na<sub>2</sub>O-FeO-MgO-Al<sub>2</sub>O<sub>3</sub>-SiO<sub>2</sub>-H<sub>2</sub>O. *Contrib Mineralog Petrol* 104:8598
- Harley SL (2008) Refining the P-T records of UHT crustal metamorphism. *J Metamorph Geol* 26:125–154
- Heck ET (1943) Regional metamorphism of coal in southeastern West Virginia. *Bull Am Assoc Petrol Geol Bull* 27:1194–1227
- Hodges KV, Spear FS (1982) Geothermometry, geobarometry and the Al<sub>2</sub>SiO<sub>5</sub> triple point at Mt. Moosilauke, New Hampshire. *Am Mineralog* 67:1118–1134
- Hokada T (2001) Feldspar thermometry in ultrahigh-temperature metamorphic rocks: evidence of crustal metamorphism attaining ≈ 1100°C in the Archean Napier Complex, East Antarctica. *Am Mineralog* 86:932–938
- Holdaway MJ (2000) Application of new experimental and garnet Margules data to the garnet-biotite geothermometer. *Am Mineralog* 85:881–892
- Holdaway MJ (2004) Optimization of some key geothermobarometers for pelitic metamorphic rocks. *Mineralog Mag* 68:1–14
- Holdaway MJ, Mukhopadhyay B (1993) Geothermobarometry in pelitic schists: a rapidly evolving field. *Am Mineralog* 78:681–693
- Hollis JA, Harley SL (2003) Alumina solubility in orthopyroxene coexisting with sapphirine and quartz. *Contrib Mineralog Petrol* 144:473–483
- Hood A, Gutjar CCM, Heacock RL (1975) Organic metamorphism and the generation of petroleum. *Am Assoc Petrol Geol Bull* 59:986–996
- Hoschek G (2004) Comparison of calculated P-T pseudosections for a kyanite eclogite from the Tauern Window, Eastern Alps, Austria. *Eur J Mineralog* 16:59–72
- Huckenholtz HG, Lindhuber W, Fehr KT (1981) Stability of grossular + quartz + wollastonite + anorthite: the effect of andradite and albite. *Neues Jahrb Mineral Abh* 142:223–247
- Indares AD, Martignole J (2003) Towards the upper limits of the granulite facies. *J Metamorph Geol* 21:1–2
- Jamieson RA, Craw D (1987) Sphalerite geobarometry in metamorphic terranes: an appraisal with implications for metamorphic pressure in the Otago Schist. *J Metamorph Geol* 5:87–99
- Kaneko Y, Miyano T (2004) Recalibration of mutually consistent garnet-biotite geothermometer. *Lithos* 73:255–269

- Katayama I, Parkinson CD, Okamoto K, Nakajima Y, Maruyama S (2000) Supersilicic clinopyroxene and silica exsolution in UHPM eclogite and pelitic gneiss from the Kokchetav massif, Kazakhstan. *Am Mineralog* 85:1368–1374
- Kirschner DL, Sharp ZD, Masson H (1995) Oxygen isotope thermometry of quartz-calcite veins: unraveling the thermal-tectonic history of the subgreenschist facies Morcles nappe (Swiss Alps). *Geol Soc Am Bull* 107:1145–1156
- Kitchen NE, Valley JW (1995) Carbon isotope thermometry in marbles of the Adirondack Mountains, New York. *J Metamorph Geol* 13:577–594
- Kohn MJ, Spear FS (1989) Empirical calibration of geobarometers for the assemblage garnet + hornblende + plagioclase + quartz. *Am Mineralog* 74:77–84
- Kretz R (1991) A note on transfer reactions. *Can Mineralog* 29:823–832
- Kroll H, Evangelakakis C, Voll C (1993) Two-feldspar geothermometry, a review and revision for slowly cooled rocks. *Contrib Mineralog Petrol* 114:510–518
- Lal RK (1997) Internally consistent calibrations for geothermobarometry of high-grade Mg-Al rich rocks in the system MgO-Al<sub>2</sub>O<sub>3</sub>-SiO<sub>2</sub> and their application to sapphirine-spinel granulites of Eastern Ghats, India and Enderby Land, Antarctica. *Earth Planet Sci Lett* 106:91–113
- Letargo CMR, Lamb WM, Park J-S (1995) Comparison of calcite + dolomite thermometry and carbonate + silicate equilibria: constraints on the conditions of metamorphism of the Llano uplift, central Texas, U.S.A. *Am Mineralog* 80:131–143
- Liogys VA, Jenkins DM (2000) Hornblende geothermometry of amphibolite layers of the Popple Hill gneiss, north-west Adirondack Lowlands, New York, USA. *J Metamorph Geol* 18:513–530
- Mahar EM, Baker JM, Powell R, Holland TJB (1997) The effect of Mn on mineral stability in metapelites. *J Metamorph Geol* 15:223–238
- Manning CE, Bohlen SR (1991) The reaction titanite + kyanite = anorthite + rutile and titanite-rutile barometry in eclogites. *Contrib Mineralog Petrol* 109:1–9
- Martignole J, Martelat JE (2003) Regional-scale Grenvillian-age UHT metamorphism in the Mollendo-Camana block (basement of the Peruvian Andes). *J Metamorph Geol* 21:99–120
- Miyashiro A (1972) Pressure and temperature conditions and tectonic significance of regional and ocean floor metamorphism. *Tectonophys* 13:141–159
- Moecher DP, Essene EJ, Anovitz LM (1988) Calculation of clinopyroxene-garnet-plagioclase-quartz geobarometers and application to high grade metamorphic rocks. *Contrib Mineralog Petrol* 100:92–106
- Newton RC, Smith JV (1967) Investigations concerning the breakdown of albite at depth in the earth. *J Geol* 75:268–286
- Paria P, Bhattacharya A, Sen A (1988) The reaction garnet + clinopyroxene + quartz = 2 orthopyroxene + anorthite: a potential geobarometer for granulites. *Contrib Miner Petrol* 100:126–133
- Parkinson CD, Katayama I, Liou JG, Maruyama S (2002) The diamond-bearing Kokchetav Massif, Kazakhstan: Petrochemistry and tectonic evolution of a unique ultrahigh-pressure metamorphic terrane. Universal Academy Press, Tokyo, Japan, p 527
- Patiño Douce AE, Johnston AD, Rice JM (1993) Octahedral excess mixing properties in biotite: a working model with applications to geobarometry and geothermometry. *Am Mineralog* 78:113–131
- Pattison DRM (2003) Petrogenetic significance of orthopyroxene-free garnet + clinopyroxene + plagioclase ± quartz-bearing metabasites with respect to the amphibolite and granulite facies. *J Metamorph Geol* 21:21–34
- Pattison DRM, Spear FS, Cheney JT (1999) Polymetamorphic origin of muscovite + cordierite + staurolite + biotite assemblages: implications for the metapelitic petrogenetic grids and for P-T paths. *J Metamorph Geol* 17:685–703
- Pattison DRM, Spear FS, DeBuhr CL, Cheney JT, Guidotti CV (2002) Natural assemblage and thermodynamic analysis of the reaction muscovite + cordierite = Al<sub>2</sub>SiO<sub>5</sub> + biotite +

- quartz + H<sub>2</sub>O: implications for the metapelitic petrogenetic grid. *J Metamorph Geol* 20(1): 99–118
- Perkins EH, Brown TH, Berman RG (1986) PT-system, TX-system, PX-system: three programs which calculate pressure-temperature-composition phase diagrams. *Comput Geosci* 12:749–755
- Powell R, Condliffe DM, Condliffe E (1984) Calcite-dolomite geothermometry in the system CaCO<sub>3</sub>-MgCO<sub>3</sub>-FeCO<sub>3</sub>: an experimental study. *J Metamorph Geol* 2:33–41
- Powell R, Holland T (1995) Optimal geothermometry and geobarometry. *Am Mineralog* 79: 120–133
- Powell R, Holland T (2001) Course notes for “THERMOCALC workshop 2001: calculating metamorphic phase equilibria” on CD-ROM (available from the authors)
- Powell R, Holland TJB (1985) An internally consistent dataset with uncertainties and correlations: 1. Methods and a worked example. *J Metamorph Geol* 3:327–342
- Powell R, Holland TJB (1990) Calculated mineral equilibria in the pelite system, KFMASH (K<sub>2</sub>O-FeO-MgO-Al<sub>2</sub>O<sub>3</sub>-SiO<sub>2</sub>-H<sub>2</sub>O). *Am Mineralog* 75:367–380
- Powell R, Holland TJB (2008) On thermobarometry. *J Metamorph Geol* 26:155–179
- Ramberg H (1952) The origin of metamorphic and metasomatic rocks. University of Chicago Press, Chicago, p 317
- Rebay G, Powell R (2002) The formation of eclogite facies metatroctolites and a general petrogenetic grid in Na<sub>2</sub>O-CaO-FeO-MgO-Al<sub>2</sub>O<sub>3</sub>-SiO<sub>2</sub>-H<sub>2</sub>O (NCFMASH). *J Metamorph Geol* 20(9):813–826
- Repetski JE, Ryder RT, Weary DJ, Harris AG, Trippi MH (2008) Thermal maturity patterns (CAI and %Ro) in the Upper Ordovician and Lower-Middle Devonian Rocks of the Appalachian Basin: a major revision of USGS Map I-917-E using new subsurface collections. U.S. Geological Survey Scientific Investigations Map SIM-3006
- Ruppert LF, Hower JC, Ryder RT, Levine JR, Trippi MH, Grady WC (2010) Geologic controls on thermal maturity patterns in Pennsylvanian coal-bearing rocks in the Appalachian basin. *Int J Coal Geol* 81:169–181
- Sengupta P, Dasgupta S, Bhattacharya PK, Mukherjee M (1990) An orthopyroxene-biotite geothermometer and its application in crustal granulites and mantle-derived rocks. *J Metamorph Geol* 8:191–198
- Shulters JC, Bohlen SR (1989) The stability of hercynite and hercynite-gahnite spinels in corundum- or quartz-bearing assemblages. *J Petrol* 30:1017–1031
- Simpson GDH, Thompson AB, Connolly JAD (2000) Phase relations, singularities and thermobarometry of metamorphic assemblages containing phengite, chlorite, biotite, K-feldspar, quartz and H<sub>2</sub>O. *Contrib Mineralog Petrol* 139:555–569
- Song SG, Zhang LF, Niu Y, Su L, Jian P, Liu DY (2005) Geochronology of diamond-bearing zircons from garnet peridotite in the North Qaidam UHPM belt, Northern Tibetan Plateau: record of complex histories from oceanic lithosphere subduction to continental collision. *Earth Planet Sci Lett* 234:99–118
- Soto JJ (1993) PTMAFIC: software for thermobarometry and activity calculations with mafic and ultramafic assemblages. *Am Mineralog* 78:840–844
- Spear FS (1989) Relative thermobarometry and metamorphic P-T paths. In: Daly JS, Cliff RA, Yardley BWS (eds) Evolution of metamorphic belts. Geological Society Special Publication 43: Blackwell, Oxford, pp 63–82
- Spear FS (1992) On the interpretation of peak metamorphic temperatures in light of garnet diffusion during cooling. *J Metamorph Geol* 9:379–388
- Spear FS, Ferry JM, Rumble D III (1982) Analytical formulation of phase equilibria: the Gibbs’ method. In: Ferry JM (ed) Characterization of metamorphism through mineral equilibria. Reviews in mineralogy, vol 10. Mineralogical Society of America, Washington, DC, pp 105–152
- Spear FS, Kohn MJ, Cheney JT (1999) P-T paths from anatectic pelites. *Contrib Mineralog Petrol* 134:17–32
- Spear FS, Menard T (1989) Program GIBBS: a generalized Gibbs method algorithm. *Am Mineralog* 74:942–943

- Spear FS, Peacock SM, Kohn MJ, Florence FP, Menard T (1991) Computer programs for petrologic P-T-t path calculations. *Am Mineralog* 76:2009–2012
- Spear FS, Selverstone J, Hickmont D, Crowley P, Hodges KV (1984) P-T paths from garnet zoning: a new technique for deciphering tectonic processes in crystalline terranes. *Geology* 12:87–90
- Stephenson NCN (1984) Two-pyroxene thermometry of Precambrian granulites from Cape Riche, Albany-Fraser Province, Western Australia. *J Metamorph Geol* 2:297–314
- Streckeisen A, Wenk E (1974) On steep isograds surfaces in the Simplon area. *Contrib Mineralog Petrol* 47:81–95
- Stüwe K, Sandiford M (1994) Contribution of deviatoric stresses to metamorphic P-T paths: an example appropriate to low-P, high-T metamorphism. *J Metamorph Geol* 12:445–454
- Symmes GH, Ferry JM (1992) The effect of whole-rock MnO content on the stability of garnet in pelitic schists during metamorphism. *J Metamorph Geol* 10:221–237
- Tilley CE (1925) Metamorphic zones in the southern Highlands of Scotland. *Q J Geol Soc* 81: 100–112
- Triboulet C, Thiéblemont D, Audren C (1992) The (Na-Ca) amphibole- albite- chlorite- epidote-quartz geothermobarometer in the system S- A- F- M- C- N- H<sub>2</sub>O. 2. Applications to metabasic rocks in different metamorphic settings. *J Metamorph Geol* 10:557–566
- Vidal O, Goffé B, Theye T (1992) Experimental study of the stability of sudoite and magnesio-carpholite and calculation of a new petrogenetic grid for the system FeO-MgO-Al<sub>2</sub>O<sub>3</sub>-SiO<sub>2</sub>-H<sub>2</sub>O. *J Metamorph Geol* 10:603–614
- Vielzeuf D (1983) The spinel and quartz associations in high grade xenoliths from Tallante (S.E. Spain) and their potential use in geothermometry and barometry. *Contrib Mineralog Petrol* 82:301–311
- Waters DJ (1989) Metamorphic evidence for the heating and cooling path of Namaqualand granulites. In: Daly JS, Cliff RA, Yardley BWS (eds) *Evolution of metamorphic belts*. Geological Society Special Publication 43: Blackwell, Oxford, pp 357–363
- Will T, Okrush M, Schmaedicke E, Chen G (1998) Phase relations in the greenschist-blueschist-amphibolite-eclogite facies in the system Na<sub>2</sub>O-CaO-FeO-MgO-Al<sub>2</sub>O<sub>3</sub>-SiO<sub>2</sub>-CO<sub>2</sub>-H<sub>2</sub>O. (NCFMASH) with application to metamorphic rocks from Samos, Greece. *Contrib Mineralog Petrol* 104:353–386
- Will TM, Powell R, Holland T, Guiraud M (1990a) Calculated greenschist facies mineral equilibria in the system CaO-FeO-MgO-Al<sub>2</sub>O<sub>3</sub>-SiO<sub>2</sub>-CO<sub>2</sub>-H<sub>2</sub>O. *Contrib Mineralog Petrol* 104:353–368
- Will TM, Powell R, Holland TJB (1990b) A calculated petrogenetic grid for ultramafic rocks in the system CaO-FeO-MgO-Al<sub>2</sub>O<sub>3</sub>-SiO<sub>2</sub>-CO<sub>2</sub>-H<sub>2</sub>O at low pressures. *Contrib Mineralog Petrol* 105:347–358
- Worley B, Powell R (1998a) Making movies; phase diagrams changing in pressure, temperature, composition and time. In: Treloar PJ, O'Brien PJ (eds) *What drives metamorphism and metamorphic relations?* Vol 138. Geological Society Special Publications, London, pp 269–280
- Worley B, Powell R (1998b) Singularities in NCKFMASH (Na<sub>2</sub>O-CaO-K<sub>2</sub>O-FeO-MgO-Al<sub>2</sub>O<sub>3</sub>-SiO<sub>2</sub>-H<sub>2</sub>O). *J Metamorph Geol* 16:169–188
- Worley B, Powell R (2000) High-precision relative thermobarometry; theory and a worked example. *J Metamorph Geol* 18:91–101
- Yui T-F, Huang E, Xu J (1996) Raman spectrum of carbonaceous material: a possible metamorphic grade indicator for low-grade metamorphic rocks. *J Metamorph Geol* 14:115–124







## Part II Metamorphism of Specific Rock Types

Garnet-granulite (*coronite*) from Ytre Arna, Bergen Arcs, Norway. Matrix of rock: plagioclase (*white*), clinopyroxene (*green*), garnet (*brown*). Protolith: Igneous olivine – plagioclase rock (*troctolite*). Sites of coarse igneous olivine transformed to concentric structures (*corona structures*) with orthopyroxene cores, dark clinopyroxene and brown rims (*coronas*) of garnet. The texture resulted from the reaction of olivine with plagioclase at pressures of the lower continental crust. Reaction products are  $\text{Cpx} + \text{Grt}$ . The texture also shows that metamorphic reactions often involve small-scale transport processes



# Chapter 5

## Metamorphism of Ultramafic Rocks

### 5.1 Introduction

Ultramafic rocks are magnesium silicate rocks that normally contain no felsic minerals or very little (<10 vol%) normative feldspar. The Earth's mantle consists predominantly of ultramafic rocks. The mantle is, with the exception of some small anomalous regions, in a solid state. The ultramafic rocks undergo continuous recrystallization due to large-scale convection in sub-lithosphere mantle and as a result of tectonic processes in the lithosphere. The bulk of the mantle rocks, therefore, meet the criteria of metamorphic rocks. Metamorphic ultramafic rocks represent the largest volume of rocks of the planet.

Most of the ultramafic rocks found in the Earth's crust and consequently found in surface outcrops have been tectonically emplaced from the mantle during orogenesis. Such ultramafic mantle fragments are often referred to as Alpine-type peridotites (Fig. 5.1a). Ultramafic rocks of igneous origin do occur in the crust but are relatively rare (Fig. 5.1b). Most are formed from fractional crystallization from basic (gabbroic, basaltic) magmas in crustal magma chambers (olivine-saturated cumulate layers).

There are two basic types of mantle fragments in the crust: (1) mantle fragments from beneath oceanic crust. These constitute integral members of ophiolite sequences and are often lherzolitic in bulk composition (see below); (2) mantle fragments from sub-continental mantle occur in rock associations typical of continental crust. Such ultramafites are usually of harzburgitic (or dunitic) composition.

### 5.2 Ultramafic Rocks

Ultramafic mantle rock fragments experience strong mineralogical and structural modifications during emplacement in the crust and subsequent crustal deformation and metamorphism. Two different situations can be conceived.

1. Mantle fragments may retain parts of the original minerals and structure. Equilibration may be incomplete, because of limited access of water or slow

**Fig. 5.1** (a) World largest olivine (dunite) mine, Almklovdalen, Norway. Alpine type peridotite in Caledonian continental basement. The 8 m high bench in the quarry consists of coarse grained pure olivine (forsterite) rock. Note green color of fresh rock. (b) Layered peridotites in gabbro magma chamber. Leka Island, Norwegian Caledonides. Note typical *yellow-brown weathering crust* on peridotite matrix



reaction kinetics at low temperature. The ultramafics may not (or only partially) display mineral assemblages that equilibrated at the same conditions as the surrounding crustal rocks. Such ultramafic rocks may be termed **aliofacial**. Aliofacial ultramafics are particularly typical members of ophiolite complexes, metamorphosed under relatively low grade conditions.

2. Ultramafic rocks may completely equilibrate at the same  $P-T$  conditions as the surrounding crustal rocks. They may show rare relics of original minerals and structure (e.g., cores of mantle Cr-spinel in crustal magnetite). The ultramafic rocks register identical  $P-T$  histories as their crustal envelope. Ultramafic rocks showing such characteristics may be designated **isofacial**. Most ultramafics in higher grade terrains conserve very little of their mantle heritage. On the other hand, transitions between the two extremes, as usual, do occur (or are probably the rule). For example, the assemblage Fo + Atg + Di (see below) found in antigorite schists may be isofacial but structures and relict minerals often permit a fairly confident reconstruction of the pre-crustal state of the ultramafics (chlorite exsolution from mantle high-Al Cpx, Cr-spinel, polygonization of mantle olivine megacrysts, etc.).

### 5.2.1 Rock Types

Some examples of metamorphic ultramafic rocks are listed below. **Serpentinites** are massive or schistose rocks containing abundant minerals of the serpentine group. They represent hydrated low-temperature versions of mantle lherzolites, dunites or harzburgites. **Peridotite** is often used for olivine-rich ultramafic mantle rocks. This includes the main varieties spinel-peridotite and garnet-peridotite (Fig. 5.2). Partially serpentinized allofacial mantle peridotite may still be called peridotite, a recrystallized isofacial olivine-bearing antigorite-schist is described as serpentinite but not as peridotite. Rocks containing prograde metamorphic olivine and enstatite are named enstatite-forsterite **felses**. Carbonate-bearing serpentinites are often designated as **ophicarbonates** (ophicalcite, etc.). Carbonate-bearing talc schist (**talc fels**) is known as **soapstone**. The name **sagvandite**, from the type-locality

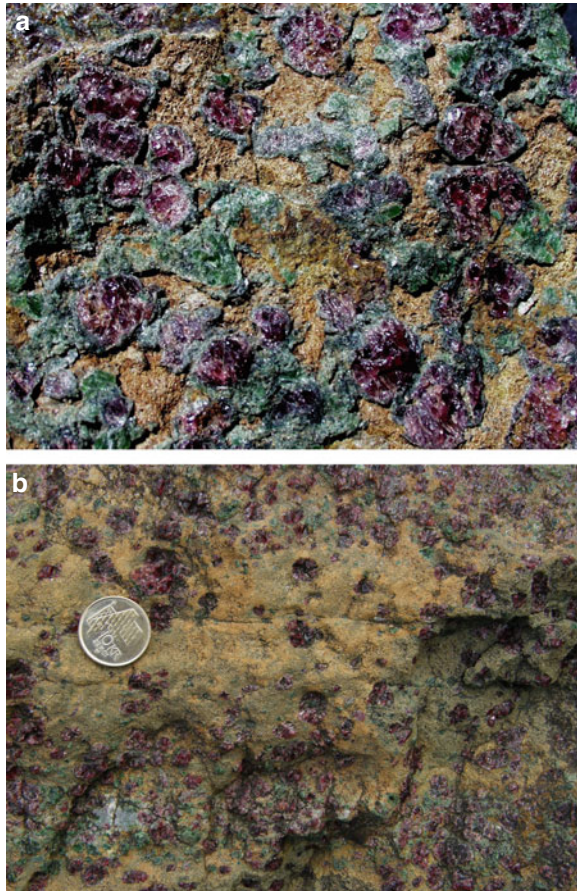


**Fig. 5.2** (a) Garnet peridotite at Gurskøya, Western Gneiss Region Norway, containing *red pyrope garnet* and *green diopside* (Cpx) in orthopyroxene-forsterite matrix. Note the characteristic *yellow weathering rind* on the Opx-Ol matrix. (b) Garnet peridotite (Grt lherzolite, Grt dunite) of the Almklovdalen ultramafic body, Norway. The rock matrix contains predominantly forsteritic olivine and some enstatite. Note typical *yellow-brown weathering crust* on peridotite matrix

Sagelv vatnet in Northern Norway, is often used for carbonate-bearing enstatite fels. In the Scandinavian Caledonides, sagvandite is widespread.

The very characteristic yellow-brownish or even reddish weathering rind of ultramafic rocks make peridotite outcrops very special. Such places have fascinated and attracted people at all times. Knobs and hills with peridotite outcrops have been favorite cult sites in many cultures. This is often still discernable from geographic place names. For example, the type locality of **dunite** (dun = brownish-gray color) is named after Dun Mountain in New Zealand.

Soapstone have been a sought after material in all ancient cultures where it was used to build stoves and utensils for cooking and as material for cult objects. Many place names on modern topographic maps still indicate the presence or the former presence of a soapstone occurrence.

### 5.2.2 Chemical Composition

Ultramafic rocks consist predominantly of ferro-magnesian silicates. Anhydrous ultramafic rocks contain the three minerals, olivine, orthopyroxene and calcic clinopyroxene in various proportions. Olivine, Opx and Cpx together dominate the modal composition of anhydrous ultramafites. Consequently, the system components,  $\text{SiO}_2$ , FeO, MgO and CaO constitute >95 wt% of almost all anhydrous ultramafites. Iron represents an important component in most ultramafic rocks. Much of it is normally present in a spinel phase (magnetite, spinel, chromite) and consequently Fe occurs in two different oxidation states. In the silicates, Fe–Mg substitution in Ol and Opx seldom exceeds 5–15 mol% ( $X_{\text{Mg}} \sim 0.85\text{--}0.95$ ). Thus, phase relationships in ultramafic rocks can be discussed in terms of Fe-free systems as a first approximation. We will discuss possible effects of additional components such as iron where necessary and appropriate. Most ultramafic rocks contain hydrates (amphiboles, sheet silicates, etc.) and very often also carbonates. Therefore,  $\text{H}_2\text{O}$  and  $\text{CO}_2$  must be added to the set of components in order to describe phase relationships in partially or fully hydrated (and/or carbonated) versions of Ol + Opx + Cpx rocks.

The system  $\text{SiO}_2\text{--MgO--CaO--H}_2\text{O--CO}_2$  (CMS-HC system) or subsystems thereof is adequate for a discussion of metamorphism of ultramafic rocks (note: the same system will be used to describe reactions and assemblages in sedimentary carbonate rocks, Chap. 6). Figure 5.3 shows the chemography of the CMS-HC system projected from  $\text{H}_2\text{O}$  and  $\text{CO}_2$  onto the  $\text{SiO}_2\text{--CaO--MgO}$  plane. The composition of mantle rocks with the anhydrous assemblage Ol + Opx + Cpx is restricted to the shaded area defined by forsterite (Ol), enstatite (Opx) and diopside (Cpx). Rocks with compositions inside the triangle Fo–En–Di are usually termed lherzolites (undepleted mantle peridotite). Rocks falling on the Fo–En join are harzburgites (depleted mantle peridotites) and rocks falling close to the Fo-corner in Fig. 5.3 are referred to as dunites (Fig. 5.1a). Pyroxenites are rocks with compositions along the Di–En join (including the Di- and En-corners).

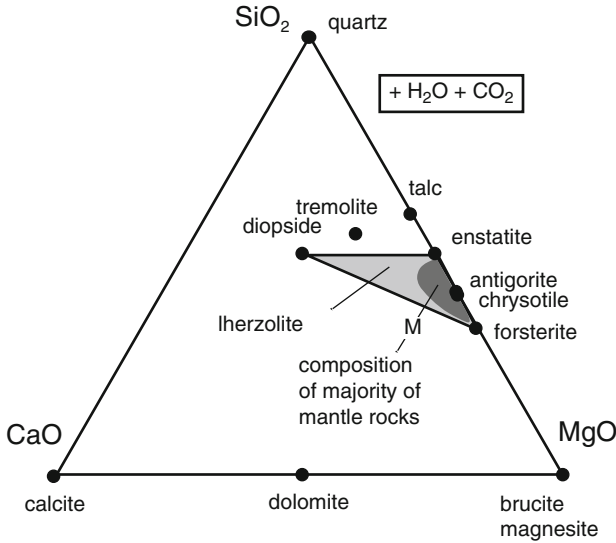


**Fig. 5.3** Chemography of the system CMS-HC projected from  $\text{CO}_2$  and  $\text{H}_2\text{O}$  onto the plane  $\text{CaO-MgO-SiO}_2$ , showing typical ultramafic rock and mineral compositions

Most of the accessible mantle material (tectonic fragments in the crust, xenoliths in basalts and other mantle-derived volcanic rocks) and of the ultramafic cumulate material, is olivine normative. In this chapter, we will not consider metamorphism of pyroxenites and their hydrated equivalents. In addition, mantle lherzolites are often rich in  $\text{Ol} + \text{Opx}$ , whereas  $\text{Cpx}$  ( $\text{Di}$ ) occurs in modal amounts below 20–30%. The composition of the majority of mantle rocks is restricted to the heavy shaded range (labeled “M”) in Fig. 5.3 and this chapter deals with such rock compositions.

All important minerals occurring in ultramafic rocks are shown in Fig. 5.3. The minerals chrysotile ( $\text{Ctl}$ ) and lizardite ( $\text{Lz}$ ) are structural varieties of serpentine of very similar composition, whereas antigorite ( $\text{Atg}$ ), a third form of serpentine, is slightly less magnesian than  $\text{Ctl}$  or  $\text{Lz}$ . Minerals of the serpentine group are related by (5.2) in Table 5.1.  $\text{Ctl}$  and  $\text{Lz}$  represent the low temperature serpentine minerals and typically occur at metamorphic grades below the middle greenschist facies.  $\text{Atg}$  is the typical greenschist, blueschist, eclogite and lower amphibolite facies serpentine mineral. All three carbonate minerals,  $\text{Cal}$ ,  $\text{Dol}$ ,  $\text{Mgs}$  in Fig. 5.3 occur in ultramafic rocks. It is apparent from Fig. 5.3 that a large number of potential mineral assemblages in this system are excluded on rock compositional grounds. For example, as the assemblage  $\text{En} + \text{Tr} + \text{Tlc}$  is outside the composition range of “normal” ultramafic rocks, it will not occur in such rocks and all mineral reactions leading to this assemblage are not relevant for meta-lherzolites and are therefore not considered in subsequent phase diagrams. Other examples of assemblages outside the lherzolite composition are  $\text{Brc} + \text{Fo}$  and  $\text{Di} + \text{En} + \text{Tlc}$  (Fig. 5.3). We do not consider assemblages of the type,  $\text{Dol} + \text{Fo} + \text{Brc}$  for the same reason.



**Table 5.1** Reactions in ultramafic rocks

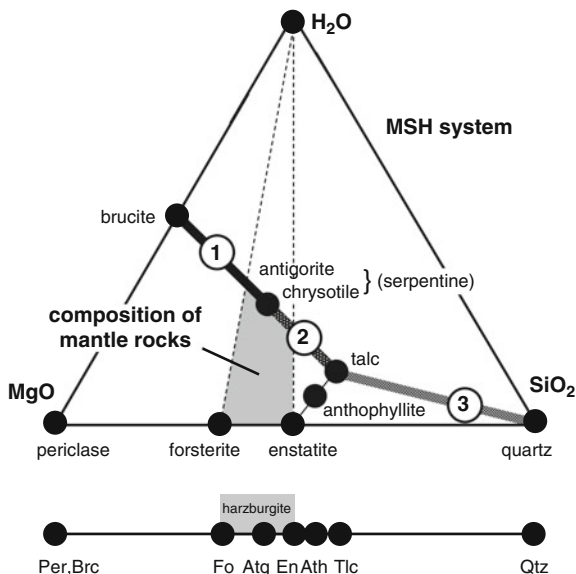
Composition of phase components			
Chrysotile	Ctl		$Mg_3Si_2O_5(OH)_4$
Antigorite	Atg		$Mg_{48}Si_{34}O_{85}(OH)_{62}$
Brucite	Brc		$Mg(OH)_2$
Talc	Tlc		$Mg_3Si_4O_{10}(OH)_2$
Forsterite	Fo		$Mg_2SiO_4$
Enstatite	En		$Mg_2Si_2O_6$
Anthophyllite	Ath		$Mg_7Si_8O_{22}(OH)_2$
Diopside	Di		$CaMgSi_2O_6$
Tremolite	Tr		$Ca_2Mg_5Si_8O_{22}(OH)_2$
Chlorite	Chl		$Mg_5Al_2Si_3O_{10}(OH)_8$
Anorthite	An		$CaAl_2Si_2O_8$
Pyrope	Py		$Mg_3Al_2Si_3O_{12}$
<b>MSH</b>	$15Ctl + Tlc \Rightarrow Atg$	(5.1)	First antigorite
	$17Ctl \Rightarrow Atg + 3Brc$	(5.2)	Last chrysotile
	$Atg + 20Brc \Rightarrow 34Fo + 51H_2O$	(5.3)	First forsterite (low T limit of olivine)
	$Atg \Rightarrow 18Fo + 4Tlc + 27H_2O$	(5.4)	Last antigorite (high T-limit of serpentinites)
	$9Tlc + 4Fo \Rightarrow 5Ath + 4H_2O$	(5.5)	Tlc-out (at lower P)
	$2Tlc + 2Fo \Rightarrow 5En + 2H_2O$	(5.6)	Tlc-out (at higher P)
	$2Ath + 2Fo \Rightarrow 9En + 2H_2O$	(5.7)	Ath-out
	$Atg \Rightarrow 10En + 14Fo + 31H_2O$	(5.8)	Last antigorite at high pressures
<b>CMSH</b>	$Atg + 8Di \Rightarrow 18Fo + 4Tr + 27H_2O$	(5.9)	Upper limit of Di in serpentinites
	$2Tr + 2Fo \Rightarrow 5En + 4Di + 2H_2O$	(5.10)	Tremolite-out, lherzolite assemblage
<b>MASH</b>	$Chl \Rightarrow Fo + En + Spl + 4H_2O$	(5.11)	Chlorite-out
	$Py + Fo \Rightarrow 2En + Spl$	(5.12)	Garnet-spinel boundary
<b>CMASH</b>	$En + Di + Spl \Rightarrow 2Fo + An$	(5.13)	Spinel-plagioclase boundary
	$4Spl + 2Tr \Rightarrow 6Fo + En + 4An + 2H_2O$	(5.14)	Tr + Spl-out

### 5.3 Metamorphism in the MSH System

#### 5.3.1 Chemographic Relations in the MSH System

The chemography of the three-component MSH system is shown in Fig. 5.4. The base line is anhydrous. Mantle rocks are normally restricted to the composition range between Fo and En (= harzburgites) and hydrated varieties of harzburgites occupy the shaded area in Fig. 5.4. H<sub>2</sub>O in the system may be stored in solid hydrous minerals such as amphiboles (orthoamphibole, anthophyllite), sheet silicates (talc, antigorite), hydroxide (brucite) or as a free fluid phase, depending on *P–T* conditions and the hydrologic situation. In an equilibrium situation, many three-phase assemblages that represent hydrated ultramafic rocks are possible, some of which contain three solid phases but no fluid (fluid-absent situation), some others contain two solids (minerals) and an aqueous fluid phase (fluid-present

**Fig. 5.4** Chemography of the system MSH showing mineral compositions relevant to metamorphosed rocks derived from harzburgite (depleted subcontinental upper mantle; *shaded area*). Maximum hydrated ultramafics contain the assemblages labeled 1, 2, and 3. Projection of the MSH system from  $H_2O$  onto the  $MgO-SiO_2$  binary is shown below together with the composition range for harzburgites (*shaded area*)



condition). For instance, the three minerals Fo + Tlc + Atg may represent the composition of an  $H_2O$ -bearing ultramafic rock. The same composition can also be made from Fo + Tlc +  $H_2O$ . In the first case, there is no free fluid present, in the second case  $H_2O$  is present as a distinct fluid phase. In the following, we only deal with fluid-present metamorphism.

Mantle harzburgites may, during weathering or other near-surface hydration processes, reach a state of maximum hydration. Three maximum hydrated assemblages are possible in the MSH system. The assemblages are shown in Fig. 5.4: (1) Brc + Ctl, (2) Ctl + Tlc, (3) Tlc + Qtz. The latter assemblage is outside the meta-harzburgite composition. However, a “super” hydrated assemblage, Ctl + Qtz, (tie line Ctl–Qtz in Fig. 5.4) occasionally occurs in near-surface modifications of harzburgites. This assemblage is probably metastable under all geological conditions relative to Ctl + Tlc. Evans (2004) suggested that the mineral chrysotile is thermodynamically a metastable phase thus all assemblages containing it would also be metastable. The assemblage Brc + Qtz is still more hydrous than Ctl + Qtz, and it is definitely metastable under metamorphic  $P$ – $T$ -conditions. All three hydrated assemblages coexist with free water at sub-critical conditions.

Meta-harzburgites are often discussed by using projections onto the binary  $MgO-SiO_2$  from  $H_2O$ . The resulting figures can be used for fluid-present conditions. Figure 5.4 also shows such a binary projection of the chemical compositions of the relevant phases in the MSH system for  $H_2O$ -excess situations. The harzburgite restriction is also shown on the binary chemography in that assemblages such as En + Ath, Tlc + Ath, Fo + Brc fall outside the composition range of mantle rocks and they will, therefore, not be discussed further.

### 5.3.2 *Progressive Metamorphism of Maximum Hydrated Harzburgite*

Understanding progressive metamorphism of ultramafic rocks is somewhat more difficult than metamorphism of sedimentary rocks. Most sedimentary rocks are normally in a maximum hydrated state when formed and progressive metamorphism systematically reduces the water-content of sediments as the  $P$ – $T$ -conditions increase progressively. Ultramafic rocks, in contrast, are often anhydrous mantle rocks and are initially converted to hydrous low grade serpentinites. Serpentinization is a retrograde process and normally occurs at the ocean floor (see Sect. 5.7). As a result, anhydrous or partially hydrated mantle assemblages are first converted into the maximum hydrated equivalents (1)–(3) (Fig. 5.4) before the onset of progressive metamorphism. This, in turn, means that prograde metamorphism of serpentinites always affects rocks that have been previously metamorphosed (and metasomatized).

Let us examine prograde metamorphism of the two possible maximum hydrated versions of harzburgite. The rocks are assumed to be in structural and chemical equilibrium in a very low-grade terrain. Two assemblages are possible: Brc + Ctl and Ctl + Tlc (or metastable Ctl + Qtz) respectively. The equilibrium distribution of assemblages is shown in Fig. 5.5 and the relevant reactions are listed in Table 5.1.

The assemblage Ctl + Tlc is replaced by Atg (+ Tlc) at the onset of prograde metamorphism [reaction (5.1), Table 5.1]. Antigorite forms already at temperatures below 200°C. At 250–300°C the maximum temperature for chrysotile is reached and the fibrous serpentine is replaced by antigorite [reaction (5.2)]. Chrysotile represents a very low temperature weathering or alteration product of ultramafic rocks and the stable serpentine mineral with the beginning of greenschist facies conditions is antigorite. Chrysotile and antigorite occur together (metastable) over a wide temperature range of about 100°C in the sub-greenschist facies. Serpentinites in low-grade Alpine ophiolite complexes may contain both chrysotile and antigorite.

Antigorite serpentinites occur over a wide temperature range (Fig. 5.5). The lower limit is given by reaction (5.2) and the antigorite breakdown reactions (5.4) and (5.8) mark the upper boundary. In regional scale orogenic metamorphism, antigorite schist may occur over a  $T$ -interval of  $>300^\circ\text{C}$ . Above about 250°C, MSH rocks may contain two different assemblages depending on bulk composition: Brc + Atg and Atg + Tlc and bulk chemical control on the assemblages can be seen in Fig. 5.4. Harzburgite with a molar Fo/En ratio  $> 0.7$  will contain Brc + Atg, harzburgite with Fo/En  $< 0.7$  consists of Atg + Tlc, and harzburgite with Fo/En = 0.7 will occur as monomineralic antigorite serpentinite.

In regional metamorphism, the assemblage Brc + Atg is replaced by Fo + Atg at about 400°C [reaction (5.3), Table 5.1]. Brucite–antigorite schists are diagnostic rocks for the lower to middle greenschist facies. Note, however, that brucite-bearing antigorite schists normally contain little brucite and careful microscopic examination is required so as not to overlook the mineral (Fig. 5.6a). It is recommended to examine brucite in a reference section before working with unknown samples. The low modal content of brucite in Brc–Atg schists is a consequence of

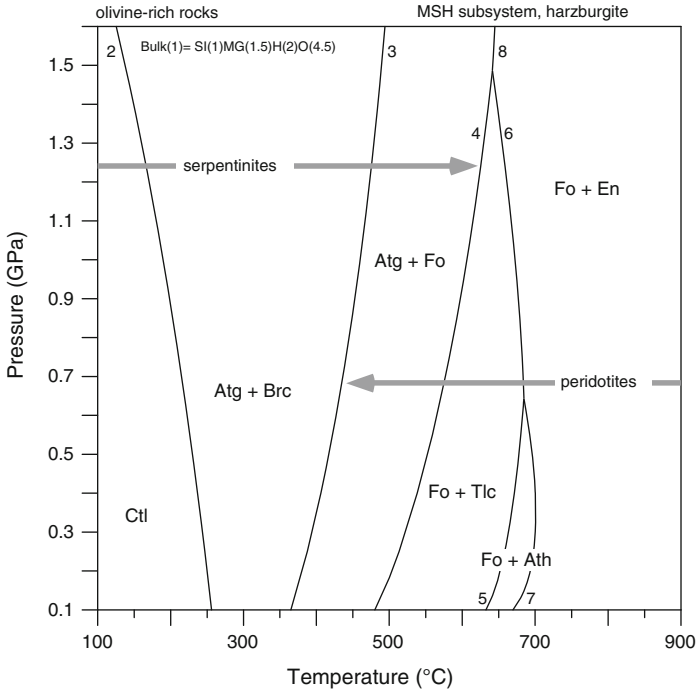


**Fig. 5.5** Assemblage stability diagram for harzburgites showing equilibria in the MSH system, [reactions (5.1)–(5.9); Table 5.1]. The diagram is valid only if pure H<sub>2</sub>O is present as a fluid phase. Reaction (5.4) = upper boundary of serpentinite; Reaction (5.3) = lower limit of peridotite

the chemographic relationships shown in Fig. 5.4. Isochemical serpentinization of dunite should produce a fair amount of brucite. The lack of the Mg-hydroxide is probably caused in meta-dunites by loss due to dissolution in hot water or to reaction with dissolved SiO<sub>2(aq)</sub> in the fluid to form serpentine.

The product assemblage Fo + Atg is diagnostic for upper greenschist to lower amphibolite facies conditions. The upper T-limit of the assemblage Fo + Atg in orogenic metamorphism is about 570–620°C depending on the pressure. Therefore, antigorite serpentinite occurs well within the middle amphibolite facies, but also under blueschist and low-T eclogite conditions (Fig. 5.5). In Alpine ophiolites, for example, that have undergone subduction zone metamorphism, serpentinites occur together with eclogites and blueschists. These are isofacial occurrences and all three rock types formed at the same *P–T* conditions (e.g. 2.7 GPa and 600°C in the Zermatt ophiolite of the Central Alps, Switzerland).

Reaction (5.3) also represents the low-temperature limit for forsterite (Ol) in the presence of an aqueous fluid phase. Olivine represents a stable mineral in ultramafic rocks at conditions as low as middle greenschist facies (~400°C) even if water is present. Pure dunite will not develop any new mineral assemblage and will not be serpentinized above reaction curve (5.3). This is shown in Fig. 5.5 by the peridotite arrow.

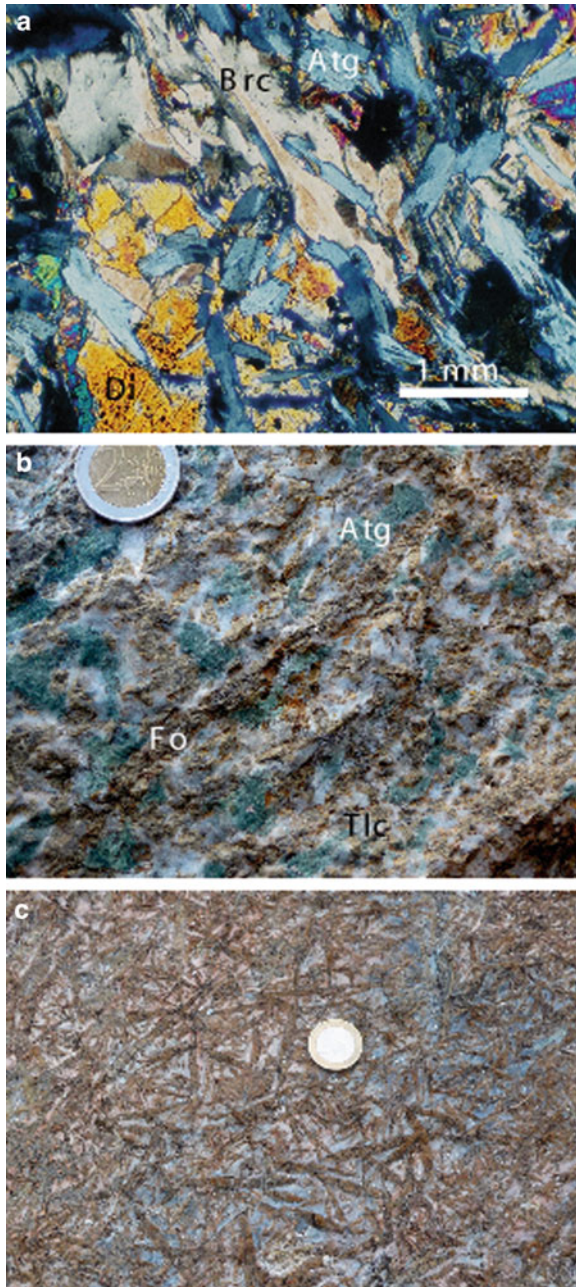


**Fig. 5.6** (a) Lower greenschist facies serpentinite with the diagnostic assemblage brucite–antigorite–diopside. Sognefjell, Jotunheimen, Norway (thin section, crossed polarizers). (b) Antigorite breakdown to talc and olivine [reaction (5.4)]. Relic serpentinite persists as green patches in a matrix made up from the reaction products (Tlc white, Ol brownish). Note elongated shape of olivine. Malenco Serpentinite, Alpe Zocca, Val Ventina, Italian Alps. (c) Needle shaped olivine formed by overstepping of reaction (5.4) boundary in the Bergell contact aureole (Pseudospinifex texture, Evans 1977)

It is important to remember that reaction (5.3) only affects rocks with normative  $Fo/En > 0.7$ . As the widespread assemblage  $Atg + Tlc$  is unaffected by reaction (5.3), such rocks are, in contrast to  $Brc + Atg$  rocks, inappropriate for locating the 400°C boundary in terrains with abundant ultramafic rocks.

The upper thermal boundary for antigorite is given by reactions (5.4) and (5.8) (Table 5.1). The high-temperature limit for serpentinite is ~620°C in subduction zone metamorphism, ~570°C in regional orogenic metamorphism, ~550°C in low-P high-T metamorphism and near 510°C in contact aureoles at 200 MPa. The antigorite breakdown reaction (5.4) may produce spectacular textures that can be easily recognized on outcrop scale (Fig. 5.6b, c). Generally, the last serpentinite disappears approximately with the beginning of middle amphibolite facies conditions in orogenic belts. However, because of the positive slope of equilibrium (5.4) in Fig. 5.5, serpentinites are stable at fairly high temperatures if pressure is high, e.g. in subduction and crustal thickening settings. In high-pressure low-temperature ophiolite complexes produced by subduction of oceanic lithosphere, antigorite schist (serpentinites) often occurs in isofacial associations with 600–650°C eclogite. In recent years, new experimental studies have defined the upper limit of  $Atg$  at super-high pressures (see references and further reading). Furthermore, field evidence supported by new experimental data indicates that the periodicity of the antigorite structure and, consequently, its composition systematically varies with increasing grade (see references).

Reaction (5.8) defines the high-T limit of  $Atg$  at pressures greater than ~1.4 GPa. The reaction produces enstatite from antigorite. The assemblage  $Atg + En$  has not been reported as a stable equilibrium assemblage in rocks to our knowledge.

The assemblage  $Fo + Tlc$  occupies a ~100–150°C-wide temperature interval along  $P$ – $T$ -paths typical of regional orogenic metamorphism.  $Tlc + Fo$  is the characteristic assemblage at middle amphibolite facies conditions. It is replaced by either  $En + Fo$  [reaction (5.6)] or by  $Fo + Ath$  [reaction (5.5)], depending on the  $P$ – $T$ -path taken during prograde metamorphism. The upper T-limit of the  $Tlc + Fo$  assemblage is near 670°C and relatively independent of pressure.

The invariant point at the intersection of reactions (5.5), (5.6), and (5.7) (Fig. 5.5) defines the maximum pressure for anthophyllite in meta-harzburgites. The precise pressure position of the invariant point depends, among other factors, on the amount of Fe–Mg exchange in the involved minerals. The effect is very small on the temperature position of the equilibria (5.5), (5.6), and (5.7). However, because of the low-angle of intersection of equilibria (5.5) and (5.7), the invariant point may be displaced by several hundred MPa along the slightly displaced equilibrium (5.6).

Nevertheless, anthophyllite + forsterite schists and felses occur in contact aureoles and low-P type metamorphism. The assemblage is often related to partial hydration (retrogression) of  $En + Fo$  rocks during cooling and uplift in regional orogenic metamorphism. Prograde sequences in typical collision belts (such as the Scandinavian Caledonides) are characterized by enstatite forming from  $Fo + Tlc$ , and with anthophyllite as a product of retrogression. Reactions (5.5) and (5.6) mark the approximate beginning of upper amphibolite facies conditions.

In contact aureoles, anthophyllite decomposes in the presence of forsterite according to reaction (5.7) at temperatures near 700°C. The harzburgite assemblage En + Fo has a low-temperature limit (~670°C) in the presence of an aqueous fluid. The limit is defined by reactions (5.6) and (5.7), respectively. Towards higher temperatures, the assemblage Fo + En remains stable at all geologically possible temperatures in the crust.

## 5.4 Metamorphism in the CMASH System

### 5.4.1 Progressive Metamorphism of Hydrated Al-Bearing Lherzolite

Assemblage stabilities and CMASH equilibria appropriate for ultramafic rocks are presented in Fig. 5.7 for the average bulk composition of serpentinites from the Zermatt-Saas meta-ophiolite (Li et al. 2004). Calcium, if present, is stored in ultramafic rocks in three minerals; tremolite (Tr), diopside (Di) and under rather extreme conditions plagioclase (An). At low temperatures of the sub-greenschist

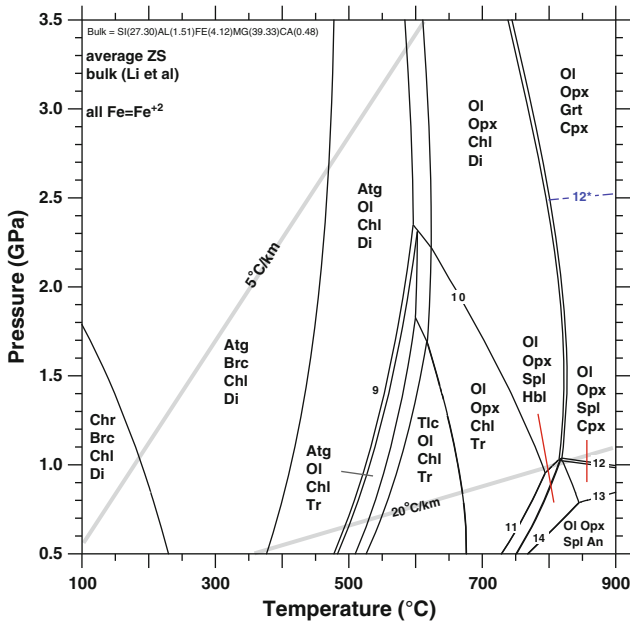


**Fig. 5.7** Assemblage stability diagram for the average serpentinite composition of the Zermatt-Saas ophiolite (Li et al. 2004). Reaction numbers refer to Table 5.1. Reaction (5.12)\* is an example of a displaced reaction (5.12) limiting Grt peridotite towards lower pressure for rocks that contain components stabilizing spinel relative to garnet (see text)

and greenschist facies the presence of the pyroxene diopside is perhaps somewhat surprising. However, chemically pure, white-colored diopside is widespread in serpentinites and occurs in Atg + Brc, Atg + Tlc and Atg + Fo schists. Thus metamorphic low-T diopside should not be confused with relic augitic Cpx that is also commonly present in such rocks. The latter Cpx, often displaying diallag lamellae, represents a relic mineral from the mantle assemblage.

Diopside is consumed by reaction (5.9) at about 20–30°C below the upper limit of antigorite [reaction (5.4)]. This has the consequence that rocks containing the product assemblage of reaction (5.9), namely Atg + Fo + Tr, are diagnostic for a narrow range of temperature. The temperature for this assemblage is near 540°C in regional orogenic metamorphism and 500°C in contact aureoles at 200 MPa.

Tremolite is the only calcic mineral in isofacial ultramafic rocks of amphibolite facies grade and disappears from En + Fo rocks at the onset of granulite facies conditions. Tremolite is replaced by diopside in lherzolitic rocks according to reaction (5.10) and the product assemblage Fo + En + Di corresponds to the primary minerals in mantle lherzolite, Ol + Opx + Cpx. The onset of Cpx production in the pure CMASH system is at about 800°C. However, examples of pure CMASH ultramafics are rare. The presence of minor Al<sub>2</sub>O<sub>3</sub>, FeO (Chl, Spl), TiO<sub>2</sub> (Ilm), Na<sub>2</sub>O (fluid), and other elements in natural lherzolites has the consequence that calcic amphibole (Cam) becomes increasingly aluminous, sodic and titaniferous (etc.) at high temperatures. Also, the Cpx product of reaction (5.10) will not be pure diopside. Partitioning of the “extra components” between Ca-amphibole and clinopyroxene results in a substantial increase of the amphibole field towards higher temperatures so that the precise position of equilibrium (5.10) is composition dependent. Reaction (5.10) marks the amphibolite to granulite facies transition in ultramafic rocks and curve (5.10) in Fig. 5.7 is only valid for the rock composition used. The breakdown of amphibole with a moderate departure from a tremolite end-member composition (~30% tremolite + 70% pargasite components) is at higher T than the model shown in Fig. 5.7.

**Aluminum**, if present, occurs almost exclusively in Mg-chlorite in low-temperature hydrated ultramafic rocks. Mg-chlorite is a very stable mineral in quartz-free rocks such the ultramafic rocks. At 1.0 GPa, corresponding to the base of the crust, Mg-chlorite is stable to temperatures exceeding 800°C, that is to granulite facies conditions. During orogenic and contact metamorphism, it decomposes to Fo + En and spinel according to reaction (5.11) in the MASH system. However, the presence of “extra” components has a dramatic effect on the thermal stability of chlorite (Fig. 5.7). In the case of chlorite breakdown, iron strongly partitions into the spinel phase (as hercynite and magnetite components), so that equilibrium (5.11) becomes divariant. The assemblages Fo + Opx + Tr + Chl and Fo + Opx + Tr + Spl are separated by a marked divariant assemblage field for Fo + Opx + Tr + Chl + Spl in Fig. 5.7. Prograde spinel is often present as a spinel-hercynite overgrowth on low-grade magnetite originally produced by serpentinization.

In regional orogenic metamorphism at higher pressures, chlorite begins to decompose near 700°C, and amphibole is not removed from the ultramafics below a temperature of about 850°C. Experimental evidence indicates that pure tremolite



decomposes at a temperature about 50°C lower than the maximum temperature for pure Mg-clinochlore, but in rocks, chlorite begins to decompose 150°C before the last amphibole disappears. “Extra” components in ultramafic rocks have opposite effects on the tremolite- and chlorite-out reactions, respectively. They tend to increase the upper limit for Ca-amphibole (Cam) but decrease the upper stability limit for chlorite. In the low-pressure high-temperature region of Fig. 5.7 additional reactions delineate the field for plagioclase in ultramafic rocks. Textural evidence for both reactions are found in nature. Commonly, evidence for reactions (5.13) and (5.14) in olivine- (and Opx-) bearing rocks is indicated by the widespread occurrence of Spl + Cpx and Spl + Cam ± Chl symplectites and rims around decomposing plagioclase. We are not aware of evidence indicating *prograde* plagioclase formation by these reactions. Plagioclase + olivine formed initially by crystallization from a mafic melt and Pl + Ol is widespread in basalts and gabbros (Ol-basalt, Ol-gabbro, troctolite). The same reactions (5.13) and (5.14) also limit the mineral pair in these rocks (see reference to the Allalin gabbro in Chap. 9).

#### 5.4.2 *Effects of Rapid Decompression and Uplift Prior to Cooling*

In many orogenic belts metamorphic rocks experience a period of rapid decompression and uplift after equilibration at T-max of the reaction history. Possible effects related to rapid decompression must always be considered. Suppose a tectonically-emplaced isofacial ultramafic rock has equilibrated (Fig. 5.7) at 700°C and 800 MPa and contains the assemblage Ol + Opx + Tr + Chl. The rock may subsequently follow an isothermal decompression path. In that case, the chlorite breakdown reaction (5.11) may begin to produce some Mg-Fe spinel at pressures below about 600 MPa. The decompression and cooling path may also cross the stability field of the assemblage Ath + Fo that requires access of H<sub>2</sub>O. Indeed, late Ath + Fo is often developed along fractures and in vein systems that have provided access for aqueous fluids during the decompression and cooling history of a regional metamorphic terrain. See also decompression effects in soapstone and sagvandite (Sect. 5.10.2).

### 5.5 Isograds in Ultramafic Rocks

A DOMINO/THERIAK model (see Chap. 4) for prograde metamorphism of ultramafic rocks in the CMASH system is shown in Fig. 5.8. It describes the development of the modal composition as a result of reactions along the 20°C/km shown in Fig. 5.7 for the same bulk composition of the initial serpentinite as used in Fig. 5.7. Metamorphism begins with a serpentinite containing chrysotile, chlorite, brucite, diopside and magnetite. The assemblages successively replace one another as *P-T* conditions gradually increase. The final end product is a peridotite containing

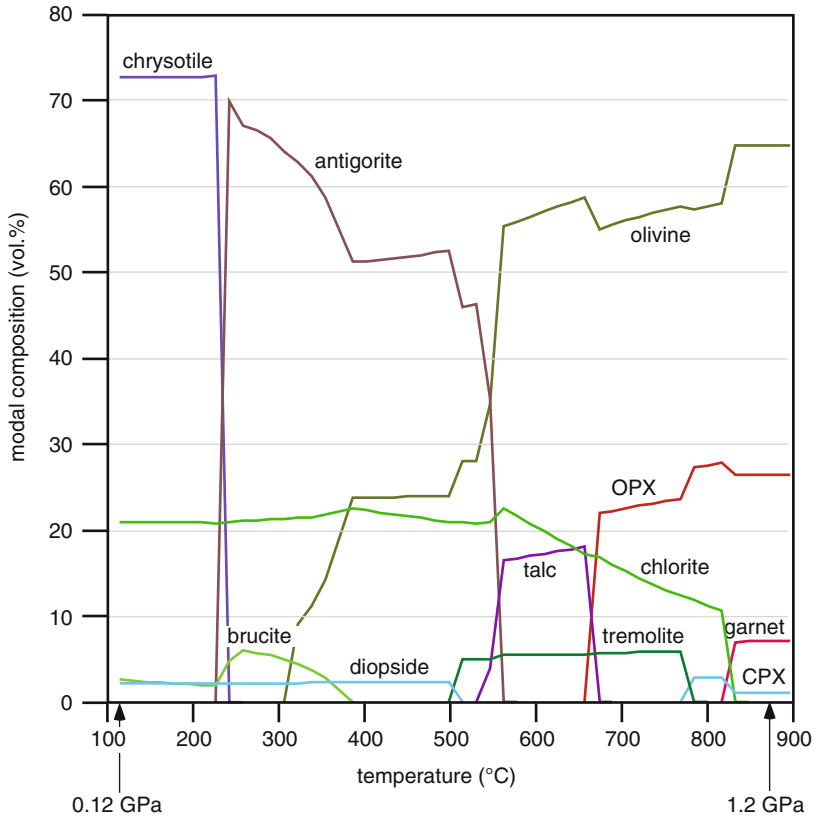


**Fig. 5.8** Model metamorphism of the bulk composition used in Fig. 5.7 along a geothermal gradient of 20°C/km

olivine, enstatite (Opx), garnet and diopside (Cpx). It can clearly be seen on Fig. 5.8 that some modal changes are rather gradual, whilst other changes occur over a narrow  $P$ - $T$  interval and the associated modal changes are rather dramatic. These discontinuities in modal composition of the rock can be used to define isograds in ultramafic rocks (Fig. 5.9).

The successive presence of different minerals in progressively metamorphosed ultramafic rocks is shown in Fig. 5.9 using the data displayed in Fig. 5.8 (same bulk and same  $P$ - $T$  gradient). The discontinuous assemblage boundaries (zone boundaries) shown in Fig. 5.8 are all very well suited for isograd mapping and isograd definition. They are equivalent to reaction isograds because all boundaries are related to well-defined reactions (Table 5.1) in relatively simple chemical systems. As discussed above, there is some overlap of the chlorite and spinel fields, as well as of the tremolite and diopside fields. In low- $P$  metamorphism, (e.g. the contact aureole example shown in Fig. 5.10), reaction isograds at lower grades are displaced to somewhat lower temperatures and a Ath + Fo field may appear near

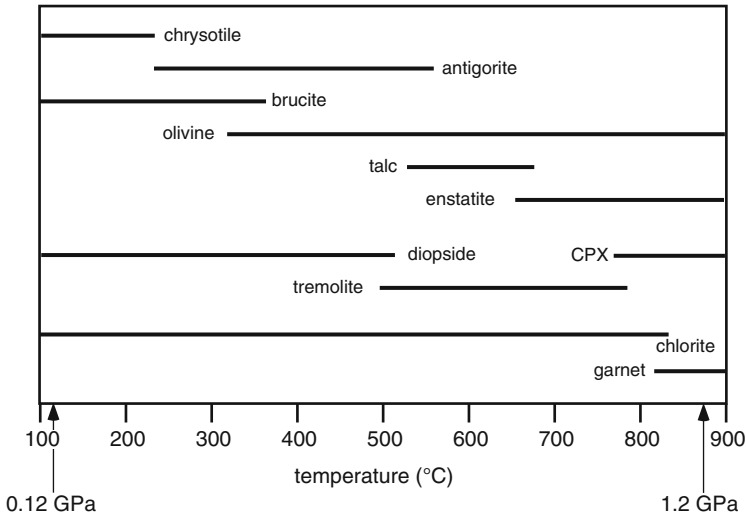


**Fig. 5.9** Mineral zones and isograds in Al-bearing lherzolite (bulk as in Figs. 5.7 and 5.8)

700°C. In such settings, amphibole decomposes at a higher temperature compared to that indicated in Fig. 5.9.

An example of prograde metamorphism of serpentinite is provided by the Malenco serpentinite of the Central Alps that has been heated by the Bergell tonalite intrusion (Trommsdorff and Evans 1972). Field relations are illustrated in Fig. 5.10. Lowest grade rocks are characterized by the assemblage, Atg + Brc + Di. The assemblage occurs outside the map shown on Fig. 5.10. Towards the granite contact, Atg + Ol + Di, Atg + Ol + Tr, Tlc + Ol + Tr and Ath + Ol + Tr progressively form. This sequence can be explained by reactions (5.4), (5.5) and (5.9), respectively, in Table 5.1 and an isobaric heating path between ~450°C and 650°C at an inferred P of ~300 MPa (Fig. 5.5). The antigorite decomposition to talc and forsterite according to the reaction (5.4) is texturally well preserved at Alpe Zocca (Fig. 5.6b, c). The product assemblage is characterized by extremely elongated olivine crystals (so-called pseudo-spinifex texture, Evans 1977). The texture has been described from similar settings and may be related to rapid heating in contact aureoles and consequently resulting in significant overstepping of the equilibrium conditions of reaction (5.4) and a very rapid reaction progress once the first olivine nucleates (Evans 1977).

## 5.6 Mineral Assemblages in the Uppermost Mantle

The top of the upper mantle is situated at a depth of 30–40 km beneath stable continental crust. In tectonically active areas (subduction, collision, rifting), the boundary to the upper mantle may be found anywhere between the surface

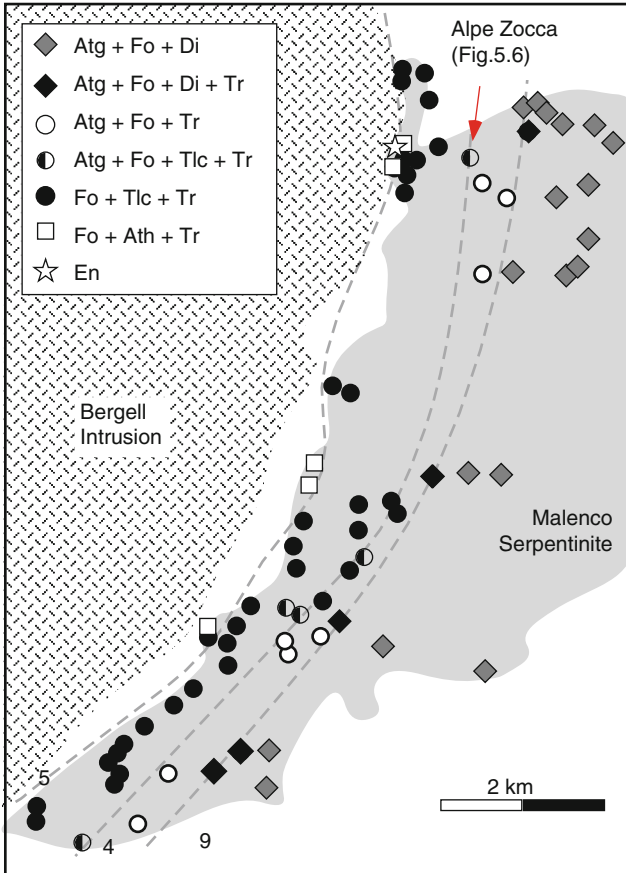


**Fig. 5.10** Map showing distribution of mineral reaction isograds in antigorite schist contact metamorphosed at about 300 MPa by tonalite of the Bergell Intrusion, Western Alps (Trommsdorff and Evans 1972). Isograd reactions (5.4), (5.5) and (5.9) (Table 5.1) are also shown on the models Figs. 5.5 and 5.7. The outcrop Alpe Zocca showing the Atg breakdown texture of Fig. 5.6b, c is indicated

and 70 km depth or even deeper. The precise location of the crust–mantle boundary depends on the state and geological history of the continent. The average depth in stable continental areas corresponds to a pressure of about 1.0 GPa. Since the subcontinental mantle predominantly consists of harzburgite with subordinate lherzolite, a number of interesting conclusions regarding mantle petrology can be drawn from Fig. 5.7.

The 1.0 GPa isobar of the continent–mantle boundary on Fig. 5.7 implies that spinel lherzolite is not stable in the presence of  $H_2O$  at temperatures below  $\sim 820^\circ C$ . Such unusually high temperatures occur in active rift zones or in collision belts undergoing thermal relaxation or in other anomalous hot regions. Harzburgite in the MSH system (Opx–Ol) is not stable below  $\sim 670^\circ C$  if an  $H_2O$ -rich fluid is present at

35 km depth. The temperature at the crust-mantle boundary in Central Europe, for instance, is typically between 600°C and 700°C. Any water reaching the mantle at  $T < 670^\circ\text{C}$  will be consumed by hydration reaction (5.6) [reactions (5.9), (5.10) consume  $\text{H}_2\text{O}$  at even much higher temperatures but affect only lherzolites and/or Al-phases in the rocks]. The assemblage  $\text{Tlc} + \text{Fo} + \text{Tr} + \text{Chl}$  represents the stable mantle assemblage under fluid-present conditions ( $\text{H}_2\text{O}$  fluid) beneath most young continental areas. Under Precambrian shields, the upper mantle temperature usually ranges between 350°C and 450°C (blueschist facies conditions). The upper mantle rocks will, therefore, be transformed into stable serpentinites ( $\text{Brc} + \text{Atg}$ ;  $\text{Atg} + \text{Tlc}$ ;  $\text{Atg} + \text{Fo}$ ) if water crosses the crust–mantle boundary along deep faults and shear zones. Very prominent seismic reflectors observed in the mantle beneath the Celtic Sea and Great Britain (Warner and McGeary 1987) are probably caused by partially hydrated mantle rocks (serpentinites).

Beneath most continental areas there are two types of mantle rocks: (1) weakly hydrated or completely anhydrous peridotites may occur under fluid-absent conditions or in areas with absolutely abnormally high geothermal gradients; and (2) partially or fully hydrated ultramafic rocks (serpentinites and talc-schists) under fluid present conditions.

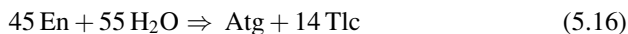
## 5.7 Serpentinization of Peridotite

Serpentinization of mantle rocks occurs normally in three different environments: (1) in oceanic ophiolite complexes where serpentinization is related to oceanic metamorphism, (2) in the crust during formation of collision belts, and (3) in the mantle itself (see above). Low temperature alteration of peridotites in ophiolite and other associations is a process of retrogression and hydration.

Generally, if an ultramafic rock (e.g., mantle lherzolite, harzburgite or dunite) is subjected to conditions to the left of reaction (5.4) and (5.8) in Figs. 5.5 and 5.7 it will be partially or fully serpentinized in the presence of an aqueous fluid. It follows from Fig. 5.7 that the first serpentine forms between 620°C (2.5 GPa) and 520°C (0.5 GPa). At 100 MPa the first serpentinization may occur at 580°C (Fig. 5.5). The reaction (5.4) (Table 5.1) describes the equilibrium serpentinization process at low pressure where enstatite has been completely hydrated to the  $\text{Tlc} + \text{Fo}$  assemblage during cooling [reaction (5.6), Table 5.1]. If  $\text{H}_2\text{O}$  is introduced to dry peridotite ( $\text{Fo} + \text{En}$ ) at  $T$  below reaction equilibrium (5.4), serpentinization of enstatite at low  $P$  occurs through the metastable reaction (5.15):



Serpentinization by reaction (5.15) produces either  $\text{Atg} + \text{En}$  (all  $\text{Fo}$  used up) or  $\text{Atg} + \text{Fo}$  (all  $\text{En}$  used up). The assemblage  $\text{Atg} + \text{En}$  is metastable at pressures where serpentinization normally occurs. The remaining  $\text{En}$  is then removed by the metastable reaction (5.16):



If the product assemblage of serpentinization by reaction (5.15) is Atg + Fo, then the olivine is removed by the reaction (5.3):

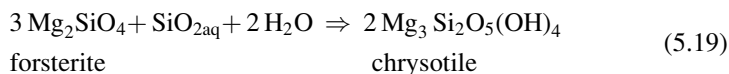
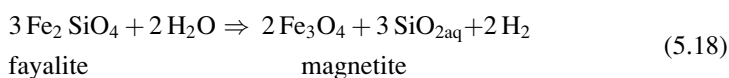


Equilibrium of reaction (5.3) is at about 400°C at low pressures (Fig. 5.5). The last olivine, also mantle olivine, is not serpentinized before the peridotite has cooled to conditions at the beginning of the lower greenschist facies. Very common is, however, that some portions of peridotite mantle slices remain anhydrous and cool to near surface temperature. Serpentinization of peridotite in very low-T environments occurs initially via the metastable reaction (5.17) that produces the metastable low-T serpentine mineral chrysotile:



Remaining Fo or En is then hydrated by reactions involving talc and chrysotile or by open system reactions that remove or add components dissolved in water (e.g. reaction (5.19)).

The presence of iron in ultramafic rocks complicates somewhat the general serpentinization process described above. Both chrysotile and antigorite are Fe-pure minerals that are unable to accommodate the iron present in mantle olivine and orthopyroxene. Although the reactions above describe serpentinization of the Mg-end members of olivine (Fo) + orthopyroxene (En), they do not describe the decomposition of the respective fayalite (Fa) and ferrosilite (Fs) components in these minerals. The following reaction scheme illustrates the serpentinization of Fe-bearing olivine, e.g. with the composition  $\text{Fo}_{90} \text{Fa}_{10}$ .



Reaction (5.18) oxidizes the Fa-component to magnetite and releases  $\text{SiO}_2$  that, in turn, is consumed by reaction (5.19) to form serpentine from the Fo-component. Because olivine in mantle rocks always contains much more Fo than Fa, all  $\text{SiO}_2$  released by reaction (5.18) will be consumed by reaction (5.19). Equilibrium of reaction (5.18) depends on the hydrogen pressure in the fluid. Oxidation of the Fa-component to magnetite is written with  $\text{H}_2\text{O}$  as an oxidizing agent and with  $\text{H}_2$  gas as a reaction product because hydrogen gas has been observed in settings that undergo present day serpentinization (see references).  $\text{H}_2$  can readily be linked to  $\text{O}_2$  and oxygen activity (fugacity) via the equation  $2 \text{H}_2\text{O} = 2 \text{H}_2 + \text{O}_2$ . Three to five

vol. % magnetite typically occurs in many serpentinites and often nucleates on primary chromite (Cr-spinel). The resulting assemblage of the overall process is chrysotile (serpentine) + magnetite, with some remaining unreacted, partly resorbed grains of olivine.) The reaction of 1 mol Fa produces enough silica to serpentinize 3 mol of Fo. Hence, a  $\text{Fo}_{75}\text{Fa}_{25}$  olivine can be turned into serpentine and magnetite without leaving any residual, unreacted olivine. However, most olivine is more magnesian than this, and a small amount of brucite may appear as an additional product (Fig. 5.6a). Because  $\text{Mg}(\text{OH})_2$  (Brc) is highly soluble in water, the excess Mg-component is normally lost by the ultramafic rock during low-T serpentinization. The extra Mg-component may also combine with additional components in the serpentinization fluid to form a variety of secondary minerals such as dolomite, sepiolite or saponite, for example.

With progressive metamorphism of such a Ctl + Mag rock, the iron remains fixed in magnetite and does not dissolve in the product phases of the reactions listed in Table 5.1. As a result, olivine and orthopyroxene produced by prograde metamorphism of serpentinites are usually very Mg-rich in contrast to primary mantle peridotites where Ol and Opx normally have lower  $X_{\text{Mg}}$ .

Low-temperature alteration of high-T clinopyroxene (Al, Ti-rich Cpx) results in the decomposition of the pyroxene and the formation of chlorite and a pure diopside (the latter is stable in very low-temperature environments as discussed above). A frequent byproduct of this process is titanoclinohumite a dark-red-brown mineral that is widespread in serpentinites of some orogenic belts e.g. the Alps and absent in others e.g. the Scandinavian Caledonides (see references).

## 5.8 Ultramafic Rocks at High Temperature

At temperatures above about 700°C ultramafic rocks contain some very characteristic mineral assemblages. The assemblage stabilities of some of these are shown in Fig. 5.7. Ultramafic rocks with characteristic anhydrous high-T assemblages occupy three *P-T*-fields in Fig. 5.7. All contain the assemblage Ol–Opx–Cpx but three different Al-minerals: garnet at high pressure, spinel at intermediate pressure and anorthite at low pressure. These rocks are referred to as garnet lherzolite, spinel lherzolite and plagioclase lherzolites, respectively. If the peridotite does not contain Ca, spinel is the Al-mineral also at low pressure. Towards lower temperatures, the three anhydrous assemblages are limited by hydration reactions that produce chlorite from the respective Al-mineral and amphibole from Cpx.

Rocks containing olivine + plagioclase are diagnostic for low pressure of formation. Because the assemblage requires very high temperatures (>800°C), olivine + plagioclase rocks are typically found in crustal mafic intrusions (i.e. <600 MPa) containing olivine gabbro and troctolite, and are therefore igneous. As mentioned earlier, no prograde metamorphic example of plagioclase formation in olivine-rich rocks has, to our knowledge, been reported to date, but it could be expected to form in a low-P granulite facies terrain containing ultramafic rocks.

Spinel-lherzolites contain Spl + Cpx in addition to Opx + Ol and are related to plagioclase-lherzolite by reaction (5.13). Such rocks are widespread in granulite facies terranes and in hot regions of the uppermost mantle.

Garnet replaces spinel as the Al-bearing phase in anhydrous ultramafic rocks at higher pressures, i.e.  $> \sim 1$  GPa (Fig. 5.7) and reaction (5.12) (given in Table 5.1 for pure MASH components) limits the low pressure stability of Grt + Ol in Al-bearing harzburgites. The presence of calcium in lherzolites has the consequence that garnet which is a reactant phase of reaction (5.12), contains Ca as grossular component, thus expanding the stability field for Ca-Mg-garnet + olivine. However,  $\text{Fe}^{2+}$ ,  $\text{Fe}^{3+}$ , Zn, Cr and some other elements that have been fixed mostly in chlorite at lower grade are strongly fractionated into the spinel phase, which has the effect that the assemblage stability for spinel lherzolite is dramatically expanded to higher pressure compared to the simple model shown on Fig. 5.7. Typically, garnet peridotites are associated with pressures of 3 GPa and more, corresponding to mantle depth of about 80–100 km, but they may form at pressures of 2 GPa or even lower in relatively pure MASH rocks.

Garnet-lherzolite bodies (lenses of a meter to kilometer size) originating from  $> 50$  km, or often even  $> 100$  km depth occur sporadically in orogenic belts, e.g. the UHP Western Gneiss region of Norway (Fig. 5.2), the Western Alps and the Dabie–Sulu metamorphic belts, China (see references). Many of these garnet-peridotites preserve mineralogical evidence (e.g. microdiamonds) of very high pressure metamorphism ( $P > 6$  GPa). These UHP Grt peridotites can be related to deep subduction of continental crustal host rocks into which they have become entrained.

## 5.9 Thermometry and Geobarometry in Ultramafic Rocks

Geothermobarometers applicable to ultramafic rocks include: intercrystalline Fe–Mg exchange between any pair of anhydrous Fe–Mg phases in ultramafic rocks, e.g. Ol–Spl, Ol–Grt, Opx–Cpx; intracrystalline Fe–Mg exchange in Cpx; temperature dependence of miscibility gap between En–Di, Mg–Tschermak content in Opx in various defining assemblages, e.g. Opx–Grt; Ca–Tschermak content in Cpx in a number of assemblages, e.g. Cpx–Ol–Spl.

Most of the listed geothermobarometers obviously can only be used for estimating equilibration  $P$  and  $T$  for ultramafic rocks metamorphosed in the eclogite- and granulite-facies (also contact metamorphic pyroxene-hornfels), but in greenschist- and amphibolite-facies ultramafic rocks, thermobarometers are lacking. Estimates of  $P$ – $T$  from such rocks depend entirely on petrogenetic grids and reactions involving volatile species and this requires assumptions or estimates of the activities of volatile species ( $\text{H}_2\text{O}$ ). For progressive metamorphism,  $\text{H}_2\text{O}$ -saturated conditions are usually assumed (as in Figs. 5.5–5.8), but in terrains with a poly-metamorphic (polyphase) evolution, it is difficult to estimate the activity of  $\text{H}_2\text{O}$  during equilibration of the ultramafic rocks. In many ultramafic rocks the presence of carbonate minerals (magnesite, dolomite) indicates that the fluid cannot be treated as a pure  $\text{H}_2\text{O}$  fluid.



The problem may not be as severe as it first appears. Consider a specific example; a Fo–En-fels contains scattered flakes of talc apparently replacing enstatite and lacking carbonates. The rock also contains veins of talc. Is it possible to estimate the temperature at which talc-formation occurred? The presence of vein-structures can be used as evidence that the talc formation is related to the infiltration of an aqueous ( $\text{H}_2\text{O}$ -rich) fluid. By reference to Fig. 5.5, direct talc formation from enstatite by reaction (5.6) requires pressures in excess of 600 MPa and temperatures below 640–670°C. The minimum temperature is given by the position of reaction (5.4) in Fig. 5.5 because the alteration did not produce antigorite.

## 5.10 Carbonate-Bearing Ultramafic Rocks

Carbonate minerals (magnesite, calcite and dolomite) are found in many ultramafic rocks. In the Scandinavian Caledonides, for example, almost all Alpine-type ultramafic rocks contain carbonate in a wide variety of associations with silicates and oxides. Although in some cases the carbonate minerals are probably of mantle origin, most ultramafic rocks in the crust are carbonated in the same way as they are hydrated. Infiltration of external  $\text{CO}_2$  into ultramafic rocks leads to the production of carbonate minerals. Maximum hydrated and carbonated low temperature varieties of ultramafic rocks such as talc + magnesite + dolomite rocks or antigorite + talc + dolomite rocks still fall within the composition field of typical mantle rocks (see chemographical relationships in Fig. 5.3).

Phase relationships in carbonate-bearing ultramafic rocks are relatively complex and can provide excellent information about  $P$ – $T$  regimes in a particular metamorphic terrain. Two specific geologic settings will be used to demonstrate the usefulness of analyzing phase relationships in carbonate-bearing ultramafic rocks, although it is obvious that they cannot cover all possible geological situations. We therefore recommend modification of phase diagrams Figs. 5.11 and 5.12 for use in other metamorphic environments.

### 5.10.1 Metamorphism of Ophicarbonates

Serpentinites containing carbonate minerals in appreciable amounts are referred to as ophicarbonates (ophicalcite, ophimagnesite, ophi..) that typically form from carbonate-free serpentinites by reaction with crustal  $\text{CO}_2$  given off by progressive decarbonation reactions in carbonate-bearing metasediments. Serpentinites are very efficient  $\text{CO}_2$  buffers and small amounts of  $\text{CO}_2$  in a fluid are sufficient to convert serpentine assemblages into carbonate-bearing assemblages.

As an example, Fig. 5.11 shows an isobaric assemblage stability  $T$ – $X$ -diagram at 100 MPa relevant to ophimagnesite rocks. Stoichiometries of some carbonate-involving reactions are given in Table 5.2 and two dehydration reactions relevant

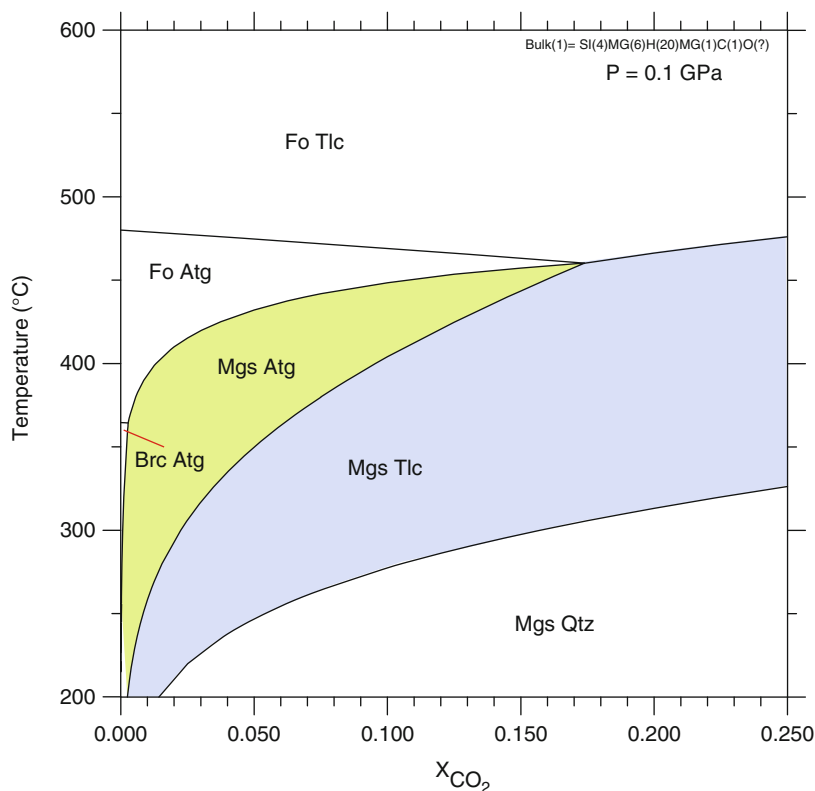


**Fig. 5.11** Assemblage stability diagram for magnesite-bearing ultramafic rocks in the system MS-HC at 100 MPa. The ophimagnesite assemblage is shown in *green*, the soapstone assemblage in *blue*

**Table 5.2** Selected carbonate-involving reactions in serpentinite, soapstone and sagvandite

$45\text{Mgs} + 17\text{Tlc} + 45\text{H}_2\text{O} \Rightarrow 45\text{CO}_2 + 2\text{Atg}$	(5.20)
$\text{Atg} + 20\text{Mgs} \Rightarrow 31\text{H}_2\text{O} + 20\text{CO}_2 + 34\text{Fo}$	(5.21)
$\text{Tlc} + 5\text{Mgs} \Rightarrow 4\text{Fo} + 5\text{CO}_2 + \text{H}_2\text{O}$	(5.22)
$\text{Tlc} + \text{Mgs} \Rightarrow 2\text{En} + \text{CO}_2 + \text{H}_2\text{O}$	(5.23)
$2\text{Mgs} + \text{En} \Rightarrow 2\text{Fo} + 2\text{CO}_2$	(5.24)

to Fig. 5.11 involving antigorite [reactions (5.3) and (5.4)] have been discussed previously and are listed in Table 5.1. The  $T$ - $X_{\text{CO}_2}$  diagram shows fields for the ophimagnesite Atg + Mgs assemblage in green and for the soapstone assemblage Tlc + Mgs in blue. It follows from Fig. 5.11 that Atg + Brc tolerates almost no  $\text{CO}_2$  and is converted to Atg + Mgs at very low levels of  $\text{CO}_2$  in the fluid. The ophimagnesite Atg + Mgs assemblage reacts with  $\text{CO}_2$  to soapstone. Also Atg + Fo is not stable in fluids with  $X_{\text{CO}_2} > 0.17$  and reacts with  $\text{CO}_2$  to yield Tlc + Mgs. On the other hand, soapstone decomposes to ophimagnesite at  $X_{\text{CO}_2} < 0.17$  and to Tlc + Fo at higher a  $\text{CO}_2$  content of the fluid during prograde metamorphism.

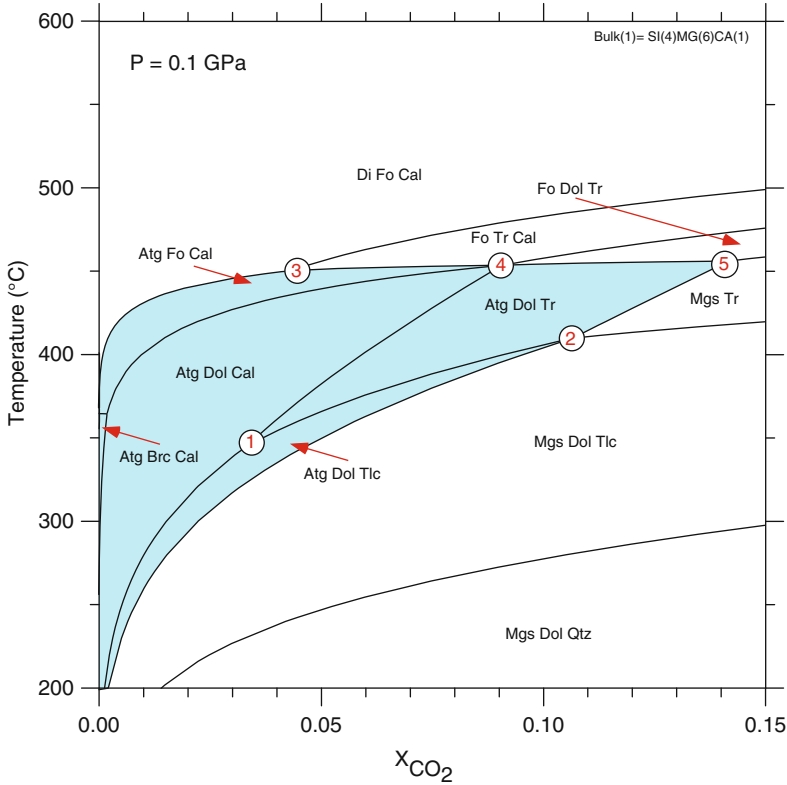
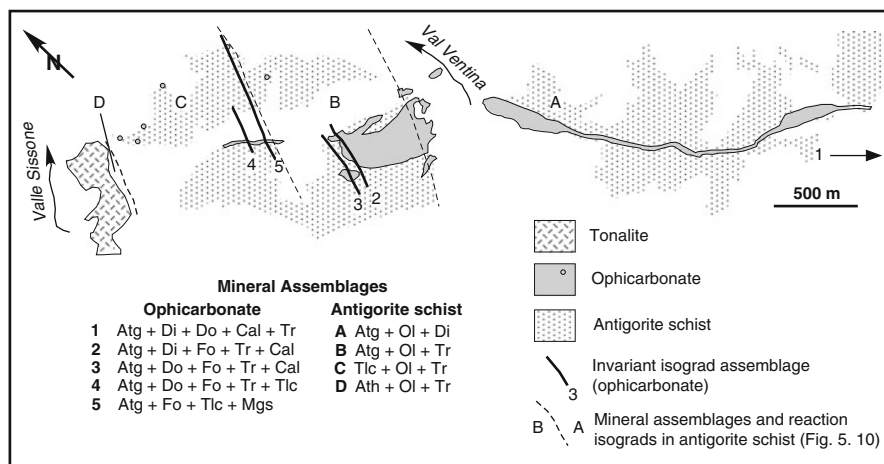


**Fig. 5.12** Assemblage stability diagram for carbonate-bearing ultramafic rocks in the system CMS-HC at 100 MPa. The opihcarbonate assemblages are shown in *blue*

The positions of the equilibria are displaced to higher  $T$  with increasing  $P$  while at lower pressure other topologic configurations may become stable so that the figure needs to be recalculated for higher or lower pressure terrains.

Figure 5.12 is an example of an assemblage stability diagram for rocks in the CMS-HC system at 100 MPa. The blue field on Fig. 5.12 indicates that antigorite-bearing rocks are stable at  $X_{\text{CO}_2} < 0.14$  (point 1) and  $T < 450^\circ\text{C}$ . Prograde metamorphism replaces the Atg-bearing assemblages with three different carbonate-bearing assemblages all with olivine and a Ca-silicate (Tr or Di). Because antigorite is stable only under condition of low  $\text{CO}_2$  in the fluid phase, serpentinites emplaced in the crust can be very efficient  $\text{CO}_2$  absorbers with the opihcarbonate field in blue separated from carbonate-free serpentinite essentially along the pure  $\text{H}_2\text{O}$  axis of Fig. 5.12. The assemblage antigorite + calcite is diagnostic for extremely  $\text{H}_2\text{O}$ -rich fluids.

The invariant points shown in Fig. 5.12 comprise five minerals each. These isobaric invariant assemblages can be used to map isograds in opihcarbonate rocks. The isograd temperatures at 100 MPa for the isobaric invariant assemblages on



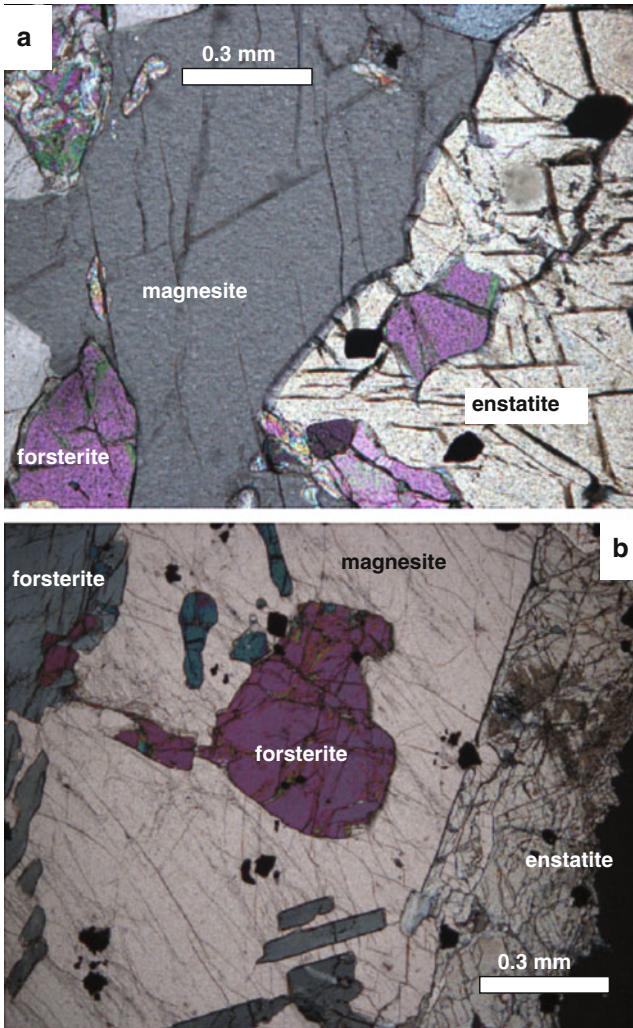
**Fig. 5.13** Map showing distribution of isobaric invariant assemblage isograds in ophicarbonate and reaction isograds in host antigorite schist (see also Fig. 5.10) metamorphosed by tonalite of the Bergell Intrusion, Western Alps (combined and simplified from Fig. 2 of Trommsdorff and Evans 1977 and Fig. 2 of Trommsdorff and Evans 1972)

Fig. 5.12 are: (1) 350°C: Atg–Tlc–Tr–Dol–Cal, (2) 410°C: Atg–Tlc–Tr–Mgs–Dol, (3) 450°C: Atg–Fo–Tr–Di–Cal, (4) 455°C: Atg–Fo–Tr–Dol–Cal, (5) 450°C: Atg–Fo–Tr–Mgs–Dol.

The positions of a set of isograds have been mapped by Trommsdorff and Evans (1977) in a band of ophicarbonate within antigorite schist that has been contact metamorphosed by tonalite, Central Alps (Fig. 5.13; see also with Fig. 5.10). The temperature resolution of the isograds is considered to be within a few degree Celsius. A petrologic tool with such a high temperature resolution is unusual and where possible we strongly recommend to study and map ophicarbonate assemblages for investigating the detailed thermal structure of a metamorphic terrain. Note that the isobaric invariant assemblage (2) of Fig. 5.13 corresponds to the assemblage (3) in Fig. 5.12 and assemblage (3) on Fig. 5.13 is identical with assemblage (4) on Fig. 5.12. The other mapped isograd assemblages of Fig. 5.13 do not appear on Fig. 5.12 because the estimated pressure in the Bergell aureole (Fig. 5.13) is 300 MPa and not 100 MPa as on Fig. 5.12. This shows that for detailed analysis of ophicarbonate rocks one needs to compute the assemblage stability diagrams at the appropriate pressure.

### 5.10.2 Soapstone and Sagvandite

Soapstone is an ultramafic rock containing predominantly talc + magnesite (or dolomite). Sagvandite is an ultramafic rock consisting of abundant enstatite + magnesite (Fig. 5.14). Both rock types usually develop from ordinary carbonate-free ultramafic rocks by interaction with an externally-derived CO<sub>2</sub>–H<sub>2</sub>O fluid



**Fig. 5.14** Textural expression of the sagvandite reaction (5.24) (Table 5.2). Olivine reacts with  $\text{CO}_2$  and binds the volatile into magnesite. Olivine is very strongly resorbed and product enstatite perfectly euhedral as a result of progress of carbonation reaction:  $\text{Ol} + \text{CO}_2 = \text{Mgs} + \text{En}$ . (a) Resorbed forsterite in euhedral enstatite, (b) Resorbed forsterite in magnesite. Ørnes sagvandite body, Nordland, Norway

phase. Fragments of ultramafic mantle rocks emplaced in the crust are normally accompanied by partly carbonated versions of these rocks.

Relevant reactions in harzburgite involving a binary  $\text{CO}_2\text{--H}_2\text{O}$  fluid are shown on two isothermal  $P\text{--}X_{\text{CO}_2}$  diagrams at  $650^\circ\text{C}$  and  $675^\circ\text{C}$ , respectively (Fig. 5.15). Magnesite is the only carbonate mineral considered. The two diagrams show the distribution of diagnostic assemblages for harzburgite (Fo + En) rock compositions

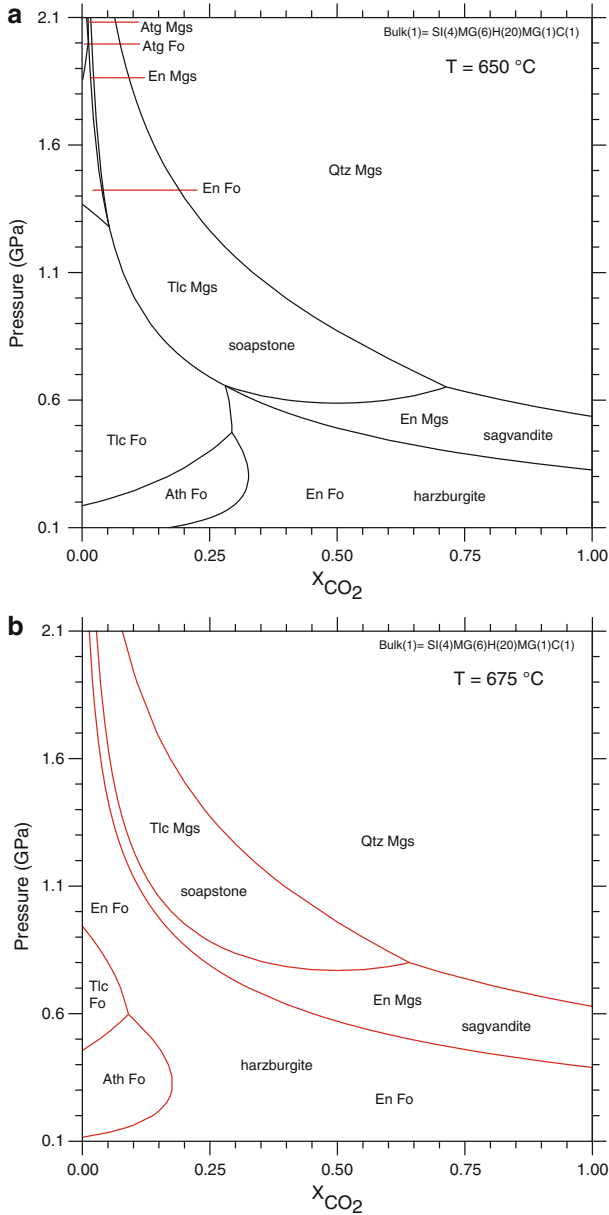


**Fig. 5.15** Magnesite-bearing ultramafic rocks. (a) isothermal section at  $650^\circ C$ : sagvandite = En + Mgs; soapstone = Tlc + Mgs; ophicarbonates = Atg + Mgs. (b) isothermal section at  $675^\circ C$ . *Note:* the very different P–X-topologies at a  $\Delta T$  of only  $25^\circ C$ . Harzburgite is not stable at mantle pressures in the presence of a fluid phase at  $T = 650^\circ C$  and below. At  $T = 675^\circ C$ , harzburgite may coexist with an extremely  $H_2O$ -rich fluid at mantle depth (it is not stable in the presence of  $CO_2$ )

at middle amphibolite facies temperatures as a function of pressure (depth). The magnesite-absent reactions (5.4), (5.7), (5.8), and (5.9) (Table 5.1) have been discussed above (e.g. Fig. 5.5) and reactions (5.21), (5.22) and (5.24) (Table 5.2) separate magnesite-bearing from carbonate-free assemblages. The three major types of carbonate-bearing ultramafic rocks are (see also Fig. 5.11), Atg + Mgs (ophimagnesite), Tlc + Mgs (soapstone) and En + Mgs (sagvandite) (shaded fields in Fig. 5.15). Ophicarbonates are linked to soapstones by reaction (5.20), the soapstones are separated from sagvandites by reaction (5.30) (Table 5.2).

At low pressures carbonate saturation is not reached even in pure CO<sub>2</sub> fluids. For instance, in Fig. 5.15a at 200 MPa fluid pressure and 650°C, the stable assemblage in pure H<sub>2</sub>O fluids is Fo + Tlc (compare with Fig. 5.5). In the fluid composition range X<sub>CO<sub>2</sub></sub> 0.05–0.42, Fo + Ath replaces Fo + Tlc and Fo + En represents the stable assemblage in CO<sub>2</sub>-rich fluids (X<sub>CO<sub>2</sub></sub> up to 1.0). At higher pressures, carbonate-free rocks coexist with H<sub>2</sub>O-rich fluids and magnesite forms at the expense of forsterite if the fluid contains CO<sub>2</sub>. With increasing pressure forsterite breakdown in CO<sub>2</sub>-bearing fluids produces first enstatite [reaction (5.24)], then talc [reaction (5.22)] and finally antigorite [reaction (5.21)]. In most carbonate-bearing ultramafic rocks the composition of the fluid phase is controlled by reactions (5.21), (5.22), and (5.24). Magnesite + quartz assemblages are extremely rare, which suggests that in most metamorphosed ultramafic rocks forsterite is not completely exhausted by the three reactions above.

At 650°C, there exists an isothermal invariant point at 600 MPa and X<sub>CO<sub>2</sub></sub> = 0.45. The invariant assemblage Fo + En + Tlc + Mgs is widespread in Alpine-type ultramafic rocks from many orogenic belts and different processes may lead to its formation. With increasing pressure, harzburgite may, in the presence of a CO<sub>2</sub>–H<sub>2</sub>O fluid, undergo partial carbonation by reaction (5.24) to produce En + Mgs from Fo (Fig. 5.14). The progressing reaction buffers the fluid composition to the invariant point and, finally, the invariant reaction produces Tlc. In contrast, soapstone and a CO<sub>2</sub>–H<sub>2</sub>O fluid may reach reaction (5.23) along a decompression path by which enstatite is formed. The rock may eventually reach the invariant reaction point at which new forsterite will also form.

At a temperature that is only 25°C higher, i.e. 675°C, the invariant assemblage (at the intersection of reactions 24 and 25 in Fig. 5.15b) is at very high pressure and outside the *P*–*X* window indicated for 650°C. The significant difference between the two *T*–*X*<sub>CO<sub>2</sub></sub> diagrams can best be appreciated by focusing on the Fo + En (=harzburgite) stability field. At 650°C, harzburgite is not stable at mantle depths in the presence of a fluid phase. This means that in the mantle, harzburgite would efficiently bind all CO<sub>2</sub>–H<sub>2</sub>O fluids and convert to either soapstone or ophicarbonate depending on depth. It also means that there is no free fluid phase in the mantle at this temperature (because there is abundance forsterite). In contrast, at 675°C harzburgite at mantle depth can coexist with a fluid phase, but the composition of the fluid is H<sub>2</sub>O-rich. CO<sub>2</sub>-rich fluids would be consumed by reaction (5.24) to form sagvandite and no CO<sub>2</sub>-rich fluids can survive in the mantle under these conditions. If the typical crust–mantle boundary is at about 1.0 GPa, the 650–675°C temperature range is an important interval for the transition from fluid-absent to fluid-present

conditions in the uppermost mantle beneath continents. Temperatures of 650–675°C at the crust–mantle boundary are characteristic for younger continental areas, but beneath Precambrian shields the temperature is significantly less and in areas that experience active extension and rifting it can be much warmer (and even CO<sub>2</sub>-rich fluids may cross the interface).

The above discussion of mineral reactions and phase relations in soapstone and sagvandite has been restricted to the MS-HC system. Ca-bearing ultramafic rocks give rise to a number of additional reactions and diagnostic assemblages, particularly important being reactions involving Dol, Tr, and Di. However, the relationships, reactions and assemblages presented above for the MS-HC system are also valid in a more complex system (e.g. CMAS-HC) and phase equilibria of carbonate-bearing spinel–lherzolitic bulk compositions are very useful for deciphering details of the metamorphic evolution of a particular terrane.

## 5.11 Open System Reactions in Ultramafic Rocks

Alpine-type peridotite bodies incorporated in collision belts are chemically dissimilar from surrounding crustal gneiss and granite that enclose them. As a result, ultramafic rock lenses are vulnerable to metasomatism and open system reactions. Along the contacts of the ultramafic rock fragments to the crustal rocks exchange of components between the dissimilar rocks result in the formation of so-called black-walls (see Fig. 3.3). Typically SiO<sub>2</sub> is added to the ultramafic rocks as SiO<sub>2aq</sub> dissolved in crustal fluids and the ultramafic rocks may give off magnesium that then migrates to the crustal rocks. Characteristic examples of open system (allochemical) reactions are: Serpentinization of forsterite by reaction (5.19) as discussed above (Sect. 5.7), and talcization of forsterite by the analogous reaction (5.25):

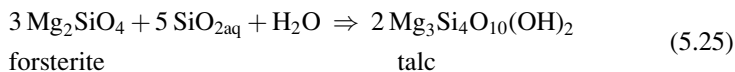
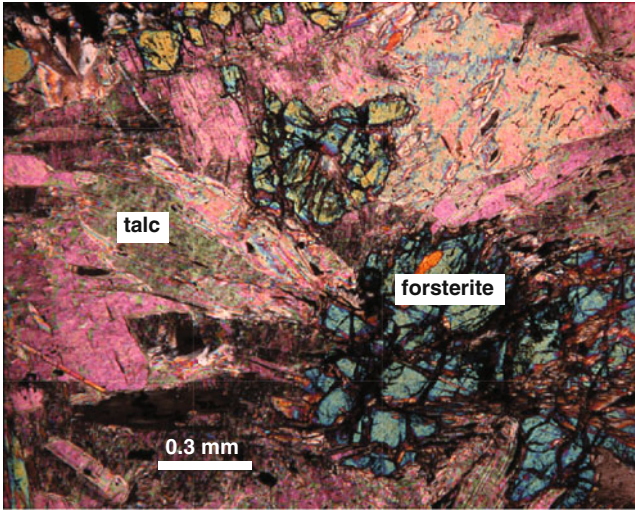


Figure 5.16 shows the textural manifestation of reaction (5.25) in a lens of amphibolite-facies ultramafic rock in the Scandinavian Caledonides (Bucher et al. 2005). Very strongly resorbed forsterite is replaced by talc and the reaction is supported by the supply of SiO<sub>2aq</sub> dissolved in an infiltrating aqueous fluid.

The diagram shown as Fig. 5.17 quantitatively displays the equilibrium conditions of reactions (5.19) (boundary between Fo and Atg if it forms stable Atg rather than metastable Ctl) and reaction (5.25) (boundary between Fo and Tlc). Quartz-saturation occurs along the y-axis at the right-hand side of Fig. 5.17. Note that the standard state for the activity of SiO<sub>2</sub> on Fig. 5.17 is the pure solid at P and T, whereas the open system reactions (5.19) and (5.25) have been written with SiO<sub>2aq</sub>. If one prefers to express the activity of SiO<sub>2</sub> related to the molality of dissolved





**Fig. 5.16** Talcization of olivine by the open system reaction  $Fo + SiO_{2aq} + H_2O = Tlc$ . Murusjøen, N-Trøndelag, Norway

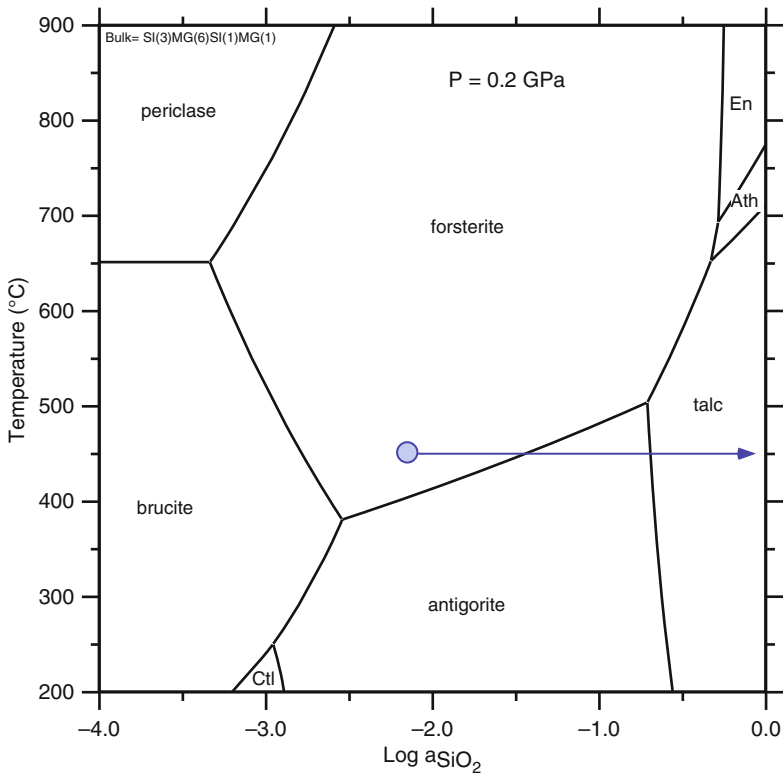


**Fig. 5.17** T- $a_{SiO_{2aq}}$  Diagram at 0.2 GPa for equilibria in the system MSH

$\text{SiO}_{2\text{aq}}$  in the fluid then the x-axis needs to be converted to another standard state. It follows from Fig. 5.17 that talcization of forsterite is restricted to temperatures between 650° and 500°C during cooling of a peridotite (at 200 MPa). Talcization of forsterite (e.g. Fig. 5.16) occurs along the field boundary Fo–Tlc and buffers  $a_{\text{SiO}_2}$  to progressively lower values during cooling. At  $T < 500^\circ\text{C}$  (invariant assemblage Fo–Tlc–Atg), forsterite is converted to antigorite by the Atg-equivalent reaction (5.19). Serpentinization of Fo commences at 500°C and progresses to about 400°C [reaction (5.2)] buffering  $a_{\text{SiO}_2}$  to very low values. However, open system reactions are typically short lived isobaric and isothermal processes. This means that a forsterite rock infiltrated by an  $\text{SiO}_2$ -rich fluid for example at 600°C reaches the Tlc-forming reaction at  $\log a_{\text{SiO}_2}$  about  $-0.4$ . The conversion of forsterite to talc buffers  $a_{\text{SiO}_2}$  to this value. If forsterite finally disappears from the rock  $a_{\text{SiO}_2}$  may continue to increase in the talc rock. A similar process describes isothermal (isobaric) serpentinization of forsterite. However, with increasing  $a_{\text{SiO}_2}$  is also newly formed antigorite converted to talc. The path of  $\text{SiO}_2$  metasomatism of dunite at e.g. 450°C is shown by a blue arrow on Fig. 5.17. Similar diagrams may be computed for other pressures and other mobile components in order to explore open system metamorphism in ultramafic rocks. Also useful are isobaric isothermal activity–activity diagrams.

## 5.12 Potassium-Bearing Peridotites

Some rare mantle peridotites may contain K-bearing phases such as phlogopite and K-amphibole (K-richterite variety). K (and Na) has been introduced to peridotite by devolatilization of felsic rocks during deep subduction of continental crust. Phlogopite stability is controlled by the reaction,  $\text{Phl} + \text{Di} \pm \text{En} = \text{K-amphibole} + \text{Grt} + \text{Fo} + \text{fluid}$  with K-amphibole appearing between 6 and 6.5 GPa at 800°C in the KNCMASH system (Konzett and Ulmer 1999).

## References and Further Reading

### *Cited References*

- Bucher K, de Capitani Ch, Grapes R (2005) The development of a margarite-corundum blackwall by metasomatic alteration of a slice of mica schist in ultramafic rock, Lake Kvesjøen, Norwegian Caledonides. *Can Mineralog* 43:129–156
- Evans BW (1977) Metamorphism of alpine peridotite and serpentine. *Ann Rev Earth Planet Sci* 5:397–447
- Konzett J, Ulmer P (1999) The stability of hydrous potassic phases in the Earth's upper mantle: an experimental study to 9.5 GPa in simplified and natural bulk compositions. *J Petrol* 40:629–652
- Li X-P, Rahn M, Bucher K (2004) Serpentinites of the Zermatt-Saas ophiolite complex and their texture evolution. *J Metamorph Geol* 22:159–177

- Trommsdorff V, Evans BW (1972) Progressive metamorphism of antigorite schist in the Bergell tonalite aureole (Italy). *Am J Sci* 272:487–509
- Trommsdorff V, Evans BW (1977) Antigorite–ophicarbonates: contact metamorphism in Valmalenco, Italy. *Contrib Miner Petrol* 62:301–312
- Warner M, McGeary S (1987) Seismic reflection coefficients from mantle fault zones. *Geophys J R Astron Soc* 89:223–230

### ***Further Reading and Recommended Literature***

- Ballhaus C, Berry RF, Green DH (1990) Oxygen fugacity controls in the Earth's upper mantle. *Nature* 348:437–440
- Barnes I, O'Neil JR (1969) The Relationship between fluids in some fresh alpine-type ultramafics and possible modern serpentinization, Western United States. *Geol Soc Am Bull* 80:1947–1960
- Bodinier J-L, Godard M (2004) Orogenic, ophiolitic, and abyssal peridotites. In: Carlson RW, Holland HD, Turekian KK (eds) *The mantle and core. Treatise on geochemistry*, vol 2. Elsevier-Pergamon, Oxford, pp 103–170
- Brey G, Brice WR, Ellis DJ, Green DH, Harris KL, Ryabchikov ID (1983) Pyroxene-carbonate reactions in the upper mantle. *Earth Planet Sci Lett* 62:63–74
- Brey GP, Köhler T (1990) Geothermobarometry in Four-phase Lherzolites II. New Thermobarometers, and practical assessment of existing thermobarometers. *J Petrol* 31:1353–1378
- Brey GP, Köhler T, Nickel KG (1990) Geothermobarometry in four-phase lherzolites I. Experimental results from 10 to 60 kb. *J Petrol* 31:1313–1352
- Bromiley GD, Pawley AR (2003) The stability of antigorite in the systems MgO-SiO<sub>2</sub>-H<sub>2</sub>O (MSH) and MgO-Al<sub>2</sub>O<sub>3</sub>-SiO<sub>2</sub>-H<sub>2</sub>O (MASH): the effects of Al<sup>3+</sup> substitution on high pressure stability. *Am Mineralog* 88:99–108
- Brueckner HK, Carswell DA, Griffin WL (2002) Paleozoic diamonds within a Precambrian peridotite lens in UHP gneisses of the Norwegian Caledonides. *Earth Planet Sci Lett* 203:805–816
- Bucher-Nurminen K (1990) Transfer of mantle fluids to the lower continental crust: constraints from mantle mineralogy and MOHO temperature. In: Nelson BK, Vidal P (eds) *Development of continental crust through geological time. Chem Geol* 83:249–261
- Bucher-Nurminen K (1991) Mantle fragments in the Scandinavian Caledonides. *Tectonophysics* 190:173–192
- Carswell DA, Curtis CD, Kanaris-Sotiriou R (1974) Vein metasomatism in peridotite at Kalskaret near Tafjord, South Norway. *J Petrol* 15:383–402
- Carswell DA, Cuthbert SJ (2003) Ultrahigh pressure metamorphism in the Western Gneiss Region of Norway. In: Carswell DA, Compagnoni R (eds) *Ultrahigh pressure metamorphism*, vol 5, European Mineralogical Union Notes in Mineralogy. Eötvös University Press, Budapest, pp 51–73
- Chidester AH, Cady WM (1972) Origin and emplacement of alpine-type ultramafic rocks. *Nature* 240:27–31
- Coleman RG (1971) Plate tectonic emplacement of upper mantle peridotites along continental edges. *J Geophys Res* 76:1212–1222
- Coleman RG, Keith TE (1971) A chemical study of serpentinization – Burro Mountain, California. *J Petrol* 12:311–328
- Dódy I, Pósfai M, Buseck PR (2002) Revised structure models for antigorite: an HRTEM study. *Am Mineralog* 87:1443–1457

- Dymek RF, Boak JL, Brothers SC (1988) Titanian chondroditite- and titanian clinohumite-bearing metadunite from the 3800 Ma Isua supracrustal belt, West Greenland: chemistry, petrology, and origin. *Am Mineralog* 73:547–558
- Evans BW (2004) The serpentinite multisystem revisited: chrysotile is metastable. *Int Geol Rev* 46:479–506
- Evans BW (2008) Control of the products of serpentinization by the Fe<sup>2+</sup>Mg-1 exchange potential of olivine and orthopyroxene. *J Petrol* 49:1873–1887
- Evans BW, Trommsdorff V (1974) Stability of enstatite + talc, and CO<sub>2</sub>-metasomatism of metaperidotite, Val d'Efra, Lepontine Alps. *Am J Sci* 274:274–296
- Evans BW, Trommsdorff V (1978) Petrogenesis of garnet lherzolite, Cima di Gagnone, Lepontine Alps. *Earth Planet Sci Lett* 40:333–348
- Ferry JM (1995) Fluid flow during contact metamorphism of ophicarbonate rocks in the Bergell aureole, Val Malenco, Italian Alps. *J Petrol* 36:1039–1053
- Friend CRL, Bennett VC, Nutman AP (2002) Abyssal peridotites > 3, 800 Ma from southern West Greenland: field relationships, petrography, geochronology, whole-rock and mineral chemistry of dunite and harzburgite inclusions in the Itsaq Gneiss Complex. *Contrib Mineralog Petrol* 143:71–92
- Frost BR (1985) On the stability of sulfides, oxides and native metals in serpentinite. *J Petrol* 26:31–63
- Frost BR, Beard JS (2007) On silica activity and serpentinization. *J Petrol* 48:1351–1368
- Fumagalli P, Poli S (2005) Experimentally determined phase relations in hydrous peridotites to 6.5 GPa and their consequences on the dynamics of subduction zones. *J Petrol* 46:555–578
- Grobety B (2003) Polytypes and higher-order structures of antigorite: a TEM study. *Am Mineralog* 88:27–36
- Katzir Y, Avigad D, Matthews A, Garfunkel Z, Evans BW (1999) Origin and metamorphism of ultrabasic rocks associated with a subducted continental margin, Naxos (Cyclades, Greece). *J Metamorph Geol* 17:301–318
- Kostenko O, Jamtveit B, Austrheim H, Pollok K, Putnis C (2002) The mechanism of fluid infiltration in peridotites at Almklovdalen, western Norway. *Geofluids* 2:203–215
- Liou JG, Zhang RY, Ernst WG (2007) Very high-pressure orogenic garnet peridotites. *PNAS (Nat'l Acad Sci USA)* 104:9116–9121
- Medaris LG (1984) A geothermobarometric investigation of garnet peridotites in the Western Gneiss Region of Norway. *Contrib Miner Petrol* 87:72–86
- Mellini M, Trommsdorff V, Compagnoni R (1987) Antigorite polysomatism: behaviour during progressive metamorphism. *Contrib Miner Petrol* 97:147–155
- O'Hanley DS, Dyar MD (1993) The composition of lizardite 1T and the formation of magnetite in serpentinites. *Am Mineralog* 78:391–404
- O'Hara MJ, Mercy ELP (1963) Petrology and petrogenesis of some garnetiferous peridotites. *Trans R Soc (Edinb)* 65:251–314
- Pawley A (2003) Chlorite stability in mantle peridotite: the reaction clinocllore + enstatite = forsterite + pyrope + H<sub>2</sub>O. *Contrib Mineralog Petrol* 144:449–456
- Peacock SM (1987) Serpentinization and infiltration metasomatism in the Trinity peridotite, Klamath province, northern California: implications for subduction zones. *Contrib Mineralog Petrol* 95:55–70
- Peretti A, Dubessy J, Mullis J, Frost BR, Trommsdorff V (1992) Highly reducing conditions during Alpine metamorphism of the Malenco peridotite (Sondrio, northern Italy) indicated by mineral paragenesis and H<sub>2</sub> in fluid inclusions. *Contrib Mineralog Petrol* 112:329–340
- Rahn MK, Bucher K (1998) Titanian clinohumite formation in the Zermatt-Saas ophiolites, Central Alps. *Mineral Petrol* 64:1–13
- Ringwood AE (1975) Composition and petrology of the Earth's mantle. McGraw-Hill, New York, 532 pp
- Scambelluri M, Hoogerduijn Strating EH, Piccardo GB, Vissers RLM, Rampone E (1991) Alpine olivine- and titanian clinohumite-bearing assemblages in the Erro-Tobbio peridotite (Voltri Massif, NW Italy). *J Metamorph Geol* 9:79–91

- Schmädicke E (2000) Phase relations in peridotitic and pyroxenitic rocks in the model system CMASH and NCMASH. *J Petrol* 41:69–86
- Schreyer W, Ohnmacht W, Mannchen J (1972) Carbonate-orthopyroxenites (sagvandites) from Troms, northern Norway. *Lithos* 5:345–363
- Snoke AW, Lewis CC (1978) Jackstraw-textured talc-olivine rocks, Preston Peak area, Klamath Mountains, California. *Geol Soc Am Bull* 89:223–230
- Song SG, Su L, Niu Y, Zhang LF (2007) Petrological and geochemical constraints on the origin of garnet peridotite in the North Qaidam ultrahigh-pressure metamorphic belt, Northwestern China. *Lithos* 96:243–265
- Song SG, Zhang LF, Niu Y (2004) Ultra-deep origin of garnet peridotite from the North Qaidam ultrahigh-pressure belt, Northern Tibetan Plateau, NW China. *Am Mineralog* 89:1330–1336
- Soto JJ (1993) PTMAFIC: software for thermobarometry and activity calculations with mafic and ultramafic assemblages. *Am Mineralog* 78:840–844
- Trommsdorff V, Evans BW (1980) Titanian hydroxyl – clinohumite: formation and breakdown in antigorite rocks (Malenco, Italy). *Contrib Miner Petrol* 72:229–242
- Trommsdorff V, López Sánchez-Vizcaíno V, Gómez-Pugnaire MT, Müntener O (1998) High pressure breakdown of antigorite to spinifex-textured olivine and orthopyroxene, SE Spain. *Contrib Mineralog Petrol* 132:139–148
- Trommsdorff V, Nimis PN (2001) Revised thermobarometry of Alpe Arami and other garnet peridotites from the Central Alps. *J Petrol* 42:103–115
- Ulmer P, Trommsdorff V (1995) Serpentine stability to mantle depths and subduction related magmatism. *Boch Geol Geotech Arb* 44:248–249
- Ulmer PTV (1995) Serpentine stability to mantle depths and subduction-related magmatism. *Science* 268:858–861
- van Roermund HLM, Drury MR (1998) Ultra-high pressure ( $P > 6$  GPa) garnet peridotites in western Norway: exhumation of mantle rocks from  $> 185$  km depth. *Terra Nova* 10:295–301
- Viti C, Mellini M (1998) Mesh textures and bastites in the Elba retrograde serpentinites. *Eur J Miner* 10:1341–1359
- Wunder B, Schreyer W (1997) Antigorite: high pressure stability in the system  $MgO-SiO_2-H_2O$  (MSH). *Lithos* 41:213–227
- Yang TN, Jahn BM (2000) Deep subduction of mantle-derived garnet peridotites from the Su-Lu UHP metamorphic terrane in China. *J Metamorph Geol* 18:167–180
- Zhang RY, Liou JG, Cong BL (1995) Talc-, magnestite- and Ti-clinohumite-bearing ultrahigh-pressure meta-mafic and ultramafic complex rocks in the Dabie Mountains, China. *J Petrol* 36:1011–1037

# Chapter 6

## Metamorphism of Dolomites and Limestones

### 6.1 Introduction

#### 6.1.1 Rocks

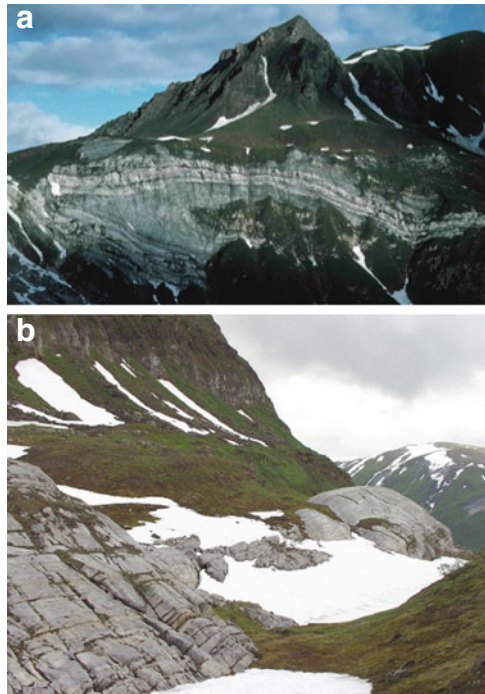
Sedimentary carbonate rocks consist predominantly of carbonate minerals (as the name implies). There are two main types of carbonate rocks, dolomites and limestones. The first is modally dominated by dolomite ( $\text{CaMg}(\text{CO}_3)_2$ ), the second by calcite ( $\text{CaCO}_3$ ) and there is a complete gradation between the pure dolomite and limestone “end members” indicated by the rock names, calcitic dolomite, dolomitic limestone, magnesian limestone. As the rocks often also contain variable amounts of quartz they are sometimes referred to as siliceous dolomites and siliceous limestones.

Magnesite-bearing sedimentary carbonate rocks occur occasionally in evaporite environments, but they are extremely rare and are not considered further. In contrast, siliceous dolomites and limestones represent a large portion of the sedimentary record, particularly in Phanerozoic sediments. Their metamorphic equivalents are termed **marbles**. If the marbles are very poor in silicate minerals marbles are named after the dominant carbonate mineral, e.g., dolomitic marbles, dolomite marbles; calcitic marbles, calcite marbles. Particularly dolomitic marbles contain Mg-silicates in places even modally abundant. Such marbles are named after the significant metamorphic silicate mineral; tremolite marble, diopside marble, forsterite (olivine) marble end so on. Dolomite marbles often contain also very pale brown colored biotite, and typical rocks are phlogopite marbles. High-grade olivine marbles may also contain spinel and (or) humite minerals. Marbles are widespread in metamorphic terrains associated with orogenic belts. Marbles occur commonly interlayered with other metasediments (Fig. 6.1). They often form distinct massive bands in gneissic country rocks (Fig. 6.2). There are also many examples of marbles occurring in contact aureoles around shallow level magmatic intrusions into dolomite and limestone sequences.



**Fig. 6.1** Folded and banded marble sequence of the Svartisen Nappe Complex (Scandinavian Caledonides) at Engabreen (Nordland, Norway). The outcrop shows highly ductile deformation patterns typical of calcite marbles. Lighter colored bands of tremolite marble alternate with phlogopite-rich dark marble layers

**Fig. 6.2** (a) Large recumbent fold in tremolite dolomite marble at Camplungo (Ticino, Central Alps). This is the tremolite type locality (see also Fig. 6.3). The Triassic dolomite marble is underlain by basement gneisses of the North Penninic nappe complex and covered by younger Cenozoic metasediments. All units have been metamorphosed at middle amphibolite facies conditions during the Oligocene collision phase of the Alpine orogeny. (b) Prominent band of homogeneous coarse grained tremolite marble in the gneissic basement of the Svartisen Nappe Complex of the Scandinavian Caledonides (Nordland, Norway)



### 6.1.2 Minerals and Rock Composition

The dominant mineralogy of sedimentary carbonate rocks (dolomite, calcite, quartz), defines a very simple chemical composition space. Water-bearing minerals are often absent in sedimentary carbonate rocks but do occur in their metamorphic equivalents. Talc and particularly tremolite are modally abundant hydrous minerals in many marbles (Fig. 6.3). In collision belts tremolite marbles occur widespread (Fig. 6.2). Therefore, H<sub>2</sub>O was either present as water in the pore space at low grade or was introduced into the marbles during metamorphism. In order to discuss the phase relationships of marbles, H<sub>2</sub>O must be added to the components of Cal, Dol, and Qtz. The five components of the siliceous dolomite system used in the discussion below are CaO–MgO–SiO<sub>2</sub>–H<sub>2</sub>O–CO<sub>2</sub> (CMS–HC system).

Dolomitic limestones are generally iron-poor rocks and metamorphic ferromagnesian minerals in dolomitic marbles commonly have compositions of  $X_{Mg} > 0.95$  or even  $> 0.99$ . As a consequence white tremolite, colorless diopside and olivine are characteristic minerals in marbles. Thus, iron can be ignored in the discussion of phase relationships of most marbles. On the other hand, this compositional restriction also precludes the use of Fe–Mg exchange thermometry in marble assemblages. Other chemical impurities, e.g., K<sub>2</sub>O, Al<sub>2</sub>O<sub>3</sub> present as clay minerals, and their effect on the phase relationships in marbles, e.g., formation of phlogopite, K-feldspar, Mg-rich chlorite, hornblende and spinel with metamorphism, will be discussed at the end of the chapter.

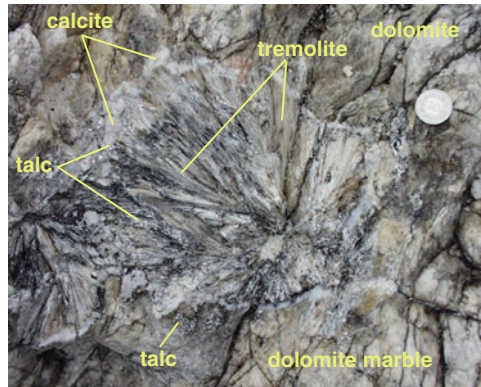


**Fig. 6.3** Tremolite marble from the Campolungo outcrop (see Fig. 6.2a). Radial bundles of cm-long tremolite with a thin veneer of pure calcite at the front tips of the needles. Late talc crusts cover partly the tremolite. Both Tlc and Tr contain much fluorine but virtually no iron. The dolomite marble contains very little quartz. Tremolite formed by reaction of the dolomite rock matrix with SiO<sub>2(aq)</sub> dissolved in an aqueous phase that entered the rock along fractures. The fluid provided SiO<sub>2</sub> and H<sub>2</sub>O for the making of the tremolite and removed the CO<sub>2</sub> and a part of the calcite produced by the reaction



### 6.1.3 Chemographic Relationships

A chemographic representation of the siliceous carbonate system is shown in Fig. 6.4 which is a projection of the five-component system onto the CaO–MgO–SiO<sub>2</sub> plane from CO<sub>2</sub> and H<sub>2</sub>O. The diagram shows the composition of the most important minerals found in marbles that can be described in this system. Other Mg-silicate minerals of this system such as enstatite and anthophyllite, do not occur in marbles. High grade marbles often contain minerals of the humite group, in particular chondrodite and clinohumite. In the pure CMS-HC system the humites are metastable relative to forsterite and brucite. The occurrence is related to the presence of the extra components TiO<sub>2</sub> and F that can be incorporated in the humites but not in forsterite. Some minerals of the CMS-HC system, e.g., anhydrous CaMg-silicates such as monticellite, åkermanite, merwinite, anhydrous Ca-silicates such as larnite, rankinite, the CO<sub>2</sub>-bearing Ca-silicates spurrite, tilleyite, and CaO or lime) are only found in very high-T, low-P contact aureoles around mafic intrusions (hydrous granite is too cold) or in xenoliths. Their phase relationships will not be considered in this book, but the reader is referred to Grapes (2006) for details of their paragenesis and examples of this sanidinite facies-type contact metamorphism.

The shaded areas in Fig. 6.4 represent the compositional range of sedimentary silica-bearing carbonate rocks within the triangle Dol–Cal–Qtz and Table 6.1 lists all stable reactions among the minerals that occur within the CMS-HC system. The composition space can be subdivided into dolomite-rich rocks (6.1) and quartz-rich rocks (6.2). The boundary that separates the two composition fields is the tie line between calcite and diopside and metamorphosed rocks with compositions falling in field 2 are typically referred to as calcsilicate marbles or rocks, particularly if they contain Al<sub>2</sub>O<sub>3</sub> as an additional component. Siliceous dolomites and calcitic dolomites plot within field 1, whereas siliceous limestone, magnesian limestone and dolomitic limestone plot within either field 1 or 2. In most instances, bulk SiO<sub>2</sub> contents of siliceous carbonate rocks are typically < 50 wt% and often < 20 wt%. Primary bulk compositions that plot in field 2 above 50 mol% SiO<sub>2</sub> (i.e., above the

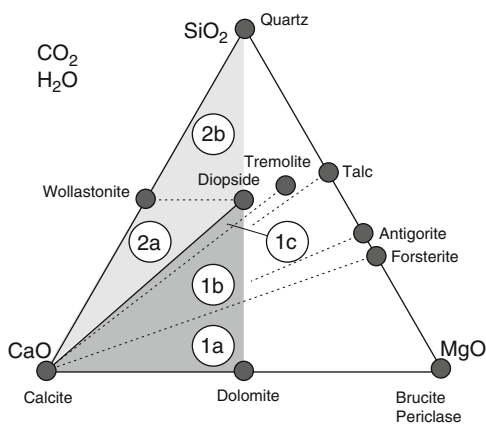


**Fig. 6.4** Chemography of the siliceous dolomite system projected from CO<sub>2</sub> and H<sub>2</sub>O onto the CaO–MgO–SiO<sub>2</sub> plane. Dolomite marbles are represented by the composition fields 1a, 1b and 1c, calcsilicate marbles by the fields 2a and 2b

**Table 6.1** Reactions in siliceous dolomites

Dolomite-rich rock compositions (1)		
Upper limit of quartz		
$3\text{Dol} + 4\text{Qtz} + \text{H}_2\text{O} \Rightarrow \text{Tlc} + 3\text{Cal} + 3\text{CO}_2$	(6.1)	Talc
$5\text{Dol} + 8\text{Qtz} + \text{H}_2\text{O} \Rightarrow \text{Tr} + 3\text{Cal} + 7\text{CO}_2$	(6.2)	Tremolite
$\text{Dol} + 2\text{Qtz} \Rightarrow \text{Di} + 2\text{CO}_2$	(6.3)	Diopside
Upper limit of talc		
$2\text{Tlc} + 3\text{Cal} \Rightarrow \text{Tr} + \text{Dol} + \text{CO}_2 + \text{H}_2\text{O}$	(6.4)	Tremolite
Upper limit of tremolite		
$3\text{Cal} + \text{Tr} \Rightarrow \text{Dol} + 4\text{Di} + \text{H}_2\text{O} + \text{CO}_2$	(6.5)	Diopside
$11\text{Dol} + \text{Tr} \Rightarrow 13\text{Cal} + 8\text{Fo} + 9\text{CO}_2 + \text{H}_2\text{O}$	(6.6)	Forsterite
$5\text{Cal} + 3\text{Tr} \Rightarrow 11\text{Di} + 2\text{Fo} + 5\text{CO}_2 + 3\text{H}_2\text{O}$	(6.7)	Fo + Di
$107\text{Dol} + 17\text{Tr} + 107\text{H}_2\text{O} \Rightarrow 141\text{Cal} + 4\text{Atg} + 73\text{CO}_2$	(6.8)	Antigorite
Upper limit of diopside		
$3\text{Dol} + \text{Di} \Rightarrow 4\text{Cal} + 2\text{Fo} + 2\text{CO}_2$	(6.9)	Forsterite
Upper limit of antigorite		
$20\text{Cal} + \text{Atg} \Rightarrow 20\text{Di} + 34\text{Fo} + 20\text{CO}_2 + 31\text{H}_2\text{O}$	(6.10)	Forsterite
Upper limit of dolomite		
$\text{Dol} \Rightarrow \text{Cal} + \text{Per} + \text{CO}_2$	(6.11)	Periclase
$\text{Dol} + \text{H}_2\text{O} \Rightarrow \text{Cal} + \text{Brc} + \text{CO}_2$	(6.12)	Brucite
Upper limit of brucite		
$\text{Brc} \Rightarrow \text{Per} + \text{H}_2\text{O}$	(6.13)	Periclase
Quartz-rich rock compositions (2)		
Upper limit of dolomite		
$3\text{Dol} + 4\text{Qtz} + \text{H}_2\text{O} \Rightarrow \text{Tlc} + 3\text{Cal} + 3\text{CO}_2$	(6.1)	Talc
$5\text{Dol} + 8\text{Qtz} + \text{H}_2\text{O} \Rightarrow \text{Tr} + 3\text{Cal} + 7\text{CO}_2$	(6.2)	Tremolite
$\text{Dol} + 2\text{Qtz} \Rightarrow \text{Di} + 2\text{CO}_2$	(6.3)	Diopside
Upper limit of talc		
$5\text{Tlc} + 6\text{Cal} + 4\text{Qtz} \Rightarrow 3\text{Tr} + 6\text{CO}_2 + 2\text{H}_2\text{O}$	(6.14)	Tremolite
Upper limit of tremolite		
$3\text{Cal} + 2\text{Qtz} + \text{Tr} \Rightarrow 5\text{Di} + \text{H}_2\text{O} + 3\text{CO}_2$	(6.15)	Diopside
Upper limit of quartz + calcite		
$\text{Cal} + \text{Qtz} \Rightarrow \text{Wo} + \text{CO}_2$	(6.16)	Wollastonite

Wo–Di tie line) are not common. They typically occur as either siliceous layers or concretions within psamitic–pelitic sediments that have been partly replaced by carbonate or as silicified carbonates. It is also important to note that the term “siliceous carbonate” can also mean an association of nearly pure dolomites and/or limestone that contain chert nodules. The reason for a separate discussion of the two main carbonate rock compositions is because of the different reactions affecting them at higher metamorphic grades. Both compositions form Di, Tr, Tlc, but additional Fo, Atg, Per and Brc can form from dolomite-rich carbonates, and Wo from quartz-rich carbonates. Reactions (6.3) ( $\text{Qtz} + \text{Dol} \Rightarrow \text{Di} + \text{CO}_2$ ) and (6.16) ( $\text{Cal} + \text{Qtz} \Rightarrow \text{Wo} + \text{CO}_2$ ) of Table 6.1 define the 50 mol% SiO<sub>2</sub> separation of the composition space. A sedimentary carbonate rock consisting of Cal + Dol + Qtz will, after completion of reaction (6.3), consist of either Cal + Dol + Di (no Qtz remaining) and plot in field 1, or Cal + Qtz + Di (no Dol remaining) and plot in

field 2. At higher temperature, the Cal–Dol–Di assemblage of the Dol-rich marble will undergo transformation according to reaction (6.9) ( $3\text{Dol} + \text{Di} \Rightarrow 4\text{Cal} + 2\text{Fo} + \text{CO}_2$ ), whereas the Cal–Qtz–Di assemblage of the Cal-rich siliceous marble will undergo reaction (6.16) to form wollastonite. Note that the first three reactions of Table 6.1 describe the upper limit of the sedimentary Dol–Cal–Qtz assemblage and they are identical for the two composition fields 1 and 2. Reactions (6.1), (6.2) and (6.3) all involve Dol + Qtz as reactants and if the reactions run to completion the rock will contain the product silicate (Tlc, Tr, Di) and calcite plus unused reactants which can be either Dol or Qtz.

The equilibrium conditions of the reactions listed in Table 6.1 depend on P, T and on the activities of  $\text{CO}_2$  and  $\text{H}_2\text{O}$  in binary  $\text{CO}_2$ – $\text{H}_2\text{O}$  fluid phase. The composition of this fluid can be expressed in terms of  $X_{\text{CO}_2}$  (see Chap. 3).

## 6.2 Orogenic Metamorphism of Siliceous Dolomite

The P–T– $a_{\text{CO}_2}$  relationships of siliceous dolomite-rich marbles in orogenic belts are shown in Fig. 6.5. The figure has been constructed for a field gradient typical of collision belts (Kyanite-type geotherm). The model molar bulk composition is:

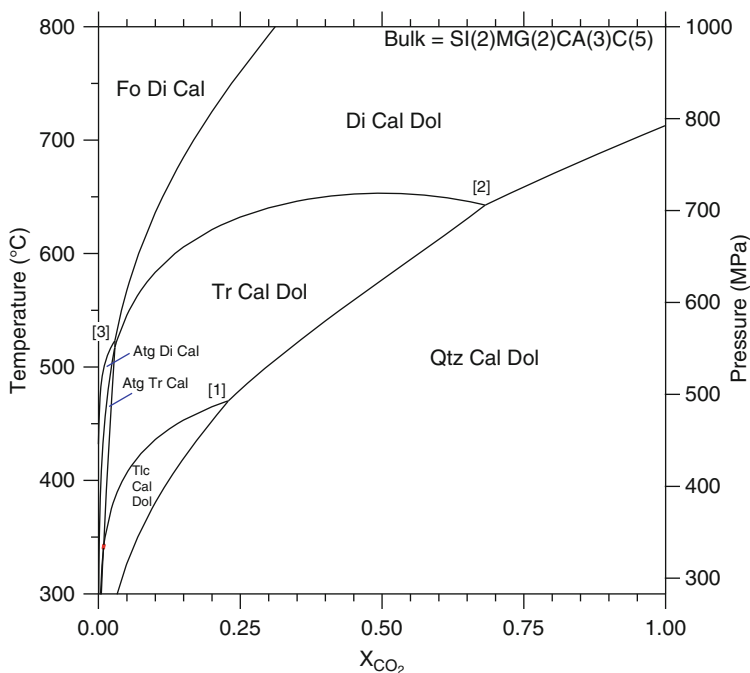


**Fig. 6.5** P–T– $a_{\text{CO}_2}$  diagram showing phase equilibria of siliceous dolomites for the composition  $2\text{Qtz} + 2\text{Dol} + 1\text{Cal}$  (field 1b Fig. 6.4). The vertical axis represents an orogenic geotherm characteristic of regional metamorphism in collision belts

40% Dol, 20% Cal, 40% Qtz. Dol + Qtz will react to form Tlc, Tr or Di according to reactions (6.1), (6.2), and (6.3) depending on the composition of the fluid phase initially present in the pore space or introduced into the marble during metamorphism. Under most conditions, the initial pore fluid is probably H<sub>2</sub>O-rich at low grade. The rock will, therefore, be buffered along the reaction boundaries (6.1), (6.2), and (6.3) until all quartz is used up. Note that both the Tlc- and Tr-forming reactions consume H<sub>2</sub>O. The widespread occurrence of abundant coarse grained tremolite in marbles is compelling evidence of the availability and presence of H<sub>2</sub>O in prograde metamorphism.

**Talc** will form in H<sub>2</sub>O-rich fluids at  $T < 470^{\circ}\text{C}$  and talc-bearing marbles are restricted to  $T < 470^{\circ}\text{C}$ . However, talc in marbles of orogenic belts is usually associated with late hydrothermal activity or it is of retrograde origin. It is the only metamorphic mineral in dolomites at lower metamorphic grades. The steep equilibrium position of reaction (6.1) in P–T–a space (Fig. 6.5) has the consequence that only a small amount of Tlc is produced by this reaction under closed system conditions. Therefore, tremolite is usually the first recognizable metamorphic mineral in marbles. Talc is removed from marbles at invariant point [1] of Fig. 6.5. The upper limit for talc is defined by reaction (6.4).

**Tremolite** first occurs at invariant point [1] involving Qtz + Tlc + Tr (+ Dol + Cal) at about  $470^{\circ}\text{C}$  and 500 MPa. The first occurrence of tremolite represents an excellent mapable isograd in the field and coincides approximately with the beginning of the amphibolite facies (= tremolite-in isograd). The temperature of the isograd is rather independent of the precise position of the geotherm and close to  $500^{\circ}\text{C}$ . Reaction (6.2) will continue to produce tremolite with increasing temperature and the rock will effectively control the composition of the fluid phase along the boundary of the Qtz Cal Dol and Tr Cal Dol fields of Fig. 6.5 (the rock contains the univariant assemblage Dol + Cal + Qtz + Tr). Finally, reactant Qtz will be exhausted and the rock will enter the divariant Tr field. The assemblage Tr + Dol + Cal is the characteristic assemblage in amphibolite facies siliceous dolomite marbles (Fig. 5.3). At a typical mid-amphibolite facies temperature (e.g.,  $600^{\circ}\text{C}$ , 650 MPa, Fig. 6.5), dolomite marbles may contain three assemblages: Tr–Dol–Cal (common), Tr–Dol–Cal–Qtz [reaction (6.2)], Dol–Cal–Qtz (rare).

**Diopside** forms in dolomite marbles from reactions (6.3) and (6.5), and from the reaction at invariant point [2]. The position of this invariant point defines the lowest possible T for the occurrence of diopside in dolomite marbles (closed system). In other words, the first occurrence of diopside represents a distinct mapable boundary in the field (diopside-in isograd) and indicates a temperature of about  $650^{\circ}\text{C}$  along the P–T–a section of Fig. 6.5.

If a rock does not reach the invariant point along a prograde metamorphic path because reaction (6.2) consumes all quartz at lower temperature, then diopside will form from reaction (6.5). This reaction replaces the divariant assemblage Tr + Dol + Cal by Di + Dol + Cal and separates the corresponding fields in Fig. 6.5 (and also in the field). The maximum temperature of the assemblage Tr + Dol + Cal is given by  $T_{\text{max}}$  ( $650^{\circ}\text{C}$ ) of reaction (6.5). Along a collision-type P–T path, no

tremolite-bearing dolomite marbles are stable at  $T > 650^{\circ}\text{C}$  (= tremolite-out isograd). In the P–T interval between the Di-in and Tr-out isograd ( $\Delta T$  is about  $20^{\circ}\text{C}$ ), tremolite- and diopside-bearing marbles may occur together and the four minerals of reaction (6.5) present.

Diopside can also form from reaction (6.3) if the rock is sufficiently quartz-rich to leave the invariant point along the quartz-diopside boundary [= equilibrium of reaction (6.3)] during prograde metamorphism or if the initial fluid contains more than about 80 mol%  $\text{CO}_2$ . Reaction (6.3) will also produce diopside in rocks devoid of a fluid phase. Reaction (6.3) will create a pure  $\text{CO}_2$  fluid in such rocks and impose the maximum P–T limit for the Dol + Qtz assemblage ( $\sim 710^{\circ}\text{C}$  at 800 MPa). No mineralogical changes will occur in fluid-free siliceous dolomitic marble until P–T conditions of the upper amphibolite facies are reached.

**Forsterite** will not form during regional metamorphism of siliceous dolomites along the P–T path of Fig. 6.5. Diopside will be removed from dolomitic marbles by reaction (6.9). This reaction replaces the Di + Dol + Cal assemblage of by the Fo + Di + Cal assemblage for the selected rock composition of Fig. 6.5. However, this reaction will take place at temperatures much higher than  $800^{\circ}\text{C}$  for the  $a_{\text{CO}_2}$  of progressively metamorphosed high-grade marbles. At temperatures  $< 800^{\circ}\text{C}$ , forsterite can only be produced by interaction of the marble with an externally derived  $\text{H}_2\text{O}$ -rich fluid phase, e.g., along fractures or shear zones and veins. As an example, at  $700^{\circ}\text{C}$   $a_{\text{CO}_2}$  must be below 0.17 (Fig. 6.5) in order to form forsterite from reaction (6.9). Closed system marbles will be free of forsterite if metamorphism occurred at the P–T conditions of Fig. 6.5. At pressures in the range 500–800 MPa (sillimanite-grade metamorphism), forsterite may form in dolomite marbles at granulite facies conditions ( $T > 800^{\circ}\text{C}/800$  MPa, or  $T > 700^{\circ}\text{C}/500$  MPa).

### 6.2.1 Modal Evolution Model

A model for the progressive collision type metamorphism is shown on a modal composition versus P–T diagram (Fig. 6.6) for a metamorphic path ending at  $900^{\circ}\text{C}$  and 0.9 GPa. The rock composition is the same as used in Fig. 6.5. It shows that at low grade the reaction progress per  $\Delta T$  is low and increases dramatically near  $600^{\circ}\text{C}$  finally resulting in a marble with 40 vol% tremolite. It also can be clearly seen that at invariant point [1] (Fig. 6.5) all Tlc abruptly disappears and about 7 vol% tremolite in the rock result from the reaction in [1]. Reaction (6.2) produces rapidly increasing amounts of tremolite until all Qtz is used up at about  $615^{\circ}\text{C}$  and the rock enters the divariant Tr Dol Cal field (Fig. 6.5). The rock does not reach invariant point [2]. Reaction (6.5) removes very efficiently all Tr and replaces it by Di. The transformation occurs in a very small temperature interval due to the nearly isothermal position of the equilibrium of reaction (6.5) at the P–T conditions of the rock during this metamorphic stage (Fig. 6.5). The resulting Di + Dol + Cal assemblage remains stable up to upper granulite facies conditions. At  $820^{\circ}\text{C}$  forsterite forms and reaction (6.9) uses up all dolomite in this bulk rock composition, leaving the Fo + Di + Cal

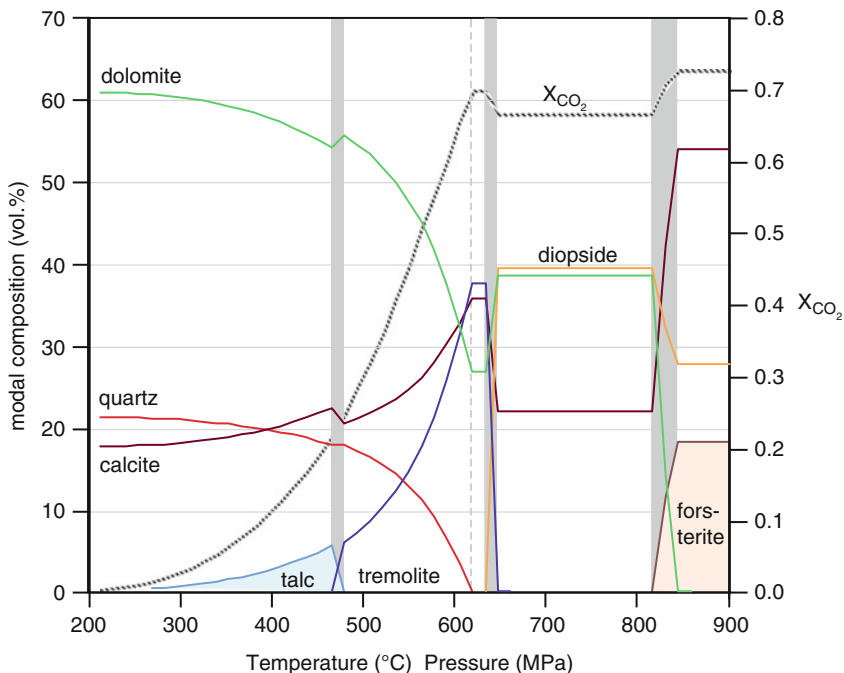


**Fig. 6.6** Modal composition versus P–T diagram showing the metamorphic development of a siliceous dolomite of the composition 2Qtz–2Dol–1Cal (field 1b Fig. 6.4). The horizontal axis represents an orogenic geotherm characteristic of regional metamorphism in collision belts. Note that the isograd (invariant point) transitions appear not as sharp boundaries as they should because of the finite step size used in the model (50)

assemblage typical of high-grade marbles. The initial marble contained 80 vol% carbonate minerals thereof 60% dolomite, the final rock still contains more than 50 vol% of carbonates but now exclusively calcite. Metamorphism replaces dolomite marble by calcite marble.

In summary, dolomite-rich marbles in regional metamorphic terrains of orogenic belts may contain small amounts of talc in addition to Dol + Cal + Qtz in the upper greenschist facies. Tremolite-bearing marbles are characteristic of lower to middle amphibolite facies and diopside-bearing marbles are stable from the upper middle amphibolite facies. Forsterite marbles are diagnostic of granulite facies conditions or imply infiltration of the marble by H<sub>2</sub>O-rich fluids.

### 6.3 Orogenic Metamorphism of Limestone

Orogenic metamorphism of calcsilicate marbles (composition field 2 in Fig. 6.4) is modeled by Fig. 6.7 for the rock composition 25% Dol, 12.5% Cal and 62.5% Qtz. Dolomite is the limiting mineral in the reactions (6.1), (6.2), and (6.3) for this

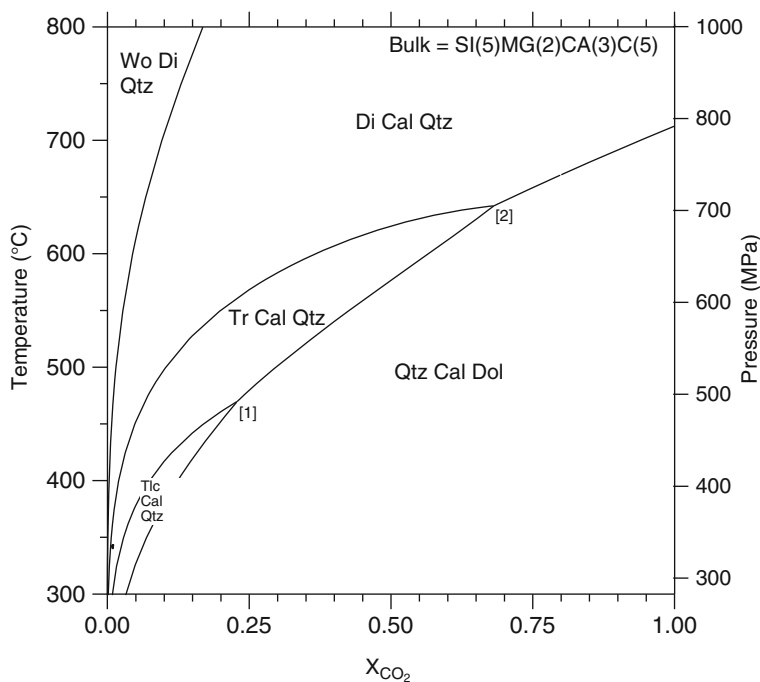


**Fig. 6.7** P–T– $a_{\text{CO}_2}$  diagram showing phase equilibria of siliceous limestones (or calcareous sandstones) for the composition 5Qtz–2Dol–1Cal (Di–Wo join Fig. 6.4). The vertical axis represents an orogenic geotherm characteristic of regional metamorphism in collision belts

composition. The production of Tlc, Tr, and Di by reactions (6.1), (6.2), and (6.3) is identical to the dolomite-rich rocks described above. The upper limit for talc is, however, given by reaction (6.14) in such rocks.

The **tremolite**-producing reaction (6.2) will consume all dolomite and the resulting assemblage, after completion of reaction (6.2), is Tr + Cal + Qtz. Here, tremolite will be removed from the rocks at higher grades by reaction (6.15). It occurs at significantly lower temperatures than reaction (6.5) which removes tremolite in dolomite-excess rocks. The tremolite stability field in such rocks is diminished in comparison to that in dolomite-rich marbles.

**Diopside** is usually produced by reaction (6.15). For the same reason as above, diopside may appear in calc-silicate marbles at lower temperature than in dolomite marbles (~600°C). The highest grade assemblage in calc-silicate marbles is Di + Cal + Qtz (Fig. 6.7). In contrast to dolomite-rich rocks, there is very little overlap between the tremolite and diopside stability fields in calc-silicate marbles.

A minor complication may occur if reaction (6.15) consumes all quartz, leaving a rock with the assemblage Cal + Tr + Di (composition 1c in Fig. 6.4). Tremolite is then removed from the rocks at higher grade by reaction (6.5). This reaction produces new metamorphic dolomite, the rock again becomes saturated with dolomite and the assemblage boundaries shown in Fig. 6.5 apply. The conversion

from Qtz-saturated to Dol-saturated conditions as metamorphism progresses affects only rocks with a composition of (1c) and not the rock composition displayed on Fig. 6.7.

**Wollastonite** does not form in regional metamorphic rocks under closed system conditions. Even under granulite facies conditions the assemblage Cal + Qtz remains stable. Figure 6.7 shows that wollastonite may only form from reaction (6.16) by interaction of the marble with an H<sub>2</sub>O-rich fluid. Such externally derived fluids may invade the marbles along fractures or shear zones.

Thus, in regional metamorphic terrains, Qtz-rich marbles (Fig. 6.4) may contain small amounts of talc in addition to Dol + Cal + Qtz in the upper greenschist facies. Tremolite-bearing marbles are characteristic of lower to middle amphibolite facies. Diopside-bearing marbles are stable upgrade from middle amphibolite facies. Wollastonite marbles are diagnostic for interaction with externally derived fluids or for certain P–T paths after maximum metamorphic conditions (see below).

## 6.4 Contact Metamorphism of Dolomites

There are numerous examples of siliceous dolomitic rocks metamorphosed by igneous intrusions at relatively shallow levels in the crust (see references). The igneous rocks are commonly granite, granodiorite, quartz diorite or monzonite and maximum temperatures attained at the country rock contacts are on the order of 600–700°C. Assemblage stabilities of siliceous dolomites at 100 MPa are shown in a T- $a_{\text{CO}_2}$  diagram in Fig. 6.8 for the bulk rock composition also used in Figs. 6.5 and 6.6). The diagram models progressive metamorphism of dolomites in a typical contact aureole surrounding a granitic pluton at a depth of *ca.* 3–4 km (100 MPa). The size (thickness) of the distinct mineral zones in the contact aureole depends on the heat given off by the granite which, in turn, depends on its size, composition, magma temperature and convective transfer of heat by hydrothermal fluids. Typically, contact effects of shallow level intrusions can be recognized in the country rocks to distances ranging from a few hundred meters to 1 or 3 km.

Compared with the corresponding Fig. 6.5 for regional metamorphism, Fig. 6.8 shows increased assemblage stabilities for the hydrates Tlc, Tr and Atg. All hydrates are stable to higher  $a_{\text{CO}_2}$ . Invariant points [4], [5] and [6] were not present in Fig. 6.5. However, as on Fig. 6.5, reactions (6.1), (6.2) and (6.3) (Table 6.1) define the upper limit for the sedimentary Dol + Cal + Qtz assemblage. However, invariant point [1] occurs at  $a_{\text{CO}_2} = 0.6$  and reaction (6.1) has a low dT/dX slope in Fig. 6.8. These features potentially result in the development of a recognizable zone with **talc**-bearing dolomites in the outer (cooler) parts of an aureole. Such a talc zone is diagnostic of temperatures below 410°C (at 100 MPa).

A zone with **tremolite**-bearing dolomites may develop from reactions (6.2) and (6.4), or the reaction at invariant point [1]. The low temperature limit for tremolite coincides with the upper limit for talc (~410°C). All tremolite will subsequently be removed from dolomite marbles by reactions (6.5) and (6.6) and the maximum



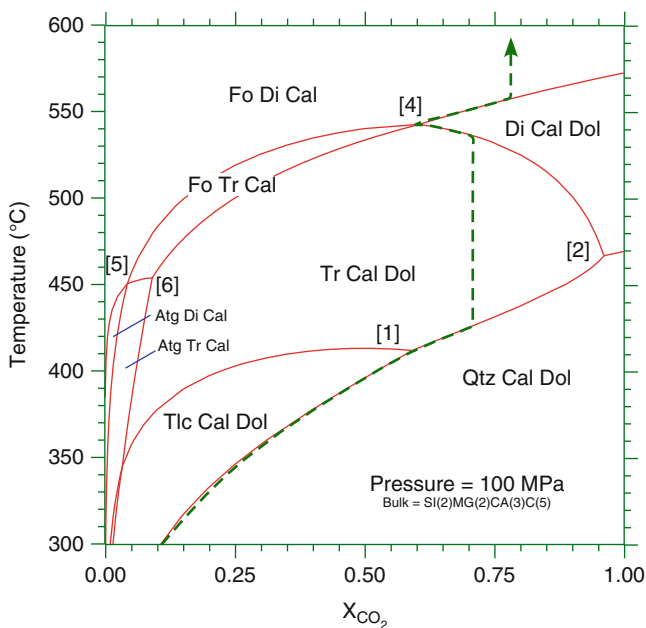


**Fig. 6.8**  $T$ - $x_{\text{CO}_2}$  diagram showing phase equilibria of siliceous dolomites for the composition  $2\text{Qtz}-2\text{Dol}-1\text{Cal}$  (field 1b Fig. 6.4) at a constant pressure of 100 MPa typical of shallow level contact aureoles. Progressive closed system metamorphism of rocks of the chosen composition would follow the dashed and arrowed path. The modal evolution of the rock along that path is shown on Fig. 6.10

temperature for tremolite is given by the position of invariant point [4] at about  $540^\circ\text{C}$ . Reaction (6.6), which is metastable in Fig. 6.5, produces forsterite in tremolite-bearing marbles in low pressure aureoles.

**Forsterite** appears in marbles in significant amounts at about  $540^\circ\text{C}$  (at 100 MPa). Forsterite assemblages (Fo + Dol + Cal, Fo + Di + Cal) are therefore characteristic of dolomites close to the igneous contact. Reaction (6.6), if gone to completion, results in the assemblage Fo + Dol + Cal in dolomite-rich rocks of composition (1a) in Fig. 6.4. The rock remains dolomite-saturated. However, reaction (6.6) may also consume all dolomite present in the rock and the resulting assemblage is Cal + Fo + Tr. This applies to rocks of composition (1b) in Fig. 6.4. The assemblage is present in Fig. 6.8 because of the specific bulk composition used for its construction. In this assemblage, tremolite is removed from the marble by reaction (6.7). The equilibrium curve for this reaction emerges from invariant point [4] in Fig. 6.8. The maximum temperature for tremolite in rocks of composition (1b) coincides with that of composition (1a), it is given by the position of the invariant point [4]. However, the high-temperature assemblage for the (1b) compositions is Cal + Di + Fo instead of Dol + Cal + Fo. However, most of the forsterite of Fo-marbles is formed by the diopside consuming reaction (6.9) discussed below.

**Diopside**, if present in dolomite-rich rocks, is restricted to a narrow T interval near 540°C (at 100 MPa). It will form by reaction (6.5) or at the invariant point [4]. Diopside may also occur where H<sub>2</sub>O had no access to the marbles and the Dol + Cal + Qtz assemblage is replaced by Di + Dol + Cal according to reaction (6.3) near 470°C. Diopside will be removed from the marbles by reaction (6.9) in the temperature interval 540–570°C. Rocks of composition (1a) will, after completion of the reaction, contain Dol + Cal + Fo, and rocks of composition (1b) the assemblage Cal + Di + Fo (see above).

Rocks with Fo assemblages are the typical high-grade rocks in contact aureoles. In many contact metamorphic fields, periclase- or brucite-bearing marbles occur close to the igneous contact or in marble xenoliths and roof pendants within the intrusion. A classic example is the contact aureole around the monzonite intrusion at Monzoni (N Italy) where pure periclase (brucite) marbles, so called predazzites, occur near Predazzo. **Periclase** usually forms from decomposition of dolomite according to reaction (6.11). **Brucite** may form by direct decomposition of dolomites by reaction (6.12) or, more commonly, by retrograde hydration of previously formed periclase by a reversal of reaction (6.13). It is apparent from Fig. 6.9, that both periclase and brucite can only form by interaction of dolomite-marble with an externally-derived H<sub>2</sub>O-rich fluid. The minimum temperature required for periclase to form is 600°C at 100 MPa (Fig. 6.9). It is given by invariant point [7]. Under closed system conditions, dolomite remains stable in “normal” contact aureoles

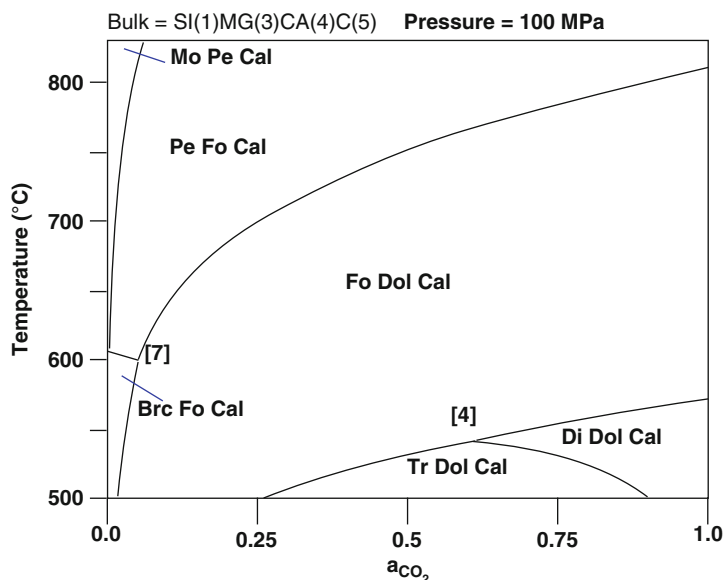


**Fig. 6.9** T–a<sub>CO2</sub> diagram showing some high-temperature phase equilibria of siliceous dolomites for the composition 2Qtz–2Dol–1Cal (field 1b Fig. 6.4) at a constant pressure of 100 MPa typical of shallow level contact aureoles

around granitoid intrusions. The minimum temperature required for the decomposition of dolomite in closed systems is close to 800°C at 100 MPa (Fig. 6.9).

Periclase and brucite are most often found in pure dolomites (SiO<sub>2</sub>-free rocks) because such compositions do not have the capacity to create and control their own (relatively CO<sub>2</sub>-rich) fluid phase. Pure dolomites are, therefore, most likely to produce periclase by H<sub>2</sub>O flushing from magmatic fluids close to igneous contacts. Note that olivine marbles that normally form near invariant point [4] at ~550°C require a further temperature increase to >600°C before H<sub>2</sub>O flushing can transform them to Pkl marbles (Fig. 6.9).

Stability fields for **antigorite** assemblages are present in Fig. 6.8 which also cannot be accessed by progressively metamorphosed siliceous dolomites under closed system conditions. However, antigorite may form in dolomites at peak conditions by interaction of the marble with an external fluid. Reaction (6.8) replaces Tr + Dol + Cal by Atg + Tr + Cal. Antigorite may be consumed under more H<sub>2</sub>O-rich conditions by reaction (6.10) (but also forms by reversing reaction (6.10) during retrograde replacement of a Fo + Di + Cal assemblage.

#### 6.4.1 Modal Evolution Model

A model for the metamorphic evolution of a dolomitic rock of the same composition (1b) as used in Figs. 6.5, 6.6, and 6.8 is presented on Fig. 6.10. The model shows the modal composition of the rock at a given temperature at 100 MPa pressure. By comparison with the companion Fig. 6.6 for regional metamorphism a number of features are quite different in low P contact aureoles. Talc is modally more prominent and reaches 20 vol% at about 410°C. The reaction at invariant point [1] removes all talc and replaces it by tremolite. About 30 vol% of tremolite is present right after leaving [1] upgrade. The sudden appearance of a large amount of Tr defines an excellent and easy recognizable isograd in the field. Note that the modal changes at [1] are isothermal, the apparent transitional zone on Fig. 6.10 is an artifact of the stepwise computation of the diagram (50 steps from 200°C to 700°C). With increasing step numbers the model would approach isothermal reactions at invariant points on Figs. 6.6 and 6.10. Upgrade from [1] the rock used in Fig. 6.10 rapidly consumes all remaining Qtz and then traverses the divariant Tr Dol Cal field for a > 100°C interval. Then some dramatic changes occur within a 30°C temperature interval at about 550°C. First all Tr is replaced by Di [reaction (6.5)] and the resulting rock reaches [4] with 40 vol% Di. At this point forsterite production sets in [reaction (6.9)] and rapidly uses up all remaining dolomite. At about 560°C the final rock with ~20% Fo and ~30% Di and 55% Cal can be heated to 700°C without undergoing further changes.

The Alta Stock in the Wasach Range (Utah, USA) is an excellent example of a low-pressure contact aureole in dolomites (Fig. 6.11). The sequence of metamorphic minerals begins in the outer aureole with the occurrence of talc, which is then replaced by tremolite. Forsterite appears in the inner aureole. Locally clinohumite

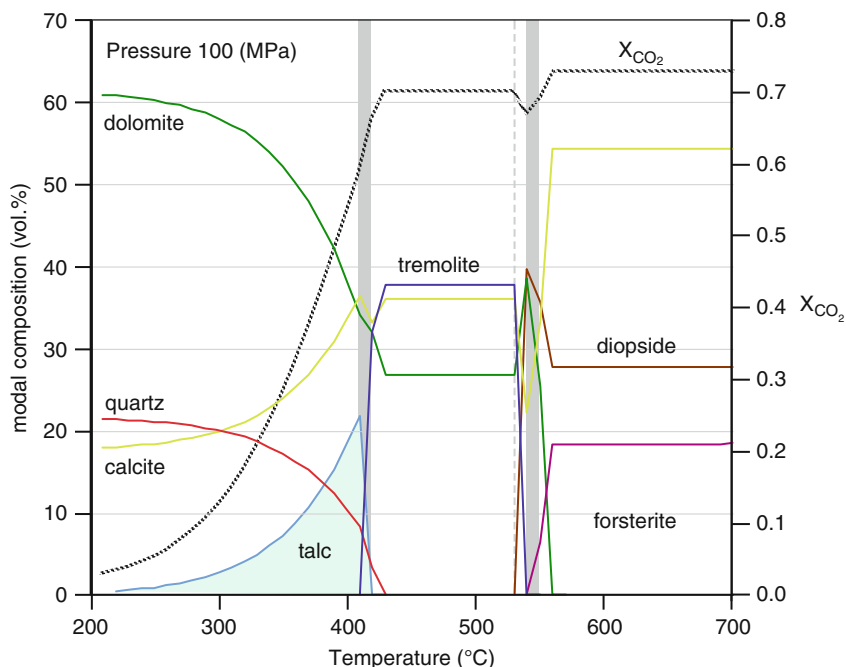


**Fig. 6.10** Modal composition versus temperature diagram at 100 MPa pressure showing the contact metamorphic development of a siliceous dolomite of the composition  $2Qtz-2Dol-1Cal$  (field 1b Fig. 6.4). Note that the isograd (invariant point) transitions appear not as sharp boundaries as they should because of the finite step size used in the model (50). Compare with EQUILAS model shown on Fig. 3.17

takes the place of forsterite (see below). A periclase zone is developed immediately at the contact. Diopside is not important in the Alta aureole because the bulk marble is very dolomite-rich (field 1a in Fig. 6.4).

In summary, under low pressure contact metamorphism, siliceous dolomites may develop the following mineral zonation (from low to high T, listing only the silicates): Qtz, Tlc, Tr, (Di), Fo (or Fo + Di). Periclase may form in pure dolomite close to the igneous heat source at  $T > 600^{\circ}C$ . Periclase, brucite and antigorite also commonly form by interaction of the marble with an externally controlled  $H_2O$ -rich fluid.

## 6.5 Contact Metamorphism of Limestones

Rocks of composition field (2) in Fig. 6.4 undergo progressive transformations visualized in Fig. 6.12. The specific rock composition used is the same as in Fig. 6.7 ( $5Qtz\ 2Dol\ 1Cal$ ). The three low-T reactions (6.1), (6.2) and (6.3) (Table 6.1) limit

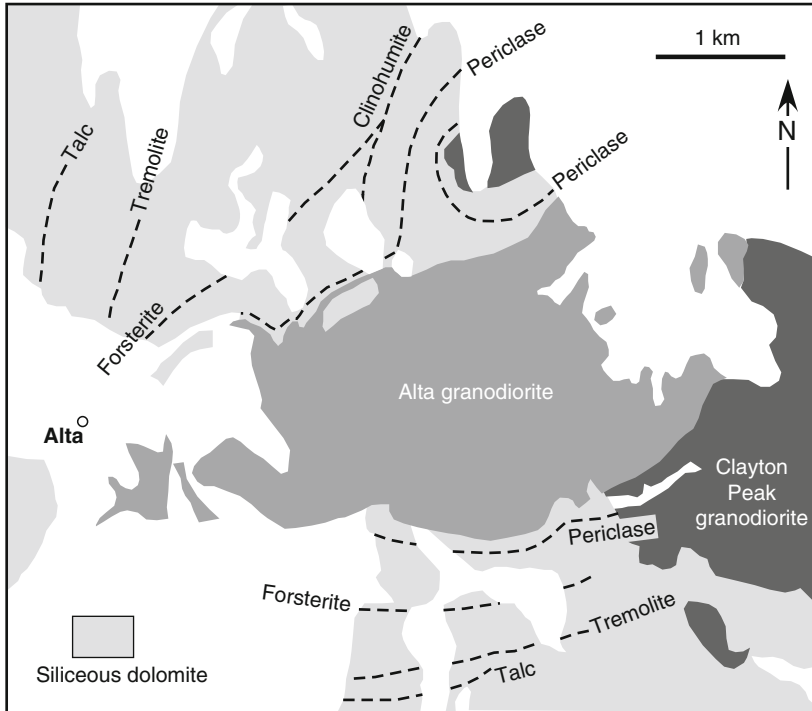


**Fig. 6.11** Map showing distribution of talc, tremolite, forsterite, clinohumite and periclase isograds developed in  $\text{SiO}_2$ -poor siliceous dolomite surrounding the Alta granodiorite, central Wasatch range, Utah, USA (Redrawn from Fig. 1 of Cook and Bowman 1994)

the sedimentary Qtz + Dol + Cal assemblage as in the previous cases. **Talc** is subsequently removed by reaction (6.14).

**Tremolite** has a distinctly lower maximum temperature of occurrence compared with dolomite-rich rocks. Tremolite is replaced by diopside by reaction (6.15), which has a temperature maximum at about  $490^\circ\text{C}$ . Tremolite occurs in a relatively narrow temperature interval of  $<80^\circ\text{C}$ . For the sake of completeness, if reaction (6.15) consumes all quartz, the resulting assemblage will be Cal + Tr + Di. For this to occur, a rock composition of (1c) in Fig. 6.1 is required (and not (2a) as used on Fig. 6.12). The fate of this assemblage with progressive metamorphism is discussed in Sect. 6.4 [reactions (6.5), (6.7), and (6.9)].

It follows from the above that **diopside** first appears in calcisilicate marbles further away from the intrusive contact than in dolomite marbles (if it occurs at all in the latter). The assemblage Di + Cal + Qtz is typical for calcisilicate marbles of the CMS-HC system near igneous contacts.

**Wollastonite** may form in contact metamorphic calcisilicate marbles even under closed-system conditions. For example, in siliceous limestones with the sedimentary assemblage Qtz + Cal and an  $\text{H}_2\text{O}$ -rich pore fluid, wollastonite will form in small but petrographically detectable amounts at temperatures as low as  $500^\circ\text{C}$ . In

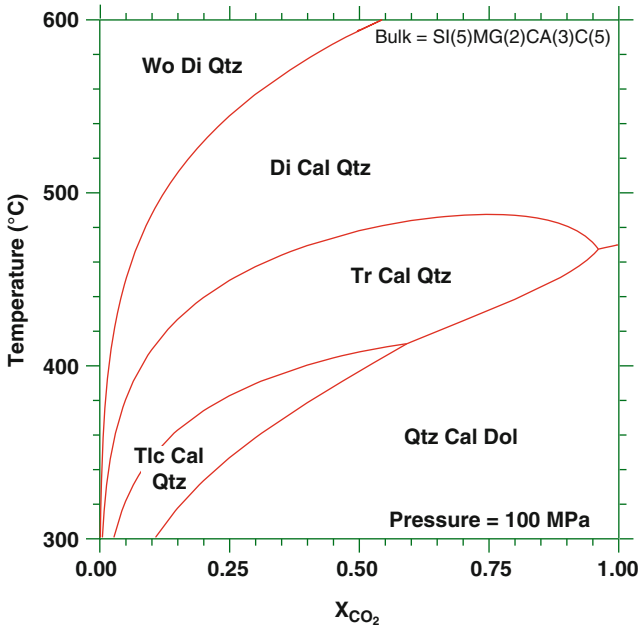


**Fig. 6.12** T- $a_{\text{CO}_2}$  diagram showing phase equilibria of siliceous limestones (or calcareous sandstones) for the composition 5Qtz-2Dol-1Cal (Di-Wo join Fig. 6.4) at a constant pressure of 100 MPa typical of shallow level contact aureoles

more siliceous carbonate-bearing rocks, significant amounts of wollastonite may form according to reaction (6.16).

In rocks which initially contain dolomite and consequently undergo a series of CO<sub>2</sub>-producing reactions, the fluid may have the composition of the T-maximum of reaction (6.15) when entering the diopside field under closed-system conditions ( $a_{\text{CO}_2} = 0.75$ ). In this case, a temperature of about 620°C is required for the onset of the wollastonite-producing reaction (6.16) and  $T > 650^\circ\text{C}$  (at 100 MPa) the coexistence of Cal + Qtz is not possible. Such temperatures are occasionally reached in the vicinity of the immediate igneous contact. It is about the same temperature that is required for making periclase marbles (see above). However, wollastonite may form by interaction of the Di + Cal + Qtz assemblage with an infiltrating H<sub>2</sub>O-rich fluid phase but it also may form from closed system metamorphism in low pressure aureoles.

If the wollastonite-forming reaction (6.16) runs to completion, composition field (2) of Fig. 6.4 can be subdivided into two subfields, i.e., defined by the Wo-Di tie-line. Rocks of composition (2a) (below the Wo-Di tie-line) contain Cal + Wo + Di, and reaction (6.16) has used up all quartz. Rocks of composition (2b) (above the Wo-Di tie-line) contain Qtz + Wo + Di, reaction (6.16) has consumed all calcite and consequently such rocks cannot be termed marbles (e.g., the quartz-calcite sandstone example quoted below). At a typical temperature of about 600°C

at the immediate contact of granitoid intrusions, three assemblages characterize calcisilicate marbles:  $\text{Cal} + \text{Qtz} + \text{Di}$ ,  $\text{Cal} + \text{Di} + \text{Wo}$  and  $\text{Qtz} + \text{Di} + \text{Wo}$ .

An excellent field example for extensive formation of  $\text{Wo}$  marbles is the Convict Lake aureole in the Eastern Sierra Nevada in California (Fig. 6.13a). Wollastonite formed from a calcite-quartz rock (Devonian Mt. Morrison sandstone with 62–79%  $\text{Qtz}$  and 13–32%  $\text{Cal}$ ) that forms part of a  $\sim 200 \text{ km}^2$  roof pendant contact metamorphosed by the Round Valley Peak granodiorite intrusion 89 Ma ago (Fig. 6.13b). The calcite-quartz sandstone has been infiltrated by an  $\text{H}_2\text{O}$ -rich (magmatic) fluid mainly parallel to bedding and the distribution of wollastonite (as wollastonite hornfels with 18–60%  $\text{Wo}$ ) near the igneous contact appears to directly reflect the paths of fluid flow (see Fig. 6.13a with inserted schematic cross section A–B). The wollastonite hornfels also contains small amounts of diopside and K-feldspar and the peak temperature of formation is inferred to be  $\sim 560^\circ\text{C}$  at  $\sim 150 \text{ MPa}$  that implies a low  $a_{\text{CO}_2}$  of  $\sim 0.2$  ( $\sim 0.3$  on Fig. 6.12 at 100 MPa).

In summary, calcisilicate marbles with compositions plotting within composition field (2) of Fig. 6.4 may contain talc in the outer aureole, tremolite in a middle zone and diopside in a relatively wide inner zone around an intrusive body. Wollastonite is often present in marbles or calcite-quartz-rich rocks close to an igneous contact and usually forms from interaction of the rocks with  $\text{H}_2\text{O}$ -rich fluids of magmatic, metamorphic or meteoric origin.

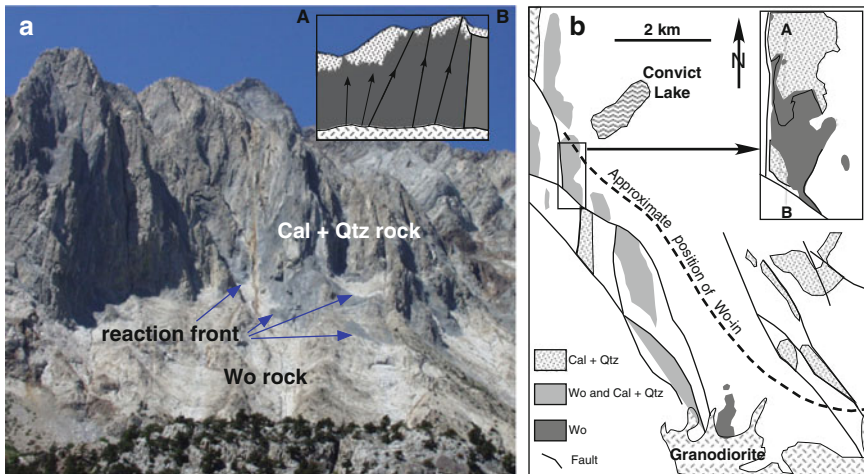


**Fig. 6.13** Contact metamorphism and fluid infiltration of the Devonian Mt. Morrison formation (Ferry et al. 2001) (a) View from Convict Lake to the SW showing gray  $\text{Cal} + \text{Qtz}$  rocks in the upper portion of the mountain wall and white wollastonite rock at the base (Fotograph Bucher). The two rocks are separated by a sharp reaction boundary (reaction (6.16); Table 6.1) which is driven by fluid infiltration. (b) Maps and section showing the occurrence of wollastonite in the Mt. Morrison quartz-calcite sandstone that forms part of a roof pendant within the Sierra Nevada batholith, California (simplified after Figs. 1 and 14 of Ferry et al. 2001). The N–S section line (A–B) of the cross section is indicated on the map. The cross section approximately corresponds to the picture 6.12a. Arrows in cross section indicate direction of fluid flow

## 6.6 Isograds and Zone Boundaries in Marbles

Isograds and zone boundaries in mixed volatile systems such as siliceous marbles can be related to unique points on isobaric T–a sections. For example, invariant point [2] marks the first occurrence of diopside in marbles and it can be expected that the first-appearance of diopside in marble can be delineated as an isograd on a map. Likewise, the last occurrence of tremolite in dolomite-rich marbles can be mapped as an isograd that is related to invariant point [4]. The pressure dependence of singular points that limit a unique assemblage on a T–a section can be shown on a P–T diagram as a univariant curve (Fig. 6.14). For instance, maximum P–T conditions of the assemblage Tr + Dol + Cal given by the maximum T of reaction (6.5) in Fig. 6.5 (last Tr in Dol-marble) is at about 660°C and 730 MPa. If a flat P–T path (geotherm) is chosen for constructing Fig. 6.5, the T and P for the last tremolite would have also been lower. A steeper P–T path results in a higher T at a higher P. All P–T conditions at which the last tremolite disappears from Dol-marbles are consequently given by a curve on Fig. 6.14. Note also that  $a_{\text{CO}_2}$  varies along the curves in Fig. 6.14. Other upper or lower limits of assemblages in marbles are also shown in Fig. 6.14. A prograde path of metamorphism in a given terrain will intersect the boundaries displayed on Fig. 6.14 at specific P–T points and these intersections are mappable isograds in marbles as shown by the contact metamorphic example illustrated in Fig. 6.11 and described above.

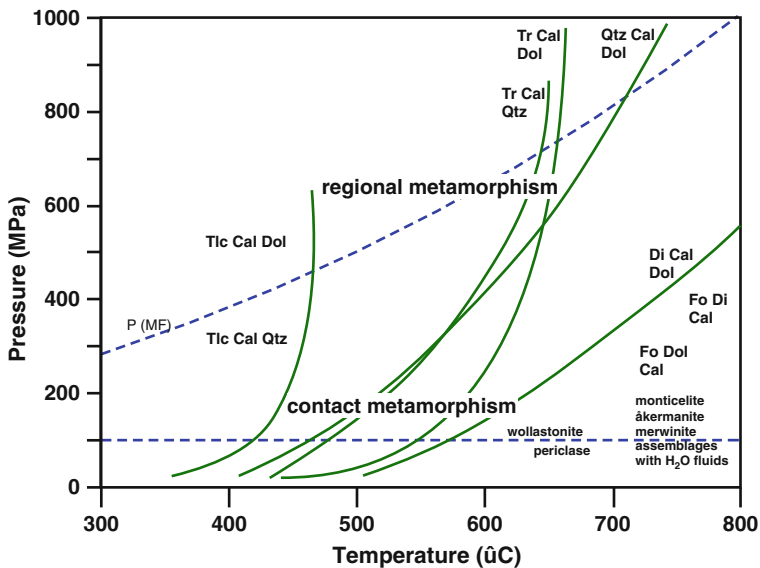


**Fig. 6.14** Isograds in siliceous dolomites and limestones projected into the P–T-plane. The P–T-trajectory (*curved stippled line*) signifies a metamorphic field gradient typically found in regional metamorphic areas in collision belts and shown on Figs. 6.5–6.7. The isobaric line at 100 MPa correspond to the low-pressure contact metamorphic conditions shown on Figs. 6.8–6.11



The **diopside-in isograd** can correspond to the upper limit of  $\text{Tr} + \text{Cal} + \text{Qtz}$  or to the invariant point [2] assemblage (coexistence of  $\text{Dol} + \text{Cal} + \text{Tr} + \text{Qtz} + \text{Di}$ ). The assemblage coexists with increasingly  $\text{H}_2\text{O}$ -rich fluids as pressure increases. This is a general relationship and holds for all polybaric traces of isobaric invariant assemblages. Fig. 6.14 shows that a diopside-in isograd mapped in a contact aureole at 100 MPa marks  $450^\circ\text{C}$ , in a low-P regional metamorphic area it coincides with about  $550^\circ\text{C}$  and in a kyanite-type regional metamorphic field the diopside-in isograd is coincident with about  $640^\circ\text{C}$ . The assemblage  $\text{Dol} + \text{Cal} + \text{Qtz} + \text{Tlc} + \text{Tr}$  defines the **talco-out isograd** and **tremolite-in isograd**. Its temperature is about  $420^\circ\text{C}$  at low P and  $470^\circ\text{C}$  in regional metamorphism and rather independent of the precise position of the P–T trajectory of a particular orogenic metamorphic region. The upper limit for  $\text{Tr} + \text{Cal} + \text{Qtz}$  (**Tr + Cal + Qtz-out isograd**) coincides with the diopside-in isograd at pressures above about 300 MPa. Below this pressure the isograd occurs at slightly higher T than the diopside-in isograd. The **Dol + Qtz-out isograd** is defined by the T maximum of reaction (6.3) at a given pressure (pure  $\text{CO}_2$  fluid). It marks the maximum conditions for the sedimentary  $\text{Dol} + \text{Cal} + \text{Qtz}$  assemblage. The **Di + Dol-out isograd** marks the last occurrence of diopside in dolomite-rich rocks. The curve also marks approximately the **Fo + Cal-in isograd**.

The position of isograd assemblages in P–T space (Fig. 6.14) for regional metamorphism shows that there are only two potentially useful isograds that may be found in field studies. At about  $450^\circ\text{C}$  corresponding to upper greenschist facies conditions tremolite appears abruptly in marbles with many vol% (see also Fig. 6.6). The second one is the abrupt first occurrence of diopside (Di-in isograd) at  $630^\circ\text{C}$  (at 700 MPa). Di-in is an easily mapable isograd in regional metamorphic areas and it marks the beginning of the upper amphibolite facies. In low-pressure contact aureoles the isograd boundaries are more evenly distributed (between  $430^\circ\text{C}$  and  $580^\circ\text{C}$  at 100 MPa) and give rise to well defined and mapable isograds (see also example Fig. 6.11).

## 6.7 Metamorphic Reactions Along Isothermal Decompression Paths

As outlined in Chap. 3, the metamorphic evolution of rocks during orogenesis follows distinct P–T–time paths. After the maximum temperature has been reached during metamorphism associated with continental collision, a marked period of rapid uplift and decompression often follows and a nearly isothermal decompression stage has been documented from many such orogenic belts. Below we examine transformations which may occur in middle amphibolite facies grade marbles during uplift and isothermal decompression.

This geological situation is best modeled by isothermal P– $a_{\text{CO}_2}$  sections. Figure 6.15 shows two model sections at a constant temperature of  $600^\circ\text{C}$ , one for (a)

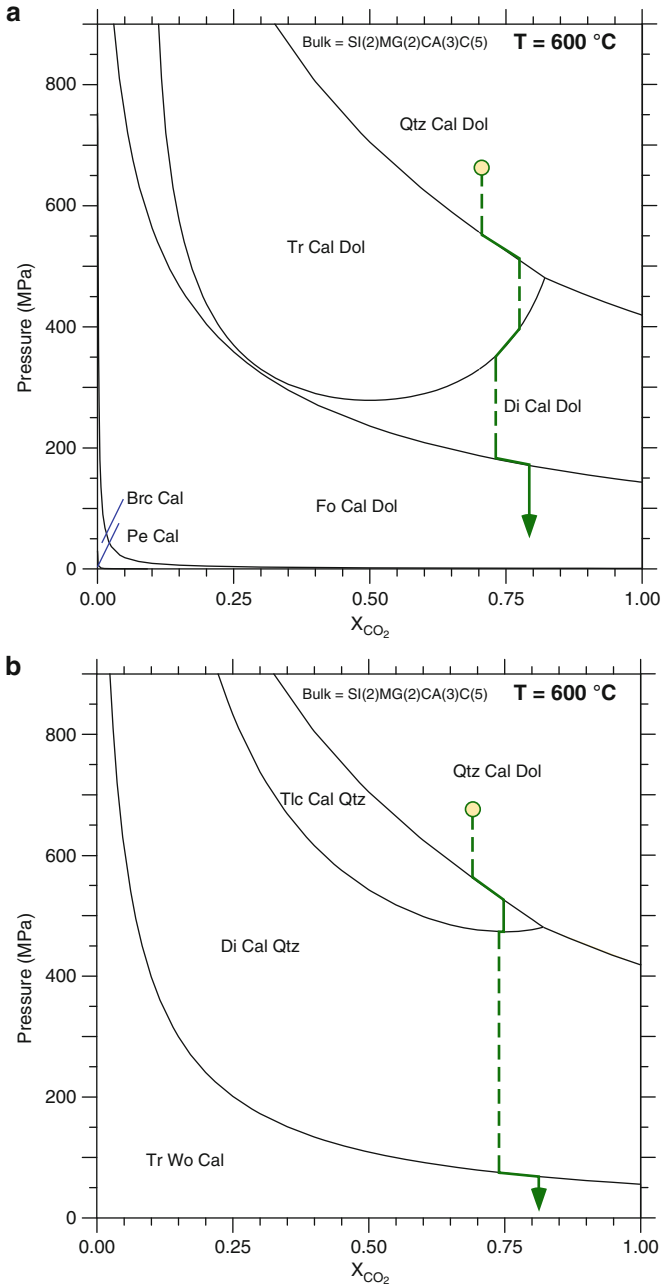


**Fig. 6.15** P- $a_{CO_2}$  phase relationships for (a) siliceous dolomites and (b) limestones (calcareous sandstone) at a constant temperature of 600°C. On both figures: the stipled and arrowed path is followed by the respective rocks during isothermal decompression. It shows that high-grade assemblages in regional metamorphic marbles can be formed along late decompression paths

dolomite-rich marbles and one for (b) calcsilicate marbles. The figure is valid for all carbonate rocks that were initially composed of Dol + Cal + Qtz. Before decompression begins, the marbles may contain a number of different assemblages at 600°C and, for instance 650 MPa, depending on the composition of the rock and the fluid present in the pore space (or introduced during metamorphism). For example a rock composed of Dol + Cal + Qtz at the position marked with an open circle on Fig. 6.15 will travel along a complex path upon decompression to a final pressure of say 100 MPa before the onset of cooling. The precise path depends on the modal abundance of Dol, Cal and Qtz in the initial rock (the path on Fig. 6.14 is a possible example).

Tremolite will appear at pressures around 500 MPa. Later tremolite is replaced by diopside at pressures below 500 MPa in calcsilicate marbles and below 400 MPa in dolomite marble. Ultimately, forsterite may appear in the marbles via reaction (6.9) at pressures below 200 MPa. In Cal + Qtz marbles, wollastonite may be produced by reaction (6.16) in detectable amounts at pressures below about 100 MPa (e.g., along a path taken by the rock in Fig. 6.15b). The effect may be further enhanced by introducing H<sub>2</sub>O-rich fluids during decompression. For example, wollastonite observed in granulite facies marbles may have formed during rapid uplift along a path of nearly isothermal decompression together with infiltration of the marbles by late H<sub>2</sub>O-rich fluids.

In summary, rapid uplift along isothermal decompression paths may drastically modify marble assemblages that originally formed during prograde orogenic metamorphism. Assemblages produced by reactions during isothermal decompression may be difficult to distinguish from assemblages produced at “peak” conditions. The best way to detect the presence of decompression assemblages in marbles is by an integral evaluation of the metamorphic evolution of the entire region (e.g., comparison with thermobarometry data from associated metapelites). Decompression assemblages may form in all type of rocks. Generally, they form if a rock follows a path from maximum P–T that crosses devolatilization reactions in a prograde direction. The least hydrated state (or in the case of marbles: the state with the least volatile content) is typically reached at the low-P end of an isothermal decompression period before significant cooling sets in (especially if the isothermal decompression portion of the path follow max-T). It is this point along the P–T path that may be best preserved in metamorphic assemblage of the rocks.

## 6.8 Marbles Beyond the CMS-HC System

In the following section the consequences of additional components in marbles, usually in amounts of typically less than 5 wt% of combined Al<sub>2</sub>O<sub>3</sub> + Fe<sub>2</sub>O<sub>3</sub> + FeO + MnO + TiO<sub>2</sub> + Na<sub>2</sub>O + K<sub>2</sub>O + F, is discussed.

### 6.8.1 Fluorine

As mentioned above, marbles are often extremely poor in iron. Consequently, hydrous Mg-silicates such as Tlc and Tr are usually very close to their end member composition. However, metamorphic fluids commonly have a small but essential partial pressure of hydrofluoric acid (HF). Fluorine is strongly partitioned into solid hydrate phases. In other words, a small amount of HF in the fluid coexists with rather fluorine-rich minerals. Campolungo tremolite (Fig. 6.3), the type tremolite, for example contains 1.4 wt% F. In addition,  $X_{\text{Fe}}$  and  $X_{\text{F}}$  in hydrate silicates (e.g., talc and tremolite) are negatively correlated, which means that at a given  $P_{\text{HF}}$  the replacement of hydroxyl groups by fluorine rapidly decreases with increasing  $X_{\text{Fe}}$ . The consequence of the  $\text{F}(\text{OH})_{-1}$  exchange in talc and tremolite is a general increase of their respective stability fields on the phase diagrams presented above. The net effect on the talc-tremolite boundary is an increase of the talc field.

In forsterite-grade marbles, a small HF pressure may lead to the formation of minerals of the humite group, i.e., clinohumite (Chu; low  $P_{\text{HF}}$ ) and chondrodite (Chn; high  $P_{\text{HF}}$ ). Both minerals are not stable in pure  $\text{CO}_2\text{-H}_2\text{O}$  fluids, but their stability fields roughly coincide with the forsterite fields on the  $P\text{-T-a}$  diagrams above. However, their occurrence is restricted to the  $\text{H}_2\text{O}$ -rich side of the phase diagrams. The precise location of the phase boundaries involving Chu or Chn depends on the prevailing HF pressure during metamorphism. Typical assemblages in dolomite marbles are: Dol + Cal + Fo + Chu (clinohumite marbles) or Dol + Cal + Chu + Chn (chondrodite marbles, humite marbles). Chn and Fo do not occur together. Chu and Chn may also be stabilized by the presence of titanium (giving rise to the presence of titano-clinohumite or titano-chondrodite), but both minerals always contain some fluorine if occurring in marbles (Fig. 6.16). It is strongly advised to analyze minerals for fluorine when studying marble samples with the electron microprobe.

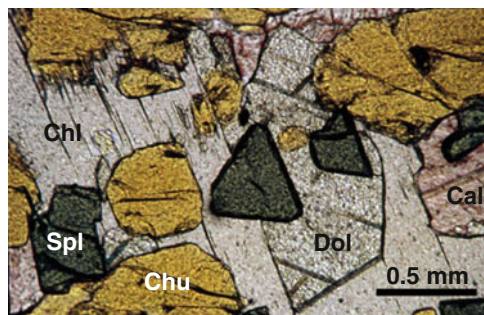
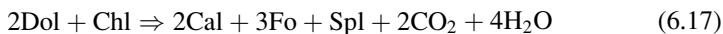


**Fig. 6.16** Fotomicrograph of high-grade contact metamorphic dolomite marble from the Bergell contact aureole (Central Alps). Yellow Ti- and F-bearing clinohumite, green  $\text{MgAl}_2\text{O}_4$  spinel with about 10 mol% hercynite component, clinocllore, dolomite and calcite (stained, red). The forsterite-grade marble formed at about  $600^\circ\text{C}$  and 200–300 MPa

### 6.8.2 Aluminium

Dolomitic limestones usually contain various amounts of Mg-chlorite (clinochlore). The mineral is stable at all metamorphic grades except in the granulite facies and in low-pressure contact aureoles where it may decompose according to the two spinel-producing reactions:



or



At 100 MPa, reaction (6.17) has a T-maximum of 555°C that marks the chlorite-out isograd in rocks containing Dol + Cal + Fo + Chl. Reaction (6.18) has its maximum temperature at 580°C at 100 MPa corresponding to the chlorite-out isograd in rocks containing Cal + Di + Fo + Chl. Forsterite-grade marbles in contact aureoles may contain clinohumite (F and Ti) + spinel (Al) in addition to carbonate (Fig. 6.16). They may also contain clinochlore as a reactant (prograde) or as a retrograde product of the reactions (6.17) or (6.18).

The maximum temperature for the two reactions increases with increasing pressure, which means that chlorite remains stable in regionally metamorphosed rocks up to granulite facies conditions. At 700 MPa chlorite-out occurs at 715°C in Dol-rich rocks, and at 715°C in Dol-poor marbles.

In contact aureoles, clintonite (Cli), a trioctahedral calcium brittle mica, occasionally occurs in dolomite marbles of the forsterite zone. Typical assemblages are (for example): Cal + Fo + Di + Spl + Cli and Cal + Fo + Chu + Spl + Cli.

The presence of aluminum in calcsilicate marbles may lead to the appearance of a number of additional minerals such as margarite, zoisite, grossular, scapolite, vesuvianite and anorthite. The phase relationships of such rocks will be discussed in Chap. 8 on metamorphism of marls that contain significantly greater amounts of the additional oxides listed above, particularly Al<sub>2</sub>O<sub>3</sub> and iron.

### 6.8.3 Potassium

Potassium in sedimentary dolomites is present in the form of detrital or autigenic K-feldspar and/or muscovite. These are two of the first minerals of the sedimentary assemblage to be removed from marbles undergoing progressive metamorphism. The reaction that consumes K-feldspar to form phlogopitic biotite is,



In natural systems, the equilibrium of reaction (6.19) runs approximately parallel to and a few degrees below reactions (6.1) and (6.2) on the (P)–T–a phase diagrams

above. After completion of the reaction, dolomite marble contains the assemblage Dol + Cal + Qtz + Phl. The assemblage subsequently undergoes reactions (6.1) or (6.2) as discussed above. Reaction (6.19) also increases  $a_{\text{CO}_2}$  in the fluid and may run to completion at  $a_{\text{CO}_2}$  greater than that of the invariant point [1]. Thus, rocks undergoing reaction (6.19) are potentially deflected around the talc field and talc will not form in phlogopite-bearing marbles. With increasing grade, such rocks contain the following assemblages: Dol + Cal + Qtz + Kfs, Dol + Cal + Qtz + Phl, Dol + Cal + Tr + Phl (phlogopite marbles). Phlogopite remains stable in rocks containing excess Dol and Cal to very high grades. For example, the assemblage Dol + Cal + Fo + Chu (F) + Spl (Al) + Phl (K) often occurs in contact metamorphic marbles near the contact of an intrusive body. Note also that phlogopite stability is significantly affected by the  $\text{F}(\text{OH})_{-1}$  exchange.

An example of phlogopite and K-feldspar reactions in *impure* siliceous dolomite (contain detrital Kfs) is afforded by the contact aureole developed around the Marysville granodiorite, Montana, shown in Fig. 6.17 (field data from Rice 1977). The initial assemblage Dol + Cal + Qtz + Kfs is successively replaced by

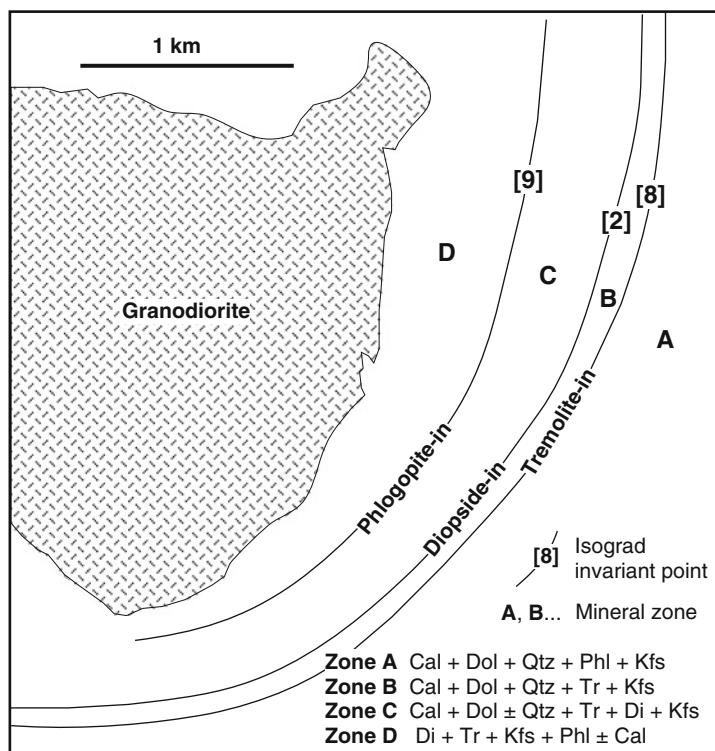
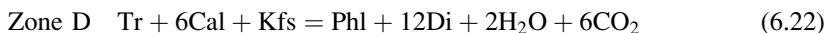
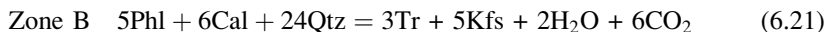
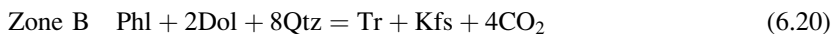


**Fig. 6.17** Distribution of isograds and mineral zones developed in impure siliceous dolomite surrounding a granodiorite pluton (Marysville pluton, Montana). Simplified and modified after Fig. 2 of Rice (1977). Note that zone C is a combination of zones C and D and isograd [9] replaces isograd IV of Rice (1977)

a sequence of assemblages linked by reactions (6.19)–(6.23) in addition to (6.2), (6.3), (6.5) and (6.14) listed in Table 6.1.



The Kfs- and Phl-involving equilibria are shown on Fig. 6.18 at the estimated  $P$  of the Marysville areole. The observed sequence of assemblages (Fig. 6.17) is linked to the consistent metamorphic path on Fig. 6.18. The reaction path runs across the three invariant points [8], [2] and [9] (Fig. 6.18) representing the mapable

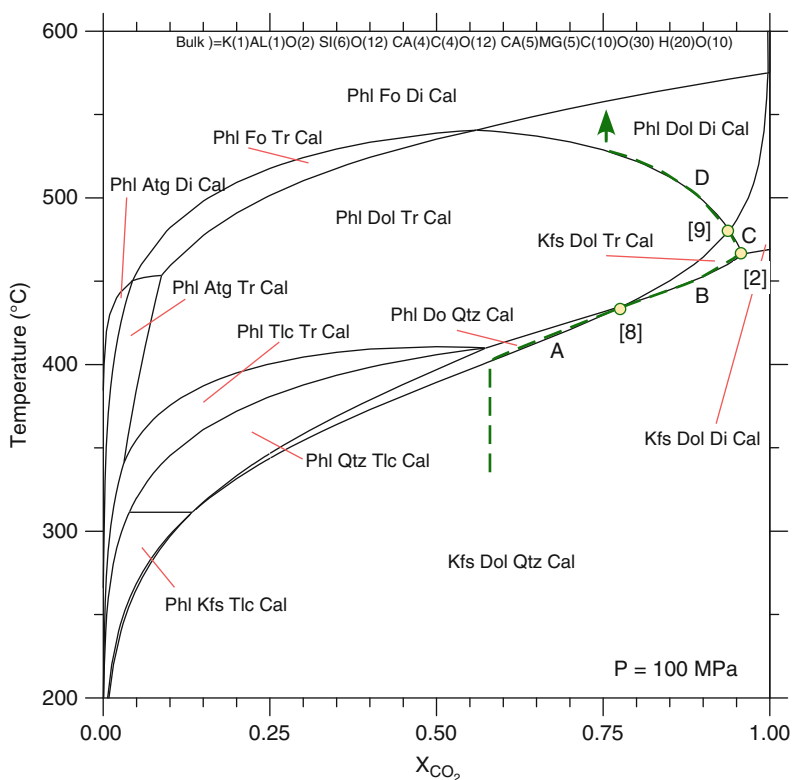


**Fig. 6.18**  $T$ - $x_{\text{CO}_2}$  diagram at 100 MPa for the rock composition of 1Kfs–4Cal–5Dol–3Qtz with labeled mineral assemblage fields. Circles indicate invariant points [8], [2] and [9] corresponding to the isograd positions of Fig. 8.16 together with mineral zones A, B, C, D as indicated. Prograde metamorphism of the rock with the indicated composition follows the dashed arrowed path

isograds in the field (Fig. 6.17). The three isograds section the path and the field area in three zones (A)–(D). The lowest grade contact metamorphic zone (A) is characterized by the assemblage Cal + Dol + Qtz + Phl + Kfs. The temperature of Phl-in is at about 400–425°C, but the first appearance of phlogopite could not be determined in the field because of very fine grain size ( $\ll 0.1$  mm) that makes unambiguous identification of the stable mineral assemblage difficult. Zone (B) is marked by the appearance of Tr and the disappearance of Phl (isograd, invariant point [8];  $a_{\text{CO}_2} = \sim 0.78/435^\circ\text{C}$ ) giving rise to the diagnostic assemblage Cal + Dol + Qtz + Tr + Kfs. At higher grade Zone (C) is defined by the appearance of Di (isograd, invariant point [2];  $a_{\text{CO}_2} = 0.96/465^\circ\text{C}$ ) where the rocks become coarser grained and develop a hornfelsic texture. The characteristic assemblage in Zone (C) is Cal + Qtz + Tr + Di + Kfs although Qtz disappears in the higher grade part of the zone. The boundary between Zones (C) and (D) is marked by a second incoming of Phl (isograd, invariant point [9];  $a_{\text{CO}_2} = 0.93/475^\circ\text{C}$ ) and Zone (D) has the characteristic silicate assemblage Phl + Di + Kfs + Tr. The final fluid became fixed at around  $a_{\text{CO}_2} = 0.75$  and T-max of metamorphism must have been below that of Fo formation at about 560°C (Fig. 6.18). Thus, with progressive metamorphism the fluid was buffered to a more CO<sub>2</sub>-rich composition up to the Di-in isograd and then back towards more H<sub>2</sub>O-rich values at higher grade. MgCO<sub>3</sub> contents of Cal coexisting with Dol indicate a temperature of 450–475°C for isograd [2] (Rice 1977), which brackets the T indicated from Fig. 6.18.

Phase equilibria involving Phl and Kfs with additional Ms, Zo, An and Mg-Chl, in calc-silicate rocks will be discussed further in Chap. 8 dealing with the metamorphism of marls.

### 6.8.4 Sodium

Sodium may be present as NaCl in the metamorphic fluid (albite in low grade dolomites is rare). Its presence complicates the phase relationships in Al-bearing dolomite marbles because it continuously modifies the composition of tremolite with increasing temperature. The compositional changes of calcic amphibole are closely described by the tremolite-pargasite exchange reaction ( $\# \text{Mg } 2\text{Si} = \text{Na } 3\text{Al}$ ; # denotes a vacancy) which produces pargasitic amphiboles at high temperature. Consequently, the upper limit of amphibole in marbles is displaced to higher temperatures compared to the pure CMS-HC system.

## 6.9 Thermobarometry of Marbles

There is only one useful geological thermometer available for temperature estimates in marbles.



### 6.9.1 Calcite–Dolomite Miscibility Gap

In rocks containing excess dolomite, the solubility of  $\text{MgCO}_3$  in calcite is a function of temperature and to a lesser degree also of pressure. The temperature dependence of the  $\text{MgCa}_{-1}$  exchange in calcite (and because of the asymmetry of the miscibility gap with some restrictions also the  $\text{CaMg}_{-1}$  exchange in dolomite) represents a widely used geological thermometer. Various calibrations exist in the geological literature (see Chap. 4).

## 6.10 High-Pressure and Ultrahigh-Pressure Metamorphism of Carbonate Rocks

High-pressure (HP) and ultrahigh-pressure (UHP) subduction related metamorphism is not normally well preserved in marbles. Carbonate rocks recrystallize relatively easily and HP/UHP assemblages are lost due to retrogression during exhumation. Marbles are also often strongly deformed (e.g., Fig. 6.1) and deformation facilitates fluid access and retrogression. Marbles are associated with eclogites in many HP/UHP terrains but eclogite facies mineral assemblages are rarely preserved in the marbles and other carbonate-dominated rocks (e.g., calcareous micaschists).

However, marbles with glaucophane, omphacite, high-Si phengite and other minerals typical of HP-conditions have been reported in association with eclogites (see references). In addition, the carbonate minerals calcite and dolomite undergo phase transitions to HP-phases and thus have restricted stability with increasing pressure. The products of these HP-transitions are often best preserved in silicate rocks (e.g., Cal- or Dol-bearing eclogites) and not in marbles.

*Cal–Arg transition.*  $\text{CaCO}_3$  undergoes a phase transition from trigonal calcite to orthorhombic aragonite at high pressures. At  $400^\circ\text{C}$  the transition pressure is close to 1.0 GPa, and at  $800^\circ\text{C}$  aragonite is stable at pressures greater than 1.5 GPa. However, aragonite is easily converted to calcite during decompression of carbonate-bearing high-pressure rocks. Occasionally, the mineral is preserved in rocks that were metamorphosed in a subduction zone and rapidly returned to the surface without being substantially heated. The presence of aragonite in metamorphic rocks indicates minimum pressures in excess of 1.0 GPa (also see comments on the Arg = Cal transition in Chap. 4).

*Cal–Arg–Dol assemblage.* In UHP rocks (e.g., Dabie Mountains, China, and the Kokchetav massif, Kazakhstan), dolomite + aragonite are the stable carbonate phases at peak P–T conditions of metamorphism. The compositions of Mg-rich calcite and Ca-rich dolomite coexisting with aragonite can be used to derive minimum P–T conditions along the equilibrium reaction, aragonite + dolomite = Mg-rich calcite.

*Dol breakdown.* The breakdown of dolomite to form aragonite + magnesite seems to indicate extremely high pressures of metamorphism, i.e., >quartz/coesite and graphite-diamond phase transitions. However, the P–T conditions of the

transition is very difficult to locate experimentally (e.g., Sato and Katsura 2001; Shirasaka et al. 2002; Morlidge et al. 2006). The Dol = Arg + Mgs reaction is a solid–solid reaction and very sensitive to small amounts of impurities in the carbonates and to the structural state of the solids (ordering state of dolomite). This holds true for the other solid phase transitions of the carbonates as well. The textures of the Dol–Arg–Mgs-bearing rocks are often ambiguous (Smit et al. 2008) and presently there is little agreement on the significance of the assemblage in a specific rock. Experimental and computed Dol-breakdown curves are located in the field characterized by geothermal gradients  $<5^{\circ}\text{C}/\text{km}$  (Zhang et al. 2003). A consequence is that the dolomite breakdown requires a special tectonic process to bring the rocks into the zone with  $<5^{\circ}\text{C}/\text{km}$  gradients (which has been named “forbidden zone” by Zhang et al. 2003).

## References and Further Reading

### *Cited References*

- Cook SJ, Bowman JR (1994) Contact metamorphism surrounding the Alta Stock: thermal constraints and evidence of advective heat transport from calcite-dolomite geothermometry. *Am Mineralog* 79:513–525
- Ferry JM, Boswell AW, Rumble D (2001) Formation of wollastonite by chemically reactive fluid during contact metamorphism. Mt. Morrison pendant, Sierra Nevada, California, USA. *J Petrol* 42:1705–1728
- Grapes RH (2006) *Pyrometamorphism*. Springer, Berlin, Heidelberg, New York, 275 pp
- Morlidge M, Pawley A, Droop G (2006) Double carbonate breakdown reactions at high pressures: an experimental study in the system CaO–MgO–FeO–MnO–CO<sub>2</sub>. *Contrib Mineralog Petrol* 152:365–373
- Rice JM (1977a) Progressive metamorphism of impure dolomitic limestone in the Marysville aureole, Montana. *Am J Sci* 277:1–24
- Sato K, Katsura T (2001) Experimental investigation on dolomite dissociation into aragonite + magnesite up to 8.5 GPa. *Earth Planet Sci Lett* 184:529–534
- Shirasaka M, Takahashi E, Nishihara Y, Matsukage K, Kikegawa T (2002) In situ X-ray observation of the reaction dolomite = aragonite + magnesite at 900–1300 K. *Am Mineralog* 87:922–930
- Smit MA, Bröcker M, Scherer EE (2008) Aragonite and magnesite in eclogites from the Jæren nappe, SW Norway: disequilibrium in the system CaCO<sub>3</sub>–MgCO<sub>3</sub> and petrological implications. *J metamorph Geol* 26:959–979
- Zhang L, Ellis DJ, Arculus RJ, Jiang W, Wei C (2003) ‘Forbidden zone’ subduction of sediments to 150 km depth – the reaction of dolomite to magnesite + aragonite in the UHPM metapelites from western Tianshan, China. *J Metamorph Geol* 21:523–529

### *Further Reading and Recommended Literature*

- Anovitz LM, Essene EJ (1987) Phase equilibria in the system CaCO<sub>3</sub>–MgCO<sub>3</sub>–FeCO<sub>3</sub>. *J Petrol* 28:389–414
- Bickle MJ, Powell R (1977) Calcite-dolomite geothermometry for iron-bearing carbonates. The Glockner area of the Tauern window, Austria. *Contrib Mineralog Petrol* 59:281–292

- Bowen NL (1940) Progressive metamorphism of siliceous limestones and dolomite. *J Geol* 48:225–274
- Bowman JR, Essene EJ (1982) P-T-X(CO<sub>2</sub>) conditions of contact metamorphism in the Black Butte aureole, Elkhorn, Montana. *Am J Sci* 282:311–340
- Bucher-Nurminen K (1981) Petrology of chlorite-spinel marbles from NW Spitsbergen (Svalbard). *Lithos* 14:203–214
- Bucher-Nurminen K (1982) On the mechanism of contact aureole formation in dolomitic country rock by the Adamello intrusion (N Italy). *Am Mineralog* 67:1101–1117
- Cartwright I, Buick IS (1995) Formation of wollastonite-bearing marbles during late regional metamorphic channelled fluid in the Upper Calcisilicate Unit of the Reynolds Range Group, central Australia. *J Metamorph Geol* 13:397–417
- Castelli D (1991) Eclogitic metamorphism in carbonate rocks: the example of impure marbles from the Sesia-Lanzo zone, Italian Western Alps. *J Metamorph Geol* 9:61–78
- Castelli D, Rolfo F, Groppo C, Compagnoni R (2007) Impure marbles from the UHP Brossasco-Isasca Unit (Dora-Maira Massif, western Alps): evidence for Alpine equilibration in the diamond stability field and evaluation of the X(CO<sub>2</sub>) fluid evolution. *J Metamorph Geol* 25:587–603
- Connolly JAD, Trommsdorff V (1991) Petrogenetic grids for metacarbonate rocks: P-T phase-diagram projection for mixed-volatile systems. *Contrib Mineralog Petrol* 108:93–105
- Cook SJ, Bowman JR (2000) Mineralogical evidence for fluid-rock interaction accompanying prograde contact metamorphism of siliceous dolomites: Alta Stock Aureole, Utha, USA. *J Petrol* 41:739–758
- Dunn SR, Valley JW (1992) Calcite-graphite isotope thermometry: a test for polymetamorphism in marble, Tudor gabbro aureole, Ontario, Canada. *J Metamorph Geol* 10:487–502
- Eggert RG, Kerrick DM (1981) Metamorphic equilibria in the siliceous dolomite system: 6 kbar experimental data and geologic implications. *Geochim Cosmochim Acta* 45:1039–1049
- Ehlers K, Hoinkes G (1987) Titanian chondrodite and clinohumite in marbles from the Ötztal crystalline basement. *Mineral Petrol* 36:13–25
- Eveney B, Shermann D (1962) The application of chemical staining to the study of diagenesis in limestones. *Proc Geol Soc Lond* 1599:10 pp
- Fernández-Caliani JC, Galán E (1998) Effects of fluid infiltration on wollastonite genesis at the Mérida contact-metamorphic deposits, SW Spain. *Mineral Petrol* 62:247–267
- Ferry JM, Rumble D (1997) Formation and destruction of periclase by fluid flow in two contact aureoles. *Contrib Mineralog Petrol* 128:313–334
- Gieré R (1987) Titanian clinohumite and geikielite in marbles from the Bergell contact aureole. *Contrib Mineralog Petrol* 96:496–502
- Goldsmith JR, Newton RC (1969) P-T-X Relations in the system CaCO<sub>3</sub>-MgCO<sub>3</sub> at high temperatures and pressures. *Am J Sci* 267A:160–190
- Harker RI, Tuttle OF (1956) Experimental data on the P<sub>CO2</sub>-T curve for the reaction: calcite + quartz = wollastonite + carbon dioxide. *Am J Sci* 254:239–256
- Harley SL, Buick IS (1992) Wollastonite-scapolite assemblages as indicators of granulite pressure-temperature-fluid histories: the Rauer Group, East Antarctica. *J Petrol* 33:693–728
- Holness MB (1997) Fluid flow path and mechanisms of fluid infiltration in carbonates during contact metamorphism: the Beinn an Dubhaich aureole, Skye. *J Metamorph Geol* 15:59–70
- Jamtveit B, Dahlgren S, Austrheim H (1997) High grade contact metamorphism of calcareous rocks from the Oslo Rift, Southern Norway. *Am Mineralog* 82:1241–1254
- Jansen JBH, van den Kratts AH, van der Rijst H, Schuiling RD (1978) Metamorphism of dolomites at Naxos, Greece. *Contrib Mineralog Petrol* 67:279–288
- Kato T, Enami M, Zhai M (1997) Ultra-high-pressure (UHP) marble and eclogite in the Su-Lu UHP terrane, eastern China. *J Metamorph Geol* 15:169–182
- Letargo CMR, Lamb WM, Park J-S (1995) Comparison of calcite + dolomite thermometry and carbonate + silicate equilibria: constraints on the conditions of metamorphism of the Llano uplift, central Texas, U.S.A. *Am Mineralog* 80:131–143

- Lieberman JE, Rice JM (1986) Petrology of marble and peridotite in the Seiad ultramafic complex, northern California, USA. *J Metamorph Geol* 4:179–199
- Liu L-G, Lin C-C (1995) High-pressure phase transformations of carbonates in the system CaO-MgO-SiO<sub>2</sub>-CO<sub>2</sub>. *Earth Planet Sci Lett* 134:297–305
- Moore JN, Kerrick DM (1976) Equilibria in siliceous dolomites of the Alta aureole, Utah. *Am J Sci* 276:502–524
- Mposkos E, Baziotis I, Proyer A, Hoinkes G (2006) Dolomitic marbles from the ultrahigh-pressure metamorphic Kimi complex in Rhodope, N.E.Greece. *Mineral Petrol* 88:341–362
- Ogasawara Y, Ohta M, Fukosawa K, Katayama I, Maruyama S (2000) Diamond-bearing and diamond-free metacarbonate rocks from Kumdy-Kol in the Kokchetav massif, northern Kazakhstan. *Island Arc* 9:400–416
- Omori S, Liou JG, Zhang RY, Ogasawara Y (1998) Petrogenesis of impure dolomitic marble from the Dabie Mountains, Central China. *Island Arc* 7:98–114
- Powell R, Condcliffe DM, Condcliffe E (1984) Calcite-dolomite geothermometry in the system CaCO<sub>3</sub>-MgCO<sub>3</sub>-FeCO<sub>3</sub>: an experimental study. *J Metamorph Geol* 2:33–41
- Proyer A, Mposkos E, Baziotis I, Hoinkes G (2008) Tracing high-pressure metamorphism in marbles: phase relations in high-grade aluminous calcite-dolomite marbles from the Greek Rhodope massif in the system CaO-MgO-Al<sub>2</sub>O<sub>3</sub>-SiO<sub>2</sub>-CO<sub>2</sub> and indications of prior aragonite. *Lithos* 104:119–130
- Rice JM (1977b) Contact metamorphism of impure dolomitic limestone in the Boulder Aureole, Montana. *Contrib Mineralog Petrol* 59:237–259
- Roselle GT, Baumgartner LP, Valley JW (1999) Stable isotope evidence of heterogeneous fluid infiltration at the Ubehebe Peak contact aureole, Death Valley National Park, California. *Am J Sci* 299:93–138
- Schmid J, Flammer I (2002) How grey limestones become white marbles. *Eur J Mineralog* 14:837–848
- Skippen G (1974) An experimental model for low pressure metamorphism of siliceous dolomitic marbles. *Am J Sci* 274:487–509
- Skippen G, Trommsdorff V (1986) The influence of NaCl and KCl on phase relations in metamorphosed carbonate rocks. *Am J Sci* 286:81–104
- Slaughter J, Kerrick DM, Wall VJ (1975) Experimental and thermodynamic study of equilibria in the system CaO-MgO-SiO<sub>2</sub>-H<sub>2</sub>O-CO<sub>2</sub>. *Am J Sci* 275:143–162
- Suzuki K (1977) Local equilibrium during the contact metamorphism of siliceous dolomites in Kasuga-mura, Gifu-ken, Japan. *Contrib Mineralog Petrol* 61:79–89
- Tilley CE (1951) A note on the progressive metamorphism of siliceous limestones and dolomites. *Geol Mag* 88:175–178
- Trommsdorff V (1972) Change in T-X during metamorphism of siliceous dolomitic rocks of the central Alps. *Schweiz Mineral Petrogr Mitt* 52:567–571
- Valley JW, Peterson EU, Essene EJ, Bowman JR (1982) Fluorophlogopite and fluortremolite in Adirondack marbles and calculated C-O-H-F fluid compositions. *Am Mineralog* 67:545–557



# Chapter 7

## Metamorphism of Pelitic Rocks (Metapelites)

### 7.1 Metapelitic Rocks

Metapelites are probably the most distinguished family of metamorphic rocks. Typical examples include characteristic rocks and minerals such as chlorite–kyanite–schist, staurolite–garnet micaschist, chloritoid–garnet micaschist, kyanite–staurolite schist, biotite–garnet–cordierite gneiss, sillimanite–biotite gneiss and orthopyroxene–garnet granulite.

In many metamorphic terrains, characteristic minerals in metapelites show a regular spatial distribution that can be readily related to the intensity of metamorphism. The pattern of metapelitic mineral distribution reflects the general metamorphic style and structure of many metamorphic terrains in orogenic collision belts. Mineral zones and mineral assemblages in metapelites often permit a fine-scale analysis of the intensity and nature of metamorphism in a given area. A number of well-established and calibrated geological thermometers and barometers can be applied to mineral assemblages in metapelitic rocks.

### 7.2 Pelitic Sediments

#### 7.2.1 *General*

Metapelitic rocks are derived from fine-grained (typically  $<2\ \mu\text{m}$ ) clay-rich sedimentary rocks such as shale, claystone and mudstone. Shale represents  $> 80\%$  of all sedimentary rocks (Table 2.2). With incipient metamorphism, these pelitic rocks are collectively termed **argillite** and further weak metamorphism transforms them into slate.

Semi-pelitic rocks with a high proportion of silt (siltstones) and less clay transform to metamorphic equivalents with less interesting and diagnostic mineral assemblages.

## 7.2.2 Chemical Composition

Of the two types of pelitic rocks (platform shale and pelagic clay) listed in Table 2.3, the characteristic composition of pelitic rocks is best represented by the pelagic clay deposited in deep sea basins. Aluminum is very high at 16.6 wt%  $\text{Al}_2\text{O}_3$ , total iron is significant at 10 wt%, and moderate amounts of MgO (3.4 wt%) and alkalis (4 wt%) are present. Calcium is extremely low (0.7 wt% CaO or lower). Water is high with 5 mol of  $\text{H}_2\text{O}/\text{kg}$  rock reflecting (along with the high  $\text{Al}_2\text{O}_3$ ) the high clay-content. From the viewpoint of a metamorphic geologist, this is a positive aspect because it can be expected that  $\text{H}_2\text{O}$  released during metamorphism helps to maintain chemical equilibrium in the rocks during recrystallisation. Prograde metamorphism of pelitic sediments thus begins with rocks in a maximum hydrated state. This is often not the case in other rock compositions (e.g., ultramafic and mafic rocks). In contrast, platform shales often deviate from pure clay compositions because of a higher silt fraction (higher  $\text{SiO}_2$  reflecting greater amounts of detrital quartz and feldspar), and/or the presence of carbonate (higher CaO and  $\text{CO}_2$ ), and there is a complete transition between pure clay (pelagic) compositions and arkose or marl. In chapter 7 the metamorphism of *carbonate-free* claystone and shale compositions is described.

## 7.2.3 Mineralogy

The mineralogy of claystone and shale is dominated by clay minerals such as montmorillonite, smectite and kaolinite. Muscovite and paragonite of detrital or autigenic origin are also an important group of minerals and contribute to bulk alkali and alumina contents with abundant chlorite accounting for much of the Mg and Fe present. Together, the above sheet silicates usually represent much more than 50 vol% of the rock. Quartz occurs in modal proportions of typically between 10–30 vol%. As a consequence, most metamorphic equivalents of shales contain quartz despite the fact that many of the prograde mineral reactions in pelitic rocks consume quartz. Shales also contain detrital and/or autigenic feldspars and sometimes a substantial amount of zeolite. An additional complication arises from high modal amounts of Fe-oxides-hydroxides (hematite–goethite) in some shales and sulfides and organic carbonaceous matter in others (oil shale). This has the consequence that REDOX-reactions and sulfur-involving reactions can be important in metapelitic rocks.

## 7.3 Pre-metamorphic Changes in Pelitic Sediments

During compaction and diagenesis, primary clays and shales undergo significant chemical and mechanical changes. The very large (e.g., >50%) porosity of clays is continuously reduced during burial and compaction. Typical shales may still

contain several percent pore space filled with formation water when metamorphism starts at approximately 200°C and about 6 km depth = 160 MPa. Original clay minerals, such as smectite are replaced by illite (a precursor mineral of the white K-micas) and chlorite. Lattice ordering of the sheet silicates, particularly of illite, progressively increases with increasing temperature and pressure. Illite “crystallinity” can be used as a measure of the degree of diagenetic and very low-grade metamorphic recrystallization. Carbonaceous matter undergoes a series of reactions which ultimately destroy the organic compounds to eventually form graphite or are completely transferred to the vapor phase as CO<sub>2</sub> or CH<sub>4</sub> under oxidizing and reducing conditions respectively. Optical reflectivity of carbonaceous matter is also used as a sensitive indicator of the thermal regime during diagenesis and incipient metamorphism (Sect. 4.10.2.2). Compaction and recrystallization during burial and diagenesis also produce a distinct fissility and cleavage (slaty cleavage) resulting from pressure-induced parallel orientation of the sheet silicate minerals.

Consequently, during the initial stage of metamorphism, shale is transformed to slate and phyllite with a mineralogy that typically includes Kln, Ill (Ms), Chl, Qtz and feldspar (Ksp and Ab), Hem or sulfides and graphite. The bulk chemical composition of the shale remains more or less unchanged during pre-metamorphic processes with the exception of H<sub>2</sub>O-loss.

Below, we detail the mineralogical changes that occur in slate and phyllite when they are subjected to an increase in T and P during a tectono-metamorphic event such as a typical orogenic cycle.

## 7.4 Intermediate-Pressure Metamorphism of Pelitic Rocks

Metapelites formed by intermediate-P (IP) metamorphism (see Sect. 4.3.3) include the well-known schists and gneisses mentioned in Sect. 7.1. The distinct zonal pattern of mineral assemblages in metapelitic rocks that is produced by IP orogenic metamorphism has been found and extensively studied in a large number of metamorphic terrains from many orogenic belts (fold belts, mountain belts, mobile belts in cratonic areas) ranging in age from Precambrian to Tertiary. Intermediate-P metamorphism is also referred to as “Barrovian” metamorphism referred to in Sect. 4.2, Figs. 4.1 and 4.2, after being first described from the Scottish Highlands by G Barrow (1893, 1912) (Fig. 7.1). It corresponds approximately to a prograde metamorphic path along a Ky-type field gradient.

### 7.4.1 *Chemical Composition and Chemography*

Reactions and assemblages in metapelites can be discussed by means of selected simple chemical subsystems. By reference to the average composition of pelagic clays (Table 2.3), the components occur in the following order of abundance: SiO<sub>2</sub>,



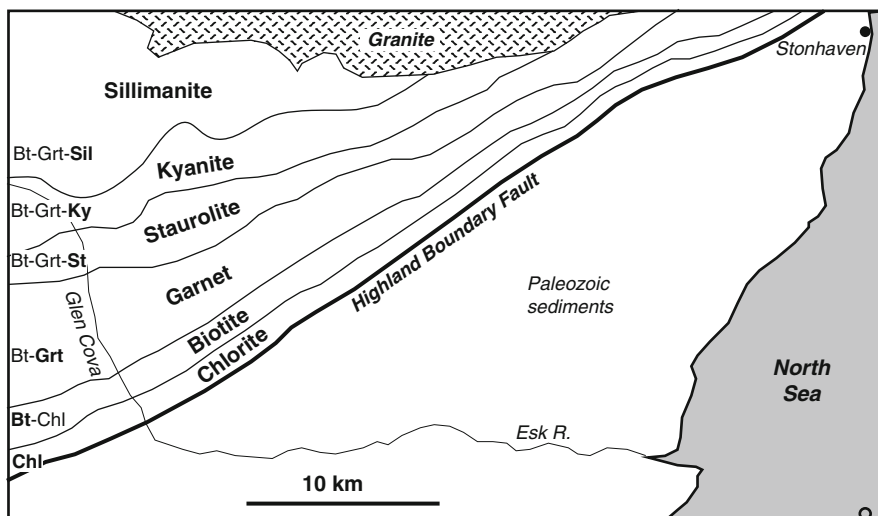


**Fig. 7.1** Map showing distribution of mineral zones in pelitic rocks mapped by G. Barrow, SE Scottish Highlands, and later defined as the typical sequence of Barrovian metamorphism (After Barrow 1893, 1912; Tilley 1925). See Fig. 4.1 for location. Diagnostic minerals of each zone are listed below (see also Fig. 4.2). Note that in the chlorite and biotite zones, plagioclase is albite (Ab); in the garnet zone, Ab + oligoclase; in the staurolite, kyanite and sillimanite zones Pl changes from oligoclase to andesine with increasing metamorphic grade. The staurolite-in isograd marks the beginning of amphibolite facies conditions (no Ab)

$\text{Al}_2\text{O}_3$ ,  $\text{FeO} + \text{Fe}_2\text{O}_3$ ,  $\text{H}_2\text{O}$ ,  $\text{MgO}$ ,  $\text{K}_2\text{O}$ ,  $\text{Na}_2\text{O}$ ,  $\text{TiO}_2$ ,  $\text{CaO}$ . This ten-component system can be subdivided into manageable subsystems. Metapelite compositions are often approximated by a six-component system that include the six most abundant oxides above and representing total iron as FeO. This system can be graphically represented in AFM diagrams as outlined in Chap. 2. Sodium is mainly stored in feldspar (Ab) and paragonite. Reactions involving Na-bearing minerals will be discussed separately below. The low amount of CaO in clays is, in metapelitic rocks, present in garnet (Grs component) and plagioclase (An component). Complications arising from CaO and other minor components in metapelites will be discussed in Sect. 7.9.

#### 7.4.2 Mineral Assemblages at the Beginning of Metamorphism

The AFM-chemography of shales at the onset of metamorphism is represented in Fig. 7.2. The requirements of the AFM-projection are met by many shales. As outlined above, most shales contain modally abundant quartz and illite (white mica such as Ms and Ser) and excess  $\text{H}_2\text{O}$ . Because pelitic sediments are at a maximum hydrated state (at least when metamorphosed for the first time!), they will experience

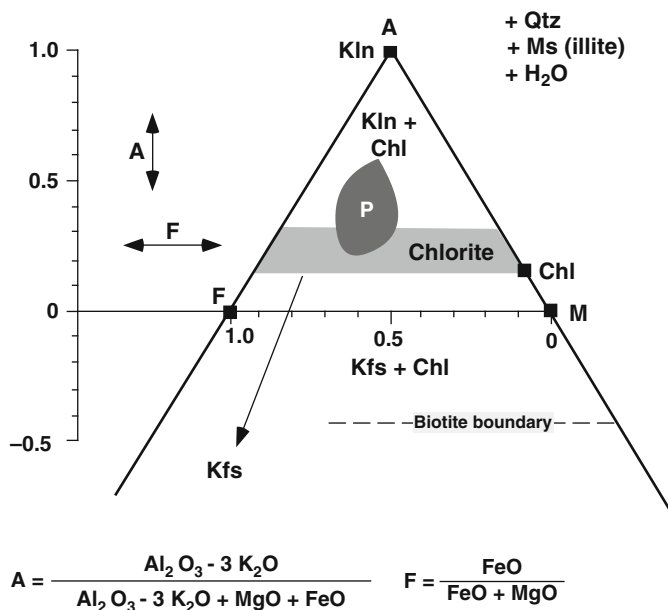


Fig. 7.2 AFM diagram for low-grade shales. Compositions of pelagic clays and muds fall into the dark shaded area and the average pelagic clay (Table 2.3) is represented by P. AFM coordinates of minerals and rocks can be calculated from equations given below the figure (molar basis)

a series of dehydration reactions when heat is added during prograde metamorphism. Thus, during much of their prograde metamorphic evolution, metapelites may remain water-saturated.

The average composition of typical shales (Table 2.3) falls into the dark shaded area of Fig. 7.2 and has the following AFM-coordinates:  $A = 0.41$ ;  $F = 0.62$ . It is represented by point P in Fig. 7.2 and this composition can be regarded as the reference “normal” pelite composition. Such a shale contains Kao/Prl + Chl in addition to Qtz, Ms (Ill, Ser) and water at the beginning of metamorphism. The prerequisite of the AFM diagram requires that Qtz and Ms is present during the course of prograde metamorphism. At high-grade conditions Ms may be replaced by Kfs. This means that “true” metapelites should always contain Ms (or Kfs). Metapelite composition P of Fig. 7.2 has the TS-component in Chl buffered by the assemblage, whereas the FM-component is constrained by the bulk composition. This follows from the fact that P plots in the Kao + Chl univariant field. Shale compositions falling into the divariant Chl field contain Chl as the only AFM phase. The Chl composition is given by the bulk composition and can vary within the horizontal shaded field representing the range of compositional variation observed in low temperature chlorites (Chl solid solution). Shales with A-values below about 0.17 (clinocllore composition), contain the univariant assemblage Chl + feldspar. Such compositions will not develop the characteristic and diagnostic mineral assemblages that one usually associates with metapelites unless the bulk composition

is much more magnesian than compositions within the dark shaded area. If the A-coordinate is below  $-0.5$ , diagnostic assemblages will not develop in such rocks irrespective of their F-coordinate. This compositional restriction may be designated as the **biotite boundary**. Biotite-gneiss and schist, garnet-biotite gneiss and two mica gneiss are typical metamorphic products of low-Al shales/siltstones and are often referred to as semi-pelitic gneisses and shales. The most typical assemblage  $\text{Qtz} + \text{Kfs} + \text{Ms} + \text{Bt} \pm \text{Pl}$  is widespread in meta-arkoses and metagranitoid rocks. Reactions and assemblage variations with grade in such rocks will be in Chap. 10 on quartzofeldspathic rocks.

### 7.4.3 The ASH System

The two most abundant components of pelites ( $\text{SiO}_2$  and  $\text{Al}_2\text{O}_3$ ), together with  $\text{H}_2\text{O}$  (ASH), make up a group of typical minerals in metapelites: Kao, Prl, the three aluminosilicate polymorphs (Ky, Sil, And) and Qtz (and its polymorphs). The ASH system is a subsystem of the KFMASH system portrayed by AFM diagrams. It describes all phase relations and reactions in the A-apex of an AFM diagram.

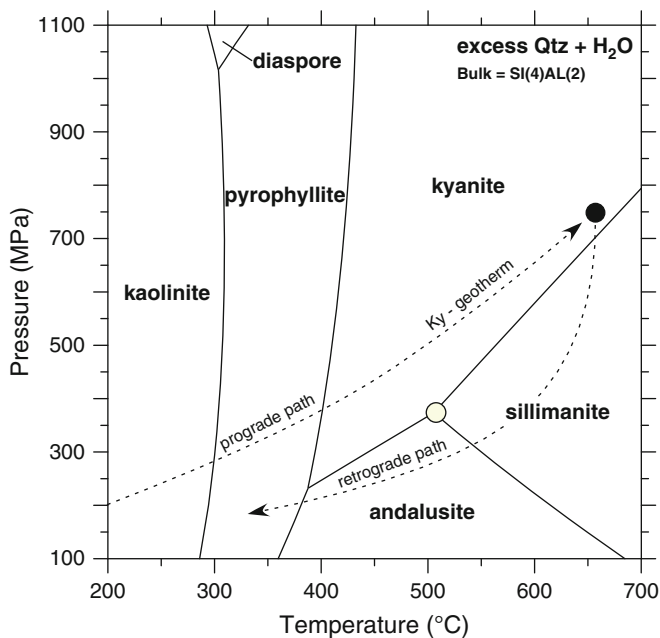


**Fig. 7.3** Distribution of stable assemblages in the ASH-system. Typical prograde and retrograde paths of metamorphism are shown as *arrowed dashed lines*. Maximum  $P$ - $T$  conditions are at *black dot*. The retrograde path shows initial near isothermal decompression (see also Chap. 3)

**Table 7.1** Reactions in the ASH system

Sillimanite, kyanite, andalusite	$\text{Al}_2\text{SiO}_5$
Pyrophyllite	$\text{Al}_2\text{Si}_4\text{O}_{10}(\text{OH})_2$
Kaolinite	$\text{Al}_2\text{Si}_2\text{O}_5(\text{OH})_4$
Quartz	$\text{SiO}_2$
And = Ky	(7.1)
And = Sil	(7.2)
Sil = Ky	(7.3)
$\text{Kln} + 2\text{Qtz} = \text{Pr1} + \text{H}_2\text{O}$	(7.4)
$\text{Pr1} = \text{Ky} + 3\text{Qtz} + \text{H}_2\text{O}$	(7.5)
$\text{Pr1} = \text{And} + 3\text{Qtz} + \text{H}_2\text{O}$	(7.6)

Reaction equilibria in the ASH system are shown in Fig. 7.3 and listed in Table 7.1 in relation to bulk compositions with excess quartz and  $\text{H}_2\text{O}$  (as for AFM diagrams).

Prograde metamorphism will replace Kao by Pr1 at about 300°C and the new stable mineral at the A apex of an AFM diagram is Pr1. At about 400°C and in the presence of a pure  $\text{H}_2\text{O}$ -fluid, Pr1 reaches its upper thermal limit and decomposes to Al-silicate + Qtz (Ky at  $P > 230$  MPa, And at  $P < 230$  MPa). At higher temperatures, the stable divariant assemblage in the ASH system is quartz +  $\text{H}_2\text{O}$  + Al-silicate. The nature of the stable Al-silicate polymorph depends on pressure and temperature (along a Ky-type path:  $\text{Qtz} + \text{Ky} + \text{H}_2\text{O}$ ) and the stable mineral at the A apex of an AFM diagram is Ky, Sil or And depending on the  $P$ - $T$  conditions selected for the AFM diagram. Andalusite is not stable at pressures greater than 370 MPa; Sil is not stable below about 500°C. Aluminosilicates are not stable below about 350–400°C in the presence of  $\text{H}_2\text{O}$  and Qtz [reactions (7.5) and (7.6), Table 7.1]. In low- $P$  orogenic metamorphism, Pr1 decomposes to And + Qtz at about 380°C. Andalusite is replaced by Sil at about 530°C.

Note, however, that in rocks containing abundant organic material (a situation that is not uncommon in pelites) the fluid phase may contain significant  $\text{CH}_4$  at low temperature. Under this condition, the equilibrium of any dehydration reaction will be displaced to lower temperatures compared with the pure  $\text{H}_2\text{O}$ -fluid case shown in Fig. 7.3. Therefore, pyrophyllite usually forms at much lower temperature than indicated in Fig. 7.3. In metapelites, pyrophyllite is common at  $T < 200^\circ\text{C}$ , whereas kaolinite is extremely rare in rocks metamorphosed at  $T > 200^\circ\text{C}$ .

The polymorphic transitions [reactions (7.1), (7.2) and (7.3)] require a complete reconstruction of the Al-silicate structure. Because these “solid-solid” reactions involve only small changes in Gibbs free energy, metastable persistence of one polymorph in the field of another more stable polymorph is common. For example, prograde metamorphism along a Ky-type path to conditions near 650°C and 750 MPa (black dot on Fig. 7.3) produces a rock with the assemblage  $\text{Ky} + \text{Qtz} (+\text{H}_2\text{O})$ . From this  $P$ - $T$  maximum the rock may follow a typical decompression and cooling path (retrograde path on Fig. 7.3). Along the decompression path (retrograde metamorphism) excess water conditions cannot be taken for granted. Lack of water has important consequences for the presence or absence of the stable Al-silicate polymorph even though reactions (7.1), (7.2) and (7.3) are nominally water-absent reactions. At about 700 MPa, coarse-grained Ky that has originally

formed along the prograde path becomes less stable than Sil and under equilibrium conditions all Ky should now be replaced by Sil. In nature, this is normally not the case. Fine Sil needles may grow on Ky or precipitate from Al-silicate-saturated fluids in fractures and nodules and most of the originally-formed Ky remains in the rock. At about 540°C and 310 MPa along the decompression path in Fig. 7.3, both Ky and Sil become less stable with respect to And. However, in most cases, no spontaneous formation of andalusite from kyanite or sillimanite occurs in the rock matrix. Andalusite, like Sil, may form in nodules, veins and fissures by direct precipitation from a fluid phase. Thus, all three Al-silicates can occasionally be observed at a given locality or even in a single hand-specimen. Obviously, this does not necessarily mean that the rocks have been metamorphosed at or near the Al-silicate triple point as the three Al-silicates found at one locality are normally not isochronous as each began to form at different depths along a metamorphic  $P$ - $T$ - $t$ -path.

The observation of metastable persistence of one polymorph in the stability field of another suggests that water, although not a species in the stoichiometric reaction equation, is present in the rock as both, a solvent and catalyst. If water is present along a decompression path, metastable Ky (for example) can be dissolved and stable Sil may precipitate. This is further supported by the frequent observation of Sil or And in veins, fractures and nodules in otherwise massive kyanite-bearing rocks, i.e., in structures that are clearly late in the metamorphic history.

#### 7.4.4 Metamorphism in the FASH System

Addition of FeO (as total iron) to the ASH system permits discussion of phase relationships among a number of additional minerals: Fe-chlorite (daphnite, amesite), chloritoid, staurolite, almandine garnet, Fe-cordierite, hercynite-spinel. Additional minerals in the FASH system include Fe-orthoamphiboles (Oam) and Fe-orthopyroxene (Opx). Phase relationships involving Oam- and Opx-bearing assemblages are presented in Sects. 7.5 and 7.6.

The distribution of stable phase fields for an Al-rich bulk composition in the FASH system is shown in Fig. 7.4. The presence of staurolite in the assemblage is highlighted with gray shading. Some additional important equilibria for Fe-rich bulks are also shown as dashed curves. As Fe-chlorite has the lowest  $X_{Al}$  of all minerals of interest, its decomposition at higher temperature produces an Fe-oxide in addition to a product silicate. Iron-oxides in metapelitic rocks are either Hem or/and Mag and both contain trivalent iron. Consequently, terminal chlorite decomposition depends on oxygen activity in the rocks. Two important chlorite-involving REDOX reactions are shown in Fig. 7.4 and they are explained below. The stoichiometric equations of all reaction equilibria shown in Fig. 7.4 are listed in Tables 7.1 and 7.2.

Consider prograde Ky-type metamorphism of a pelitic rock containing the assemblage Chl + Prl with excess quartz and H<sub>2</sub>O (gray thick line in Fig. 7.4).

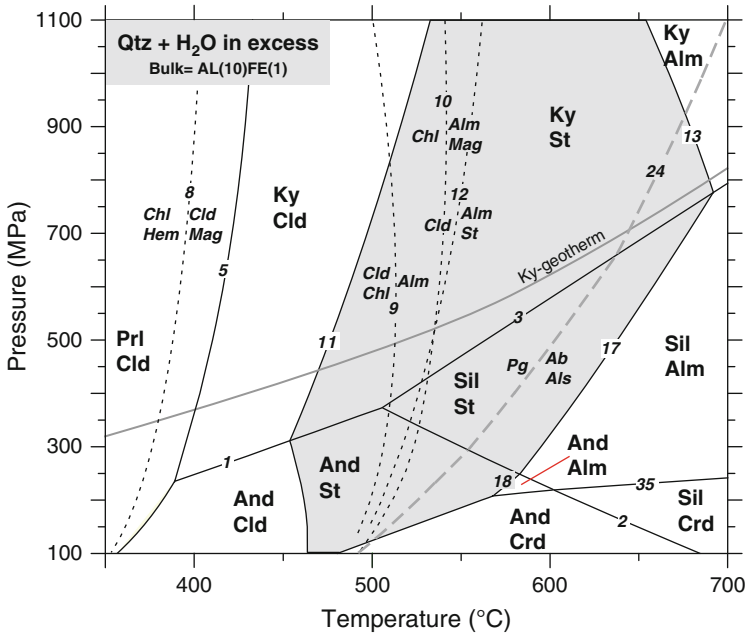


**Fig. 7.4** Stable assemblages in the FASH-system. Numbers refer to reactions listed in Tables 7.1 and 7.2. *Shaded field* – coexistence of St + Qtz, and *Dashed line* – prograde metamorphic path discussed in text

At about 280°C, the Chl–Prl pair is replaced by chloritoid (Cld) by reaction (7.7) (the equilibrium is outside the P–T-window of Fig. 7.4). The appearance of Cld in metapelites coincides with the transition from subgreenschist to greenschist facies. Under lower greenschist facies (~350°C) conditions, Fe-rich metapelites contain the assemblages Chl–Cld or Cld–Prl depending on  $X_{Al}$  of the bulk rock. In “normal” metapelites, Cld will usually appear at somewhat higher temperatures (see below).

At about 380°C, Chl reacts with Hem, the later is often present in low-grade slates and phyllites, and produces Mag and more Cld [reaction (7.8)]. The oxygen activity is controlled by the Hem–Mag pair through the reaction:  $6 \text{Fe}_2\text{O}_3 = 4 \text{Fe}_3\text{O}_4 + \text{O}_2$ . This is the Hem–Mag oxygen buffer (Sect. 3.6.2.4) and it defines relatively high oxygen activities at a given temperature (Fig. 3.20). Since Chl is modally more abundant than Fe-oxides in low-grade phyllites, all Hem will normally be consumed by reaction (7.8). The assemblage Chl–Cld–Mag is now stable above 380°C.

At 400°C, Prl is replaced by Ky and Cld–Ky becomes the diagnostic assemblage in Al-rich rocks [reaction (7.5)].

At about 470°C, Cld and Ky react according to reaction (7.11) and form staurolite (St). The first occurrence of St marks the transition from greenschist facies to amphibolite facies in pelitic rocks. The diagnostic assemblage in lower amphibolite

**Table 7.2** Reactions in the FASH system

Sillimanite, kyanite, andalusite	$\text{Al}_2\text{SiO}_5$
Quartz	$\text{SiO}_2$
Pyrophyllite	$\text{Al}_2\text{Si}_4\text{O}_{10}(\text{OH})_2$
Kaolinite	$\text{Al}_2\text{Si}_2\text{O}_5(\text{OH})_4$
Chlorite (daphnite)	$\text{Fe}_5\text{Al}_2\text{Si}_3\text{O}_{10}(\text{OH})_8$
Chloritoid	$\text{FeAl}_2\text{SiO}_6(\text{OH})_2$
Staurolite	$\text{Fe}_4\text{Al}_{18}\text{Si}_{17.5}\text{O}_{44}(\text{OH})_4$
Almandine	$\text{Fe}_3\text{Al}_2\text{Si}_3\text{O}_{12}$
Hercynite	$\text{FeAl}_2\text{O}_4$
Magnetite	$\text{FeFe}_2\text{O}_4$
Hematite	$\text{Fe}_2\text{O}_3$
Reactions with excess quartz + $\text{H}_2\text{O}$	
And = Ky	(7.1)
And = Sil	(7.2)
Sil = Ky	(7.3)
Kln + 2Qtz = Prl + $\text{H}_2\text{O}$	(7.4)
Prl = Ky + 3Qtz + $\text{H}_2\text{O}$	(7.5)
Prl = And + 3Qtz + $\text{H}_2\text{O}$	(7.6)
Chl + 4Prl = 5Cld + 2Qtz + 3 $\text{H}_2\text{O}$	(7.7)
Chl + 4Hem = Cld + 4Mag + 2Qtz + 3 $\text{H}_2\text{O}$	(7.8)
Chl + Cld + 2Qtz = 2Alm + 5 $\text{H}_2\text{O}$	(7.9)
3Chl = 3Alm + 2Mag + 12 $\text{H}_2\text{O}$ (+QFM)	(7.10)
8Cld + 10Ky = 2St + 3Qtz + 4 $\text{H}_2\text{O}$	(7.11)
23Cld + 7Qtz = 2St + 5Alm + 19 $\text{H}_2\text{O}$	(7.12)
75St + 312Qtz = 100Alm + 575Ky + 150 $\text{H}_2\text{O}$	(7.13)
3Cld + 2Qtz = Alm + 2Ky + 3 $\text{H}_2\text{O}$	(7.14)
3Cld + 2Qtz = Alm + 2And + 3 $\text{H}_2\text{O}$	(7.15)
8Cld + 10And = 2St + 3Qtz + 4 $\text{H}_2\text{O}$	(7.16)
75St + 312Qtz = 100Alm + 575Sil + 150 $\text{H}_2\text{O}$	(7.17)
75St + 312Qtz = 100Alm + 575And + 150 $\text{H}_2\text{O}$	(7.18)
Decomposition of staurolite in qtz-free rocks	
2St = Alm + 12Sil + 5Hc + 4 $\text{H}_2\text{O}$	(7.19)
2St = Alm + 12And + 5Hc + 4 $\text{H}_2\text{O}$	(7.20)

grade metapelite is Cld–St. For the Al-rich bulk used in Fig. 7.4 St–Ky forms at the greenschist facies to amphibolite facies transition and remains the stable until it is replaced by the high-grade Ky–Alm assemblage by reaction (7.13) at a temperature close to 700°C (upper amphibolite facies). Almandine garnet is formed by the decomposition of Chl–Cld [reaction (7.9)] and two additional diagnostic assemblages are Chl–Alm and Alm–Cld with garnet-formation in the pure FASH system at about 520°C (Note: these reactions shown as dashed curves refer to less Al-rich bulk compositions than used for the background grid of Fig. 7.4). At 540°C, Cld disappears from Qtz-bearing rocks by reaction (7.12). This means that Cld, which is the most characteristic mineral in greenschist facies metapelites, extends into the lower amphibolite facies. The disappearance of Cld-bearing assemblages marks the upper boundary of the lower amphibolite facies. The greater part of amphibolite facies pelitic rocks is characterized by the assemblages St + Ky and St + Alm.

Chlorite decomposes in Qtz-bearing rocks at about 540°C by reaction (7.10) Alm + Mag. The disappearance of Chl coincides with that of Cld. In Fig. 7.4,

oxygen activity along reaction (7.10) is controlled by the QFM buffer and it is implicitly assumed that oxygen activities in metapelites at the beginning of the amphibolite facies are close to those defined by the QFM assemblage. Depending on the  $X_{Al}$  of the rock, stable assemblages at this metamorphic grade are: Mag + Alm, Alm + Cld, Cld + St and St + Ky.

Finally, at 690°C St decomposes in Qtz-bearing rocks and the characteristic high-grade assemblage is Alm + Ky [reaction (7.13)]. The  $P$ - $T$  field with stable St + Qtz is shaded in Fig. 7.4. It follows from Fig. 7.3 that metamorphism along prograde paths at very low and very high pressures will remain in the St + Qtz field only over a small temperature interval. Chloritoid is replaced directly by Alm-And at very low pressure [reaction (7.15)] and by Alm-Ky at pressures greater than 1.4 GPa [reaction (7.14)]. In Qtz-free rocks, St survives to much higher temperatures than in Qtz-bearing rocks. Reactions (7.19) and (7.20) describe St decomposition in Qtz-free rocks to form Alm + Al-silicate + Hc-spinel. In high-T contact metamorphism a number of Fe-Crd- and Hc-involving assemblages appear in Fe-rich metapelites (lower-right area of Fig. 7.4). Crd-Spl assemblages will be discussed in Sect. 7.5.

The sequence of diagnostic assemblages and their  $P$ - $T$  limits during metamorphism along other prograde  $P$ - $T$  paths can be determined from Fig. 7.4. For example, the temperature interval of St + Qtz is much smaller along a low- $P$  metamorphic path compared to the Ky-type path. Thus extensive zones with staurolite-bearing metapelites are characteristic for typical “Barrovian-style” (Ky-type) regional metamorphic terrains, in agreement with Fig. 7.4. In Al-rich rocks, the prograde sequence of two-mineral assemblages is: Chl + Prl, Cld + Prl, Cld + Ky, St + Ky and Alm + Ky, and these can also be used to define characteristic metamorphic zones in a “Barrovian-style” regional metamorphic terrain.

### 7.4.5 Mica-Involving Reactions

Micas (muscovite, paragonite, biotite) are the most important mineral group in metapelitic rocks. Typical metapelitic rocks are, for this reason, termed micaschists and mica gneisses. Muscovite and paragonite are commonly designated white micas (dioctahedral micas) and their distinction under the microscope is difficult (use X-ray patterns). All micas show compositional variation along the  $FeMg_{-1}$  (FM) and  $MgSiAl_{-2}$  (TS) exchange directions. Sedimentary and diagenetic illite rapidly recrystallizes to K-white mica with various amounts of TS- and FM-components. Low-temperature (high-pressure) K-white mica contains a significant amount of TS-component. Such micas are termed **phengites**. Increasing temperature removes much of the TS-component and high-grade white micas are close to the muscovite end member composition. The  $NaK_{-1}$  exchange is important in metapelites because Ms and Pg commonly coexist in many micaschists, and it is also significant in pelitic rocks containing the widespread assemblage Ms and Ab.



Reaction (7.21) in Table 7.3 replaces the sedimentary assemblage  $Ksp + Chl$  that characterizes arkoses (or very low-grade granites) by  $Bt + Ms$ . The reaction affects rocks with low  $X_{Al}$  that do not contain  $Prl$  (Fig. 7.2). Equilibrium conditions of this reaction in the pure KFMASH system are shown in Fig. 7.5. The equilibrium

**Table 7.3** Additional important reactions in the KNFASH system (in addition to reactions in Tables 7.1 and 7.2)

Annite (biotite)	$KFe_3AlSi_3O_{10}(OH)_2$
Muscovite	$KAl_3Si_3O_{10}(OH)_2$
Paragonite	$NaAl_3Si_3O_{10}(OH)_2$
K-feldspar	$KAlSi_3O_8$
Albite	$NaAlSi_3O_8$
All reactions with excess quartz + $H_2O$	
$3Chl + 8Kfs = 5Ann + 3Ms + 9Qtz + 4H_2O$	(7.21)
$2Pg + 3Chl + 6Qtz = 5Alm + 2Ab + 14H_2O$	(7.22)
$1Ms + 3Chl + 3Qtz = 4Alm + 1Ann + 12H_2O$	(7.23)
$Pg + Qtz = Ab + Als + H_2O$	(7.24)
$1Ms + 1Ann + 3Qtz = 1Alm + 2Kfs + 2H_2O$	(7.25)
$Ms + Qtz = Kfs + Als + H_2O$	(7.26)
Discontinuous reactions in the KFMASH-system	
$Cld = St + Grt + Chl$	(7.27)
$Grt + Chl = St + Bi$	(7.28)
$St + Chl = Bt + Als$	(7.29)
$St = Grt + Bt + Als$	(7.30)
$St + Bt = Grt + Als$	(7.31)
$St + Chl = Als + Grt$	(7.32)
$Grt + Chl = Bt + Als$	(7.33)
$Cld + Als = St + Chl$	(7.34)

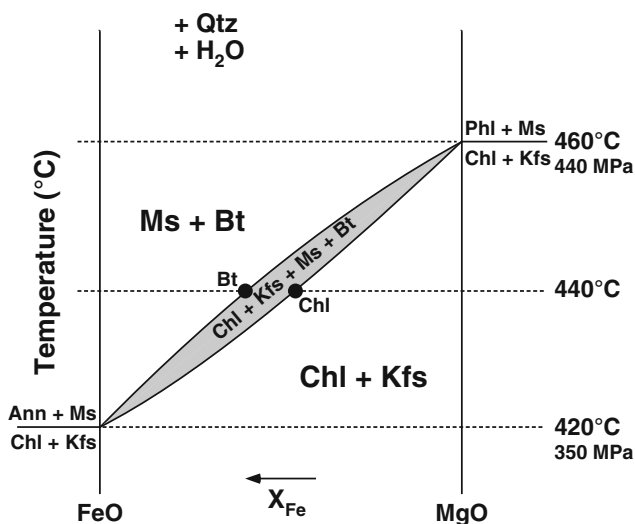


**Fig. 7.5**  $P$ - $T$ - $X_{Fe}$  diagram representing the  $Kfs$ - $Ms$ - $Bt$ - $Chl$  assemblage [reaction (7.21); Table 7.3]. The  $P$ - $T$  gradient corresponds to the  $Ky$ -type path used in previous diagrams

conditions of such reactions depend on the Fe/Mg ratio of the rock. Therefore, the equilibrium conditions of reaction (7.21) can be discussed as a function of  $X_{\text{Fe}}$  (Fig. 7.5). The reaction equilibrium in the pure KFASH system is given on the left hand side of Fig. 7.5 (420°C), whereas the reaction equilibrium in the pure KMASH system (pure Mg-end member) is located on the right hand side of Fig. 7.5 (460°C). In the temperature interval between the two limiting equilibria, all four minerals (Chl + Kfs + Ms + Bt) may occur stably together. For example, at a temperature of 440°C (Fig. 7.5) rocks with an appropriate A-coordinate may consist of Bt + Ms, Bt + Ms + Kfs + Chl, or Kfs + Chl depending on the  $X_{\text{Fe}}$  of the rock. The composition of Bt and Chl in the assemblage Bt + Ms + Kfs + Chl is given by the filled circles. It can be seen from Fig. 7.5 that the three phase field Bt + Kfs + Chl moves across the entire AFM diagram from Fe-rich compositions to Mg-rich compositions over a temperature interval of only 40°C. The product Bt is Fe-rich (typically green biotite under the microscope) that first appears at about 420°C. Since Kfs is modally subordinate to Chl in Al-poor metapelites, all Kfs is consumed by reaction (7.21) and such rocks typically contain the assemblage: Ms + Chl + Bt + Pg + Qtz at  $T > 420^\circ\text{C}$ .

Muscovite remains stable along the Ky-type path to  $T > 700^\circ\text{C}$ . Reaction (7.26) represents the upper limit of Ms in the presence of Qtz and the product assemblage is Kfs + Sil (or And). However, because reactions (7.22) and (7.24) produce Ab (plagioclase) at lower temperature (see below) and reactions (7.25) and (7.26) produce Kfs, the stable assemblage at high temperatures is Kfs + Ab + Qtz. In the presence of excess water, this assemblage begins to melt at rather low temperatures ( $< 700^\circ\text{C}$ ). Partial melting of metapelites and in quartzofeldspathic rocks will be discussed separately in Chap. 11.

#### 7.4.6 Metamorphism in the KFMASH System (AFM System)

The six-component system  $\text{K}_2\text{O}-\text{FeO}-\text{MgO}-\text{Al}_2\text{O}_3-\text{SiO}_2-\text{H}_2\text{O}$  is useful and appropriate to discuss metamorphism of pelites. In contrast to the discussion so far, the effects of the FM component in Fe-Mg-bearing minerals on the distribution of assemblages is considered in this section. The following diagrams show the distribution of mineral assemblages for typical bulk rock compositions in the KFMASH system. Figure 7.6 has been computed for a Chl-Ms schist with  $X_{\text{Fe}} = 0.8$ . In all fields Qtz, Ms and  $\text{H}_2\text{O}$ -fluid are present in addition to the minerals indicated. Note that Kfs replaces Ms in the assemblage fields in the lower right area of Fig. 7.6. The heavy black curve represents the Ms-breakdown reaction (7.26) that replaces Ms by Kfs. The rocks are composed of the three excess phases and one, two or three AFM minerals.

Prograde metamorphism along a Ky-type geotherm produces Bt at about 520°C, the first Grt appears at 540°C and finally St forms at 560°C. The three-phase assemblage Grt-Bt-St is characteristic for much of the amphibolite facies. Finally increasing  $X_{\text{Mg}}$  of all three phases with T brings the bulk composition into the

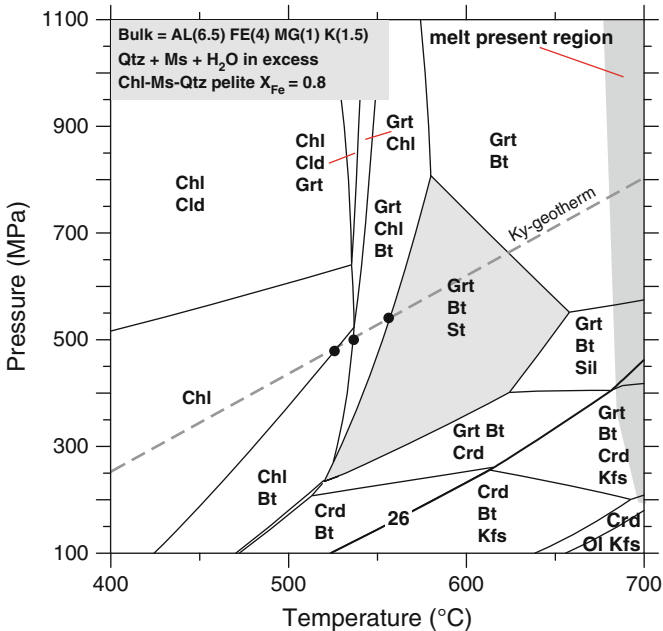


**Fig. 7.6** Stable assemblages in Fe-rich metapelitic rocks that originally contained Chl–Ms–Qtz (model system KFMASH). The mineral zone boundaries along a Ky-geotherm are marked with *black dots*. Note that this type of rock (see also Fig. 7.2) will not develop Sil along a Ky-type geotherm and that it will not contain Ky at any P and T. The fields that contain Kfs do not carry Ms (high T low P). The central amphibolite facies assemblage is Grt–Bt–St (highlighted in gray). Note there is no St at P > 800 MPa and that Chl–Cld–Grt does not occur at P < 650 MPa

Bt–Grt field. The modeled composition of Fig. 7.6 reproduces the “Barrovian” mineral zones of Scotland (Fig. 7.1) quite well. The zones along the dashed path are: chlorite, biotite, garnet, staurolite (the zone boundaries are indicated with small black dots). The path runs inside the kyanite field (Fig. 7.2). However, Ky requires more Al-rich rock compositions than the one used in Fig. 7.6. The sillimanite zone of Fig. 7.1 could also be modeled by the rock composition of Fig. 7.6 as a result of decompression after peak metamorphism (compare also with path on Fig. 7.2). The presence of cordierite in metapelite assemblages is restricted to low-pressure and high-temperature conditions.

Metamorphism of pelitic sediments can be favorably modeled with (P)TX<sub>Fe</sub> sections (Fig. 7.7). The horizontal axis shows the Fe–Mg variation of the rock and on the vertical axis either the temperature at constant pressure or a P–T gradient can be represented. For the (P)TX sections the A-coordinate (see Fig. 7.2) must be specified and the bulk composition is further constrained by the requirement of excess Qtz, Ms and H<sub>2</sub>O. The PTX-section (Fig. 7.7) represents the stable assemblages in metapelites along a the Ky-type geotherm used previously for the A-coordinate (0.4) of the mean pelite compositions shown as “P” on Fig. 7.2. Note that at temperatures above about 700°C partial melting occurs and a melt is present (gray shaded area on Fig. 7.7).

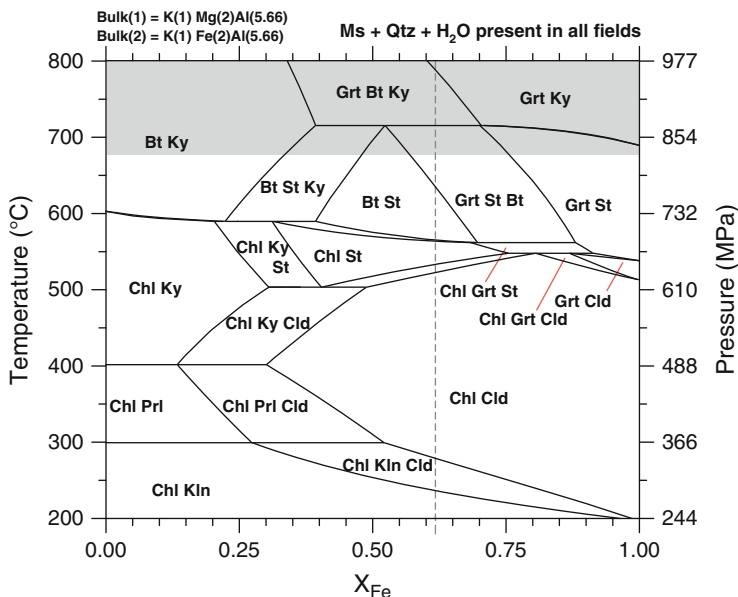


**Fig. 7.7** Fe–Mg dependence of the distribution of stable assemblages in the system KFMASH along a Ky-type geotherm (continent collision type metamorphism).  $X_{\text{Fe}}$  of average pelites shown by *dashed line*. Note that the average pelite would define a mineral zone sequence: Cld, St, Bt, Grt, Ky, quite different from Fig. 7.1 because of different Al content of the rocks and probably also because of a different  $P$ – $T$  path. The *gray shaded area* above 680°C marks the melt present region where Ms melts and is no longer present in the assemblage fields. Note that in very Mg-rich metapelites Chl–Ky decomposes not before middle amphibolite facies is reached (600°C) and that the highest grade assemblage is phlogopite + kyanite

The PTX-window is subdivided into a series of field where two and three AFM minerals are stable, respectively. The fields with three AFM minerals correspond to three-phase fields in AFM-diagrams. It can be seen on Fig. 7.7 that some boundaries of three-phase fields have negative slopes and some have positive slopes. Fields with negative slopes correspond to triangles in AFM-diagrams that rotate to more Mg-rich compositions with increasing temperatures, fields with positive slopes correspond to AFM triangles that rotate to more Fe-rich compositions with T. As an example: All minerals of the Grt + St + Bt assemblage decrease in  $X_{\text{Fe}}$  with increasing T, all minerals of the Bt + St + Ky gradually increase in  $X_{\text{Fe}}$  with T, thus the two phase field Bt + St is progressively reduced until it disappears at 710°C. This is the temperature at which the discontinuous AFM reaction  $\text{St} + \text{Bt} = \text{Grt} + \text{Ky}$  occurs (horizontal line in Fig. 7.7) leaving the three-phase assemblage Grt + Bt + Ky that is diagnostic for upper amphibolite facies metapelites. The assemblage again shows field-boundaries with negative slopes thus consuming Bt and replacing it with Grt + Ky with increasing T. Note that the  $P$ – $T$  gradient intersects the Ky–Sil phase boundary at about 800°C.

The pelite model (Fig. 7.7) shows some general patterns that characterize the succession of mineral assemblages in typical metapelitic rocks: There are

characteristic sequences of prograde assemblages in Fe- and Mg-rich bulk compositions, respectively, that are distinct and remarkably different from each other. The series in Fe-rich rocks is: Chl + Cld, Grt + Cld, Grt + St, Grt + Ky, Grt + Sil. No biotite develops in Fe-rich compositions. In Mg-rich rocks a quite different sequence evolves: Chl + Prl, Chl + Ky, Bt + Ky, Bt + Sil. No garnet, staurolite and chloritoid is formed in Mg-rich rocks. Biotite is generally favored by Mg-rich compositions. Chl + Ky and Bt + Ky are indicative for Mg-rich rocks. The most Fe-rich assemblage with biotite is Grt + St + Bt allowing for the presence of Bt in rocks with a maximum  $X_{\text{Fe}}$  of 0.88. The low-temperature boundary (560°C) of this three phase field represents also the lowest temperature at which Bt occurs. It is 10°C higher than the maximum temperature for the occurrence of Cld. The terminal temperature for Chl is 100°C higher in Mg- than in Fe-rich rocks.

The sequence of assemblages for rocks with the typical  $X_{\text{Fe}}$  of 0.62 (point "P" on Fig. 7.2) can be read from Fig. 7.7 along the gray dashed line (ignoring two very narrow two phase fields). The assemblages with their lower T-limit are: Chl + Cld (280), Chl + St (525), Bt + St (560), Grt + St + Bt (640), Grt + Bt + Ky (710), Grt + Bt + Sil, Grt + Sil. Consequently, Cld is the characteristic mineral in greenschist facies metapelites and staurolite dominates the amphibolite facies. If we tie the onset of amphibolite facies metamorphism to the first appearance of staurolite in metapelitic rocks of average composition this would correspond to a temperature of about 520°C along a Ky-type isotherm. The lowest possible temperature for St is given by the assemblages Chl + St and Chl + St + Ky, which terminate at 500°C but require  $X_{\text{Fe}}$  to be below 0.4. The most typical amphibolite facies metapelitic rocks with increasing grade are: St–Chl micaschist, St–Bt micaschist and Grt–St–Bt micaschist. The upper temperature limit of St is close to or within the melt-present field (Fig. 7.7). The highest-grade St schists are found in areas where gneisses show migmatitic textures.

Al-poor pelites develop prograde sequences of assemblages that are quite different from the sequence shown for pelites with  $A = 0.4$  (Fig. 7.7). Figure 7.8 shows a PTX diagram for  $A = -0.11$  pelites. Again the dashed line for  $X_{\text{Fe}} = 0.62$  marks the average pelite on Fig. 7.2. At low grade the only AFM phase present is chlorite. At about 400°C biotite appears and chlorite reacts out of the rock at  $T < 550^\circ\text{C}$  for the average  $X_{\text{Fe}}$  of pelite. Chlorite persists in Mg-rich rocks up to 600°C and is then replaced by the assemblage Ky + Bt. In  $X_{\text{Fe}} = 0.62$  pelites chlorite is replaced by the characteristic St + Grt + Bt assemblage of amphibolite facies metapelites at about 550°C. In contrast to more Al-rich pelites the assemblage Grt + Bt appears just above 500°C and it is present also in very Fe-rich rock compositions. The striking difference is, however, that no chloritoid appears in Al-poor metapelites during prograde metamorphism.

Very Al-rich pelites are characterized by assemblages that all contain a stable Al-silicate. For  $A = 0.89$  pelites the distribution of stable assemblages is shown on Fig. 7.9. Al-rich metapelites contain chloritoid and one of the Al-silicate minerals according to Fig. 7.3. Under the conditions of the diagram, Chl + Cld is present in addition to Ms + Qtz up to ~500°C. Kyanite appears in the rock at 400°C and at 470°C the first St forms. At 500°C, all Cld has disappeared and the diagnostic assemblages are St + Ky (+ Chl) and Chl + Ky in very Mg-rich rocks.

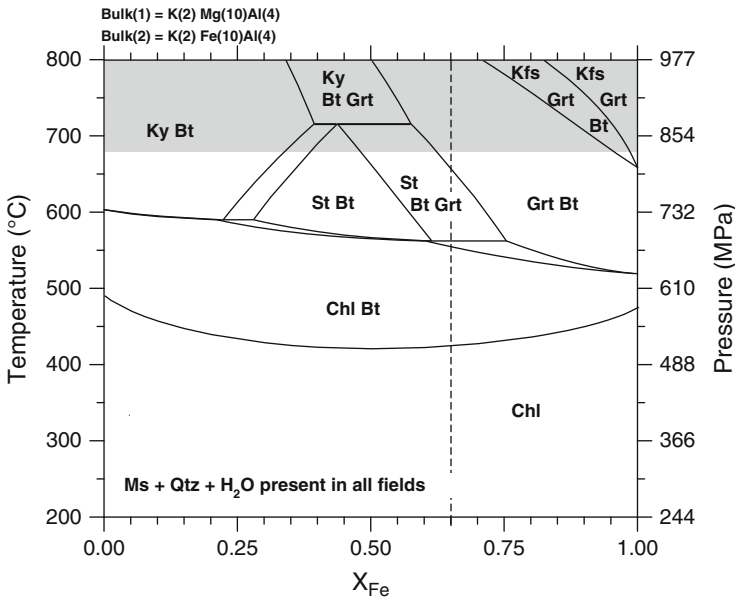


**Fig. 7.8** Distribution of stable assemblages in the system KFMASH along a Ky-type geotherm (continent collision type metamorphism) for variable  $X_{Fe}$  (average pelites shown by *dashed line*). The mineral zone sequence defined by this composition: Cld, Bt, Grt, St. The *gray shaded area* above 680°C marks the melt present region where Ms melts and is no longer present in the assemblage fields

In this Al-rich rock biotite does not form until the temperature has reached ~580°C. With the onset of the amphibolite facies staurolite + kyanite forms and remains the characteristic assemblage to the upper amphibolite facies (~700°C on Fig. 7.9). A typical staurolite + kyanite micaschist from Alpe Sponda (Central Alps) is shown on Fig. 7.10. It formed at about 600°C and 700 MPa. Biotite does not form at  $T < 600^\circ\text{C}$  and is absent from Fe-rich rocks.

Metamorphism of pelitic sediments can also be presented by a series of AFM diagrams (see Chap. 2 and above). The development of mineral assemblages along a medium pressure geotherm (“Barrovian-type”, Ky-geotherm) is represented by the AFM projections shown in Fig. 7.11. Prograde metamorphism will now be discussed, step by step, by reference to Fig. 7.11. The AFM diagrams are schematic and qualitative (computed AFM diagrams look rather unfamiliar because of the changing composition of K-mica used as a projection point).

As outlined above, all mineralogical changes occurring at the A apex of AFM diagrams are described in the ASH system. The FASH system, also discussed above, refers to the FA binary on the left hand side of the AFM diagrams in Fig. 7.11. All reactions in the FASH system represent limiting reactions in the KFMASH system and provide the basic framework of the following discussion. Therefore, much of the topological changes in the AFM diagrams can be understood by reference to Figs. 7.3–7.5. It is important to note that the treatment refers

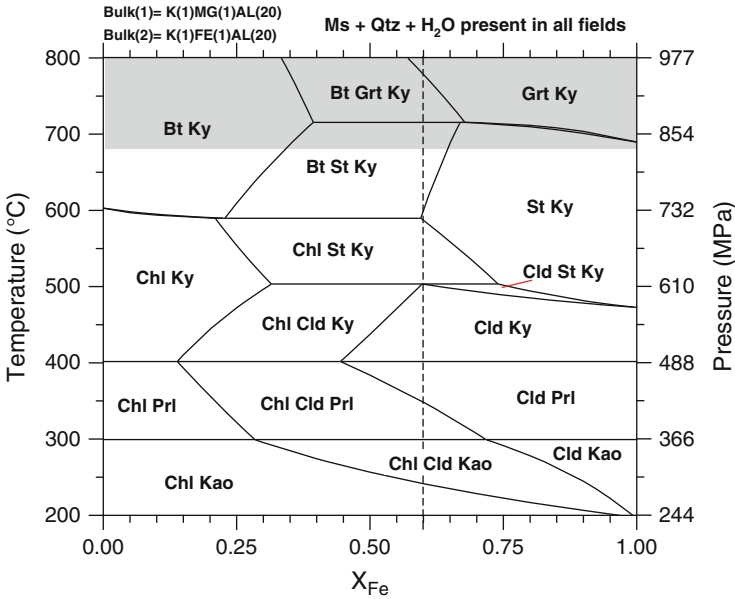


**Fig. 7.9** Stable assemblages in the system KFMASH along a Ky-type geotherm (continent collision type metamorphism) for very Al-rich rock compositions and for variable  $X_{\text{Fe}}$  (average pelites shown by *dashed line*). The mineral zone sequence defined by this composition: Cld, Prl, Ky, St, Bt, Grt. The *gray shaded area* above 680°C marks the melt present region where Ms melts and is no longer present in the assemblage fields. Note that this diagram shows the relationships of Fig. 7.3 plus the sequence of AFM minerals. This sequence is for Fe-rich compositions Cld, St, Grt and for Mg-rich compositions Chl, Bt. Also note that there is a large field for St–Ky, which is not present on Figs. 7.7 and 7.8

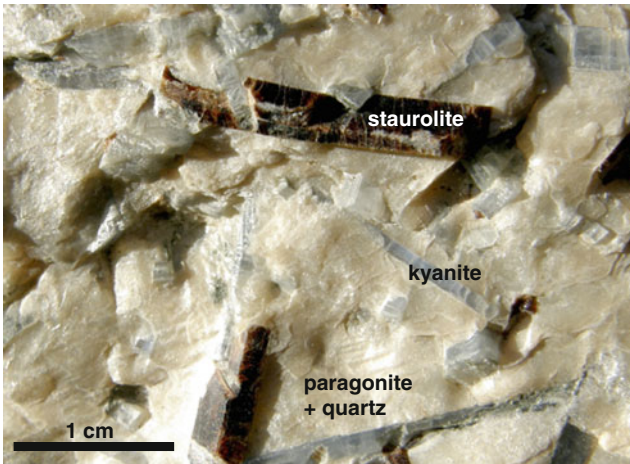


**Fig. 7.10** Staurolite–kyanite schist from Alpe Sponda in the Ticino area of the Central Alps (5 × 3 cm). The rock has been metamorphosed at about 600°C and 700 MPa (see Fig. 7.9) under amphibolite facies conditions during Tertiary continent collision. The rock also contains muscovite and paragonite and excess quartz

**Sequence of mineral assemblages in meta-pelitic rocks during progressive metamorphism**

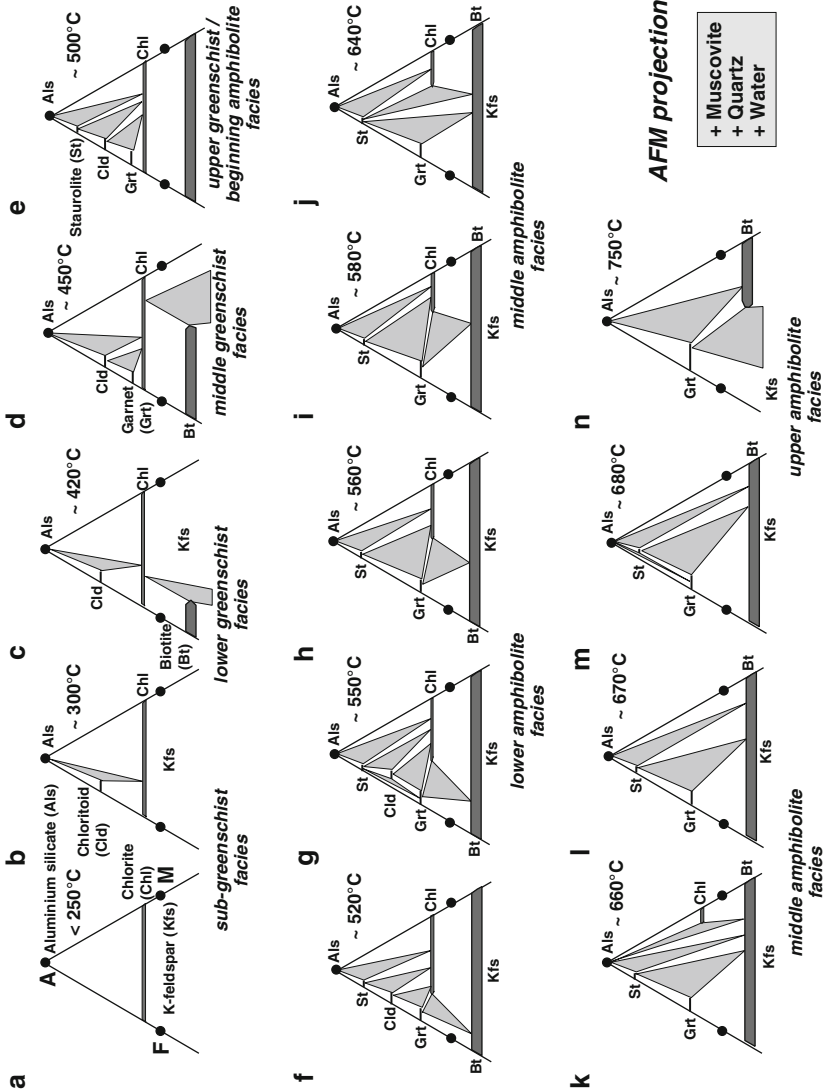


**Fig. 7.11** Sequence of assemblages displayed as a sequence of schematic AFM diagrams in the KFMASH system (AFM-system) along a Ky-type path of metamorphism that corresponds to the previous figures (see text)



strictly to the six-component KFMASH system. However, metapelitic rocks usually contain small but not negligible amounts of other components that may give rise to some “extra” complications (see Sect. 7.9).

1. At temperatures below about 250°C, the stable assemblage in “normal” pelites is Qtz–Ill (Ms)–Chl–Prl (or Kln)–Pg. Semi-pelitic compositions with less alumina may contain abundant Kfs instead of Prl.
2. The first truly metamorphic mineral formed is **chloritoid**. In “normal” pelites chloritoid appears at about 300°C. Assemblages at this stage are: Cld + Chl, Cld + Prl, Chl + Prl and Cld + Prl + Chl.
3. Near 400°C, the first **biotite** appears in Al-poor metapelites. Biotite forms at the expense of Kfs and Chl. The reaction has equilibrium conditions of 420°C at about 350 MPa along the Ky-type path in the pure KFMASH system. However, the reaction, as most other reactions discussed here, is a continuous divariant reaction in the AFM system. Details of this reaction are discussed above as an example for all divariant equilibria in the AFM system (Fig. 7.5). The low-grade assemblage Kfs + Chl is replaced by Bt + Chl over a temperature interval of about 40°C (Fig. 7.11b–e). At the conditions of AFM (b) Kfs–Chl is stable across the entire range of  $X_{Fe}$ , at (c) and (d) some intermediate positions of the three phase field are shown, and at AFM (e) the entire range of  $X_{Fe}$  is covered by Chl–Bt (in the presence of excess Ms + Qtz).
4. The **first garnet** appears in metapelites at temperatures of around 450°C (Fig. 7.11d). This temperature is in conflict with the information provided by the pure FASH system. However, in rocks garnets preferentially incorporate manganese in the form of spessartine (Sps) component at low temperatures. Therefore, Mn–Fe-garnet appears at significantly lower temperatures than pure almandine (Alm). In addition, garnets in metapelites also always contain small amounts of Ca that further lowers the temperature of the first appearance of garnet in prograde metamorphism. This has been taken into account in Fig. 7.11.
5. At 500°C, the Kfs–Chl assemblage disappeared also from Mg-rich rock compositions (Fig. 7.11e). The **first staurolite** forms and this marks the transition to **amphibolite facies** conditions of metamorphism. New diagnostic assemblages at this stage are: Ky–St–Chl and St–Cld–Chl.
6. Fe-rich chlorite begins to be replaced by **garnet + biotite** between 500°C and 520°C (Fig. 7.11f). The new assemblage Grt + Bt remains stable to very high grades, and Fe–Mg partitioning between the two minerals is a popular geothermometer. Note, however, the succession of critical mineral assemblages shown in Fig. 7.11(f–n) probably has a better temperature resolution than the Grt–Bt thermometer. Because Grt is stabilized by the incorporation of Mn (that is preferentially fractionated into the first prograde Grt), the Grt + Bt assemblage may also occur in rocks at significantly lower temperatures. The first Grt + Bt pair may form at temperatures as low as 470°C.
7. Fe-chloritoid breaks down to **garnet + staurolite** and the diagnostic three phase assemblage Grt + St + Cld occurs over a narrow temperature interval and in special bulk compositions (about 550°C).

8. **Chloritoid disappears.** The terminal reaction that removes Cld is the first discontinuous AFM reaction in the sequence [reaction (7.27), Table 7.3]. The equilibrium temperature of reaction (7.27) (Fig. 7.11g–h) is only a few degrees C above equilibrium (7.12) in the pure FASH system (Fig. 7.4).
9. Figure 7.11h represents the characteristic AFM topology at the transition from lower- to mid-amphibolite facies conditions.
10. The AFM discontinuous reaction (7.28) has removed the Grt + Chl tie-line and replaced it with a two-phase field between St + Bt (Fig. 7.11i–j). The **first staurolite + biotite** appears at temperatures slightly above 600°C and marks the beginning of **middle amphibolite facies**. The discontinuous nature of reaction (7.28) makes it well suited for isograd mapping. In metamorphic terrains, the Chl + Grt zone is separated from the St + Bt zone by a well-defined isograd. The temperature at the boundary is about 600°C and it is rather insensitive on pressure (along Sil- or Ky-paths).
11. The discontinuous AFM-reaction (7.29) replaces the St + Chl tie-line by the new assemblage **kyanite (sillimanite) + biotite** (Fig. 7.11j–k).
12. Mg-chlorite decomposes to Bt + Ky (Sil). All Chl disappears from Qtz + Ms-saturated rocks at about 670°C (Fig. 7.11k–l). Note however, some additional complications appear in extremely Mg-rich composition because Tlc and Mg-rich Crd are additional stable minerals near the AM-binary at various conditions. Phase relationships in extremely Mg-rich rocks as shown on (7.23) will be discussed in Sect. 7.7, as they are not relevant to “normal” pelite compositions (Fig. 7.2) in regional metamorphism.
13. Fe-rich staurolite breaks down to Grt + Ky (Sil) (Fig. 7.11m). The new diagnostic assemblage is Ky + St + Grt, although this is restricted to a small range of bulk compositions.
14. Staurolite has disappeared from Qtz-bearing rocks (Fig. 7.11n). The new diagnostic assemblage is **garnet + biotite + kyanite (sillimanite)**. The appearance of the assemblage by the discontinuous AFM-reaction (7.30) also marks the beginning of the **upper amphibolite facies**. Note that this boundary also coincides with the production of the **first melt** in rocks of suitable composition at H<sub>2</sub>O-saturated conditions.

Fe-rich biotite decomposes to Grt + Kfs and from about 720°C, Kfs + Grt + Bt constitutes a stable assemblage in semi-pelitic gneisses. Three assemblages cover the full range of Fe–Mg-variations in Al-poor rocks: Kfs + Grt (in Fe-rich compositions), Kfs + Grt + Bt (in intermediate compositions), and Kfs + Bt (in Mg-rich compositions). Note however, that over the pressure range of a Ky-type metamorphic path partial melting will form migmatite gneisses under these conditions.

Metamorphism along a higher pressure path shows an inverted sequence of reactions limiting the assemblages Chl + Grt and Chl + St respectively. Reaction (7.32) (Table 7.3) breaks down the St + Chl tie line at slightly lower temperature than reaction (7.33), which limits the occurrence of Grt + Chl.

## 7.5 Low-Pressure Metamorphism of Pelites

In low-pressure metamorphic terrains ( $\leq 600$  MPa at  $700^\circ\text{C}$ ), the sequence of stable mineral assemblages in metapelitic rocks is different from those found in orogenic “Barrovian” type terrains. The heat source in low-pressure terrains is magma that intrudes the upper crust from depth. Large volumes of ascending magma may accumulate in the depth range of 3–12 km ( $\sim 100$ – $400$  MPa) below surface where  $\text{H}_2\text{O}$ -saturated granitoid magma loses dissolved  $\text{H}_2\text{O}$  and crystallizes. Thermal contact aureoles are typically developed around such magma bodies. The maximum temperature to which sediments can be heated depends on a number of factors, including the composition of magma and the size of the body. However, maximum contact temperatures at the contacts of shallow-level  $\text{H}_2\text{O}$ -saturated granitic and granodioritic magmas (“wet” magma) rarely exceed  $650^\circ\text{C}$ . On the other hand, at somewhat deeper levels in the upper crust large scale accumulation of granitic magma can result in temperatures up to about  $750^\circ\text{C}$ . Intrusion of large amounts of hot and dry mafic magma from the mantle may result in extensive high-temperature contact aureoles with temperatures in the metamorphic envelope reaching  $900$ – $1,000^\circ\text{C}$ . High-temperature contact aureoles are typically found around large mafic intrusions (gabbros, troctolites), intrusions of charnockite and mangerite bodies, and anorthosite complexes that occur in Precambrian continental crust.

A first overview shows that metapelites contain andalusite-bearing assemblages over a wide range of temperatures at very low pressure. At higher temperatures cordierite is the characteristic mineral of low pressure metapelites. Cordierite may occur together with biotite and sillimanite forming typical cordierite gneisses that occur widespread in some Precambrian terrains. At still higher grades orthopyroxene and ultimately hercynite spinel, sapphirine and other ultra-high temperature minerals may form. At somewhat higher pressure garnet can be present in cordierite gneisses and metapelitic granulites.

### 7.5.1 FASH System

In the pure FASH system (Fig. 7.12) the sequence of mineral assemblages at low temperatures is similar to orogenic metamorphism, although andalusite replaces kyanite in Al-rich metapelites. Andalusite may form at pressures slightly below 400 MPa (Fig. 7.3). Its maximum P stability limit varies with composition ( $\text{Fe}^{3+}$ ) and structural details (e.g., dislocation density) but is around 350–450 MPa. However, And is the characteristic Al-silicate polymorph at even lower pressure. At 200 MPa, for example, And may occur in Al-rich metapelites from below  $400^\circ\text{C}$  to more than  $600^\circ\text{C}$ , a temperature range of more than  $200^\circ\text{C}$  (Fig. 7.3). Sillimanite may occur in metapelites of granite aureoles at the immediate contact to the igneous rocks.

At about  $500^\circ\text{C}$ , cordierite may occur together with And in Al rich metapelites (Fig. 7.12). Cordierite is the characteristic mineral in high-grade low-pressure terrains.

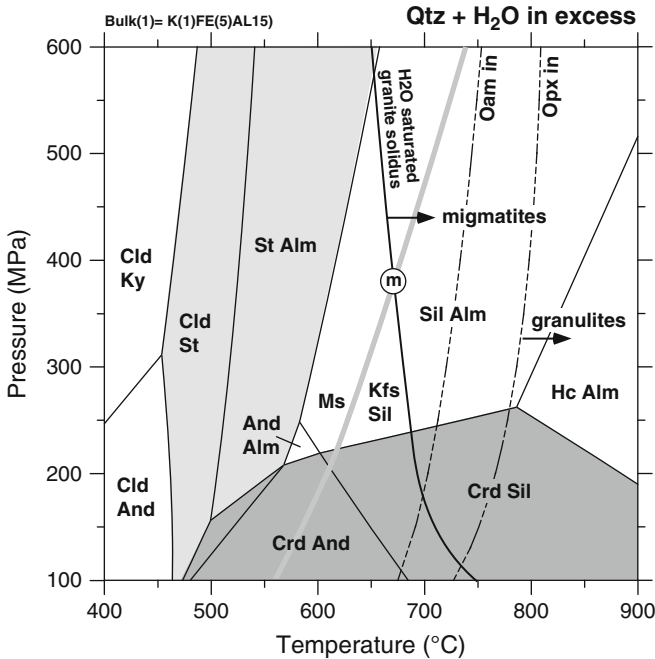


**Fig. 7.12** Low-P, high-T assemblages and reactions in metapelites in the KFLASH-system (reactions are listed in Tables 7.1 through 7.4). For reactions involving St see Fig. 7.4. The Ms breakdown is shown as *dark shaded curve*. It intersects the H<sub>2</sub>O-saturated solidus for granite (the lower boundary for the formation of migmatites) at about 400 MPa (point “m”). The first occurrence of Opx + Qtz defines the beginning of the granulite facies. Note Fe-cordierite is restricted to low pressures (250 MPa, *gray shaded field*). Also note that Hc + Qtz is diagnostic for very high temperatures (>800°C)

The assemblage is replaced by cordierite + sillimanite at higher temperatures. The first stable Sil appears between about 600°C and 700°C. In many contact aureoles such high temperatures are not realized even at the close contact to the igneous rock. However, Crd + Sil is widespread in regional high-grade terrains at mid-crustal depth. Finally, at very high temperatures hercynite appears in Qtz-excess rocks. The assemblage Spl + Qtz marks the beginning of ultra-high temperature metamorphism. The minimum temperature of the assemblage is about 800°C at 250 MPa (Fig. 7.12). It rapidly increases with decreasing or increasing pressure and with decreasing  $X_{\text{Fe}}$  (see below).

The overview Fig. 7.12 shows also the upper limit of Ms [reaction (7.26)] (Table 7.3) as a thick gray line above which Ms + Qtz is replaced by Kfs and Als is stable. This leads to the assemblage Crd + And + Kfs in low pressure aureoles. Crd + Sil always occur with Kfs and never with Ms. The solidus for granites at H<sub>2</sub>O-saturation (Fig. 7.12) shows that high grade Crd + Sil + Kfs gneisses may be associated with migmatitic textures. Above about 700°C cordierite gneisses may contain orthoamphibole, such as anthophyllite or gedrite.

Orthoamphibole-bearing assemblages are produced from Chl- and Bt-consuming reactions. Reaction (7.39) is an example of an Oam-producing reaction. The reaction is metastable in the pure FASH system, but it is important in natural systems. It generates Crd–Ath (anthophyllite) rocks that occur in Precambrian shield areas. Note that the term orthoamphibole (Oam) is used here for all Fe–Mg-amphiboles and includes also cummingtonite and gedrite. More than one type of Fe–Mg-amphibole may occur in high-grade rocks. Gedrite may occur in rocks metamorphosed close to granulite facies conditions. The precise conditions for the first occurrence of Fe–Mg-amphiboles in metapelites depends on the rock and fluid compositions. The Oam-in curve in Fig. 7.12 represents an approximate boundary above which metapelites (and related rocks) may contain various Fe–Mg-amphiboles in a number of associations formed by several reactions. Note that there is no overlap of the orthoamphibole and muscovite fields, respectively. In addition, Bt appears to be distinctly more stable than the alternative assemblage Kfs + Oam in metapelites and to our knowledge, Kfs + Oam have not been reported from metapelitic rocks, even if the mineral pair is predicted to be stable by the thermodynamic datasets (Sect. 3.8.1). A typical stable natural Oam assemblage at low- to intermediate-pressures (300–500 MPa) is Bt + Oam + Crd ± Grt. Widespread but subordinate Crd + Ath gneisses are characteristic rocks of many Precambrian shield areas. At about 800°C, orthopyroxene becomes important in metapelites. Its occurrence in Qtz-saturated rocks defines granulite facies conditions.

### 7.5.2 *KFMASH System*

The sequence of successive mineral assemblages in low-pressure metamorphism of iron-rich metapelites can be summarized as follows. At low temperatures, the sequence is similar to that produced in pelitic rocks during orogenic metamorphism (with And instead of Ky). Important here is reaction (7.21) which divides the cooler parts of a contact aureole into an outer zone with Chl + Kfs and a higher-grade inner zone with Bt + Ms. The temperature of the boundary between the two zones is at about 400°C. Around very shallow level intrusions, such as for example the Oslo rift zone ( $P \sim 0.5$  MPa), this is the only mineralogical change taking place in most metapelitic sediments. The maximum temperature that can be reached at the contact to shallow H<sub>2</sub>O-rich granitic magma is below 500°C (magma  $T < 800^\circ\text{C}$ , country rock temperature  $T^\circ = 200^\circ\text{C}$ ,  $\Delta T < 600^\circ\text{C}$ . Rule of thumb: maximum  $T$  in sediments =  $T^\circ + 1/2 \Delta T \Rightarrow < 500^\circ\text{C}$ ). The final contact metamorphic assemblage is Bt + Chl + Ms + Qtz.

Between about 500°C and 550°C, cordierite appears in various assemblages involving Chl, Ms and Bt. Staurolite is absent and also garnet may not be present. Andalusite is the characteristic Al-silicate. Above about 600°C, metapelites contain the diagnostic assemblage Crd + Kfs + Bt ± And (at higher  $T$ , Sil). Andalusite + Crd + Kfs represents the highest grade assemblage close to the contact of shallow-level granitoids. Metastable Sil can occasionally be found close to the contact of

shallow level igneous rock as a result of structural disorder and chemical impurities that stabilize Sil relative to And. Cordierite + Bt + Sil + Kfs + Qtz is the high-T stable assemblage.

Iron-magnesium exchange in Fe–Mg minerals has profound effects in high-temperature metamorphism of metapelitic rocks. The Crd-involving reactions [reactions (7.35), (7.36) and (7.37)] are fluid-absent reactions and as such strongly depend on the compositions of the participating minerals (geological thermometers and barometers). Cordierite may also contain molecular fluid species such as H<sub>2</sub>O and CO<sub>2</sub> in channels of its atomic structure with the number of moles of water (“n” in Table 7.4) varying between 0 and 2. The amount depends on the total pressure, the H<sub>2</sub>O pressure, the composition of Crd and T. The presence of H<sub>2</sub>O in Crd stabilizes the mineral relative to the respective reactant assemblage. The water is relatively loosely bound and can be compared with molecular water contained in many zeolites. However, the reactions involving Crd can also be formulated for H<sub>2</sub>O-free environments (n = 0). In addition, the Fe–Mg content of the bulk rock is

**Table 7.4** Cordierite-spinel-orthopyroxene-orthoamphibole-reactions (KFASH system)

Cordierite	Fe <sub>2</sub> Al <sub>3</sub> [AlSi <sub>5</sub> O <sub>18-n</sub> H <sub>2</sub> O
Spinel (hercynite)	FeAl <sub>2</sub> O <sub>4</sub>
Orthopyroxene (ferrosilite)	FeSiO <sub>3</sub>
Orthoamphibole (ferro-anthophyllite)	Fe <sub>7</sub> Si <sub>8</sub> O <sub>22</sub> (OH) <sub>2</sub>
Sapphirine (ferro-sapphirine)	Fe <sub>2</sub> Al <sub>4</sub> SiO <sub>10</sub>
Osumilite (ferro-osumilite)	KFe <sub>2</sub> Al <sub>3</sub> [Al <sub>2</sub> Si <sub>10</sub> ]O <sub>30</sub>
All reactions with excess quartz + H <sub>2</sub> O	
2Alm + 4Als + 5Qtz + nH <sub>2</sub> O = 3Crd	(7.35)
2Spl + 5Qtz = Crd	(7.36)
Alm + 2Als = 3Spl + 5Qtz	(7.37)
Oam = 7Opx + Qtz + H <sub>2</sub> O	(7.38)
14Chl + 57Qtz = 8Oam + 7Crd + 48H <sub>2</sub> O	(7.39)
Ann + 3Qtz = 3Opx + Kfs + H <sub>2</sub> O	(7.40)
6Alm(Grt) + 12Qtz = 4Crd + 10Fs (Opx)	(7.41)
Some important cordierite reactions involving sheet silicates (in the order of increasing grade)	
Continuous reactions	
2Chl + 8And/Sil + 11Qtz = 5Crd + 8H <sub>2</sub> O	(7.42)
Chl + Ms + 2Qtz = Crd + Bt + 4H <sub>2</sub> O	(7.43)
3Crd + 2Ms = 8Sil + 2Bt + 7Qtz	(7.44)
3Crd + 2Bt = 4Grt + 2Ms + 3Qtz	(7.45)
3Crd + 4Bt + 3Qtz = 6Grt + 4Kfs + 4H <sub>2</sub> O	(7.46)
2Bt + 6Ms + 15Qtz = 3Crd + 8Kfs + 8H <sub>2</sub> O	(7.47)
6Sil + 2Bt + 9Qtz = 3Crd + 2Kfs + 2H <sub>2</sub> O	(7.48)
Discontinuous reactions	
Chl + Sil + Ms + Qtz = Crd + Bt + H <sub>2</sub> O	(7.49)
Bt + Sil + Qtz = Crd + Grt + Kfs + H <sub>2</sub> O	(7.50)
Bt + Grt + Qtz = Crd + Opx + Kfs + H <sub>2</sub> O	(7.51)
Bt + Grt + Qtz = Opx + Sil + Kfs + H <sub>2</sub> O	(7.52)
Bt + Sil + Qtz = Crd + Opx + Kfs + H <sub>2</sub> O	(7.53)
Opx + Sil + Qtz = Crd + Grt	(7.54)
Crd + Grt + Sil = Spl + Qtz	(7.55)
Crd + Sil + Kfs + Qtz = Osm + Opx	(7.56)

strongly fractionated between Crd, Grt and Spl with Crd being much more magnesian than coexisting Grt or Spl. As a consequence, stability of Crd is greatly expanded relative to the pure FAS system.

The FM assemblages can best be shown on an isobaric TX section (Fig. 7.13). The section has been computed at 300 MPa (about 10 km in the continental upper crust) for  $A = 0.5$ . It shows assemblages at low temperature ( $<500^{\circ}\text{C}$ ) we are already familiar with. Not much above  $500^{\circ}\text{C}$  cordierite appears in rocks with high-Mg to very Fe-rich compositions ( $X_{\text{Fe}} \sim 0.9$ ) in various assemblages. At  $T = 600^{\circ}\text{C}$  Mg-rich rocks contain Crd + Bt + Ms, typical metapelites with  $X_{\text{Fe}} \sim 0.7$  are Crd + Grt + two-mica gneisses, whereas Fe-rich compositions contain Crd + Grt + Sil but no Bt. At  $700^{\circ}\text{C}$ , Ms has been replaced by Kfs. In Mg-rich rocks the stable assemblage is Crd + Bt + Kfs, the average metapelite would contain Crd + Grt + Kfs, while very Fe-rich rocks contain Crd + Grt + Sil + Kfs. At very high temperatures ( $900^{\circ}\text{C}$ ), the stable assemblages are: Bt + Crd + Kfs (Mg-rich rocks), Opx + Crd + Kfs (normal metapelites) and Crd + Grt + Spl + Kfs (Fe-rich compositions). The minimum T of the Opx + Crd (+ Qtz + Kfs)

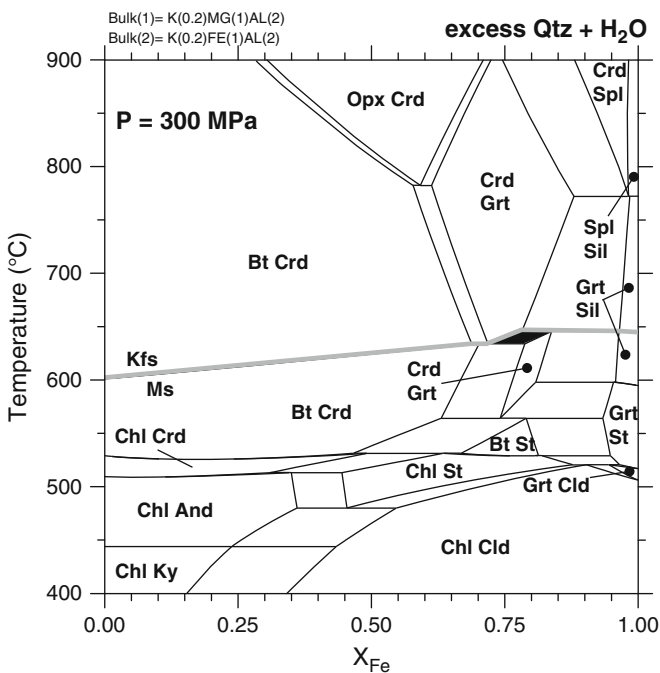


**Fig. 7.13** Isobaric  $T$ - $X_{\text{Fe}}$  section at 300 MPa showing the distribution of stable assemblages in metapelites in the KFMASH system in contact metamorphic terrains. All assemblages contain Qtz and  $\text{H}_2\text{O}$  in excess, at  $T$  lower than the Ms breakdown boundary (thick gray shaded line) they also contain Ms, above that line they all contain Kfs. Note that assemblages with St, Bt, Grt, and Crd typical of the amphibolite facies occur above about  $500 \pm 20^{\circ}\text{C}$ . Cordierite is the characteristic and dominant mineral in all metapelites from about  $500^{\circ}\text{C}$  upward, except in extremely Fe-rich rocks

granulite facies assemblage is about 780°C at 300 MPa. Figure 7.14 shows an example texture of Bt replacement by Opx + Kfs, where Opx encrusts Bt in Opx + Crd + Kfs gneiss. The prograde reaction (7.40) separates the Bt + Crd from the Opx + Crd field on Fig. 7.13. The high-grade assemblage Crd + Grt is replaced by Opx + Crd by reaction (7.41) on Fig. 7.13. Figure 7.15 shows a granulite from the Alps where garnet is replaced by a fine-grained intergrowth of

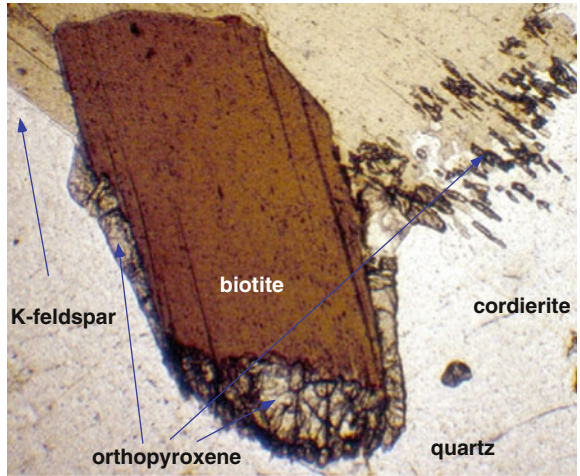


**Fig. 7.14** Photomicrograph showing textural evidence for the biotite breakdown reaction  $Bt + Qtz = Opx + Kfs + H_2O$  in a granulite from the Gruf Complex, Central Alps (picture diagonal 2mm). The brown biotite crystal is encrusted by orthopyroxene (hypersthene). Biotite shows characteristic lobate resorption contacts to Opx showing that Bt is reactant and Opx is product of the reaction. Kfs and Qtz make up the gray matrix, where Kfs is in contact to Bt no Opx formed (*upper left corner*). The rock shows no structures that would indicate partial melting. The texture suggests low  $a_{H_2O}$  conditions (see text)

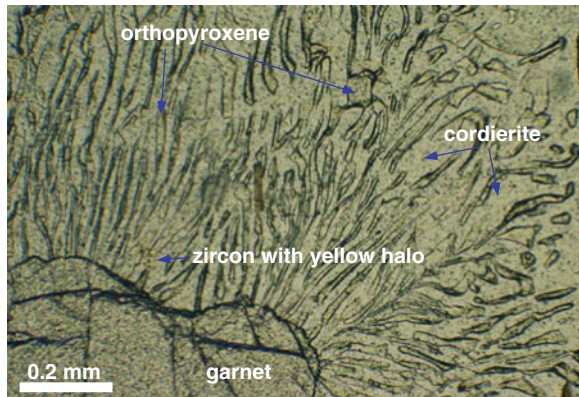


**Fig. 7.15** Photomicrograph showing garnet (*lower left*) replacement by Opx (high relief “worms”) and Crd (matrix between Opx) in a granulite from the Gruf Complex, Central Alps. This so called symplectite texture suggests low  $a_{H_2O}$  conditions (see text)



cordierite and worm-like orthopyroxene. The so-called symplectite texture of intergrown Opx–Crd is characteristic for H<sub>2</sub>O-deficient conditions typical of granulite facies metamorphism. Note the characteristic yellow halos in cordierite around radioactive small zircon grains causing radiation damage in Crd. More information on high-T metamorphism of pelites is presented below in a separate Sect. 7.6.

In  $P$ – $T$ -space, the Grt + Als + Qtz + Crd assemblage [reaction (7.35)] intersects a number of Ms- and Chl-involving reactions and this brings about some sheet silicate reactions (and orthoamphibole reactions) that involve Crd. These reactions are listed in Table 7.4. Reactions (7.42) and (7.43) are continuous Crd-producing dehydration reactions that are terminated by the discontinuous reaction Chl + And = Crd + Bt [reaction (7.50)] which intersects the 200 MPa isobar at about 530°C. Above this temperature Crd + Bt may be present in metapelites. Reactions (7.44) and (7.45) are H<sub>2</sub>O-absent reactions with equilibria characterized by very low  $dP/dT$  slopes. Equilibrium conditions are independent of temperature and the assemblages have potential as geobarometers. The assemblages Crd + Ms and Crd + Bt occur on the low-pressure side of the equilibria.

At higher temperatures, a number of continuous dehydration reactions (7.46)–(7.48) produce Kfs that may enter a melt phase together with Qtz and H<sub>2</sub>O. The reactions are linked by the discontinuous reaction (7.51) which ultimately produces the characteristic assemblages Crd + Grt + Kfs + Bt and Crd + Grt + Kfs + Al-silicate (And or Sil). These assemblages are diagnostic of high-grade Crd-gneisses and are widespread in low- to medium- $P$  terrains metamorphosed in the range of 700°C ± 50°C at 200–500 MPa. Crd–Grt–Kfs–Bt gneisses are transitional between upper amphibolite and granulite facies conditions and the assemblage often indicates equilibration under conditions of reduced  $P_{H_2O}$ .

Very commonly, however, Crd-gneisses do not contain Kfs. Bt is then the only K-bearing mineral in the rock. Biotite assemblages in rocks lacking Kfs (Ms) **cannot** be represented on AFM diagrams (Kfs projection), so that Bt becomes an “extra” phase and typical assemblages involve four (or even more) “AFM” minerals. The representative assemblage in such rocks is: Crd + Grt + Sil + Bt. It forms at  $P$ – $T$  conditions similar to the Kfs-bearing Crd-gneisses. They are most typically found in terrains that have been metamorphosed at 300–500 MPa and 650–750°C (see Fig. 4.18).

## 7.6 High-Temperature Metamorphism of Pelites: Metapelitic Granulites

It was shown in the previous section that distinct high-T assemblages are formed in metapelites in unusually hot contact aureoles (Fig. 7.13). In the following we shall explore the assemblages and assemblage relationships that may form in high-grade

and granulite facies metamorphism of pelitic rocks. Very high-T contact aureoles that create low-pressure high-T hornfelses are related to shallow level basaltic magma chambers and, thus, they are relatively rare. Some of these mafic often layered complexes intruded old metamorphic gneisses and the polymetamorphic assemblages and assemblage development is difficult to separate into distinct metamorphic events. Geothermal gradients in high-T low-P environments may exceed 100°C/km. However, at about 20 km depth corresponding to 600 MPa pressure, temperatures of 800°C and more may be reached in extensive areas of the crust that receives heat in the form of many magma pulses from greater depth. The conditions correspond to average linear gradients of 40°C/km that characterize many granulite facies terrains.

### 7.6.1 Cordierite–Garnet–Opx–Spinel–Olivine Equilibria

Cordierite is the key mineral in high-grade metapelites at low- to medium-pressures. It occurs in many different mineral associations and together with minerals including garnet, orthopyroxene, spinel (hercynite), olivine, aluminosilicate, sapphirine and others in quartz- and in corundum-bearing gneisses.

Cordierite-bearing assemblages can be used to derive reliable pressure and temperature estimates for high-grade metapelites. Because of the large composition contrast between Mg-rich Crd and Fe-rich Grt, the mineral pair Crd + Grt can be used as a geothermometer. The assemblage Crd + Grt + Sil + Qtz is linked by the reaction (7.35). The reaction equilibrium (7.35) is used as a geobarometer.

The pressure dependence of equilibria among some of these minerals in Qtz-rich rocks is shown on two  $P$ - $X_{\text{Fe}}$  diagrams at 700°C and 860°C respectively (Fig. 7.16a, b). The assemblage Crd + Grt + Sil + Qtz, shown as a shaded field on Fig. 7.16, is an excellent barometer. An example pair of coexisting Crd + Grt is shown on the 700°C figure at 500 MPa. At 700°C the assemblage terminates at  $P = 600$  MPa, while at 860°C the assemblage extends close to 800 MPa. At 860°C hercynite spinel is present in metapelites with high  $X_{\text{Fe}}$  ( $>0.75$ ) at pressures below 400 MPa. At both isothermal sections, the assemblage cordierite + olivine is present over a wide range of rock  $X_{\text{Fe}}$  at pressures below 300 MPa. The relatively rare assemblage Ol + Crd has been described from high-T contact aureoles. Mg-rich rocks tend to contain Crd + Opx and Crd + Opx + Grt is typical of intermediate rock  $X_{\text{Fe}}$ . Cordierite-bearing assemblages are restricted to pressures below 700 MPa at 700°C and to below 850°C at 860°C. At the pressure maximum cordierite is pure Mg-endmember Crd. The assemblage orthopyroxene + aluminosilicate is diagnostic for high-pressure granulites. The pair Opx + Sil is restricted to  $P > 600$  MPa at 700°C and to  $P > 750$  MPa at 860°C. The pair Opx + Ky requires  $P > 800$  MPa at 700°C.

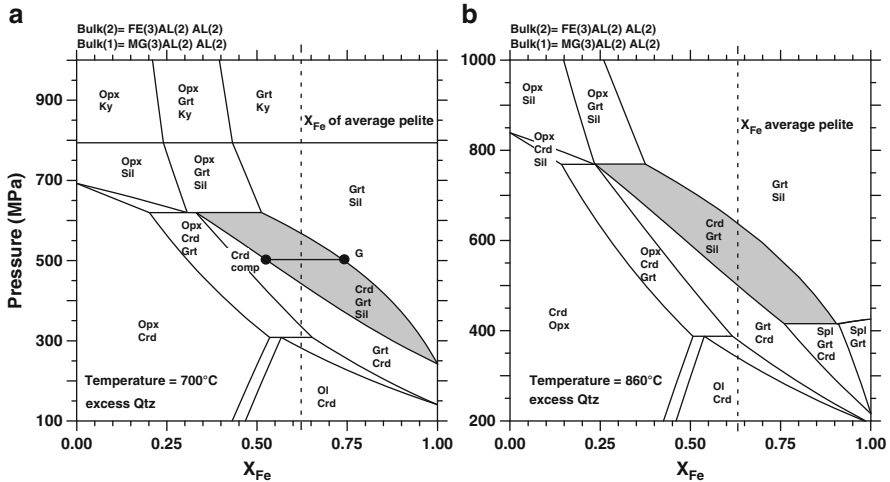


**Fig. 7.16** Two isothermal  $P$ - $X_{\text{Fe}}$  section: (a) at  $700^\circ\text{C}$  (*upper amphibolite facies*) and (b) at  $860^\circ\text{C}$  (*granulite facies*) showing the distribution of stable assemblages in metapelites in the FMASH system for high-grade metamorphism. All assemblages contain excess Qtz. At high  $X_{\text{Fe}}$  and low  $P$  Ol-Crd is the characteristic assemblage. The assemblage Opx-Crd occurs in low- $X_{\text{Fe}}$  rocks over a wide range of pressures. The sequence of assemblages with progressively increasing pressure for metapelites with average  $X_{\text{Fe}}$  can be read from the *dashed line*. The assemblage Crd-Grt-Sil (*gray shaded loop*) can be used as a geologic barometer (see text). Grt-Als is stable over a very large  $P$ -range. In contrast: Opx-Als is a typical assemblage of lower crustal granulites

### 7.6.2 The Excess Quartz Condition

The discussion of metamorphism of pelitic rocks outlined above requires the presence of  $\text{SiO}_2$  in the form of quartz in the rocks at all stages of prograde metamorphism. Consequently all diagrams used for this discussion were constructed for excess Qtz conditions. The excess Qtz condition is also a precondition for the legitimate use of AFM diagrams. Many pelitic sediments are sufficiently rich in  $\text{SiO}_2$  as to contain excess quartz, or one of its stable polymorphs, at all stages of prograde metamorphism. Some metapelites may, however, become deficient in free quartz during prograde metamorphism and in the following the consequences of the loss of free quartz on mineral assemblages shall be explored.

The crucial element is aluminum, because it is stored in Si-poor sheet silicates such as chlorite at low grade. During prograde metamorphism Al is transferred from sheet silicates to feldspars that contain three times more Si per Al than for instance micas and two times more Si per Al than chlorite. Consequently, sheet silicate consuming reactions use up free quartz during transformation to feldspar. It is clear from this general association that some pelites may become devoid of free quartz during prograde metamorphism.

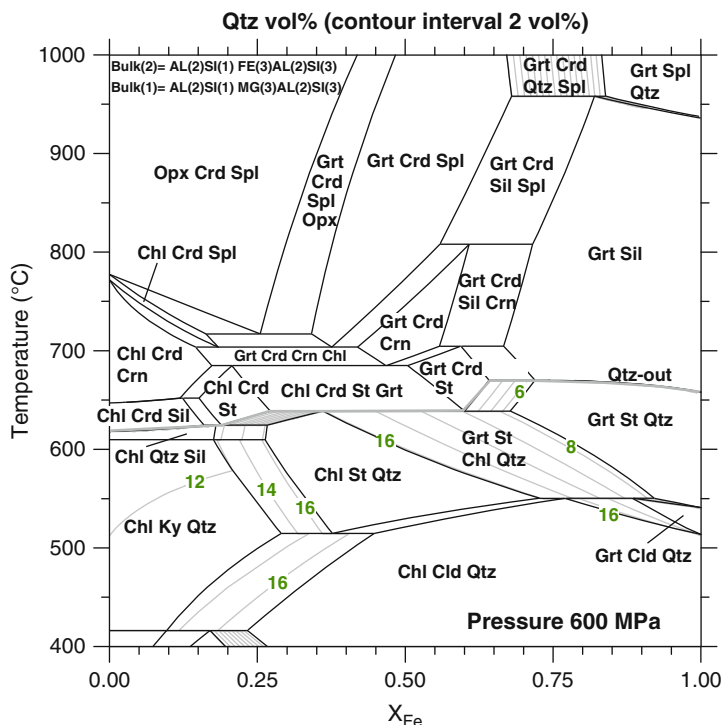


**Fig. 7.17** Isobaric  $T$ - $X_{\text{Fe}}$  section at 600 MPa showing the distribution of stable assemblages in metapelites in the FMASH system illustrating the Qtz-saturation problem. At  $T$  lower than the Ms breakdown boundary (*thick gray shaded line*) all assemblages include Ms, above that line they all contain Kfs. The bulk rock composition has sufficient  $\text{SiO}_2$  that the low-grade rock contains ~ 17 mol% quartz ( $X_{\text{Fe}} > 0.25$ ). As a result of  $\text{SiO}_2$ -consuming reactions free  $\text{SiO}_2$  decreases (labeled vol% contours) and finally the rocks run out of free quartz (*gray thick Qtz-out line* at about 650°C). Note that corundum is present in various assemblages (Crn gneisses, Crn schists). Spinel is not present below 800°C

The situation is depicted on Fig. 7.17 showing an isobaric  $T$ - $X_{\text{Fe}}$  diagram at 600 MPa for a pelitic rock that contains about 16 vol% of free quartz at low grade and Fe-rich bulk rock compositions. The rock is a simple Chl + Prl schist at very low grade and alkalis have been neglected for simplicity. It can be seen that at low grade the assemblages are well-known from the presentation above. The rock contains Chl + Cld and excess quartz. With increasing grade, however, chlorite-consuming reactions reduce also the amount of free quartz in the rock. The gray-shaded lines in the 4-phase fields (rotating 3-phase triangles in AFM diagrams) indicate constant vol% of Qtz present. Quartz rapidly diminishes with increasing temperature and the rocks loose quartz between 620°C (Mg-rich) and 670°C (Fe-rich) (gray thick line Qtz-out). Above that temperature an entirely new assemblage world opens up. Corundum is here a member of many assemblages. Corundum occurs frequently in Qtz-deficient gneisses and schists in the upper amphibolite facies. At about 700°C (at 600°C), that is at conditions normally associated with

the upper amphibolite facies, spinel appears at medium  $X_{\text{Fe}}$  in assemblages such as Spl + Grt + Crd. Spinel appears at a temperature 250°C lower than in Qtz-saturated rocks. Also orthopyroxene develops in Mg-rich rocks at a temperature slightly above 700°C. The assemblage Grt + Crd + Opx + Spl (Fig. 7.17) is characteristic for ultra-high grade metamorphism in Qtz-bearing rocks, here in Qtz-free rocks it is consistent with temperatures as low as 700°C.

It is interesting to note that at very high temperature (>950°C) the considered rock develops free quartz as a result of Al-transfer from Als to Spl leaving behind excess quartz in high- $X_{\text{Fe}}$  compositions. This shows that the pair Spl + Qtz is the essential assemblage for UHT metamorphism not the occurrence of spinel (hercynite) alone in Qtz-deficient rocks.

### 7.6.3 Partial Melting and Migmatite

Partial melting begins to be important in rocks containing feldspar and quartz (Fig. 7.12) at about 650–700°C if metamorphism occurs in the presence of excess  $\text{H}_2\text{O}$ . The solidus curve marks the onset of partial melting in “granitic” systems and the beginning of migmatite formation. This means that at temperatures above this curve, the Kfs-component produced by dehydration reactions (Table 7.4) dissolve in a melt phase that in some cases may leave the site of production. The melt segregates and removes Kfs and Ab produced by mica-involving dehydration reactions. The remaining rock (restite) may be devoid of Kfs and consequently also poor in alkalis. It has lost its “granite” component.

Particularly important is the decomposition of Ms in the presence of Qtz. The melt-absent reaction (7.25) that produces And or Sil and Kfs at low- $P$  intersects the minimum melt curve at about 300 MPa (point “m” in Fig. 7.12). At higher pressures, Ms decomposes to Sil and a Kfs-bearing melt. The melt-absent decomposition of muscovite (+ Qtz) is an ordinary dehydration reaction and has the characteristic curve shape on a  $P$ – $T$  diagram (Fig. 3.13) with a positive  $dP/dT$  slope at all pressures of geological interest. At  $a_{\text{H}_2\text{O}} = 1$ , Ms + Qtz has its maximum stability. With decreasing  $a_{\text{H}_2\text{O}}$ , Kfs + Sil forms at progressively lower temperature. The formation of Sil by reaction (7.25) is occasionally referred to as “the second sillimanite isograd” (in contrast to Sil from the phase transitions  $\text{Ky} = \text{Sil}$  and  $\text{And} = \text{Sil}$  respectively, that may or may not form Sil because of metastable survival of And or Ky!). In contrast to the dehydration curve, the solidus for Ms-granite at  $\text{H}_2\text{O}$ -saturated conditions has a negative slope in a  $P$ – $T$  diagram at the pressures of interest. At the minimum melt curve shown on the Fig. 7.12, Qtz + feldspar begin to melt. Muscovite of the solidus assemblage dissolves in the melt and contributes a Kfs component and  $\text{H}_2\text{O}$  to the melt, leaving Sil as a solid residue. Compared with the melt-absent reaction, decreasing  $a_{\text{H}_2\text{O}}$  has an opposite effect on the Ms + Qtz breakdown curve and the minimum  $T$  of Ms melting increases with decreasing  $a_{\text{H}_2\text{O}}$ .

The consequences for the Ms-out isograd in Qtz-bearing rocks are as follows: At pressures below about 400 MPa, that is below the intersection of the water-saturated melt-present and melt-absent Ms-breakdown curves, (point “m” in Fig. 7.12), muscovite disappears by reaction (7.25) to form Kfs + Als + H<sub>2</sub>O. At pressures above the intersection, Ms disappears by partial melting. The quantitative position of the intersection point “m” of the two reactions is shown in Fig. 7.12 at ~380 MPa and 670°C.

The melt produced by prograde metamorphism of micaschists is close to the eutectic composition in the granite system and it is H<sub>2</sub>O-saturated. The fate of this melt depends primarily on the amount produced in the partial melting process but also on accompanying deformation and other factors. Small amounts of melt may not migrate over long distances and will remain as leucocratic quartzofeldspathic bands, pods, lenses and patches termed **leucosomes**. If a significant amount of anatectic “granitic” melt is produced by local in-situ partial melting of pelitic and semi-pelitic gneiss and schist, the melt may eventually collect to form large masses of granite that may either show a discordant relationship to the primary host rock foliation or bedding (implying movement), or a gradational contact with highly migmatized rocks (formed in-situ as a result of extensive melting). The leucocratic Qtz–Fsp-rich component in gneisses representing the anatectic melt phase typically shows randomly oriented minerals and fabrics typical of igneous rocks. The unmelted **restite** material has a high modal proportion of mafic minerals (mainly Al-silicate (sillimanite), biotite and garnet) and has a dark appearance (**melanosome**). The leucosome and melanosome components are the result of **anatexis** and occur in countless proportions and as an infinite number of different light-dark meso- to megascopic-scale structures that typify migmatite rocks.

An example of migmatite formation resulting from the action of muscovite dehydration melting is the St. Malo migmatite-granite terrane, Brittany, France (Brown 1979; Milord et al. 2001) that involved partial melting (<40%) of Ms + Bt + Pl + Qtz rocks with more Al-rich varieties containing up to 30% Ms. The disappearance of Ms to form Sil coincides with the appearance of migmatite that is characterized by the assemblage Qtz + Pl + Bt + Kfs + rare fibrolitic Sil and sometimes Crd, indicating that melting occurred within the stability field of Bt (T < 800°C). The migmatite zone can be subdivided into two types: low melt-fraction **metatexite** which is defined as migmatite preserving unmelted original layering, foliation or banding. The metatexite contains <20% leucosome veins and pods composed of Qtz + Pl + Kfs + (Bt) sometimes with Bt-rich selvages (melanosomes); **diatexite** defined as migmatite in which original structures are destroyed and having a more homogeneous, coarse-grained igneous-looking texture indicating significant melting. Biotite-rich parts exhibit flow banding with schlieren development, and the most evolved, granite-like lighter parts show flow alignment of Pl and Kfs phenocrysts. The diatexite is associated with **anatectic granite** (Bt-, Ms–Bt-, and tourmaline-bearing varieties), which is the most leucocratic and homogeneous rock type, although pegmatitic layers and patches also occur locally. Contacts between diatexite and anatectic granite are gradational indicating a process of granite formation by in-situ melting and melt retention.

The  $P$ - $T$  conditions of many migmatite terranes indicate that they formed at depths of between 10 and 30 km at temperatures between about 630°C and 800°C, i.e., at temperatures above the pelitic “wet” solidus (= Ms-granite solidus, Fig. 7.12), the Ms and/or Bt-dehydration melting curves within the Sil stability field and, as expected, there is complete overlap of the  $P$ - $T$  conditions of migmatite and granite formation (Fig. 7.18).

Orthoamphibole that may have formed during upper amphibolite grade metamorphism decomposes to Opx + Qtz [reaction (7.38)] at about 750–800°C (Fig. 7.12) which marks the transition to **granulite facies** conditions. However, the diagnostic granulite facies assemblage Opx + Qtz may originate from a number of different reactions, the most important being reaction (7.40), which eventually removes the last remaining sheet silicate, Bt, from metapelites. In general, Bt breaks down in the presence of Qtz at about 800°C to Opx + Kfs (Fig. 7.14). Replacement of Bt by Opx actually takes place over a fairly wide  $T$ -interval, depending on the composition of Bt and fluid. According to reaction (7.40), Bt decomposition

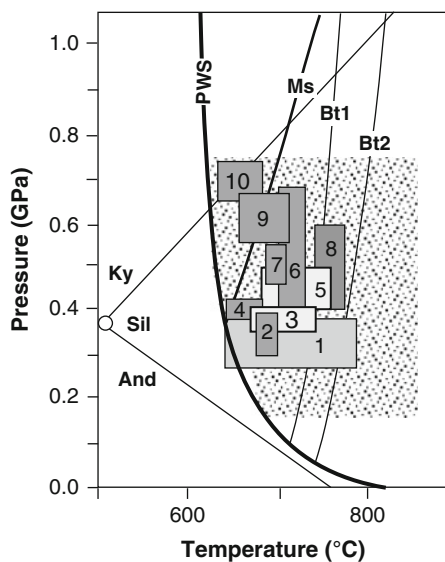


**Fig. 7.18**  $P$ - $T$  conditions of some migmatite terranes (numbered) shown in relation to the model pelitic wet solidus (PWS; Thompson 1982), muscovite + plagioclase + quartz = aluminum silicate + K-feldspar + liquid dehydration melting reaction (Ms; Thompson and Tracy 1979), biotite dehydration melting reactions; biotite + aluminum silicate + plagioclase + quartz = garnet + K-feldspar + liquid (Bt1; Le Breton and Thompson 1988; Vielzeuf and Holloway 1988), and biotite + plagioclase + quartz = orthopyroxene + K-feldspar + liquid (Bt2; Clemens and Wall 1981), and field of crystallization of granites (stippled area, Anderson 1996). 1 Mt. Stafford, Australia (White et al. 2003b); 2 Pyrenees (Wickham 1987); 3 Cooma, Australia (Ellis and Obata 1992); 4 Maine (De Yoreo et al. 1989); 5 Broken Hill, Australia (White et al. 2003a, 2004); 6 St. Malo, Brittany (Brown 1979); 7 South Brittany (Jones and Brown 1989); 8 Calabria (Graessner and Schenk 2001); 9 West-central Massachusetts (Tracy 1978); 10 Sevier hinterland (Patino-Douce et al. 1990)

produces Kfs that together with H<sub>2</sub>O released commonly enters a melt phase. The melt-absent version of reaction (7.40) is metastable at pressures above a few tens of MPa and in the presence of H<sub>2</sub>O-rich fluids relative to corresponding Bt melting reaction. The relationships are analogous to those of the Ms breakdown. Biotite melting boundaries are also shown on Fig. 7.18. K-feldspar may dissolve in a melt phase (H<sub>2</sub>O-rich conditions) or it may remain in the rock (dry conditions). Under upper amphibolite facies conditions, typical metapelitic gneisses with Bt + Grt + Sil + Kfs + Pl + Qtz may have lost a free fluid phase after the main dehydration reactions have gone to completion. Biotite remains as the last hydrate in the rocks and it survives in relatively low a<sub>H<sub>2</sub>O</sub> environments. However, if the rocks experience further heating, fluid-absent melting in high-grade gneisses becomes important and this process is responsible for much of the Opx found in granulite terrains.

The above reactions and assemblages are illustrated to a large extent by the low-P/high-T (Crd-bearing) gneiss and migmatite of the Mt. Stafford area, Central Australia, where a prograde sequence in metapelitic and semi-pelitic rocks extends from greenschist (Zone 1), through amphibolite (Zones 2–3) to granulite (Zones 4–5) (Fig. 7.19) over a P–T range of 200–400 MPa and ~640–800°C, respectively (Greenfield et al. 1998; White et al. 2003b). Leucosomes appear upgrade of the inferred pelitic solidus and increase in abundance upgrade of the And = Sil transition. The transition to Zone 3 is indicated by the formation of Crd + Spl-bearing

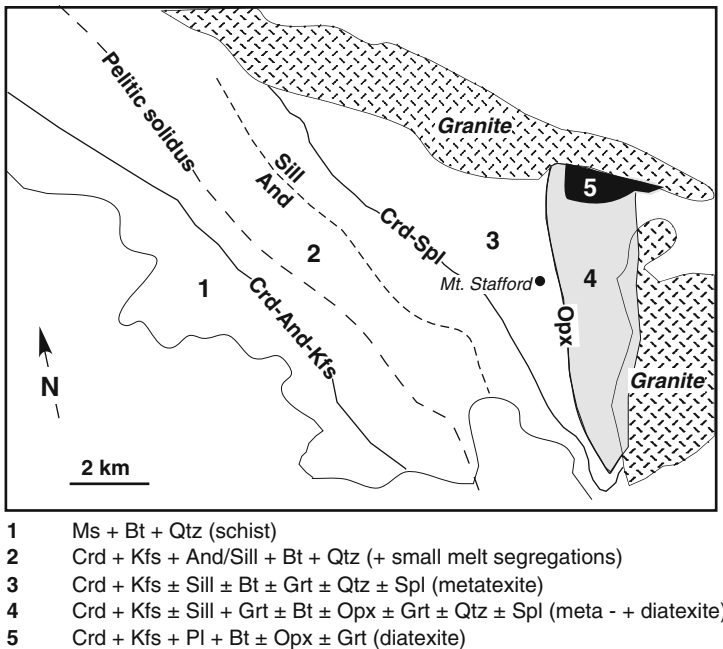


**Fig. 7.19** Map showing the distribution of granulite facies rocks and related migmatite, Mt Stafford area, Central Australia (simplified after Fig. 1 of Greenfield et al. 1998). Zone mineral assemblages are listed below (see text)



symplectites that mantle Al-silicate porphyroblasts and Grt becomes more abundant in the high-T part of Zone 3.

The Crd + Spl symplectites mantle large grains of sillimanite. The absence of quartz from the symplectite reaction sites is consistent with these silica-undersaturated domains having formed during the breakdown of sillimanite + biotite + quartz, and with available quartz being consumed at lower grade. As leucosomes also occur with the symplectites a suggested melt-producing reaction is:  $Bt + Sil + Qtz = Spl + Crd + \text{leucosome (Kfs + Qtz + water)}$ . The breakdown of biotite and sillimanite in these rocks can occur over a large temperature range, from subsolidus conditions to temperatures of close to 750°C.

The transition to Zone 4 (Fig. 7.19) is marked by the appearance of the granular Grt + Opx + Crd assemblage and the highest grade zone, Zone 5, is largely a diatexite. Partial melting to form the Kfs + Qtz-bearing leucosomes that also contain melt-derived Crd, Grt and Bt, appear to be related to multivariant dehydration melting of Bt that occurred over a considerable T-interval (~660–780°C) and can be characterized with increasing T as,  $Bt + Sil + Qtz = Crd + Kfs + \text{melt}$ ,  $Bt + Sil = Crd + Spl + Kfs + \text{melt}$ ,  $Bt + Qtz + Crd = Grt + Kfs + \text{melt}$  and  $Bt + Grt + Qtz = Opx + Crd + Kfs + \text{melt}$  (White et al. 2003b).

### 7.6.4 More About Granulites

Metamorphism of metapelitic rocks is strongly affected by partial melting reactions at high temperatures and increased formation of partial melts has severe consequences for the bulk composition of the rocks in that they become depleted in their “granite” component, i.e., in feldspar and Qtz. Iron is also strongly fractionated into the melt phase and consequently the residuum (restite) is enriched in Mg and Al. Recurring dehydration reactions along a prograde P–T path also inevitably leaves the rocks devoid of an aqueous fluid phase. Accordingly, extreme high-grade “metapelites” are often quartz-free Al–Mg-rich restites of the partial melting processes consisting of minerals such as Opx, Crd, Sil (Ky), Spr, Spl, Grt, Crn, etc. Water-deficient conditions are often reflected in disequilibrium micro-structures including symplectites, replacement structures and coronites.

Partial melting of metapelites produces a melt phase the so called neosome and leaves behind a refractory residue. The components making up the original composition of the metapelite are distributed into a melt phase that is enriched in K, Fe, Si and H<sub>2</sub>O that later becomes the granitoid neosome and into unmelted residue enriched in Mg and Al relative to the subsolidus metapelite. This has the consequence that the prograde path of metamorphism on the TX<sub>Fe</sub> diagrams does not follow an isochemical path (vertical path on the diagrams) but rather tends to evolve to the Mg-rich side of the diagrams in the fields where partial melting occurs. The unmelted residue is depleted in H<sub>2</sub>O and Qtz and contains typically assemblages associated with granulite facies metamorphism.

Most Bt and also the assemblage Bt + Sil found in higher grade amphibolite facies rocks may form from Kfs + Grt and Kfs + Opx assemblages by retrograde rehydration of granulite facies rocks. Water-rich fluids often become available when these rocks cool through the “wet” granite/pelitic solidus. Water dissolved in granitoid melts that formed during migmatization (see above) is released and may pervasively retrograde granulites to Bt + Sil + Grt gneisses or Bt + Sil + Crd gneisses. Conventional geothermobarometry will yield 650–700°C and 300–500 MPa for such rocks and the P–T conditions mimic the “wet” granite/pelitic solidus that is actually responsible for the pervasive retrogression under these conditions (see Figs. 4.18 and 7.18).

Granulites are, however, not always associated with partial melting. In fact, granulites typically do not show migmatite structures. Thus few granulites actually represent residues of a partial melting process. The processes described above generate granulite facies assemblages on a relatively small scale in the middle crust (400–700 MPa) related to the heat transferred by melts ascending from the lower crust. However, large granulite terrains (Norway, India, Labrador, Antarctica) formed at typical pressures indicating lower crust (800 MPa and more). This is particularly the case for mafic granulites (see Chap. 8). But also rocks of pelitic and semipelitic composition may recrystallize to granulites under appropriate conditions. Granulites are formed in crustal areas where the activity of H<sub>2</sub>O is smaller than 1 (standard state = pure compound at P and T), that is under conditions where a pure H<sub>2</sub>O fluid phase is not present in the rocks. If H<sub>2</sub>O deficiency is the case the rocks will not melt at the water-saturated solidus but at higher temperature. How much higher depends on the actual value of  $a_{\text{H}_2\text{O}}$ . The crucial point is that the subsolidus dehydration reactions also depend on  $a_{\text{H}_2\text{O}}$  and the isobaric equilibrium temperature decreases with decreasing  $a_{\text{H}_2\text{O}}$ . For example, the biotite breakdown reaction to orthopyroxene in the presence of Qtz and Kfs occurs at about 925°C at 500 MPa in the presence of pure H<sub>2</sub>O (Fig. 7.20; note that the Figure shows only one reaction, Opx may be metastable relative to other assemblages at lower T even at low  $a_{\text{H}_2\text{O}}$ ). The reaction is metastable relative to the biotite melting reaction, which starts to decompose Bt at T as low as 750°C under water-saturated conditions at the same pressure. However, subsolidus Bt decomposition becomes stable at T < 850°C (Fig. 7.20). The consequence is that Bt decomposes isothermally to Opx with decreasing  $a_{\text{H}_2\text{O}}$ . As a result, at a given P–T migmatitic gneisses form at high  $a_{\text{H}_2\text{O}}$  (up to saturation with a pure H<sub>2</sub>O fluid), at lower  $a_{\text{H}_2\text{O}}$  partial melting may not occur and the rocks preserve amphibolite-facies assemblages (e.g., Qtz–Kfs–Bt on Fig. 7.20). At very low  $a_{\text{H}_2\text{O}}$  assemblages form that are typical of the granulite facies (e.g., Qtz–Kfs–Opx on Fig. 7.20). Felsic granulites may form in the absence of partial melting as a result of low  $a_{\text{H}_2\text{O}}$ .

There are several feasible circumstances that may lead to low  $a_{\text{H}_2\text{O}}$ . For example, the fluid phase may contain components other than H<sub>2</sub>O. The most common extra volatile component in metamorphic fluids is CO<sub>2</sub> (see also Chaps. 3 and 6), resulting from CO<sub>2</sub> producing reactions progressing in carbonate bearing metasediments associated with pelitic schists such as calcareous micaschists or marbles. In the lower continental crust, CO<sub>2</sub> may also be derived from degassing of the mantle.

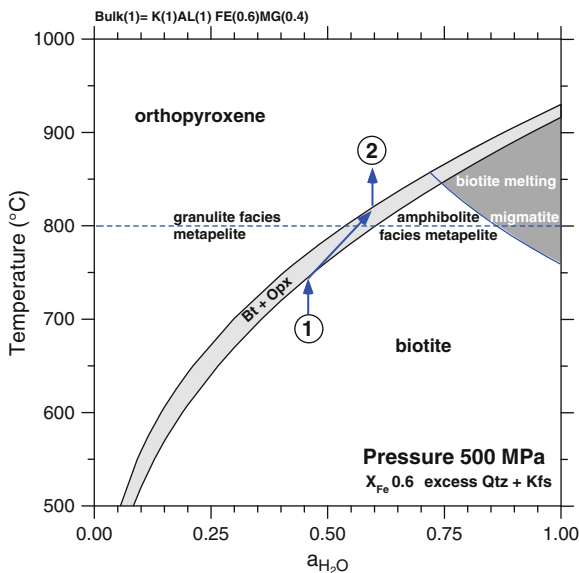


**Fig. 7.20** Isobaric  $T$ - $a_{\text{H}_2\text{O}}$  section at 500 MPa for a bulk rock  $X_{\text{Fe}}$  of the average metapelite of 0.6 and Qtz-Kfs excess conditions. At  $a_{\text{H}_2\text{O}} = 1$ , biotite begins to melt in Qtz-bearing rocks at about 750°C. However, the melting  $T$  increases dramatically with decreasing  $a_{\text{H}_2\text{O}}$  and it reaches the melt-absent Bt-breakdown reaction at about 850°C and  $a_{\text{H}_2\text{O}} = 0.75$ . At  $a_{\text{H}_2\text{O}} < 0.75$  Bt decomposes to Opx-Kfs without the participation of a melt. The  $X_{\text{Fe}}$  loop of the Bt-Opx reaction is shown as a *gray shaded zone*. If in low  $a_{\text{H}_2\text{O}}$  environments Bt (at position 1) is heated, it will decompose to Opx (at position 2) along a buffered path and no melt is involved. Bt decomposition to Opx may also occur strictly isothermally (see also Fig. 7.14)

Low  $a_{\text{H}_2\text{O}}$  may also be related to situations where rocks are devoid of a fluid phase due to progressive loss of volatile components during prograde metamorphism. In the upper amphibolite facies the rocks may have lost a fluid phase and  $a_{\text{H}_2\text{O}}$  is low (point 1 on Fig. 7.20). Through further  $T$  increase, Bt is converted to Opx over a certain interval and the assemblage Opx-Bt-Kfs-Qtz is capable of buffering  $a_{\text{H}_2\text{O}}$ . Finally, an Opx-Qtz granulite formed (point 2 on Fig. 7.20) in the absence of partial melting and migmatization.

Further effects of low  $a_{\text{H}_2\text{O}}$  common in high grade metamorphism is shown on Fig. 7.21 for a low Al metapelite with  $X_{\text{Fe}} = 0.6$ . At a typical upper amphibolite facies temperature of 680°C (dashed horizontal line on Fig. 7.21), the rock consists of Kfs-Qtz-Bt-Ms at  $a_{\text{H}_2\text{O}} > 0.8$  and is a two mica gneiss. At  $0.8 < a_{\text{H}_2\text{O}} < 0.5$  rock is made up of Grt-Bt-Sil-Kfs-Qtz, a garnet sillimanite gneiss. In the small interval  $0.5 < a_{\text{H}_2\text{O}} < 0.3$ , cordierite is now present in the rock that is characterized by the assemblage Grt-Crd-Bt-Kfs-Qtz. At  $a_{\text{H}_2\text{O}} < 0.3$  no biotite is present in the stable assemblage and the rock is a mica-free Grt-Crd gneiss. It is obvious from Fig. 7.21 that a wide variety of rocks and assemblages may be formed all of the same rock composition and all formed at the same pressure and temperature. It also follows from Fig. 7.21 that the assemblage Grt-Bt-Crd may form at 750°C in the

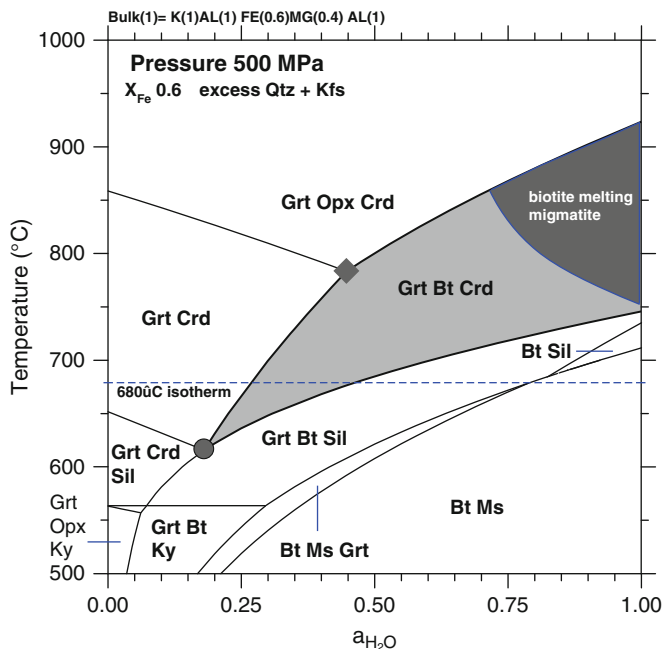
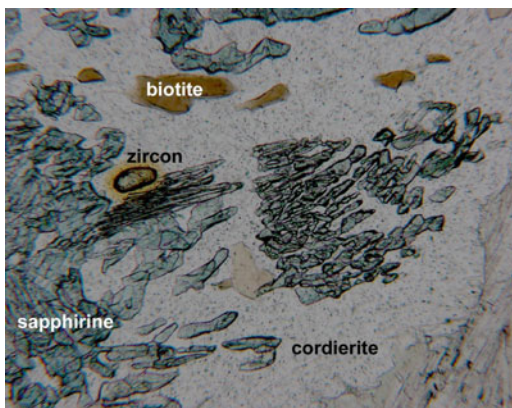


**Fig. 7.21** Isobaric  $T$ - $a_{\text{H}_2\text{O}}$  section at 500 MPa for a bulk rock  $X_{\text{Fe}}$  of the average metapelite of 0.6 and Qtz-Kfs excess conditions. Biotite melting is indicated by dark shading. Note that the granulite facies assemblage Grt-Opx-Crd-Qtz terminates at about 800°C (black diamond). The first occurrence of Grt-Bt-Crd (black circle; light shaded field) is possible at 620°C at low  $a_{\text{H}_2\text{O}}$ , more than 100°C lower than at  $a_{\text{H}_2\text{O}} = 1$ . Assemblages along the 680°C isotherm (dashed line) are discussed in the text

presence of pure  $\text{H}_2\text{O}$ , however, it also may occur at a temperature as low as 620°C at low  $a_{\text{H}_2\text{O}}$ . (black circle on Fig. 7.21). Similarly, the diagnostic granulite facies assemblage Grt-Crd-Opx (-Kfs-Qtz) replaces the Grt-Crd-Bt assemblage at 925°C at  $a_{\text{H}_2\text{O}} = 1$ . The lowest possible temperature for the assemblage (at 500 MPa) is 780°C (black diamond on Fig. 7.21) at an  $a_{\text{H}_2\text{O}}$  of about 0.45. It marks the low temperature limit of the granulite facies in felsic rocks for the rock composition of the diagram. This minimum temperature varies with pressure and rock composition between about 700°C and 800°C in middle to lower crustal metamorphism in accordance with the amphibolite-granulite facies boundary in mafic rocks (Chaps. 4 and 8).

The pressure dependence of high-grade and granulite facies assemblages is shown on the isothermal section (Fig. 7.16). At pressures below about 300 MPa, Fe-rich rocks contain cordierite and olivine. The Ol-Crd assemblage has been reported in several field studies (e.g., Abraham and Schreyer 1973). With increasing pressure Ol-Crd is replaced by Grt-Crd in Fe-rich rocks and by Opx-Crd in Mg-rich compositions. The gray shaded loop represents the field for the assemblage Grt-Crd-Sil-Qtz. If the equilibration temperature is known (here for example from

**Fig. 7.22** Photomicrograph ( $0.4 \times 0.3$  mm) showing Crd (low relief and with characteristic yellow radiation damage halo around zircon grain) and sapphirine (bluish high-relief grains) in a granulite from the Gruf Complex, Central Alps. This symplectite texture suggests low  $a_{\text{H}_2\text{O}}$  conditions (see text). It may have formed from Opx–Sil or from Grt–Sil decomposition. Small brown grains are retrograde biotite



the Grt–Crd Fe–Mg exchange thermometer), the composition of Grt and Crd also define an equilibrium pressure (500 MPa on Fig. 7.16). The barometer can be used in the range from 250 to 600 MPa (at 700°C). The diagnostic assemblage Opx–Sil appears in granulites at pressures above 600 MPa. The Opx + Sil forms from reactions (7.52) and (7.54). Possible assemblages include Opx + Sil + Qtz + Grt + Kfs and Opx + Sil + Qtz + Bt + Kfs, both of which are diagnostic for high-P granulites. Orthopyroxene + Sil + Qtz + Grt granulites typically form at pressures greater than 800 MPa at temperatures above 800°C, i.e., characteristic for metapelitic granulites in the lower continental crust. The Opx + Ky pair requires even higher pressures to form ( $P > 0.8$ – $1.0$  GPa). The diagnostic Opx + Sil assemblage is often (partly) replaced during the later stages of metamorphism, for example during isothermal decompression, by Crd-bearing assemblages such as Grt–Crd, Crd + Spl or sapphirine (Spr) + Crd symplectites (Fig. 7.22).

At very high T, diagnostic granulite assemblages are Spl + Qtz ( $>850^\circ\text{C}$ ) that may form by reaction (7.55), Spr + Qtz ( $>900^\circ\text{C}$ ), osumilite (Os) + Qtz ( $>950^\circ\text{C}$ ). Pigeonite (ternary clinopyroxene) may also appear in high-grade rocks at temperatures above 850–900°C. High-grade metamorphic rocks with assemblages that are diagnostic for crustal temperatures above 850–900°C are rare and have been reported from Precambrian terrains where massive heat transfer from the mantle to the middle continental crust took place by means of dry igneous intrusions, e.g., contact aureoles around anorthosite complexes.

## 7.7 Metamorphism of Mg-rich “Pelites”

Extremely Mg-rich primary sedimentary shale compositions ( $\text{MgO} > 15\%$ ) are unusual (see Sect. 7.2), but Mg-rich micaschists and other rocks such as Crd–Ath-bearing rocks with unusually high Mg/Fe ratios can occasionally be found as layers, boudins and lenses in other schists and gneisses in many metamorphic terrains.

The Mg-rich rocks may derive from evaporitic sediments containing Mg-clay minerals such as sepiolite, palygorskite, chlorite or corrensite, or have resulted from fluid/rock interaction (metasomatism) during metamorphism, or represent restites of partial melting. Nevertheless, the assemblages of these rocks resemble those of “normal” metapelites and bulk compositions may show a continuous transition to more Fe-rich metapelites. A number of features are, however, special to Mg-rich pelitic schists and some selected equilibria in the pure KMAH system are shown in Fig. 7.23. Note that the phase diagram is valid for rocks that contain Qtz and for the condition  $P_{\text{tot}} = P_{\text{H}_2\text{O}}$ . The latter condition has the consequence that some equilibria at high temperatures become metastable relative to melt producing reactions (see also Sects. 7.5 and 7.6).

Mg-cordierite can be found over a wide range of  $P$ - $T$  conditions and occurs in rocks that were metamorphosed at pressures in excess of 1 GPa, in sharp contrast to  $P$ - $T$  conditions of Fe-Crd stability in Fe-rich metapelites. The light-shaded area in Fig. 7.23 indicates the  $P$ - $T$  range for Mg-Crd in various assemblages. Note that

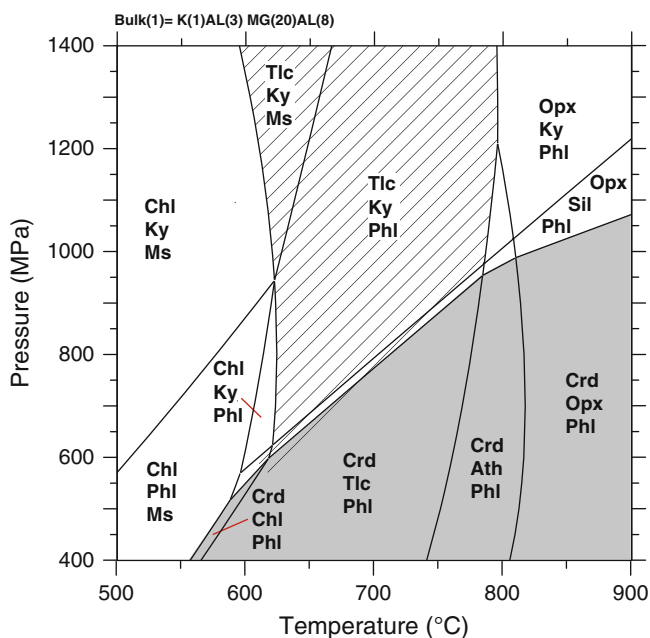


**Fig. 7.23** Metamorphism of Mg-metapelites (Ms-Mg-Chl-Qtz):  $P$ - $T$  diagram showing assemblages in the KMAH system for conditions of excess Qtz and  $\text{H}_2\text{O}$ . Mg-cordierite (*gray shaded field*) is present over a very large range of  $P$ - $T$  (compare with Fig. 7.12). Mg-Crd extends to pressures in excess of 1 GPa in the granulite facies ( $T > 800^\circ\text{C}$ ). Mg-Crd does not reach into the Ky-field. Ky present in Crd rocks may be metastable (see  $P$ - $T$  path on Fig. 7.3). The characteristic whiteschist assemblage Tlc-Ky (*diagonally ruled pattern*) indicates lower crustal metamorphism (high-pressure amphibolite facies). Granulites with Opx-Als (Ky, Sil) imply  $P > 1$  GPa. Rocks with Crd-Ath-Phl, widespread in shield areas, indicate upper amphibolite facies conditions at any pressure in the crust ( $P$  up to 1 GPa)

there is a small area of overlap of the Mg–Crd and Ky fields (dark gray field in Fig. 7.23). The assemblage Crd–Ky is metastable on Fig. 7.23, however, it has been observed in amphibolite facies schists from “Barrovian-type” metamorphic terrains. The diagnostic high-pressure granulite facies assemblage Opx + Al-silicate is restricted to temperatures  $>800^{\circ}\text{C}$  and pressures  $>1$  GPa. The indicative granulite facies assemblage Opx (enstatite) + Qtz requires minimum temperatures of  $800^{\circ}\text{C}$ . However, one must be aware that this is true only in the presence of a pure  $\text{H}_2\text{O}$ -fluid. Also note that in extremely Mg-rich rocks, talc may appear in a number of new assemblages. Talc is not present in Fe-rich metapelites and the mineral has little Fe–Mg substitution and therefore promptly disappears with increasing  $X_{\text{Fe}}$  of the bulk rock. The most interesting and diagnostic assemblage present in Mg-rich metapelites is Tlc + Ky which is restricted to high- P above 700–1,000 MPa at temperatures of  $700^{\circ}\text{C} \pm 50^{\circ}\text{C}$ . The so-called **whiteschist** assemblage Tlc + Ky, appears during high-P low-T metamorphism associated with lithosphere subduction (see below) but also forms in many Precambrian granulite facies terrains by isobaric cooling of lower crustal granulites. In the lower right corner of Fig. 7.23, the position of the metastable Phl + Qtz breakdown curve is shown. This reaction takes place at about  $100^{\circ}\text{C}$  above the corresponding Ann (Fe-biotite) + Qtz breakdown temperature. Both biotite-consuming, Opx-forming reactions are metastable relative to the corresponding melt-producing reactions in rocks containing feldspar and as mentioned above, the maximum temperature for Bt + Qtz is about  $850^{\circ}\text{C}$ .

## 7.8 High Pressure: Low Temperature Metamorphism of Pelites

High-pressure, low-temperature metamorphism (HPLT) is most commonly associated with subduction of oceanic lithosphere along convergent plate margins. Metapelites that are found in HPLT ophiolite complexes and but also in continental HPLT terrains contain few distinct metamorphic minerals and characteristic assemblages that are unique for HPLT metamorphism are rare. Of course, coesite inclusions in garnet are normally taken for unequivocal evidence of ultra-high pressure metamorphism (by definition).

However, some rather unusual minerals and special mineral composition features are associated with low grade high-pressure metamorphism. The mineral **sudoite** (sud), a dioctahedral Al–Mg chlorite, appears to be typical in very low grade high-pressure rocks. With increasing P the distinctive mineral **carpholite** (Cp) may replace Sud. The  $\text{H}_2\text{O}$ -conserving reaction (7.56) describes this transition in terms of the end member phase components given in Table 7.5. Carpholite also forms from Chl + Prl by reaction (7.57) although nominally this reaction is a dehydration reaction that decomposes rather than forms Cp. However, the steep  $P$ – $T$  paths of HPLT metamorphism may, in some situations, cross dehydration equilibria from the dehydrated to the hydrated side with increasing P. The effect is shown in Fig. 3.13, where the “dehydration by decompression” path is followed in the reverse direction during HPLT metamorphism (“hydration by compression”).

**Table 7.5** Reactions at high pressure and low temperature

Chlorite (clinocllore, daphnite)	$(\text{Mg,Fe})_5\text{Al}_2\text{Si}_3\text{O}_{10}(\text{OH})_8$
Sudoite	$\text{Mg}_2\text{Al}_3[\text{AlSi}_3\text{O}_{10}](\text{OH})_8$
Chloritoid	$(\text{Mg,Fe})\text{Al}_2\text{Si}_2\text{O}_6(\text{OH})_2$
Magnesiocarpholite	$\text{MgAl}_2[\text{Si}_2\text{O}_6](\text{OH})_4$
Ferrocapholite	$\text{FeAl}_2[\text{Si}_2\text{O}_6](\text{OH})_4$
Celadonite (phengite)	$\text{K}(\text{Mg,Fe})\text{AlSi}_4\text{O}_{10}(\text{OH})_2$
Talc	$\text{Mg}_3\text{Si}_4\text{O}_{10}(\text{OH})_2$
Pyrope	$\text{Mg}_3\text{Al}_2\text{Si}_3\text{O}_{12}$
Coesite	$\text{SiO}_2$
Reactions with excess quartz + H <sub>2</sub> O	
Sud + Qtz = 2Mcp	(7.56)
5Mcp + 9Qtz = Chl + 4Pr1 + 2H <sub>2</sub> O	(7.57)
Fcp(Mcp) = Cld + Qtz + H <sub>2</sub> O	(7.58)
5Mcp = Chl + 4Ky + 3Qtz + 6H <sub>2</sub> O	(7.59)
3Chl + 14Qtz = 5Tlc + 3Ky + 7H <sub>2</sub> O	(7.60)
Chl + 3Qtz = 2Cld + Tlc + H <sub>2</sub> O	(7.61)
4Cel + Mcp = Chl + 4Kfs + 3Qtz + 2H <sub>2</sub> O	(7.62)
5Cel + Ms = Chl + 6Kfs + 2Qtz + 2H <sub>2</sub> O	(7.63)
3Cel = Phl + 2Kfs + 3Qtz + 2H <sub>2</sub> O	(7.64)
4Cel + Chl = 3Phl + Ms + 7Qtz + 4H <sub>2</sub> O	(7.65)

For this reason, carpholite may form by hydration of a Chl + Ky assemblage by reaction (7.59). Note, however, that the formation of Cp by these mechanisms requires that a free H<sub>2</sub>O fluid is available and that Cp-forming reactions will cease when water is used up.

Fe-rich carpholite decomposes to Cld [reaction (7.58)] whereas Mg-rich Cp is replaced by Chl + Ky [reaction (7.59)] if the rocks are not carried to greater depth but rather follow a “normal” clockwise *P–T* path through the greenschist facies field. If HPLT metamorphism continues, Cp decomposition produces magnesiochloritoid [Mg-version of reaction (7.58)]. Chloritoid may, in fact, become very Mg-rich in HPLT, and Cld with  $X_{\text{Mg}} > 0.5$  is not uncommon. As one would expect, it is a general observation that the typical Fe-rich AFM-phases Cld, St and Grt become increasingly magnesian at very high P. Also talc is a characteristic mineral in HPLT metapelites and it often occurs together with K-white mica (the two minerals are difficult to distinguish under the microscope). Chloritoid + Tlc forms from the continuous Chl-consuming reaction (7.61) and the two minerals finally combine to form a pyrope-component in Grt at very high P. The diagnostic whiteschist assemblage Tlc + Ky results from the Chl-breakdown reaction (7.60) or analogous Cld- and Cp-involving reactions.

Stable high-pressure assemblages of a Fe-rich metapelite are shown on Fig. 7.24. Between the geothermal gradients of 5 and 10°C/km there are larger *P–T* fields for three assemblages with two AFM minerals separated by two narrow zones with three AFM minerals present. Starting the metamorphic path at 400°C and 1.6 GPa, the sequence of stable AFM assemblages (at constant 7.5°C/km) is: Cld–Chl, Grt–Cld–Chl, Grt–Cld, Grt–Cld–Ky, and Grt–Ky. In addition, all rocks contain a stable SiO<sub>2</sub> mineral, a phengitic white mica and excess H<sub>2</sub>O. At 600°C and 2.6 GPa



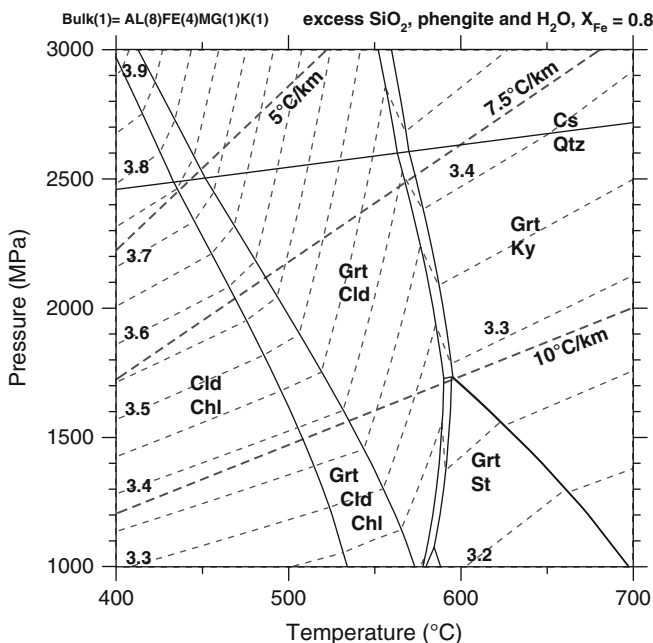


**Fig. 7.24** High-pressure metamorphism of metapelites.  $P$ - $T$  diagram showing assemblages in the KFMASH system for conditions of an excess  $\text{SiO}_2$  phase, phengite and  $\text{H}_2\text{O}$  at a rock  $X_{\text{Fe}} = 0.8$ . At high- $P$ , three large two-phase fields are present: Chl-Cld, Cld-Grt and Grt-Ky. Grt-St terminates at  $P \sim 1,700$  MPa. Grt-Cld-Phe is a diagnostic high pressure assemblage ( $P > 1$  GPa). Isopleths for constant Si p.f.u. in phengite are labeled *dashed thin lines*. *Heavy dashed lines* represent three different subduction geotherms. Most of garnet growth occurs in the Grt-Cld-Chl field from the Chl-Grt reaction. Coesite (Cs) inclusions in Grt require very low- $T$  geotherms

this path crosses the quartz-coesite phase transition boundary. At pressures  $>2.6$  GPa this metapelite contains Grt-Ky-Phe-Cs. Cs will be preserved during decompression and exhumation if it is included in garnet. However, in the Grt-Ky field of Fig. 7.24 no garnet growth occurs and the chances of preserving the UHP evidence are slim. Along the  $5^\circ\text{C}/\text{km}$  geotherm, most of the garnet growth occurs in the narrow Grt-Cld-Chl field at about  $430^\circ\text{C}$ , coinciding with the Qtz-Cs transition. Once the garnet has formed it continues to grow within the Grt-Cld and Cs fields. The garnet growth occurs in the Grt-Cld field as a result of Cld breakdown. Thus coesite may be enclosed in garnet particularly in garnet rims in metamorphism that is characterized by very low geothermal gradients (specifically  $<7^\circ\text{C}/\text{km}$ ).

The assemblage Grt-Cld is typical of high-pressure pelites (Fig. 7.24). Its stability field closes towards lower pressures ( $\sim 1$  GPa for the bulk of Fig. 7.24) and at the Qtz-Cs boundary the assemblage occurs over a temperature interval of more than  $100^\circ\text{C}$ . Also visible is that staurolite is not a mineral that occurs in normal Fe-rich high-pressure metapelites and the field for the Grt-St assemblage closes toward high  $P$  at about 1.7 GPa.

Micas in high pressure metapelites also show some characteristic diagnostic features. Particularly notable is the absence or scarcity of Bt in HPLT metapelites. Biotite persists only in extremely Mg-rich high-P rocks in the form of Phl. The main reason for this is that K-white mica experiences significant TS substitution with increasing P. Thus, Mg- and Fe-free muscovite changes its composition systematically towards celadonite (Cel) (Table 7.5) with increasing pressure. Celadonite-rich K-white micas are commonly termed phengite (Phe). It is the characteristic mica in HPLT rocks. Phengite is present in all assemblages displayed on Fig. 7.24. The Cel component is produced by a number of continuous reactions such as (7.62) through (7.65) (Table 7.5). The number of Si per formula unit (per 12 oxygen) in phengite varies between 3 in muscovite and 4 in celadonite. This the number of Si atoms characterizes the Ms–Cel series and the amount of tschermak component in phengite. The  $P$ – $T$  window on Fig. 7.24 is contoured for Si in phengite isopleths. They show that at high T and low P Si is about 3.2 corresponding to 20 mol% celadonite component in the white mica. In contrast, at low T and high P Si may be as high as 3.9 (90% celadonite component). The iso-Si contours also show that white mica composition depends on the assemblage of coexisting minerals. It is also evident from Fig. 7.24 that an equilibrium pressure can be derived from the phengite composition if the equilibrium temperature of the assemblage is known from another geothermometer. For example, if the temperature of a Cld–Grt micaschist has been determined to 550°C and the analyzed phengite contains 3.4 Si p.f.u. an equilibrium pressure of about 2 GPa can be read from Fig. 7.24. Furthermore, it also follows from Fig. 7.24 that, e.g., along the 5°C geotherm, Si in phengite first increases, reaches a maximum of 3.75 at the onset of garnet formation, then Si decreases continuously in the Grt–Cld field with increasing grade.

The pressure dependence of metapelitic assemblages over the full range of  $X_{\text{Fe}}$  at 600°C is shown on Fig. 7.25. For Fe-rich metapelites (such as the bulk used in Fig. 7.21) the sequence of successive assemblages with increasing pressure is (all with phengite, an  $\text{SiO}_2$  phase and  $\text{H}_2\text{O}$ ): (Bt–St–Grt), Grt–St, Grt–Ky with Qtz then with Cs. The high-pressure indicator assemblage Grt–Cld terminates at about 1.4 GPa. The Grt and Cld become increasingly more magnesian with increasing pressure. The  $X_{\text{Fe}}$  of coexisting Grt and Cld can be used for pressure estimates if T is known independently (dashed line Cld composition, heavy line Grt composition in Fig. 7.25). In Mg-rich rocks, talc appears in the HP and UHP assemblages, first together with Cld and in very Mg-rich rocks with Ky (whiteschist assemblage of Fig. 7.23). It is also evident that with increasing pressure the assemblage Grt–Ky–(Phe– $\text{SiO}_2$ ) represents an increasing range of rock  $X_{\text{Fe}}$ .

Mineral assemblages in HPLT metapelites offer a considerable potential for the analysis of metamorphic conditions under which they have formed. Thus metapelites can be successfully used to supplement information in eclogite terrains and can contribute to the analysis of subduction zone metamorphism and the understanding of the geodynamic processes that cause it. However, successive sequences of mineral assemblages must be quantitatively modeled for each HPLT terrain.

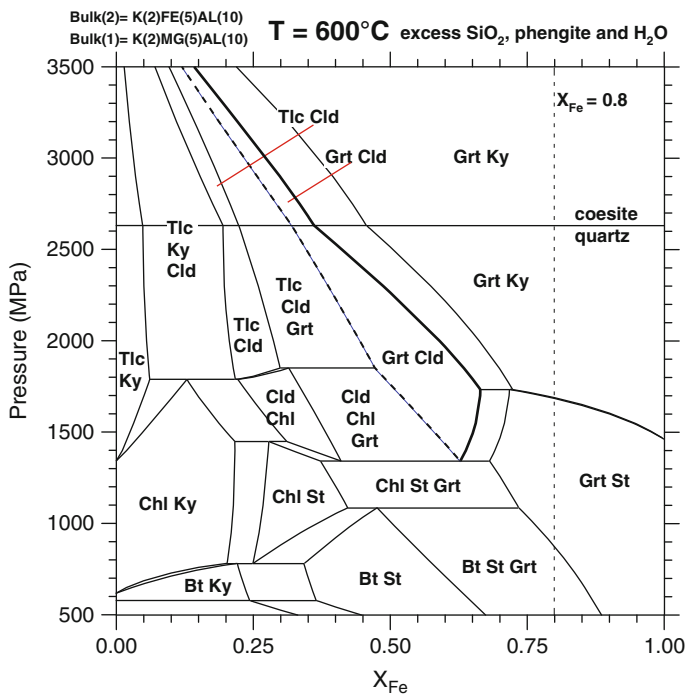


**Fig. 7.25** High-pressure metamorphism of metapelites. Isothermal  $P$ - $X_{Fe}$  diagram showing assemblages in the KFMASH system for conditions of an excess  $SiO_2$  phase, phengite and  $H_2O$  at  $T = 600^\circ C$ . Grt-Ky-Phe is the dominant assemblage at high  $P$ . The Grt-Cld assemblage is highlighted because of its potential as a geobarometer in high- $P$  metapelites. In low- $X_{Fe}$  rocks talc is the characteristic mineral in different assemblages, including the whiteschist assemblages Tlc-Ky

## 7.9 Additional Components in Metapelites

Until now we have discussed the metamorphism of pelitic sediments in the six-component AFM system that typically accounts for more than 95 wt% oxide components of "normal", i.e., mature pelagic shales. However, pelites may also contain many additional elements that give rise to complex solid solutions in AFM phases or to the formation of separate minerals with metamorphic recrystallization. Such "extra" phases may provide valuable information about the metamorphic evolution of a rock.

With respect to the idealized 6-component pelite, it is obvious that the widespread and abundant elements Ca, Na, Mn, Ti, P and  $Fe^{3+}$  are also present in minor amounts even in the most "mature" end-member pelitic composition. These "extra" elements can account for the presence of additional major minerals such as Na-Ca feldspar, paragonite, epidote-group minerals and accessory minerals like apatite, titanite, rutile, ilmenite, magnetite, monazite, and many others. With respect to typical AFM minerals, Grt normally incorporates Ca and Mn in significant amounts,

but also  $\text{Fe}^{3+}$  and sometimes OH may be present. The spessartine (Sps) component in prograde low-grade garnet is particularly important. The Pl present in metapelites carries large amount of the bulk rock's Na and Ca content at higher grades. At lower grades and in the absence of Pl the carrier of Na is Pg, whereas the Ca may be incorporated in Grt as a grossular (Grs) component or in Ca-minerals, such as Zo, Czo or Ep. Biotite usually contains Ti, Mn, halogens and  $\text{Fe}^{3+}$ . It can take up more than 6 wt%  $\text{TiO}_2$  and it may be the only significant Ti-bearing mineral present. If the bulk rock  $\text{TiO}_2$ -content exceeds Ti-saturation of biotite or if no Bt is present in the assemblage, some extra Ti-phase will be present (usually Rt, Ttn or Ilm). Staurolite in metapelitic rocks tends to contain Mn and particularly Zn (sometimes up to several percent!) Cordierite often accommodates Li and Be that replace Mg, Fe, and Al on regular crystallographic cation sites and Na, K,  $\text{CO}_2$ , and  $\text{H}_2\text{O}$  in the structural channels. Li and Be are difficult to analyze using standard electron microprobe techniques. Muscovite, as discussed above, is often phengitic, i.e., contains Mg and Fe as Cel component. Spinel may contain a large variety of "non-AFM elements" including  $\text{Fe}^{3+}$ , Zn, Mn, Cr, and V with Zn concentrations, in particular that may be several wt%.

There are two major effects of extra components in "AFM minerals". Equilibrium conditions of mineral reactions can be displaced in  $P$ - $T$  space relative to the pure AFM system and, in the most extreme case, the topology of phase relationships can be altered and inverted. In other words, mineral assemblages that are not stable in the pure AFM system can become possible as a result of strong fractionation of an "extra" element (e.g., zinc) into one "AFM mineral". Strong partitioning of Mn into Grt for example, causes the Grt to appear in a prograde metamorphic sequence at a temperature about 50–100°C lower than in the pure AFM system. The other major effect of extra components is that more minerals appear in an assemblage than expected in the pure AFM system. For example, in a typical AFM situation, the minerals Chl + Bt + St can be found in a rock with Ms + Qtz. In such a rock it will not be unusual to also find Grt as an additional mineral because of its Mn-content. In this case, the coexistence of the four minerals does not mean, that the rock equilibrated at the conditions of the AFM discontinuous reaction (7.28) (Table 7.3). In reality, Grt is not a co-planar phase in terms of the AFM projection but rather defines a phase volume in AFM + Mn space.

Particularly complicated are high-grade assemblages involving spinel because this mineral often deviates significantly from pure Spl-Hc solid solutions and because it is usually involved in fluid-absent reactions which are especially sensitive to small deviations from the pure AFM system. Therefore, great care must be taken in the interpretation of Spl-bearing assemblages.

In conclusion, the observed common deviation of metapelites from the pure AFM composition may have significant consequences on the  $P$ - $T$  distribution of stable assemblages. The interpretation of assemblages in metapelites, therefore, requires common petrologic sense and a great deal of professional experience. These difficulties, however, certainly do not invalidate the use of an AFM model for the prediction of phase relationships in metapelites.

In the following some specific consequences of the presence of Na and Ca will be illuminated. First let us consider the component Na, which may be present in the percentage-range even in mature pelites. Paragonite is the mineral that stores Na at low grade, that is in rocks that typically also contain much chlorite. Reaction (7.22) replaces the Pg + Chl with Grt and Ab. The temperature at which this reaction occurs along the chosen model metamorphism is about 520°C. The reaction may use up either one of the reactants leaving two possible product assemblages: Chl + Grt + Ab or Pg + Grt + Ab, that both coexist with Ms + Qtz in most metapelites. Reaction (7.23) limits the presence of Chl in Ms-bearing pelitic rocks. The assemblage is replaced by Grt + Bt at about 540°C. Sedimentary (diagenetic) in Barrowian metamorphism. Na-white mica (Pg) breaks down in the presence of Qtz at about 625°C [reaction (7.24)] to form Ab + Ky at mid-crustal 600 MPa (560°C at 300 MPa, 670°C at 900 MPa). It follows that Pg is present in large portions of the field of the stable assemblage St + Qtz so that paragonite generally is widespread in micaschists and that one typical metamorphic rock of the mid-amphibolite facies zone of the Central European Alps contains St–Ky–Pg (Fig. 7.10).

The distribution of stable phases in the simple KNASH system is shown in Fig. 7.26 at a constant pressure of 600 MPa (middle crust). At low temperature,

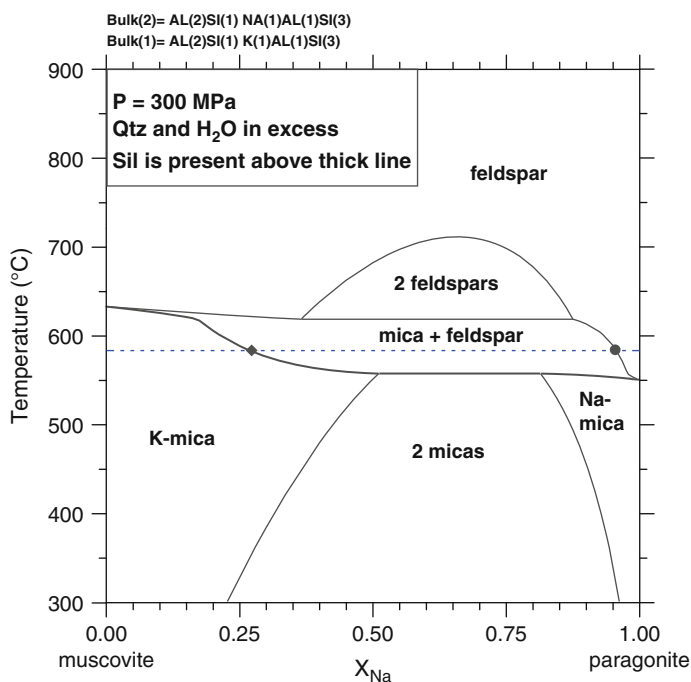


**Fig. 7.26** Isobaric  $T$ - $X_{Na}$  diagram showing stable assemblages in the KNASH system at 300 MPa. As an example, along the isotherm at ~680°C (*dashed line*) the assemblages with increasing  $X_{Na}$  (Na/(Na + K)) are: Ms–Qtz, Ms–Ab–Sil–Qtz, and Ab–Sil–Qtz. The composition of the K-mica in the assemblage Ms–Ab–Sil–Qtz is given as *black diamond*, and of the coexisting feldspar as a *black circle*

there are two micas present, a K-rich white mica (muscovite) and Na-rich white mica (paragonite). For intermediate Na–K compositions, the two micas coexist and the coexisting micas become more K-rich (paragonite) and more Na-rich (muscovite) as temperature increases. The composition of the two micas are defined by the solvus relationship. Muscovite may dissolve more than 50 mol% Pg at  $T \sim 550^\circ\text{C}$ . At  $550^\circ\text{C}$  pure Pg decomposes to pure Ab and Als (here Sil). At a very slightly higher temperature the two-mica solvus is capped by a new field for K-mica and Na-feldspar. At the  $\sim 580^\circ\text{C}$  isotherm (dashed line), for example, a feldspar of the composition of the black circle coexists with a mica of the composition of the black diamond. It can be seen that both minerals, feldspar and mica, become more K-rich with increasing temperature. At  $620^\circ\text{C}$  the situation is further complicated by the alkali feldspar solvus. At  $630^\circ\text{C}$ , for example, rocks with a high  $X_{\text{Na}}$  ( $\text{Na}/(\text{Na} + \text{K})$ ) contain a Na-rich feldspar, rocks with  $X_{\text{Na}}$  between about 0.4 and 0.85 contain two feldspars with compositions given by the solvus. Rocks with  $X_{\text{Na}}$  between about 0.1 and 0.4 contain a K-rich alkali feldspar and in rocks with  $X_{\text{Na}}$  in the range of 0.05–0.1 a K-feldspar and muscovite is present, whereas at  $X_{\text{Na}} < 0.05$  only muscovite but no feldspar is present. Pure endmember muscovite decomposes to K-feldspar and Als at  $640^\circ\text{C}$ . Remember that this reaction is metastable relative to the Ms melting reaction at pressures greater than 300 MPa (see above).

The “world average” pelagic pelite (taken from a compilation of rock data by Carmichael, 1989) has the following composition (in atoms):  $\text{Si}_{58.16}\text{Al}_{20.73}\text{Fe}_{7.97}\text{Mg}_{5.37}\text{Ca}_{0.82}\text{Na}_{2.67}\text{K}_{3.65}\text{O}_{164.75}$ . As expected, the KFMAS components make up most of the rock composition ( $X_{\text{Fe}} = 0.6$ ). Ca is present but its concentration is low and the amount of Na is significant ( $X_{\text{Na}} = 0.42$ ). The distribution of stable assemblages for this average pelite is shown on Fig. 7.27 for  $\text{H}_2\text{O}$  saturated conditions. In addition to the labeled assemblages in each field, there is Ms and Qtz present in all fields except in the lower right corner where there is no Ms present. There are two geothermal gradients representing Barrovian mid-crustal collision metamorphism shown as dashed lines. Along the  $30^\circ\text{C}/\text{km}$  geotherm, the succession of Barrovian mineral zones can easily be recognized: chlorite, biotite, garnet, staurolite, sillimanite. The kyanite zone is lacking because the average pelite is not aluminous enough to develop a kyanite zone. The general behavior of the Ca and Na extra components is: At low grade, Na is contained in mica and Ca forms a small amount of epidote/clinozoisite. At higher pressures, actinolite may replace epidote. In the upper greenschist facies, biotite forms, actinolite transforms to hornblende (tschermakitic) and plagioclase turns into oligoclase and takes up much of the Ca and Na (see also Chap. 8). In higher grade rocks also garnet may contain some Ca. For example, for  $650^\circ\text{C}$  and 700 MPa (black circle on Fig. 7.27) the computed mode and the mineral compositions are listed in Table 7.6. At this  $P$ – $T$  point the average pelagic pelite consists of more than 50 vol% Qtz and plagioclase. The two micas, muscovite and biotite, represent 30% of the rock volume. The typical AFM minerals in addition to 17 vol% Bt are represented by 11% garnet and 8% staurolite. Thus it can be expected that the average pelite will be metamorphosed to a St–Grt two-mica-gneiss at upper amphibolite facies conditions. The plagioclase contains 19 mol% anorthite component (oligoclase) and garnet has 5 mol% grossular

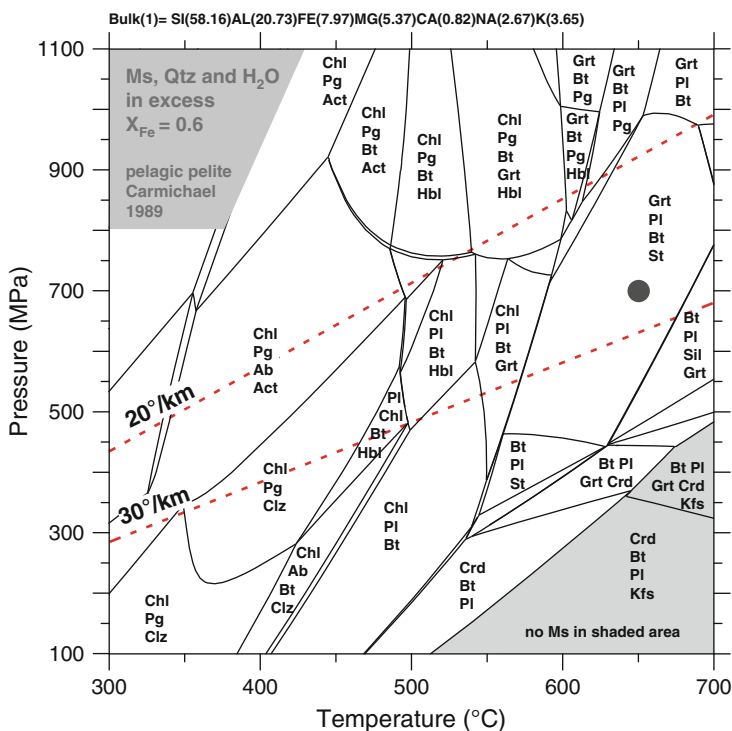


**Fig. 7.27** Metamorphism of impure pelites (KFMASH system + Na + Ca). Model for the average pelagic pelite composition of Carmichael (1989). Two typical continental collision geotherms are shown as *dashed lines* (see text)

**Table 7.6** Mode and mineral composition of pelagic pelite at 650°C and 700 MPa

Mineral	Vol%	Computed composition
Garnet	11	Alm 74, Prp 21, Grs 05
Plagioclase	16	Ab 79, An 19, Kfs 02
Biotite	17	Phl 59, Ann 41
Staurolite	8	Fe–St 76, Mg–St 24
Muscovite	13	Ms 75, Pg 16, Fe–Mg Cel 09
Quartz	35	Qtz

component. These computed mineral compositions (Table 7.6) closely match those of field samples from the same metamorphic grade.

## References and Further Reading

### *Cited References*

Abraham K, Schreyer W (1973) Petrology of a ferruginous hornfels from Riesensglück, Harz mountains, Germany. *Contrib Mineralog Petrol* 40:275–292

- Anderson JL (1996) Status of thermobarometry in granite batholiths. *Trans R Soc Edinb Earth Sci* 87:125–138
- Barrow G (1893) On an intrusion of muscovite biotite gneiss in the S.E. Highlands of Scotland and its accompanying metamorphism. *Q J Geol Soc Lond* 49:330–358
- Barrow G (1912) On the geology of lower deeside and the southern Highland border. *Proc Geol Assoc* 23:268–284
- Brown M (1979) The petrogenesis of the St. Malo migmatite belt, American Massif, France. *N Jb Mineral Abh* 135:48–74
- Carmichael RS (1989) Practical handbook of physical properties of rocks and minerals. CRC Press, Boca Raton, 834 pp
- Clemens JD, Wall VJ (1981) Origin and crystallization of some peraluminous (S-type) granite magmas. *Can Mineralog* 19:111–131
- De Yoreo JJ, Lux DR, Guidotti CV (1989) The Arcadian thermal history of western Maine. *J Metamorph Geol* 7:169–190
- Ellis DJ, Obata M (1992a) Migmatite and melt segregation at Cooma, New South Wales. *Trans R Soc Edinb* 83:95–106
- Graessner T, Schenk V (2001) An exposed Hercynian deep crustal section in the Sila Massif of southern Calabria: mineral chemistry, petrology and a P-T path of granulite-facies metapelitic migmatites and metabasites. *J Petrol* 32:931–961
- Greenfield JE, Clarke GL, White RW (1998) A sequence of partial melting reactions at Mt. Stafford, central Australia. *J Metamorph Geol* 16:363–378
- Jones KA, Brown M (1989) The metamorphic evolution of the Southern Brittany metamorphic belt, France. In: Daly JS, Cliff RA, Yardley BWD (eds) *Evolution of metamorphic belts*, Geological Society of London, Special Publication, vol 43, pp 187–202
- Le Breton N, Thompson AB (1988) Fluid-absent (dehydration) melting of biotite in metapelites in the early stages of crustal anatexis. *Contrib Mineralog Petrol* 99:226–237
- Milord I, Sawyer EW, Brown M (2001) Formation of diatexite migmatite and granite magma during anatexis of semi-pelitic metasedimentary rocks: an example from St. Malo, France. *J Petrol* 42:487–505
- Patino-Douce AE, Humphreys ED, Johnson AD (1990) Anatexis and metamorphism in tectonically thickened continental crust exemplified by the Sevier hinterland, western North America. *Earth Planet Sci Lett* 97:290–315
- Thompson AB (1982) Dehydration melting of pelitic rocks and the generation of H<sub>2</sub>O-undersaturated granitic liquids. *Am J Sci* 282:1567–1595
- Thompson AB, Tracy RJ (1979) Model systems for anatexis of pelitic rocks. II. Facies series melting and reactions in the systems CaO-KAlO<sub>2</sub>-NaAlO<sub>2</sub>-Al<sub>2</sub>O<sub>3</sub>-SiO<sub>2</sub>-H<sub>2</sub>O. *Contrib Mineralog Petrol* 70:429–438
- Tracy RJ (1978) High grade metamorphic reactions and partial melting of pelitic schist, west-central Massachusetts. *Am J Sci* 278:150–178
- Vielzeuf D, Holloway JR (1988) Experimental determination of the fluid-absent melting relations in pelitic systems: consequences for crustal differentiation. *Contrib Mineralog Petrol* 98:257–276
- White RW, Pomroy NE, Powell R (2003a) An in situ metatexite-diatexite transition in upper amphibolite facies rocks from Broken Hill, Australia. *J Metamorph Geol* 23:579–602
- White RW, Powell R, Clarke GL (2003b) Prograde metamorphic assemblage evolution during partial melting of metasedimentary rocks at low pressures: migmatites from Mt. Stafford, central Australia. *J Petrol* 44:1937–1960
- White RW, Powell R, Halpin JA (2004) Spatially-focused melt formation in aluminous metapelites from Broken Hill, Australia. *J Metamorph Geol* 22:825–845
- Wickham SM (1987) Crustal anatexis and granite petrogenesis during low-pressure regional metamorphism: the Trois Seigneurs Massif, Pyrenees, France. *J Petrol* 28:127–169



### ***Further Reading and Additional References***

- Albee AL (1972) Metamorphism of pelitic schists: reaction relations of chloritoid and staurolite. *Geol Soc Am Bull* 83:3249–3268
- Allaz J, Maeder X, Vannay J-C, Steck A (2005) Formation of aluminosilicate-bearing quartz veins in the Simano nappe (Central Alps): structural, thermobarometric and oxygen isotope constraints. *Schweiz Miner Petrogr Mitt* 85:191–214
- Aranovich LY, Podlesskii KK (1983) The cordierite-garnet-sillimanite-quartz equilibrium: experiments and applications. In: Saxena SK (ed) *Kinetics and equilibrium in mineral reactions*. Springer, Berlin, Heidelberg, New York, pp 173–198
- Arkai P, Sassi FP, Sassi R (1995) Simultaneous measurements of chlorite and illite crystallinity: a more reliable tool for monitoring low- to very low grade metamorphism in metapelites. A case study from the Southern Alps (NE Italy). *Eur J Mineralog* 7:115–128
- Ashworth JR (1985) *Migmatites*. Blackie, Glasgow, 301 pp
- Bestel M, Gawronski T, Abart R, Rhede D (2009) Compositional zoning of garnet porphyroblasts from the polymetamorphic Wölz Complex, Eastern Alps. *Mineral Petrol* 97:173–188
- Bhattacharya A, Sen SK (1986) Granulite metamorphism, fluid buffering and dehydration melting in the Madras charnockites and metapelites. *J Petrol* 27:1119–1141
- Black PM, Maurizot P, Ghent ED, Stout MZ (1993) Mg-Fe carpholites from aluminous schists in the Diaphot region and implications for preservation of high-pressure/ low-temperature schists, northern new Caledonia. *J Metamorph Geol* 11:455–460
- Blenkinsop TG (1988) Definition of low-grade metamorphic zones using illite crystallinity. *J Metamorph Geol* 6:623–636
- Bohlen SR (1991) On the formation of granulites. *J Metamorph Geol* 9:223–230
- Bucher K, Droop GTR (1983) The metamorphic evolution of garnet-cordierite-sillimanite gneisses of the Gruf-Complex, Eastern Pennine Alps. *Contrib Mineralog Petrol* 84:215–227
- Carrington DP (1995) The relative stability of garnet-cordierite and orthopyroxene-sillimanite-quartz assemblages in metapelitic granulites: experimental data. *Eur J Mineralog* 7:949–960
- Carrington DP, Harley SL (1995a) Partial melting and phase relations in high-grade metapelites: an experimental petrogenetic grid in the KFMASH system. *Contrib Mineralog Petrol* 120:270–291
- Carrington DP, Harley SL (1995b) The stability of osumilite in metapelitic granulites. *J Metamorph Geol* 13:613–625
- Cesare B (1994) Hercynite as the product of staurolite decomposition in the contact aureole of Vedrette di Ries, eastern Alps, Italy. *Contrib Mineralog Petrol* 116:239–246
- Chamberlain CP, Lyons JB (1983) Pressure, temperature, and metamorphic zonation studies of pelitic schists in the Merrimack synclinorium, south-central New Hampshire. *Am Mineralog* 68:530–540
- Chopin C (1981) Talc-phengite, a widespread assemblage in high-grade pelitic blueschists of the Western Alps. *J Petrol* 22:628–650
- Chopin C (1983) Magnesiochloritoid, a key-mineral for the petrogenesis of high-grade pelitic blueschists. *Bull Minéral* 106:715–717
- Chopin C (1984) Coesite and pure pyrope in high-grade blueschists of the western Alps: a first record and some consequences. *Contrib Mineralog Petrol* 86:107–118
- Chopin C, Schreyer W (1983) Magnesio-carpholite and magnesio-chloritoid: two index minerals of pelitic blueschists and their preliminary phase relations in the model system MgO-Al<sub>2</sub>O<sub>3</sub>-SiO<sub>2</sub>-H<sub>2</sub>O. *Am J Sci* 283A:72–96
- Connolly JAD, Cesare B (1993) C-O-H-S fluid composition and oxygen fugacity in graphitic metapelites. *J Metamorph Geol* 11:379–388
- Currie KL, Gittins J (1988) Contrasting sapphirine parageneses from Wilson Lake, Labrador and their tectonic implications. *J Metamorph Geol* 6:603–622
- Curtis CD (1985) Clay mineral precipitation and transformation during burial diagenesis. *Philos Trans R Soc Lond A* 315:91–105

- Daczko NR, Clarke GL, Klepeis KA (2002) Kyanite-paragonite-bearing assemblages, northern Fiordland, New Zealand: rapid cooling of the lower crustal root to a Cretaceous magmatic arc. *J Metamorph Geol* 20:887–902
- Das K, Dasgupta S, Miura H (2001) Stability of osumilite coexisting with spinel solid solution in metapelitic granulites at high oxygen fugacity. *Am Mineralog* 86:1423–1434
- Dempster TJ (1985) Garnet zoning and metamorphism of the Barrovian type area, Scotland. *Contrib Mineralog Petrol* 89:30–38
- Droop GTR, Bucher-Nurminen K (1984) Reaction textures and metamorphic evolution of sapphirine-bearing granulites from the Gruf complex, Italian Central Alps. *J Petrol* 25:766–803
- Droop GTR, Harte B (1995) The effect of Mn on the phase relations of medium-grade pelites: constraints from natural assemblage on petrogenetic grid topology. *J Petrol* 36:1549–1578
- Dunoyer de Segonzac G (1970) The transformation of clay minerals during diagenesis and low grade metamorphism: a review. *Sedimentology* 15:281–346
- Earley D III, Stout JH (1991) Cordierite-cumingtonite facies rocks from the Gold Brick District, Colorado. *J Petrol* 32:1169–1201
- Ellis DJ (1987) Origin and evolution of granulites in normal and thickened crusts. *Geology* 15:167–170
- Ellis DJ, Obata M (1992) Migmatite and melt segregations at Cooma, New South Wales. In: Brown PE, Chappell BW (eds) *The second Hutton symposium on the origin of granites and related rocks*, Proceedings of the Geological Society of America Special Paper, vol 272, pp 95–106
- El-Shazly AK, Aley El-Din K (1995) Petrology of Fe-Mg-carpholite-bearing metasediments from NE Oman. *J Metamorph Geol* 13:379–396
- Enami M (1983) Petrology of pelitic schists in the oligoclase-biotite zone of the Sanbagawa metamorphic terrain, Japan: phase equilibria in the highest grade zone of a high-pressure intermediate type of metamorphic belt. *J Metamorph Geol* 1:141–161
- Ferri F, Poli S, Vielzeuf D (2009) An experimental determination of the effect of bulk composition phase relationships in metasediments at near-solidus conditions. *J Petrol* 50:909–931
- Fitzsimons ICW (1996) Metapelitic migmatites from Brattstrand Bluffs, East Antarctica – metamorphism, melting and exhumation of the mid crust. *J Petrol* 37:395–414
- Florence FP, Spear FS (1993) Influences of reaction history and chemical diffusion on P-T calculations for staurolite schists from the Littleton Formation, northwestern New Hampshire. *Am Mineralog* 78:345–359
- Foster CT Jr (1991) The role of biotite as a catalyst in reaction mechanisms that form sillimanite. *Can Mineralog* 29:943–964
- Fransolet A-M, Schreyer W (1984) Sudoite, di/trioctahedral chlorite: a stable low-temperature phase in the system MgO–Al<sub>2</sub>O<sub>3</sub>–SiO<sub>2</sub>–H<sub>2</sub>O. *Contrib Mineralog Petrol* 86:409–417
- Frey M (1987) The reaction-isograd kaolinite + quartz = pyrophyllite + H<sub>2</sub>O, Helvetic Alps, Switzerland. *Schweiz Miner Petrogr Mitt* 67:1–11
- Frost BR, Frost CD, Touret JLR (1989) Magmas as a source of heat and fluids in granulite metamorphism. In: Bridgewater D (ed) *Fluid movements – element transport, and the composition of the deep crust*. Kluwer, Dordrecht, pp 1–18
- Gharrabi M, Velde B, Sagon J-P (1998) The transformation of illite to muscovite in pelitic rocks: constraints from X-ray diffraction. *Clays Clay Miner* 46:79–88
- Giaramita MJ, Day HW (1991) The four-phase AFM assemblage staurolite–aluminum–silicate–biotite–garnet: extra components and implications for staurolite-out isograds. *J Petrol* 32:1203–1230
- Giaramita MJ, Day HW (1992) Buffering in the assemblage staurolite–aluminium silicate–biotite–garnet–chlorite. *J Metamorph Geol* 9:363–378
- Grant JA (1981) Orthoamphibole and orthopyroxene relations in high-grade metamorphism of pelitic rocks. *Am J Sci* 281:1127–1143
- Grant JA (1985) Phase equilibria in low-pressure partial melting of pelitic rocks. *Am J Sci* 285:409–435

- Grew ES (1980) Sapphirine and quartz association from Archean rocks in Enderby Land, Antarctica. *Am Mineralog* 65:821–836
- Grew ES (1988) Kornerupine at the Sar-e-Sang, Afghanistan, whiteschist locality: implications for tourmaline-kornerupine distribution in metamorphic rocks. *Am Mineralog* 73:345–357
- Harley SL (1986) A sapphirine-cordierite-garnet-sillimanite granulite from Enderby Land Antarctica: implications for FMAS petrogenetic grids in the granulite facies. *Contrib Mineralog Petrol* 94:452–460
- Harley SL (1989) The origins of granulites: a metamorphic perspective. *Geol Mag* 126: 215–247
- Harley SL, Fitzsimons IC (1991) P-T evolution of metapelitic granulites in a polymetamorphic terrane: the Rauer Group, East Antarctica. *J Metamorph Geol* 9:231–244
- Henry DJ, Guidotti CV (2002) Titanium in biotite from metapelitic rocks: temperature effects, crystal-chemical controls, and petrologic applications. *Am Mineralog* 87:375–382
- Hirsch DM, Prior DJ, Carlson WD (2003) An overgrowth model to explain multiple, dispersed high-Mn regions in the cores of garnet porphyroblasts. *Am Mineralog* 88:131–141
- Hodges KV, Spear FS (1982) Geothermometry, geobarometry and the  $\text{Al}_2\text{SiO}_5$  triple point at Mt. Moosilauke, New Hampshire. *Am Mineralog* 67:1118–1134
- Holdaway MJ, Mukhopadhyay B (1993) Geothermobarometry in pelitic schists: a rapidly evolving field. *Am Mineralog* 78:681–693
- Hollis JA, Harley SL, White RW, Clarke GL (2006) Preservation of evidence for prograde metamorphism in ultrahigh-temperature, high-pressure kyanite-bearing granulites, South Harris, Scotland. *J Metamorph Geol* 24:263–279
- Hollister LS (1966) Garnet zoning: an interpretation based on the Rayleigh fractionation model. *Science* 154:1647–1651
- Hudson NFC (1980) Regional metamorphism of some Dalradian pelites in the Buchan area, N.E. Scotland. *Contrib Mineralog Petrol* 73:39–51
- Kawakami T, Ikeda T (2003) Boron in metapelites controlled by the breakdown of tourmaline and retrograde formation of borosilicates in the Yanai area, Ryoke metamorphic belt, SW Japan. *Contrib Mineralog Petrol* 145:131–150
- Kerrick DM (1988)  $\text{Al}_2\text{SiO}_5$ -bearing segregations in the Lepontine Alps, Switzerland: aluminum mobility in metapelites. *Geology* 16:636–640
- Klaper EM, Bucher-Nurminen K (1986) Alpine metamorphism of pelitic schists in the Nufenen Pass area, Lepontine Alps. *J Metamorph Geol* 5:175–195
- Labotka TC, Kath RL (2001) Petrogenesis of the contact-metamorphic rocks beneath the Stillwater Complex, Montana. *Geol Soc Am Bull* 113:1312–1323
- Lancaster PJ, Fu B, Page FZ, Kita NT, Bickford ME, Hill BM, McLelland JM, Valley JW (2009) Genesis of metapelitic migmatites in the Adirondack Mountains, New York. *J Metamorph Geol* 27:41–54
- Lang HM (1991) Quantitative interpretation of within-outcrop variation in metamorphic assemblage in staurolite-kyanite-grade metapelites, Baltimore, Maryland. *Can Mineralog* 29:655–672
- Likhanov II, Reverdatto VV, Sheplev VS, Vershinin AE, Kozlov PS (2001) Contact metamorphism of Fe- and Al-rich graphitic metapelites in the Transangarian region of the Yenisei Ridge, eastern Siberia, Russia. *Lithos* 58:55–80
- Livi KJT, Ferry JM, Veblen DR, Frey M, Connolly JAD (2002) Reactions and physical conditions during metamorphism of Liassic aluminous black shales and marls in central Switzerland. *Eur J Mineralog* 14:647–672
- Lonker SW (1980) Conditions of metamorphism in high-grade pelites from the Frontenac Axis, Ontario, Canada. *Can J Sci* 17:1666–1684
- Lonker SW (1981) The P-T-X relations of the cordierite-garnet-sillimanite-quartz equilibrium. *Am J Sci* 281:1056–1090
- Loomis TP (1986) Metamorphism of metapelites: calculations of equilibrium assemblages and numerical simulations of the crystallization of garnet. *J Metamorph Geol* 4:201–229

- Mahar EM, Baker JM, Powell R, Holland TJB (1997) The effect of Mn on mineral stability in metapelites. *J Metamorph Geol* 15:223–238
- Mather JD (1970) The biotite isograd and the lower greenschist facies in the Dalradian rocks of Scotland. *J Petrol* 11:253–275
- McDade P, Harley SL (2001) A petrogenetic grid for aluminous granulite facies metapelites in the KFMASH system. *J Metamorph Geol* 19:45–59
- Miyashiro A, Shido F (1985) Tschermak substitution in low- and middle-grade pelitic schists. *J Petrol* 26:449–487
- Mohr DW, Newton RC (1983) Kyanite-staurolite metamorphism in sulfidic schists of the Anakeesta Formation, Great Smoky Mountains, North Carolina. *Am J Sci* 283:97–134
- Motoyoshi Y, Hensen BJ (2001) F-rich phlogopite stability in ultra-high-temperature metapelites from the Napier Complex, East Antarctica. *Am Mineralog* 86:1404–1413
- Munz IA (1990) Whiteschists and orthoamphibole-cordierite rocks and the P-T-t path of the Modum Complex, S. Norway. *Lithos* 24:181–200
- Nair R, Chacko T (2002) Fluid-absent melting of high-grade semi-pelites: P-T constraints on orthopyroxene formation and implications for granulite genesis. *J Petrol* 43:2121–2142
- Nichols GT, Berry RF, Green DH (1992) Internally consistent gahnitic spinel-cordierite-garnet equilibria in the FMASHZn system: geothermobarometry and applications. *Contrib Mineralog Petrol* 111:362–377
- Nyman MW, Pattinson DRM, Ghent ED (1995) Melt extraction during formation of K-feldspar + sillimanite migmatites, west of Revelstoke, British Columbia. *J Petrol* 36:351–372
- Okuyama-Kununose Y (1994) Phase relations in andalusite-sillimanite type Fe-rich metapelites: Tono contact metamorphic aureole, northeast Japan. *J Metamorph Geol* 12:153–168
- Pattinson DRM (2001) Instability of  $Al_2SiO_5$  “triple point” assemblages in muscovite + biotite + quartz-bearing metapelites, with implications. *Am Mineralog* 86:1414–1422
- Pattinson DRM, Tracy RJ (1991) Phase equilibria and thermometry of metapelites. In: Kerrick DM (ed) *Contact metamorphism, Reviews in Mineralogy*. Mineralogical Society of America, Washington DC, pp 105–206
- Pattinson DRM, Vogl JJ (2005) Contrasting sequences of metapelitic mineral-assemblages in the aureole of the tilted Nelson batholith, British Columbia: implications for phase equilibria and pressure determination in andalusite-sillimanite-type settings. *Can Mineralog* 43:51–88
- Pattinson DRM, Spear FS, Cheney JT (1999) Polymetamorphic origin of muscovite + cordierite + staurolite + biotite assemblages: implications for the metapelitic petrogenetic grids and for P-T paths. *J Metamorph Geol* 17:685–703
- Powell R, Holland T (1990) Calculated mineral equilibria in the pelite system, KFMASH ( $K_2O$ -FeO-MgO- $Al_2O_3$ - $SiO_2$ - $H_2O$ ). *Am Mineralog* 75:367–380
- Prenzel JD, Abart R (2009) Garnet reaction rims from the breakdown of staurolite in polymetamorphic micaschists from the Rappold complex, Austroalpine basement, Eastern Alps. *Mineral Petrol* 97:189–201
- Reinhardt J (1987) Cordierite-anthophyllite rocks from north-west Queensland, Australia: metamorphosed magnesian pelites. *J Metamorph Geol* 5:451–472
- Robinson D, Warr LN, Bevins RE (1990) The illite ‘crystallinity’ technique: a critical appraisal of its precision. *J Metamorph Geol* 8:333–344
- Schreyer W (1977) Whiteschists: their compositions and pressure – temperature regimes based on experimental, field and petrographic evidence. *Tectonophysics* 3:127–144
- Schumacher JC, Hollocher KT, Robinson P, Tracy RJ (1990) Progressive metamorphism and melting in Central Massachusetts and Southwestern New Hampshire, USA. In: Ashworth JR, Brown M (eds) *High-temperature metamorphism and crustal anatexis*, vol 2, The mineralogical society series. Unwin Hyman, London, pp 198–234
- Selverstone J, Spear FS (1985) Metamorphic P-T paths from pelitic schists and greenstones from the south-west Tauern Window, eastern Alps. *J Metamorph Geol* 3:439–465
- Sharma RS, MacRae ND (1981) Paragenetic relations in gedrite-cordierite-staurolite-biotite-sillimanite-kyanite gneisses at Ajitpura, Rajasthan, India. *Contrib Mineralog Petrol* 78:48–60

- Shaw DM (1956) Geochemistry of pelitic rocks. Part III: major elements and general geochemistry. *Geol Soc Am Bull* 67:919–934
- Spear FS (1999) Real-time AFM diagrams on your Macintosh. *Geol Mater Res* 1:1–18
- Spear FS, Cheney JT (1989) A petrogenetic grid for pelitic schists in the system  $\text{SiO}_2\text{-Al}_2\text{O}_3\text{-FeO-MgO-K}_2\text{O-H}_2\text{O}$ . *Contrib Mineralog Petrol* 101:149–164
- Spear FS, Kohn MJ, Cheney JT (1999) P-T paths from anatectic pelites. *Contrib Mineralog Petrol* 134:17–32
- Spear FS, Kohn MJ, Florence FP, Menard T (1990) A model for garnet and plagioclase growth in pelitic schists: implications for thermobarometry and P-T path determination. *J Metamorph Geol* 8:683–696
- Spear FS, Kohn MJ, Paetzold S (1995) Petrology of the regional sillimanite zone west-central New Hampshire, U.S.A., with implications for the development of inverted isograds. *Am Mineralog* 80:361–376
- Symmes GH, Ferry JM (1992) The effect of whole-rock MnO content on the stability of garnet in pelitic schists during metamorphism. *J Metamorph Geol* 10:221–238
- Symmes GH, Ferry JM (1995) Metamorphism, fluid flow and partial melting in pelitic rocks from the Onawa contact aureole, Central Maine, USA. *J Petrol* 36:587–612
- Theye T, Seidel E, Vidal O (1992) Carpholite, sudoite, and chloritoid in low-grade high-pressure metapelites from Crete and the Peloponnese, Greece. *Eur J Mineralog* 4:487–507
- Theye T, Chopin C, Grevel KD, Ockenga E (1997) The assemblage diaspore + quartz in metamorphic rocks: a petrological, experimental and thermodynamic study. *J Metamorph Geol* 15:17–28
- Thompson AB (1976) Mineral reactions in pelitic rocks: II. Calculation of some P-T- $X_{(\text{Fe-Mg})}$  phase relations. *Am J Sci* 276:425–454
- Tilley CE (1925) A preliminary survey of metamorphic zones in the southern Highlands of Scotland. *Q J Geol Soc Lond* 81:100–112
- Tinkham DK, Zuluaga CA, Stowell HH (2001) Metapelite phase equilibria modeling in MnNCKFMASH: the effect of variable  $\text{Al}_2\text{O}_3$  and  $\text{MgO}/(\text{MgO} + \text{FeO})$  on mineral stability. *Geol Mater Res* 3:1–42
- Tomkins HS, Pattison DRM (2007) Accessory phase petrogenesis in relation to major phase assemblages in pelites from the Nelson contact aureole, southern British Columbia. *J Metamorph Geol* 25:401–421
- Torre Dalla M, Livi KJT, Veblen DR, Frey M (1996) White K-mica evolution from phengite to muscovite in shales and shale matrix melange, Diablo Range, California. *Contrib Mineralog Petrol* 123:390–405
- Touret J, Dietvorst P (1983) Fluid inclusions in high-grade anatectic metamorphites. *J Geol Soc Lond* 140:635–649
- Tracy RJ, Robinson P (1983) Acadian migmatite types in pelitic rocks of Central Massachusetts. In: Atherton MP, Gribble CD (eds) *Migmatites, melting and metamorphism*. Shiva, Nantwich, pp 163–173
- Tracy RJ, Robinson P (1988) Silicate-sulfide-oxide-fluid reaction in granulite-grade pelitic rocks, Central Massachusetts. *Am J Sci* 288A:45–74
- Vidal O, Goffe B, Theye T (1992) Experimental study of the stability of sudoite and magnesio-carpholite and calculation of a new petrogenetic grid for the system  $\text{FeO-MgO-Al}_2\text{O}_3\text{-SiO}_2\text{-H}_2\text{O}$ . *J Metamorph Geol* 10:603–614
- Vidal O, Parra T, Trotet F (2001) A thermodynamic model for Fe-Mg aluminous chlorite using data from phase equilibrium experiments and natural pelitic assemblages in the 100° to 600°C, 1 to 15 kb range. *Am J Sci* 301:557–592
- Vinograd VL, Perchuk LL, Gerya TV, Putins A, Winkler B, Gale JD (2007) Order/disorder phase transition in cordierite and its possible relationship to the development of symplectite reaction textures in granulites. *Petrology* 5:459–473
- Waters DJ (1991) Hercynite-quartz granulites: phase relations and implications for crustal processes. *Eur J Miner* 3:367–386

- Waters DJ, Charnley NR (2002) Local equilibrium in polymetamorphic gneiss and the titanium substitution in biotite. *Am Mineralog* 87:383–396
- Waters DJ, Lovegrove HT (2002) Assessing the extent of disequilibrium and overstepping of prograde metamorphic reactions in metapelites from the Bushveld Complex aureole, South Africa. *J Metamorph Geol* 20:135–149
- Waters DJ (1988) Partial melting and the formation of granulite facies assemblages in Namaqualand, South Africa. *J Metamorph Geol* 6:387–404
- Weaver BL, Tarney J (1983) Elemental depletion in Archaean granulite facies rocks. In: Atherton MP, Gribble CD (eds) *Migmatites, melting and metamorphism*. Shiva, Nantwich, pp 250–263
- White RW, Powell R, Holland TJB, Worley BA (2000) The effect of  $\text{TiO}_2$  and  $\text{Fe}_2\text{O}_3$  on metapelitic assemblages at greenschist and amphibolite facies conditions: mineral equilibria calculations in the system  $\text{K}_2\text{O}\text{-FeO}\text{-MgO}\text{-Al}_2\text{O}_3\text{-SiO}_2\text{-H}_2\text{O}\text{-TiO}_2\text{-Fe}_2\text{O}_3$ . *J Metamorph Geol* 18:497–511
- Whitney DL (2002) Coexisting andalusite, kyanite and sillimanite: sequential formation of three polymorphs during progressive metamorphism near the  $\text{Al}_2\text{SiO}_5$  triple point, Sivrihisar, Turkey. *Am Mineralog* 84:405–416
- Whitney DL, Dilek Y (2000) Andalusite-sillimanite-quartz veins as indicators of low pressure-high temperature deformation during late-stage unroofing of a metamorphic core complex. *J Metamorph Geol* 18:59–66
- Whitney DL, Mechum TA, Kuehner SM, Dilek YR (1996) Progressive metamorphism of pelitic rocks from protolith to granulite facies, Dutchess County, New York, USA: constraints on the timing of fluid infiltration during regional metamorphism. *J Metamorph Geol* 14:163–181
- Xu G, Will TM, Powell R (1994) A calculated petrogenetic grid for the system  $\text{K}_2\text{O}\text{-FeO}\text{-MgO}\text{-Al}_2\text{O}_3\text{-SiO}_2\text{-H}_2\text{O}$ , with particular reference to contact-metamorphosed pelites. *J Metamorph Geol* 12:99–119
- Yardley BWD (1977) The nature and significance of the mechanism of sillimanite growth in the Connemara Schists, Ireland. *Contrib Mineralog Petrol* 65:53–58
- Yardley BWD, Leake BE, Farrow CM (1980) The metamorphism of Fe-rich pelites from Connemara, Ireland. *J Petrol* 21:365–399
- Zuluaga CA, Stowell HH, Tinkham DK (2005) The effect of zoned garnet on metapelite pseudo-section topology and calculated metamorphic P-T paths. *Am Mineralog* 90:1619–1628



# Chapter 8

## Metamorphism of Marls

### 8.1 General

Marls are carbonate-bearing pelitic sediments covering a wide range of composition between “impure” carbonate rocks and “true” pelites. In the Anglo-American literature, this group of sedimentary rocks is better known as argillaceous carbonate rocks, calcareous sediments, calcic pelitic rocks, or calcareous pelites. The sediments are widespread and typical of shelf and platform areas. An average composition of a platform marl (shale) is given in Table 2.2.

Unmetamorphosed marls are mainly composed of mixtures of clay minerals (smectite [Sm], illite [Ill], kaolinite [Kln], chlorite [Chl], etc.), carbonates (mainly Cal and/or Dol), Qtz, and feldspars in varying proportions. In metamorphosed marls (metamarls), most minerals occurring in metapelites and metacarbonates may be present, plus additional Ca–Al-bearing silicates such as Ca-pyroxenes (Cpx), Ca-amphiboles (Cam), epidote-group minerals (Zo, Czo, Ep), lawsonite (Lws), margarite (Mrg), scapolite (Scp), vesuvianite (Ves) and others. The many possible mineral constituents result from the complex chemical composition of calcareous pelites in the system:  $K_2O$ – $Na_2O$ – $CaO$ – $FeO$ – $MgO$ – $Al_2O_3$ – $SiO_2$ – $H_2O$ – $CO_2$ . This system has a pelite component (KFMASH + N) and a limestone component ( $CaCO_3$ ). Therefore calcareous micaschists are the prime example of metamarl. We expect that at low grade the pelite component contributes Qtz, micas (Ms and Pg) and chlorite to the rock (see Chap. 7), whereas the limestone component is simply present as calcite (dolomite, ankerite). With increasing grade we also suspect that the sheet silicates of the pelite component will react with calcite to form the wide variety of Ca-silicates introduced above. The resulting rocks are high-grade calc-silicate marbles or calc-silicate gneisses. Examples of an amphibolite facies metamarl and contact metamorphic calc-silicate marble are shown on Fig. 8.1.

Metamarls are chemically the most complex type of rocks. A full quantitative model of marl metamorphism must be developed for the specific composition of an investigated rock. Some generalities of marl metamorphism, however, can be derived from models of chemical subsystems. In this chapter, three subsystems of the full and very complex 9-component marl system will be discussed, one dealing



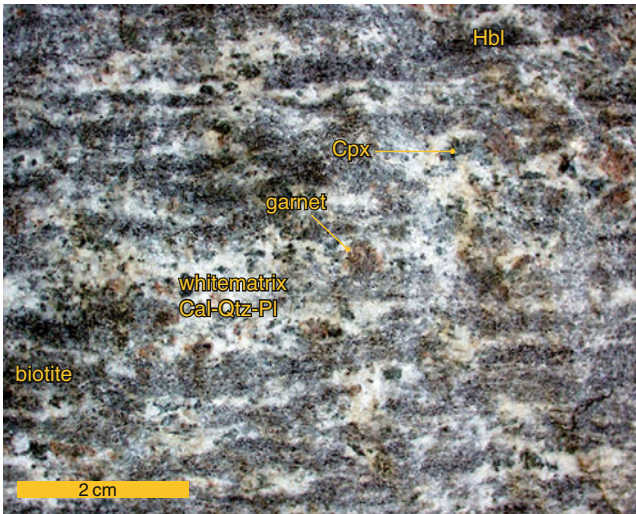
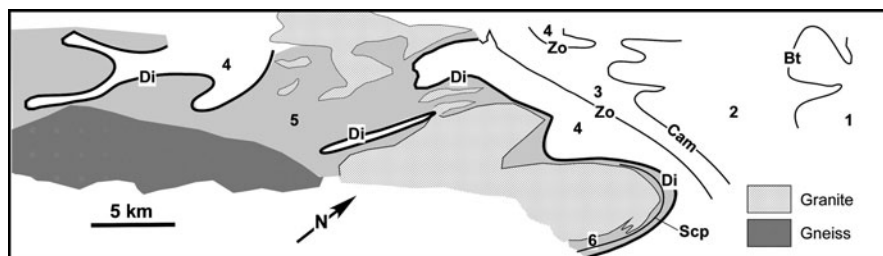


**Fig. 8.1** Calc-silicate gneiss from Castione, Central Alps. This middle amphibolite facies metamarl formed from Mesozoic calcareous shales. It was a calcareous micaschist at lower grade during prograde Alpine collision phase metamorphism. The rock contains Qtz + Pl + Cal + Bt + Kfs + Cpx + Cam + Grt

with Al-poor and two to describe Al-rich metamarls. In all three subsystems, Qtz and Cal will be considered to be present in excess, which is true for most low- and medium-T metamarls (although Qtz and/or Cal may be used up in reactions at high-T). Therefore, SiO<sub>2</sub> will be treated as an excess component. In addition, a H<sub>2</sub>O–CO<sub>2</sub>-bearing fluid phase is assumed to have been present during metamorphism. Chemographic relationships of any particular metamarl system can then be projected from SiO<sub>2</sub>, H<sub>2</sub>O and CO<sub>2</sub>.

## 8.2 Orogenic Metamorphism of Al-Poor Marls

Al-poor marls are common in many orogenic belts. In the northern Appalachians, as an example, the prograde metamorphism of such rocks has been studied in great detail (e.g., Hewitt 1973; Ferry 1976, 1983a, b, 1992; Zen 1981). In the Vassalboro Formation in Maine, USA, Ferry mapped six mineral zones, each characterized by an index mineral and separated by reaction-isograds (Fig. 8.2). With increasing metamorphic grade, the following index minerals are encountered: Ank, Bt, Cam, Zo, Di, Scp. A summary of mineral assemblages and related reactions is given by Yardley (1989, pp. 143–145), and here we refer to five of these reactions and present a simplified model for progressive metamorphism of Al-poor marls.



Zone	Mineral assemblage	Zone	Mineral assemblage
1	Ank + Qtz + Ab + Ms ± Chl ± Cal	4	Zo + Cal + Cam + Qtz + Pl + Cal ± Bt ± Kfs
2	Bt + Ank + Qtz + Ab + Ms + Cal + Chl	5	Di + Zo + Cam + Cal + Qtz + Pl ± Bt ± Kfs
3	Bt + Qtz + Pl + Cal ± Ms ± Chl	6	Scp + Di + Zo + Cam + Qtz + Pl + Cal
	Cam + Qtz + Pl + Cal + Bt ± Chl		

**Fig. 8.2** Map showing distribution of mineral zones (numbered 1 to 6) and isograds (labelled) in metamarls of the Vassalboro Formation, south-central Maine (simplified after Fig. 1. of Ferry 1983c). Diagnostic zone mineral assemblages are listed below. Note that Pl compositions are: oligoclase-labradorite (upper Bt zone); andesine-anorthite (Cam, Zo, Di zones)

### 8.2.1 Phase Relationships in the KCMAS-HC System

For the system  $K_2O-CaO-MgO-Al_2O_3-SiO_2-H_2O-CO_2$ , phase relationships are considered among An, Cal, Mg-Chl (clinocllore), Di, Dol, Kfs, Ms, Phl, Qtz, Tr and Zo. The chemography of these phases is shown as the inset in Fig. 8.3 projected from  $SiO_2 + CaO + H_2O + CO_2$ . Reaction equilibria in the KCMAS-HC system with excess Qtz, Cal and  $H_2O-CO_2$  are listed in Table 8.1 and depicted in Fig. 8.3 in an isobaric  $T-X_{CO_2}$ -section. The pressure of 350 MPa has been chosen in accordance with Ferry (1983a, b), derived from associated metapelites near the Sil-isograd. The range of  $X_{CO_2} < 0.2$  has been chosen according to Ferry (1983b, Table 2).

The petrogenetic grid shown in Fig. 8.3 is considered in some detail. First, we characterize certain reactions followed by an analysis of the stability fields of selected phases. Mixed-volatile reactions with steep (at  $X_{CO_2} < 0.05$ ) to gentle (at  $X_{CO_2} > 0.1$ ) positive slopes are predominant. Reactions (8.6) and (8.10) have been discussed in Chap. 6 in relation to the metamorphism of dolomite and limestone. Reactions (8.11) and (8.14) with gentle negative slopes are dehydration reactions, and reaction (8.11) has been referred to in Chap. 7 dealing with the metamorphism of pelites. Reaction (8.4), with a steep negative slope and crossing the whole diagram of Fig. 8.3, is a special case of a mixed-volatile reaction of the type  $a + CO_2 = b + H_2O$  (cf. Fig. 3.19). This reaction divides Fig. 8.3 into Zo- and An(Pl)-bearing assemblages. Because Di, Dol and Tr coincide in the chemographic projection with excess Qtz, Cal and fluid (see inset of Fig. 8.3), the  $T-X$  stability fields of these three phases do not overlap. Diopside is stable above reaction (8.6), Tr is stable between reactions (8.6) and (8.10), and Dol is stable below reaction (8.10). K-feldspar is stable over the  $T-X$  range of Fig. 8.3 because of its single corner position in the chemography. For Mg-Chl, reaction (8.7) defines its lower and reactions (8.3) and (8.13) its upper stability limits. Phlogopite is stable

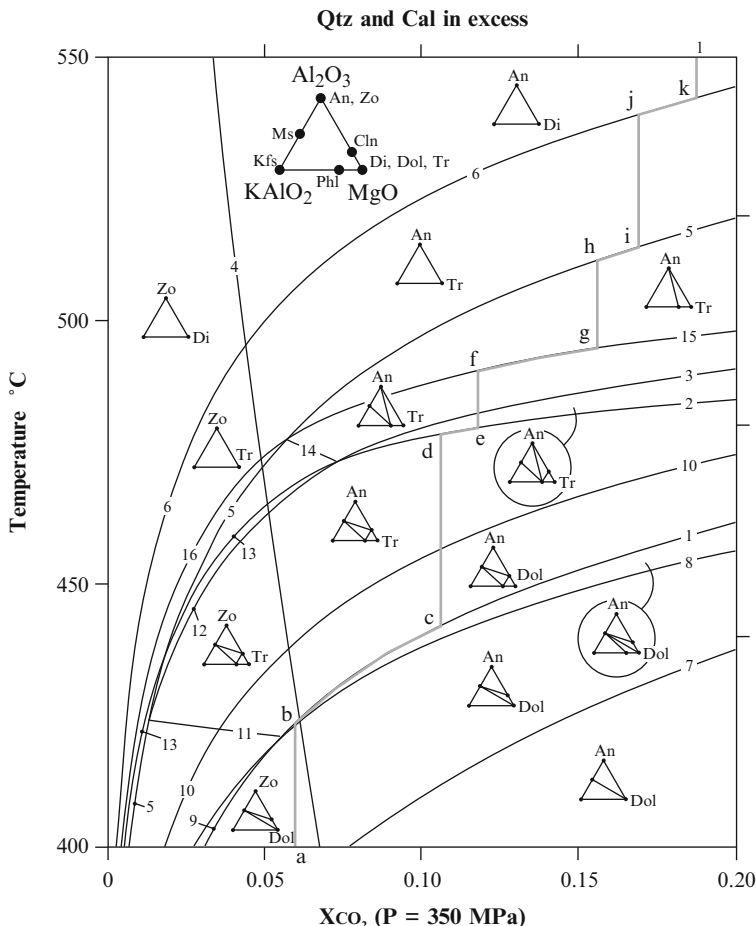


**Fig. 8.3** T–X section of the KCMAS-HC system with excess Qtz and Cal at  $0 < X_{CO_2} < 0.2$  and a constant pressure of 350 MPa. Pure end member mineral compositions are used. The inset shows the chemography projected from Qtz, Cal, H<sub>2</sub>O and CO<sub>2</sub> onto the KAIO<sub>2</sub>–MgO–Al<sub>2</sub>O<sub>3</sub> plane. Compatibility diagrams are shown for some selected divariant fields only. Reactions are numbered as in Table 8.1. The prograde path “a–l” is emphasized and discussed in Sect. 8.2.2

between reactions (8.8) and (8.5). Finally, for Ms, reactions (8.15) and (8.16) limit its T–X stability field towards high-T and very low  $X_{CO_2}$ .

The sequence of index minerals observed in the Vassalboro Formation, i.e., Ank, Bt, Cam, Zo, Di (Fig. 8.2) is approximated in the KCMAS-HC system by Dol, Phl, Tr, Zo, Di as shown in Fig. 8.3. The sequence is consistent in terms of T– $X_{CO_2}$  values with first an increase in T and then, after leaving the Tr zone in prograde metamorphism, a decrease in  $X_{CO_2}$  in order to reach the Zo zone. The decrease in  $X_{CO_2}$  may have been caused by an infiltration of externally derived H<sub>2</sub>O (see Ferry 1976, 1983a, b). Furthermore, the relative positions of reactions (8.1)–(8.6) in T–X space of Fig. 8.3 closely match the sequence of reaction-isograds shown in Fig. 8.2. The main difference between the isograd-reactions as formulated by Ferry (1976) and reactions

**Table 8.1** Reactions in the KCMAS-HC system

Anorthite	$\text{CaAl}_2\text{Si}_2\text{O}_8$
Calcite	$\text{CaCO}_3$
Clinocllore	$\text{Mg}_5\text{Al}_2\text{Si}_3\text{O}_{10}(\text{OH})_8$
Diopside	$\text{CaMgSi}_2\text{O}_6$
Dolomite	$\text{CaMg}(\text{CO}_3)_2$
K-feldspar	$\text{KAlSi}_3\text{O}_8$
Muscovite	$\text{KAl}_3\text{Si}_3\text{O}_{10}(\text{OH})_2$
Phlogopite	$\text{KMg}_3\text{AlSi}_3\text{O}_{10}(\text{OH})_2$
Quartz	$\text{SiO}_2$
Tremolite	$\text{Ca}_2\text{Mg}_5\text{Si}_8\text{O}_{22}(\text{OH})_2$
Zoisite	$\text{Ca}_2\text{Al}_3\text{Si}_3\text{O}_{12}(\text{OH})$
All reactions with excess quartz, calcite, and fluid:	
$\text{Ms} + 8\text{Dol} + 3\text{Qtz} + 4\text{H}_2\text{O} = \text{Phl} + \text{Cln} + 8\text{Cal} + 8\text{CO}_2$	(8.1)
$5\text{Ms} + 3\text{Cln} + 7\text{Qtz} + 8\text{Cal} = 5\text{Phl} + 8\text{An} + 12\text{H}_2\text{O} + 8\text{CO}_2$	(8.2)
$\text{Cln} + 7\text{Qtz} + 3\text{Cal} = \text{Tr} + \text{An} + 3\text{H}_2\text{O} + 3\text{CO}_2$	(8.3)
$2\text{Zo} + \text{CO}_2 = 3\text{An} + \text{Cal} + \text{H}_2\text{O}$	(8.4)
$5\text{Phl} + 24\text{Qtz} + 6\text{Cal} = 5\text{Kfs} + 3\text{Tr} + 2\text{H}_2\text{O} + 6\text{CO}_2$	(8.5)
$\text{Tr} + 2\text{Qtz} + 3\text{Cal} = 5\text{Di} + \text{H}_2\text{O} + 3\text{CO}_2$	(8.6)
$\text{Cln} + 6\text{Cal} + 4\text{CO}_2 = 5\text{Dol} + \text{An} + \text{Qtz} + 4\text{H}_2\text{O}$	(8.7)
$\text{Phl} + 3\text{Cal} + 3\text{CO}_2 = \text{Kfs} + 3\text{Dol} + \text{H}_2\text{O}$	(8.8)
$\text{Ms} + 5\text{Dol} + 3\text{Qtz} + 3\text{H}_2\text{O} = \text{Kfs} + \text{Cln} + 5\text{Cal} + 5\text{CO}_2$	(8.9)
$5\text{Dol} + 8\text{Qtz} + \text{H}_2\text{O} = \text{Tr} + 3\text{Cal} + 7\text{CO}_2$	(8.10)
$8\text{Kfs} + 3\text{Cln} = 3\text{Ms} + 5\text{Phl} + 9\text{Qtz} + 4\text{H}_2\text{O}$	(8.11)
$5\text{Phl} + 5\text{Cln} + 49\text{Qtz} + 16\text{Cal} = 5\text{Ms} + 8\text{Tr} + 12\text{H}_2\text{O} + 16\text{CO}_2$	(8.12)
$3\text{Cln} + 21\text{Qtz} + 10\text{Cal} = 3\text{Tr} + 2\text{Zo} + 8\text{H}_2\text{O} + 10\text{CO}_2$	(8.13)
$5\text{Ms} + 3\text{Tr} + \text{CO}_2 = 5\text{Phl} + 5\text{An} + 14\text{Qtz} + \text{Cal} + 3\text{H}_2\text{O}$	(8.14)
$\text{Ms} + 2\text{Qtz} + \text{Cal} = \text{Kfs} + \text{An} + \text{H}_2\text{O} + \text{CO}_2$	(8.15)
$3\text{Ms} + 6\text{Qtz} + 4\text{Cal} = 3\text{Kfs} + 2\text{Zo} + 2\text{H}_2\text{O} + 4\text{CO}_2$	(8.16)

(8.1)–(8.6) in Table 8.1 concerns Pl. Albite and oligoclase–anorthite compositions (designated in Fig. 8.2) are reactants in reactions (8.2) and (8.3), but the Ab-component in Pl is not considered in the KCMAS-HC system dealt with here. Note also that the highest-grade isograd, Scp-in, shown in Fig. 8.2 indicating the reaction  $\text{Pl} + \text{Cal} = \text{Scp}$  (in this case with  $\text{Ca}/(\text{Ca} + \text{Na}) = 0.75$  in Scp), cannot be modeled in the above system because of the Na-component in Pl and Scp.

In summary, progressive metamorphism of Al-poor marls such as those in the Vassalboro Formation, Maine, can be modeled in the system KCMAS-HC, at least in a qualitative way. A quantitative treatment would require two additional components, FeO and  $\text{Na}_2\text{O}$ .

### 8.2.2 Prograde Metamorphism in the KCMAS-HC System at Low $X_{\text{CO}_2}$

In this section, prograde metamorphism of rocks consisting originally of  $\text{Ms} + \text{Dol}$  with excess  $\text{Qtz} + \text{Cal}$  and an initial fluid composition of  $X_{\text{CO}_2} = 0.06$  will be considered. The prograde path in  $T$ – $X_{\text{CO}_2}$  space at 350 MPa is shown in Fig. 8.3 by

a curve extending from a to l and the changing mineral modal composition is displayed in Fig. 8.4. The prograde path can be divided into several sections as follows.

a–b. The starting mineral assemblage Dol + Ms + Qtz + Cal is heated at a constant  $X_{CO_2}$  of 0.06.

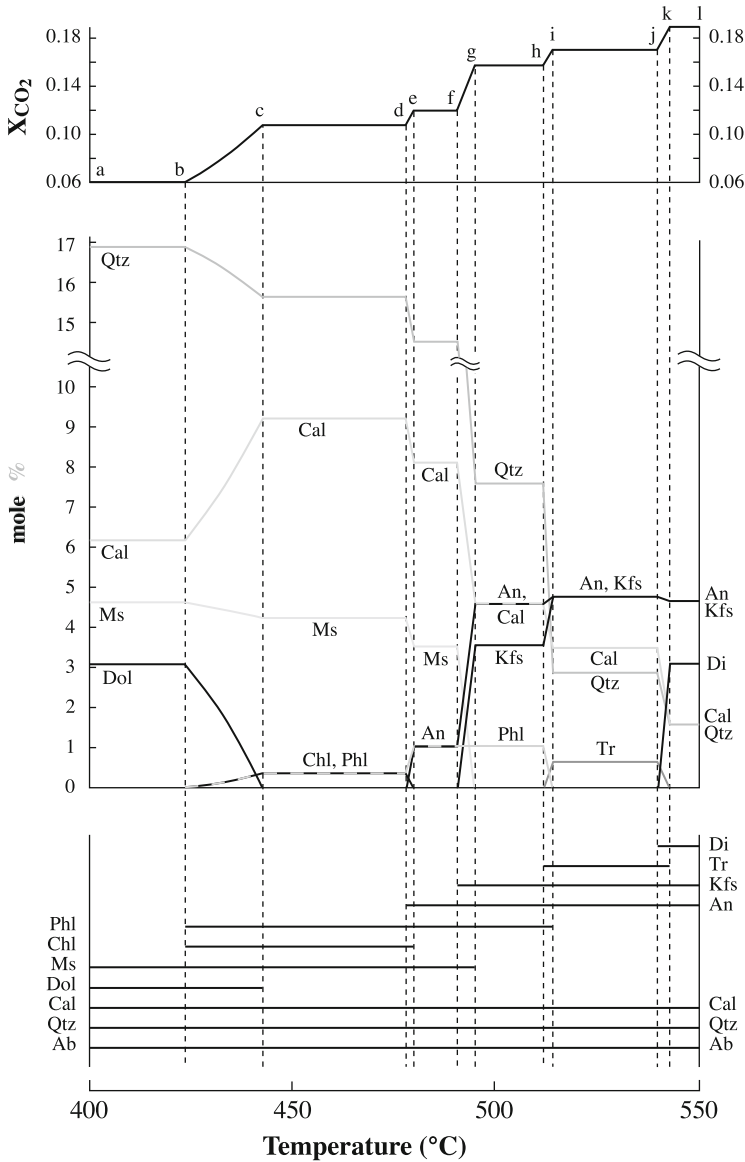


**Fig. 8.4** Modal composition (mol%), fluid composition ( $X_{CO_2}$ ) and mineral distribution along the prograde path “a–l” shown in Fig. 8.3

- b–c. Equal amounts (on a mole basis) of Mg–Chl (clinochlore) and Phl are formed according to reaction (8.1) between 424 and 443°C while  $X_{\text{CO}_2}$  increases to 0.107.
- c–d. At point **c**, all Dol is used up. The rock is now composed of Phl + Ms + Chl + Qtz + Cal and is heated up at a constant  $X_{\text{CO}_2}$  of 0.107.
- d–e. The first An and additional Phl are formed according to reaction (8.2) between 478°C and 480°C while  $X_{\text{CO}_2}$  increases to 0.119.
- e–f. At point **e**, all Chl is used up. The rock is now composed of Phl + Ms + An + Qtz + Cal and heating continues at a constant  $X_{\text{CO}_2}$  of 0.119.
- f–g. The first Kfs and additional An are formed according to reaction (8.15) between 491°C and 495°C while  $X_{\text{CO}_2}$  increases to 0.156.
- g–h. At point **g**, all Ms is used up. The rock is now composed of Phl + An + Kfs + Qtz + Cal and is heated at a constant  $X_{\text{CO}_2}$  of 0.156.
- h–i. The first Tr and additional Kfs are formed according to reaction (8.5) between 512°C and 514°C while  $X_{\text{CO}_2}$  increases to 0.167.
- i–j. At point **i**, all Phl is used up. The rock is now composed of Tr + An + Kfs + Qtz + Cal and heating continues at a constant  $X_{\text{CO}_2}$  of 0.167.
- j–k. The first Di is formed according to reaction (8.6) between 540°C and 543°C while  $X_{\text{CO}_2}$  increases to 0.188.
- k–l. At point **k**, all Tr is used up. The rock is now composed of Di + An + Kfs + Qtz + Cal and is further heated at a constant  $X_{\text{CO}_2}$  of 0.188.

The model metamorphism of the assemblage Ms + Dol with excess Qtz + Cal in the system KCMAS-HC described above shows several interesting features. Firstly,  $X_{\text{CO}_2}$  increases by steps from 0.06 to 0.188 because all acting reactions have a positive slope in  $T$ – $X_{\text{CO}_2}$  space. Secondly, most reactions [(8.2), (8.5), (8.6), (8.15)] take place within a very narrow temperature range of a few degree centigrade because of the gentle slope of reaction curves at  $X_{\text{CO}_2} > 0.1$  and because a relatively large amount of fluid was assumed. In a metamorphic terrain, this leads to the formation of sharp and mapable reaction-isograds. Thirdly, with increasing metamorphic grade sheet silicates (Chl, Ms, and Phl in this example) are replaced by feldspars and chain silicates (Tr and Di).

### 8.3 Orogenic Metamorphism of Al-Rich Marls

Al-rich marls are present in many orogenic belts. In the European Alps for example, such rocks are widespread, both in platform sediments of the Helvetic zone and in deep-sea metasediments of the Penninic zone. Their metamorphism has been studied in some detail (e.g., Frey 1978; Bucher et al. 1983; Frank 1983), and an example of progressive metamorphism of calcareous mica schist, western Lepontine Alps, is shown in Fig. 8.5, where mineral-in (Bt, Grt, Cam, Scp) and mineral-out (Pg, Mrg, Ms) isograds have been mapped. The metamorphism spans greenschist to amphibolite facies grade and is estimated to have occurred between ~400–420°C/200–300 MPa and 580–620°C/600–800 MPa.



### 8.3.1 Phase Relationships in the CAS-HC System

The system  $\text{CaO-Al}_2\text{O}_3\text{-SiO}_2\text{-H}_2\text{O-CO}_2$  permits description of phase relationships among An, Cal, Czo, Grs, Ky, Mrg, Prl, Qtz, and Wo as shown in the inset chemography in Fig. 8.6 projected from  $\text{H}_2\text{O} + \text{CO}_2$ . Note the presence of several colinearities among three phases in this system, e.g., Ky–Prl–Qtz, Ky–Mrg–Cal, An–Czo–Cal. Reaction equilibria in the CAS-HC system with excess Qtz, Cal and  $\text{H}_2\text{O-CO}_2$  are listed in Table 8.2 and depicted in Fig. 8.6 as a polybaric T– $X_{\text{CO}_2}$  section along a regional Ky-geotherm. According to the phase rule (cf. Sect. 3.8.1), each divariant assemblage consists of one single phase in addition to Qtz + Cal + fluid.

In the CAS-HC system, the assemblage Prl–Qtz–Cal represents the characteristic assemblage in Al-rich marls at the onset of metamorphism. The fluid composition will be  $\text{H}_2\text{O}$ -rich because carbonates have not yet liberated  $\text{CO}_2$  by reacting with sheet silicates, and interstitial water is therefore not yet diluted by reaction generated  $\text{CO}_2$ .

Margarite will form during prograde metamorphism according to reaction (8.18) at temperatures below  $390^\circ\text{C}$  and this temperature will be lower than  $350^\circ\text{C}$

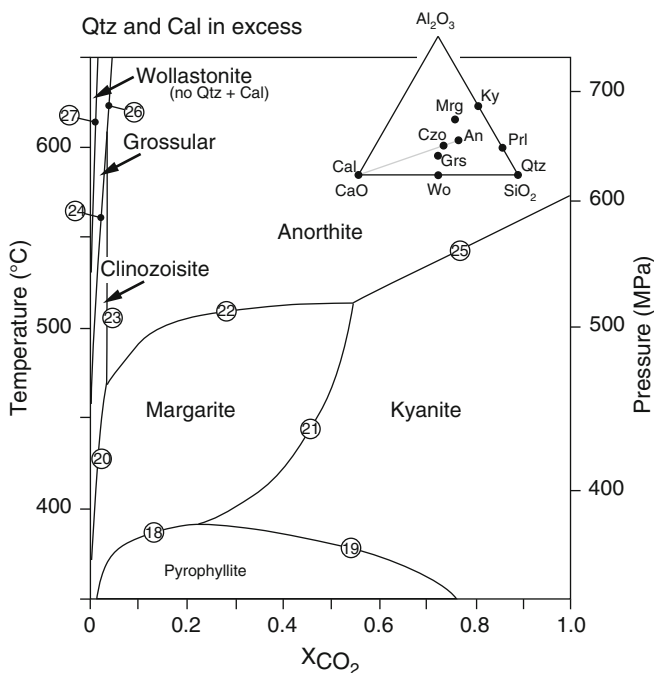


**Fig. 8.6** P–T–X diagram of the CAS-HC system with excess Qtz and Cal. The vertical axis represents an orogenic geotherm characteristic for Ky-type terrains. The inset shows the chemography projected from  $\text{H}_2\text{O}$  and  $\text{CO}_2$  onto the  $\text{CaO-Al}_2\text{O}_3\text{-SiO}_2$  plane. Two colinearities corresponding to reactions (8.21) and (8.23) are indicated. Reactions are numbered as in Table 8.2



**Table 8.2** Reactions in the CAS-HC system

Anorthite	$\text{CaAl}_2\text{Si}_2\text{O}_8$
Calcite	$\text{CaCO}_3$
Clinzoisite	$\text{Ca}_2\text{Al}_3\text{Si}_3\text{O}_{12}(\text{OH})$
Grossular	$\text{Ca}_3\text{Al}_2\text{Si}_3\text{O}_{12}$
Kyanite	$\text{Al}_2\text{SiO}_5$
Margarite	$\text{CaAl}_4\text{Si}_2\text{O}_{10}(\text{OH})_2$
Pyrophyllite	$\text{Al}_2\text{Si}_4\text{O}_{10}(\text{OH})_2$
Quartz	$\text{SiO}_2$
Wollastonite	$\text{CaSiO}_3$
All reactions with excess quartz, calcite, and fluid:	
$2\text{Pr}_l + \text{Cal} = \text{Mrg} + 6\text{Qtz} + \text{H}_2\text{O} + \text{CO}_2$	(8.1)
$\text{Pr}_l = \text{Ky} + 3\text{Qtz} + \text{H}_2\text{O}$	(8.2)
$3\text{Mrg} + 5\text{Cal} + 6\text{Qtz} = 4\text{Czo} + \text{H}_2\text{O} + 5\text{CO}_2$	(8.3)
$\text{Mrg} + \text{CO}_2 = 2\text{Ky} + \text{Cal} + \text{H}_2\text{O}$	(8.4)
$\text{Mrg} + 2\text{Qtz} + \text{Cal} = 2\text{An} + \text{H}_2\text{O} + \text{CO}_2$	(8.5)
$2\text{Czo} + \text{CO}_2 = 3\text{An} + \text{Cal} + \text{H}_2\text{O}$	(8.6)
$2\text{Czo} + 3\text{Qtz} + 5\text{Cal} = 3\text{Gr}_s + \text{H}_2\text{O} + 5\text{CO}_2$	(8.7)
$\text{Ky} + \text{Qtz} + \text{Cal} = \text{An} + \text{CO}_2$	(8.8)
$\text{An} + \text{Qtz} + 2\text{Cal} = \text{Gr}_s + 2\text{CO}_2$	(8.9)
$\text{Qtz} + \text{Cal} = \text{Wo} + \text{CO}_2$	(8.10)

for very  $\text{H}_2\text{O}$ -rich fluid compositions ( $X_{\text{CO}_2} < 0.02$ ). However, as a consequence of the steep equilibrium position of reaction (8.1) at  $X_{\text{CO}_2} < 0.05$  (Fig. 8.6), a noticeable amount of Mrg will only be produced between 375°C and 390°C. Therefore, the first occurrence of Mrg should represent a mapable reaction-isograd at low grade greenschist facies conditions. Assuming low modal Prl and closed system behavior, reaction (8.18) will consume all Prl before reaching the invariant point involving Prl + Mrg + Ky (+ Qtz + Cal). The metamarl will now enter the divariant Mrg field, the assemblage Mrg + Qtz + Cal being characteristic of the greenschist facies. It should be pointed out that at such low metamorphic grade, Mrg will be very fine-grained and may be easily missed during thin section observation, and X-ray diffraction work is needed to identify it (e.g., see Frey 1978, p. 110).

Next, the rock will undergo reaction (8.22) between 470°C and 510°C depending on fluid composition, producing the An-component in plagioclase. However, as discussed in Sect. 8.3.2, in Mrg-bearing rocks Pl will have already formed at considerably lower temperatures if Na is present as an additional component.

Clinzoisite is formed by reaction (8.20), but the steep slope of this reaction in P–T–X space and the corresponding small change in  $X_{\text{CO}_2}$  allows only a very small amount of Czo to form. At the invariant point involving Czo + Mrg + An (+ Qtz + Cal), the An-component in Pl is produced at the expense of all other solid phases present. Depending on whether Czo or Mrg is used up first, reaction (8.22) or (8.23) would occur respectively. Because of the small amount of Czo formed by reaction (8.20), it is conceivable that this phase will be used up first. Following reaction (8.22), more calcic plagioclase is produced. Another and more effective way of

producing Czo is by interaction of a metamarl with an externally derived H<sub>2</sub>O-rich fluid to initiate reactions (8.20) or (8.23).

Grossular and Wo do not form in orogenic metamorphic rocks under closed system conditions. According to Fig. 8.6, these minerals may be generated by reactions (8.24) or (8.26) in case of Grs and by reaction (8.27) in case of Wo by interaction with a H<sub>2</sub>O-rich fluid. Metamarls with Grt + Wo + Cpx + Pl + Cal are typical of low-P contact metamorphism (Fig. 8.1). If they occur in regional metamorphic settings, the assemblage formed by infiltration of an external H<sub>2</sub>O-rich fluid. Thus, in orogenic metamorphic terrains, relatively Al-rich but Qtz- and Cal-bearing metamarls (Fig. 8.4) will be characterized by two index minerals with prograde metamorphism: Prl under sub-greenschist and Mrg under greenschist facies conditions.

### 8.3.2 Phase Relationships in the KNCAS-HC System

Calcareous micaschists typically contain Ms and Pg in addition to Mrg. The micas will decompose with increasing grade to feldspar, Kfs and Ab. The chemography

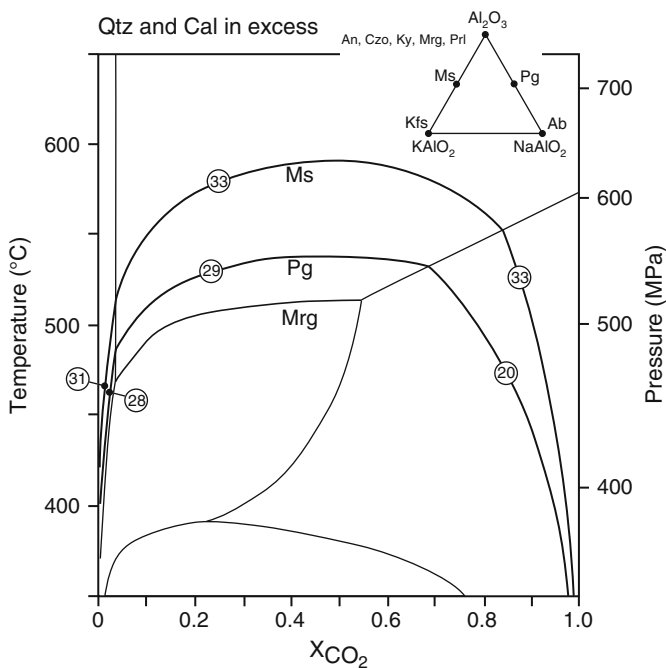


**Fig. 8.7** P-T-X section of the KNCAS-HC system with excess Qtz and Cal. Pure end member mineral compositions are used. The vertical axis represents a prograde metamorphic path typical of Ky-type terrains. Note the maximum thermal stabilities for Mrg, Pg and Ms. The inset shows the chemography projected from Qtz, Cal, H<sub>2</sub>O and CO<sub>2</sub> onto the KAlO<sub>2</sub>-NaAlO<sub>2</sub>-Al<sub>2</sub>O<sub>3</sub> plane. Reactions are numbered as in Table 8.3

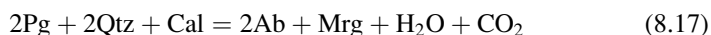
**Table 8.3** Reactions in the KNCAS-HC system (in addition to reactions of Table 8.2)

Muscovite	$\text{KAl}_3\text{Si}_3\text{O}_{10}(\text{OH})_2$
Paragonite	$\text{NaAl}_3\text{Si}_3\text{O}_{10}(\text{OH})_2$
K-feldspar	$\text{KAlSi}_3\text{O}_8$
Albite	$\text{NaAlSi}_3\text{O}_8$
All reactions with excess quartz, calcite, and fluid:	
$3\text{Pg} + 6\text{Qtz} + 4\text{Cal} = 3\text{Ab} + 2\text{Czo} + 2\text{H}_2\text{O} + 4\text{CO}_2$	(8.11)
$\text{Pg} + 2\text{Qtz} + \text{Cal} = \text{Ab} + \text{An} + \text{H}_2\text{O} + \text{CO}_2$	(8.12)
$\text{Pg} + \text{Qtz} = \text{Ab} + \text{Ky} + \text{H}_2\text{O}$	(8.13)
$3\text{Ms} + 6\text{Qtz} + 4\text{Cal} = 3\text{Kfs} + 2\text{Czo} + 2\text{H}_2\text{O} + 4\text{CO}_2$	(8.14)
$\text{Ms} + 2\text{Qtz} + \text{Cal} = \text{Kfs} + \text{An} + \text{H}_2\text{O} + \text{CO}_2$	(8.15)
$\text{Ms} + \text{Qz} = \text{Kfs} + \text{Ky} + \text{H}_2\text{O}$	(8.16)

for the system KNCAS-HC is shown as an inset in Fig. 8.7. Grossular and Wo have been omitted for simplicity, and all remaining phases considered in the CAS-HC system plot at the  $\text{Al}_2\text{O}_3$  apex (projection from excess Qtz + Cal +  $\text{H}_2\text{O}$  +  $\text{CO}_2$ ). The six additional equilibria are listed in Table 8.3 and depicted in Fig. 8.7. Maximum T for pure end-member white mica in the presence of excess Qtz and Cal: 515°C for Mrg, 540°C for Pg, and 590°C for Ms. These temperatures are valid only for Ky-type *P-T* paths. Note that reaction equilibria (8.22), (8.29), and (8.32) are all mixed volatile reactions with identical coefficients for all the phases involved, except for feldspars: 2 mol An are produced from Mrg + 2Qtz + Cal, 1 mol each of Ab and An from Pg + 2Qtz + Cal, and 1 mol each of Kfs and An from Ms + 2Qtz + Cal.

The petrogenetic grid of Fig. 8.7 is not directly applicable to natural rocks because of solid solution in the white micas and feldspars, but for simplicity, only the effect of Pl solid solution is quantified below. Anorthite-involving reactions in Fig. 8.8 are contoured for different An-content in Pl. The stability field of Pl + Mrg + Qtz + Cal is indicated with its low-T boundary fixed by reaction (8.22) contoured for  $\text{An}_{30}$  based on the field observations of Frey and Orville (1974). The effect of Mrg-Pg solid-solution shifts the Pl + Mrg + Qtz + Cal stability field to higher T, but also enlarges it (because of increasing solubility of the Pg- component in Mrg with increasing T). Compared with Fig. 8.7, the stability field of Mrg + Qtz + Cal in Fig. 8.8 is considerably reduced, with an upper T of about 470°C.

In contrast to Mrg-bearing rocks, Ab does occur in Pg-bearing metamarls of the greenschist facies (e.g., Ferry 1992). According to Fig. 8.8, the equilibrium curve of reaction (8.29) for  $\text{An}_{30}$  is stable up to about 490°C, i.e., about 40°C lower than the maximum T stability of Pl + Pg + Qtz + Cal. An interesting feature concerns the breakdown of the assemblage Pg + Qtz + Cal in the presence of intermediate Pl compositions of between about  $\text{An}_{50}$ – $\text{An}_{70}$ . The assemblage Pg + Qtz + Cal breaks down at a lower T than the assemblage Mrg + Qtz + Cal (compare with Fig. 8.7), and reaction (8.29) is then replaced by the reaction:



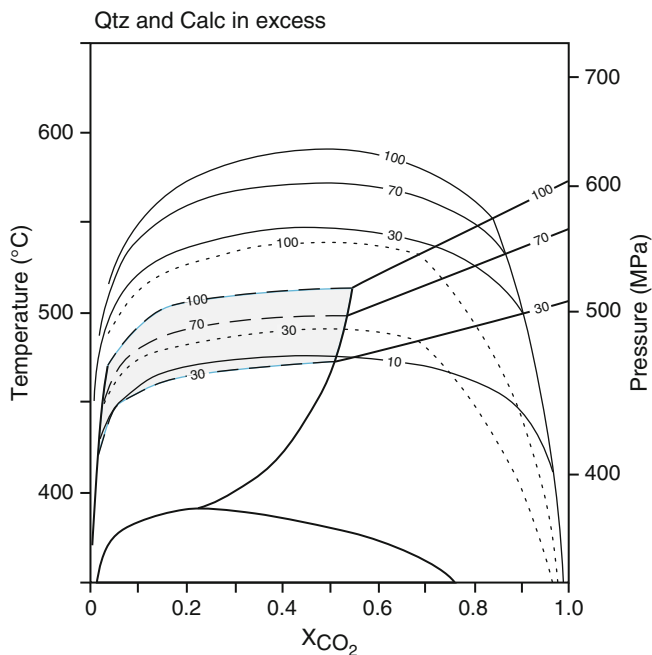


**Fig. 8.8** P–T–X section of the KNCAS–HC system with excess Qtz and Cal. The vertical axis represents a prograde metamorphic path characteristic of Ky-type terrains. Polybaric divariant equilibria for a particular Pl-composition ( $An_x$ ) are shown as full lines (Ms-involving reactions), stippled lines (Pg-involving reactions) or dashed lines (Mrg-involving reactions). Numbers refer to mole percent An-content in Pl. Most Czo-involving equilibria from Fig. 8.6 have been omitted for clarity. The stability field for the assemblage Mrg + Pl (+ Qtz + Cal) is emphasized by gray shading

For a given Pl composition, contours of reactions (8.22) and (8.17) are separated by only a few degrees. For example, for a composition of  $An_{70}$  and for fluid compositions of  $X_{CO_2} = 0.2–0.5$ , reaction (8.17) is located 5°C below reaction (8.22), but for graphical reasons this is not shown in Fig. 8.8. The formation of Kfs and Pl from Ms + Qtz + Cal for plagioclase compositions  $>An_{30}$  takes place at higher T than the breakdown of Pg + Qtz + Cal (Fig. 8.8).

### 8.3.2.1 Prograde Metamorphism at Low $X_{CO_2}$

Let us now consider a subgreenschist facies rock consisting of Ms + Pg + Prl + Qtz + Cal and an initial fluid composition of  $X_{CO_2} = 0.1$  and evaluate prograde regional metamorphism along a Ky-type geotherm. The beginning of metamorphism will be identical to that described for the CAS–HC system in Fig. 8.6, i.e., formation of Mrg according to reaction (8.18) (Table 8.2). The resulting mineral assemblage with Ms + Pg + Mrg + Qtz + Cal is characteristic for the lower

greenschist facies. Such assemblages with three coexisting white micas have been described by Frey (1978). Whether a small amount of sodic Pl is already formed from Pg + Qtz + Cal at this grade of metamorphism is not documented in the literature. Between 450°C and 470°C, the first Pl of composition An<sub>30</sub> is produced by reaction (8.22). Within the stability field of Mrg + Pl + Qtz + Cal (gray shaded area in Fig. 8.8), phase relationships are complex and besides *P-T-X* conditions, depend on the modal mineral composition of the rock considered, including the amount of fluid. Margarite and Pg will react, together with Qtz and Cal, to form Pl according to reactions (8.22) and (8.29), respectively. On the other hand, reaction (8.17) will produce additional Mrg. Concomitantly, the fluid composition, X<sub>CO<sub>2</sub></sub>, will slightly increase. If during prograde metamorphism the upper limit of the gray shaded area in Fig. 8.8 is reached, the net result will be the consumption of all Mrg. For most marl compositions, all Pg will also be used up at this stage. However, for rocks rich in Al and Na, remaining Pg + Qtz + Cal will react to An-rich plagioclase above the gray shaded area in Fig. 8.8, between 515°C and 540°C. Thus, the following mineral assemblages result from middle and upper greenschist facies conditions: Ms + Mrg + Pl + Qtz + Cal ± Pg and Ms + Pg + Pl + Qtz + Cal (for Al- and Na-rich compositions only). After the final breakdown of Mrg and Pg in the presence of Qtz and Cal, at temperatures up to 590°C, the mineral assemblage in Al-rich metamarls will be Ms + Pl + Kfs + Qtz + Cal. Finally, at even higher temperatures, after the final breakdown of Ms in the presence of Qtz and Cal, the remaining assemblage is Pl + Kfs + Qtz + Cal.

The contouring of reactions (8.22), (8.29), (8.15) and (8.17) in Fig. 8.8 shows that they simultaneously produce Pl of different An-content at a given T and P. Provided that differences in Pl composition are not eliminated by diffusion processes, it is to be expected that Al-rich metamarls of greenschist and amphibolite facies grade will show a range of Pl An-content within a single thin section, e.g., in Central Alpine marl compositions described by Frank 1983; Fig. 8.5 and see below). However, variation in Pl composition may also be due to miscibility gaps, e.g., Bøggild (compositions ~ An<sub>39-48</sub> and An<sub>53-64</sub>) and Huttenlocher (compositions ~ An<sub>65</sub> and An<sub>95</sub>) intergrowths, within the plagioclase solid solution series.

### 8.3.2.2 Prograde Metamorphism at Very Low X<sub>CO<sub>2</sub></sub>

Phase relationships for the system KNCAS-HC involving the phases Ab, An, Czo, Grs, Kfs, Mrg, Ms, Pg, Prl with excess Qtz and Cal are shown in Fig. 8.9. Calculation of this petrogenetic grid was performed using pure end-member mineral compositions, except for Czo, where an activity of 0.64 was computed based on mineral composition data of Frank (1983) with Czo containing about 6 wt% Fe<sub>2</sub>O<sub>3</sub>. Note that Fig. 8.9 is similar to the H<sub>2</sub>O-rich portion of Fig. 8.7, but with an enlarged stability field for Czo [reaction (8.23)] is now at X<sub>CO<sub>2</sub></sub> of ca. 0.13 instead of 0.035 in Fig. 8.7 [and with addition of reaction (8.24)].

Figure 8.10 shows phase relationships as in Fig. 8.9, complemented by contours for reactions involving An as discussed earlier for Fig. 8.8. The stability field of

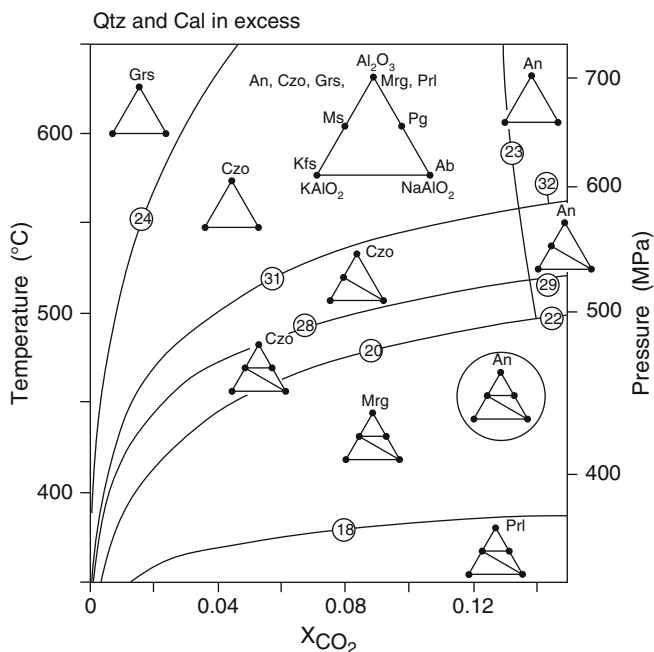


**Fig. 8.9** P-T-X phase relationships for the KNCAS-HC system with excess Qtz and Cal at  $0 < X_{\text{CO}_2} < 0.15$ . Pure end member mineral compositions are used, except for Czo ( $a_{\text{Czo}} = 0.64$ ). The vertical axis represents a prograde Ky-type path of orogenic metamorphism. The inset shows the chemography projected from Qtz, Cal,  $\text{H}_2\text{O}$  and  $\text{CO}_2$  onto the  $\text{KAlO}_2$ - $\text{NaAlO}_2$ - $\text{Al}_2\text{O}_3$  plane. Compatibility diagrams are given for each divariant field. Reactions are numbered as in Tables 8.2 and 8.3

the assemblage  $\text{Pl} + \text{Mrg} + \text{Qtz} + \text{Cal}$  is emphasized by the gray-shaded area in Fig. 8.10 and is limited by reaction (8.22): high- and low-T boundaries are given by the  $\text{An}_{100}$  and  $\text{An}_{30}$  contours, respectively. As already discussed above for Fig. 8.8, the assemblage  $\text{Pg} + \text{Qtz} + \text{Cal}$  in the presence of intermediate Pl composition breaks down by reaction (8.17), and not by reaction (8.29). This is indicated in Fig. 8.10 for the  $\text{An}_{70}$  contours of reactions involving Mrg- and Pg which meet at an invariant point at about  $470^\circ\text{C}$  and  $X_{\text{CO}_2} = 0.11$  as shown by the configuration in the inset diagram. Prograde metamorphism of a rock consisting of  $\text{Ms} + \text{Pg} + \text{Prl} + \text{Qtz} + \text{Cal}$  and an initial fluid composition of  $X_{\text{CO}_2} = 0.02$  is now considered. The prograde path in  $P$ - $T$ - $X_{\text{CO}_2}$  space is shown in Fig. 8.10 by a line extending from **a** to **k** with changing modal mineral composition illustrated in Fig. 8.11.

a-b. The starting assemblage  $\text{Ms} + \text{Pg} + \text{Prl} + \text{Qtz} + \text{Cal}$  is heated at a constant  $X_{\text{CO}_2}$  of 0.020.

b-c. Margarite is formed according to reaction (8.18), between  $359^\circ\text{C}$  and  $364^\circ\text{C}$  and  $X_{\text{CO}_2}$  increases to 0.025.

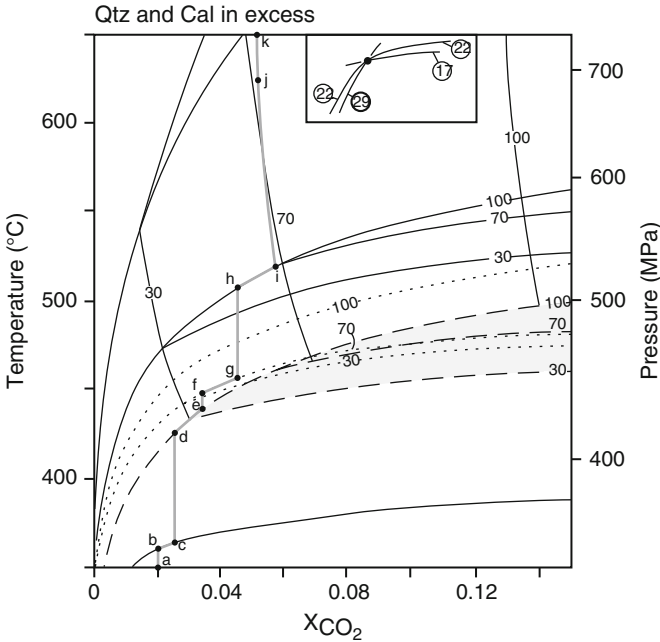


**Fig. 8.10** P–T–X diagram of the KNCAS–HC system with excess Qtz and Cal at  $0 < X_{CO_2} < 0.15$ . The vertical axis represents a prograde path of Ky-type terrains. Pure end member mineral compositions are used, except for Czo ( $a_{Czo} = 0.64$ ) and Pl. Polybaric divariant equilibria for a particular Pl-composition of ( $An_x$ ) are shown as *full lines* (Ms-involving reactions), *stippled lines* (Pg-involving reactions) or *dashed lines* (Mrg-involving reactions). Numbers refer to mole percent An-content in Pl. The stability field for the assemblage Mrg + Pl (+ Qtz + Cal) is shown in gray. The prograde path from “a” to “k” is emphasized and discussed in the text

- c–d. At point c, Pl is exhausted. The rock is now composed of Ms + Pg + Mrg + Qtz + Cal and is subjected to further heating at a constant  $X_{CO_2}$  of 0.025. The mineral assemblage is characteristic of the lower greenschist facies grade.
- d–e. Clinzoisite is formed for the first time according to reaction (8.20) between 425°C and 436°C and  $X_{CO_2}$  increases to 0.034.
- e–f. At point e, Mrg is used up and the resulting mineral assemblage Ms + Pg + Czo + Qtz + Cal undergoes continued heating at a constant  $X_{CO_2}$  of 0.034.
- f–g. Plagioclase of composition  $An_{33-36}$  forms according to reaction (8.28) between 450°C and 458°C and  $X_{CO_2}$  increases to 0.045.
- g–h. At point g, all Pg is used up. The mineral assemblage Ms + Pl + Czo + Qtz + Cal is present between 458 and 507°C and is characteristic of upper greenschist facies grade. Over this T interval, reactions (8.23), (8.28) and (8.29) result in only minor changes in the mode and mineral composition of the rock (note that these three reactions are linearly dependent). Reactions (8.28) and (8.29) are responsible for a decrease in the Pg-component of Ms, and all three reactions produce additional Pl. The very small increase in  $X_{CO_2}$  is not visible in Figs. 8.10 and 8.11.

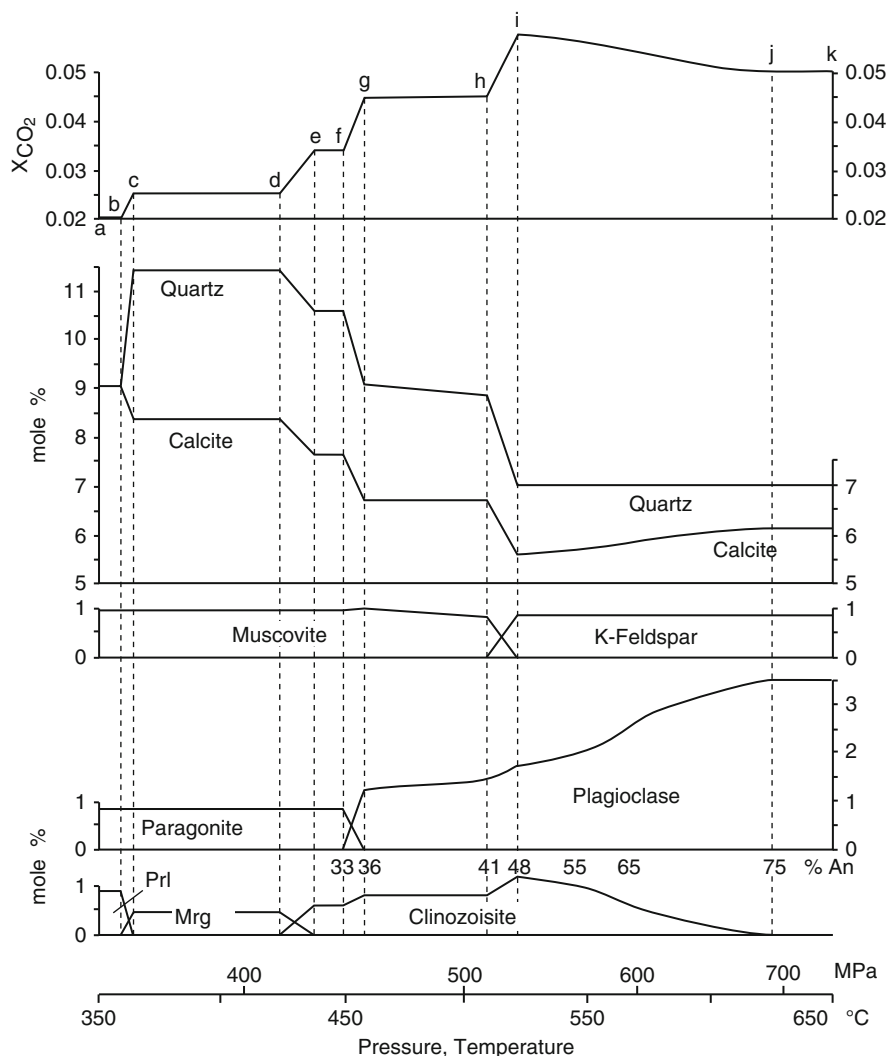


**Fig. 8.11** Modal composition (mol%), fluid composition ( $X_{\text{CO}_2}$ ) and Pl-composition (An %) along the prograde path “a”–“k” shown in Fig. 8.9

h–i. K-feldspar and additional Czo are formed by reaction (8.31) between 507°C and 520°C and  $X_{\text{CO}_2}$  increases to 0.058. Some additional Pl is produced as in the previous segment of the prograde path.

i–j. At point **i**, all Ms is used up. The stable mineral assemblage is Kfs + Pl + Czo + Qtz + Cal that is characteristic of lower and middle amphibolite facies grade. Additional Pl is produced by reaction (8.23), An-content of Pl increases from 48 to 75 mol%, and  $X_{\text{CO}_2}$  decreases slightly.



j–k. At point **k** and 625°C, all Czo c is exhausted and the resulting mineral assemblage Kfs + Pl + Qtz + Cal undergoes continued heating at a constant  $X_{\text{CO}_2}$  of 0.051 without further reaction.

In summary, although phase relationships of relatively Al-rich metamarls with excess Qtz and Cal are complex, several diagnostic assemblages (always with excess Qtz + Cal) are found along a Ky-type path of regional metamorphism. The assemblage Ms + Pg + Prl is characteristic for sub-greenschist facies conditions. The assemblage Ms + Pg + Mrg is characteristic for the lower greenschist facies, and Ms + Mrg + Pl and Ms + Czo + Pl for upper greenschist facies conditions. The assemblages Ms + Pl + Kfs and Czo + Pl + Kfs indicate lower and middle amphibolite facies, and Pl + Kfs indicate upper amphibolite facies grade. The first Pl to form has an An-content of ca. 30 mol%, and becomes more calcic with increasing metamorphic grade. In short, sheet silicate-rich assemblages containing two or three white micas at low grade are replaced by feldspar-rich assemblages at high grade. In comparison with mineral stabilities in the progressively metamorphosed calcareous mica schist from the western Lepontine Alps (Fig. 8.5), Pg begins to disappear before Mrg implying a higher  $X_{\text{CO}_2}$  in the fluid phase with reference to Fig. 8.10. Scapolite stability which not shown in Fig. 8.10, is controlled by the reaction  $\text{Pl} + \text{Cal} = \text{Scp}$  as in the Vassalboro marls described above, in rocks with Pl compositions  $< \text{An}_{60-68}$ . The distribution of Rt and Ttn shown in Fig. 8.5 reflects overgrowths of Ttn on Rt in high grade rocks and the reaction  $\text{Rt} + \text{Cal} + \text{Qtz} = \text{Ttn} + \text{CO}_2$ .

## 8.4 Increasing Complexity of Metamarls

Metamarls, as defined in the introduction to the marl chapter, are typically rocks of a nine component chemical system. The arising complexity is difficult to represent graphically on well arranged diagrams. Mg and Fe are always present in chlorite or ankerite in low-grade metamarls. Thus in the course of metamorphism various CFM minerals are typically present in metamarls in addition to the white micas and feldspars from the simple subsystems discussed above. In addition, excess Cal and Qtz was a precondition of the discussion above. Both minerals are consumed by most reactions and their modal abundance decreases stepwise in the course of metamorphism (e.g., Fig. 8.4). Thus many metamarls loose in fact free carbonate and become pure silicate rocks, typically in the amphibolite facies. An example is the Grt–Hbl-gneiss shown on Fig. 8.1a. The texture shows domains of the rock where Chl is still present. Also Czo is abundant in other domains of the rock matrix. Large hornblende and garnet formed from Chl and Czo as is evident from the halos of Chl depletion particularly around the Hbl crystals. The reactions that produce the observed texture are: (a)  $\text{Chl} + \text{Czo} \pm \text{Qtz} = \text{Hbl} + \text{Pl} + \text{H}_2\text{O}$  and (b)  $\text{Chl} + \text{Czo} \pm \text{Qtz} = \text{Hbl} + \text{Grt} + \text{H}_2\text{O}$ . Hornblende growth occurred clearly after the last penetrative deformation as indicated by the orientation of some crystals across the foliation. The specific

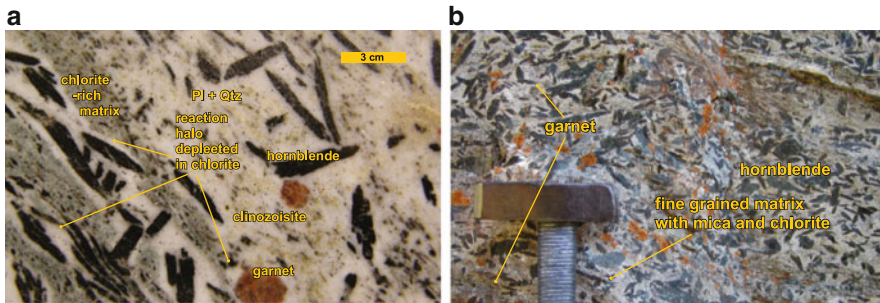


**Fig. 8.12** Amphibolite facies metamarls: (a) Grt–Hbl gneiss from the Tremola series of the southern Gotthard Massif of the Central Alps (outcrop N of Airolo). The white matrix of the rock contains Pl + Qtz, Bt is abundant, in some domains of the matrix are rich in beige-colored Czo, in Chl is present in the greenish zones. Note Chl depleted reaction halos around Hbl and Grt. Hbl crystals grow also across the foliation. (b) Hornblende gneiss at the Frodalera locality, Lukmanier area, Central Alps. The rock formed from a Mesozoic marl (“Quartenschiefer”, Upper Triassic (Keuper), cover of the Gotthard basement) at lower amphibolite facies condition. The foliated fine-grained matrix consists of Qtz + Pl + Ms + Chl ± Cal. Very coarse grained tschermakitic hornblende grows across the foliation. Some Grt is also present

rock may have run out of calcite originally present at relatively early stages of metamorphism as a result of Czo formation (e.g., reaction (8.3) Table 8.2).

The upper Triassic “Quartenschiefer” of the Central Alps is a similar metamarl that originally contained free carbonate (Fig. 8.12). The outcrop photograph shows the marly sediment after it has been metamorphosed to 520°C at 500 MPa at the beginning of the amphibolite facies. Coarse grained tschermakitic hornblende is modally dominant and a few garnet grains are scattered in the matrix of fine-grained mica, chlorite and quartz. Carbonate has been completely used up in the Hbl producing reactions. Total consumption of calcite during metamorphism has profound effects on the fluid composition. As explained above (Figs. 8.3, 8.10, and 8.11), in closed system metamorphism of marls with excess calcite  $X_{\text{CO}_2}$  increases progressively during most reactions such that fluids tend to be  $\text{CO}_2$ -rich in high-grade metamarls. If, as in the two field examples above, calcite is used up by the reactions no additional  $\text{CO}_2$  can be released. Because the rock still may contain abundant mica and even chlorite at this point further metamorphism will be characterized by pure dehydration reactions. These reactions will dilute the  $\text{CO}_2$ -rich fluid by  $\text{H}_2\text{O}$  und buffer the fluid composition back to low values of  $X_{\text{CO}_2}$ .

## 8.5 Low Pressure Metamorphism of Marls

In low pressure contact aureoles metamarls from distinct rocks, so called calc-silicate marbles and calc-silicate hornfelses. Depending on the original mineral composition of the sediment, such rocks contain various assemblages among minerals including Cal, Qtz, Cpx, Grt, An and Kfs at the contact to granite intrusions.

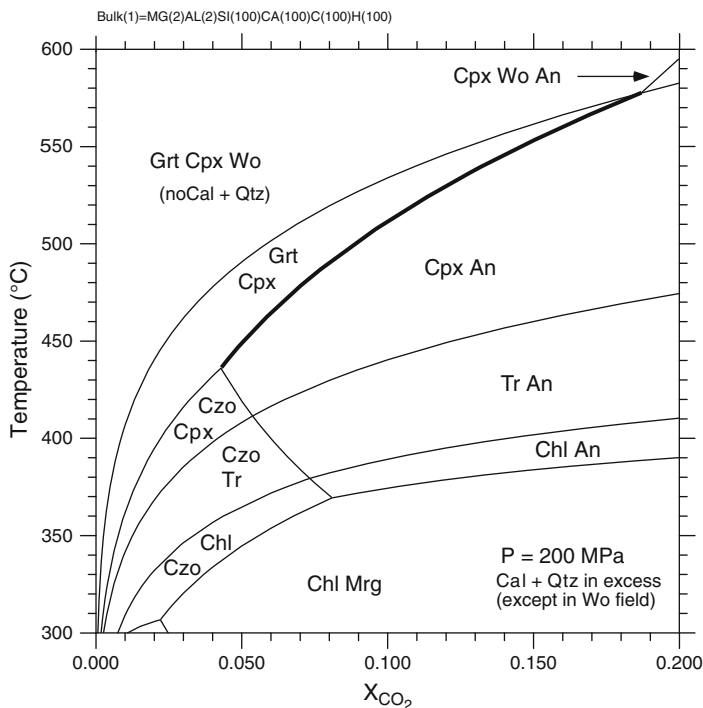


**Fig. 8.13** Isobaric  $T$ - $X_{\text{CO}_2}$  diagram of the CMAS-HC system with excess Qtz and Cal at 200 MPa showing the distribution of stable assemblages in contact metamorphism. Note that in the upper left of the diagram Wo is present instead of Cal + Qtz. Equilibrium of reaction (8.9) (Table 8.2)  $\text{An} + \text{Cal} + \text{Qtz} = \text{Grs} + \text{CO}_2$  is highlighted (see text)

The rocks often characterized by abundant grossular garnet. In addition, wollastonite is typically present in metamarl outcrops close to the intrusive contacts as a result of reaction (8.10) (Table 8.2) the terminates the assemblage calcite + quartz.

The simple model for metamarls on the  $T$ - $X_{\text{CO}_2}$  diagram shows the distribution of stable assemblages in the system CMAS-HC for 200 MPa contact metamorphism (Fig. 8.13). The chosen rock composition is represented by the minerals calcite, quartz chlorite and kaolinite in the sediment. The model shows that assemblages typical of calc-silicate contact rocks indicate the presence of a low- $\text{CO}_2$  fluid. Temperatures close to the contacts to the most common granite plutons (crystallized from  $\text{H}_2\text{O}$ -rich melts) range between  $450^\circ\text{C}$  und  $550^\circ\text{C}$  at 200 MPa (see Chaps. 6 and 7). The model predicts that the marly rock contains the assemblage Cal + Qtz + Cpx + An, for example at  $500^\circ\text{C}$  and an of 0.15, as a result of prograde closed system metamorphism.

An outcrop with banded metasedimentary contact rocks from the Adamello aureole shows greenish bands consisting of Qtz + Cpx + An + Kfs + some relic Tr (Fig. 8.14). The green bands do not contain Cal, it has been used up by

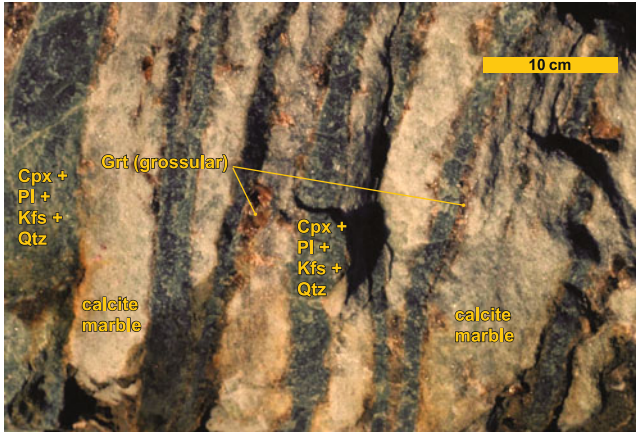


**Fig. 8.14** Outcrop of a contact metamorphic marl (and shale) – limestone sequence (Upper Triassic) at Monte Frerone, southern aureole of the Tertiary Adamello pluton, Northern Italy. Limestone bands were transformed into pure white calcite marble, the low-grade minerals of the marly layers reacted to green bands of calc-silicate rock containing Cpx + An + Qtz  $\pm$  Cal  $\pm$  Kfs. Along the contacts between the rock bands some brownish grossular garnet has formed

the Tr-consuming reaction (that also removed almost all Tr). However, at the direct contact to the white bands of pure calcite marble the assemblage Qtz + An + Cal is present having the potential to form grossular garnet by reaction (8.9) (Table 8.2). Grossular seams are present along most of the direct contacts of the green and white layers showing the effect of reaction (8.9). The equilibrium of this reaction is highlighted on Fig. 8.13 as thick heavy line separating the Cpx + An from the Cpx + Grt field. In principle, grossular growth could have been buffered along the thick curve with increasing T. It seems more likely that progress of reaction (8.9) has been caused by an infiltrating H<sub>2</sub>O-rich fluid that isothermally moved the Qtz + Cal + Cpx + An assemblage at the lithological contact to the reaction boundary. Evidence for this conclusion is the lack of thin Grs layers along some of the contacts between the green and white layer. The Cal-free green bands would not form garnet even if they would be heated to very high T (the green bands would form garnet at high pressures though).

Finally we return to the beginning, namely to Fig. 1.1. The figure shows an outcrop of shale with nodules of limestone (Fig. 1.1a). The contact zone of the two rocks is marl as defined above. Permian contact metamorphism of the Palaeozoic sediments caused by the rift-related intrusion of a syenite pluton resulted in the formation of zoned concentric structures at the sites of the former limestone nodules. The concentric rings of Ca-silicate rocks were formed by typical reactions of the marl system and contain assemblages with Bt and Kfs toward the metapelitic hornfels and Cpx + An in the core of the structure but no Qtz (compare with example above). The reactions consumed all calcite of the former limestone nodule and replaced it with pure Ca-silicate rock. The structure shows that components other than H<sub>2</sub>O and CO<sub>2</sub> (here specifically MgO, FeO, AlO<sub>1.5</sub>, SiO<sub>2</sub>) can be mobile

in metamorphic processes and migrate along chemical potential gradients. However, it also shows that, at least in this example, transport and homogenization distances are small and the original structure of the sedimentary rock still can be recognized.

## References and Further Reading

### *Cited References*

- Bucher K, Frank E, Frey M (1983) A model for the progressive regional metamorphism of margarite-bearing rocks in the Central Alps. *Am J Sci* 283A:370–395
- Ferry JM (1976) Metamorphism of calcareous sediments in the Waterville-Vassalboro area, south-central Maine: mineral reactions and graphical analysis. *Am J Sci* 276:841–882
- Ferry JM (1983a) Applications of the reaction progress variable in metamorphic petrology. *J Petrol* 24:343–376
- Ferry JM (1983b) Mineral reactions and element migration during metamorphism of calcareous sediments from the Vassalboro Formation, south-central Maine. *Am Mineralog* 68:334–354
- Ferry JM (1983c) Regional metamorphism of the Vassalboro Formation, south-central Maine, USA: a case study of the role of fluid in metamorphic petrogenesis. *J Geol Soc Lond* 140:551–576
- Ferry JM (1992) Regional metamorphism of the Waits River Formation, eastern Vermont: delineation of a new type of giant metamorphic hydrothermal system. *J Petrol* 33:45–94
- Frank E (1983) Alpine metamorphism of calcareous rocks along a cross-section in the Central Alps: occurrence and breakdown of muscovite, margarite and paragonite. *Schweiz Miner Petrogr Mitt* 63:37–93
- Frey M (1978) Progressive low-grade metamorphism of a black shale formation, Central Swiss Alps, with special reference to pyrophyllite and margarite bearing assemblages. *J Petrol* 19:93–135
- Frey M, Orville PM (1974) Plagioclase in margarite-bearing rocks. *Am J Sci* 274:31–47
- Hewitt DA (1973) The metamorphism of micaceous limestones from south-central Connecticut. *Am J Sci* 273A:444–469
- Yardley BWD (1989) *An introduction to metamorphic petrology*. Longman, Edinburgh, 248 pp
- Zen E-an (1981) *A study of progressive regional metamorphism of pelitic schists from the Taconic allochthon of southwestern Massachusetts and its bearing on the geologic history of the area*. US Geological Survey Professional Paper 1113, US Government Printing Office, Washington DC, 128 pp

### *Further Reading*

- Aines RD, Rossman GR (1984) The hydrous component in garnets: pyralispites. *Am Mineralog* 69:1116–1126
- Bucher K (1976) Occurrence and chemistry of xanthophyllite in roof pendants of the Bergell granite, Sondrio, N Italy. *Schweiz Miner Petrogr Mitt* 56:413–426
- Castelli D (1991) Eclogitic metamorphism in carbonate rocks: the example of impure marbles from the Sesia-Lanzo Zone, Italian Western Alps. *J Metamorph Geol* 9:61–77

- Connolly JAD, Memmi I, Trommsdorff V, Franceschelli M, Ricci CA (1994) Forward modeling of calc-silicate micro-inclusions and fluid evolution in a graphitic metapelite, northeastern Sardinia. *Am Mineralog* 79:960–972
- Dasgupta S (1993) Contrasting mineral parageneses in high-temperature calc-silicate granulites: examples from the Eastern Ghats, India. *J Metamorph Geol* 11:193–202
- Harley SL, Buick IS (1992) Wollastonite-scapolite assemblages as indicators of granulite pressure-temperature-fluid histories: the Rauer Group, East Antarctica. *J Petrol* 33:693–728
- Jamtveit B, Bucher K, Stijfhoorn DE (1992) Contact metamorphism of layered metasediments in the Oslo rift: I. Buffering, infiltration and the mechanisms of mass transport. *J Petrol* 33:377–422
- Joesten R (1974) Local equilibrium and metasomatic growth of zoned calc-silicate nodules from a contact aureole, Christmas Mountains, Big Bend region, Texas. *Am J Sci* 274:876–901
- Kohn MJ, Spear FS (1993) Phase equilibria of margarite-bearing schists and chloritoid + hornblende rocks from western New Hampshire, USA. *J Petrol* 34:631–651
- Labotka TC (1987) The garnet + hornblende isograd in calcic schists from an andalusite-type regional metamorphic terrain, Panamint Mountains, California. *J Petrol* 28:323–254
- Labotka TC (1995) Evidence for immiscibility in Ti-rich garnet in a calc-silicate hornfels from northeastern Minnesota. *Am Mineralog* 80:1026–1030
- Labotka TC, Nabelek PI, Papike JJ, Hover-Granath VC, Laul JC (1988) Effects of contact metamorphism on the chemistry of calcareous rocks in the Big Horse Limestone Member, Notch Peak, Utah. *Am Mineralog* 73:1095–1110
- Léger A, Ferry JM (1991) Highly aluminous hornblende from low-pressure metacarbonates and a preliminary thermodynamic model for the Al content of calcic amphibole. *Am Mineralog* 76:1002–1017
- Letargo CMR, Lamb WM (1993) P-T-X conditions of calc-silicate formation: evidence from fluid inclusions and phase equilibria; Llano Uplift, central Texas, USA. *J Metamorph Geol* 11:89–100
- Livi KJT, Ferry JM, Veblen DR, Frey M, Connolly JAD (2002) Reactions and physical conditions during metamorphism of Liassic aluminous black shales and marls in central Switzerland. *Eur J Mineralog* 14:647–672
- Lopez Sanchez-Vizcaino V, Connolly JAD, Gomez-Pugnaire MT (1997) Metamorphism and phase relations in carbonate rocks from the Nevado-Filabride Complex (Cordilleras Beticas, Spain): application of the  $Ttn + Rt + Cal + Qtz + Gr$  buffer. *Contrib Mineralog Petrol* 126:292–302
- Mathavan V, Fernando GVAR (2001) Reactions and textures in grossular-wollastonite-scapolite calc-silicate granulites from Maligawila, Sri Lanka: evidence for high-temperature isobaric cooling in the metasediments of the Highland Complex. *Lithos* 59:217–232
- Melson WG (1966) Phase equilibria in calc-silicate hornfels, Lewis and Clark County, Montana. *Am Mineralog* 51:402–421
- Menard T, Spear FS (1993) Metamorphism of calcic pelitic schists, Stafford Dome, Vermont: compositional zoning and reaction history. *J Petrol* 34:977–1005
- Misch PM (1964) Stable association wollastonite-anorthite and other calc-silicate assemblages in amphibolite-facies crystalline schists of Nanga Parbat, northwest Himalayas. *Beitr Mineral Petrogr (Contrib Mineral Petrol)* 10:315–356
- Motoyoshi Y, Thost DE, Hensen BJ (1991) Reaction textures in calc-silicate granulites from the Bolingen Islands, Prydz Bay, East Antarctica: implications for the retrograde P-T path. *J Metamorph Geol* 9:293–300
- Sillanpää J (1986) Mineral chemistry study of progressive metamorphism in calcareous schists from Ankarvattnet, Swedish Caledonides. *Lithos* 19:141–152
- Svensen H, Jamtveit B (1998) Contact metamorphism of shales and limestones from the Grua area, the Oslo Rift, Norway: a phase – petrological study. *Norsk Geol Tidsskrift* 78:81–98
- Tanner PWG (1976) Progressive regional metamorphism of thin calcareous bands from the Moinian rocks of N.W. Scotland. *J Petrol* 17:100–134

- Thompson PH (1973) Mineral zones and isograds in "impure" calcareous rocks, an alternative means of evaluating metamorphic grade. *Contrib Mineralog Petrol* 42:63–80
- Thompson AB (1975) Mineral reactions in a calc-mica schist from Gassetts, Vermont, U.S.A. *Contrib Mineralog Petrol* 53:105–127
- Valley JW, Peacor DR, Bowman JR, Essene EJ, Allard MJ (1985) Crystal chemistry of a Mg-vesuvianite and implications of phase equilibria in the system CaO-MgO-Al<sub>2</sub>O<sub>3</sub>-SiO<sub>2</sub>-H<sub>2</sub>O-CO<sub>2</sub>. *J Metamorph Geol* 3:137–154
- Will TM, Powell R, Holland T, Guiraud M (1990) Calculated greenschist facies mineral equilibria in the system CaO-FeO-MgO-Al<sub>2</sub>O<sub>3</sub>-SiO<sub>2</sub>-CO<sub>2</sub>-H<sub>2</sub>O. *Contrib Mineralog Petrol* 104:353–368
- Winchester JA (1972) The petrology of Moinian calc-silicate gneisses from Fannich Forest, and their significance as indicators of metamorphic grade. *J Petrol* 13:405–424

# Chapter 9

## Metamorphism of Mafic Rocks

### 9.1 Mafic Rocks

Metamorphic mafic rocks (e.g., mafic schist or greenschist and mafic gneiss, amphibolite) are derived from mafic igneous rocks, mainly basalts and andesites, and of lesser importance, gabbro and mafic diorite (Chap. 2). Metamorphic assemblages in mafic rocks are particularly useful in defining the intensity of metamorphism within the metamorphic facies concept (Chap. 4).

Extrusive mafic igneous rocks comprise the largest volume of mafic rocks in comparison to their plutonic equivalents (Tables 2.1 and 2.2). Basalts and andesites occur as massive lava flows, pillow lavas, sills, dykes, hyaloclastic breccias and tuff layers. Basaltic rocks constitute a major portion of the oceanic crust and most basalts appear to have been subjected to ocean-floor metamorphism immediately after formation at a spreading ridge. When transported to a continental margin via plate motion, oceanic mafic rocks are again recrystallized at or near convergent plate junctions and are typically retained as fragments within the subduction complex; the change in mineralogy depends on whether the oceanic crust was subducted beneath a continental plate or was obducted onto continental crust. On the other hand, andesitic rocks and related calc-alkaline volcanics together with associated volcanogenic sediments (e.g. typically graywacke) are the dominant lithologies within island arcs and Pacific-type continental margins. These rocks are subjected to alteration by hydrothermal fluids as evidenced by present-day geothermal activity in many island arc areas or are transformed during burial and orogenic metamorphism.

Metamorphosed mafic rocks (Fig. 9.1) are particularly susceptible to changes in T and P and this is the main reason why most names of individual metamorphic facies are derived from mineral assemblages of this rock group, e.g. greenschist, amphibolite, granulite, blueschist, and eclogite (cf. Chaps. 2 and 4). In addition, mafic rocks that are metamorphosed under very weak conditions below greenschist and blueschist facies grade often show systematic variations in mineralogy that permits a further subdivision into characteristic metamorphic zones. These distinct low-grade zones have been given separate metamorphic facies names such as zeolite, prehnite–pumpellyite and pumpellyite–actinolite, that are here simply grouped as subgreenschist facies for very-low grade conditions of incipient metamorphism.



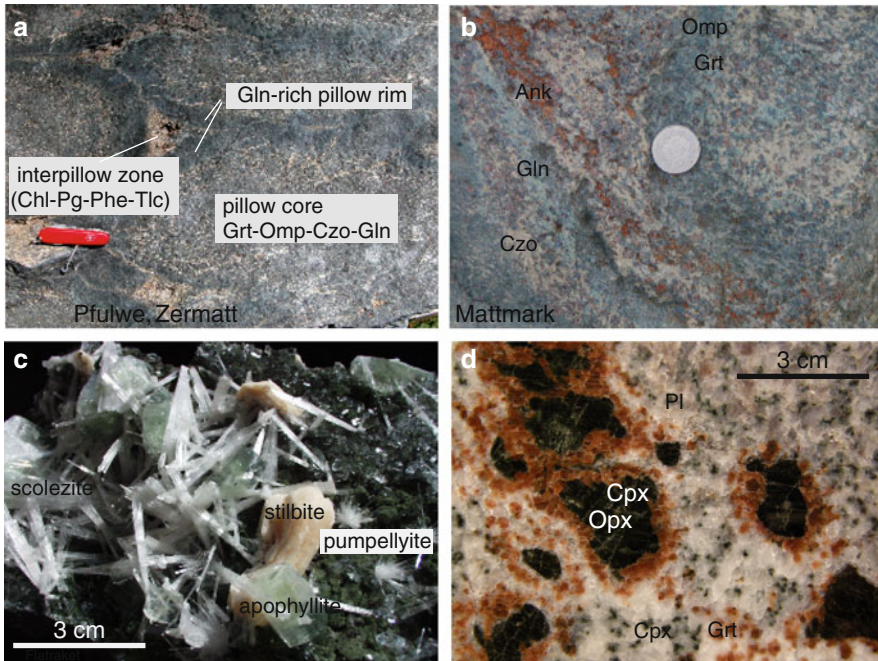


**Fig. 9.1** Metamorphic mafic rocks: (a) Eclogite facies basaltic pillow lava from Pfulwe (Zermatt, Alps). Pillow cores contain Grt–Omp + Ep/Czo–Gln–Cld, dark pillow rims contain Gln–Cld–Grt–Omp + minor Czo–Pg–Tlc, interpillow zones are rich in Chl–Pg–Phe and Tlc (Bucher et al. 2005). The compositional zoning probably resulted from seafloor metasomatism. (b) Eclogite facies metabasalt from the Saas valley (Alps) with Grt–Omp–Gln–Czo/Ep–Ank–Cld. The rock is typical of fast subduction of oceanic lithosphere ( $\sim 7^\circ\text{C}/\text{km}$  geothermal gradient). The rock reached 100 km depth (2.7 GPa) at a very low temperature of only  $600^\circ\text{C}$ . (c) Low temperature alteration minerals cover basaltic volcanic rocks at Poona (India). A continuous thin layer of *dark green* pumpellyite covers the basaltic rock. On this early reaction product younger (and at lower T) Ca-zeolites scolezite and stilbite were precipitated from thermal water together with apophyllite. (d) Granulite facies troctolite from Holsnøy (Bergen Arcs, Norway). Rock matrix contains predominantly plagioclase and fine grained Cpx and Grt. Large coronitic structures with occasionally Opx in the core, rimmed by dark Cpx and a corona of coarser grained clear garnet represent sites of former olivine megacrysts. The low-P igneous assemblage Ol–Pl has been replaced by the high-P Grt–Cpx–Pl granulite assemblage

### 9.1.1 Hydration of Mafic Rocks

Basalts and gabbros have solidus temperatures on the order of  $1,200^\circ\text{C}$ . Consequently, hydrous minerals are not typical members of the solidus assemblage of basalts and other mafic rocks. Therefore, at the onset of metamorphism, mafic rocks, including pyroclastic rocks, are in their least hydrated state as opposed to “wet” sedimentary rocks that start metamorphism in a maximum hydrated state. Because newly formed minerals in metamafics at low-T are predominantly hydrous phases, access of water is essential to initiate metamorphism (see Fig. 3.16), otherwise,

igneous rocks would persist relatively unchanged in metamorphic terrains. Partial or complete hydration of mafic rocks may occur during ocean-floor metamorphism (Fig. 9.1), with hydrothermal activity in island arc settings, or during orogenic metamorphism where deformation facilitates the influx of water. During metamorphism of mafic rocks it is not self-evident that the condition  $P_{\text{tot}} = P_{\text{H}_2\text{O}}$  is continuously maintained during their prograde reaction history. On the other hand, mafic rocks in many metamorphic terranes show that partial persistence of igneous minerals and microstructures is common in subgreenschist facies rocks and that such features are typically absent in rocks metamorphosed to conditions of greenschist facies and higher. Nevertheless, primary igneous meso-structures such as magmatic layering and pillow structures may be preserved even in eclogite and granulite facies terrains. Coarse-grained gabbroic rocks have the best chance to retain primary igneous minerals up to high-grade metamorphic conditions. Gabbro bodies often escape pervasive internal deformation and this, in turn, prevents access of water, hampers recrystallization and hinders hydration of the igneous minerals.

As pointed out in Chap. 3, dehydration reactions are strongly endothermic. Consequently, hydration of basalt is exothermic and releases large amounts of heat. The heat of reaction released by replacing a basalt assemblage  $\text{Cpx} + \text{Pl}$  by low-T hydrous minerals such as  $\text{Prh} + \text{Chl} + \text{zeolites}$  could raise the temperature by as much as  $100^\circ\text{C}$  (in a heat-conserving system). Another interesting aspect of exothermic reactions is their self-accelerating and feedback nature. Once initiated, they will proceed as long as water is available. Increasing temperature will initially make the reactions go faster, but it will also bring the reaction closer to its equilibrium where it would eventually stop. Also, note that reactions that partially or completely hydrate mafic rocks are metastable reactions and as such tend to occur far from equilibrium. Consider, for instance, the reaction  $\text{Di} + \text{An} + \text{H}_2\text{O} \rightleftharpoons \text{Chl} + \text{Prh} \pm \text{Qtz}$  mentioned above. In the presence of water at low-T, this reaction will always run to completion and the product and reactant assemblage will never attain reaction equilibrium. Thus, the unstable or metastable nature of the hydration reactions that replace high-T anhydrous igneous assemblages by low-T hydrate assemblages has the consequence that low-grade mafic rocks often show disequilibrium assemblages. Unreacted high-T igneous assemblages may occur together with various generations of low-T assemblages in subgreenschist facies rocks. The hydration process commonly leads to the development of zoned metasomatic structures, e.g. networks of veins and concentric shells of mineral zones that reflect progressive hydration of basaltic pillow lavas. In this case, the highly permeable inter-pillow zones serve as water-conducting structures for hydration water and the hydration process progresses towards the pillow centers. The nature of the product assemblages depends on the P and T during the hydration process but also on the chemical composition of the hydration fluid.  $\text{CO}_2$  in the fluid plays a particularly important role.  $\text{CO}_2$ -rich aqueous fluids may result in altered basalts with modally abundant carbonates such as Cal and Ank.  $\text{CO}_2$ -rich fluids also tend to favor the formation of less hydrous assemblages compared with pure  $\text{H}_2\text{O}$  fluids. The cation composition of aqueous fluids that have already reacted with large volumes of basalt is dramatically different from that of seawater. Fluid that moves rapidly through

permeable fractured rocks will have a different composition than fluid that moves slowly through porous basalt. Fluid-rock interaction typically also leads to extensive redistribution of chemical elements, such as in piles of basaltic pillow lavas. Mineralogical evidence for this may still be observed in high-grade metabasaltic rocks. For example, in the Saas–Zermatt ophiolite complex of the Central Alps, Switzerland, mesoscopic pillow lava structures are often preserved with pillow cores of 2.5 GPa eclogite and inter-pillow material of nearly monomineralic Gln (Fig. 9.1a). Finally, the alteration products of the fluid-basalt interaction process will, of course, reflect these compositional differences of the hydration fluid.

A heterogeneous degree of hydration also results in features such as incipient to extensive development, sporadic distribution, and selective growth of low-grade minerals in vesicles and fractures, and the topotaxial growth of these minerals after igneous Pl, Cpx, Ol, Hbl, Fe–Ti oxides, and glass. From the viewpoint of the igneous petrologist, these minerals are usually referred to as “secondary or deuteritic minerals”. Depending on the effective bulk composition of local domains of a mafic rock, different associations of secondary minerals may develop in vesicles, veins and patches replacing primary phases very irregularly even on the scale of a single thin section. Furthermore, relic igneous phases such as Pl and Cpx as well as their preserved textural relations are common (e.g. ophitic textures). From the viewpoint of the metamorphic petrologist, the low-grade hydrates and carbonates, the “secondary or deuteritic minerals”, constitute the stable low-grade assemblage and the starting material of prograde metamorphism. In the conceptually simplest case, no relic igneous minerals remain in the mafic rock and its igneous assemblage has been completely replaced by a stable low-T assemblage and the rock is in its maximum hydrated state at low T.

### 9.1.2 Chemical and Mineralogical Composition of Mafic Rocks

The characteristic composition of alkali–olivine basalt is listed in Table 2.1 and of a mid-ocean ridge basalt (MORB) in Table 2.3. MORB that is produced along ocean spreading centers, is by far the most common type of mafic rock and will serve as a reference composition for all mafic rocks discussed in this chapter. Mafic rocks are characterized by SiO<sub>2</sub> contents of about 45–60 wt% and are also relatively rich in MgO, FeO, CaO and Al<sub>2</sub>O<sub>3</sub>. It is general custom in petrology to term igneous rocks with 45–52 wt% SiO<sub>2</sub> *basic*, and their metamorphic derivatives are then called metabasic or metabasaltic rocks, in short, metabasites. Andesitic rocks, on the other hand, contain higher SiO<sub>2</sub>, Al<sub>2</sub>O<sub>3</sub>, and alkalis, but lower MgO, FeO, and CaO than basalts (e.g. Carmichael 1989); basaltic andesites and andesites belong to the *intermediate* igneous rocks, defined by SiO<sub>2</sub> contents of 52–63 wt%.

Basic or mafic igneous rocks contain appreciable amounts of at least the following eight oxide components: SiO<sub>2</sub>, TiO<sub>2</sub>, Al<sub>2</sub>O<sub>3</sub>, Fe<sub>2</sub>O<sub>3</sub>, FeO, MgO, CaO, Na<sub>2</sub>O, with K<sub>2</sub>O, MnO, P<sub>2</sub>O<sub>5</sub>, H<sub>2</sub>O, and CO<sub>2</sub> also present in small amounts. These components are stored in relatively few minerals. The mineral inventory of the

mafic protolith comprises the major constituents Pl and Cpx. In addition, Qtz, Opx, Ol and Ne can be present in various associations with Cpx + Pl. Plagioclase and Cpx are the most common minerals of most mafic rocks and many gabbros and basalts contain more than 90–95 vol% of these minerals. Other basalts and gabbros may be composed of Pl + Cpx + Opx + Qtz or Pl + Cpx + Ol + Ne, troctolites contain Pl + Ol, anorthosites have more than 90 vol% Pl, etc. However, all mafic rocks are always combinations of only a few mineral species. A large variety of minor and accessory minerals including Ilm, Mag, Chr, sulphides, Grt, Ap, carbonate, and even Hbl and Bt can also occur in mafic rocks. The later two hydrous minerals are often poor in OH as a result of oxidation and/or halogen substitution.

The complex chemical bulk rock composition of basalts will be redistributed from the few igneous mineral species into a variety of new minerals during metamorphism. The high CaO content of the chief basalt minerals Cpx and Pl results in the formation of numerous separate calcium-bearing metamorphic minerals such as Prh, Pmp, Ttn, Ep, Pl, Am and Grt. This is the essential difference from metapelitic rocks (Chap. 7) where CaO is very low and does not form separate calcic phases but rather occurs as a minor component in ordinary Fe–Mg minerals such as garnet. The most important minerals found in metamafic rocks are listed in Table 9.1.

### 9.1.3 *Chemographic Relationships and ACF Projection*

The composition space that must be considered in an analysis of phase relationships in metamafic rocks is rather complex and requires eight or more system components. This follows from above and from the chemical analysis of MORB in Table 2.3. A graphical analysis of phase relationships in metamafic rocks is often made by means of the ACF projection, the principles of which were introduced in Sect. 2.5.3 and shown in Figs. 2.13 and 2.14. In general, the ACF diagram is used for the representation and analysis of phase relationships that involve calcic minerals. Because of its importance for the subsequent treatment of metamafic rocks some important features of the ACF projection are briefly reviewed.

The following discussion makes extensive use of Fig. 9.2a that is a pseudo-3D display of the NACF tetrahedron, and Fig. 9.2b, a conventional ACF diagram. As usual, the ACF diagram represents a mole fraction triangle and displays the three composition variables  $Al_2O_3$ , CaO and FeO. Any mineral that is composed of only these three components can be directly shown on an ACF diagram (e.g. hercynite). Any other mineral composition is projected onto the ACF triangle or is used as a projection point. In the latter case, the mineral must be present in all assemblages in order to deduce meaningful phase relationships. As ACF diagrams are projections from  $SiO_2$ , this means that at any given  $P$ – $T$  the stable polymorph of  $SiO_2$  (e.g. Qtz) must be present in all assemblages. This restriction often causes a problem when dealing with metamorphic silica-poor igneous mafic rocks such as troctolite, olivine gabbro, olivine basalt and nepheline basalt. However, other meaningful diagrams

**Table 9.1** Minerals and compositions in metabasaltic rocks

Nesosilicates	
Garnet	$(\text{Fe,Mg,Ca})_3(\text{Al,Fe})_2\text{Si}_3\text{O}_{12}$
Sorosilicates	
Kyanite	$\text{Al}_2\text{SiO}_5$
Zoisite	$\text{Ca}_2\text{Al}_3\text{Si}_3\text{O}_{12}(\text{OH})$
Epidote	$\text{Ca}_2\text{FeAl}_2\text{Si}_3\text{O}_{12}(\text{OH})$
Pumpellyite	$\text{Ca}_4\text{Mg}_1\text{Al}_3\text{Si}_6\text{O}_{23}(\text{OH})_3 \bullet 2\text{H}_2\text{O}$
Vesuvianite	$\text{Ca}_{19}\text{Mg}_2\text{Al}_{11}\text{Si}_{18}\text{O}_{69}(\text{OH})_9$
Lawsonite	$\text{CaAl}_2\text{Si}_2\text{O}_7(\text{OH})_2 \bullet \text{H}_2\text{O}$
Chloritoid	$\text{Mg}_1\text{Al}_2\text{Si}_1\text{O}_5(\text{OH})_2$
Pyroxenes	
Diopside	$\text{CaMgSi}_2\text{O}_6$
Jadeite	$\text{NaAlSi}_2\text{O}_6$
Hypersthene	$(\text{Mg,Fe})_2\text{Si}_2\text{O}_6$
Omphacite	$(\text{Ca,Na})(\text{Mg,Fe,Al})\text{Si}_2\text{O}_6$
Amphiboles	
Tremolite	$\text{Ca}_2\text{Mg}_5\text{Si}_8\text{O}_{22}(\text{OH})_2$
Actinolite	$\text{Ca}_2(\text{Fe,Mg})_5\text{Si}_8\text{O}_{22}(\text{OH})_2$
Glaucophane	$\text{Na}_2(\text{Fe,Mg})_3(\text{Al})_2\text{Si}_8\text{O}_{22}(\text{OH})_2$
Barroisite	$(\text{Ca,Na})_2(\text{Fe,Mg,Al})_5\text{Si}_8\text{O}_{22}(\text{OH})_2$
Tschermakite	$\text{Ca}_2(\text{Fe,Mg})_3(\text{Al})_2(\text{Al}_2\text{Si}_6\text{O}_{22}(\text{OH})_2)$
Hornblende	$(\text{Na,K})\text{Ca}_2(\text{Fe,Mg,Al})_5(\text{Si,Al})_8\text{O}_{22}(\text{OH,F,Cl})_2$
Sheet silicates	
Muscovite	$\text{KAl}_3\text{Si}_3\text{O}_{10}(\text{OH})_2$
Celadonite	$\text{KMgAlSi}_4\text{O}_{10}(\text{OH})_2$
Paragonite	$\text{NaAl}_3\text{Si}_3\text{O}_{10}(\text{OH})_2$
Phlogopite	$\text{KMg}_3[\text{AlSi}_3\text{O}_{10}](\text{OH})_2$
Biotite	$\text{K}(\text{Mg,Fe,Al,Ti})_3[(\text{Al,Si})_3\text{O}_{10}](\text{OH,F,Cl})_2$
Clinchlore	$\text{Mg}_5\text{Al}_2\text{Si}_3\text{O}_{10}(\text{OH})_8$
Chlorite	$(\text{Fe,Mg})_5\text{Al}_2\text{Si}_3\text{O}_{10}(\text{OH})_8$
Prehnite	$\text{Ca}_2\text{Al}_2\text{Si}_3\text{O}_{10}(\text{OH})_2$
Tectosilicates	
Quartz	$\text{SiO}_2$
Anorthite	$\text{CaAl}_2\text{Si}_2\text{O}_8$
Albite	$\text{NaAlSi}_3\text{O}_8$
Analcite	$\text{NaAlSi}_2\text{O}_6 \bullet \text{H}_2\text{O}$
Scapolite	$\text{Ca}_4(\text{Al}_2\text{Si}_2\text{O}_8)_3(\text{CO}_3,\text{SO}_4,\text{Cl}_2)$
Zeolites	
Stilbite	$\text{CaAl}_2\text{Si}_7\text{O}_{18} \bullet 7\text{H}_2\text{O}$
Heulandite	$\text{CaAl}_2\text{Si}_7\text{O}_{18} \bullet 6\text{H}_2\text{O}$
Laumontite	$\text{CaAl}_2\text{Si}_4\text{O}_{12} \bullet 4\text{H}_2\text{O}$
Wairakite	$\text{CaAl}_2\text{Si}_4\text{O}_{12} \bullet 2\text{H}_2\text{O}$
Carbonates	
Calcite	$\text{CaCO}_3$
Aragonite	$\text{CaCO}_3$
Dolomite	$\text{Ca}(\text{Mg,Fe})(\text{CO}_3)_2$

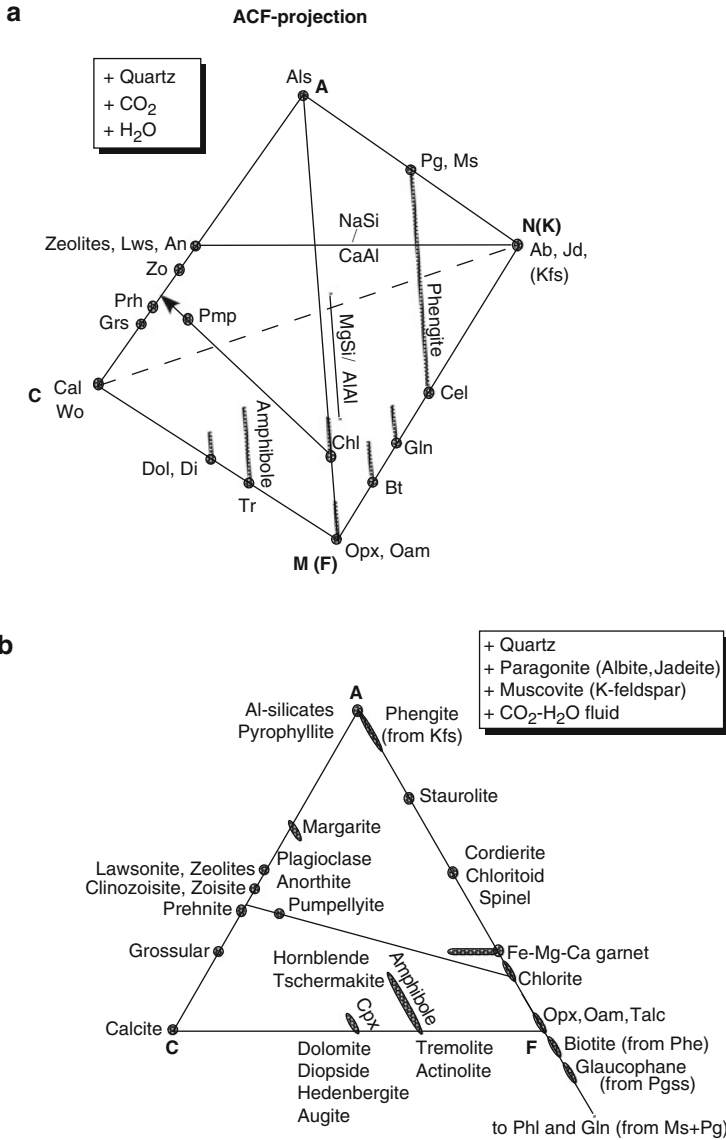


**Fig. 9.2** ACF projections for metamafic rocks

may be designed for such quartz-free metamafics following the suggestions given in Sect. 2.5. ACF diagrams are also projections from H<sub>2</sub>O and CO<sub>2</sub> in order to permit the display of hydrous and carbonate minerals. This means that a fluid phase of a specified composition must be present, or the chemical potentials of H<sub>2</sub>O and CO<sub>2</sub> must be defined. This again may cause problems, particularly at low metamorphic grades, because the universal presence of a fluid phase is not obvious in anhydrous

igneous protolith rocks (see discussion above). Note also that Pmp plots on the ACF surface in Fig. 9.2a and its composition projects between Zo and Prh as viewed from the Mg–Chl (clinocllore) composition.

ACF diagrams also represent projections parallel to the  $MgFe_{-1}$  exchange vector. This is a rigid and lamentable feature of ACF diagrams. All complex relationships, continuous and discontinuous reactions arising from variations in the Fe–Mg ratio of Fe–Mg silicate minerals cannot be properly analyzed and understood with the aid of such diagrams. The AF binary is identical on ACF and AFM diagrams. Consequently, many of the relationships discussed in Chap. 7 with respect to metapelites are also valid here. In Chap. 7 the AF binary is expanded to the AFM triangle and in order to include Ca-minerals, to the ACF triangle in this chapter. Although an ACFM tetrahedron would permit a rather thorough analysis of phase relationships in metamafic rocks, it is very inconvenient to work with three-dimensional composition phase diagrams.

The  $MgFe_{-1}$  projection on ACF diagrams has the consequence that crossing tie-line relationships among Fe–Mg silicates (with contrasting  $X_{Fe}$ ) and Ca-minerals do not necessarily represent a discontinuous reaction relationship but rather span a composition volume in the ACFM space. For example (Fig. 9.2b), the presence of four minerals Grt, Hbl, Ky, and Zo can be related to the reaction,  $2Ts + 1Ky = 2Grt + 2Zo + 1Qtz + 1H_2O$ . This important reaction in high-P amphibolites is not discontinuous, as may be concluded erroneously from Fig. 9.2b. The four minerals actually occupy corners of a composition volume in ACFM space and may occur as a stable assemblage over a certain P–T interval. The reaction formulated above is thus a continuous reaction. Another effect of the  $MgFe_{-1}$  projection is that Fe- and Mg-endmembers of a given mineral species project to identical positions (and of course any intermediate  $X_{Fe}$  composition of that mineral as well, e.g. Prp and Alm garnet). The consequences of the  $MgFe_{-1}$  projection on ACF diagrams must always be kept in mind.

About 3 wt% of  $Na_2O$  is present in typical basalts (Table 2.3) and Na-bearing minerals such as Pl, Na–Am, Na–Cpx and Na–mica, are important in metamafic rocks. If one wants to represent sodic phases on ACF diagrams, the ACF triangle of Fig. 9.2a requires expanding to a tetrahedron with  $NaAlO_2$  as an additional apex. At this apex plot the compositions of Ab, Jd and Anl (Qtz,  $H_2O$  projection). In a similar fashion, Kfs will plot at the  $KAlO_2$  apex of an analogous K-tetrahedron. End member Pg and Ms project onto the AN and AK binary, respectively. All Pl compositions project onto the ACN ternary as the compositional variation of Pl is mainly related to the  $NaSiAl_{-1}Ca_{-1}$  exchange that relates Ab and An in Fig. 9.2a. The same exchange component can also be found in, for example, Am, Cpx and Mrg. End member Cel, Gln and Phl (Bt) project onto the MN- and MK binary, respectively. The micas and amphiboles also show strong P–T- and assemblage-dependent compositional variations along the  $MgSiAl_{-1}Al_{-1}$ -exchange direction. This Ts-exchange is parallel to the AM–(AF)binary. Phengite projects onto the AMN- (AFN) ternary and the solid solution series connects Ms and Cel. Sodic phases are often depicted on ACF diagrams by projecting from the  $NaAlO_2$  apex of the ACFN tetrahedron onto the ACF triangle. This means that Ab, Jd, Anl

(whatever is stable at the P and T of the diagram) is present as an extra mineral or that the chemical potentials of these phase components is fixed. It can be seen in Fig. 9.2a that Ab cannot be shown on ACF diagrams and that any Ca-bearing plagioclase will plot at the An position. This means that the consequences of the Pl composition on phase relationships in metamafic rocks cannot be analyzed on ACF diagrams. Muscovite and Pg will project to the A apex of ACF diagrams, whereas, Phe will occupy the entire AF-binary when projected from Kfs (Ab). However, as Kfs is very rare in metamafics, Kfs projections are not usually used. In analogy to AFM diagrams, one may project from the white micas rather than from the feldspar components, particularly for blueschist facies mafic rocks. In this case, the feldspars do not project onto the ACF plane with the exception of An and neither does Phe, whereas Gln projects onto the AF binary with a negative A coordinate, like Bt projected from Ms (Fig. 9.2a, b). In metamafic rocks, only one of the K-micas, Phe or Bt, is generally present, which means that the small amount of  $K_2O$  present can be ignored. One may also choose to project from Ab (Jd) and Ms. The consequences of the large number of alternatives can be understood by a careful consideration of Fig. 9.2a. Also note that not all possible compositional variations of minerals are shown in Fig. 9.2a (e.g. Jd–Di solid solution). Whatever projection is preferred, it is important to specify the projections on any phase diagrams constructed.

Another complication when dealing with metamafic rocks is the fact that they tend to be much more oxidized than, for example, metapelites. Redox reactions that involve phase components with ferric iron are common and important. Notably, in Grt (Adr-component), Am (e.g. riebeckite- and crossite-components) and Cpx (e.g. Ac-component) a considerable amount of the total iron is usually present as  $Fe_2O_3$ . Also, considerable substitution of  $Fe_2O_3$  for  $Al_2O_3$  occurs in most of the low-grade Ca–Al hydrosilicates such as Prh and Ep. The presence of Ep in particular always signifies the presence of  $Fe^{3+}$ . Magnetite is a widespread oxide phase in metamafics as is ilmenite, and sometimes hematite in very oxidized rocks. A separate treatment of REDOX reactions will not be given in this book but one of the effects of variable  $Fe^{3+}/Fe^{2+}$  ratios in minerals is a further increase of the variance of the considered assemblages. Consequently, the assemblages can occur over a wider P–T range compared to the situation where all, or most of the iron is present as  $Fe^{2+}$ . One may also construct ACF diagrams for a fixed oxygen activity. For instance, the coexistence of Hem and Mag in a rock at a particular P and T will fix  $a_{O_2}$  (as discussed in Sect. 3.6.2.4) and the conditions will be rather oxidizing with a significant amount of the total iron of the rock present as  $Fe^{3+}$ . The effects on mineral stabilities and compositions can be related, to a large extent, to the  $Fe^{3+}Al_{-1}$  exchange which forms, for example, Ep from Czo, Mag from Hc and Rbk from Gln. By considering ACF projections as projections parallel to the  $Fe^{3+}Al_{-1}$  exchange vector, important minerals in metamafics such as Ep, grandite (Ca– $Fe^{3+}$ ) Grt, Mag and crossite can be represented. Note that Mag does not project to the F apex but to the same projection point as Hc and Mg–Al Spl.

Carbonates are widespread and abundant in low-grade metamafics. Fe-bearing Cal and Ank (Dol) are predominant. Carbonates are also often present in high-grade



rocks. Carbonates can be represented on ACF diagrams as explained above. However, any reactions that involve carbonates are in general mixed volatile reactions and must be analyzed accordingly (see Chaps. 3, 6 and 8). The presence of significant  $\text{CO}_2$  in an aqueous fluid phase also has effects on pure dehydration reactions that do not involve carbonate minerals (Chap. 3). Compared with pure  $\text{H}_2\text{O}$  fluids, in  $\text{CO}_2$ -rich fluids hydrates (e.g. Chl, Am) may also break down at much lower  $T$  in rocks that do not contain carbonates.

Basalts also contain  $\text{TiO}_2$  in the percentage range that usually occurs in one major Ti-phase, i.e. Ttn, Ilm or Rt. If two of these minerals are present, Ti-balanced reactions may be useful for  $P$ - $T$  estimates, e.g.  $\text{Ky} + 3 \text{Ilm} + 2 \text{Qtz} = 3 \text{Rt} + \text{Grt}$ . Titanium is also present in significant amounts in silicates such as Bt, Am and Grt, with unavoidable consequences for solution properties and equilibrium conditions of reactions.

In conclusion, the composition of metamafic rocks is complex and minerals that typically occur in the assemblages show extensive chemical variation along several exchange directions. This makes comprehensive graphical analysis of phase relationships in metamorphic mafic rocks difficult. The complex chemical variation of solid-solution minerals can be simplified for graphical analysis by projecting parallel to some of the exchange components but the choice of projection depends entirely on the problem one wants to solve and the kind of rocks one is working with. For many metamafic rocks, it turns out that a very advantageous and powerful projection can be made from  $\text{SiO}_2$ ,  $\text{NaAlO}_2$ ,  $\text{H}_2\text{O}$  and  $\text{CO}_2$ , parallel to  $\text{MgFe}_{-1}$  and  $\text{Fe}^{3+}\text{Al}_{-1}$  onto the  $\text{Al}_2\text{O}_3$ - $\text{CaO}$ - $\text{FeO}$ -mole fraction triangle. This ACF projection will be used below.

The chemical complexity of mafic rocks also makes it difficult to discuss phase relationships by means of chemical subsystems and comprehensive petrogenetic grids and phase diagrams in  $P$ - $T$  space (as for example such as those used in previous chapters). Note, however, that although the complexity of mafic rocks can be quantitatively analyzed, this must be done individually for each given suite of rocks. The presentation below is thus mainly a discussion of the ACF system and MORB composition with some important reactions discussed separately where necessary.

## 9.2 Overview of Metamorphism of Mafic Rocks

The best overview of the metamorphism of mafic rocks can be gained from the metamorphic facies scheme shown in Fig. 4.3. As the characteristic assemblages in metabasalts are used for the definition of metamorphic facies they serve as a reference frame for all other rock compositions and metamafic rock mineral assemblages that are diagnostic for different facies are given in Chap. 4. From Fig. 4.3 it is evident that basalt undergoing prograde metamorphism along a Ky- or Sil-type prograde path will first produce diagnostic assemblages of the subgreenschist facies,

followed by greenschist, amphibolite and finally end up as a mafic granulite. High-P/low-T metamorphism (HPLT metamorphism) transforms basalt into blueschist and then to eclogite. Any geologic process that transports mafic rocks to great depth (>50 km) will result in the formation of eclogite. In contact metamorphism (LPHT metamorphism), basalts are converted to mafic hornfelses. Partial melting of H<sub>2</sub>O-saturated metamafics begins at temperatures significantly higher than for metagranitoids, metapsammites and metapelites, e.g. ~850–700°C between 200 and 700 MPa, respectively.

Prograde metamorphism of mafic rocks produces sequences of mineral zones that can be compared with mineral zones defined by metapelite minerals such as the example from the low-P northern Michigan terrane shown in Fig. 9.3. The metapelites contain Ms and Qtz throughout with And or Sil as the Al-silicates.

Metamorphic facies	Greenschist		Amphibolite		
	Chlorite	Biotite	Garnet	Staurolite	Sillimanite
<b>Mineral zoning</b>					
<b>Metamafites</b>					
Albite	—————	-----			
Albite-oligoclase		-----	—————		
Oligoclase-andesine			—————	—————	
Andesine				—————	—————
Epidote	—————	—————	—————		
Actinolite	—————	—————			—————
Hornblende		—————		—————	—————
Chlorite	—————	—————			
Calcite	-----	—————			
Biotite		—————		—————	-----
Muscovite	-----	-----	-----	-----	-----
Quartz	-----	-----	-----	-----	-----
<b>Metapelites</b>					
Chlorite	—————	-----			
Muscovite	—————	—————			
Biotite		—————	—————		
Garnet			—————		
Staurolite				—————	-----
Alumosilicate				—————	—————
Chloritoid	-----	-----			
Plagioclase	—————	—————	—————	—————	
Quartz	—————	—————	—————	—————	—————

**Fig. 9.3** Progressive mineral changes in metamafic and metapelitic rocks of northern Michigan (After James 1955)

The corresponding prograde mineral zonation in metabasites shows a series of features that are very characteristic of metamafic rocks.

- There are very few different mineral species present in metamafic rocks. The greenschist facies rocks contain:  $Ab + Chl + Act + Ep \Rightarrow$  greenschist. In the amphibolite facies, the minerals are:  $Pl (>An_{17}) + Hbl \pm Bt \pm Ep \Rightarrow$  amphibolite.
- Most minerals occur in many of the mineral zones defined by metapelites.
- The characteristic prograde changes in metabasites relate to the compositions of plagioclase and amphibole.
- Plagioclase systematically changes its composition from Ab at low grade to more calcic plagioclase (andesine). The transition from albite to oligoclase is abrupt and marks a sharp mapable boundary in the field. The discontinuous nature is caused by a miscibility gap in the plagioclase system as shown in Fig. 4.5a, b. This discontinuity can be used to define the greenschist–amphibolite facies boundary, which is clearly transitional and can be designated as a transitional facies (see Fig. 4.5a). Along a Ky-type path the oligoclase-in boundary coincides with the staurolite zone boundary that marks the beginning of the amphibolite facies in metapelites. In low-P metamorphism (e.g. Fig. 9.3), St occurs for the first time inside the amphibolite facies.
- Amphibole systematically changes its composition from Act at low grade to Na- and Al-bearing Hbl at higher grade (the Hbl color information in Fig. 9.3 relates to the changing mineral composition).
- Quartz is only occasionally present and hence, ACF diagrams must be used with care.
- Biotite is present as an extra K-bearing mineral from the greenschist to upper amphibolite facies and systematically changes its composition during prograde metamorphism, e.g. becomes more Ti and Mg-rich.
- Calcite is present in low-grade rocks but is used up by mixed volatile reactions during prograde metamorphism.

A comprehensive representation of the effects of metamorphism on mafic rocks is shown in Fig. 9.4. The figure depicts the characteristic assemblages in metabasalts in the form of ACF diagrams representative for the respective position in  $P$ – $T$  space. The ACF diagrams are arranged along three typical paths of prograde metamorphism and the  $9^\circ\text{C}/\text{km}$  geotherm limits the geologically accessible  $P$ – $T$  space. The Al-silicate phase relations are given for reference. The inset in the upper left corner shows the composition of typical mid-ocean ridge basalt ( $Pl + Cpx \pm Opx \pm Qtz$ ). Many metabasalts are expected to lie compositionally within the horizontally ruled field. Shown on the ACF diagrams in Fig. 9.4, assemblages that represent the approximate composition of MORB have been shaded. Metabasalts that have been strongly metasomatized during ocean-floor metamorphism may project to other compositions in the ACF diagram. In the following presentation, details of the phase relations in each of the represented ACF chemographies will be discussed separately.

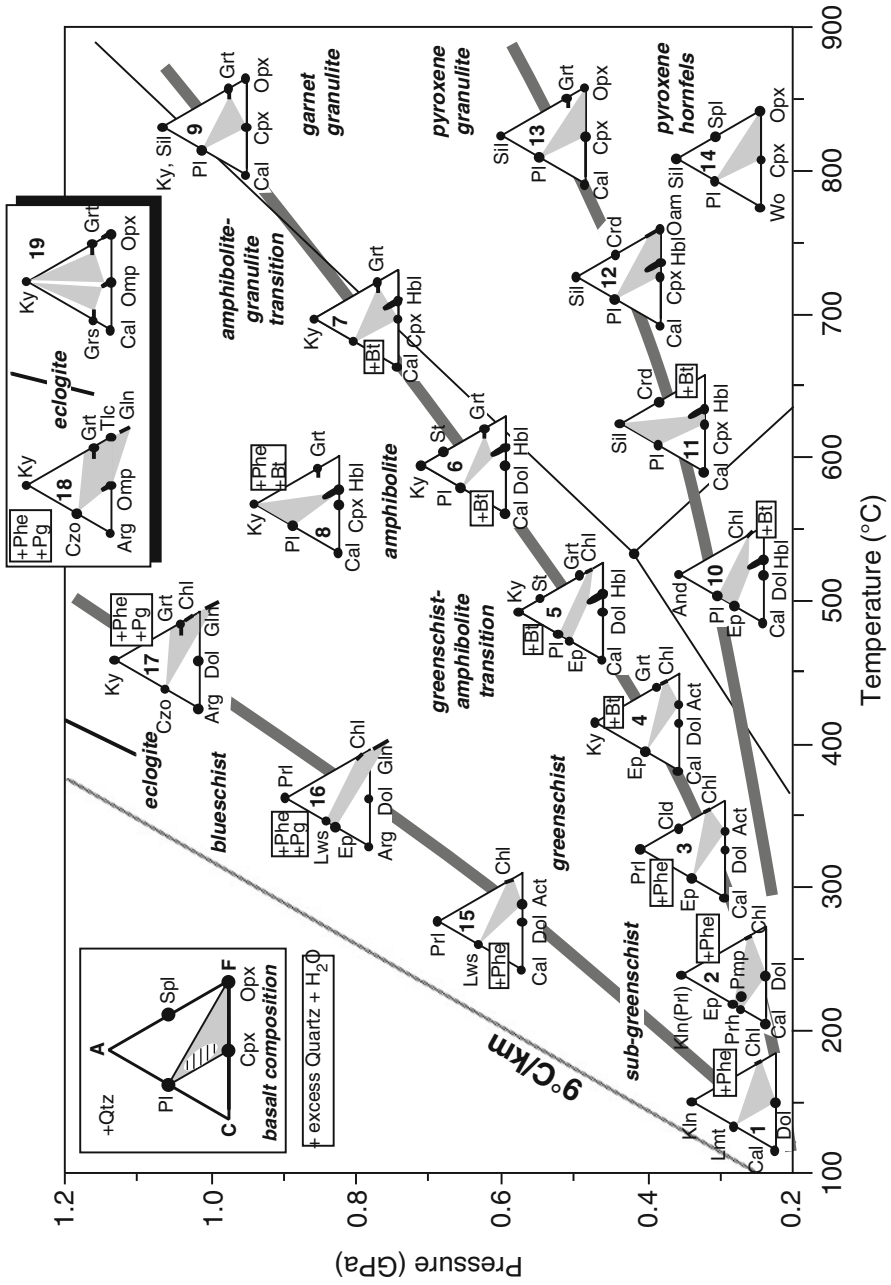
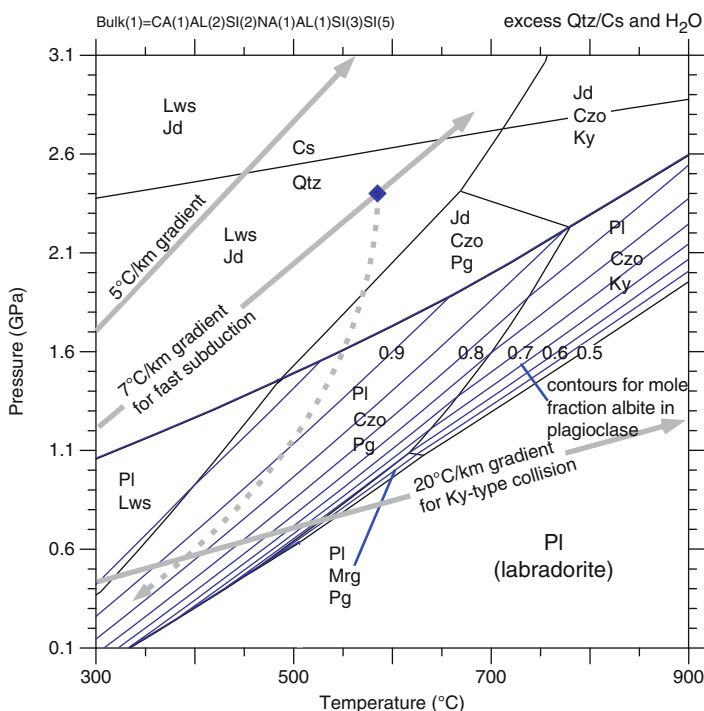


Fig. 9.4 Metamorphism of mafic rocks (metabasalts) represented by ACF diagrams

### 9.2.1 Plagioclase in Mafic Rocks, Equilibria in the Labradorite System (NCASH System)

Figure 9.5 depicts assemblage stabilities in the NCASH system, specifically for the composition of labradorite (1Ab + 1An). The composition represents the typical plagioclase of mafic igneous rocks such as basalts and gabbros. This composition and the model of Fig. 9.5 fully describe metamorphism of anorthosite and a large part of the behavior of basalts and gabbros. In the  $P$ – $T$  range of Fig. 9.5 plagioclase changes its composition systematically. In the lower right area of Fig. 9.5 Pl is a homogeneous solid solution of labradorite composition. With increasing pressure Pl becomes increasingly sodic and the An component of labradorite is transferred to other calcic minerals such as clinozoisite and margarite. In the  $T$ -range of the greenschist facies (300–500°C) and a given Barrovian  $Ky$ -type geotherm of 20°C/km the labradorite composition is represented by the assemblage albite–clinozoisite



**Fig. 9.5** Distribution of stable assemblages for the labradorite composition and excess Qtz and  $H_2O$ . Thin blue lines are mole fraction contours for the Ab-content of plagioclase. Three different geotherms are shown as gray lines. Blue diamond on the fast subduction geotherm is an arbitrary pressure (depth) of detachment from the slab followed by an exhumation path indicated by a dashed gray curve

(epidote)–paragonite–Qtz. As temperature approaches about 520°C plagioclase drastically increases its An-content and in a small T-interval near 530°C the stable assemblage is margarite–paragonite–andesine (Fig. 9.5). Above 550°C labradorite is stable.

Along a constant 7°C/km geotherm for fast subduction, the labradorite bulk composition will be represented by an albite–lawsonite assemblage at temperatures significantly below 300°C. At  $T > 300^\circ\text{C}$  jadeite is stable rather than albite (Fig. 9.5). Lws + Jd is the characteristic assemblage in very low-T and high-P metamorphism. At 650°C and 2.6 GPa the geotherm crosses the boundary to the coesite-stable field.

The considered labradorite-bearing material may detach from the subducting slab at the position indicated by an open diamond on the 7°C/km geotherm (2.4 GPa). From there it may follow a characteristic exhumation path along the subduction interface (indicated by a dashed arrow on Fig. 9.5). The typical path is described by an initial stage marked decompression (see Chap. 3). The consequence is that the HPLT assemblage Lws + Jd is replaced by Jd + Czo + Pg at 1.9 GPa [reaction (9.69), Table 9.2]. This dehydration reaction typically runs to completion and replaces all Lws by Czo + Pg. The latter mineral pair forms very commonly pseudomorph textures after Lws, indicating the former presence of the diagnostic HPLT minerals lawsonite in the rocks. Further decompression brings the rock back to the plagioclase present field of Fig. 9.5. The initial Pl so formed at 1.6 GPa along the dashed decompression path is rather pure albite.

Metamorphism along geotherms that reach high-P granulite facies condition produces the characteristic assemblage Czo + Ky and the plagioclase becomes more albitic with increasing pressure. Eclogite facies metamorphism creates the same assemblage Czo + Ky in the Pl-absent field of Fig. 9.5. The Czo + Ky is typical of high-T eclogites (see below).

## 9.3 Subgreenschist Facies Metamorphism

### 9.3.1 General Aspects

ACF chemographies #1 and #2 (Fig. 9.4) represent mineral assemblages typical of the subgreenschist facies of metamorphism. At very low grade, the characteristic assemblage includes Ab + Chl + carbonate + a variety of zeolites. On the ACF chemography #1, zeolite is typified by Lmt but any of the four zeolites listed in Table 9.1 would project to the same point. In addition, clay (e.g. smectite, Vrm) and “white mica” (Ill, Ser) may be present as well as Kln. At slightly higher grade (ACF chemography #2), zeolites are replaced by Prh, Pmp and Ep in a number of different combinations. Still Ab, Chl and carbonates are major minerals in prehnite–pumpellyite facies rocks. Pyrophyllite may be present instead of Kln. Zeolite-bearing metamafics indicate temperatures of 150–200°C or lower, and metabasalts with Prh and Pmp are characteristic for the temperature range 150–300°C.

Mineral zonation in metamafic rocks from the Tanzawa Mountains, central Japan, is shown in Fig. 9.6. The low-P Sil-type metamorphic terrain has been subdivided into five zones ranging from lower subgreenschist facies to amphibolite facies. The two lowest-grade zones are characterized by the presence of zeolites, low-T zeolites in zone I and high-T zeolites in zone II. Zone I zeolites are typically stilbite (Stb) and heulandite (Hul); Zone II zeolites are laumontite (Lmt) and wairakite (Wa). This is

Mineral zonation	zone I	zone II	zone III	zone IV	zone V
Clinoptililite	— — — —	X	X		
Stilbite	— — — —	X	X		
Heulandite	- — — —				
Mordenite	- - - - -				
Chabazite		X	X		
Laumontite		— — — —	X	X	X
Thompsonite		- - - - -			
Wairakite		— — — —			
Yugawaralite		— — — —			
Analcime		- - - - -	- - - - -		
Montm.-verm.	— — — —				
Verm.-chlorite	— — — —	- - - - -			
Chlorite		- - - - -	- - - - -	- - - - -	- - - - -
Sericite		- - - - -	- - - - -	- - - - -	- - - - -
Biotite			- - - - -	— — — —	— — — —
Pumpellyite			- — — —	- - - - -	
Prehnite			- — — —	- - - - -	
Epidote			- — — —	— — — —	- - - - -
Piemontite				- - - - -	- - - - -
Actinolite				— — — —	
Hornblende				— — — —	— — — —
Cummingtonite					- - - - -
Diopside					- - - — —
Ca-garnet					- - - — —
Plagioclase				An <sub>10</sub> An <sub>20</sub> An <sub>30</sub>	
Opalline silica	- - - -				
Quartz	— — — —				
Magnetite	— — — —			— — — —	- - - - -
Hematite	- - - - -			- - - - -	- - - - -
Pyrite	- - - - -			- - - - -	- - - - -
Calcite	- - - - -			- - - - -	- - - - -

**Fig. 9.6** Occurrence of some metamorphic minerals in metamafic rocks, Tanzawa Mountains, central Japan (After Seki et al. 1969). *Zone I* Stilbite (clinoptilolite)–vermiculite; *Zone II* Laumontite–“mixed layer”–chlorite; *Zone III* Pumpellyite–prehnite–chlorite; *Zone IV* Actinolite–greenschist; *Zone V* Amphibolite. × = only in veins. Map showing distribution of contact metamorphic zones surrounding quartz diorite below

understandable by reference to Table 9.1 where it can be seen that zone I zeolites clearly contain more crystal water (zeolite water) than zeolites of zone II. The transition from zone I to zone II is therefore related to dehydration reactions involving zeolites. For the same reason, it is also clear that Wa is typically the highest-T zeolite of prograde metamorphism. Analcite occurs sporadically in both zones and mixed-layer clays are typically present. Plagioclase is present in all zones with the composition of Ab in the zones I–IV. As the mafic protolith is SiO<sub>2</sub>-rich, quartz is present as an excess phase throughout (ACF diagrams). No zeolites survive in zone III, which is characterized by three new metamorphic minerals: Prh, Pmp and Ep. Also, Chl has transformed into a well-defined Fe–Mg sheet silicate. Sericite is sporadically present. Several zeolite- and Chl-consuming reactions are responsible for the generation of the new metamorphic minerals Prh, Pmp, and Ep. In zone IV, typical greenschist facies assemblages replace the zone III mineralogy. In particular, Pmp and Prh disappear and the characteristic greenschist facies mineral association Chl + Ep + Act + Ab ± Qtz becomes dominant. In zone V, close to the igneous contact, the minerals are diagnostic of the amphibolite facies. Calcic plagioclase and Hbl are dominant but Bt, Grt and Cpx may appear as well. In low-P terrains such as the Tanzawa Mountains, cummingtonite or other Fe–Mg amphiboles typically occur together with calcic amphibole (Hbl).

The Tanzawa mineral zonation is similar in many respects to that described from recent geothermal systems (<100,000 years old) such as the Nesjavellir geothermal field developed within a sequence of hyaloclastites, basalt flows, dykes and sills of the Hengill central volcano, Iceland. Although the system is now cooling, a highest subsurface T of > 380°C and structures indicate that ascending boiling water from a heat source (probably diorite as at Tanzawa) has mixed with descending cold ground water resulting in the formation of a systematic depth zonation of mineral assemblages ranging from zeolite to amphibolite facies grade in vesicles, veins and within the host basalt near zones of high permeability such as brecciated-vesiculated flow tops and fractures (Fig. 9.5). Noteworthy is the sequence of zeolite zonation with Lmt and Wa forming at the highest T of >120 and >200°C, respectively; the other zeolites forming below about 100°C. At shallow depths, smectite-type clay minerals occur. With depth they are replaced by interstratified smectite–chlorite at ~200°C, and finally Chl at 230–240°C. Unlike Tanzawa, Pmp is absent (as in ocean floor metamorphism); Prh appears at >200°C, Act at >280°C and Hbl at >350°C. Albite is the most common feldspar with oligoclase and andesine occurring at deeper levels.

Another well-documented example of prograde zeolite to amphibolite facies thermal metamorphism of metamorphic rocks is a >6 km-thick sequence of massive lava flows, pillow lava, breccia and tuff known as the Karmutsen Volcanics at Vancouver Island, British Columbia (Fig. 9.7a, b). Metamorphism occurred at 100–250 MPa and 250–550°C. The size of inferred equilibrium metamorphic mineral domains in the rocks is very small and relates to incipient replacement of igneous Cpx, Ca-plagioclase, with more extensive replacement of fine-grained mesostasis and glass. Vesicle (amygdules) assemblages are also considered to represent equilibrium domains and provide the best evidence of prograde metamorphism under subgreenschist facies conditions. The diagnostic calcite-free zeolite facies assemblage is Lmt + Pmp + Chl + Ep + Ab + Qtz + Ttn ± Prh. Prehnite–pumpellyite facies



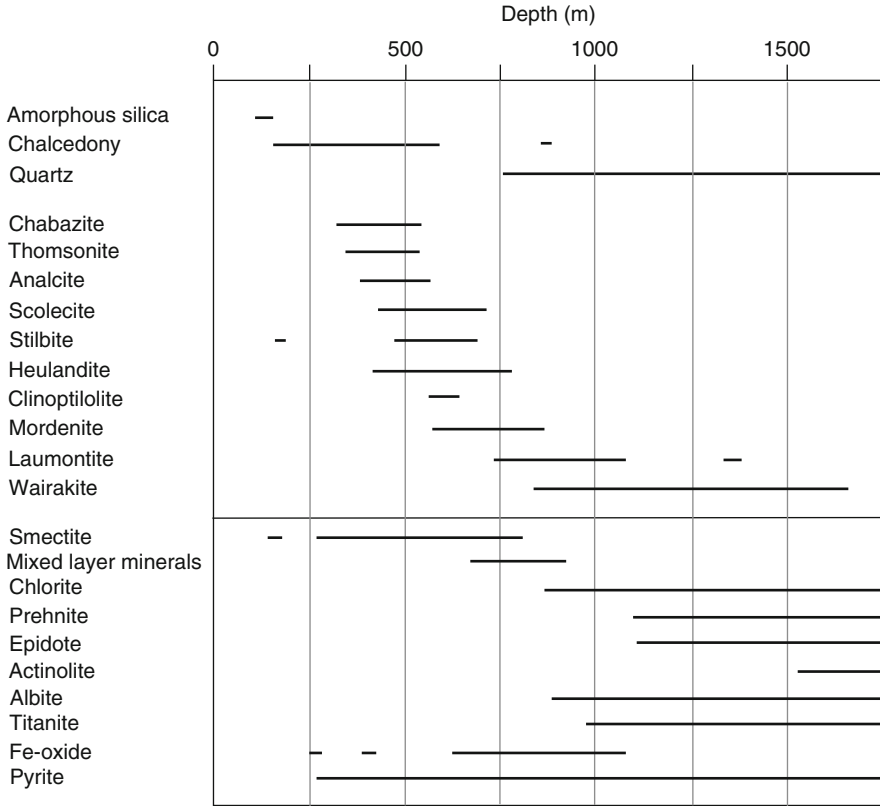


**Fig. 9.7** Hydrothermal mineral stabilities with depth in the Nesjavellir geothermal field, Iceland (well NJ-15) (Modified after Fig. 13. of Arnórsson 1995)

rocks are widespread and contain  $Ab + Chl + Pmp + Ttn + Mag \pm Qtz \pm Prh \pm Ep$  with trace  $Phe \pm hydro\text{-}Grt \pm Wa \pm Cal$ , and with vesicles (amygdules) containing  $Pmp + Chl \pm Ep \pm Prh \pm Qtz \pm K\text{-white mica} \pm Lmt \pm Wa$ . The prehnite–pumpellyite facies – greenschist facies transition is marked by the appearance of Act without Pmp and a narrow transition zone can be mapped where both Act + Pmp without Prh (and with  $Ab + Chl + Ep + Cal$ ) define a pumpellyite–actinolite zone (Fig. 9.7a, b).

### 9.3.2 Metamorphism in the CMASH and NCMASH Systems

Assemblage stabilities in the simple CMASH system in low-grade metamorphism are shown in Fig. 9.9 together with three different geothermal gradients. The stoichiometries of some of the reactions limiting the assemblage fields can be found in Table 9.2. The predicted sequence of Ca-zeolites in progressively metamorphosed metamafic rocks along a “very hot”  $>30^\circ\text{C}$  geotherm is: Stb, Hul, Lmt

**Table 9.2** Stoichiometries of reactions in mafic rocks

Subgreenschist facies	
CASH system (Fig. 9.8)	
Stb = Lws + 5Qtz + 5H <sub>2</sub> O	(9.1)
Lmt = Lws + 2Qtz + 2H <sub>2</sub> O	(9.2)
Stb = Lmt + 3Qtz + 3H <sub>2</sub> O	(9.3)
Stb = Hul + H <sub>2</sub> O	(9.4)
Hul = Lmt + 3Qtz + 2H <sub>2</sub> O	(9.5)
Hul = Wa + 3Qtz + 4H <sub>2</sub> O	(9.6)
Lmt = Wa + 2H <sub>2</sub> O	(9.7)
Wa = Lws + 2Qtz	(9.8)
Lws = An + 2H <sub>2</sub> O	(9.9)
Wa = An + 2Qtz + 2H <sub>2</sub> O	(9.10)
Stb + Grs = 2Prh + 4Qtz + 5H <sub>2</sub> O	(9.11)
2Prh = Lws + Grs + Qtz	(9.12)
5Prh = 2Czo + 2Grs + 3Qtz + 4H <sub>2</sub> O	(9.13)
5Lws + Grs = 4Czo + Qtz + 8H <sub>2</sub> O	(9.14)
2Lws + Prh = 2Czo + Qtz + 4H <sub>2</sub> O	(9.15)
Prh + 2Lmt = 2Czo + 5Qtz + 8H <sub>2</sub> O	(9.16)
Prh + 2Wa = 2Czo + 5Qtz + 4H <sub>2</sub> O	(9.17)
NCMASH system (Fig. 9.9)	
4Hul + Tr = 3Prh + Chl + 24Qtz + 18H <sub>2</sub> O	(9.18)
4Lmt + Tr = 3Prh + Chl + 12Qtz + 10H <sub>2</sub> O	(9.19)
20Pmp + 3Tr + 6Qtz = 43Prh + 7Chl + 2H <sub>2</sub> O	(9.20)
86Lmt + 17Tr = 30Pmp + 11Chl + 267Qtz + 212H <sub>2</sub> O	(9.21)
86Lws + 17Tr = 30Pmp + 11Chl + 95Qtz + 40H <sub>2</sub> O	(9.22)
5Pmp + 3Qtz = 7Prh + 3Czo + Chl + 5H <sub>2</sub> O	(9.23)
6Lmt + 17Prh + 2Chl = 10Pmp + 21Qtz + 14H <sub>2</sub> O	(9.24)
14Lmt + 5Pmp = 17Czo + Chl + 32Qtz + 61H <sub>2</sub> O	(9.25)
86Stb + 17Tr = 30Pmp + 11Chl + 525Qtz + 470H <sub>2</sub> O	(9.26)
Subgreenschist to greenschist facies transition	
Essential reactions	
5Prh + Chl + 2Qtz = 4Czo + Tr + 6H <sub>2</sub> O	(9.27)
25Pmp + 2Chl + 29Qtz = 7Tr + 43Czo + 67H <sub>2</sub> O	(9.28)
Additional reactions	
4Wa + Ab = Pg + 2Czo + 10Qtz + 6H <sub>2</sub> O	(9.29)
4Lws + Ab = Pg + 2Czo + 2Qtz + 6H <sub>2</sub> O	(9.30)
14Lws + 5Pmp = 17Czo + Chl + 4Qtz + 33H <sub>2</sub> O	(9.31)
4Lmt + Ab = Pg + 2Czo + 10Qtz + 14H <sub>2</sub> O	(9.32)
Reactions involving carbonates (examples)	
3Chl + 10Cal + 21Qtz = 2Czo + 3Tr + 10CO <sub>2</sub> + 8H <sub>2</sub> O	(9.33)
15Pmp + 9Qtz + 4CO <sub>2</sub> = 4Cal + 25Czo + 3Tr + 37H <sub>2</sub> O	(9.34)
Greenschist facies	
CMASH reactions	
2Czo + 5Prl = 4Mrg + 18Qtz + 2H <sub>2</sub> O	(9.35)
Mrg + 2Qtz + 2Czo = 5An + 2H <sub>2</sub> O	(9.36)
Mrg + Qtz = An + And + H <sub>2</sub> O	(9.37)
4Mrg + 3Qtz = 2Czo + 5Ky + 3H <sub>2</sub> O	(9.38)
2Chl + 2Czo + 2Qtz = 2Tr + 5Ky + 7H <sub>2</sub> O	(9.39)
6Czo + 7Qtz + Chl = 10An + Tr + 6H <sub>2</sub> O	(9.40)
2An + Chl + 4Qtz = Tr + 3Sil + 3H <sub>2</sub> O	(9.41)
Example of reaction producing Tschermak (Ts) component	
7Chl + 14Qtz + 12Czo = 12Tr + 25TS(Al <sub>1</sub> Al <sub>1</sub> Si <sub>-1</sub> Mg <sub>-1</sub> ) + 22H <sub>2</sub> O	(9.42)

*(continued)*

**Table 9.2** (continued)

<b>Greenschist facies</b>	
Mica-involving reactions	
$16\text{Tr} + 25\text{Ms} = 25\text{Phl} + 16\text{Czo} + 1\text{Chl} + 77\text{Qtz} + 4\text{H}_2\text{O}$	(9.43)
$4\text{Tr} + 6\text{Chl} + 25\text{Cel} = 25\text{Phl} + 4\text{Czo} + 63\text{Qtz} + 26\text{H}_2\text{O}$	(9.44)
$1\text{Chl} + 4\text{Cel} = 3\text{Phl} + 1\text{Ms} + 7\text{Qtz} + 4\text{H}_2\text{O}$	(9.45)
$2\text{Chl} + 2\text{Czo} + 5\text{Ab} + 4\text{Qtz} = 2\text{Tr} + 5\text{Pg} + 2\text{H}_2\text{O}$	(9.46)
Carbonate-involving reaction (examples)	
$1\text{Ms} + 3\text{Qtz} + 8\text{Dol} + 4\text{H}_2\text{O} = 1\text{Phl} + 1\text{Chl} + 8\text{Cal} + 8\text{CO}_2$	(9.47)
$9\text{Tr} + 2\text{Cal} + 15\text{Ms} = 15\text{Phl} + 10\text{Czo} + 42\text{Qtz} + 2\text{CO}_2 + 4\text{H}_2\text{O}$	(9.48)
$19\text{Cal} + 3\text{Chl} + 11\text{CO}_2 = 15\text{Dol} + 2\text{Czo} + 3\text{Qtz} + 11\text{H}_2\text{O}$	(9.49)
<b>Greenschist-amphibolite facies transition</b>	
$4\text{Chl} + 18\text{Czo} + 21\text{Qtz} = 5\text{Ts} - \text{amphibole} + 26\text{An} + 20\text{H}_2\text{O}$	(9.50)
$7\text{Chl} + 13\text{Tr} + 12\text{Czo} + 14\text{Qtz} = 25\text{Ts} - \text{amphibole} + 22\text{H}_2\text{O}$	(9.51)
$\text{Ab} + \text{Tr} = \text{Ed} + 4\text{Qtz}$	(9.52)
$12\text{Czo} + 15\text{Chl} + 18\text{Qtz} = 8\text{Gr} + 25\text{Prp} + 66\text{H}_2\text{O}$	(9.53)
<b>Amphibolite facies</b>	
$4\text{Tr} + 3\text{An} = 3\text{Prp} + 11\text{Di} + 7\text{Qtz} + 4\text{H}_2\text{O}$	(9.54)
$1\text{Ts} - \text{amphibole} + 6\text{Czo} + 3\text{Qtz} = 10\text{An} + 4\text{Di} + 4\text{H}_2\text{O}$	(9.55)
$3\text{Ts} - \text{amphibole} + 7\text{Ky} = 6\text{An} + 4\text{Prp} + 4\text{Qtz} + 3\text{H}_2\text{O}$	(9.56)
$7\text{Ts} - \text{amphibole} + 7\text{Sil} + 4\text{Qtz} = 14\text{An} + 4\text{Ath} + 3\text{H}_2\text{O}$	(9.57)
$7\text{Tr} = 3\text{Ath} + 14\text{Di} + 4\text{Qtz} + 4\text{H}_2\text{O}$	(9.58)
<b>Amphibolite-granulite facies transition</b>	
$\text{Tr} = 2\text{Cpx} + 3\text{Opx} + \text{Qtz} + \text{H}_2\text{O}$	(9.59)
$\text{Ts} = \text{Cpx} + 3\text{Opx} + \text{An} + \text{H}_2\text{O}$	(9.60)
$\text{Tr} + 7\text{Gr} = 27\text{Cpx} + \text{Prp} + 6\text{An} + \text{H}_2\text{O}$	(9.61)
$\text{Tr} + \text{Gr} = 4\text{Cpx} + \text{Opx} + \text{An} + \text{H}_2\text{O}$	(9.62)
<b>Granulite facies</b>	
$4\text{En} + 1\text{An} = 1\text{Di} + 1\text{Qtz} + 1\text{Prp}$	(9.63)
<b>Blueschist facies</b>	
$\text{Tr} + 10\text{Ab} + 2\text{Chl} = 2\text{Lws} + 5\text{Gln}$	(9.64)
$6\text{Tr} + 50\text{Ab} + 9\text{Chl} = 25\text{Gln} + 6\text{Czo} + 7\text{Qtz} + 14\text{H}_2\text{O}$	(9.65)
$13\text{Ab} + 3\text{Chl} + 1\text{Qtz} = 5\text{Gln} + 3\text{Pg} + 4\text{H}_2\text{O}$	(9.66)
$12\text{Lws} + 1\text{Gln} = 2\text{Pg} + 1\text{Prp} + 6\text{Czo} + 5\text{Qtz} + 20\text{H}_2\text{O}$	(9.67)
$4\text{Pg} + 9\text{Chl} + 16\text{Qtz} = 2\text{Gln} + 13\text{Prp} + 38\text{H}_2\text{O}$	(9.68)
$4\text{Lws} + 1\text{Jd} = 2\text{Czo} + 1\text{Pg} + 1\text{Qtz} + 6\text{H}_2\text{O}$	(9.69)
<b>Blueschist-eclogite facies transition</b>	
$\text{Jd} + \text{Qtz} = \text{Ab}$	(9.70)
$1\text{Gln} + 1\text{Pg} = 1\text{Prp} + 3\text{Jd} + 2\text{Qtz} + 2\text{H}_2\text{O}$	(9.71)
<b>Granulite- and amphibolite-eclogite facies transition</b>	
$\text{CaTs} + \text{Qtz} = \text{An}$	(9.72)
$2\text{Czo} + \text{Ky} + \text{Qtz} = 4\text{An} + \text{H}_2\text{O}$	(9.73)
$1\text{Gr} + 2\text{Ky} + 1\text{Qtz} = 3\text{An}$	(9.74)
$4\text{Tr} + 3\text{An} = 3\text{Prp} + 11\text{Di} + 7\text{Qtz} + 4\text{H}_2\text{O}$	(9.75)
$4\text{En} + 1\text{An} = 1\text{Prp} + 1\text{Di} + 1\text{Qtz}$	(9.76)
$3\text{Di} + 3\text{An} = 1\text{Prp} + 2\text{Gr} + 3\text{Qtz}$	(9.77)
$1\text{An} + 2\text{Di} = 2\text{En} + 1\text{Gr} + 1\text{Qtz}$	(9.78)

*(continued)*

**Table 9.2** (continued)

Granulite- and amphibolite-eclogite facies transition

Eclogite facies

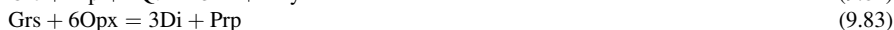
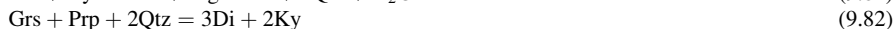
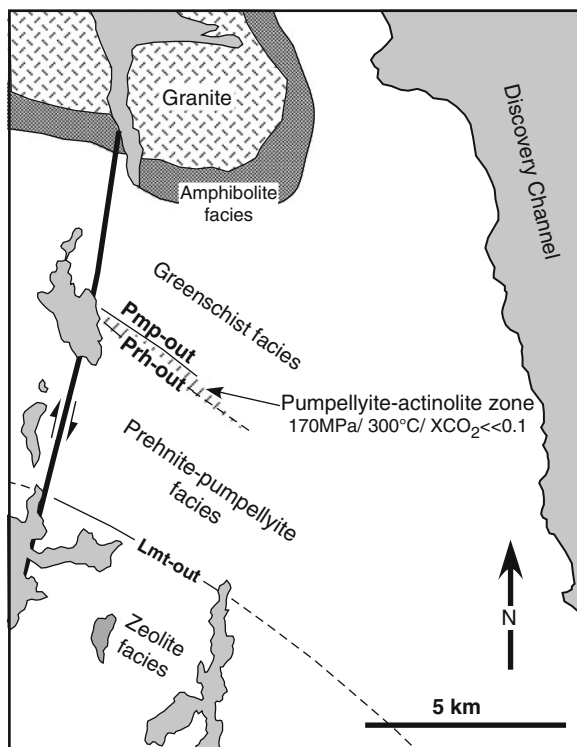


**Fig. 9.8** Map showing distribution of facies and pumpellyite–actinolite zone in metamorphosed Karmutsen Volcanics, Vancouver Island, British Columbia (After Fig. 1 of Cho and Liou 1987; Fig. 1. of Liou et al. 1985 and Fig. 1 of Kuniyoshi and Liou (1976))



and Wa. This sequence is clearly consistent with the sequence of observed mineral zones in the Tanzawa Mountains shown in Fig. 9.6. This sequence with wairakite as the highest-T zeolite is characteristic for “hot” geothermal environments (geothermal fields, young volcanic areas). Wairakite disappears from the rocks at about 340°C (Fig. 9.9) and is replaced by the greenschist facies assemblage Chl–Act (Tr)–Ab–Qtz. In CFMASH rocks Tr is Act and Chl is Fe–Mg chlorite but the assemblages do not shift significantly with Fe as an additional component. Pumpellyite is lacking in hydrothermal hot geothermal sequences (Fig. 9.9). In areas characterized by still “hot” 30°C/km gradients the zeolite sequence is: Stb–(Hul)–Lmt but Wairakite does not appear (Fig. 9.9). The zeolite Lmt is

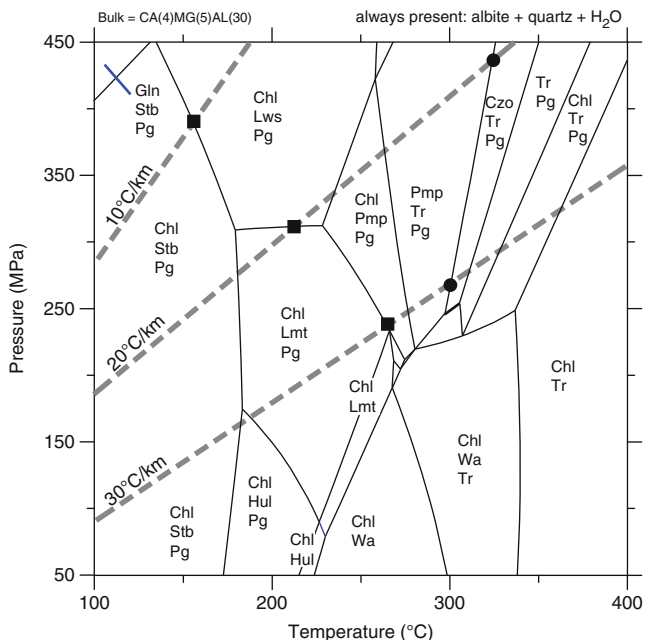


**Fig. 9.9** Low-grade metamorphism of metamafic rocks containing Ab and Qtz in excess. Three type-geotherms are shown as *dashed lines*. Upper T-limit of zeolite indicated by *black squares*, beginning of greenschist facies marked by *black circles*

replaced by pumpellyite at about 270°C (black square on dashed 30°C/km gradient) defining the zeolite–pumpellyite facies boundary. At 300°C (black circle) pumpellyite is replaced upgrade by Czo and Tr that form, together with excess albite, the characteristic assemblage of the greenschist facies. Along “cooler” gradients, the zeolite facies grades into the pumpellyite facies at lower temperatures. At close to 20°C/km the facies transition occurs at about 220°C and the transition to the greenschist facies is located at T close to 325°C. Along “cool” geotherms the pumpellyite facies is lacking. Zeolite assemblages are replaced by lawsonite assemblages. The low-pressure limit of lawsonite assemblages on Fig. 9.9 is near 300 MPa. Along a fast subduction geotherm of 10°C/km stilbite decomposes to lawsonite at T as low as 170°C. The lawsonite assemblages are characteristic for very “cool” low-T high-P geotherms. They finally grade into blueschist facies and finally eclogite facies assemblages (see below).

Below follows a brief discussion of the typical  $P$ – $T$  conditions under which some diagnostic index minerals may form and subsequently decompose during prograde metamorphism of metamafic rocks. The discussion is based on Fig. 9.9 with reaction stoichiometries given in Table 9.2.

**Analcite** (Anl) is commonly found in quartz-bearing diagenetic and low-grade metamorphic rocks. The Anl–Qtz assemblage, along with stilbite (Stb) + Qtz, can be used as an indicator of the initial stage of zeolite facies metamorphism. In the

NASH model system, Anl decomposes in the presence of Qtz to Ab according to the reaction:  $\text{Anl} + \text{Qtz} = \text{Ab} + \text{H}_2\text{O}$  (reaction is not listed in Table 9.2). The equilibrium conditions of the Anl breakdown reaction very nearly coincide with the three reactions that limit the Stb field towards higher temperature in Fig. 9.9 [reactions (9.1), (9.2), (9.3) in Table 9.2]. In order to avoid overcrowding, the Anl reaction has not been shown in Fig. 9.9. Natural Anl often shows extensive solid solution with Wa, thus expanding its stability field to higher T. This has the consequence that the  $P$ - $T$  fields of Anl and Hul overlap.

**Stilbite**, a widespread zeolite mineral, it dehydrates to Hul, Lmt or Lws with increasing T and successively higher P in the CASH model system (Fig. 9.9). However, Stb is occasionally associated with Hul and/or Lmt, e.g. geothermal areas in Iceland (Fig. 9.7). Although little is known about the composition of Stb in low-grade metamorphic rocks, this association may result from solid solution effects. In Alpine fissures Stb may occur together with Lmt and Hul but it always texturally younger than the other zeolites and forms during postorogenic cooling as the latest and “coldest” zeolite.

**Heulandite** is one of the most common zeolites besides Stb and Lmt. In Fig. 9.9, its stability field is located at temperatures around 200°C and at pressures below 200 MPa; and limited by the stability fields of three other zeolites, i.e. Stb towards low-T, Wa towards high-T, and Lmt towards high- $P$ - $T$ . Heulandite and Lmt appear to be equally abundant in ocean-floor thermal, hydrothermal, and burial metamorphism. Laumontite, but not Hul, has been described from subduction zone metamorphism, e.g. from the metabasaltic rocks of the Franciscan terrane, California, and the Sanbagawa Belt, Japan (see Liou et al. 1987 for a summary). This may indicate that Hul is a low- $P$  zeolite consistent with the topology shown in Fig. 9.9.

Natural Hul commonly contains Na or K or both substituting for Ca, and its chemical composition may extend to those of clinoptilolite and alkali-clinoptilolite. This effect, together with other variables (e.g. pore-fluid chemistry), may explain the considerable overlap between the stability regions of Hul and other zeolites (see Fig. 9.7).

**Laumontite** is widespread in ocean-floor, burial, and subduction zone metamorphism. In Fig. 9.9, its field of stable occurrence is limited by five univariant reactions. With increasing T, Lmt is formed from Hul at lower P and from Stb at higher P. The upper P limit of Lmt with respect to Lws is about 300 MPa, and the upper T limit with respect to Wa and Ep (Czo) is about 230–260°C. Compositionally, Lmt is near the ideal composition,  $\text{CaAl}_2\text{Si}_4\text{O}_{12} \cdot 4\text{H}_2\text{O}$ , but solid solution in Hul and Wa will allow the coexistence of Lmt + Hul and Lmt + Wa.

The presence of Lmt is often taken to indicate low-grade metamorphic conditions, and thus its lower thermal stability limit is of interest. In the CASH model system, this limit is about 180°C. From field evidence, however, it has been inferred that Lmt could have formed at temperatures as low as 50–100°C (e.g. Boles and Coombs 1975).

In Alpine fissures Lmt is very common, although rarely observed in surface outcrops because of its susceptibility to fast decay if exposed to the atmosphere. However, laumontite is the absolutely dominant zeolite in basement rocks found during tunnel constructions in the Alps where the fissure minerals have not been in contact with the atmosphere.

**Wairakite** is restricted to areas with high thermal gradients, including geothermal systems and areas with intrusive igneous bodies. In the CMASH model system, Wa is produced from Hul or Lmt at temperatures between 220°C and 260°C. As stated above, Wa has the highest thermal stability of any zeolite (Fig. 9.7) and, in the presence of excess Ab + Qtz, its upper thermal stability is between 220°C and 340°C. Wairakite also shows considerable solid solution with Anl that may explain the natural occurrence of Wa + Anl and Wa + Lmt (+ Ab + Qtz). It is remarkably absent from Alpine type orogenic belts.

**Lawsonite** is one of the most definitive of blueschist facies minerals.

**Pumpellyite** is a very common mineral in metamafics and is found in various associations in low-grade rocks (Fig. 9.1 and text). Pmp stability in Fig. 9.9 ranges from 220°C to 320°C at  $P > 300$  MPa. Reactions forming and consuming Pmp are listed in Table 9.2. In rocks that depart from the average meta-MORB, Pmp may occur over a much larger or much smaller  $P$ - $T$  interval. However, for all rock compositions the center of the Pmp stability fields clusters around 270°C  $\pm$  20°C and 400  $\pm$  200 MPa. Most Pmp-bearing rocks probably formed close to 250°C and at pressures of 300 MPa.

**Prehnite** occurs widespread in low-grade metamafic rocks as a part of the matrix assemblage but also very often in vesicles, veins and open fractures. Prh fields do not appear for the chosen bulk in Fig. 9.9. The assemblage prehnite + pumpellyite has been used to define a separate Prh-Pmp facies between the zeolite and the greenschist facies. However, it is evident from Fig. 9.9 and also from field occurrences that Prh rarely occurs in stable equilibrium with Pmp and thus the 2-phase assemblage is not well suited to define a metamorphic facies. It is in contrast manifest from Fig. 9.9 that Pmp-involving assemblages may occur characteristically in the T-range between zeolite-bearing rocks and greenschist facies rocks. Pmp assemblages may, however, be absent at very high- and very low-T geotherms (Fig. 9.9).

### 9.3.3 Transition to Greenschist Facies

The transition to the greenschist facies is marked by the first appearance of the diagnostic assemblage Act + Ep in the presence of Chl, Ab and Qtz. The assemblage is produced from Wa decomposition at low- $P$  (<200 MPa) and Pmp decomposition at higher  $P$  (>200 MPa). Both reactions [reactions (9.27) and (9.28)] produce the typical greenschist facies mineralogy at about 320°C  $\pm$  30°C. Along the characteristic prograde metamorphic paths (20 and 30°C/km), the occurrence of Act + Ep + Chl + Ab + Qtz without Pmp defines the beginning of the greenschist facies. The greenschist facies assemblage is shown on chemography #3 in Fig. 9.4. Chemography #3 also suggests that the greenschist facies assemblage may also form from Dol- or Cal-involving reactions [an example is reaction (9.33)]. As carbonates are present in many low-grade mafic rocks, these mixed volatile reactions are important in removing carbonate minerals at an early stage of prograde metamorphism in

connection with the formation of greenschist facies minerals. Typically, these reactions consume Chl and carbonate and produce Act + Ep and are maximum-type mixed volatile reactions (see Chap. 3). Note, however, that Pmp- and Prh-consuming reactions *produce* rather than consume carbonates. Reaction (9.34) is an example that limits Pmp formation in the presence of CO<sub>2</sub>-bearing fluids and produces the greenschist facies assemblage. Accordingly, if fluids contain CO<sub>2</sub>, greenschist facies assemblages may appear at lower T compared to pure H<sub>2</sub>O fluids.

At high P (e.g., along a low-T 10°C/km subduction geotherm), subgreenschist facies assemblages are replaced by assemblages diagnostic of blueschist facies conditions. These rocks contain Gln, Lws, Pg, Ep, and other minerals in various assemblages and will be discussed below.

## 9.4 Greenschist Facies Metamorphism

### 9.4.1 Introduction

Greenschist facies mafic rocks are, as the name suggests, green schists. The green color of greenschist results from the modal dominance of green minerals in the rocks notably Chl, Act, Ep and these minerals together with Ab ± Qtz are the most characteristic assemblage of greenschist as stated above. The term *greenschist* is exclusively reserved for schistose chlorite-rich rocks derived from mafic igneous rocks that were metamorphosed under greenschist facies conditions. Note, however, that Pmp + Ep + Chl schist or semi-schist of the subgreenschist facies are also green schists, though obviously not of greenschist facies grade. Schistose serpentinites may also be green schists of the greenschist facies, but they are not classified as greenschist.

Chemographies #3 and #4 (Fig. 9.4) represent the typical range of assemblages in the greenschist facies. In addition to the most important minerals named above, other phases such as Ms (Phe), Bt, Stp, Ttn, Cal, Mag or Hem can often be present in minor amounts. Greenschists have also commonly lost all relic structures from previous metamorphic and magmatic stages so that they are both mineralogically and structurally equilibrated.

### 9.4.2 Mineralogical Changes Within the Greenschist Facies

The difference between chemography #3 and #4 (Fig. 9.4) is the presence of Prl and Phe in the lower greenschist facies and of Ky and Bt in the upper greenschist facies. Phase relationships in the ASH system that covers changes at the A apex of ACF diagrams has been discussed in Chap. 7 and are shown in Fig. 7.2.

Inside the Chl–Ep–Act triangle of Fig. 9.4, there are also reactions that modify the typical greenschist facies assemblage. The processes are best explained by



using reaction (9.42) as an example. This reaction describes the production of the TS-component in Am and Chl and the Al-contents of both minerals change systematically (become more Al-rich) with increasing grade across the greenschist facies. The effect can be shown on ACF diagrams by a displacement of the Chl + Ep + Act triangle along the TS vector, but note that concurrent rotations of FM relationships cannot be displayed. AF relationships are complex and can be evaluated along the lines described in Chap. 7. Furthermore, REDOX reactions may change the composition of Ep and other Fe-bearing minerals.

### 9.4.2.1 Reactions Including Micas

Muscovite (K-white mica, sericite, phengite) is the most common K-bearing mineral in low-grade metamafic rocks and this is also true for the lower greenschist facies. However, in the middle of the greenschist facies (~400°C), Bt appears for the first time in metamafics replacing K-white mica. This is shown in Fig. 9.4 (chemographies #3 and #4). Biotite formation can be modeled by reaction (9.43), which involves all greenschist minerals and transfers Ms component to Phl component. The equilibrium of reaction (9.43) is close to 600°C in the pure KCMASH system and it is rather pressure insensitive. For real mineral compositions of greenschist facies rocks, the formation of Bt from reaction (9.43) takes place around 400°C. The color of the first Bt that appears during prograde metamorphism of mafic rocks is often green. This is an indication of high Fe<sup>3+</sup> and demonstrates the importance of REDOX reactions in low-grade metamafics (one must bear this in mind when calculating phase relationships involving Bt).

The production of Bt is a continuous process. The Bt-producing reaction (9.44) is similar to reaction (9.43) except that it consumes the celadonite (Cel) component in K-white mica in order to produce Bt and leaves behind a white mica that is closer to the Ms end-member composition. This is in accordance with field evidence that K-white mica becomes progressively depleted in the Cel-component and enriched in Ms-component along a Ky-type path of prograde metamorphism. The effect can also be understood by investigating reaction (9.45), where the Cel-component is consumed in white mica and Bt + Ms components are formed with prograde metamorphism.

Again, Bt forms in metamafics at about 400–450°C. K-white mica is typically celadonitic (Phe, Ser) in low-grade rocks and becomes more muscovitic (Ms) at the upper grade limit of the greenschist facies. The small amount of K<sub>2</sub>O in mafic rocks is usually bound in K-white mica below 400°C and in Bt at temperatures above 400°C, and there is little overlap of the two micas.

Paragonite occurs in greenschists at high-P. The equilibrium conditions of reaction (9.46) are extremely sensitive to small compositional variations in the protolith and the resulting metamorphic minerals. However, the typical Act + Pg assemblage forms, at pressures above about 600 MPa, and at this P its stability is insensitive to T.

### 9.4.2.2 Garnet, Stilpnomelane and Carbonate

**Garnet** may form in mafic schist from reactions very similar to those that form Grt in pelitic schist. The first Grt to form is manganiferous and contains only a small Grs-component. Garnet first appears in the higher-grade part of the greenschist facies at relatively high-P, but Grt (typically less Mn-rich) is not common in mafic rocks until amphibolite facies conditions are attained.

**Stilpnomelane** is a characteristic mineral in many low-grade mafic schists and, if present, is diagnostic of lower greenschist facies conditions (or blueschist facies). The brown color of this pleochroic mineral (the oxidized ferristilpnomelane variety) often resembles Bt under the microscope and can easily be mistaken for such. Stilpnomelane is replaced by green Bt at around 400°C and mafic rocks containing both Stp and Bt occur over a narrow temperature interval near this temperature.

**Carbonate** minerals such as Dol (Ank) and Cal are commonly present in greenschists and participate in many mixed volatile reactions that involve the characteristic greenschist facies silicates, Act, Chl and Ep. The reactions may also involve micas such as reaction (9.47) that replaces K-white mica by Bt in Dol- and Cal-bearing metamafic rocks. Another example is reaction (9.48) where the assemblage Act + Ms + Cal is replaced by Ep + Bt. Reaction (9.49) involves two carbonates in rocks containing Ep + Act. Some of the carbonate-involving reactions are also relevant for marbles (CMS-HC system) or for marly rocks and these have been discussed in Chaps. 6 and 8. There is, however, a great potential for obtaining useful information regarding fluid compositions in carbonate-bearing greenschists.

### 9.4.3 *Greenschist–Amphibolite Facies Transition*

Between about 450°C and 550°C depending on P, the greenschist facies assemblage experiences two basic mineralogical changes:

- Ab disappears and it is replaced by oligoclase (typically An<sub>17–20</sub>).
- Act takes up increasing amounts of Al and Na and is eventually replaced by Na-bearing aluminous Hbl.

The combined transformation results in the replacement of the Ab + Act pair by the Pl + Hbl pair. This transformation designates the transition from greenschist facies to amphibolite facies conditions. In orogenic metamorphism along a Ky-type prograde path, the greenschist-amphibolite facies transition occurs at temperatures at 500°C ± 50°C (400–500 MPa).

The An-component in Pl is produced by a series of continuous reactions. However, greenschist Ab does not continuously change its composition along the albite-anorthite binary. At upper greenschist facies conditions, the Pl solid-solution series is not continuous but rather shows a miscibility gap (the peristerite

gap) between Ab (up to An<sub>10</sub>) and oligoclase (An<sub>17</sub>). Because of the abrupt appearance of oligoclase due to the miscibility gap, the first appearance of plagioclase of An<sub>17</sub> can be used to define an *oligoclase-in isograd* in mafic as well as pelitic and psammitic schist and denotes the *lower grade limit* of the greenschist–amphibolite facies transition zone. With increasing grade, Ab and oligoclase coexist, with Ab becoming more Ca-rich and oligoclase becoming more Ab-rich defining the miscibility gap solvus until it closes with the disappearance of Ab. The disappearance of Ab also represents an isograd, the *Ab-out isograd* that marks the *upper grade limit* of the transition zone and the beginning of amphibolite facies conditions where oligoclase is the only plagioclase. Unfortunately, the oligoclase-in and albite-out isograds can only be determined by microscope examination. With high-T gradients of contact metamorphism, the transition from greenschist to amphibolite facies can be abrupt with only a narrow, or no transition zone containing coexisting albite and oligoclase, such as in the Karmutsen Volcanics (Fig. 9.8). In this case, an abrupt change from Ab (An<sub>0-4</sub>) to oligoclase (An<sub>20</sub>) occurs that reflects the peristerite composition gap. The systematic compositional changes in the Am solid-solution series are generally more continuous in nature (although an Act–Hbl miscibility gap also exists). Throughout the *T–P* range of the transition zone Act composition changes by: (1) taking up Ts-component produced by a series of continuous reactions, (2) incorporation of edenite (Ed)-component produced by Ab-consuming reactions, and, (3) the inevitable FM-exchange. Other effects are related to incorporation of Ti and REDOX reactions. The resulting single amphibole is a green tschermakitic to pargasitic hornblende that together with Pl constitutes, by definition, an amphibolite and defines the beginning of the amphibolite facies. Chemography #5 (Fig. 9.4) shows this new situation; Am has changed its composition along the TS-exchange direction and Pl appears on the ACF projections. The most important mineralogical changes within the greenschist–amphibolite transition can be related to three main reactions (Table 9.2). Reaction (9.50) consumes greenschist Ep and Chl and produces the An-component of Pl and Ts- component of Am. Although the reaction will eventually consume all Ep or all Chl, Chl-, and/or Ep-bearing amphibolites may be present in the lowest grade amphibolite facies. All three main minerals of the greenschist facies assemblage (Act, Chl, Ep) are consumed by reaction (9.51) to produce Ts-component in Am, and reaction (9.52) describes the formation of the Ed-component in amphibolite facies Hbl. Thus, the combined effect of the three reactions results in the gradual disappearance of Chl + Ep, increasing Ca-enrichment of Pl, and a systematic change in Am composition from Act to Hbl.

Garnet may also appear in metamafic rocks transitional to the amphibolite facies. Its formation, as in metapelitic and psammitic rocks, mainly occurs at the expense of Chl. Reaction (9.53) indicates that Chl contributes the Prp- (and Alm-) components and Ep produces the Grs- (and Adr) components in the Grt. The Mn (Sps)-component (higher in early-formed Grt) is also supplied by the breakdown of Chl or in some cases, from Ank decomposition. In metamafic rocks, Grt may appear at temperatures of 400–450°C, depending on P.

## 9.5 Amphibolite Facies Metamorphism

### 9.5.1 Introduction

The amphibolite facies is characterized by chemography #6, #7 and #8 (Fig. 9.4) and Pl and Hbl make up the bulk volume of amphibolitic metamafic rocks. Much smaller amounts of other silicate minerals include Qtz, Ep, Ms, Bt, Ttn, Grt, and Cpx. Calcite can be found in some amphibolites. Mineralogical changes within the amphibolite facies mostly result from continuous reactions that operate over wide a  $P$ - $T$  range. The main effect of these continuous reactions produces systematic variations in the compositions of Pl and Hbl, and decreasing amounts of Ep-Czo and Ms if they persist beyond greenschist facies conditions. Garnet becomes modally more important with increasing grade to form garnet amphibolites and Cpx appears at higher temperatures in the amphibolite facies.

In principle, given a MORB composition and the compositions of Pl and Hbl, the  $P$ - $T$  conditions of equilibration are uniquely defined. However, at present, experimental data do not permit a rigorous treatment of Pl-Hbl relationships. In particular, solution properties of amphiboles are still poorly known and few end-member phase components are well constrained. Surprisingly, the low- $T$  behavior of the plagioclase system is also not quantitatively known (e.g. quantitative thermodynamic description of the several miscibility gaps and structural transitions along the Ab-An binary at low  $T$ ). This remains true also for the 2011 edition of this book.

### 9.5.2 Mineralogical Changes Within the Amphibolite Facies

In prograde orogenic metamorphism of metabasalts, the rocks contain Hbl and Pl (oligoclase) at the beginning of the amphibolite facies ( $\sim 500^\circ\text{C}$ ) as explained in Sect. 9.4.3. In addition, amphibolites may still contain some Ep and/or Chl that has not been completely consumed by reactions that produced the An- and Ts-components in Pl and Hbl, respectively. Biotite may be present as well. The same continuous reactions that produced the amphibolite facies mineralogy initially continue to consume Chl and Ep within the lower grade part of the amphibolite facies until Chl eventually disappears at about  $550^\circ\text{C}$  and Ep is not typically found in amphibolites that were metamorphosed to  $\sim 600^\circ\text{C}$ . Some of the Ep- and Chl-consuming reactions produce Grt that, in general, becomes modally more important with increasing grade. Chemography #6 in Fig. 9.4 is characteristic for the middle grade part of the amphibolite facies at  $\sim 600^\circ\text{C}$ . Here, amphibolites are characterized by andesine and green Hbl  $\pm$  Grt  $\pm$  Bt. At still higher temperatures, chemography #7 indicates the appearance of Cpx of the Di-Hd series at  $\sim 650^\circ\text{C}$  (along a prograde Ky-path) [reaction (9.54)]. The reaction simultaneously produces Cpx and Grt, and is typical of relatively high- $P$ . However, Cpx is also often found in amphibolites lacking Grt and a typical assemblage is Hbl + Pl + Cpx + Bt. Reaction (9.55)

produces Di- and An- components from Am and Ep or Zo. This important reaction has several significant effects: (1) it continuously consumes Ep or Czo that may still be present in mid-amphibolite facies grade rocks and eventually eliminates them, (2) the reaction consumes the amphibole, a process typical in the higher amphibolite facies, (3) the reaction produces Cpx that appears in higher-grade amphibolites, (4) the reaction produces more An-component that is incorporated in plagioclase in high-grade amphibolites. Plagioclase in high-grade amphibolites thus becomes progressively more calcic and in the upper amphibolite facies, andesine-labradorite compositions ( $An_{30-70}$ ) are typical, although bytownite or anorthite compositions have also been reported.

The first appearance of Cpx in amphibolites can be used to define the lower grade boundary of the upper amphibolite facies. Reactions in the upper amphibolite facies, such as (9.54) and (9.55), begin to break down Am components and replace them with pyroxene components. This is a continuous process, and the first appearance of Cpx in mafic rocks is not usually designated as a sharp isograd in the field. Nevertheless, the “Cpx-in” transition zone marks the beginning of the upper amphibolite facies and indicates a representative temperature of about 650°C. Under upper amphibolite facies conditions in water-saturated environments, metamafic rocks show the first structural evidence in the field of local partial melt formation, migmatization and appearance of quartzofeldspathic seams, patches, veins (leucosomes) and similar mobilisate structures. The migmatization processes removes Qtz, Pl, Hbl (and Bt if present) from the rocks and transfers their oxide components to a granitic (trondjemite, tonalite, granodiorite, = TTG) melt phase (leucosome) and a granulite Grt ± Cpx restite. In a generalized form, migmatization of metabasalts (oceanic crust) produces igneous rocks that are typical constituents of continental crust (TTG).

At higher P than that of the ordinary Ky-geotherm (Fig. 9.4), mafic amphibolites may contain the diagnostic Ky + Hbl assemblage Hbl which may have formed by reaction (9.39) earlier in the course of prograde metamorphism. The link to the more common Pl + Grt assemblage found in amphibolites is given by reaction (9.56). This reaction replaces the Grt + Pl tie-line of chemographies #6 and #7 by the Ky + Hbl tie-line of chemography #8. The continuous dehydration reaction runs typically between chemography #6 and chemography #8 in Fig. 9.4 for typical metabasaltic compositions. Therefore, Ky-bearing amphibolites are diagnostic of high-P amphibolite facies (typically greater than 700 MPa). It should be remembered, however, that a Ky–Hbl–Grt–Pl assemblage is not normally co-planar (as one may erroneously conclude from ACF figures in Fig. 9.4) but rather defines a phase volume that occurs over a relatively wide  $P$ – $T$  interval.

### 9.5.3 Low-Pressure Series Amphibolites

At low metamorphic grades, mafic rocks that are metamorphosed along a prograde Ky-type and Sil-type path have very similar mineral assemblages. The most

significant difference is the composition of Chl and, especially, K-white mica. The Cel-component of K-white mica is relatively sensitive to variations in P and is controlled by reactions such as (9.45). The Ts-component in mica (and in principle also Chl or Bt) can be used to monitor P conditions in low-grade metamorphism.

The transition to amphibolite facies at low-P is similar to the one described in Sect. 9.4.3. In Al-rich rocks, And may appear instead of Ky (chemography #10 in Fig. 9.4). However, examples of And + Am are rare. Because the reactions that produce amphibolite from greenschist are ordinary continuous dehydration reactions, the transition to the amphibolite facies occurs at slightly lower T for low-P metamorphism. The lower boundary of the amphibolite facies along a Sil-path is typically at about 450°C (at 300 MPa). Reactions (9.36), (9.37), (9.40) and the And-equivalent of reaction (9.41) pass through the And field in Fig. 9.4. The reactions generally produce An and Hbl components from greenschist facies mineralogy. At 550°C (Fig. 9.4), Ep and Chl typically disappear from low-P amphibolites and the characteristic assemblage is Hbl + Pl ± And ± Bt.

Compared with orogenic metamorphism along a prograde Ky-path, Cpx forms at significantly lower T in low-P amphibolites (600°C or lower). Chemography #11 in Fig. 9.4 is characteristic of amphibolites that formed in the range of 300–400 MPa. It shows the usual Hbl + Pl assemblage together with Cpx and Bt. Sillimanite may be present in Al-rich amphibolites and the Sil + Hbl pair forms a stable, though rare, assemblage. However, Grt is scarce or even absent in low-P amphibolites.

Chemography #12 in Fig. 9.4 is representative for amphibolites of upper amphibolite facies grade at low-P (Sil-path). The most significant feature is the presence of Fe–Mg amphiboles such as anthophyllite (Ath), cummingtonite (Cum), gedrite (Ged) in addition to the Cam (Hbl). In some amphibolites even three different amphibole species may be present such as, e.g. Hbl, Ged and Ath. The abbreviation “Oam” for orthoamphibole in Fig. 9.4 includes all Fe–Mg amphiboles and Ged. Phase relationships in such multi-amphibole rocks can be very complex and miscibility gaps in various amphibole series as well as structural changes in amphiboles are additional complications. However, such low-P amphibolites possess a great potential for detailed analysis of relationships among minerals and assemblages and for the reconstruction of the reaction history of low-P amphibolites. Fe–Mg-amphiboles may form by a number of different conceivable mechanisms. The first and obvious one is reaction (9.57) that links chemographies #11 and #12. The reaction breaks down a Hbl + Sil assemblage to produce an An component in Pl and it also produces Ath-component in any Fe–Mg-amphibole. As metamorphic grade increases, reaction (9.58) becomes more important in producing the Ath-component. The reaction consumes Cam and replaces it with Cpx and Oam. The equilibrium of reaction (9.58) in metamafic rocks involves phase components of the typical assemblage: Hbl + Oam + Cpx + Pl ± Qtz. As a general rule of thumb, this assemblage is characteristic for temperatures of 650–750°C along a prograde Sil-type geotherm.

An example of Sil-type amphibolite facies metamorphism is the area of central Massachusetts, USA, where Qtz- and Pl-bearing upper amphibolite facies mafic

rocks contain assemblages with a number of coexisting amphiboles; Hbl, Hbl + Cum, Hbl + Oam, Hbl + Oam + Cum (Oam includes Ged and Ath) depending on rock Mg/(Mg + Fe) ratios. In addition to forming single, homogeneous crystals, Hbl contains exsolution lamellae of Cum, Cum contains exsolution lamellae of Hbl, and Ged has exsolved Ath. Metamorphism is estimated to have occurred over an interval of about 580–660°C, and at higher T the amphibolite assemblages were transformed into two pyroxene (Opx + Cpx) ± Grt granulites (Hollocher 1991).

### 9.5.4 Amphibolite–Granulite Facies Transition

Much of the Qtz that has been produced during subgreenschist facies to greenschist facies metamorphism is consumed by continuous reactions in the amphibolite facies so that many amphibolites are quartz-free (use ACF diagrams with care!). Most of the water bound in hydrous minerals has also been released by dehydration reactions during prograde metamorphism and metamafic rocks that have been progressively metamorphosed to 700°C, contain Pl + Hbl ± Cpx ± Grt ± Bt (Ky-path) and Pl + Hbl ± Cpx ± Oam ± Bt (Sil-path). Amphibole is the last remaining hydrous phase and further addition of heat to the rock by tectono-thermal processes will ultimately remove it. The transition from a relatively hydrous amphibolite facies assemblage to a completely anhydrous granulite facies assemblage is gradual and takes place over a temperature interval of at least 200°C (from about 650°C to 850°C). The first clear and unequivocal indication that granulite facies conditions have been attained is the appearance of Opx in Cpx-bearing Qtz-free rocks. Granulite facies conditions are obvious if Opx occurs in Qtz-bearing amphibolites. Orthopyroxene is most common in low-P mafic granulites, whereas at higher P the typical anhydrous granulite facies assemblage is Pl + Cpx + Grt ± Qtz. The reactions that eventually produce this assemblage are continuous in nature and the T-interval is very wide. Hornblende gradually decreases in modal amount, leaving behind an anhydrous granulite facies assemblage. Note, however, that Pl + Cpx + Grt may also occur in the amphibolite facies and that such an assemblage is not necessarily diagnostic of granulite facies conditions. If pressures are too high for Opx to form, then the ultimate granulite facies conditions are reached when Am has disappeared from the rock. Reactions (9.59) to (9.62) in Table 9.2 consume the major Am-components Tr and Ts and produce pyroxene-, Grt- and An-components and, hence, represent the transition of amphibolite to granulite facies (Fig. 9.10a, b). In particular, reaction (9.60) is important as it decomposes Hbl to form the two-pyroxene (Cpx + Opx) assemblage diagnostic of the granulite facies in Qtz-absent mafic rocks. In addition, the reaction produces An-component that ultimately leads to the presence of Ca-rich plagioclase (labradorite) in mafic granulites.

What happens to Bt during the amphibolite to granulite facies transition? Biotite is a subordinate (accessory) hydrous phase in high-grade amphibolites. The small

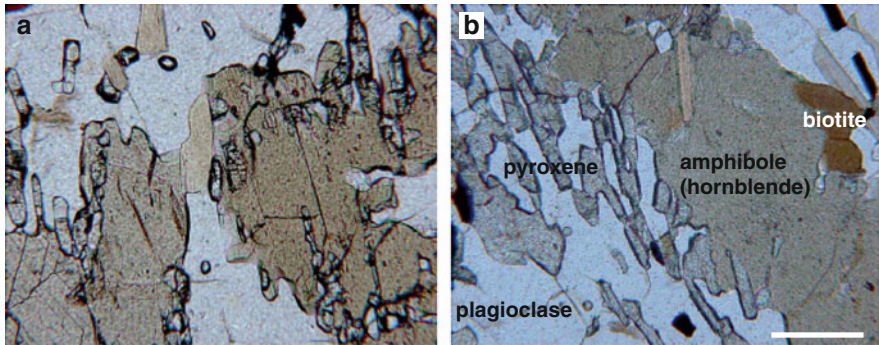


**Fig. 9.10** photomicrographs of mafic rocks from the Thor Range (Antarctica) showing structures that indicate the breakdown of hornblende to pyroxene and plagioclase [reactions (9.59) and (9.60) Table 9.2]. The texture indicates prograde transition from amphibolite to granulite facies (Bucher and Frost 2006)

amount of  $K_2O$  typically present in amphibolitic metamafic rocks is mostly stored in Bt and will either be taken up by pyroxene and ternary feldspar or become incorporated into a Kfs–Ab–Qtz melt during migmatization. However, as the total amount of water that can be stored in high-grade amphibolites is also very small (on the order of 0.4 wt%  $H_2O$  or less), mafic rocks are less susceptible to partial melting compared to their metapelitic, metapsammitic or metagranitoid counterparts.

## 9.6 Granulite Facies and Mafic Granulites

Granulite facies metamorphism of mafic rocks is represented by chemographies #9 and #13 in Fig. 9.4. At high-P the characteristic assemblage is: Pl + Cpx (augite) + Grt. At lower P the typical granulite facies assemblage is: Pl + Cpx (augite) + Opx (hypersthene). The two assemblages are linked by the important reaction (9.63) which separates a field of pyroxene granulites at P below about 500–700 MPa from a field of garnet granulites below the eclogite field at high-P. The continuous nature of reaction (9.63) generates a wide overlap zone where both Grt and Opx are present in Pl + Cpx rocks. If restricted to meta-MORB compositions, however, the overlap is smaller and the boundary between the two fields occurs close to 600–700 MPa at 800°C.

Because high-grade brown hornblende is an extremely stable mineral, very high temperatures are necessary to destroy this last hydrous phase in mafic rocks. Completely anhydrous mafic granulites normally form above 850°C or at even higher temperatures. Amphibole dehydration is often aided by interaction of the rocks with an  $H_2O$ -poor external fluid phase. Alternatively, dehydration of amphibole may be triggered by partial melting and removal of  $H_2O$  in a melt phase (see also Chap. 7),



where aspects of granulite facies metamorphism have been discussed. The relationships that are important in high-grade and granulite facies metamorphism of mafic rocks are shown in Fig. 9.11, which is a schematic T versus fluid composition diagram at an approximate  $P_{\text{total}}$  of 600 MPa. Along the 750°C isotherm, three different assemblage fields are intersected. If H<sub>2</sub>O-rich fluids are present (section A), mafic rocks undergo partial melting and mafic migmatites are formed (see Sect. 9.5.2). Intermediate fluid compositions are consistent with amphibolite facies rocks containing the typical assemblage: Pl + Hbl + Cpx (section B) and migmatite structures are absent. Fluids low in H<sub>2</sub>O coexist with granulite facies rocks at the same T and the characteristic assemblage is: Pl + Cpx + Opx ± Grt (section C). Note that the transition zone between the granulite and amphibolite facies assemblages in Fig. 9.11 extends over a wide range of fluid composition. However, an important observation shown in Fig. 9.11 is that at the same T (e.g. 750°C) mafic migmatites, amphibolites and mafic granulites may be intimately associated in a metamorphic complex or terrain depending on the composition of the fluid phase. The situation may be complicated by variations of fluid composition over time at a particular site. Also note that the first melt in mafic rocks forms if a pure H<sub>2</sub>O-fluid is present (wet solidus in Fig. 9.11). With increasing T, migmatites form with fluids that contain decreasing amounts of water. The amphibolite facies assemblage has a T-maximum that equates with an amphibole-out isograd at about 900°C

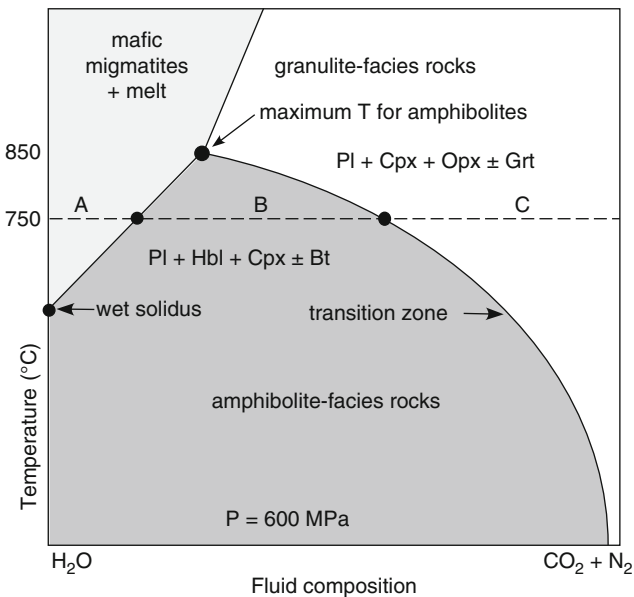


**Fig. 9.11** Schematic isobaric temperature versus fluid composition diagram showing amphibolite-granulite facies relationships in metamafic rocks

(at 600 MPa) in the presence of a pure H<sub>2</sub>O-fluid and which may be closer to 850°C if mixed volatile fluids are present at the same pressure.

Although completely anhydrous mafic granulites are common, e.g., in the Jotun nappe and the Bergen arcs of the Scandinavian Caledonides, many mafic granulites still contain prograde hornblende (as opposed to retrograde post-granulite Hbl). A case in point is the amphibolite–granulite facies transition in metamafic rocks at Broken Hill, Australia. The color of Hbl changes with increasing grade from bluish-green through green-brown in amphibolite facies rocks to dark reddish brown in granulite facies rocks that mainly reflects increasing Ti (indication of increasing T) that is coupled with □ increasing Ed-substitution (Na<sup>A</sup>Al □<sup>A</sup><sub>-1</sub>Si<sup>A</sup><sub>-1</sub>). The presence of brown Hbl in mafic rocks that contain Opx defines a lower grade granulite facies; Hbl–two pyroxene granulite. The case is more difficult at high-P where Opx does not form in mafic rocks and the typical assemblage Pl + Cpx + Grt may also be present in the amphibolite facies or where Hbl persists to very high-T (1,000°C at 1.0 GPa). Obviously, in this case, the definition of the amphibolite–granulite facies *boundary* is impossible on the basis of mafic rocks alone (see comments in Chap. 4 on metamorphic grade).

In addition to the minerals discussed so far, mafic granulites may also contain more exotic minerals such as sapphirine (Spr) or scapolite (Scp) in various assemblages. Also hercynitic spinel (Hc) is commonly present in mafic granulites and its presence is diagnostic of low-P conditions (<400 MPa).

At very low-P, such as represented by chemography #14 in Fig. 9.4, pyroxene hornfels form by high-T contact metamorphism of mafic rocks. Ultimately, with UHT contact metamorphism of mafic rocks, the assemblage Pl + Cpx + Opx ± Spl (chemography #14) will form that is identical to the basalt mineralogy shown in the upper left corner of Fig. 9.4. The upper boundary of granulite facies metamorphism of mafic rocks is given by the dry basalt liquidus at ~1,200°C.

The causes of granulite facies metamorphism at low-P are commonly attributed to intrusion of large volumes of dry or CO<sub>2</sub>-rich mafic (gabbroic/basaltic) or charnockitic magma to shallow crustal levels from the mantle or lower crust (see references for this chapter and Chap. 7). The dry or CO<sub>2</sub>-rich nature of such magma facilitates dehydration of the crustal rocks and there is little tectonic activity associated with this type of granulite facies metamorphism. After heating to high-T, the granulite facies rocks cool essentially in-situ as evidenced by many granulite facies terrains being characterized by isobaric cooling paths (and perhaps a counter clockwise *P–T* loop; see also Chap. 3). In general, exhumation of granulite facies rocks requires a later contractional orogenic event that involves stacking and tilting of crustal slices with the formation of fold-nappe structures that ultimately permit the erosion surface to intersect middle or lower crust granulite terranes. If water becomes available during slow cooling, the high-grade assemblages may be completely erased and if Opx disappears from mafic granulites during amphibolitization it is very difficult to determine if the rocks were ever recrystallized under granulite facies conditions.

## 9.7 Blueschist Facies Metamorphism

### 9.7.1 Introduction

Blueschists are rocks that contain a significant amount of blue alkali-amphibole with a very high proportion of Gln endmember component. Such rocks are, in an outcrop or hand specimen, blue in color. Note, however, that pure Gln is colorless under the microscope. If a rock contains a blue pleochroic amphibole in thin section it means that it is not a pure Gln and appreciable amounts of the riebeckite (Rbk) and other sodic ferro-ferric amphibole components are important and the overall composition of the amphibole is crossite (an amphibole name disapproved by IMA but still useful for petrologists). Note also that Cl-rich Hbl may have a blue color under the microscope. However, if metamafic rocks of basaltic bulk composition contain sodic amphibole, the rocks are likely to have been metamorphosed under the conditions of the blueschist facies.

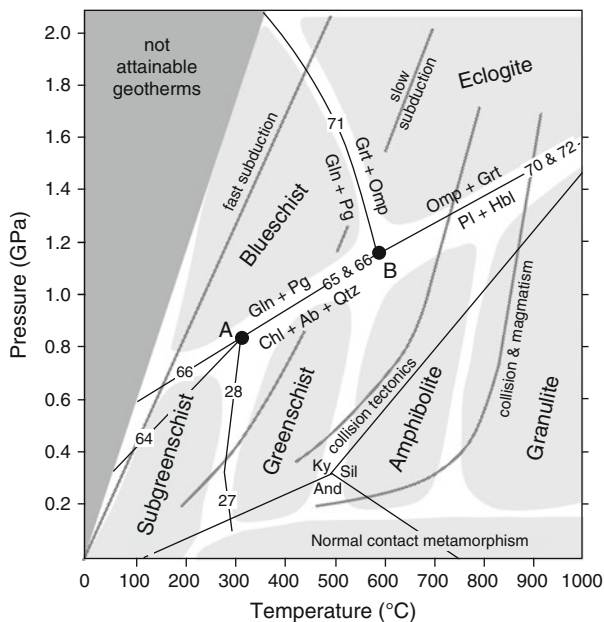
The general  $P$ - $T$  field of the blueschist facies is delineated in Fig. 4.3 and the blueschist facies mineralogy is represented by chemographies #16 and #17 in Fig. 9.4. The lower  $P$  range is characterized by Gln (Na-Am) + Lws + Chl assemblages. In the higher-grade blueschist facies chemography #17, typical metamafic rocks contain various assemblages that include Gln (Na-Am), Zo (Czo-Ep), Grt, Pa, Phe, Chl, Tlc, Ky, Rt, Ank and other minerals.

A detailed rendering of the blueschist facies field is shown in Fig. 9.12. It is bounded towards the subgreenschist and greenschist facies by reactions (9.64), (9.65) and (9.66) in Table 9.2. The high- $P$  boundary is given by reaction (9.71). Worldwide, blueschist facies terrains are associated with subduction zone metamorphism that typically occurs along destructive plate margins where basaltic oceanic crust is recycled to the mantle beneath the continental lithosphere. Two typical geotherms related to subduction tectonics are depicted in Fig. 9.12. The slow subduction geotherm only marginally passes through the blueschist field and eclogite assemblages are produced at pressures as low as 1.3 to 1.4 GPa. If subduction is fast, prominent blueschist facies terrains may develop and eclogite formation does not occur until pressures of 1.8 to 2.0 GPa are reached (corresponding to subduction depths of 50–60 km). Because there are natural limits to attainable subduction velocities in global tectonic processes,  $P$ - $T$  conditions represented by the upper left wedge area in Fig. 9.12 are not conditions accessible for metamorphism.

### 9.7.2 Reactions and Assemblages

As discussed above, reactions (9.27) and (9.28) mark the boundary between the subgreenschist facies and the greenschist facies. The boundary between subgreenschist facies and blueschist facies conditions is given by reaction (9.64) that replaces

**Fig. 9.12** Metamorphic facies scheme and reactions defining some of the field boundaries (reaction stoichiometry given on Table 9.2). The facies concept uses type assemblages of metabasaltic rocks (Chap. 4). Aluminosilicate phase transitions given for comparison



low-grade assemblage Act + Chl + Ab by the high- $P$  assemblage Gln + Lws. The reaction is  $H_2O$ -conserving, and as such independent of  $P_{H_2O}$  or fluid phase composition. Equilibrium of reaction (9.64) is shown in Fig. 9.12 for average mineral compositions found in low-grade equivalents of basaltic rocks.

Point A in Fig. 9.13 marks an important  $P$ - $T$  region where blueschist, greenschist and subgreenschist facies assemblages meet at about 800 MPa and 300°. The  $P$ - $T$  region is defined by the approximate intersection of the reactions (9.22), (9.28), (9.30), (9.31), (9.64), (9.66) and (9.70). Note, however, that point A is not an invariant point in Schreinemaker's sense but rather a relatively narrow  $P$ - $T$  range of locations of various invariant points generated by the intersection of continuous reactions in the NCMASH system.

The blueschist facies is separated from the greenschist facies by reactions (9.65) and (9.66) shown in Fig. 9.12. Reaction (9.65) consumes the low-grade assemblage Chl + Act + Ab and replaces it by the most typical blueschist facies assemblage Gln + Ep (Zo). Reaction (9.65) connects points A and B in Fig. 9.12 and almost coincides with the other important reaction (9.66) that replaces the greenschist facies assemblage Chl + Ab by the characteristic blueschist assemblage Gln + Pg. If for any reason, some Ab should still be present in the rocks after all Chl is exhausted, it will be consumed by reaction (9.70). The boundary of reaction (9.66) roughly coincides with the diagonally ruled boundary that separates a Pl-present from a Pl-absent region (Fig. 9.12). As in the eclogite facies, blueschists do not contain stable Ab (Pl). In most low-grade mafic rocks, however, Chl is much more abundant than is Ab and consequently, reactions (9.65) and (9.66) will normally remove it.

Facies	Zeolite	Prehnite-Pumpellyite	Blueschist	Eclogite
Quartz				
Albite	-----		-----	---
Laumontite	-----			
Other zeolites	-----			
Prehnite	-----	-----		
Pumpellyite	-----		-----	---
Lawsonite			-----	---
Epidote			-----	
Clinopyroxene			----- Jd -----	----- Omp -----
Glaucophane			-----	-----
Actinolite		-----	-----	
Garnet			-----	-----
Chlorite				
Stilpnomelane		-----	-----	---
Phengite	-----	-----	-----	-----
Titanite				-----
Rutile				-----
Calcite			-----	
Aragonite			-----	

**Fig. 9.13** Progressive mineral changes in high-P metabasites, Franciscan terrane, California (Data from Ernst 1965, 1971; Ernst et al. 1970; Jayko et al. 1986; Brothers and Grapes 1989)

The Gln + Pg assemblage is replaced by Omp + Grt as a result of reaction (9.71). The reaction terminates the blueschist field towards higher P where it grades into the eclogite field with the diagnostic Omp + Grt assemblage. At low grade, the Na<sub>2</sub>O present in metamafic rocks occurs in Ab, in the blueschist facies it is taken up by alkali-Am (Gln, crossite) and Pg, and in the eclogite facies it occurs in Na-Cpx (Omp, Jd). Reaction (9.71) has a negative slope on a *P-T* diagram (Fig. 9.12) and terminates at point B towards lower P where it becomes metastable relative to feldspar-involving reactions. The negative slope of reaction (9.71) means that the most favorable conditions for the development of extensive blueschist facies terrains are tectonic settings where there is fast subduction of cold (old) oceanic crust.

Inside the blueschist facies field, some additional reactions may modify the assemblages. Most important is reaction (9.67) that terminates the Lws + Gln assemblage represented by chemography #16 and produces Grt towards higher P (chemography #17). Another important Grt-producing reaction in the blueschist facies is reaction (9.68). Reaction (9.69) generates the widespread Czo + Pg pseudomorphs that is diagnostic for the former presence of lawsonite in blueschists (see Sect. 9.2.1 and Fig. 9.5).

The continuous reactions within the blueschist facies field result in a systematic, gradual change in the mineral and modal composition of metabasaltic rocks during prograde metamorphism. For example, take a metabasaltic rock with a subgreenschist facies assemblage that undergoes subduction at a rate intermediate to the slow and fast subduction geotherms shown in Fig. 9.12. Such a geotherm will cover a  $T$ - $P$  interval in the blueschist facies field from 250–500°C and 0.7–1.6 GPa. At pressures between 600–800 MPa, Lws + Na–Am will begin to replace the low-grade Chl + Act + Ab assemblage. The first-formed Na–Am is initially fairly Fe-rich containing a significant Rbk-component. With a further increase in  $P$ , Ab gradually disappears and Am becomes increasingly sodic and depleted in the Act-component. In the M(4) site of the Am structure, Na replaces Ca by way of a Gln exchange mechanism  $\text{Na}^{\text{M4}}\text{AlCa}_{-1}\text{Mg}_{-1}$  that does not involve the amphibole A-site. The continuous reaction produces a Lws + crossite + Chl + Pa  $\pm$  Phe assemblage that is characteristic for pressures around 1.0 GPa. At still higher  $P$ , Lws gradually disappears; Na–Am becomes increasingly enriched in the Gln-component, Czo and Ep become important modal components of the assemblages, while modal Chl continuously decreases. The characteristic assemblage for this intermediate blueschist facies stage is: Gln + Ep + Chl + Pg  $\pm$  Phe. Typical pressures for this assemblage are in the range of 1.2–1.4 GPa (along the fast subduction geotherm we are concerned with). With increasing  $P$ , Grt forms as a result of chlorite-involving reactions and high- $P$  blueschists most typically contain Gln + Ep (Czo, Zo) + Grt + Pg  $\pm$  Phe. Other minerals that may be present in high- $P$ /low- $T$  blueschists include Mg–Cld, Tlc and Ky. For a discussion of systematic compositional changes in the only important potassic mineral in blueschists, Phe, with increasing  $P$  see Sect. 7.8. Also note that blueschists often contain carbonate minerals that give rise to mixed volatile reactions that are not discussed here. Blueschist carbonates include Cal and its high- $P$  polymorph Arg, Ank, Dol, breunerite and Mgs. The origin of the carbonates is either related to ocean-floor metamorphism/metasomatism of basalt or they are derived from carbonate sediment deposited concurrently with the eruption of ocean floor basalt.

Blueschist facies assemblages are gradually replaced with the typical eclogite facies assemblage Omp + Grt at  $P > \sim 1.4$ –1.6 GPa. Because high- $P$  blueschists typically contain Grt at these conditions, it is the appearance of Omp that marks the transition to eclogite facies conditions. The boundary is gradual and there is a wide  $P$ -range where Gln + Pa + Ep + Grt + Omp may occur as a stable association and strictly speaking, this assemblage is diagnostic for the eclogite facies. Along an intermediate high- $P$ /low- $T$  geotherm, typical eclogite assemblages are formed at about 1.6–1.8 GPa and a corresponding  $T$  of around 500°C.

An example of progressive metamorphism from zeolite through prehnite–pumpellyite, blueschist to eclogite facies indicating a high- $P$ /low- $T$  geotherm (0.2–1.4 GPa/100–540°C) is the metabasite rocks of the Franciscan terrane, California. The sequence of mineral changes is shown in Fig. 9.13 and is constructed from assemblages in allochthonous metabasite fragments and eclogite “knockers” that occur throughout the greywacke–dominated subduction zone complex

(see Chap. 10). Note that greenschist facies field is not intersected by the steep  $P/T$  trajectory and the typical greenschist facies minerals Act + Ab + Chl occur with Pmp and Prh. Blueschist facies metabasaltic rocks are characterized by the assemblage Qtz + Ab + Gln + Lws + Jd + Chl + Pmp + Ttn + Arg that also may include Phe and Stp and with Grt and Ep in the higher grade facies assemblage.

## 9.8 Eclogite Facies Metamorphism

### 9.8.1 Eclogites

Eclogites are metamorphic mafic rocks that contain the stable mineral pair **Grt** and **Omp** in significant amounts. Eclogites are free of Pl. Eclogites are very dense rocks with a density even greater than some ultramafic mantle rocks ( $\rho_{\text{eclogite}} > 3,300 \text{ kg/m}^3$ ) and because of this their origin can be readily related to very high- $P$  conditions of formation. Omphacite + Grt is the diagnostic assemblage in metabasaltic rocks that recrystallized above about 1.2–1.4 GPa outside the stability field of Pl. Typical eclogites form at pressures of 1.8–2.2 GPa and higher. Many of the eclogites found in collisional mountain belts such as the Western Alps or the Scandinavian Caledonides still display clear compositional and structural evidence of being derived from basalt. In the Zermatt region of the Central Alps, for example, preserved MORB compositions and pillow structures may be found in eclogites that formed at pressures greater than 2.0 GPa corresponding to a subduction depth of about 60 km. This is compelling evidence that surface rocks (basaltic lava) can be transported by active tectonic processes to depths of 60 km or even to 100 km or more in the case of coesite-bearing eclogites found in UHP terranes.

The  $P$ – $T$  field of the eclogite facies shown in Fig. 9.12 can be accessed in prograde metamorphism from all three neighboring facies fields, blueschist, amphibolite and granulite facies, depending on the tectonic setting. In subduction zones, eclogites originate from blueschists, as outlined above and these eclogite types often indicate very high- $P$  formation.

In a continent-continent collision tectonic setting, the continental crust often attains twice its normal thickness and the deeper parts are exposed to pressures in the range of 1.2–2.4 GPa. Any mafic rocks of suitable composition in the deeper part of the thickened crust may be transformed to eclogite (Fig. 9.12). An example is the collision of the Eurasian and the Indian plates and the resulting formation of thickened crust underlying the Tibetan Plateau. Along a  $Ky$ -type geotherm, typical of collision tectonics shown in Fig. 9.12, eclogites will be created from amphibolites. Eclogites that form in such a tectonic setting characteristically record pressures in the range of 1.4–1.8 GPa rather than UHP.

If collision is accompanied by substantial magmatic heat transfer to the crust, eclogites may form from granulites along the “hot” geotherm in Fig. 9.12. Mantle-

derived basaltic melts often sample rocks bordering conduits during their ascent to the surface. These fragments are found as xenoliths in basaltic lavas and include ultramafic rocks from the mantle, granulites from the lower crust and eclogites from a range of depths. The xenolith association is characteristic of abnormally hot geotherms caused by collision and magmatism, the initial stages of crustal extension or by magmatism alone. In such settings, eclogites may have been created from mafic granulites or directly crystallized from basaltic magma at great depth. Although the  $P$ -range of these high- $T$  eclogites is very large, typical pressures are in the same range as those of eclogites formed from amphibolites. Basaltic magmas may also entrain eclogite xenoliths from great depth in the mantle but the ultimate origin of these deep eclogite samples is ambiguous and they could also represent fragments of recycled former oceanic crust.

From the comments above it follows that eclogites may form in a wide range of geotectonic settings and the eclogite facies comprises the widest  $P$ - $T$  region of any of the metamorphic facies fields with a  $T$ -range from about 400°C to 1000°C. It also follows that three general types of eclogites can be distinguished depending on geological setting and formation- $T$  (Fig. 9.14).

1. **Low- $T$ /high- $P$  (LT/HP) eclogites** are related to subduction tectonics and form from blueschists. This type includes eclogites in UHP metamorphic terranes.
2. Intermediate or **Medium- $T$  (MT) eclogites** formed in continent collision double-crust settings from amphibolites.
3. **High- $T$ (HT) eclogites** formed in crustal extension settings where the geotherm is abnormally “hot” due to magmatic heat transfer from the mantle (e.g., basalt magma underplating) from mafic granulites or have crystallized directly as eclogite from mafic magma.

The three different geodynamic types of eclogite are also characterized by typical mineral associations because of dramatically different temperatures and widely varying  $H_2O$  pressures associated with their formation. While LT/HP eclogites formed in subduction zones often contain modally large amounts of hydrate minerals, HT eclogites often contain “dry” assemblages.

In dealing with high- $P$  rocks, important issues also include the mechanism by which they return to the surface, the  $P$ - $T$  path of exhumation, and, most importantly, the modifications experienced by the rocks during decompression. For example, if an eclogite formed by subduction and equilibrated at 650°C and 2.0 GPa, it is crucial for the fate of the eclogite assemblages whether the rocks reach the surface via the blueschist field (cooling and decompression occur simultaneously), via the amphibolite and greenschist fields (initial decompression and subsequent cooling), or via the granulite field (initial heating and decompression followed by cooling). Most eclogites display some indications of mineral reactions along their return paths. Access of  $H_2O$  along that return path is essential to whether or not the high- $T$  assemblages are preserved or extensive retrogression occurs. On the other hand, as will be discussed below, LT/HP eclogites often contain abundant hydrate minerals such as Clid, Tlc, Czo at peak- $P$ . Such rocks will undergo extensive



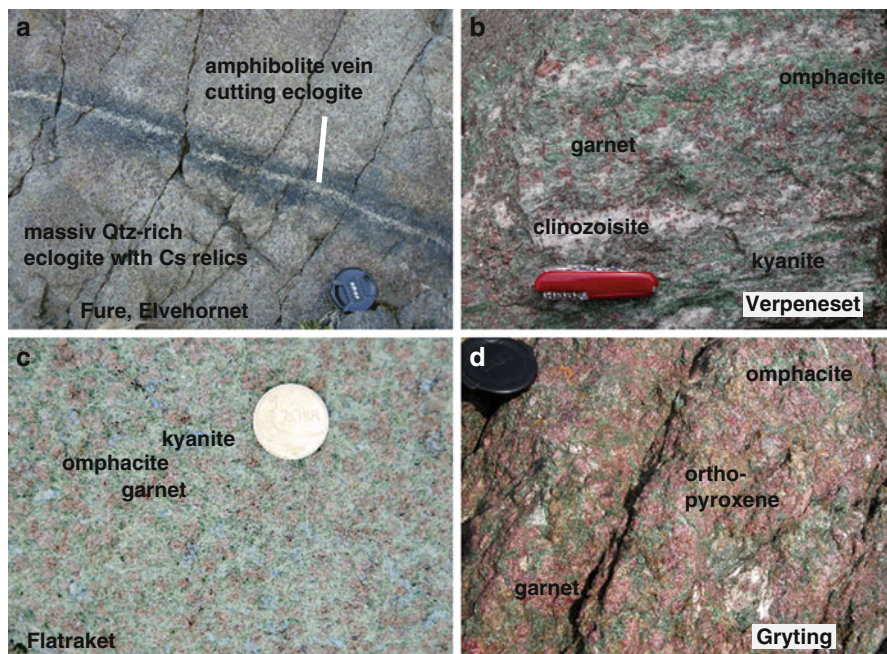


**Fig. 9.14** Field examples of MT and HT eclogites from classical eclogite outcrops in the Western Gneiss Region of Norway: (a) Coesite eclogite from Elvehornet, Fure, Stadlandet. Note amphibolitization band cutting eclogite. (b) Verpeneset eclogite, outer Nordfjord (worlds most attractive eclogite outcrop!) with the typical MT assemblage:  $\text{Omp} + \text{Grt} + \text{Czo} + \text{Ky} + \text{Qtz}$ . (c) HT eclogite at Flatraket harbour:  $\text{Omp} + \text{Grt} + \text{Ky} + \text{Qtz}$ . (d) HT eclogite at the protected Gryting outcrop:  $\text{Grt} + \text{Omp} + \text{Opx} + \text{Qtz}$ . At the same outcrop Opx-free eclogites contain coesite as inclusions in Grt

dehydration reactions that will eventually eliminate the eclogite assemblage if decompression occurs without concurrent cooling.

## 9.8.2 Reactions and Assemblages

Reactions that connect the blueschist facies to **LT/HP eclogite facies** have been discussed in Sect. 9.7.2. The most typical assemblages in LT/HP eclogites involve the following minerals (bold = essential minerals): **Grt** + **Omp** ± Czo ± Cld ± Phe ± Pg ± Gln ± Qtz ± Ky ± Tlc ± Rt ± Dol.

**Omphacite** is a sodic high-P clinopyroxene that is mainly composed of the components Jd, Acm, Di and Hd (a solid solution of:  $\text{NaAlSi}_2\text{O}_6$ – $\text{NaFe}^{3+}\text{Si}_2\text{O}_6$ – $\text{CaMgSi}_2\text{O}_6$ – $\text{CaFeSi}_2\text{O}_6$ ). In typical Omp, the M(2) site of the pyroxene structure contains about 50% Na and 50% Ca. LT/HP eclogites often contain pure Jd together

with Omp that commonly minor amounts of Cr giving the mineral a grass-green color, particularly in eclogitised metagabbros. Note that Cr–Di in garnet–peridotite also shows a characteristic grass-green color. However, because ultramafic rocks contain very little sodium, the Jd-component in Cpx of high-P ultramafic rocks is generally low.

**Garnet** in eclogite is a solid solution of the major phase components Alm, Prp and Grs, i.e.  $\text{Fe}_3\text{Al}_2\text{Si}_3\text{O}_{12}$ – $\text{Mg}_3\text{Al}_2\text{Si}_3\text{O}_{12}$ – $\text{Ca}_3\text{Al}_2\text{Si}_3\text{O}_{12}$ . However, due to its refractory nature, eclogite Grt can be inherited from earlier stages of metamorphism or be relics from the protolith, e.g. garnet–granulite.

In LT/HP eclogites, Cld is very Mg-rich and  $X_{\text{Mg}}$  may be as high as 0.9. Chloritoid and paragonite are diagnostic minerals in LT/HP eclogites. The two minerals are removed by various reactions at higher T so that they are typically absent in MT- and HT-eclogites.

Phengite and other sheet silicates that occur in LT/HP eclogites derived from gabbros also often contain small amounts of Cr giving them a green color, e.g. Cr-bearing Phe is termed fuchsite.

Ultrahigh-P eclogites, e.g. Western Alps, Bohemian Massif, Western Norway, Kokchetav Massif in Kazakhstan, Dabie Mountains and Sulu areas, China, are indicated by the presence of coesite and even diamond in some cases, most often as inclusions in garnet and zircon.

### 9.8.2.1 Amphibolite and Granulite to Eclogite Facies Transition

Under eclogite facies conditions, the An-component of Pl in amphibolites and granulites is removed by reaction (9.72) to produces the Ca–Ts component in Omp. The equilibrium of reaction (9.72) is nearly T-independent and it can be used to estimate P. Reaction (9.73) that replaces An by Czo and Ky is the most important An-consuming reaction in high-P metamorphism of both MT- and HT-eclogites. The hydration reaction consumes  $\text{H}_2\text{O}$  but the absence of water will stabilize An. Nevertheless, if water is unavailable as a solvent then reaction kinetics are so slow and transport distances so small that Ab and other low-P phases or phase components can survive to high-P. For example, in olivine gabbros of the Allalin area, Western Alps (see below), primary igneous minerals have survived pressures in excess of 2.0 GPa at around 600°C without forming eclogite except where water has had access to the rocks. Another example is the Precambrian mafic granulites of the Bergen Arcs (Norwegian Caledonides), a basement nappe complex that experienced  $P \sim 2.0$  GPa and  $T \sim 700^\circ\text{C}$  during Caledonian metamorphism. In this case, mafic granulite is perfectly preserved over large areas except along an anastomosing network of shears that permitted access of water to produce an MT eclogite assemblage.

The equilibrium conditions of reaction (9.73) shown in Fig. 9.12 indicate that it is approximately parallel to the Ab-breakdown reaction (9.70). Reaction (9.74) decomposes the An-component in Pl and produces a Grs-component in eclogite

garnet together with kyanite and quartz (Fig. 9.12). The slope of the reaction is similar to those of reactions (9.70) and (9.73).

Reaction (9.70) has been used in Chap. 3 to illustrate some general principles of chemical reactions in rocks. In high-P mafic rocks it is the most important reaction as it delineates the boundary between a Pl-present and a Pl-absent region in  $P$ - $T$  space (Fig. 9.12). If all three minerals are present (Qtz, Pl and Na-Cpx), the equilibrium conditions of reaction (9.70) can be used for  $P$ - estimates if  $T$  can be determined from a geothermometer such as Fe-Mg distribution between Grt and Omp. In the absence of Qtz, maximum  $P$  can be estimated from the pyroxene-feldspar pair. If feldspar is not present (the normal case in eclogites), the Omp + Qtz assemblage can be used to estimate a minimum  $P$  for eclogite formation assuming unit activity for the Ab-component in the equilibrium constant expression for reaction (9.70). Other important reactions of the amphibolite (or granulite) to eclogite transition zone must consume Cam or Cpx. An example is reaction (9.75) that destroys Tr- and the An-component (Hbl + Pl = amphibolite) and produces Grt + Cpx. Reactions (9.76), (9.77), and (9.78) are examples of An-consuming reactions relevant for the transition from the granulite to HT-eclogite facies rocks.

As a result of the reactions that produce MT-eclogites (from amphibolites) the typical minerals found in meta-MORB are: **Grt + Omp**  $\pm$  Zo (Czo)  $\pm$  Phe  $\pm$  Ky  $\pm$  Am (Na-Cam)  $\pm$  Qtz (Cs at UHP)  $\pm$  Rt.

**High-T eclogites (from granulites)** typically contain: **Grt + Omp**  $\pm$  Ky  $\pm$  Opx  $\pm$  Am  $\pm$  Qtz (Cs at UHP)  $\pm$  Rt.

### 9.8.2.2 Reactions in Eclogites

Prograde metamorphic mineral reactions that affect eclogites are basically ordinary dehydration reactions. The reactions transform assemblages involving hydrous minerals of LT/HP-eclogites and substitute them with less hydrous assemblages of MT-eclogites and ultimately HT-eclogites. Examples are the Pg breakdown reaction (9.79), the Czo breakdown reaction (9.80), and the replacement of Tlc + Ky by Opx reaction (9.81). Other reactions gradually remove Chl from Qtz-free MT-eclogites, some of them producing Opx. Reaction (9.80) replaces Czo and Grt to produce Ky + Cpx. This continuous reaction relates MT- to HT-eclogites and the reaction ultimately leads to the change from chemography #18 to #19 in Fig. 9.4.

Other important reactions in HT-eclogites are (9.82) and (9.83). The latter reaction is important in relatively rare Opx-bearing eclogites, e.g. eclogites of the Western Gneiss region of the Scandinavian Caledonides. Phengite is the only K-bearing phase in LT/HP-eclogites. At higher  $T$  the mica continuously decomposes to produce a K-amphibole component. K-bearing Na-Ca-amphiboles found in high-grade eclogites are very stable and remain the prime K-carrier in HT-eclogites.

### 9.8.3 Eclogite Facies in Gabbroic Rocks

Mafic rocks cover a wide range in bulk composition. Typical eclogites with Grt and Omp as the dominant minerals usually develop from basaltic protoliths. The above discussion refers to MORB-type basaltic eclogites, but many gabbros are compositionally dissimilar to MORB. In particular, gabbros are commonly much more Mg- (or Fe-rich = ferrogabbro) compared with MORB and it can be expected that high-P equivalents of troctolite and olivine–gabbro may develop mineral assemblages that are quite different from normal basaltic eclogite facies Grt + Omp rocks. In fact, Mg-rich olivine gabbro metamorphosed at 2.5 GPa and 600°C may not contain Grt + Omp as a peak assemblage because the low  $X_{\text{Fe}}$  of Mg-gabbro protoliths prevents the formation of Grt. An example of LT/HP-eclogite metamorphism of an olivine gabbro from the Western Alps is discussed in Sect. 9.8.3.1. Although such mafic rocks have been metamorphosed under eclogite facies conditions, they are not strictly eclogites, i.e. mafic eclogites. We also recommend avoiding rock names like pelitic eclogites or pelitic blueschists. The appropriate expressions for such rocks are blueschist facies metapelites or eclogite facies pelitic gneisses (see Sect. 7.7).

Anorthosites, which are also basic rocks, cannot be converted to eclogites by high-P metamorphism because the rocks contain more than 90–95% Pl. Plagioclase of the composition  $\text{An}_{70}$  will be converted into a Jd + Zo + Ky + Qtz assemblage under LT/HP and MT eclogite facies conditions (see Fig. 9.5).

#### 9.8.3.1 Blueschist and Eclogite Facies Metamorphism of Olivine Gabbro

The  $2 \times 5$  km block of gabbro that forms the Allalinhorn between Zermatt and Saas, Western Alps, Switzerland, it is referred to as the Allalin gabbro (Bearth 1967; Chinner and Dixon 1973; Meyer 1983a, b). The gabbro occurs within a typical ophiolite complex (Zermatt–Saas ophiolite) that represents the oceanic lithosphere of the Mesozoic Tethys ocean. During early Tertiary Alpine orogeny, the ophiolites and the Allalin gabbro were subducted to great depth and metamorphosed under LT/HP eclogite facies conditions. Pillow basalts were converted to ordinary LT/HP eclogites, later retrogressed to blueschists, and finally overprinted by greenschist facies metamorphism. Abundant eclogite Grt represents the only relic mineral from the eclogite stage in locally strongly retrogressed eclogites and Grt-bearing greenschists demonstrate the refractory nature of the Grt.

The Allalin gabbro is an Mg-rich olivine gabbro with irregular layers of troctolite and recent work by Bucher and Grapes (2008) indicates that it probably formed at the crust–mantle boundary during the Jurassic where it underwent granulite facies recrystallisation prior to being incorporated in the Tethys ophiolite during subduction. The succession of minerals that formed in the gabbro through its entire  $P$ – $T$  history is given in Fig. 9.15 and the  $P$ – $T$  path from magmatic crystallization, through granulite facies conditions to peak eclogite facies (return point) and retrograde eclogite, amphibolite and amphibolite–greenschist transition facies is shown in Fig. 9.16. The metamorphic

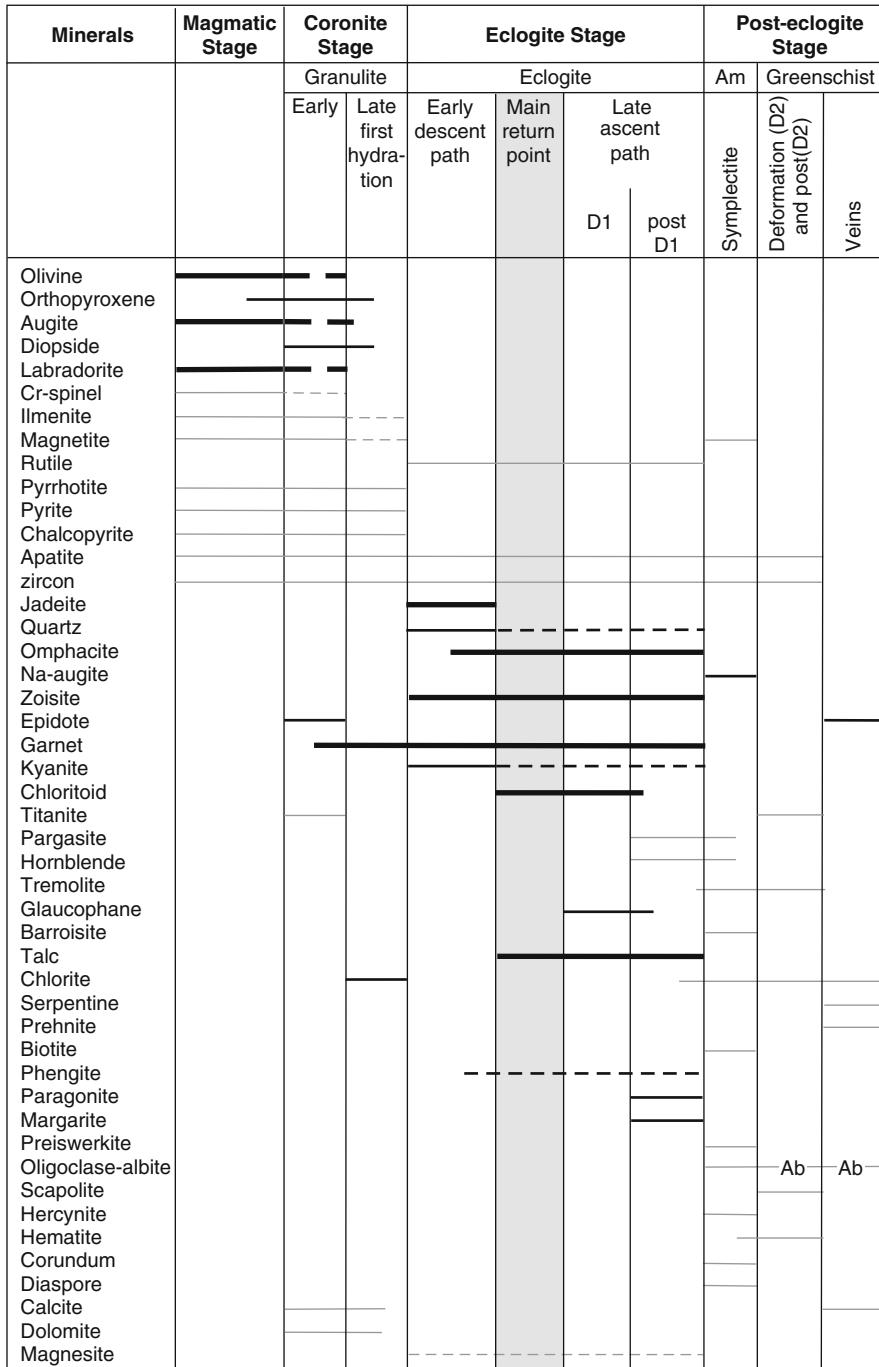
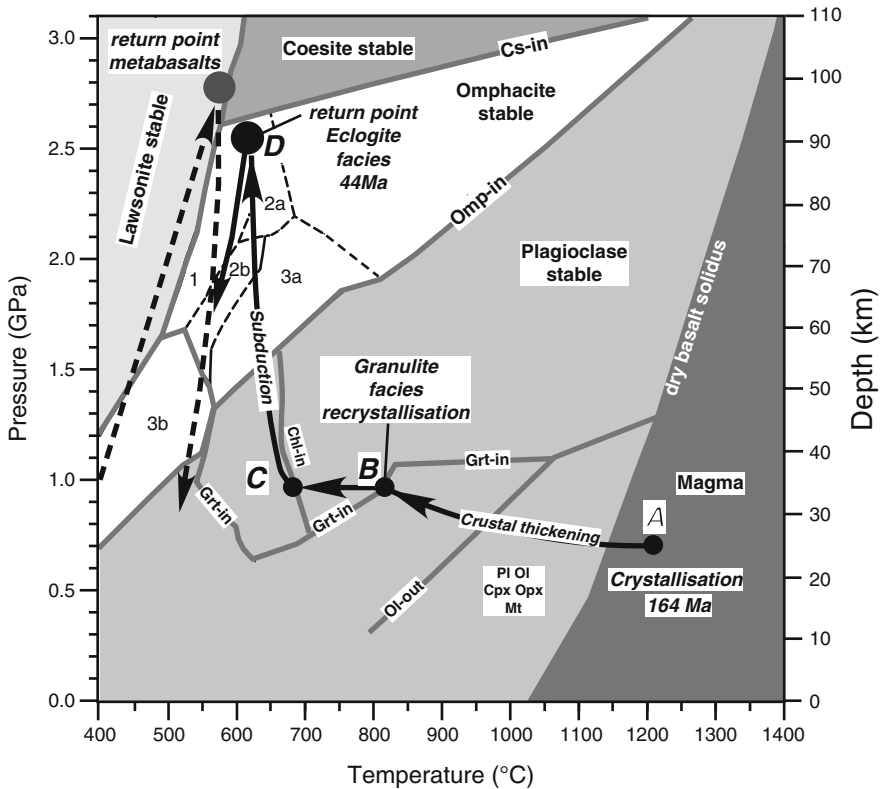


Fig. 9.15 Mineral assemblage diagram for average Allalin gabbro composition with respect to prograde-retrograde *P-T* path shown in Fig. 9.15 (After Bucher and Grapes 2008)



**Fig. 9.16** Prograde and retrograde *P*–*T* paths (arrowed solid lines) of the Allalin gabbro, Swiss Alps, shown in relation to stages (a–d) in the mineral assemblage stability diagram given in Fig. 9.14 and discussed in text. Mineral assemblage stability fields in the omphacite stable region are as follows: 1 *Cld* with *Omp* *Grt* *Zo* *Tlc* ± *Ky* ± *Qtz*; 2a *Tlc* with *Omp* *Grt* *Zo* ± *Ky* ± *Qtz*; 2b *Tlc* with *Omp* *Grt* *Zo* *Hbl* *Pg* *Qtz*; 3a *Hbl*, *Pg* with *Omp* *Grt* *Qtz* ± *Zo* ± *Ep* ± *Gln* ± *Mt* ± *Hm*; 3b *Hbl*, *Pg* with *Omp* *Zo* *Act* *Chl*. Filled circle – return point eclogite recrystallisation (After Bucher and Grapes 2008). Prograde and retrograde paths of the Zermatt–Saas metavolcanics that are now associated with the Allalin gabbro are indicated by arrowed dashed lines (After Bucher et al. 2005). Note that during the return path, the Allalin gabbro is incorporated into the Zermatt–Saas ophiolite at a depth of ~65 km and thereafter was affected by the same retrograde blueschist–greenschist facies recrystallisation

history of the gabbro can be subdivided into various stages: (a) Crystallization of a gabbroic *Pl* + *Ol* + *Cpx* + *Ilm* assemblage. These igneous minerals have survived subsequent metamorphism in undeformed areas of the rocks where  $H_2O$  never had access. (b) Recrystallisation during final cooling under granulite facies conditions caused by crustal thickening to form *Opx* and *Grt* (as corona minerals between *Ol* and *Pl*) at ~850°C/0.8–1.0 GPa. (c) Entrainment of the gabbro in subducting ophiolitic rocks and first hydration to form *Chl* that partly replaces *Ol*, *Opx* and *Cpx*. The *Chl* forms part of the *Opx* + *Grt* coronas instead of *Spl* that would normally have formed under anhydrous granulite facies conditions.

(d) Replacement of Pl by a Jd + Omp + Czo + Ky + Qtz assemblage indicating early stage eclogite facies conditions followed by Omp + Tlc + Rt after Cpx and Tlc + Cld + Ky after Ol and with corona Grt remaining stable, indicating peak eclogite facies conditions at 2.5–2.6 GPa and ~600°C. The LT/HP eclogitic gabbro thus contains a number of hydrous phases (Tlc, Cld, Czo ± Chl) and owes its existence to the access of water during subduction. (e) A highest-P retrograde blueschist facies stage is characterized by the formation of Gln, Pg, Phe that replace Omp and Cld in parts of the rocks where deformation was more intense and access of water occurred. (f) At lower-P, the rocks entered the transitional facies between blueschist and greenschist with the formation of symplectites that replace the eclogite facies minerals, i.e., barroisite + Na-Cpx + Ab + oligoclase + Chl after Omp, Mrg + Pg + preiswerkite after chloritoid, and Ab + barroisite after Gln. These assemblages are fine-grained reaction products of local hydration; (g) Greenschist facies recrystallisation resulted from the return to shallower depths and the formation of Act + Bt + Ab + Chl + Ep at ~400–500 MPa and 400–450°C. The late Alpine greenschist facies overprint is accompanied by two distinct phases of deformation. The impact of these stages on the Allalin gabbro varies from place to place and ranges from virtually nothing to complete retrogression. The greenschist facies deformation and hydration is often localized along shear zones and deformation is ductile in contrast to the eclogite-stage deformation that has been brittle. (h) Subgreenschist facies minerals, Ab, Cal, Prh, are mainly found in veins. The Allalin gabbro also contains sulfides, oxides and other accessory minerals such as Ttn, Crn and Dsp, that were stable at various stages of the  $P$ – $T$  history of the rock.

The example of the Allalin gabbro provides a complex mineral reaction history. Successive development of minerals and mineral assemblages indicate that:

- Deformation is essential in metamorphic processes. It allows water to enter dry igneous rocks. In the absence of water, igneous and metamorphic assemblages will survive under even extreme  $P$ – $T$  conditions (e.g., igneous Pl + Cpx + Ol at 2.5 GPa and 600°C).
- Mafic rocks that undergo eclogite facies metamorphism do not necessarily become eclogites. The bulk composition of many gabbros may not be favorable for the formation of Grt.
- LT eclogite facies mafic rocks that form by subduction of oceanic lithosphere, are characterized by the presence of a number of hydrous minerals at peak-P conditions of the eclogite facies (Zo, Cld, Tlc, Chl, Phe).
- LT eclogite facies rocks may pass through the blueschist facies on their return path to the surface. The blueschist facies overprint is then retrograde in nature and adds another group of hydrous minerals such as Gln and Pg to the high-P/low-T assemblage.
- All stages of the complex  $P$ – $T$  path followed by the Allalin gabbro and the reaction history involving a large number of minerals may be preserved in a single rock body. The predominant assemblage that is found in a single hand specimen or within a small area of a given outcrop depends on how much water entered the rock at a given  $P$ – $T$  stage in its metamorphic evolution.

- The availability of water is in turn related to the local extent of deformation. Given a certain stage, if much water is available, the formation of the maximum hydrated assemblage for that stage is possible. Water is consumed by hydration reactions that tend to dry out the rock. Thus, water must be continuously supplied in order to facilitate reactions that produce the maximum hydrated assemblage at that stage. Access for water to the originally dry rock is provided by micro-fractures and other brittle deformation structures during high-P metamorphism and by pervasive ductile deformation during greenschist facies metamorphism.

## References and Further Reading

### *Cited References*

- Arnórsson S (1995) Geothermal systems in Iceland; structure and conceptual models; I High-temperature area. *Geothermics* 24:561–602
- Boles JR, Coombs DS (1975) Mineral reactions in zeolitic Triassic tuff, Hokonui Hills, New Zealand. *Geol Soc Am Bull* 86:163–173
- Brothers RN, Grapes RH (1989) Clastic lawsonite, glaucophane and jadeitic pyroxene in Franciscan metagraywackes from the Diablo Range, California. *Geol Soc Am Bull* 101:14–26
- Bucher K, Fazines Y, De Capitani C, Grapes R (2005) Blueschists, eclogites, and decompression assemblages of the Zermatt-Saas ophiolite: high-pressure metamorphism of subducted Tethys lithosphere. *Am Mineralog* 90:821–835
- Bucher K, Frost BR (2006) Fluid transfer in high-grade metamorphic terrains intruded by anorogenic granites: the Thor Range, Antarctica. *J Petrol* 47:567–593
- Bucher K, Grapes R (2008) The Allalin gabbro of the Zermatt-Saas ophiolite, Western Alps: a record of subduction zone hydration. *J Petrol* 50:1405–1442
- Chinner GA, Dixon JE (1973) Some high-pressure parageneses of the Allalin gabbro, Valais, Switzerland. *J Petrol* 14:185–202
- Cho CM, Liou JG (1987) Prehnite-pumpellyite to greenschist facies transition in the Karmutsen metabasites, Vancouver island, B.C. *J Petrol* 28:417–443
- Ernst WG (1965) Mineral paragenesis in Franciscan metamorphic rocks, Panoche Pass, California. *Geol Soc Am Bull* 76:879–914
- Ernst WG (1971) Do mineral paragenesis reflect unusually high-pressure conditions in Franciscan metamorphism? *Am J Sci* 271:81–108
- Ernst WG, Seki Y, Onuki H, Gilbert MC (1970) Comparative study of low-grade metamorphism in the California Coast. Ranges and the outer metamorphic belt of Japan, vol 124. Geological Society America Memoir, Boulder, 276p
- Hollocher K (1991) Prograde amphibole dehydration reactions during high-grade regional metamorphism, Central Massachusetts, U.S.A. *Am Mineralog* 76:956–970
- James HL (1955) Zones of regional metamorphism in the Precambrian of northern Michigan. *Geol Soc Am Bull* 66:1455–1488
- Jayko AS, Blake MC, Brothers RN (1986) Blueschist metamorphism of the Eastern Franciscan belt, northern California. In: Evans BW, Brown EH (eds) *Blueschists and eclogites*, vol 164. Geological Society of America Memoir, Boulder, pp 107–123
- Kuniyoshi S, Liou JG (1976a) Burial metamorphism of the Karmutsen volcanic rocks, northeastern Vancouver Island, British Columbia. *Am J Sci* 276:1096–1119



- Liou JG, Maruyama S, Cho M (1987) Very low-grade metamorphism of volcanic and volcanoclastic rocks – mineral assemblages and mineral facies. In: Frey M (ed) Low temperature metamorphism. Blackie, Glasgow, pp 59–113
- Seki Y, Oki Y, Matsuda T, Mikami K, Okumura K (1969) Metamorphism in the Tanzawa Mountains, central Japan. *Jpn Assoc Mineralog Petrolog Econ Geol* 61(1–29):50–75

### ***Further Reading and Additional Literature***

- Apted MJ, Liou JG (1983) Phase relations amongst greenschist, epidote-amphibolite, and amphibolite in a basaltic system. *Am J Sci* 283A:328–354
- Austrheim H, Griffin WL (1985) Shear deformation and eclogite formation within granulite – facies anorthosites of the Bergen Arcs, Western Norway. *Chem Geol* 50:267–281
- Auzanneau E, Schmidt MW, Vielzeuf D, Connolly JAD (2010) Titanium in phengite: a geobarometer for high temperature eclogites. *Contrib Mineralog Petrol* 159:1–24
- Banno S (1986) The high pressure metamorphic belts in Japan: a review, vol 164. Geological Society of America Memoir, Boulder, pp 365–374
- Barnicoat AC, Cartwright I (1997) The gabbro-eclogite transformation: an oxygen isotope and petrographic study of west Alpine ophiolites. *J Metamorph Geol* 15:93–104
- Barton MD, Staude J-M, Snow EA, Johnson DA (1991) Aureole systematics. In: Kerrick DM (ed) Contact metamorphism. Reviews in mineralogy, vol 26. Mineralogical Society of America, Washington DC, pp 723–847
- Bearth P (1967) Die Ophiolithe der Zone von Zermatt-Saas Fee. Beiträge zur geologischen Karte der Schweiz N.F. 132, 130pp
- Bégin NJ (1992) Contrasting mineral isograd sequences in metabasites of the Cape Smith Belt, northern Québec, Canada: three new bathograds for mafic rocks. *J Metamorph Geol* 10:685–704
- Bégin NJ, Carmichael DM (1992) Textural and compositional relationships of Ca-amphiboles in metabasites of the Cape Smith Belt, northern Québec: implications for a miscibility gap at medium pressure. *J Petrol* 33:1317–1343
- Bevins RE, Robinson D (1993) Parageneses of Ordovician sub-greenschist to greenschist facies metabasites from Wales, U.K. *Eur J Mineralog* 5:925–935
- Bohlen SB, Liotta JJ (1986) A barometer for garnet amphibolites and garnet granulites. *J Petrol* 27:1025–1034
- Brothers RN, Yokoyama K (1982) Comparison of high pressure schists belts of New Caledonia and Sanbagawa, Japan. *Contrib Mineral Petrol* 79:219–229
- Brown EH (1974) Comparison of the mineralogy and phase relations of blueschists from the North Cascades, Washington and greenschists from Otago, New Zealand. *Geol Soc Am Bull* 85:333–344
- Brown EH (1977) The crossite content of Ca-amphibole as a guide to pressure of metamorphism. *J Petrol* 18:53–72
- Carmichael RS (1989) Practical handbook of physical properties of rocks and minerals. CRC Press, Boca Raton, 834 pp
- Cho M, Liou JG, Maruyama S (1986) Transition from the zeolite to prehnite-pumpellyite facies in the Karmutsen metabasites, Vancouver island, British Columbia. *J Petrol* 27:467–494
- Coleman RG, Lee DE, Beatty LB, Brannock WW (1965) Eclogites and eclogites: their differences and similarities. *Geol Soc Am Bull* 76:483–508
- Coombs DS, Ellis AJ, Fyfe WS, Taylor AM (1959) The zeolite facies, with comments on the interpretation of hydrothermal syntheses. *Geochim Cosmochim Acta* 17:53–107
- Cooper AF (1972) Progressive metamorphism of metabasic rocks from the Haast Schist group of southern New Zealand. *J Petrol* 13:457–492

- Cox RA, Indares A (1999) Transformation of Fe-Ti gabbro to coronite, eclogite and amphibolite in the Baie du Nord segment, Maicouagan Imbricate Zone, eastern Grenville Province. *J Metamorph Geol* 17:537–555
- Davis PB, Whitney DL (2006) Petrogenesis of lawsonite and epidote eclogite and blueschist, Sivrihisar Massif, Turkey. *J Metamorph Geol* 24:823–849
- de Haas G-JLM, Nijland TG, Valbracht PJ, Maijer C, Verschure R, Andersen T (2002) Magmatic versus metamorphic origin of olivine-plagioclase coronas. *Contrib Mineralog Petrol* 143:537–550
- de Paoli MC, Clarke GL, Klepeis KA, Allibone AH, Turnbull IM (2009) The eclogite-granulite transition: mafic and intermediate assemblages at Breaksea Sound, New Zealand. *J Petrol* 50:2307–2344
- Donato MM (1989) Metamorphism of an ophiolitic tectonic melange, northern California Klamath Mountains, USA. *J Metamorph Geol* 7:515–528
- Elmer FL, White RW, Powell R (2006) Devolatilization of metabasic rocks during greenschist–amphibolite facies metamorphism. *J Metamorph Geol* 24:497–513
- El-Shazly AK (1994) Petrology of lawsonite-, pumpellyite- and sodic amphibole-bearing metabasites from north-east Oman. *J Metamorph Geol* 12:23–48
- Ernst WG (1972) Occurrence and mineralogical evolution of blueschist belts with time. *Am J Sci* 272:657–668
- Eskola P (1921) On the eclogites of Norway. *Skr Vidensk Selsk Christiania Mat-nat Kl I* 8:1–118
- Evans BW (1990) Phase relations of epidote-blueschists. *Lithos* 25:3–23
- Evans BW, Brown EH (1986) Blueschists and eclogites. Geological Society of America Memoir, Boulder, 423 pp
- Ferry JM (1984) Phase composition as a measure of reaction progress and an experimental model for the high-temperature metamorphism of mafic igneous rocks. *Am Mineralog* 69:677–691
- Forbes RB, Evans BW, Thurston SP (1984) Regional progressive high-pressure metamorphism, Seward peninsula, Alaska. *J Metamorph Geol* 2:43–54
- Frederico L, Capponi G, Crispini L, Scambelluri M (2004) Exhumation of alpine high-pressure rocks: insights from petrology of eclogite clasts in the Tertiary Piedmontese basin (Ligurian Alps, Italy). *Lithos* 74:21–40
- Frey M, De Capitani C, Liou JG (1991) A new petrogenetic grid for low-grade metabasites. *J Metamorph Geol* 9:497–509
- Frimmel HE, Hartnady CJH (1992) Blue amphiboles and their significance for the history of the Pan-African Gariep belt, Namibia. *J Metamorph Geol* 10:651–670
- Frost BR (1980) Observations on the boundary between zeolite facies and prehnite-pumpellyite facies. *Contrib Mineralog Petrol* 73:365–373
- Gibson GM (1979) Margarite in kyanite- and corundum-bearing anorthosite, amphibolite, and hornblende from central Fiordland, New Zealand. *Contrib Mineralog Petrol* 68:171–179
- Griffin WL, Austrheim H, Brastad K, Bryhni I, Krill A, Mørk MBE, Qvale H, Tørudbakken B (1983) High-pressure metamorphism in the Scandinavian Caledonides. In: Gee DG, Sturt BA (eds) *The Caledonide Orogen – Scandinavia and related areas*. Wiley, Chichester
- Harte B, Graham CM (1975) The graphical analysis of greenschist to amphibolite facies mineral assemblages in metabasites. *J Petrol* 16:347–370
- Hartel THD, Pattison DRM (1996) Genesis of the Kapsuskasing (Ontario) migmatitic mafic granulites by dehydration melting of amphibolite: the importance of quartz to reaction progress. *J Metamorph Geol* 14:591–611
- Heinrich CA (1986) Eclogite facies regional metamorphism of hydrous mafic rocks in the central Alpine Adula Nappe. *J Petrol* 27:123–154
- Helms TS, HY Jr, McSween, Labotka TC, Jarosewich E (1987) Petrology of a Georgia Blue ridge amphibolite unit with hornblende + gedrite + kyanite + staurolite. *Am Mineralog* 72:1086–1096
- Hirajima T, Hiroi Y, Ohta Y (1984) Lawsonite and pumpellyite from the Vestgotabreen Formation in Spitsbergen. *Norsk Geol Tidsskrift* 4:267–273
- Hirajima T, Banno S, Hiroi Y, Ohta Y (1988) Phase petrology of eclogites and related rocks from the Motalafjella high-pressure metamorphic complex in Spitsbergen (Arctic Ocean) and its significance. *Lithos* 22:75–97

- Holland TJB (1979) High water activities in the generation of high pressure kyanite eclogites of the Tauern Window, Austria. *J Geol* 87:1–27
- Holland TJB, Richardson SW (1979) Amphibole zonation in metabasites as a guide to the evolution of metamorphic conditions. *Contrib Mineralog Petrol* 70:143–148
- Hosotani H, Banno S (1986) Amphibole composition as an indicator of subtle grade variation in epidote-glaucophane schists. *J Metamorph Geol* 4:23–36
- Humphris SE, Thompson G (1978) Hydrothermal alteration of oceanic basalts by seawater. *Geochim Cosmochim Acta* 42:107–125
- Johnson CD, Carlson WD (1990) The origin of olivine-plagioclase coronas in metagabbros from the Adirondack Mountains, New York. *J Metamorph Geol* 8:697–717
- Kawachi Y (1975) Pumpellyite-actinolite and contiguous facies metamorphism in the Upper Wakatipu district, southern New Zealand. *NZ J Geol Geophys* 17:169–208
- Konzett J, Hoinkes G (1996) Paragonite-hornblende assemblages and their petrological significance: an example from the Austroalpine Schneeberg Complex, Southern Tyrol, Italy. *J Metamorph Geol* 14:85–101
- Krogh Ravna EJ, Terry MP (2004) Geothermobarometry of UHP and HP eclogites and schists – an evaluation of equilibria among garnet-clinopyroxene-kyanite-phengite-coesite/quartz. *J Metamorph Geol* 22:593–604
- Kuniyoshi S, Liou JG (1976b) Contact metamorphism of the Karmutsen Volcanics, Vancouver Island, British Columbia. *J Petrol* 17:73–99
- Laird J (1980) Phase equilibria in mafic schist from Vermont. *J Petrol* 21:1–27
- Laird J, Albee AL (1981) High pressure metamorphism in mafic schist from northern Vermont. *Am J Sci* 281:97–126
- Leake BE (1964) The chemical distinction between ortho- and para-amphibolite. *J Petrol* 5:238–254
- Liogys VA, Jenkins DM (2000) Hornblende geothermometry of amphibolite layers of the Popple Hill gneiss, north-west Adirondack Lowlands, New York, USA. *J Metamorph Geol* 18:513–530
- Liou JG, Maruyama S, Cho M (1985) Phase equilibria and mineral paragenesis of metabasites in low-grade metamorphism. *Mineralog Mag* 49:321–333
- Liu X, Wei C, Li S, Dong S, Liu J (2004) Thermobaric structure of a traverse across western Dabieshan: implications for collision tectonics between the Sino-Korean and Yangtze cratons. *J Metamorph Geol* 22:361–380
- López S, Castro A (2001a) Determination of the fluid-absent solidus and supersolidus phase relationships of MORB-derived amphibolites in the range of 4–14 kbar. *Am Mineralog* 86:1396–1403
- López S, Castro A (2001b) Determination of the fluid-absent solidus and supersolidus phase relationships of MORB-derived amphibolites in the range of 4–14 kbar. *Am Mineralog* 86:1396–1403
- Lucchetti G, Cabella R, Cortesogno L (1990) Pumpellyites and coexisting minerals in different low-grade metamorphic facies of Liguria, Italy. *J Metamorph Geol* 8:539–550
- Markl G, Bucher K (1997) Eclogites from the early Proterozoic Lofoten Island, N. Norway. *Lithos* 42:15–35
- Maruyama S, Suzuki K, Liou JG (1983) Greenschist-amphibolite transition equilibria at low pressures. *J Petrol* 24:583–604
- Mattinson CG, Zhang RY, Tsujimori T, Liou JG (2004) Epidote-rich talc-kyanite-phengite eclogites, Sulu terrane, eastern China: P-T- $f_{O_2}$  estimates and the significance of the epidote-talc assemblage in eclogite. *Am Mineralog* 89:1772–1783
- Messiga B, Scambelluri M, Piccardo GB (1995) Chloritoid-bearing assemblages in mafic systems and eclogite-facies hydration of alpine Mg-Al metagabbros (Erro- Tobbio Unit, Ligurian Western Alps). *Eur J Mineralog* 7:1149–1167
- Messiga B, Kienast JR, Rebay M, Piccardi P, Tribuzio R (1999) Cr-rich magnesiochloritoid eclogites from the Monviso ophiolites (Western Alps, Italy). *J Metamorph Geol* 17:287–299
- Meyre C, Puschign AR (1993) High-pressure metamorphism and deformation at Trescolmen, Adula nappe, Central Alps. *Schweiz Mineral Petrogr Mitt* 73:277–283

- Meyre C, De Capitani C, Partsch JH (1997) A ternary solid solution model for omphacite and its application to geothermobarometry of eclogites from the Middle Adula nappe (Central Alps, Switzerland). *J Metamorph Geol* 15:687–700
- Meyer J (1983a) Mineralogie und Petrologie des Allalingabbros. Doctoral dissertation. unpublished Doctoral dissertation 329 pp. University of Basel
- Meyer J (1983b) The development of the high-pressure metamorphism in the Allalin metagabbro (Switzerland). *Terra Cognita* 3, 187
- Mongkoltip P, Ashworth JR (1986) Amphibolitization of metagabbros in the Scottish Highlands. *J Metamorph Geol* 4:261–283
- Moody JB, Meyer D, Jenkins JE (1983) Experimental characterization of the greenschist-amphibolite boundary in mafic systems. *Am J Sci* 283:48–92
- Nakamura D (2003) Stability of phengite and biotite in eclogites and characteristics of biotite- or orthopyroxene-bearing eclogites. *Contrib Mineralog Petrol* 145:550–567
- Neuhoff PS, Fridriksson T, Arnórsson S, Bird DK (1999) Porosity evolution and mineral paragenesis during low-grade metamorphism of basaltic lavas at Teigarhorn, eastern Iceland. *Am J Sci* 299:467–501
- Newton RC (1986) Metamorphic temperatures and pressures of Group B and C eclogites, vol 164. Geological Society of America Memoir, Boulder, pp 17–30
- O'Brien PJ (1993) Partially retrograded eclogites of the Münchberg Massif, Germany: records of a multistage Variscan uplift history in the Bohemian Massif. *J Metamorph Geol* 11:241–260
- Okay AI (1994) Sapphirine and Ti-clinohumite in ultra-high-pressure garnet-pyroxenite and eclogite from Dabie Shan, China. *Contrib Mineralog Petrol* 116:145–155
- Okay AI (2002) Jadeite-chloritoid-glaucophane-lawsonite blueschists in north-west Turkey: unusually high P/T ratios in continental crust. *J Metamorph Geol* 20:757–768
- Ono S, Ito E, Katsura T (2001) Mineralogy of subducted basaltic crust (MORB) from 25 to 37 GPa, and chemical heterogeneity of the lower mantle. *Earth Planet Sci Lett* 190:57–63
- Patrick BE, Day HW (1989) Controls on the first appearance of jadeitic pyroxene, northern Diablo Range, California. *J Metamorph Geol* 7:629–639
- Pattison DR (1991) Infiltration-driven dehydration and anatexis in granulite facies metagabbro, Grenville Province, Ontario, Canada. *J Metamorph Geol* 9:315–332
- Pattison DRM (2003) Petrogenetic significance of orthopyroxene-free garnet + clinopyroxene + plagioclase ± quartz-bearing metabasites with respect to the amphibolite and granulite facies. *J Metamorph Geol* 21:21–34
- Platt JP (1993) Exhumation of high-pressure rocks: a review of concepts and processes. *Terra Nova* 5:119–133
- Pognante U, Kienast J-R (1987) Blueschist and eclogite transformations in Fe-Ti gabbros: a case from the western Alps ophiolites. *J Petrol* 28:271–292
- Powell WG, Carmichael DM, Hodgson CJ (1993) Thermobarometry in a sub-greenschist to greenschist transition in metabasites of the Abitibi greenstone belt, Superior Province, Canada. *J Metamorph Geol* 11:165–178
- Raimbourg H, Goffé B, Jolivet L (2007) Garnet reequilibration and growth in the eclogite facies and geodynamical evolution near peak metamorphic conditions. *Contrib Mineralog Petrol* 153:1–28
- Ravna EK, Andersen TB, Jolivet L, de Capitani C (2010) Cold subduction and the formation of lawsonite eclogite – constraints from prograde evolution of eclogized pillow lava from Corsica. *J Metamorph Geol* 28:381–395
- Rebay G, Powell R (2002) The formation of eclogite facies metatroctolites and a general petrogenetic grid in Na<sub>2</sub>O-CaO-FeO-MgO-Al<sub>2</sub>O<sub>3</sub>-SiO<sub>2</sub>-H<sub>2</sub>O (NCFMASH). *J Metamorph Geol* 20:813–826
- Root DB, Hacker BR, Gans PB, Ducea MN, Eide EA, Mosenfelder JL (2005) Discrete ultrahigh-pressure domains in the Western Gneiss Region, Norway: implications for formation and exhumation. *J Metamorph Geol* 23:45–62

- Russ-Nabelek C (1989) Isochemical contact metamorphism of mafic schist, Laramie Anorthosite Complex, Wyoming: amphibole compositions and reactions. *Am Mineralog* 74:530–548
- Sanders LS (1988) Plagioclase breakdown and regeneration reactions in Grenville kyanite eclogite at Glenelg, NW Scotland. *Contrib Mineralog Petrol* 98:33–39
- Schmidt MW, Vielzeuf D, Auzanneau E (2004) Melting and dissolution of subducting crust at high pressures: the key role of white mica. *Earth Planet Sci Lett* 228:65–84
- Shibuya T, Kitajima K, Lomiya T, Terabayashi M, Maruyama S (2007) Middle Archean ocean ridge hydrothermal metamorphism and alteration recorded in the Cleaverville area, Pilbara Craton, Western Australia. *J Metamorph Geol* 25:751–767
- Smelik EA, Veblen DR (1989) A five-amphibole assemblage from blueschists in northern Vermont. *Am Mineralog* 74:960–964
- Smith DC, Lappin MA (1989) Coesite in the Straumen kyanite-eclogite pod, Norway. *Terra Nova* 1:47–56
- Song SG, Zhang LF, Niu Y, Wei CJ, Liou JG, Shu GM (2007) Eclogite and carpholite-bearing metasedimentary rocks in the North Qilian suture zone, NW China: implications for Early Palaeozoic cold oceanic subduction and water transport into mantle. *J Metamorph Geol* 25:547–563
- Soto JI (1993) PTMAFIC: software for thermobarometry and activity calculations with mafic and ultramafic assemblages. *Am Mineralog* 78:840–844
- Spear FS (1980) NaSi ↔ CaAl exchange equilibrium between plagioclase and amphibole. An empirical model. *Contrib Mineralog Petrol* 72:33–41
- Spear FS (1982) Phase equilibria of amphibolites from the Post Pond Volcanics, Mt. Cube quadrangle, Vermont. *J Petrol* 22:383–426
- Springer RK, Day HW, Beiersdorfer RE (1992) Prehnite-pumpellyite to greenschist facies transition, Smartville Complex, near Auburn, California. *J Metamorph Geol* 10:147–170
- Starkey RJ, Frost BR (1990) Low-grade metamorphism of the Karmutsen Volcanics, Vancouver Island, British Columbia. *J Petrol* 31:167–195
- Terabayashi M (1993) Compositional evolution in Ca-amphibole in the Karmutsen metabasites, Vancouver Island, British Columbia, Canada. *J Metamorph Geol* 11:677–690
- Thiéblemont D, Triboulet C, Godard G (1988) Mineralogy, petrology and P-T-t path of Ca-Na amphibole assemblages, Saint-Martin des Noyers formation, Vendée, France. *J Metamorph Geol* 6:697–716
- Thompson AB, Laird J (2005) Calibrations of modal space for metamorphism of mafic schist. *Am Mineralog* 90:843–856
- Thompson JB (1991) Modal space: applications to ultramafic and mafic rocks. *Can Mineralog* 29:615–632
- Thompson JB, Laird J, Thompson AB (1983) Reactions in amphibolite, greenschist, and blueschist. *J Petrol* 23:1–27
- Topuz G, Okay AI, Altherr R, Satir M, Schwarz H (2008) Late Cretaceous blueschist facies metamorphism in southern Thrace (Turkey) and its geodynamic implications. *Metamorph Geol* 26:895–913
- Triboulet C, Thiéblemont D, Audren C (1992) The (Na-Ca) amphibole- albite- chlorite- epidote-quartz geothermobarometer in the system S-A-F-M-C-N-H<sub>2</sub>O. 2. Applications to metabasic rocks in different metamorphic settings. *J Metamorph Geol* 10:557–566
- Wang Q, Zhang L, Song S (2007) p-T condition and phase equilibrium of lawsonite-blueschists in northern Qilian Mountains and its petrologic significance. *Earth Sci Front* 14:157–171
- Warren CJ, Waters DJ (2006) Oxidised eclogites and garnet-blueschists from Oman: P-T path modeling in the NCFMASHO system. *J Metamorph Geol* 24:783–802
- Wei CJ, Song SG (2008) Chloritoid-glaucophane schist in the north Qilian orogen, NW China: phase equilibria and P-T path from garnet zonation. *J Metamorph Geol* 26:301–316
- Wei CJ, Yang Y, Su XL, Song SG, Zhang LF (2009) Metamorphic evolution of low-T eclogite from the North Qilian orogen, NW China: evidence from petrology and calculated phase equilibria in the system NCKFMASHO. *J Metamorph Geol* 27:55–70

- Wolke C, Truckenbrodt J, Johannes W (1995) Beginning of dehydration-melting in amphibolites at  $P \leq 10$  kbar. *Eur J Mineralog* 7:273
- Yang J-J, Powell R (2006) Calculated phase relations in the system  $\text{Na}_2\text{O}-\text{CaO}-\text{K}_2\text{O}-\text{FeO}-\text{MgO}-\text{Al}_2\text{O}_3-\text{SiO}_2-\text{H}_2\text{O}$  with applications to UHP eclogites and whiteschists. *J Petrol* 47:2047–2071
- Zen E-an (1961) The zeolite facies: an interpretation. *Am J Sci* 259:401–409
- Zhang L, Song S, Liou JG, Ai Y, Li X (2005) Relict coesite exsolution in omphacite from Western Tianshan eclogites, China. *Am Mineralog* 90:1092–1099
- Zhang G, Song S, Zhang L, Niu Y (2008) The subducted oceanic crust within continental-type UHP metamorphic belt in the North Qaidam, NW China: evidence from petrology, geochemistry and geochronology. *Lithos* 104:99–118
- Zhang G, Ellis DJ, Christy AG, Zhang L, Niu Y, Song S (2009) UHP metamorphic evolution of coesite-bearing eclogite from the Yuka terrane, North Qaidam UHPM belt, NW China. *Eur J Mineralog* 21:1287–1300



# Chapter 10

## Metamorphism of Quartzofeldspathic Rocks

### 10.1 Quartzofeldspathic Rocks

Metamorphosed quartzofeldspathic rocks are derived from graywacke sandstone and siltstone (clastic sediments; Table 2.3), and granitoid protoliths such as granite, alkali-feldspar granite, granodiorite and tonalite (Table 2.3). They constitute the largest portion of the continental crust. For instance, quartzofeldspathic gneisses (metasedimentary paragneisses and granitic orthogneisses), commonly migmatitic, are the dominant rock type of the continents, forming extensive terranes. Because the main metamorphic constituents – Qtz, Kfs, Pl, Bt, Ms, Hbl – occur over a wide range of  $P$ – $T$  conditions, and because Al-silicates are typically absent due to a relatively high silica content (Table 2.3), quartzofeldspathic rocks may not be a particularly useful indicator of metamorphic grade and are often neglected in textbooks. However, in this chapter we examine the progressive metamorphism of metagraywacke-type rocks and describe selected mineralogical features that can be used to determine metamorphic grade in metagranitoid rocks.

### 10.2 Metagraywackes

#### 10.2.1 Introduction

Because quartzofeldspathic graywacke-type rocks originally formed as clastic sediments (often turbiditic), they contain abundant detrital minerals typically together with lithic clasts of various volcanic, plutonic and metamorphic rock types. The dominant and most obvious detrital minerals are Qtz and feldspars that account for most of the bulk rock  $\text{SiO}_2$ ,  $\text{Al}_2\text{O}_3$ ,  $\text{Na}_2\text{O}$  and  $\text{K}_2\text{O}$  contents (Table 2.3) so that they essentially equate with a granodiorite bulk composition. At low grades of metamorphic reconstitution, i.e., subgreenschist facies grade, care needs to be taken to distinguish detrital from neometamorphic minerals. Usually, this is obvious from grain size and features such as bending, cracking, strain polarization of mineral grains, but not always so especially if relatively fine-grained metamorphic detrital



minerals are present. As an example, the detrital and metamorphic mineral assemblage of two prehnite–pumpellyite facies sandstones from graywacke terranes, North Island of New Zealand, are listed in Fig. 10.1. In both cases, the component minerals and their textural relationships were carefully distinguished both optically and using the high resolution back-scattered electron imaging (BEI) technique of the electron probe microanalyser (EPMA). The rocks contain more than twenty different mineral phases and the metamorphic grade-determining minerals Ab + Ms + Chl + Pmp + Prh + Ep occur as both detrital and neometamorphic grains. Detrital Qtz, Pl, Kfs, Ms, Chl, Ep, Hbl, Ilm, and allanite even survive in semi-schistose greenschist facies rocks. In terms of bulk compositions, graywacke 1 equates with an adamellite and graywacke 2 with a granodiorite (Fig. 10.1). In other metagraywackes, e.g., the blueschist facies rocks of the Franciscan terrane, California, both detrital and neometamorphic Lws, Gln and Jd (see below) have been distinguished.

Mineral	Graywacke 1		Graywacke 2	
	Detrital	Neometamorphic	Detrital	Neometamorphic
Quartz	X	X	X	X
Plagioclase	X		X	
Albite	X	X	X	X
K-feldspar	X		X	
Muscovite	X	X	X	X
Biotite	X		X	
Stilpnomelane		X		
Chlorite	X	X	X	X
Prehnite			X	X
Pumpellyite	X	X	X	X
Hornblende			X	
Clinopyroxene			X	
Garnet	X			
Epidote	X	X	X	X
Allanite	X			
Titanite	X	X	X	X
Tourmaline	X		X	
Zircon	X		X	
Apatite	X		X	
Calcite		X		X
Ilmenite	X		X	
Pyrrhotite		X		
Pyrite		X		X
Graphite	X			

**Fig. 10.1** Detrital and neometamorphic minerals present in two prehnite–pumpellyite facies metagraywacke sandstones from New Zealand. *Graywacke 1* bulk composition: SiO<sub>2</sub> (70.9%), TiO<sub>2</sub> (0.4%), Al<sub>2</sub>O<sub>3</sub> (14.1%), Fe<sub>2</sub>O<sub>3</sub> (0.6%), FeO (2.3%), MgO (1.0%), CaO (1.3%), Na<sub>2</sub>O (4.0%), K<sub>2</sub>O (2.6%); *Graywacke 2* bulk composition: SiO<sub>2</sub> (63.7%), TiO<sub>2</sub> (0.8%), Al<sub>2</sub>O<sub>3</sub> (16.1%), Fe<sub>2</sub>O<sub>3</sub> (1.2%), FeO (5.5%), MgO (2.4%), CaO (3.1%), Na<sub>2</sub>O (4.2%), K<sub>2</sub>O (2.3%) (Data from Grapes et al. 2001)

The characteristic neometamorphic assemblage in Jd-absent metagraywackes is the blueschist assemblage Lws + Phe + Ab + Chl + Ttn ± Gln ± Arg ± Pmp.

### 10.2.2 Metamorphism of Metagraywacke (Metaspammitic) Compositions

Equilibrium mineral assemblages for a typical graywacke sandstone composition (= granodiorite) are shown in Fig. 10.2. All assemblages contain Qtz as might be expected from the silica-rich (70.9 wt%) composition of the protolith, and K-mica (Ms, Cel, Phe) is stable over most of the *P-T* field. Stauroilite is absent and Cld is restricted to very high-*P* conditions.

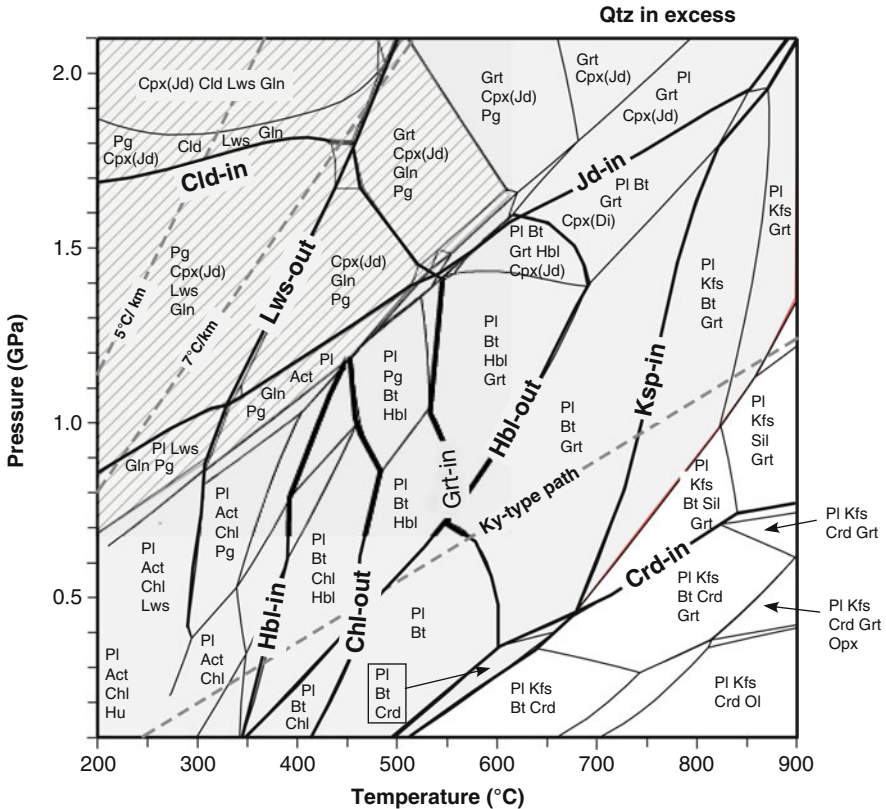


**Fig. 10.2** Calculated equilibrium mineral assemblages in *P-T* space for a graywacke sandstone (granodiorite) composition ( $\text{SiO}_2 - 73.83\%$ ;  $\text{Al}_2\text{O}_3 - 13.25\%$ ; FeO (total iron) - 3.37%;  $\text{MgO} - 1.16\%$ ;  $\text{CaO} - 1.41\%$ ;  $\text{Na}_2\text{O} - 3.10$ ;  $\text{K}_2\text{O} - 2.53\%$ ). Mineral-in and -out “isograds” are highlighted. Shaded area indicates the stability field of K-white mica (Ms, Phe, Cel). Diagonally lined area = Gln stable. Quartz occurs with all mineral assemblages

### 10.2.3 Orogenic Metamorphism of Metagraywackes

Prograde paths of high-P and medium-P, Ky-type geotherms are shown in Fig. 10.2. In high-P metamorphism, Lws, Gln and Jd are the critical minerals formed in metagraywacke lithologies. At  $P > 1.7$  GPa and  $T < 450^\circ\text{C}$ , a Cld-stability field is predicted and metaclastic schists that contain  $\text{Cld} + \text{Lws} + \text{Gln} + \text{Jd} + \text{Phe} \pm \text{Pg}$  are reported from NW Turkey where peak metamorphic conditions are inferred to have been  $> 2.0$  GPa at  $\sim 430^\circ\text{C}$  (Okay and Kelley 1994; Okay 2002). Very high-P Cld-bearing assemblages are only formed where the geothermal gradient is  $< 7^\circ\text{C}/\text{km}$  (Fig. 10.2). At lower-P, metagraywacke schist and gneiss can be subdivided into those which contain Hbl ( + Bt + Ms + Pl  $\pm$  Grt) and those without Hbl. Highest grade metagraywacke mineral assemblages are characterized by Kfs and the eventual disappearance of Ms.

#### 10.2.3.1 Medium-P Metamorphism of Graywacke

The general sequence of mineral stabilities with increasing metamorphic grade along a medium-P geotherm, e.g., near the Ky-type path shown in Fig. 10.2, can be illustrated using the New Zealand metagraywacke terrane as an example. A map showing the distribution of metamorphic facies in the South Island of New Zealand is given in Fig. 10.3 and succession of mineral assemblages shown in Fig. 10.4. Note that Hbl is not a metamorphic mineral in metagraywacke compositions although Act occurs in pumpellyite–actinolite and greenschist facies rocks. Higher grade schist of transitional and amphibolite facies grades is characterized by the non-diagnostic assemblage  $\text{Qtz} + \text{Pl} + \text{Ms} + \text{Bt} + \text{Grt}$  with the incoming of minor Kfs in the highest grade schist exposed near the Alpine Fault. Detailed structural and mineralogical studies (see references) have shown that the metagraywacke has undergone at least two main phases of metamorphic recrystallisation and deformation. An early relatively high P/T phase resulted in the formation of blue Na-amp (crossite) (in metabasite, metachert), Lws (in metagraywacke) and Mn–Grt with Ab (in metagraywacke) that has been overprinted by a higher T/P event represented by transitional and amphibolite grade schist exposed by Cenozoic uplift on the Alpine Fault to form the Southern Alps (Fig. 10.5). The highest grade amphibolite facies metagraywacke schist contains lenses/layers of granite pegmatite (Qtz, Pl, Kfs, Ms, Bt, Grt) that may represent anatexic melt.

#### 10.2.3.2 High-P Metamorphism of Graywacke

The Californian Franciscan terrane metagraywacke is an often cited example of high-P/low-T zeolite, prehnite–pumpellyite, and blueschist facies metamorphism

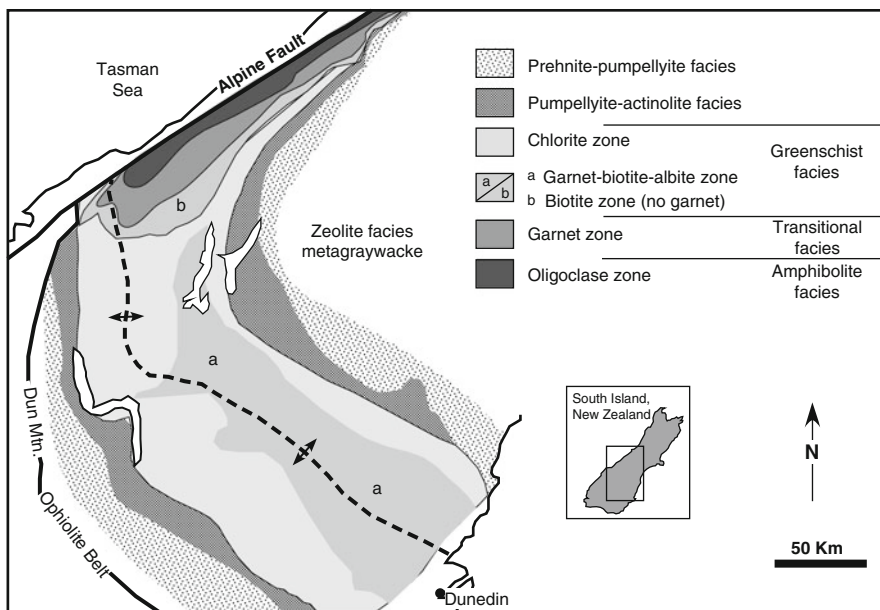


**Fig. 10.3** Map showing the distribution of prehnite–pumpellyite to amphibolite facies and mineral zones in metagraywacke-schist of the South Island of New Zealand (modified after Mortimer 2000)

(Figs. 10.6 and 10.7) indicative of a low ( $<7^{\circ}\text{C}/\text{km}$ ) geothermal gradient (Fig. 10.2). The characteristic high-P metamorphic minerals (blueschist facies) in the metagraywackes are Lws, Gln, Arg and Jd, although a detrital origin for Jd has also been argued on the basis of regional (Fig. 10.6b) and local distribution, microtextures and its replacement by Ab, Pmp, Chl and Qtz (see Brothers and Grapes 1989). If this is the case, the Franciscan metagraywackes are weakly-developed blueschist facies assemblages of  $\text{Lws} + \text{Phe} + \text{Ab} + \text{Chl} + \text{Ttn} \pm \text{Gln} \pm \text{Arg} \pm \text{Pmp}$  indicating metamorphic conditions of 350–500 MPa and 100–200°C (Fig. 10.5). In this respect, it is also worth noting that Lws and Gln occur as both detrital and neometamorphic phases in the metagraywackes. A possible detrital source as localized concentrations of Jd-pyroxene + Qtz and/or Ab clasts within well-defined areas that may represent channelled fan turbiditic sedimentation from Jd-bearing Qtz–Ab metasomatic inclusions in tectonically-emplaced ultramafic rocks and Jd–Qtz–Lws in some metabasic blocks. From Fig. 10.2, a Jd-bearing metagraywacke assemblage would form at pressures  $>0.85$  GPa at 200°C, but if  $X_{\text{Jd}}$  in pyroxene was  $< \text{Jd}_{100}$ , then it could form at lower P (Holland 1983) (Fig. 10.5). Anomalies created by the presence or absence of neometamorphic Jd with or without Ab (Fig. 10.6b) have been explained as Ab persisting as a metastable relic due to sluggish reaction rates, variation of  $\text{XH}_2\text{O}/\text{XCO}_2$  in the fluid phase, and variable metagraywacke composition, with possible jadeitic pyroxene-forming reactions

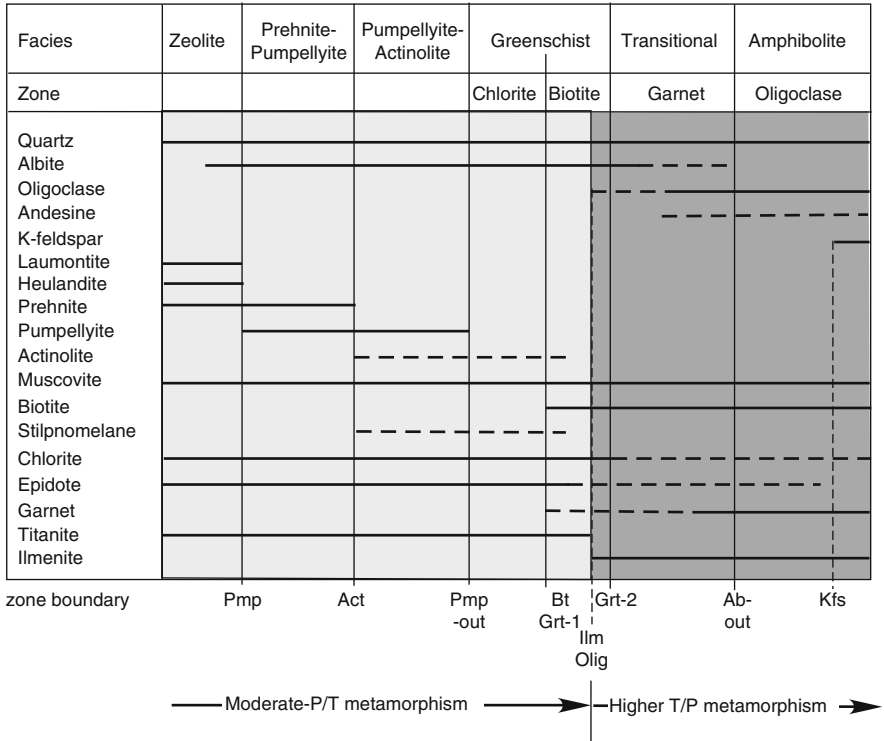
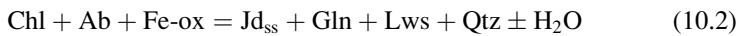


**Fig. 10.4** Mineral stability ranges in zeolite to amphibolite facies metagraywacke-schist, South Island of New Zealand. Mineral isograds are indicated. For two main stages of metamorphism see Fig. 10.5



(Ernst and Banno 1991).

### 10.2.4 Contact Metamorphism of Metagraywackes and Metapsammites

Low-P/high-T metamorphism of metagraywacke is expected to result in the formation of Kfs, Crd ± Sil, and Opx, the disappearance of K-mica, and partial melting to form migmatites (Fig. 10.2). These features are illustrated by way of two examples of contact metamorphism and one of migmatization.

At Baranof Island, SE Alaska, prehnite-pumpellyite facies metagraywacke turbidites, have been contact metamorphosed on a regional scale by granite

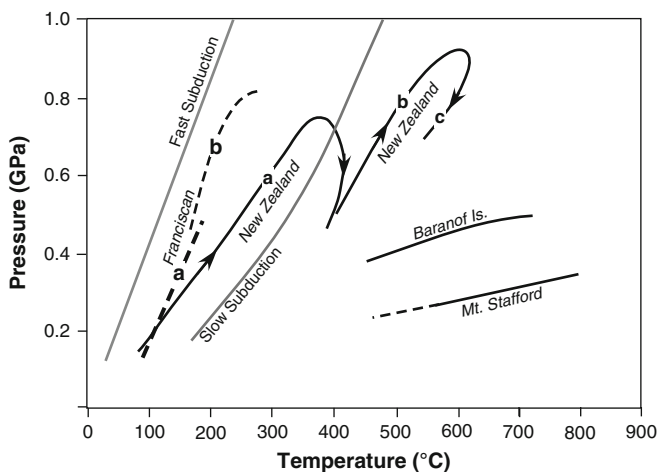


**Fig. 10.5** Prograde  $T$ - $P$  paths of metagraywacke and metapsammite rocks described in text. Franciscan metagraywacke, **a** = assuming detrital Jd (Brothers and Grapes 1989) and **b** = assuming neometamorphic Jd (Maruyama et al. 1985). New Zealand metagraywacke-schist, **a** = Late Triassic–Jurassic moderately high- $P$  subduction zone metamorphism and uplift; **b** = Cretaceous compression; **c** = Late Cretaceous uplift prior to near isothermal Cenozoic uplift on the Alpine Fault (Yardley 1982; Grapes and Watanabe 1992; Grapes 1995); Baranof Island, SE Alaska, metagraywackes (Loney and Brew 1987); Mt. Stafford, Central Australia, metapsammites (White et al. 2003)

(Fig. 10.8). Detrital phases in feldspathic, lithic and arkosic graywacke sandstones comprise mainly Qtz, Kfs, Pl, with minor Bt, Ms, Hbl, Grt, Cpx, Opx, Ap, Zrn, and 30–60% lithic fragments, i.e., similar to those in graywacke 2 listed in Fig. 10.1. Contact metamorphism has produced the zonal sequence, Grt, And–Crd–Bt, and Sil–Grt–Crd with increasing grade (Figs. 10.2 and 10.8) over a  $T$ - $P$  range of  $\sim 530$ – $720^\circ\text{C}$  and 390–450 MPa (Fig. 10.5). The assemblage And–Crd–Bt, suggests the reaction  $\text{Chl} + \text{Ms} + \text{Qtz} = \text{Bt} + \text{Crd} + \text{And} + \text{H}_2\text{O}$ . At the Sil isograd, Kfs first appears together with a decrease in modal Ms, consistent with reactions (7.26) (Table 7.3) and (7.43) (Table 7.4).

In the Mt. Stafford area of Central Australia, high- $T$ /low- $P$  metamorphism of metapsammitic rocks interbedded with metasiltstones (cordierite granofels) and metapelites are associated with migmatites associated with granitic rocks forming a regional aureole that can be subdivided into four zones (Fig. 10.9). Metapsammites of *Zone 1* have an upper greenschist facies assemblage Ms Bt Qtz. *Zone 2* is marked by the appearance of Crd, Kfs, And (lower grade) and Sil (higher grade). In *Zone 3*, Grt appears [e.g., reactions (7.45) and (7.50), Table 7.4], and in *Zone 4*, granulite facies conditions are attained with the appearance of Opx [reactions (7.51)–(7.53), Table 7.4]. Centimetre-scale leucosomes become common in rocks above mid *Zone 2* (inferred position of the wet pelite solidus shown in Fig. 10.9) and increase in size (decimeter-scale) with increasing grade. The leucosomes are essentially Kfs- and Qtz-rich with additional Crd, Bt, Grt depending on

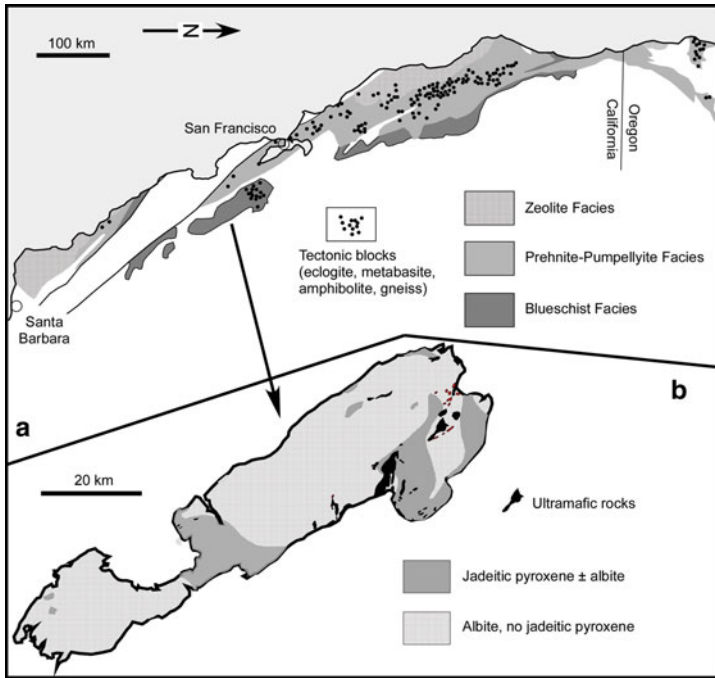
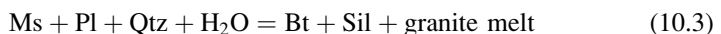


**Fig. 10.6** (a) Map showing the distribution of zeolite, prehnite–pumpellyite and blueschist facies Franciscan metagreywacke, California (After Ernst 1975). (b) Map showing distribution of jadeitic pyroxene-bearing and albite-only metagreywacke, Diablo Range, Central California Coast ranges (Modified after Ernst 1987)

metamorphic grade. In Zone 4, the presence of diatexite and schlieren migmatite indicates that a considerable amount of melting must have occurred, especially in metapelitic lithologies as metapsammitic layers are often broken and rotated within the diatexite matrix. The zonal mineralogy of the metapsammitic rocks at Mt. Stafford indicates a high T/P prograde path (Fig. 10.5) with the consecutive appearance of Crd, Ksp, Sil, Grt and Opx (Fig. 10.2).

Extensively migmatized metagraywacke schist occur in the St. Malo Terrane, Brittany (Brown 1979; Milord et al. 2001). The common mineral assemblage of non-migmatized rocks is Qtz + Pl + Ms + Bt (see Fig. 10.2) with accessory Tur, Ap, Zrn and graphite. The migmatized rocks are characterized by the assemblage Qtz + Pl + Bt ± Kfs + Ap + Zrn + Ilm + graphite with accessory Tur and rare fibrolitic Sil. Mineralogical variation in the rocks is mainly the result of variable modal proportions of the main phases. Notably absent are Grt and Opx although Crd is occasionally found. Temperatures of migmatization are estimated at <800°C within the Bt-present field and mainly involved the breakdown of Ms + Pl + Qtz according to the reactions



Facies	Zeolite	Prehnite-Pumpellyite	Blueschist
Quartz			
Albite	---		
Laumontite	---		
Prehnite		---	
Pumpellyite		---	---
Lawsonite			
Jadeite			---
Glaucophane			---
Chlorite/vermiculite			---
Chlorite			---
Phengite			
Stilpnomelane		---	---
Titanite	---		
Calcite	---		
Aragonite			---

Fig. 10.7 Mineral assemblages and mineral successions in Franciscan metagraywacke

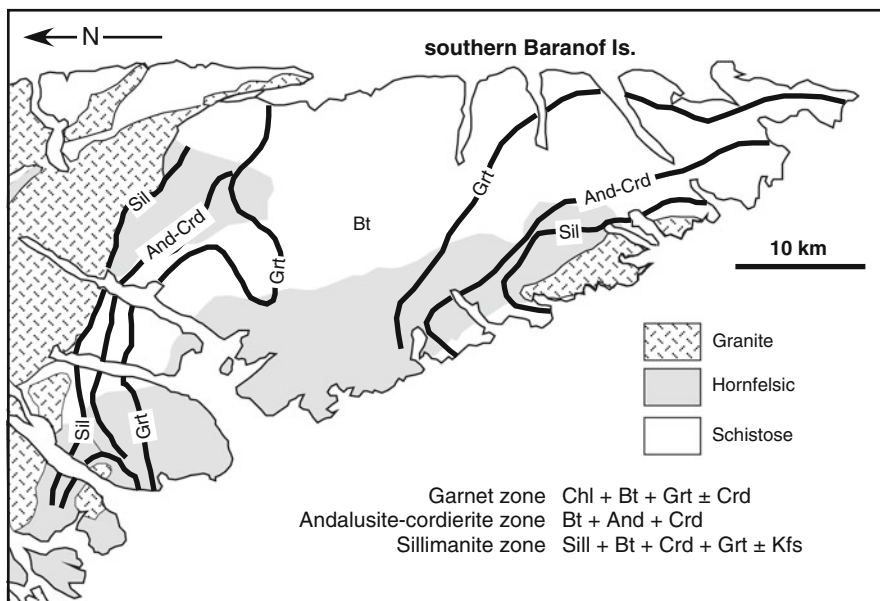
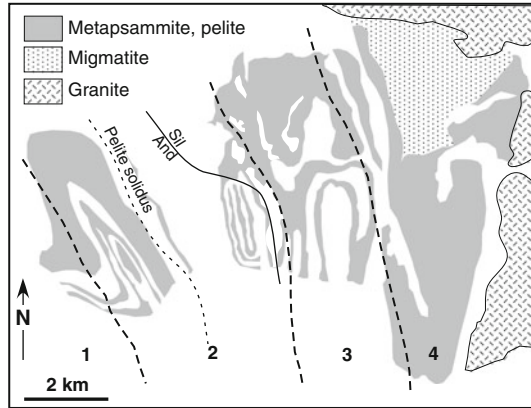


Fig. 10.8 Map showing the distribution of contact metamorphic mineral isograds in hornfelsic and schistose metagraywackes, Baranof Island, SE Alaska (After Fig. 1 of Loney and Brew 1987). Zonal assemblages are listed below

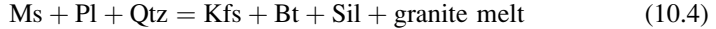


**Fig. 10.9** Map showing distribution of mineral zones in metasedimentary rocks, Mt. Stafford area, Central Australia (After Fig. 1. of White et al. 2003). Zonal assemblages are listed below



**Zone (Metapsammitic rocks)**

- 1 Ms + Bt + Qtz
- 2 Crd + Kfs + Bt + Qtz + And/Sil
- 3 Crd + Kfs + Bt + Qtz  
Crd + Kfs + Bt + Qtz + Grt
- 4 Crd + Kfs + Qtz + Grt + Opx  
Crd + Kfs + Qtz + Grt  
Crd + Kfs + Qtz + Opx



Geochemical changes of the metagraywacke protolith during migmatization to form metatexite, diatexite (melanocratic, mesocratic, leucocratic varieties) and anatectic granite are summarized in Fig. 10.10 in terms of major oxide versus silica trends. Darker rock migmatite (lower silica content) is equated with higher Bt content, lighter rock color with greater modal Qtz and feldspars (typically with  $\text{Pl} \gg \text{Kfs}$ ). With increasing  $\text{SiO}_2$  (rising modal Qtz) in the *metagraywacke protolith* (paleosome), CaO and  $\text{Na}_2\text{O}$  increase reflecting mounting modal Pl, and  $\text{Al}_2\text{O}_3$ , FeO, MgO,  $\text{TiO}_2$  and  $\text{K}_2\text{O}$  decrease indicating lower modal Bt. In relation to this variation, an evolutionary sequence of progressive melting that is also applicable to other metasedimentary, e.g., pelitic, protoliths, can be described (see also Sect. 7.6.1). Early stage migmatization involves formation of metatexite with the same  $\text{SiO}_2$  content as the metagraywacke protolith and with some melting to form Si-rich leucosomes (Qtz, feldspars, minor Bt) and Si-depleted melanosomes (Bt-rich) that typically form residual selvages around the leucosomes. With increasing melting and “homogenisation” of paleosome structures such as layering, the metatexite evolves into a coarser grained diatexite exhibiting flow structure and segregation into a Si-, Ca-, and Na-poor, Fe-, Mg-, Ti-, K-rich melanocratic variety and a Si, Ca, Na-richer leucocratic variety depending on the ratio of Bt to Qtz + Pl. Leucocratic diatexite is associated with anatectic granite (veins and larger masses that may contain pegmatitic segregations).

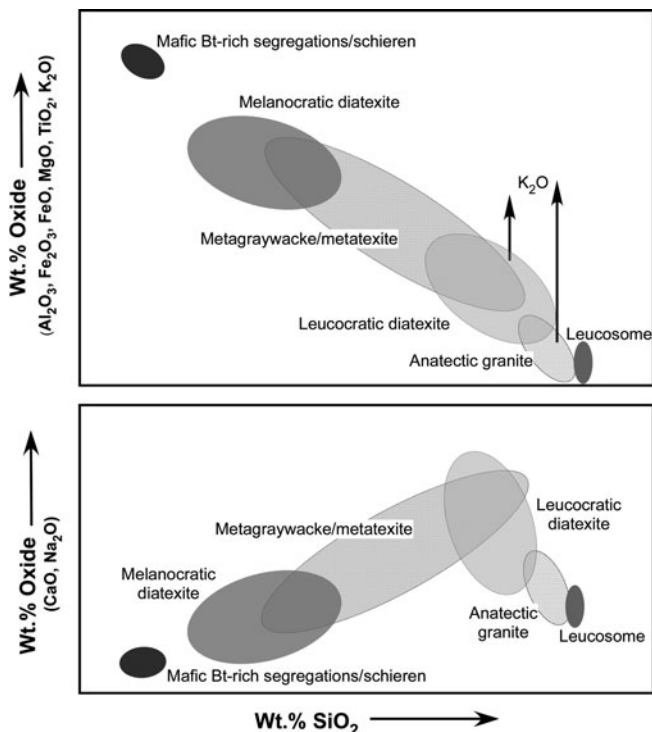


**Fig. 10.10** Generalised bulk rock oxide versus silica variation trends with progressive migmatization of metagraywacke, St. Malo Terrane, France (Modified and combined after Fig. 5 of Milord et al 2001). See text

Water-fluxed melting, i.e., at temperatures intersecting the solidus and below that of muscovite dehydration melting results in a rapid exhaustion of available water but generates enough melt to exceed the liquid percolation threshold so that it is able to migrate for short distances and accumulate in lensoid and vein-like leucosomes (in metatexites). Once temperature attains that of Ms-breakdown, significantly more and pervasive melt is formed that is able to segregate on a regional scale. Pre-migmatite structures are obliterated but are preserved in enclaves, and the rocks can be described as a diatexite. Crystalline and liquid parts of the diatexite “magma” may further become segregated leading to restite-rich (melanocratic diatexite) and melt-rich (leucocratic diatexite) portions. The melanocratic diatexite has >30% Bt and greater amounts of Zrn, Tur, Ap, Rt, Ilm and graphite compared with leucocratic diatexite with <10% Bt and a high Kfs/Pl ratio. A decreasing trend of Ca, Na with increasing Si shown by the granites, leucosomes and some leucocratic diatexites (Fig. 10.10) is due to increasing modal Qtz, and in the leucocratic diatexite and granite also to increasing Kfs as a result of K-mobility and fractional crystallization of melt yielding a Qtz + Pl-dominated cumulate and Kfs-rich liquid, respectively (arrows in Fig. 10.10). Coarser grain

size, magmatic textures and lack of foliation mark the gradational transition from leucocratic diatextite to in-situ granite that at St. Malo consist of large bodies of biotite granite, veins and patches of two-mica granite and tourmaline-bearing granite.

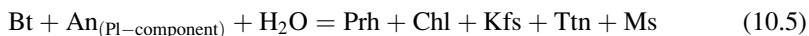
### 10.3 Granitoids

Unlike “wet” quartzofeldspathic sedimentary rocks, granitoids enter the metamorphic realm in a predominantly dry state. Thus, like mafic rocks, in order for metamorphic reactions to begin, hydration, often a significant amount, is necessary. This occurs during deformation. In the absence of penetrative deformation, primary igneous textures and structures are well preserved in metagranitoid rocks, even when subjected to UHP metamorphism.

In the following, selected mineralogical features are described which are useful in determining metamorphic grade, but no attempt is made to deal with progressive metamorphism of granitoid rocks.

#### 10.3.1 *Prehnite and Pumpellyite*

Although Prh and Pmp are commonly known from very low-grade mafic igneous rocks and graywackes, these Ca–Al silicates are sometimes also found in granitic rocks (Tulloch 1979 and references therein; AlDahan 1989). Both minerals are typically associated with Bt, secondary Chl, and Hb. In the case of Bt, Prh forms along cleavage planes that provide suitable structural sites for fluid-facilitated crystallization, although Prh replacement of Bt along its margins has also been observed, indicating the reaction:

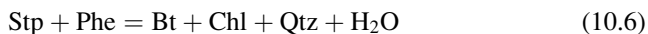


(Tulloch 1979). The presence of Prh and Pmp in granitoid rocks has been attributed to the activity of hydrothermal solutions, but alteration under prehnite–pumpellyite facies conditions is now considered to be more likely especially if indications of low-T metamorphism are also apparent in associated lithologies.

#### 10.3.2 *Stilpnomelane*

Stilpnomelane (Stp), a Fe-rich hydrous silicate with low Al and K and often mistaken for Bt, occurs as ferrostilpnomelane (Fe<sup>2+</sup>-bearing) and ferristilpnomelane (Fe<sup>3+</sup>-bearing) varieties, the latter being formed by secondary oxidation of the

former. In metagranitoids, Stp generally has a sheaf-like habit and is preferentially found within Kfs (microcline) or replaces igneous Bt and Hbl. Stilpnomelane-forming reactions in low-grade metagranitoids are poorly understood, but Bt and/or Chl are considered to be the most important reactants. Stilpnomelane occurs as a mineral of low-grade metamorphism along with Chl, Phe, Ep, Qtz, Kfs and Ab, but at slightly higher grade it also occurs together with green Bt. A possible Stp-consuming reaction in low-grade metagranitoids is



This reaction has been provisionally investigated by Nitsch (1970). In hydrothermal experiments oxygen fugacity was controlled by the HM buffer, and apparent equilibrium was obtained at 400 MPa/445°C and at 700 MPa/460°C. Thus, Stp is a diagnostic index mineral for metagranitoid rocks, formed under lower greenschist and blueschist facies conditions as in metapsammitic and metamafic rocks.

### 10.3.3 *The Microcline–Sanidine Isograd*

A discontinuity in the structural state of Kfs allows for the mapping of a microcline/sanidine transformation isograd in greenschist facies metagranitoid rocks (Bambauer and Bernotat 1982; Bernotat and Bambauer 1982; Bernotat and Morteani 1982; Bambauer 1984).

In order to understand the following, a few terms pertaining to the Kfs structure are outlined here. In the stable high-T form *sanidine*, Al and Si are distributed between the two available tetrahedral (T) sites, T<sub>1</sub> and T<sub>2</sub>, with Al slightly preferring the T<sub>1</sub> site. In the low-temperature form *microcline*, there are four T-sites, T<sub>10</sub>, T<sub>1m</sub>, T<sub>20</sub>, T<sub>2m</sub>, with Al strongly preferring the T<sub>10</sub> site. Because there exist intermediate structural states, the following Kfs-modifications are distinguished with increasing temperature: low microcline, high microcline, low sanidine, and high sanidine. For low and high microcline, the Al, Si distributions are given as Al site occupancies t<sub>10</sub>, t<sub>1m</sub>, t<sub>20</sub>, t<sub>2m</sub>. The Al, Si ordering in T<sub>1</sub> tetrahedral sites is either determined by measuring the optic axial angle, 2V<sub>x</sub> or by X-ray methods.

A microcline/sanidine transformation isograd has been mapped in metagranitoid rocks of the Central Swiss Alps where three zones, arranged with respect to increasing metamorphic grade have been distinguished;

*Zone 1* comprises unchanged, variable pre-Alpine structural states ranging from low- to high-microcline, showing a range of 2V<sub>x</sub> ~ 55–85°. Metamorphic grade is restricted to the lowest greenschist facies.

*Zone 2* comprises distinctly cross-hatched low-microcline (2V<sub>x</sub> ~ 75–88°, t<sub>10</sub>–t<sub>1m</sub> ~ 1.0, 1–4 mol% Ab). Metamorphic grade is equivalent to lower greenschist facies conditions.

*Zone 3* comprises frequent orthoclase (monoclinic bulk optics predominating, triclinic or monoclinic by X-rays) displaying a variety of high-microcline structural

states ( $2V_x \sim 53\text{--}75^\circ$ ,  $t_{10}\text{--}t_{1m} = 0.0\text{--}0.4$ , 2.5–6.5 mol % Ab) together with variable amounts of cross-hatched low-microcline ( $t_{10}\text{--}t_{1m} \sim 1.0$ ). Metamorphic grade ranges from upper greenschist facies to upper amphibolite facies conditions.

The microcline/sanidine transformation isograd separating Zone 2 from Zone 3 is interpreted as a relic of the diffusive transformation sanidine  $\Rightarrow$  microcline at the climax of the late Alpine metamorphism by the following process. K-feldspar from Zone 2 was annealed long enough at low-T during Alpine metamorphism to form low-microcline. In Zone 3, temperatures surpassed  $T_{\text{dif}}$  upon slow heating and Kfs was transformed to the high-T polymorph sanidine. During subsequent cooling, temperatures dropped below that of the phase transformation. Note that during the retrograde sanidine  $\Rightarrow$  microcline transition, triclinic domains must form within a monoclinic host. This process has a high kinetic barrier. Because of rapid cooling, diffusion became sluggish and Kfs remained as intermediate- to high-microcline. The low-microcline observed at the beginning of Zone 3 is interpreted as a relic of Zone 2.

The temperature of the microcline–sanidine phase transformation has not been determined experimentally because of the very slow kinetics of Al, Si ordering. From several lines of evidence, discussed in detail by Bambauer and Bernotat (1982), this temperature was estimated to be  $\sim 450^\circ\text{C}$  for an approximate composition  $\text{Or}_{95\text{--}90}\text{Ab}_{5\text{--}10}$ , with a negligible pressure dependence.

In the Central Swiss Alps, a microcline–sanidine transformation isograd was mapped over a distance of more than 140 km and is compatible with the general pattern of metamorphic zonation of this area in that it occurs between the Stp-out and St-in mineral zone boundaries. Furthermore, provisional results indicate that the transformation isograd surface is inclined  $\sim 15^\circ$  towards the north.

### 10.3.4 *Eclogite and Blueschist Facies Granitoids*

A rare example of granite, granodiorite and tonalite metamorphosed under eclogite facies conditions is known from the *Sesia Zone of the Western Alps* (Compagnoni and Maffeo 1973; Oberhänsli et al 1985; Compagnoni and Rolfo 2003). These granitoids are remnants of the Variscan basement and were transformed during the earliest phase of Alpine metamorphism in mid-Cretaceous time. The least deformed rocks retain well-preserved igneous textures with relict K-feldspar and biotite. Under eclogite facies conditions Pl is replaced by Jd, Qtz, Zo, Ky, Kfs, and Bt has been pseudomorphically replaced by Cel-rich, high Ti-Phe and Rt with coronitic Grt. During later decompression, Jd was replaced by Omp and Grt (chloromelanite), followed by Gln. Although coesite has not been found in the granitoids, the presence of polygonal granoblastic Qtz aggregates after igneous Qtz are inferred to be inversion products from coesite (Cs). If this textural interpretation is correct then UHP conditions of metamorphism at  $>3.5\text{ GPa}/>700^\circ\text{C}$  are implied (Compagnoni and Rolfo 2003); if not,  $P\text{--}T$  conditions for the climax of metamorphic recrystallization are lower at  $>1.4\text{ GPa}/500\text{--}600^\circ\text{C}$ . Other examples of UHP

metamorphism of granitoids (orthogneiss) are recorded from *eastern China* (Liu et al. 2002), where the undiagnostic paragenesis of Qtz + Kfs + Pl and minor Bt + Grt + Ep is typical. Only in clear overgrowth rims on zircon grains have inclusions of Cs + Phe have been identified indicating that the orthogneiss was subjected to UHP metamorphism (>3 GPa) at temperatures estimated from associated lithologies to have been between about 750°C and 800°C. These temperatures, as with possibly those of the Sesia Zone granitoids described above, are higher than the wet granite solidus, and the lack of evidence of any melting implies that  $a_{\text{H}_2\text{O}}$  was considerably less than unity and the main reason why other diagnostic HP minerals did not form.

Orthogneisses of granite, granodiorite and tonalite composition from the *Seward Peninsula, Alaska*, underwent progressive orogenic blueschist facies metamorphism followed by partial re-equilibration during decompression under greenschist facies conditions (Evans and Patrick 1987; Patrick 1995). The mineral assemblage in granitic orthogneiss is Qtz + Ab + Kfs (microcline) + (3 T) Phe + Bt; Al-rich Grt occurs in metatonalite in the absence of microcline. No typical high-P minerals such as Jd, Omp, or Gln, or obvious pseudomorphs thereof, occur in the orthogneisses, but diagnostic blueschist facies assemblages are developed in associated metabasites and metapelites indicating *P–T* conditions of ~ 0.9–1.0 GPa/420°C (Thurston 1985).

The Variscan granitic basement of *Corsica* was partly involved in early Alpine metamorphism during the middle–late Cretaceous (Gibbons and Horak 1984). Metamorphism of the basement rocks, induced by the overthrusting of a blueschist facies nappe, was confined to a major, ca. 1 km thick ductile shear zone within which deformation increases upwards towards the overlying nappe. In a mylonitized–granodiorite, Bt and Hb are replaced by Na–Am (crossite) + low-Ti Bt + Phe + Ttn ± Ep, recording metamorphic conditions transitional between blueschist and greenschist facies. *P–T* estimates for metamorphism at the base of the shear zone are given as 390–490°C at 600–900 MPa, but these values are not well constrained.

### 10.3.5 Migmatitic Granitoids and Charnockite

There are many examples of gneissic granitic rocks (orthogneiss) forming migmatite under granulite facies conditions (Mehnert 1968). Such rocks are dominated by Qtz Pl Ksp, an assemblage that is particularly suitable for producing low-T granite minimum melt compositions under water-saturated conditions (see Sect. 7.6.1) (e.g., Sawyer 1998).

Accessory amounts of Bt ± Ms ± Hbl ± Als ± Grt may also be present in gneissic granitic rocks and depending on the *P*, partial melting will typically produce granulite assemblages of Grt/Crd + Opx/Cpx + K-Nafs + Qtz + Ky/Sil ± Ca-Pl + granitic melt. Wet solidi of muscovite granite, granodiorite and tonalite compositions shown in Fig. 10.11, indicate that melting would begin over a temperature range of 650–725°C at, e.g., 300 MPa. Biotite-, Pl- and Hbl-out curves in these

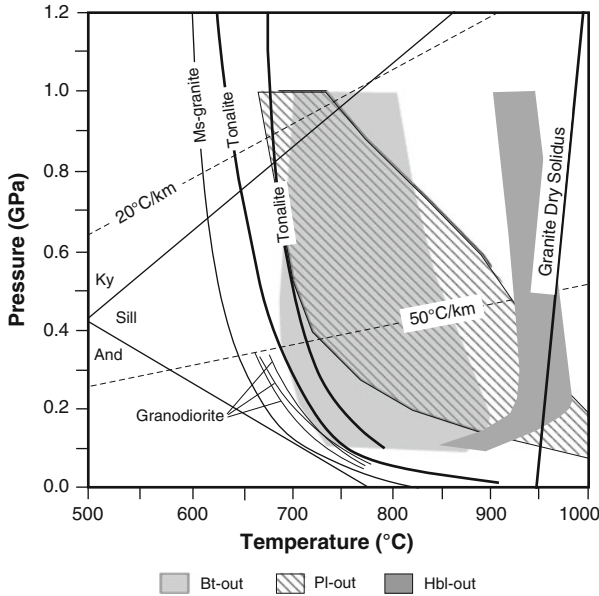
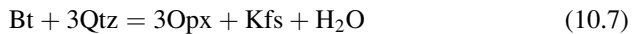


**Fig. 10.11** Wet solidi and fields of Bt-, Pl- and Hbl-out curves of granitoid compositions (granite, granodiorite, tonalite). See captions to summary diagrams Figs. 2.5 and 2.12 of Chen and Grapes (2007) for references

granitoids span T-ranges above the solidi as shown in Fig. 10.11 that reflect their variable composition.

Charnockite is an Opx- (or more rarely Fayalite- and commonly with Cpx) bearing granite (orthogneiss) that occurs within granulite terranes such as those in Antarctica, India, Sri Lanka, Africa and Madagascar. Charnockites have a characteristic dark gray, green or brown color on fresh surfaces and a “greasy” luster indicating the presence of Opx. While most charnockite gneiss massifs probably had a magmatic origin (e.g., Frost and Frost 2008 and references therein), there is also good evidence for localized formation of Opx by *solid-state dehydration* of Bt in granitic rocks by the reaction



associated with CO<sub>2</sub>-fluxing (causing the dehydration) that indicates a granulite facies metamorphic/metasomatic origin (see references). Patchy alteration, diffuse contacts, veining, alteration along shear zones, coarse grained recrystallization, and fluid-induced mineral transformation provide evidence for the contact metamorphic/metasomatic transformation of granitic rocks to a charnockite assemblage through the action of high-T magmatic fluids, notably CO<sub>2</sub>. Possible igneous sources of the CO<sub>2</sub>-rich fluid that caused dehydration of orthogneiss to form charnockite by reaction (10.3) involve exsolution of CO<sub>2</sub> during crystallization of an extensive basaltic underplate or outgassing of a subcrustal mantle diapir.

## References and Further Reading

### *Cited References*

- AlDahan AA (1989) The paragenesis of pumpellyite in granitic rocks from the Siljan area, central Sweden. *Neues Jahrb Mineral Monatsh* 8:367–383
- Bambauer HU (1984) Das Einfallen der Mikroklin/Sanidin-Isogradenfläche in den Schweizer Zentral-Alpen. *Schweiz Mineral Petrogr Mitt* 64:288–289
- Bambauer HU, Bernotat WH (1982) The microcline/sanidine transformation isograd in metamorphic regions. I. Composition and structural state of alkali feldspars from granitoid rocks of two N-S traverses across the Aar massif and Gotthard “massif”, Swiss Alps. *Schweiz Mineral Petrogr Mitt* 62:185–230
- Bernotat WH, Bambauer HU (1982) The microcline/sanidine transformation isograd in metamorphic regions. II. The region of Lepontine metamorphism, central Swiss Alps. *Schweiz Mineral Petrogr Mitt* 62:231–244
- Bernotat WH, Morteani G (1982) The microcline/sanidine transformation isograd in metamorphic regions: Western Tauern window and Merano-Mules-Anterselva complex (eastern Alps). *Am Mineralog* 67:43–53
- Brothers RN, Grapes RH (1989) Clastic lawsonite, glaucophane, and jadeitic pyroxene in Franciscan metagraywackes from the Diablo Range, California. *Geol Soc Am Bull* 101:14–26
- Brown M (1979) The petrogenesis of the St. Malo migmatite belt, Armorican Massif, France, with particular reference to diatexites. *Neus Jahrbuch Mineral Abh* 135:48–74
- Chen G-N, Grapes R (2007) Granite genesis: in-situ melting and crustal evolution. Springer, Dordrecht, The Netherlands, 273 pp
- Compagnoni R, Maffeo B (1973) Jadeite-bearing metagranites l.s. and related rocks in the Mount Mucrone area (Sesia-Lanzo zone, western Italian Alps). *Schweiz Mineral Petrogr Mitt* 53:355–378
- Compagnoni R, Rolfo F (2003) UHPM units in the Western Alps. In: Carswell DA, Compagnoni R (eds) *Ultrahigh pressure metamorphism*, vol 5, European Mineralogical Union notes on mineralogy. EMU, Italy, pp 13–49
- Ernst WG (1975) Subduction zone metamorphism. Dowden, Hutchinson and Ross, Stroudsburg
- Ernst WG (1987) Jaditized Franciscan metamorphic rocks of the Pacheco Pass – San Luis Reservoir area, central California Coast Ranges. *Geological Society of America field guide – Cordilleran section*: 245–250
- Ernst WG, Banno S (1991) Neoblastic jadeitic pyroxene in Franciscan metagraywacke from Pacheco Pass, central Diablo Range, California, and implications for the inferred metamorphic *P-T* trajectory. *NZ J Geol Geophys* 34:281–292, see also comment [Grapes] and reply [Ernst], (1992) *NZ J Geol Geophys* 35:381–387
- Evans BW, Patrick BE (1987) Phengite-3 T in high-pressure metamorphosed granitic orthogneisses, Seward Peninsula, Alaska. *Can Mineralog* 25:141–158
- Frost BR, Frost CD (2008) On charnockites. *Gondwana Res* 13:30–44
- Gibbons W, Horak J (1984) Alpine metamorphism of Hercynian hornblende granodiorite beneath the blueschist facies schistes lustrés nappe of NE Corsica. *J Metamorph Geol* 2:95–113
- Grapes RH (1995) Uplift and exhumation of Alpine Schist, Southern Alps, New Zealand: thermobarometric constraints. *NZ J Geol Geophys* 38:525–533
- Grapes R, Watanabe T (1992a) Paragenesis of titanite in metagraywackes of the Franz Josef-Fox Glacier area, Southern Alps, New Zealand. *Eur J Mineral* 3:547–555
- Grapes R, Roser B, Kifle K (2001) Composition of monocrystalline detrital and authigenic minerals, metamorphic grade, and provenance of Torlesse and Waipapa greywacke, Central North island, New Zealand. *Int Geol Rev* 43:139–175
- Holland TJB (1983) The experimental determination of activities in disordered and short-range ordered jadeitic pyroxenes. *Contrib Mineralog Petrol* 82:214–220



- Liu F, Xu Z, Liou JG, Katayama I, Masago H, Maruyama S, Yang J (2002) Ultrahigh-pressure mineral inclusions in zircons from gneissic core samples of the Chinese Continental Scientific Drilling Site in eastern China. *Eur J Mineralog* 14:499–512
- Loney RA, Brew DA (1987) Regional thermal metamorphism and deformation of the Sitka graywacke, southern Baranof Island, southeastern Alaska. *US Geological Survey Bulletin* 1779, 17 pp
- Maruyama S, Liou JG, Sasakura Y (1985) Low-temperature recrystallization of Franciscan greywackes from Pacheco Pass, California. *Mineral Mag* 49:345–355
- Mehnert KR (1968) Migmatites and the origin of granitic rocks. Elsevier, Amsterdam
- Milord I, Sawyer EW, Brown M (2001) Formation of diatexite migmatite and granite magma during anatexis of semi-pelitic metasedimentary rocks: an example from St. Malo, France. *J Petrol* 42:487–505
- Mortimer N (2000) Metamorphic discontinuities in orogenic belts: example of the garnet-biotite-albite zone of the Otago schist, New Zealand. *Int J Earth Sci* 89:295–306
- Nitsch KH (1970) Experimentelle Bestimmung der oberen Stabilitätsgrenze von Stilpnomelan. *Fortschr Mineral* 47:48–49
- Oberhänsli R, Hunziker JC, Martinotti G, Stern WB (1985) Geochemistry, geochronology and petrology of Monte Mucrone: an example of eo-alpine eclogitization of Permian granitoids in the Sesia-Lanzo zone, western Alps, Italy. *Chem Geol* 52:165–184
- Okay AI (2002) jadeite-chloritoid-glaucophane-lawsonite blueschists in north-west Turkey: unusually high P/T ratios in the continental crust. *J Metamorph Geol* 20:757–768
- Okay AI, Kelley SP (1994) Tectonic setting, petrology and geochronology of jadeite + glaucophane and chloritoid + glaucophane schists from north-west Turkey. *J Metamorph Geol* 12:455–466
- Patrick B (1995) High-pressure – low-temperature metamorphism of granitic orthogneiss in the Brooks Range, northern Alaska. *J Metamorph Geol* 13:111–124
- Sawyer EW (1998) Formation and evolution of granite magmas during crustal reworking: the significance of diatexites. *J Petrol* 39:1147–1167
- Thurston SP (1985) Structure, petrology, and metamorphic history of the Nome Group blueschist terrane, Salmon Lake area, Seward Peninsula, Alaska. *Geol Soc Am Bull* 96:600–617
- Tulloch AJ (1979) Secondary Ca-Al silicates as low-grade alteration products of granitoid biotite. *Contrib Mineralog Petrol* 69:105–117
- White RW, Rowell R, Clarke GL (2003) Prograde metamorphic assemblage evolution during partial melting of metasedimentary rocks at low pressures: migmatites from Mt. Stafford, Central Australia. *J Petrol* 44:1937–1960
- Yardley BDW (1982) The early history of the Hasst schists and related rocks in New Zealand. *Contrib Mineralog Petrol* 81:317–327

### ***Further Reading***

- Ashworth JR (1985) Migmatites. Blackie, Glasgow, 301 pp
- Bea F (1989) A method for modelling mass balance in partial melting and anatectic leucosome segregation. *J Metamorph Geol* 7:619–628
- Bohlen SR, Boettcher AL, Wall VJ, Clemens JD (1983) Stability of phlogopite – quartz and sanidine – quartz: a model for melting in the lower crust. *Contrib Mineralog Petrol* 83:270–277
- Bucher K, Frost BR (2006) Fluid transfer in high-grade metamorphic terrains intruded by anorogenic granites: the Thor Range, Antarctica. *J Petrol* 47:567–593
- Dobmeier C, Raith MM (2000) On the origin of ‘arrested’ charnockitization in the Chlika Lake area, Eastern Ghats, India: a reappraisal. *Geol Mag* 137:27–37
- Engel AEJ, Engel CE (1958) Progressive metamorphism and granitization of the major paragneiss, northwest Adirondack mountains, New York. Part 1. *Geol Soc Am Bull* 69:1369–1414
- Ernst WG (1965) Mineral paragenesis in Franciscan metamorphic rocks, Panoche Pass, California. *Geol Soc Am Bull* 76:879–914

- Ernst WG (1971) Petrologic reconnaissance of Franciscan metagraywackes from Diablo Range, central California. *J Petrol* 12:413–437
- Ferry JM (1979) Reaction mechanism, physical conditions, and mass transfer during hydrothermal alteration of mica and feldspar in granitic rocks from south-central Maine, USA. *Contrib Mineralog Petrol* 68:125–139
- Finger F, Clemens JD (1995) Migmatization and “secondary” granitic magmas: effects of emplacement and crystallization of “primary” granitoids in southern Bohemia, Austria. *Contrib Mineralog Petrol* 120:311–326
- Franz L, Harlov DE (1998) High-grade K-feldspar veining in granulites from the Ivrea-Verbano Zone, Northern Italy: fluid flow in the lower crust and implications for granulite facies genesis. *J Geol* 106:455–472
- Frey M, Hunziker JC, Jäger E, Stern WB (1983) Regional distribution of white K-mica polymorphs and their phengite content in the Central Alps. *Contrib Mineralog Petrol* 83:185–197
- Frost BR, Frost CD, Hulsebosch TP, Swapp SM (2000) Origin of the charnockites of the Louis Lake Batholith, Wind River Range, Wyoming. *J Petrol* 41:1759–1776
- Früh-Green GL (1994) Interdependence of deformation, fluid infiltration and reaction progress recorded in eclogitic metagranitoids (Sesia Zone, Western Alps). *J Metamorph Geol* 12:327–343
- Ganguly J, Singh RN, Ramana DV (1995) Thermal perturbation during charnockitization and granulite facies metamorphism in southern India. *J Metamorph Geol* 13:419–430
- Gill Ibarra JI (1995) Petrology of jadeite metagranite and associated orthogneiss from the Malpica-Tuy allocthon (Northwest Spain). *Eur J Mineralog* 7:403–415
- Grant JA (1986) Quartz-phlogopite-liquid equilibria and origins of charnockites. *Am Mineralog* 71:1071–1075
- Grapes R, Otsuki M (1983) Peristerite composition in quartzofeldspathic schists, Franz Josef Fox Glacier Area, New Zealand. *J Metamorph Geol* 1:47–61
- Grapes R, Watanabe T (1992b) Metamorphism and uplift of Alpine Schist in the Franz-Josef-Fox Glacier area of the Southern Alps, New Zealand. *J Metamorph Geol* 10:171–180
- Grapes GR, Watanabe T (1994) Mineral composition variation in Alpine Schist, Southern Alps, New Zealand: Implications for recrystallisation and exhumation. *Island Arc* 3:163–181
- Hansen EC, Janardhan AS, Newton RC, Prame WKBN, Ravindra Kumar GR (1987) Arrested charnockite formation in southern India and Sri Lanka. *Contrib Mineralog Petrol* 96:225–244
- Hirajima T, Compagnoni R (1993) Petrology of a jadeite-quartz/coesite-almandine -phengite fels with retrograde ferro-nyböite from Dora-Maira Massif, Western Alps. *Eur J Mineralog* 5:943–955
- Holtz F, Johannes W, Tamic N, Behrens H (2001) Maximum and minimum water contents of granitic melts generated in the crust: a reevaluation and implications. *Lithos* 56:1–14
- Janardhan AS, Newton RC, Hansen EC (1982) The transformation of amphibole facies gneiss to charnockite in southern Karnataka and northern Tamil Nadu, India. *Contrib Mineralog Petrol* 79:130–149
- Koons PO, Thompson AB (1985) Non-mafic rocks in the greenschist, blueschist and eclogite facies. *Chem Geol* 50:3–30
- Koons PO, Rubie DC, Früh-Green G (1987) The effect of disequilibrium and deformation on the mineralogical evolution of quartz diorite during metamorphism in the eclogite facies. *J Petrol* 28:679–700
- Kriegsman LM (2001) Partial melting, partial melt extraction and partial back reaction in anatectic migmatites. *Lithos* 56:75–96
- Le Goff E, Ballèvre M (1990) Geothermobarometry in albite-garnet orthogneisses: a case study from the Gran Paradiso nappe (Western Alps). *Lithos* 25:261–280
- Leake BE (1998) Widespread secondary Ca garnet and other Ca silicates in the Galway Granite and its satellite plutons caused by fluid movements, western Ireland. *Mineral Mag* 62:381–386
- Luth WD, Jahns RH, Tuttle OF (1964) The granite system at pressures of 4 to 10 kilobars. *J Geophys Res* 69:659–773

- Massone HJ, Chopin CP (1989) P-T history of the Gran Paradiso (western Alps) metagranites based on phengite geobarometry. In: Daly JS, Cliff RA, Yardley BWD (eds) *Evolution of metamorphic belts*. Geological Society Special Publication, Blackwell, Oxford, pp 545–550
- Morteani G, Raase P (1974) Metamorphic plagioclase crystallization and zones of equal anorthite content in epidote-bearing, amphibole-free rocks of the western Tauernfenster, eastern Alps. *Lithos* 7:101–111
- Mottana A, Carswell DA, Chopin CC, Oberhänsli R (1990) Eclogite facies mineral parageneses. In: Carswell DA (ed) *Eclogite facies rocks*. Blackie, Glasgow, pp 14–52
- Nijland TG, Senior A (1991) Sveconorwegian granulite facies metamorphism of polyphase migmatites and basic dykes, south Norway. *J Geol* 99:515–525
- Nishimoto SY, Ya H (2010) Hydrothermal alteration of deep fractured granite: effects of dissolution and precipitation. *Lithos* 115:153–162
- Olsen SN (1984) Mass-balance and mass-transfer in migmatites from the Colorado Front Range. *Contrib Mineralog Petrol* 85:30–44
- Osanai Y, Komatsu M, Owada M (1991) Metamorphism and granite genesis in the Hidaka Metamorphic Belt, Hokkaido, Japan. *J MetamorphGeol* 9:111–124
- Otamendi JE, Patiño-Douce AE (2001) Partial melting of aluminous metagreywackes in the northern Sierra de Comechingones, Central Argentina. *J Petrol* 42:1751–1772
- Patiño Douce AE, Humphreys ED, Johnston AD (1990) Anatexis and metamorphism in tectonically thickened continental crust exemplified by the Sevier hinterland, western North America. *Earth Planet Sci Lett* 97:290–315
- Plümper O, Putnis A (2009) The complex hydrothermal history of granitic rocks: Multiple feldspar replacement reactions under subsolidus conditions. *J Petrol* 50:967–987
- Proyer A (2003) The preservation of high-pressure rocks during exhumation: metagranites and metapelites. *Lithos* 70:183–194
- Santosh M, Yoshikura S (2001) Charnockite magmatism and charnockitic metasomatism in East Gondwana and Asis. *Gondwana Res* 4:768–771
- Santosh M, Jackson DH, Harris NB, Matthey DP (1991) Carbonic fluid inclusions in south Indian granulites: evidence for entrapment during charnockite formation. *Contrib Mineralog Petrol* 108:318–330
- Schreyer W, Abraham K (1979) Prehnite/chlorite and actinolite/epidote bearing mineral assemblages in the metamorphic igneous rocks of La Helle and Challes, Venn-Stavelot-Massif, Belgium. *Ann Soc Geol Belg* 101–1978:227–241
- Schwarz HP (1966) Chemical and mineralogic variations in an arkosic quartzite during progressive regional metamorphism. *Geol Soc Am Bull* 77:509–532
- Steck A (1976) Albit-Oligoklas-Mineralgesellschaften der Peristeritlücke aus alpinmetamophen Granitgneisen des Gotthardmassivs. *Schweiz Mineral Petrogr Mitt* 56:269–292
- Steck A, Burri G (1971) Chemismus und Paragenesen von Granaten aus Granitgneisen der Grünschiefer- und Amphibolitfazies der Zentralalpen. *Schweiz Mineral Petrogr Mitt* 51:534–538
- Stípská P, Powell R (2005) Does ternary feldspar constrain the metamorphic conditions of high-grade meta-igneous rocks? Evidence from orthopyroxene granulites, Bohemian Massif. *J Metamorph Geol* 23:627–647
- Török K (1998) Magmatic and high-pressure metamorphic development of orthogneisses in the Sopron area, Eastern Alps (W-Hungary). *Neues Jahrb Mineral Abh* 173:63–91
- Tropper P, Essene E, Sharp S (1999) Application of K-feldspar-jadeite-quartz barometry to eclogite facies metagranites and metapelites in the Sesia Lanzo Zone (Western Alps, Italy). *J Metamorph Geol* 17:195–209
- Tropper P, Konzett J, Finger F (2005) Experimental constraints on the formation of high-P/high-T granulites in the Southern Bohemian Massif. *Eur J Mineralog* 17:343–356
- Voll G (1976) Recrystallisation of quartz, biotite and feldspars from Erstfeld to the Leventina nappe, Swiss Alps, and its geological significance. *Schweiz Mineral Petrogr Mitt* 56:641–647
- Weisenberger T, Bucher K (2010) Zeolites in fissures of granites and gneisses of the Central Alps. *J Metamorph Geol* 28:825–847

## Appendix: Symbols for rock forming minerals

---

Ab	albite
Acm	acmite
Act	actinolite
Adr	andradite
Agt	aegirine-augite
Ak	åkermanite
Alm	almandine
Aln	allanite
Als	aluminosilicate
Am	amphibole
An	anorthite
And	andalusite
Anh	anhydrite
Ank	ankerite
Anl	analcite
Ann	annite
Ant	anatase
Ap	apatite
Apo	apophyllite
Apy	arsenopyrite
Arf	arfvedsonite
Arg	aragonite
Atg	antigorite
Ath	anthophyllite
Aug	augite
Ax	axinite
Bhm	boehmite
Bn	bornite
Brc	brucite
Brk	brookite
Brl	beryl
Brt	barite
Bst	bustamite
Bt	biotite
Cal	calcite
Cam	Ca clinoamphibole
Cbz	chabazite
Cc	chalcocite
Ccl	chrysocolla
Ccn	cancrinite
Ccp	chalcopyrite
Cel	celadonite
Cen	clinoenstatite
Cfs	clinoferrosilite
Chl	chlorite
Chn	chondrodite
Chr	chromite
Chu	clinohumite
Cld	chloritoid

---

(continued)

---

ClS	celestite
Cp	carpholite
Cpx	Ca clinopyroxene
Crd	cordierite
Crn	carnegieite
Crn	corundum
Crs	cristroballite
Cs	coesite
Cst	cassiterite
Ctl	chrysotile
Cum	cummingtonite
Cv	covellite
Czo	clinozoisite
Dg	diginite
Di	diopside
Dia	diamond
Dol	dolomite
Drv	dravite
Dsp	diaspore
Eck	eckermannite
Ed	edenite
Elb	elbaite
En	enstatite (ortho)
Ep	epidote
Fa	fayalite
Fac	ferroactinolite
Fcp	ferrocarpholite
Fed	ferroedenite
Flt	fluorite
Fo	forsterite
Fpa	ferropargasite
Fs	ferrosilite (ortho)
Fst	fassite
Fts	ferrotschermakite
Gbs	gibbsite
Ged	gedrite
Gh	gehlenite
Gln	glaucophane
Glt	glaucosite
Gn	galena
Gp	gypsum
Gr	graphite
Grs	grossular
Grt	garnet
Gru	grunerite
Gt	goethite
Hbl	hornblende
Hc	hercynite
Hd	hedenbergite
Hem	hematite
HI	halite
Hs	hastingsite
Hu	humite

---

*(continued)*

---

Hul	heulandite
Hyn	haiüyne
Ill	illite
Ilm	ilmenite
Jd	jadeite
Jh	johannsenite
Kfs	K-feldspar
Kln	kaolinite
Kls	kalsilite
Krn	kornerupine
Krs	kaersutite
Ktp	kataphorite
Ky	kyanite
Lct	leucite
Lm	limonite
Lmt	laumontite
Lo	loellingite
Lpd	lepidolite
Lws	lawsonite
Lz	lizardite
Mag	magnetite
Mcp	magnesiocarpholite
Mel	melilite
Mgh	maghemite
Mgs	magnesite
Mkt	magnesiokataphorite
Mnt	montmorillonite
Mnz	monazite
Mo	molybdenite
Mrb	magnesioriebeckite
Mrg	margarite
Ms	muscovite
Mtc	monticellite
Mul	mullite
Ne	nepheline
Nrb	norbergite
Nsn	nosean
Ntr	natrolite
Oam	orthoamphibole
Ol	olivine
Omp	omphacite
Opx	orthopyroxene
Or	orthoclase
Osm	osumilite
Pct	pectolite
Pen	protoenstatite
Per	periclase
Pg	paragonite
Pgt	pigeonite
Phe	phengite
Phl	phlogopite
Pl	plagioclase
Pmp	pumpellyite

---

*(continued)*

---

Pn	pentlandite
Po	pyrrhotite
Prg	pargasite
Prh	prehnite
Prl	pyrophyllite
Prp	pyrope
Prv	perovskite
Py	pyrite
Qtz	quartz
Rbk	riebeckite
Rdn	rhodonite
Rds	rhodochrosite
Rt	rutile
Sa	sanidine
Scp	scapolite
Sd	siderite
Sdl	sodalite
Ser	sericite
Sil	sillimanite
Sm	smectite
Sp	sphalerite
Spd	spodumene
Spl	spinel
Spr	sapphirine
Sps	spessartine
Srl	schorl
Srp	serpentine
St	staurolite
Stb	stilbite
Stp	stilpnomelane
Str	strontianite
Sud	sudoite
Tlc	talc
Tmp	thompsonite
Toz	topaz
Tr	tremolite
Trd	tridymite
Tro	troilite
Ts	tschermakite
Ttn	titanite
Tur	tourmaline
Usp	ulvöspinel
Ves	vesuvianite
Vrm	vermiculite
Wa	wairakite
Wo	wollastonite
Wth	witherite
Wus	wüstite
Zo	zoisite
Zrn	zircon

---

# Index

## A

- ACF projection
  - mafic rocks, 343–348
  - metamafic rocks, 344
  - mineral assemblages, 52–54
- AFM projections
  - low-grade shales, 261
  - mineral assemblages, 48–52
- Aluminum, 203–204
- Amphibolite
  - definition, 34
  - facies, 127
- Amphibolite–granulite facies
  - isobaric temperature vs. fluid composition diagram, 372
  - transition, 370–371
- Amphibolite–granulite facies transition, 370–371
- Analcite, 360–361
- Anatectic granite, 289
- Andalusite–kyanite–sillimanite polymorphic transitions, 142–144
- Antigorite, 196, 213
- Augen mylonite, 33

## B

- Baltic Shield, 68
- Barrovian zones, 120
- Basaltic rocks, 339
- Bathozones and bathograds, 139–141
- Bergell contact aureole
  - photomicrograph, 247
  - metamorphic dolomite marble, 247
- Bergell tonalite intrusion, 206, 207
- Blackwall rock, 34
- Blueschist, 33
- Blueschist facies, 129–130

## C

- Calcite–aragonite polymorphic transitions, 144–145
- Calc-silicate rock, 34
- Calcsilicate rocks, 3, 4
- Caledonian metasediments, 9
- CaO–MgO–Al<sub>2</sub>O<sub>3</sub>–SiO<sub>2</sub>–H<sub>2</sub>O (CMASH) system
  - chlorite breakdown reaction, 204
  - decompression and cooling path, 204
  - hydrated Al-bearing lherzolite, 202–204
  - isofacial ultramafic rock, 202, 204
  - rapid decompression and uplift, 204
  - soapstone and sagvandite, 204
- Carbonate-bearing ultramafic rocks
  - ophicarbonate rocks
    - antigorite, 196, 213
    - Atg + Brc, 213
    - Bergell aureole, 215
    - carbonate-involving reactions, 212, 213
    - isobaric assemblage stability, 212, 213
    - isobaric invariant assemblages, 214
    - rocks assemblage stability, 214
    - serpentinites, 212
    - tonalite, Central Alps, 215
    - topologic configurations, 214
  - phase relationships, 212–214
  - silicates and oxides, 212
  - soapstone and sagvandite
    - amphibolite facies temperatures, 218
    - Atg + Mgs (ophimagnesite), 218
    - crust–mantle boundary, 219
    - enstatite + magnesite, 215, 216
    - harzburgite, 216, 218
    - magnesite, 216, 217
    - mineral reactions and phase relations, 219



- ophicarbonates, 218
- talc + magnesite, 215
- Carbonate minerals, 365
- Carbonate rocks, 75–76, 109
- Cataclasite, 33
- Cataclastic metamorphism, 13–14
- Charnockite, 34, 409–410
- Combustion metamorphism, 17
- Conodont color alteration index (CAI), 174
- Contact metamorphism
  - definition, 13–14
  - dolomite
    - high-temperature phase equilibria, 237
    - modal composition vs. temperature diagram, 238–239
    - periclase/brucite-bearing marbles, 237–238
    - progressive metamorphism, 235
    - T-aCO<sub>2</sub> phase equilibrium, 235–236
  - limestone
    - contact metamorphic calcsilicate marbles, 240
    - CO<sub>2</sub>-producing reactions, 241
    - low-T reactions, 239–240
    - Mt. Morrison formation, fluid infiltration, 242
    - progressive transformations, 239
    - rocks-H<sub>2</sub>O-rich fluids interaction, 242
    - T-aCO<sub>2</sub> phase equilibrium, 240–241
    - tremolite and diopside replacement, 240
    - Wasatch range, Utah, USA, 240
    - wollastonite-forming reaction, 241–242
  - mafic rocks, 349
  - metagraywackes, 400–406
  - metapsammites, 400–406
- Continent-continent collision, 77, 78
- D**
- Dehydration reactions, 74, 79, 80
- Devolatilization reactions, 77
- Diastathermal metamorphism, 13
- Dolomite
  - chemographic relationships
    - CaO-MgO-SiO<sub>2</sub> plane, 228
    - high metamorphic grades, 229–230
    - siliceous dolomites reactions, 229
    - triangle Dol-Cal-Qtz, 228–229
  - contact metamorphism
    - high-temperature phase equilibria, 237
    - modal composition vs. temperature diagram, 238–239
    - periclase/brucite-bearing marbles, 237–238
    - progressive metamorphism, 235
    - T-aCO<sub>2</sub> phase equilibrium, 235–236
  - definition, 225
  - large recumbent fold, 225–226
  - minerals and rock composition, 227
  - modal composition vs. P-T diagram, 232–233
  - orogenic metamorphism
    - diopside, 231–232
    - forsterite, 232
    - P-T-aCO<sub>2</sub> phase equilibrium, 230–231
    - talc, 231
    - tremolite, 231
- Dunite, 194
- E**
- Earth crust and mantle
  - heat flow and geotherms
    - Baltic shield, 68
    - continental crust, 67
    - crustal volume, 68
    - Fourier's law, 66
    - heat flow unit (HFU), 66–67
    - heat transport, 66
    - model geotherms, 69
    - MOHO, 68, 69
    - steady-state heat flow, 67
    - transient geotherms, 69–70
  - pressure changes, rocks, 72–74
  - temperature changes and metamorphic reactions, 71–72
  - thermal conductivity, 66
  - transfer heat, 65
- Eclogite
  - and blueschist facies, 408–409
  - definition, 34
  - facies, 130–131
  - facies metamorphism, 378–383
- Enderbite, 34
- Enstatite-forsterite felses, 193
- F**
- Fault breccia, 33
- Felsic mineral, 33
- Felsic rock, 33
- Fe-rich metapelitic rocks, 270
- Fourier's law, 66
- G**
- Gabbroic rocks, 383
- Garnet, 81, 365, 381
- Garnet-aluminosilicate-quartz-plagioclase (GASP), 159–161

- Geologic process, 78, 79
- Geothermobarometry (GTB)
- assumptions and precautions
  - calibration quality, 151
  - cation distributions, 151
  - Fe<sup>2+</sup>/Fe<sup>3+</sup> estimation, 152–153
  - feldspar thermometry, 152
  - metamorphic mineral compositions, 151–152
  - P–T extrapolations, 151
  - retrograde effects, 150–151
  - thermobarometers sensitivity, 151
  - thermobarometry, 150
  - thermodynamic solution, 152
  - zoned poikiloblastic garnets, 150
- calcsilicate rocks, 147
- Clausius-Clapeyron slope, 148
- exchange reactions
- Fe–Mg exchange reactions, 153, 154
  - garnet–biotite thermometer, 156–157
  - garnet–clinopyroxene thermometer, 154–156
  - intracrystalline and intercrystalline exchange, 153
  - isotopic exchange thermometry, 157–158
  - metamorphic thermometry, 153
- Grt–Rt–Als (Ky)–Ilm–Qtz assemblage (GRAIL) reaction, 148, 149
- MET, 167–168
- metamorphic petrology, 146
- miscibility gaps and solvus
- thermometry, 163
  - calcite–dolomite, 165
  - definition, 162
  - mineral composition, 163
  - muscovite–paragonite, 165–166
  - orthopyroxene–clinopyroxene, 163–164
  - plagioclase–alkali feldspar, 164–165
- net-transfer
- clinopyroxene–plagioclase–quartz, 161–162
  - GASP, 159–161
  - geobarometry, 158
  - Grt + Rt + Als + Ilm + Qtz (GRAIL) assemblage, 161
  - sphalerite–pyrrhotite–pyrite, 162
  - thermobarometry, 159, 160
- plagioclase and garnet, 148
- P–T CALC eclogite, 146
- rock formation, 147
- software packages, 146
- thermobarometry, 166
- thermodynamic data, 147
- Gibbs free energy., 58–59
- Gibbs method, 168–169
- Gneiss, 31
- Granitoids, 406
- charnockite, 409–410
  - eclogite and blueschist facies, 408–409
  - microcline–sanidine isograd, 407–408
  - migmatitic granitoids, 409–410
  - prehnite and pumpellyite, 406
  - stilpnomelane, 406–407
- Granofels, 31
- Granulite
- amphibolite-facies assemblages, 293
  - definition, 34
  - facies, 127–129
  - facies rocks, 291
  - granulite facies assemblages, 295–296
  - neosome, 292
  - Opx–Qtz granulite formation, 294
  - partial melting reactions, 292–293
  - pigeonite, 296
  - prograde P–T path, 292
- Greenschist
- definition, 33
  - facies, 126–127
- Greenschist–amphibolite facies transition, 365–366
- Greenschist facies metamorphism, 126–127, 363–365
- carbonate, 365
  - garnet, 365
  - mineralogical changes, 363–364
  - reactions including micas, 364
  - stilpnomelane, 364, 365
- Greenstone, 33
- Greywakes
- high pressure metamorphism, 398–400
  - medium pressure metamorphism, 398
- H**
- Harzburgite, 216
- Heulandite, 361
- High pressure low temperature (HPLT) metamorphism, 298–299
- High-pressure metamorphism, 7–8
- High-temperature metamorphism, 5–7
- Hornfels, 34
- Hornfelsic and schistose, 403
- Hydrothermal metamorphism, 14–16
- I**
- Impact metamorphism, 16
- Isofacial ultramafic rock, 202, 204

**J**

Jotunite, 34

**K**

KFMASH system

- AFM diagram, 261, 270–271
- AFM diagrams, 275
- amphibolite facies, St + Grt + Bt assemblage, 272
- characterization, 271–272
- components, 276–277
- contact metamorphic terrains, 281–282
- Fe–Mg dependence, Ky-type geotherm, 270–271
- Fe–Mg exchange, 281
- Fe-rich metapelitic rocks, 269–270
- granulite texture, 283
- Grt + Als + Qtz + Crd assemblage, 284
- KFASH system, 281
- Ky-type geotherm, 274
- low-pressure metamorphism, 280
- medium pressure geotherm, 273
- migmatitic textures, 272
- mineral characteristic assemblages, 284
- pelites metamorphism, 269
- prograde metamorphism, 269–270
- stable assemblages, Cld, Bt, Grt, St, 273
- staurolite–kyanite schist, 274
- texture photomicrograph, 283

**L**

- Labradorite system, mafic rocks, 352–353
- Laumontite, 361
- Lawsonite, 362
- Lightning metamorphism, 16–17
- Limestone
  - contact metamorphism
    - calcisilicate marbles, 240
    - CO<sub>2</sub>-producing reactions, 241
    - low-T reactions, 239–240
    - progressive transformations, 239
    - rocks-H<sub>2</sub>O-rich fluids interaction, 242
    - T-aCO<sub>2</sub> phase equilibrium, 240–241
    - tremolite and diopside replacement, 240
    - Wasatch range, Utah, USA, 240
    - wollastonite-forming reaction, 241–242
  - definition, 225
  - minerals and rock composition 227
  - orogenic metamorphism
    - diopside, 234–235
    - P-T-aCO<sub>2</sub> phase equilibrium, 233–234
    - tremolite, 234
    - wollastonite, 235

- Low-pressure metamorphism, 7
- Low-pressure series amphibolites, 368–370
- Low-temperature metamorphism, 4–5

**M**

- Mafic mineral, 33
- Mafic rocks
  - ACF Projection, 343–348
  - amphibolite facies metamorphism
    - low-pressure series, 368–370
    - mineralogy, 367–368
  - amphibolite–granulite facies transition, 370–374
  - andesitic rocks, 339
  - basaltic pillow lava, eclogite facies, 340
  - basaltic rocks, 339
  - blueschist facies metamorphism, 374–375
    - reactions and assemblages, 375–378
  - calc-alkaline volcanics rocks, 339
  - chemical and mineralogical composition, 342–343
  - CMASH and NCMASH systems, 356–362
  - contact metamorphism, 349
  - definition, 339
  - eclogite facies in gabbroic rocks, 383–387
  - eclogite facies metamorphism
    - amphibolite and granulite, 381–382
    - eclogites, 378–380
    - gabbroic rocks, 383
    - garnet, 381
    - omphacite, 381
    - reactions in, 382–383
  - extrusive mafic igneous rocks, 339
  - greenschist–amphibolite facies transition, 365–366
  - greenschist facies metamorphism
    - carbonate, 365
    - garnet, 365
    - mineralogical changes, 363–364
    - reactions including micas, 364
    - stilpnomelane, 364, 365
  - greenschist facies transition, 362–363
  - HPLT metamorphism, 349
  - hydration, 340–342
  - labradorite system, 352–353
  - metamorphism effects, 350–351
  - NCASH system, 352–353
  - plagioclase in, 352–353
  - prograde metamorphism, 349
  - P-T fields metamorphic facies, 124, 348
  - structures, 339, 371
  - subgreenschist facies metamorphism, 353–356

- textures, 339
- Magnesite, 216, 217
- Mangerite, 34
- Marble
  - CMS-HC System
    - aluminium, 248
    - fluorine, 247
    - potassium, 248–251
    - sodium, 251
  - definition, 34
  - isograds and zone boundaries, 243–244
  - isothermal decompression paths, 244–246
  - thermobarometry
    - calcite-dolomite miscibility gap, 252
    - ultrahigh-pressure metamorphism, 252–253
- Marls
  - Al-poor orogenic metamorphism
    - KCMAS-HC system, 319–321
    - KCMAS-HC system, phase relationship, 317–319
    - prograde metamorphism, 316
  - Al-rich orogenic metamorphism
    - CAS-HC system, 323–325
    - deep-sea metasediments, 321
    - greenschist to amphibolite facies, 321
    - KNCAS-HC system, 325–327
    - low  $X_{\text{CO}_2}$  prograde metamorphism, 327–328 (*see also* Prograde metamorphism)
    - very low  $X_{\text{CO}_2}$  prograde metamorphism (*see* Prograde metamorphism)
  - composition, 315–316, 319
  - definition, 26, 315
  - low pressure metamorphism
    - calc-silicate hornfelses, 333
    - calc-silicate marbles, 333
    - CMAS-HC system, T– $X_{\text{CO}_2}$  diagram, 334
    - limestone nodules outcrop, 335
    - mineral assemblages, 333
    - outcrop, 334–335
- Matorello granite, 9, 10
- Metabasaltic rocks, 344
- Metachert, 34
- Metagraywackes, 394–397
  - contact metamorphism, 400–406
  - geochemistry, 404
  - hornfelsic and schistose, 403
  - metamorphism, 397
  - mineral assemblages and mineral successions, 403
- orogeny, 398
  - prehnite–pumpellyite and blueschist facies, 402
  - prograde T–P paths, 401
  - rock oxide vs. silica variation trends, 405
  - zeolite distribution, 402
- Metamafic rocks
  - ACF projections, 344
  - characteristics, 350
  - minerals, 349
- Metamarl
  - CFM minerals, 332
  - definition, 315–316
  - foliated fine-grained matrix, 333
  - Mesozoic marl, 333
  - Quartenschiefer, 333
- Metamorphic facies
  - amphibolite facies, 127
  - blueschist facies, 129–130
  - diagnostic mineral assemblages, 124, 125
  - eclogite facies, 130–131
  - granulite facies, 127–129
  - greenschist facies, 126–127
  - origin, 122–124
  - pressure–temperature conditions, 131, 132
  - pressure–temperature fields, 124
  - scheme, 375
  - sub-blueschist–greenschist facies, 126
- Metamorphic grade
  - assemblage stability, 170–171
  - bathozones and bathograds, 139–141
  - facies (*see* Metamorphic facies)
  - field gradient, 119, 120
  - Gibbs method, 168–169
  - GTB (*see* Geothermobarometry)
  - index minerals and mineral zones, 120–122
  - isograds
    - earth surface, 136
    - isobaric and isothermal surface, 135
    - isotherms and isobars, 136–138
    - map connecting points, 131
    - metamorphic reaction, 133
    - metamorphic structure, 137, 138
    - metamorphic zone boundary, 137
    - orogenic metamorphism, 136
    - reaction–isograds, 137
    - zone boundaries, isograds and reaction–isograds, 133–135
  - petrogenetic grid (*see* Petrogenetic grid)
  - pressure–temperature tools
    - CAI, 174
    - fluid inclusions, 173
    - magnetite–ilmenite equilibria and the QUILF system, 172–173

- phengite–biotite–K–feldspar–quartz, 171–172
  - vitrinite reflectance, 173–174
- P–T conditions, 119
- Metamorphic processes
  - calcite and quartz, 99
  - chemical reactions, 58
  - crust and mantle (*see* Earth crust and mantle)
  - gases and fluids
    - carbonate rocks, 75–76
    - dehydration reactions, 74
    - devolatilization reactions, 77
    - heat flows, 77
    - H<sub>2</sub>O isochores, 75
    - hydraulic fracturing, 76
    - mineral assemblage, 76
    - mole fraction, 76
    - sedimentary rocks, 74
  - metamorphic reaction principles
    - albite and quartz, 58, 60, 65
    - chemical thermodynamics, 58
    - equilibrium condition, 59, 61
    - forsterite+quartz, 64
    - garnet and biotite pairs, 63
    - Gibbs free energy, 58–59
    - harzburgite tectonic lens, 64
    - jadeite and quartz, 58–60, 65
    - metastable assemblages, 62
    - monomineralic, 64, 65
    - omphacite-bearing rock, 62
    - orogenic fold belts, 64
    - pressure and temperature minerals, 58
    - prograde metamorphism rocks, 63–64
    - rocks disequilibrium, 62
    - stable mineral assemblages, 61
    - stoichiometric coefficients, 60
    - textural and chemical disequilibrium, 64
    - thermodynamic laws, 60
  - metamorphic rocks (*see* Metamorphic rocks)
  - mineral assemblages, 57
  - mineral relative abundance, 57
  - phase diagrams
    - Cal–Dol thermometry, 111
    - carbonate rocks, 109
    - contact metamorphic aureole, 110, 112
    - equilibrium, 112
    - isobaric T–X<sub>CO<sub>2</sub></sub>, 109, 110
    - marble, 111
    - metamorphic mileposts, 112
    - metamorphic petrology, 102, 103
    - mineral and composition, 102
    - phase rule, 103–105
    - pressure and temperature, 102
    - Schreinemakers method (*see* Schreinemakers method)
    - stoichiometry reactions, 91, 109
    - THERIAK/DOMINO software, 102
    - thermodynamic data, 102–103
    - tremolite, 111
- pressure–temperature–time paths and reaction history
  - continent–continent collision, 77, 78
  - dehydration reactions, 79, 80
  - destructive plate margin, 77
  - garnet, 81
  - geologic process, 78, 79
  - metamorphic field gradient, 81
  - piezo–thermic array, 81
  - pressure–temperature loop, 79
  - rehydration, 81
  - steady-state geotherm, 78, 79
  - wollastonite reaction, 88, 99–101
- Metamorphic reaction, 133
- Metamorphic rocks
  - classification, 31–36
  - decarbonation reactions, 88
  - dehydration reactions
    - Clausius–Clapeyron equation, 84
    - hydrostatic pressure, 87
    - hydrous minerals, 83, 85
    - P–T space equilibria, 84, 85
    - solid–solid, 84, 85
    - talc dehydrates, 86, 87
    - zeolite minerals, 85
  - halogen reactions, 94–95
  - mineral assemblages and mineral parageneses (*see* Mineral assemblages)
  - minerals and dissolved components, aqueous solutions
    - Al–silicate, 98
    - fluid infiltration, 96–97
    - fluid–rock interaction, 96
    - hydrolysis reactions, 97
    - hydrothermal and geothermal systems, 98
    - ion exchange reaction, 98
    - K–feldspar sericitization, 97
    - margarite + calcite + quartz mineral assemblage, 89, 96
    - Na–K–Al–Si–O–H system, 98, 99
    - soapstone formation, 97
    - talc schist formation, 97

- mixed volatile reactions, 95–96
  - fluid composition, 88
  - hydrous minerals and carbonates, 88
  - isobaric T–X diagram, 89
  - margarite-bearing rock, 90
  - stoichiometry reaction, 90, 91
- oxidation/reduction reactions
  - Fe<sup>2+</sup> bearing silicate minerals, 93
  - f<sub>O<sub>2</sub></sub> (fugacity of O<sub>2</sub>), 92
  - hematite and magnetite, 91–92
  - log a<sub>O<sub>2</sub></sub>, 92
  - partial pressure, 92
  - REDOX reaction, 91–93
- protolith
  - allochemical metamorphism, 22
  - carbonate, 25
  - crustal rocks, 24
  - crust and mantle composition, 23
  - fluid–rock interaction processes, 22
  - hydrous minerals, 22
  - igneous processes, 23
  - igneous rock chemical composition, 24, 25
  - isochemical metamorphism, 23
  - mafic and quartzo-feldspathic rocks, 26
  - marls, 26
  - metasomatism, 22–23
  - pelites, 25
  - rocks abundance, 24
  - sedimentary rock chemical composition, 24, 25
  - shales deposited, 24, 25
  - ultramafic rocks, 25
- solid-phase components
  - exchange reactions, 82
  - exsolution/solvus, 83
  - net-transfer reactions, 82
  - phase transitions, polymorphic reactions, 82
- structure
  - cataclasis, 29
  - cleavage, 27, 28
  - fabric and layer, 27
  - foliation, 27
  - gneissose, 27
  - joint, 29
  - lineation, 27–28
  - metamorphic differentiation, 29
  - pressure and temperature changes, 26
  - schistosity, 27, 28
  - tectonic setting, 26
  - textural zones, 29, 30
- sulfur reactions, 94
- Metapelites. *See* Pelitic rocks
- Metapelitic granulite
  - cordierite–garnet–opx–spinel–olivine equilibria, 285–286
  - excess quartz condition, 286–288
  - granulites (*see* Granulites)
  - isobaric T–XFe section, 282
  - migmatite (*see* Migmatite)
  - partial melting (*see* Partial melting)
- Metapelitic rocks, 349
- Metapsammites
  - composition, 397
  - contact metamorphism, 400–406
  - mineral zones, 404
  - prograde T–P paths, 401
- Metasedimentary rocks, 404
- Metasomatism, 22–23
- Metatexite, 289
- MgO–SiO<sub>2</sub>–H<sub>2</sub>O (MSH) system
  - chemographic relations, 196–197
  - maximum hydrated harzburgite, 197, 198
    - antigorite serpentinites, 198, 199
    - blueschist and low-T eclogite conditions, 199
    - brucite–antigorite schists, 198, 200
  - chemographic relationships, 195, 199
  - chrysotile, 198
  - contact aureoles, 201, 202
  - Ctl + Tlc assemblage, 198, 199
  - equilibrium distribution, 198, 199
  - harzburgite, 198
  - peridotite, 199
  - prograde metamorphism, 198
  - regional metamorphism, 198
- Microcline-sanidine isograd, 407–408
- Mid Ocean Ridge Basalt (MORB), 124
- Migmatite
  - anatectic granite, 289
  - anatectic melt phase, 289
  - definition, 35
  - diatexite, 289
  - fluid-absent melting in high-grade gneisses, 291
  - granitoids, 409–410
  - granular Grt + Opx + Crd assemblage, 292
  - granulite facies rocks, 291
  - granulite facies transition, 290
  - metatexite, 289
  - micaschists, prograde metamorphism, 289
  - migmatite formation, 288
  - solid–solid and dehydration reactions, 84, 288
  - textures, 272

## Mineral assemblages

## graphical representation

- ACF projections, 52–54
- AFM projections, 48–52
- chemograph, 39
- complex projections, 44, 46–49
- composition phase diagrams, 39, 53
- mole fraction triangle, 41–43
- mole numbers, fractions and fraction line, 39–41
- simple projections, 43–45
- solid-solution phases projection, 46
- topology, 39

## and mineral parageneses

- chemical constituents, 36
- definition, 36
- electron probe microanalyser (EPMA), 37
- mafic minerals, 36
- petrogenesis and evolution, 36
- refractory minerals, 37
- staining techniques, 37
- thin-section observations, 36, 37
- wollastonite, calcite and quartz, 38
- X-ray techniques, 37

## Modal composition, 35

## MT and HT eclogites, 380

## Multi-equilibrium calculations (MET), 167–168

## Muscovite-paragonite, 165–166

## Mylonite, 33

## N

## NCASH system, 352–353

## O

## Ocean-floor metamorphism, 11

## Oceanic lithosphere, subduction of, 298

## Olivine gabbro, 383–387

## Omphacite, 381

## Omphacite-bearing rock, 62

## Ophicarbonate rocks, 193, 196, 213, 218

## Orogenic metamorphism

- banded marbles, 9, 10
- brittle deformation, 10
- diopside, 234–235
- ductile deformation, 9, 10
- mountain building/orogenic process, 8
- olivine-enstatite fractured rock, 9
- orogenic belts, 9
- P-T-aCO<sub>2</sub> phase equilibrium, 233–234
- regional metamorphism, 9
- talc-rich replacement zone, 11

## tremolite, 234

## types, 11, 12

## wollastonite, 235

## P

## Partial melting

- anatectic granite, 289
- anatectic melt phase, 289
- diatexite, 289
- fluid-absent melting, 291
- granular Grt + Opx + Crd assemblage, 292
- granulite facies rocks, 291
- granulite facies transition, 290
- metatexite, 289
- migmatite formation, 288
- prograde metamorphism, 289
- solid–solid and dehydration reactions, 84, 288

## Pelitic rocks

- AFM minerals, 303
- chemical composition, 258
- definition, 257
- examples, 257
- high-grade mineral assemblages, 303
- HPLT
  - dehydration by decompression, 298–299
  - Fe-rich AFM-phases, 299
  - low grade high-pressure metamorphism, 298
  - metapelite isothermal P–X<sub>Fe</sub> diagram, 301–302
  - metapelite P–T diagram, 299–301
  - subduction of oceanic lithosphere, 298
- impure pelites metamorphism, 305–306
- intermediate-pressure metamorphism
  - ASH System, 262–264
  - chemical composition and chemography, 259–260
  - FASH System, 264–267
  - KFMASH system/AFM system (*see* KFMASH system)
  - mica-involving reactions, 267–269
  - mineral assemblages, 260–262
- isobaric T–X<sub>Na</sub> diagram, 304–305
- low-pressure metamorphism
  - andalusite-bearing assemblages, 278
  - Barrovian type terrains, 278
  - FASH system, 278–280
  - KFMASH system (*see* KFMASH system)
- major minerals, 302–303
- mature pelagic shales, 302

- metamorphic minerals recrystallization, 302
- metapelitic granulite
  - cordierite–garnet–opx–spinel–olivine equilibria, 285–286
  - excess quartz condition, 286–288
  - granulites (*see* Granulites)
  - isobaric T–X<sub>Fe</sub> section, 282
  - migmatite (*see* Migmatite)
  - partial melting (*see* Partial melting)
- Mg-rich metamorphism, 296–298
- mineralogy, 258
- mode and mineral composition, pelagic, 305–306
- pelagic pelite, composition, 305
- pre-metamorphic changes, 258–259
- Periclase/brucite-bearing marbles, 237–238
- Peridotite, 193
- Petrogenetic grid
  - mineral assemblage, 141
  - mineral equilibria, 141
  - polymorphic transitions
    - andalusite–kyanite–sillimanite, 142–144
    - calcite–aragonite, 144–145
    - quartz–coesite, 145–146
- Phengites, 267, 381
- Phyllite, 31
- Pigeonite, 296
- Plagioclase, mafic rocks, 352–353
- Potassium-bearing peridotites, 221
- Prehnite, 362, 406
- Prehnite–pumpellyite facies, 126
- Prehnite–pumpellyite facies metagraywacke sandstones, 396
- Prograde metamorphism, 269–270, 349
  - low X<sub>CO2</sub>
    - KNCAS-HC system, excess Qtz and Cal, 327, 328
    - P–T–X diagram, CAS-HC system, 323, 327
  - mafic rocks, 349
  - rocks, 63–64
  - very low X<sub>CO2</sub>
    - clinozoisite, 330
    - KNCAS-HC system, P–T–X phase relationships, 328–329
    - margarite formation, 329
    - prograde path a–k, modal composition, 331
- Pseudotachylite, 33
- Pumpellyite, 362, 406
- Pumpellyite–actinolite facies, 126
- Q**
  - Quartz–coesite polymorphic transitions, 145–146
  - Quartzite, 34
  - Quartzofeldspathic rocks
- R**
  - REDOX reaction, 91–93, 347
  - Regional metamorphism, 11, 13
  - Restite, 35
  - Rodingite, 34
- S**
  - Sagvandite, 193–194, 204
  - Schist, 30, 31
  - Schreinemakers method
    - binary chemography, 107
    - binary system, 106, 107
    - dehydration reactions, 107
    - four-phase assemblage, 105, 106
    - hematite, magnetite, pyrothite and pyrite, 108, 109
    - metastable invariant point, 108
    - univariant and divariant assemblages, 106, 107
  - Sedimentary rocks, 74
    - chemical composition, 24, 25
    - dolomite (*see* Dolomite)
    - limestone (*see* Limestone)
  - Serpentinite, 34, 193
  - SiO<sub>2</sub>–MgO–CaO–H<sub>2</sub>O–CO<sub>2</sub> (CMS-HC) system, 194
  - Skarn, 34
  - Slate, 28, 31
  - Soapstone, 193
  - Staurolite–kyanite schist, 274
  - Stilbite, 361
  - Stilpnomelane, 364, 406–407
- T**
  - THERIAK/DOMINO software, 102
  - Thermobarometry
    - calcite–dolomite miscibility gap, 252
    - ultrahigh-pressure metamorphism, 252–253
  - Thermometry and geobarometry, 211–212
  - Tonalite, 215
- U**
  - Ultrahigh-P eclogites, 381
  - Ultra-high pressure metamorphism (UHPM), 130–131
  - Ultramafic rocks, 25



- Ultramafic rocks (*cont.*)
- allofacial, 192
  - Alpine-type peridotites, 191, 192
  - carbonate minerals (*see* Carbonate-bearing ultramafic rocks)
  - chemical composition
    - calcic clinopyroxene mineral, 194
    - calcite, dolomite and magnesium minerals, 195
    - chemography, CMS-HC system, 194, 195
    - chrysotile (Ctl) and lizardite (Lz) minerals, 195
    - dunites, 192, 194
    - ferro-magnesian silicates, 194
    - forsterite, enstatite, diopside, 194
    - lherzolites, 194, 195
    - olivine and orthopyroxene minerals, 194
    - serpentine group, 195, 196
  - CMASH system (*see* CaO–MgO–Al<sub>2</sub>O<sub>3</sub>–SiO<sub>2</sub>–H<sub>2</sub>O (CMASH) system)
  - harzburgitic composition, 191
  - high temperature, 210–211
  - igneous origin, 191, 192
  - isofacial, 192
  - isograds, 205, 206
    - Al-bearing lherzolite, 205, 206
    - antigorite decomposition, 206
    - DOMINO/THERIAK model, 204
    - Malenco serpentinite, Central Alps, 206
    - mapping and definition, 205
    - modal metamorphic composition, 205
    - serpentinite, 202, 204
  - magnesium silicate, 191
  - mantle fragments, crust, 191
  - MSH system (*see* MgO–SiO<sub>2</sub>–H<sub>2</sub>O system)
  - open system reaction, 219–221
  - peridotite serpentinization, 208–210
  - potassium-bearing peridotites, 221
  - P–T conditions, 192
  - rock types, 193–194
  - thermometry and geobarometry, 211–212
  - uppermost mantle mineral assemblages, 202, 206–208
- Ultramylonite, 33
- W**
- Wairakite, 362
  - Wollastonite, 88, 99–101
- Z**
- Zeolite facies, 126